

THIS PAGE LEFT BLANK

AN ABSTRACT OF THE DISSERTATION OF

Yohsuke Kawamata for the degree of Doctor of Philosophy in Civil Engineering presented on May 12, 2009.

Title: Seismic Performance of Pile-supported Container Wharf Structures in Rockfill

Abstract approved:

Scott A. Ashford

Recently, the concept of performance based design has become popular for many types of structures, including port facilities under seismic loading. For the case of pile-supported wharves, the level of performance is generally estimated using the displacement capacity of the structure. Therefore, understanding soil-pile interaction is one of the most critical factors for estimating performance. One of the biggest challenges on the displacement estimation is defining the soil parameters. However, only limited information is available in the literature on the behavior of laterally loaded piles in the large-diameter rockfill typically used in port dike construction, where the particle size approaches the pile diameter.

In light of this, a series of full-scale lateral load tests on piles in the rockfill were conducted in order to obtain a better understanding of the performance of the wharf deck-pile-soil system against lateral loading, and reaction mechanism in rockfill. All the tests were conducted successfully, and large amount of useful data and some important observations were obtained during and after the tests.

Following the experiments, numerical analyses were conducted with a set of soil dependant stiffness curves (i.e. p - y curves) currently used for design practice. These results were compared with the test results in order to assess the validity of the current design approach. It was concluded that those p - y curves could provide reasonable rotation

and deflection profiles along the test piles, but gave considerably underestimated ultimate lateral resistance of the pile-soil system. In order to find possible reasons for this, the observations during and after the tests were carefully reviewed. Based on the review, it was found that the lateral reaction from the rockfill under low confinement plays a very important role. Considering particulate mechanism in the rockfill, a reasonable hypothesis was developed; i.e. the lateral reaction from the rockfill is a combination of reactions due to both friction and interlocking between large rock particles. Based on this hypothesis, backcalculation of the p - y curves was carried out comparing the experimental and numerical results, and it was concluded that addition of the interlocking concept to the p - y curves used in the current design methodology significantly improved performance.

© Copyright by Yohsuke Kawamata

May 12, 2009

All Right Reserved

Seismic Performance of a Pile-Supported Container Wharf Structures
in Rockfill

by

Yohsuke Kawamata

A DISSERTATION

Submitted to

Oregon State University

in partial fulfillment of
the requirements for the
degree of

Doctor of Philosophy

Presented May 12, 2009

Commencement June 2009

Doctor of Philosophy dissertation of Yohsuke Kawamata presented on May 12, 2009.

APPROVED:

Major Professor, representing Civil Engineering

Head of School of Civil and Construction Engineering

Dean of the Graduate School

I understand that my dissertation will become part of the permanent collection of Oregon State University libraries. My signature below authorizes release of my dissertation to any reader upon request.

Yohsuke Kawamata, Author

ACKNOWLEDGMENTS

The author would like to express his sincere gratitude to the sponsor of the Seismic Performance of Container Wharf Piles Project: the Port of Los Angeles, the Port of Long Beach, the Pacific Earthquake Engineering Research Center, and Oregon State University.

Discussions with Peter Yin of the Port of Los Angeles, and Omar Jaradat and Max Weismair of PBS&J, were greatly helpful to the success of this research.

Co-researchers, Teerawut Juirnarongrit, an ex-post-doctoral researcher at the University of California at San Diego, Carlos Blandon, a visiting student from the Rose School in Italy, and Nontapat Nimityongskul, a Graduate Student at Oregon State University made a lot of efforts on this research.

The technical advice from Professor Nigel Priestly, the Rose School in Italy, Professor José Restrepo, the University of California at San Diego, and Professor Geoffrey Martin of the University of Southern California assisted to gain the correct direction for this research.

Research committees at Oregon State University, Professor Chris Higgins, Professor Marvin Pyles, Professor Jerry Yamamuro, and Professor Prasad Tadepalli gave valuable comments and advice. The advice of Dr. Stephen Dickenson is also appreciated.

All of their help is greatly acknowledged to the success of this research.

Finally, the technical advisor of the author, Professor Scott Ashford at Oregon State University, gave the chance to do this great research, advice and comments to complete this research. The author is greatly thankful for all his works.

TABLE OF CONTENTS

	<u>Page</u>
1 INTRODUCTION	1
1.1 Objectives of Research	2
1.2 Organization of Report	2
1.3 Research Overview	4
2 LITERATURE REVIEW	8
2.1 Winkler Method and the Concept of p - y Curves	10
2.1.1 Concept of p - y curves	13
2.1.2 Reese sand p - y curves	14
2.1.3 API sand p - y curves	14
2.1.4 p - y curves used for current wharf design practice	15
2.1.5 Backcalculation of p - y curves from lateral load pile tests	15
2.1.6 Influence of pile properties on p - y curves.....	17
2.2 Experimental Works of Pile-Supported Wharf Structure in Rockfill	21
2.2.1 Full-scale pile test	22
2.2.2 Centrifuge testing.....	23
2.3 Shear Behavior of Rockfill	25
2.3.1 Confining pressure	25
2.3.2 Gradation.....	27
2.3.3 Maximum particle size.....	27
2.3.4 Particle shape	28
2.3.5 Presence of water	29
2.3.6 Three dimensional failure criteria for cohesionless granular materials	29
2.4 Summary	31
3 DESIGN, CONSTRUCTION AND PROCEDURE OF PILE TEST...49	

TABLE OF CONTENTS (Continued)

	<u>Page</u>
3.1 Test Plan Update Histories	49
3.2 Prediction Analyses Prior to Construction of Test Specimens	51
3.2.1 Prediction in the original proposal (Plan Version 1)	51
3.2.2 Prediction before construction (Plan Version 2).....	52
3.3 Construction of Test Specimens and Test Procedures.....	56
3.3.1 General descriptions of test setup	56
3.3.2 Construction procedure.....	57
3.3.3 Test piles	58
3.3.4 Soil pit.....	58
3.3.5 Pile installation.....	59
3.3.6 Backfilling.....	60
3.3.7 Connections and load stubs.....	62
3.3.8 Concrete spacer, steel beam, and actuator	63
3.3.9 Data acquisition system	64
3.3.10 Testing and load protocol.....	64
3.3.11 Excavation for Single Pile Test 2.....	65
3.4 Revision of Test Plan using Single Pile Test Results	65
3.4.1 Revised prediction following the single pile tests (Plan Version 3).....	66
3.4.2 Excavation for System Tests.....	67
3.5 Description and Calibration Test of Sensors	67
3.5.1 Removable tiltmeters	68
3.5.2 Strain gages.....	70
3.5.3 String-activated linear potentiometers	70
3.5.4 Instrumented steel beam	71
3.5.5 Other sensors.....	72
3.6 Summary.....	72
4 TEST RESULTS	132
4.1 Single Pile Test 1	133

TABLE OF CONTENTS (Continued)

	<u>Page</u>
4.1.1 Load displacement behavior	134
4.1.2 Curvature along test pile	135
4.1.3 Rotation and deflection along test pile.....	136
4.1.4 Visual inspection.....	136
4.2 Single Pile Test 2	137
4.2.1 Observations during loading	137
4.2.2 Load displacement curve at pile top	138
4.2.3 Curvature along test pile	139
4.2.4 Rotation and deflection along test pile.....	139
4.2.5 In-ground inspection during pile demolition	140
4.3 System Test 1	140
4.3.1 Observations during loading	141
4.3.2 Load displacement curve at pile top	142
4.3.3 Shear and axial forces along each pile	143
4.3.4 Curvature along test pile	145
4.3.5 Rotation and deflection along test pile.....	146
4.3.6 In-ground inspection during pile demolition	147
4.4 System Test 2.....	147
4.4.1 Observations during loading	148
4.4.2 Load displacement curve at pile top	149
4.4.3 Shear and axial forces along each pile	149
4.4.4 Curvature along test pile	150
4.4.5 Rotation and deflection of pile.....	151
4.4.6 In-ground inspection during pile demolition	151
4.5 Summary	152
5 ANALYSIS FOR MODIFICATION OF DESIGN	193
5.1 Comparison between Test Results and Current Design.....	194
5.1.1 Numerical model and parameters	194
5.1.2 Comparison of the test results and the current design	195
5.2 Modification of Numerical Model and Parameters	196

TABLE OF CONTENTS (Continued)

	<u>Page</u>
5.2.1 Notable observations during and after testing	197
5.2.2 Assumptions for backcalculation of p -y curves	198
5.2.3 Settlement around the test pile	199
5.2.4 Considerations of reaction generation mechanism in rockfill	200
5.2.5 Pile responses analyzed using backcalculated p -y curves.....	205
5.3 Pushover Analyses for Whole Wharf Structure.....	211
5.3.1 Numerical model and parameters	212
5.3.2 Comparison of results of entire wharf model with various p -y curves	213
5.3.3 Conclusions and recommendations for design procedure	217
5.4 Uncertainties on Pile in Rockfill and Possible Future Research	218
5.4.1 Uncertainties on laterally loaded pile in rockfill.....	219
5.4.2 Possible future research	230
5.5 Summary	233
6 SUMMARY AND CONCLUSIONS.....	303
6.1 Summary	303
6.2 Conclusions.....	304
REFERENCES	306
APPENDIX-A UPLIFT CAPACITY OF PILE.....	311
APPENDIX-B SPECIFICATION OF ROCKFILL	314

LIST OF FIGURES

<u>Figure</u>	<u>Page</u>
Figure 1-1 Typical pile-supported wharf structure at the Port of Los Angeles	5
Figure 1-2 An example of model for pushover analysis in the current design	5
Figure 1-3 Site location.....	6
Figure 1-4 Location of soil pit for this research at the site	6
Figure 1-5 Flow chart of the research	7
Figure 2-1 Concept of Winkler's spring method for laterally loaded pile.....	38
Figure 2-2 Definition of p - y concept (after Dunnavant 1986).....	38
Figure 2-3 Shapes of p - y Curves for Sand (Reese <i>et al.</i> 1974).....	39
Figure 2-4 Coefficients needed to derive p - y curves for sand (API 1987)	39
Figure 2-5 p - y curves for the current wharf design (Martin 2005)	40
Figure 2-6 Methodology in developing p - y curves (Reese and Van Impe 2001)	40
Figure 2-7 Sketches to indicate influence of shape of cross section of pile on the ultimate resistance of soil (Reese and Van Impe 2001)	41
Figure 2-8 Configuration of Strain Wedge model (Ashour and Norris 2000).....	41
Figure 2-9 Effect of pile cross section shape on p - y curves (Ashour and Norris 2000)	42
Figure 2-10 Influence of pile diameters on dimensions of bulb pressure (Terzaghi 1995)	42
Figure 2-11 Comparison of p - y curves for different pile diameters in cemented sand (Juirnarongrit and Ashford 2005)	43
Figure 2-12 Effect of pile bending stiffness on p - y curves (Ashour and Norris 2000) ..	43
Figure 2-13 Cross section of setup of full-scale test on pile in rockfill (Diaz <i>et al.</i> 1984)	44
Figure 2-14 Back calculated moment profile and p - y curves for rockfill (Diaz <i>et al.</i> 1984)	44

LIST OF FIGURES (Continued)

<u>Figure</u>	<u>Page</u>
Figure 2-15 Centrifuge model of pile group tests (Boland <i>et al.</i> 2001b).....	45
Figure 2-16 Centrifuge model of single pile tests (Boland <i>et al.</i> 2001b)	45
Figure 2-17 Lateral pile response predicted by FLAC (McCullough <i>et al.</i> 2004)	46
Figure 2-18 Various definitions of failure envelope (Bertacchi and Bellotti 1970)	46
Figure 2-19 Examples of results from triaxial test for rockfill (Marsal 1973)	47
Figure 2-20 Effect of gradation on shear strength (Anagnosti and Popovic 1982)	47
Figure 2-21 Effect of water on shear behavior of rockfill (Bertacchi and Bellotti 1970)	48
Figure 2-22 Characteristics of failure shown in 3-dimensional stress condition (Lade 1977)	48
Figure 3-1 Test setup (Plan Version 1)	80
Figure 3-2 Potential hinge locations	81
Figure 3-3 Test setup (Plan Version 2)	82
Figure 3-4 Numerical model for single pile tests.....	83
Figure 3-5 Numerical model for system tests	83
Figure 3-6 Flow chart of analysis for system tests	84
Figure 3-7 Properties of prestressed concrete piles	85
Figure 3-8 Properties of connection between pile and load stub	85
Figure 3-9 Properties of soil-pile springs typically used for wharf design.....	86
Figure 3-10 Predicted load-displacement curves at pile top (Single Pile Test, Version 2)	87
Figure 3-11 Predicted profiles of moment and curvature (Single Pile Test, Version 2)	87
Figure 3-12 Predicted load-displacement curves at pile top (System Test 1, Version 2)	88

LIST OF FIGURES (Continued)

<u>Figure</u>	<u>Page</u>
Figure 3-13 Predicted profiles of curvature (Push, System Test 1, Version 2)	88
Figure 3-14 Predicted profiles of curvature (Pull, System Test 1, Version 2).....	89
Figure 3-15 Predicted load-displacement curves at pile top (System Test 2, Version 2)	89
Figure 3-16 Profiles of curvature (Push, System Test 2, Version 2)	90
Figure 3-17 Profiles of curvature (Pull, System Test 2, Version 2)	90
Figure 3-18 Plan view of test set-up	91
Figure 3-19 Section view for Single Pile Test at completion of construction	91
Figure 3-20 Test set-up for system tests at completion of construction	92
Figure 3-21 Flow chart of construction	93
Figure 3-22 Building test piles (Utility Vault at Fontana, CA)	94
Figure 3-23 Details of test piles	95
Figure 3-24 Soil boring log at the construction site.....	96
Figure 3-25 Location of newly excavated soil pit	97
Figure 3-26 Dimensions of newly excavated soil pit.....	97
Figure 3-27 Excavation of soil pit	98
Figure 3-28 Locations of test piles.....	99
Figure 3-29 Details of footing.....	99
Figure 3-30 Locations of steel beams fixing the pile tops	100
Figure 3-31 Pile installation.....	101
Figure 3-32 Gradation of rockfill.....	103
Figure 3-33 Details of backfilling (first stage)	104
Figure 3-34 Details of backfilling (second stage).....	104

LIST OF FIGURES (Continued)

<u>Figure</u>	<u>Page</u>
Figure 3-35 Details of backfilling in vicinity of rubber bands	105
Figure 3-36 Backfilling.....	106
Figure 3-37 Details of load stub.....	108
Figure 3-38 Details of connection.....	108
Figure 3-39 Building connections and load stubs.....	109
Figure 3-40 Details of concrete spacer block	111
Figure 3-41 Concrete spacer block	111
Figure 3-42 Dimension of steel beam.....	112
Figure 3-43 Steel beam connecting test piles (before instrumentation)	112
Figure 3-44 Hydraulic actuator	113
Figure 3-45 Aspect of test setup for Single Pile Test	113
Figure 3-46 Aspect of test setup for System Test 1	114
Figure 3-47 Data acquisition system.....	114
Figure 3-48 Load protocol	115
Figure 3-49 Section view for Single Pile Test 2 (after excavation).....	116
Figure 3-50 Test setup after 2 ft excavation (Plan Version 3).....	117
Figure 3-51 Predicted load-displacement curves at pile top (System Test 1, Version 3)	118
Figure 3-52 Predicted profiles of curvature (Push, System Test 1, Version 3)	118
Figure 3-53 Predicted profiles of curvature (Pull, System Test 1, Version 3).....	119
Figure 3-54 Predicted load-displacement curves at pile top (System Test 2, Version 3)	119
Figure 3-55 Predicted profiles of curvature (Push, System Test 2, Version 3)	120

LIST OF FIGURES (Continued)

<u>Figure</u>	<u>Page</u>
Figure 3-56 Predicted profiles of curvature (Pull, System Test 2, Version 3).....	120
Figure 3-57 Excavation for system tests.....	121
Figure 3-58 Tiltmeter sensor with housing.....	122
Figure 3-59 Cross section showing tiltmeter inside inclinometer casing.....	122
Figure 3-60 Installation of a series of tiltmeters through inclinometer casing.....	123
Figure 3-61 Locations of inclinometers for Single Pile Test.....	123
Figure 3-62 Locations of inclinometers for System Test 1.....	124
Figure 3-63 Locations of inclinometers for System Test 2.....	124
Figure 3-64 Strain gages along additional #3 rebars.....	125
Figure 3-65 Elevations of strain gages along test pile for Single Pile Test.....	125
Figure 3-66 Elevations of strain gages along test pile for System Test 1.....	126
Figure 3-67 Elevations of strain gages along test pile for System Test 2.....	126
Figure 3-68 String-activated linear potentiometer.....	127
Figure 3-69 Location of linear potentiometers on the load stub for Single Test.....	127
Figure 3-70 Location of linear potentiometers on the load stub for System Test 1.....	128
Figure 3-71 Location of linear potentiometers on the load stub for System Test 2.....	128
Figure 3-72 Instrumentation plan for steel beam.....	129
Figure 3-73 Test setup plan for calibration of the steel beam.....	129
Figure 3-74 Aspect of test setup for calibration of the steel beam.....	130
Figure 3-75 Distribution of shear force on wide flange.....	130
Figure 3-76 Calibration results of steel beam (shear strain).....	131
Figure 3-77 Calibration results of steel beam (gages on flange of steel beam).....	131
Figure 4-1 Applied load and displacement at the pile top for Single Pile Test 1.....	156

LIST OF FIGURES (Continued)

<u>Figure</u>	<u>Page</u>
Figure 4-2 Pile top force vs. displacement envelopes (Single Pile Test 1).....	156
Figure 4-3 Hysteretic loops for Cycles 1 through 5 (Single Pile Test 1).....	157
Figure 4-4 Hysteretic loops for all the loadings (Single Pile Test 1).....	157
Figure 4-5 Strain distribution to be converted to curvature of the section	158
Figure 4-6 Profile of curvature derived from strain gage arrays (Single Pile Test 1) ..	159
Figure 4-7 Profiles of rotation and deflection derived from tiltmeter readings (Single Pile Test 1)	159
Figure 4-8 Visual inspection of in-ground parts of test pile (Single Pile Test 1)	160
Figure 4-9 Applied load and displacement at the pile top for Single Pile Test 2	161
Figure 4-10 Details of the observed damage (Single Pile Test 2)	161
Figure 4-11 Deformed test pile after all the loading (Single Pile Test 2).....	162
Figure 4-12 Peak lateral load and corresponding displacement at any loading cycles (Single Pile Test 2)	162
Figure 4-13 Hysteretic loops for Cycles 1 through 3 (Single Pile Test 2).....	163
Figure 4-14 Hysteretic loops for Cycles 4 through 7 (Single Pile Test 2).....	163
Figure 4-15 Curvature profile derived from array of strain gages (Single Pile Test 2)	164
Figure 4-16 Curvature profile derived from records on tiltmeters (Single Pile Test 2)	164
Figure 4-17 Profiles of rotation and deflection derived from rotation (Single Pile Test 2)	165
Figure 4-18 General view after excavation to 3ft below ground surface (Single Pile Test 2)	166
Figure 4-19 Exposed in-ground plastic hinge on the north side of the pile (Single Pile Test 2).....	166
Figure 4-20 Applied load and displacement at the pile top for System Test 1	167

LIST OF FIGURES (Continued)

<u>Figure</u>	<u>Page</u>
Figure 4-21 Cracks at P3 for loading Cycle 3 (System Test 1)	167
Figure 4-22 Concrete crushing during Cycle 8 at P3 (System Test 1)	168
Figure 4-23 Settlement around the test pile (System Test 1).....	168
Figure 4-24 Deformed piles after the final loading (System Test 1)	169
Figure 4-25 Load displacement envelopes (System Test 1)	169
Figure 4-26 Hysteretic loops for Cycles 1 through 3 (System Test 1)	170
Figure 4-27 Hysteretic loops for all the loading cycles (System Test 1).....	170
Figure 4-28 Free body diagram of the system tests	171
Figure 4-29 Time histories of shear load at each pile top (System Test 1)	171
Figure 4-30 Distribution of the shear load (System Test 1, Push).....	172
Figure 4-31 Distribution of the shear load (System Test 1, Pull)	172
Figure 4-32 Time histories of axial load along each pile (System Test 1)	173
Figure 4-33 Axial force vs. displacement curves on each pile (System Test 1).....	173
Figure 4-34 Profiles of curvature (System Test 1).....	174
Figure 4-35 Possible mechanism of critical section migration.....	175
Figure 4-36 Profiles of rotation (System Test 1)	176
Figure 4-37 Profiles of deflection derived from rotation (System Test 1)	177
Figure 4-38 Excavation sequence at the north side (System test 1, P3)	178
Figure 4-39 Pile inspection during demolition of the piles (System Test 1, P3).....	178
Figure 4-40 Plastic hinge (System Test 1, P3).....	179
Figure 4-41 Excavation sequence on the north side (System Test 1, P5).....	179
Figure 4-42 Applied load and displacement at the pile top for System Test 2.....	180
Figure 4-43 Cracks on P2 and P4 for loading Cycles 1 to 3 (System Test 2)	180

LIST OF FIGURES (Continued)

<u>Figure</u>	<u>Page</u>
Figure 4-44 Cracks on P2 and P4 for loading Cycle 6 (System Test 2)	181
Figure 4-45 Settlement of rockfill around P2 and P4 after Cycle 8 (System Test 2) ...	181
Figure 4-46 Spalling at connection of P4 at Cycle 10 (System Test 2)	182
Figure 4-47 Deformed test piles after the final loading Cycle 11 (System Test 2)	182
Figure 4-48 Load displacement envelopes (System Test 2)	183
Figure 4-49 Hysteretic loops for Cycles 1 through 3 (System Test 2)	184
Figure 4-50 Hysteretic loops for all the loadings (System Test 2)	184
Figure 4-51 Time histories of shear load at each pile top (System Test 2)	185
Figure 4-52 Distribution of the shear load (System Test 2, Push)	185
Figure 4-53 Distribution of the shear load (System Test 2, Pull)	186
Figure 4-54 Time histories of axial force along each pile (System Test 2)	186
Figure 4-55 Axial load vs. displacement curves on each pile (System Test 2)	187
Figure 4-56 Profiles of curvature (System Test 2)	188
Figure 4-57 Profiles of rotation (System Test 2)	189
Figure 4-58 Profiles of deflection derived from rotation (System Test 2)	190
Figure 4-59 Excavation sequence on the north side (System Test 2, P2)	191
Figure 4-60 Plastic hinge on the north side (System Test 2, P2)	191
Figure 4-61 Excavation sequence on the north side (System Test 2, P4)	192
Figure 4-62 Plastic hinge on the north side (System Test 2, P4)	192
Figure 5-1 Load-displacement curve for Single Pile Test 1 with various <i>p</i> -multipliers	239
Figure 5-2 Rotation profiles for Single Pile Test 1 with various <i>p</i> -multipliers	239
Figure 5-3 Deflection profiles for Single Pile Test 1 with various <i>p</i> -multipliers	240

LIST OF FIGURES (Continued)

<u>Figure</u>	<u>Page</u>
Figure 5-4 Curvature profiles for Single Pile Test 1 with various p -multipliers	240
Figure 5-5 Load-displacement curve for Single Pile Test 2 with various p -multipliers.....	241
Figure 5-6 Rotation profiles for Single Pile Test 2 with various p -multipliers	241
Figure 5-7 Deflection profiles for Single Pile Test 2 with various p -multipliers	242
Figure 5-8 Curvature profiles for Single Pile Test 2 with various p -multipliers	242
Figure 5-9 Notable observations	243
Figure 5-10 Sketch of settlement around P5 after System Test 1	244
Figure 5-11 Concept of effect of settlement around pile on load displacement curve .	244
Figure 5-12 Possible particle movements	245
Figure 5-13 Definition of friction and interlocking	245
Figure 5-14 Concept on soil-pile spring of friction and depth independent interlocking	246
Figure 5-15 Soil-pile springs of friction and depth independent interlocking.....	246
Figure 5-16 Three-dimensional stress pass in rockfill	247
Figure 5-17 Comparison of profiles of ultimate shear resistance	247
Figure 5-18 Effect of downslope to interlocking	248
Figure 5-19 Multiplier of interlocking reduction for piles on downslope	248
Figure 5-20 Load-displacement curve for Single Pile Test 1 with p -multipliers and interlocking	249
Figure 5-21 Rotation profiles for Single Pile Test 1 with p -multipliers and interlocking	249
Figure 5-22 Deflection profiles for Single Pile Test 1 with p -multipliers and interlocking	250

LIST OF FIGURES (Continued)

<u>Figure</u>	<u>Page</u>
Figure 5-23 Curvature profiles for Single Pile Test 1 with p -multipliers and interlocking	250
Figure 5-24 Load-displacement curve for Single Pile Test 2 with p -multipliers and interlocking	251
Figure 5-25 Rotation profiles for Single Pile Test 2 with p -multipliers and interlocking	251
Figure 5-26 Deflection profiles for Single Pile Test 2 with p -multipliers and interlocking	252
Figure 5-27 Curvature profiles for Single Pile Test 2 with p -multipliers and interlocking	252
Figure 5-28 Load-displacement curve for System Test 1 with p -multipliers and interlocking	253
Figure 5-29 Load-displacement curve on each pile for System Test 1 with p -multipliers and interlocking.....	254
Figure 5-30 Axial force along each pile for System Test 1	255
Figure 5-31 Rotation profiles for System Test 1 with p -multipliers and interlocking (pushing)	256
Figure 5-32 Rotation profiles for System Test 1 with p -multipliers and interlocking (pulling)	257
Figure 5-33 Deflection profiles for System Test 1 with p -multipliers and interlocking (pushing).....	259
Figure 5-34 Deflection profiles for System Test 1 with p -multipliers and interlocking (pulling)	260
Figure 5-35 Curvature profiles for System Test 1 with p -multipliers and interlocking (pushing)	262
Figure 5-36 Curvature profiles for System Test 1 with p -multipliers and interlocking (pulling)	263
Figure 5-37 Load-displacement curve for System Test 2 with p -multipliers and interlocking	265

LIST OF FIGURES (Continued)

<u>Figure</u>	<u>Page</u>
Figure 5-38 Load-displacement curve on each pile for System Test 2 with p -multipliers and interlocking.....	266
Figure 5-39 Axial force on each pile for System Test 2	267
Figure 5-40 Rotation profiles for System Test 2 with p -multipliers and interlocking (pushing)	268
Figure 5-41 Rotation profiles for System Test 2 with p -multipliers and interlocking (pulling)	269
Figure 5-42 Deflection profiles for System Test 2 with p -multipliers and interlocking (pushing).....	271
Figure 5-43 Deflection profiles for System Test 2 with p -multipliers and interlocking (pulling)	272
Figure 5-44 Curvature profiles for System Test 2 with p -multipliers and interlocking (pushing).....	274
Figure 5-45 Curvature profiles for System Test2 with p -multipliers and interlocking (pulling)	275
Figure 5-46 Subsurface cross section of Berth 100 at the Port of Los Angeles	277
Figure 5-47 Pile layout of Berth 100 at the Port of Los Angeles	277
Figure 5-48 Numerical model of entire wharf structure	278
Figure 5-49 Flow chart of analysis for entire wharf structure	279
Figure 5-50 Load displacement curves on non-seismic piles (rows A through D)	280
Figure 5-51 Load displacement curves on seismic piles (rows E and F).....	280
Figure 5-52 Load-displacement curves for entire wharf structure.....	281
Figure 5-53 Deck displacement at certain inertial force	281
Figure 5-54 Deformed shape (Lower bound, $m_p = 0.3$; multiplied by 50)	282
Figure 5-55 Deformed shape (Standard, $m_p = 1.0$; multiplied by 50)	283
Figure 5-56 Deformed shape (Upper bound, $m_p = 2.0$; multiplied by 50).....	284

LIST OF FIGURES (Continued)

<u>Figure</u>	<u>Page</u>
Figure 5-57 Comparison of moment profiles along pile in row F in various analysis cases	285
Figure 5-58 Relationship between deck displacement and maximum moment	285
Figure 5-59 Difference of deck displacement among various analysis cases.....	286
Figure 5-60 Difference of maximum moment among various analysis cases	286
Figure 5-61 Possible mechanism on reaction generation in rockfill.....	287
Figure 5-62 Simplified p-y curves based on possible reaction generation mechanism in rockfill	288
Figure 5-63 Contact forces on a particle in poor- and well-grades rock	289
Figure 5-64 Possible relationship between particle size and ratio of interlocking to friction	289
Figure 5-65 Possible relationship between loading rate and friction/interlocking	290
Figure 5-66 Free body diagram around pile	290
Figure 5-67 Density of contacts in relatively large rockfill.....	291
Figure 5-68 Variance of reaction and relative size of soil particles	291
Figure 5-69 Expected relationship between relative size of soil particle and variance of pile response	292
Figure 5-70 Concept of probabilistic analysis on laterally loaded pile response	292
Figure 5-71 Probability density function of p -multiplier representing contact strength	293
Figure 5-72 Probability density function of gap size.....	294
Figure 5-73 Results from Monte-Carlo simulation for random contact strength	295
Figure 5-74 Results from Monte-Carlo simulation for random gap size.....	296
Figure 5-75 Results from Monte-Carlo simulation for random contact and gap size ..	297
Figure 5-76 Comparison of PDFs of various analysis cases.....	298

LIST OF FIGURES (Continued)

<u>Figure</u>	<u>Page</u>
Figure 5-77 An example of critical section migration in analysis	299
Figure 5-78 Network of experimental and numerical research	299
Figure 5-79 Examples of numerical model in DEM on pile behavior for inertial force	300
Figure 5-80 An example of numerical model in DEM on pile behavior for kinematic force	300
Figure 5-81 An example of numerical model in DEM on relative size of pile to soil particle size	301
Figure 5-82 An example of setup in centrifuge test on pile behavior for inertial force	301
Figure 5-83 An example of setup in centrifuge test on pile behavior for kinematic force	302
Figure 5-84 An example of setup in full-scale test on p - y curves of rockfill	302

LIST OF TABLES

<u>Table</u>	<u>Page</u>
Table 2-1 Summary of solutions for laterally loaded pile subjected to lateral loading in the case of constant subgrade reaction (Hetenyi 1946)	32
Table 2-2 Summary of solutions for laterally loaded pile subjected to moment loading in the case of constant subgrade reaction (Hetenyi 1946)	33
Table 2-3 Summary of Procedure in Developing Sand p - y Curves (Reese <i>et al.</i> 1974)	34
Table 2-4 Summary of Procedure in Developing API Sand p - y Curves (API 1987)	35
Table 2-5 Angle of friction between soil and pile (US Army Corps of Engineers 1991)	36
Table 2-6 Summary of full-scale lateral load pile tests in granular soils.....	36
Table 2-7 Summary of parameters in the constitutive model in three-dimensional stress condition (Lade 1977).....	37
Table 3-1 Update histories of test plan	74
Table 3-2 List of the test sets (Plan Version 1).....	75
Table 3-3 List of the test sets (Plan Version 2).....	75
Table 3-4 Summary of p -multipliers used (Plan Version 2).....	76
Table 3-5 Properties of test pile	76
Table 3-6 As-built locations of the test piles	77
Table 3-7 Specifications of compaction device	77
Table 3-8 List of the test sets (Plan Version 3).....	78
Table 3-9 Summary of p -multipliers used (Plan Version 3).....	78
Table 3-10 List of instrumentation	79
Table 4-1 Target displacement and load for Single Pile Test 1	153
Table 4-2 Target displacement and load for Single Pile Test 2	153
Table 4-3 Target displacement and load for System Test 1.....	154

LIST OF TABLES (Continued)

<u>Table</u>	<u>Page</u>
Table 4-4 Recalculated ductility for System Test 1	154
Table 4-5 Target displacement and load for System Test 2.....	155
Table 4-6 Recalculated ductility for System Test 2.....	155
Table 5-1 Summary of analysis cases for back analysis with various p -multipliers	235
Table 5-2 Summary of analysis cases for back analysis with interlocking and settlement.....	236
Table 5-3 Summary of analysis cases for entire wharf structure.....	237
Table 5-4 Numerical parameters used for analysis on entire wharf behavior	237
Table 5-5 Summary of important uncertainties on behavior of pile in rockfill	238

1 INTRODUCTION

The seismic code for port facilities approved by the Port of Los Angeles (2004) requires performance-based design for two levels of earthquake intensity: the Operating Level Earthquake (OLE) which has 50% probability of exceedance in 50 years and the Contingency Level Earthquake (CLE) having 10% probability of exceedance in 50 years. For the OLE event, the structures should remain operational with insignificant structural damage, while behavior of the structures should be in elastic and limited permanent deformations which can be repaired in an acceptable period of time for the CLE event.

At ports in the West Coast of the United States, pile-supported pier-type structure is one of the most popular types of wharves (Figure 1-1), and 2 ft (0.61 m) octagonal prestressed reinforced concrete piles are frequently used. For the pile-supported wharves, expected level of performance can be estimated by displacement capacity. In the current design practice, their displacement capacity is derived from static non-linear pushover analysis with Winkler's spring method as shown in Figure 1-2 (Winkler 1867). The analysis also gives the most critical sections of the structure at where potential damage (e.g. severe cracking or spalling of surface concrete) may develop under strong motion during earthquakes. The most possible location of damage is pile-cap connection, as well as in-ground parts of piles showing the maximum moment. Because the pile-deck connection is above the ground surface and damage there can be repaired, it is allowed even for the CLE event. On the other hand, in-ground spalling is not allowed for the CLE event because it is not repairable unless large amount of soil around the damaged piles is excavated. Once in-ground spalling occurs along piles, sea water can access to prestress strands and spiral reinforcement in the piles, and promote corrosion. In fact, allowable compressive strain in prestressed concrete piles for spalling of surface concrete is one of the most critical factors in wharf design. Therefore, appropriate nonlinear soil dependent stiffness curves, called p - y curves (e.g. Winkler 1867), and compressive strain on surface concrete when spalling occurs should be used for displacement based design with reasonable accuracy. However, information available in literature is quite limited on

behaviors of laterally loaded piles in large-diameter rockfill typically used in port facilities even though there is several literature available about full-scale pile tests in sand, clay, or liquefiable soil.

In order to supplement this shortage of information about behavior of laterally loaded wharf-foundation-dike systems in rockfill, a series of full-scale lateral load tests of piles placed in large rockfill was carried out at the Soil-Foundation-Structure-Interaction Test Facility at the University of California at San Diego's. The locations of the test site and a soil pit used for the tests are shown in Figure 1-3 and Figure 1-4, respectively. Following the series of experiments, numerical analyses were also performed in order to find better understanding on the pile-large particle rockfill interaction.

1.1 Objectives of Research

The main goals of this research program are to provide reliable numerical models and parameters for displacement based design of pile-supported wharf structures in rockfill, as well as to obtain useful information on behavior of full-scale pile-rockfill systems during lateral loading. Specifically, the objectives of this research study can be summarized as follows:

- 1) Assess the p - y curves used for the current design practice
- 2) Develop understanding of the reaction mechanism in large particle size rockfill
- 3) Modify the p - y curves with consideration of the reaction mechanism
- 4) Provide recommendations for design practice
- 5) Propose possible future research directions in this area

1.2 Organization of Report

The following outlines the organization of this dissertation.

Chapter 1 Introduction – Provides a brief description on the importance of research on the full-scale testing followed by numerical analysis of piles in large diameter rockfill. Also, research objectives, an outline of this dissertation, and research overview are described.

Chapter 2 Literature Review – Provides a review of the p - y method in predicting lateral pile response, including the concept and types of p - y curves for cohesionless soil currently available. Also, past work about the effect of pile properties on p - y curves is introduced. A summary of experimental works conducted by several researchers such as full-scale lateral pile load tests, and centrifuge pile tests, were also given, as well as numerical works based on test results. In addition, a review on shear behavior of rockfills is provided.

Chapter 3 Design, Construction and Procedure of Pile Test – Presents details of construction and testing methodology including prediction analysis for design of the test specimens, construction procedures, regulations, and dimensions are presented. In addition, details of instrumentation such as purposes, types, locations, calibration tests of sensors are described.

Chapter 4 Test Results – Presents test results obtained from the first two single pile tests and the following two system tests such as load displacement curves and profiles of rotation along the pile are presented. Some photos taken during excavation for in-ground inspection and pile removal are also shown.

Chapter 5 Analysis for Modification of Design – Shows comparisons between results from tests and the current design practice in order to verify the p - y curves used for design of pile-supported wharves. Based on test results and observations during testing, more reasonable p - y curves are proposed. In addition, magnitude of impact of the proposed modification on whole wharf design was estimated to show emergency level of more research on pile behaviors in rockfills. At the end of the chapter, some uncertainties

on behaviors of laterally loaded pile in rockfill are listed up and possible future research is briefly introduced.

Chapter 6 Summary and Conclusions - Provides the summary and conclusions of this research study.

1.3 Research Overview

The sequence of this research is shown in Figure 1-5. A series of experiments was composed of two single pile tests, and two coupled pile tests. Following the testing phase, backcalculation and parametric analyses were performed in the analysis phase in order to verify and improve parameters used for the current design. Finally, recommendations for design practice and possible future research works are proposed. Details are presented in the following chapters.

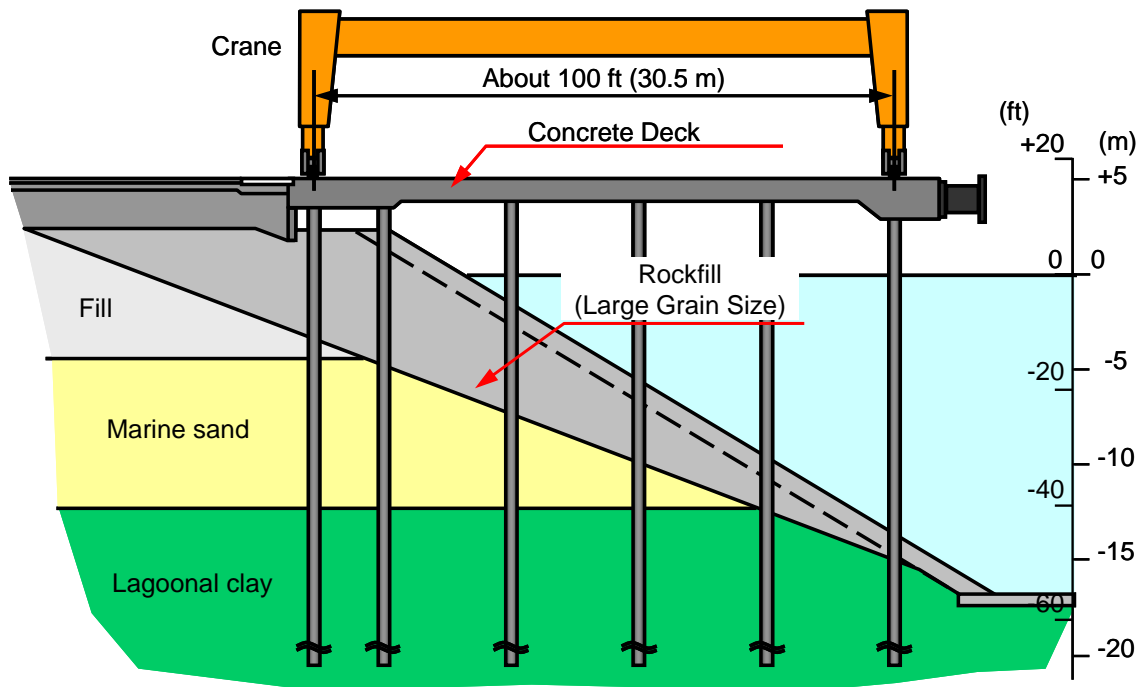


Figure 1-1 Typical pile-supported wharf structure at the Port of Los Angeles

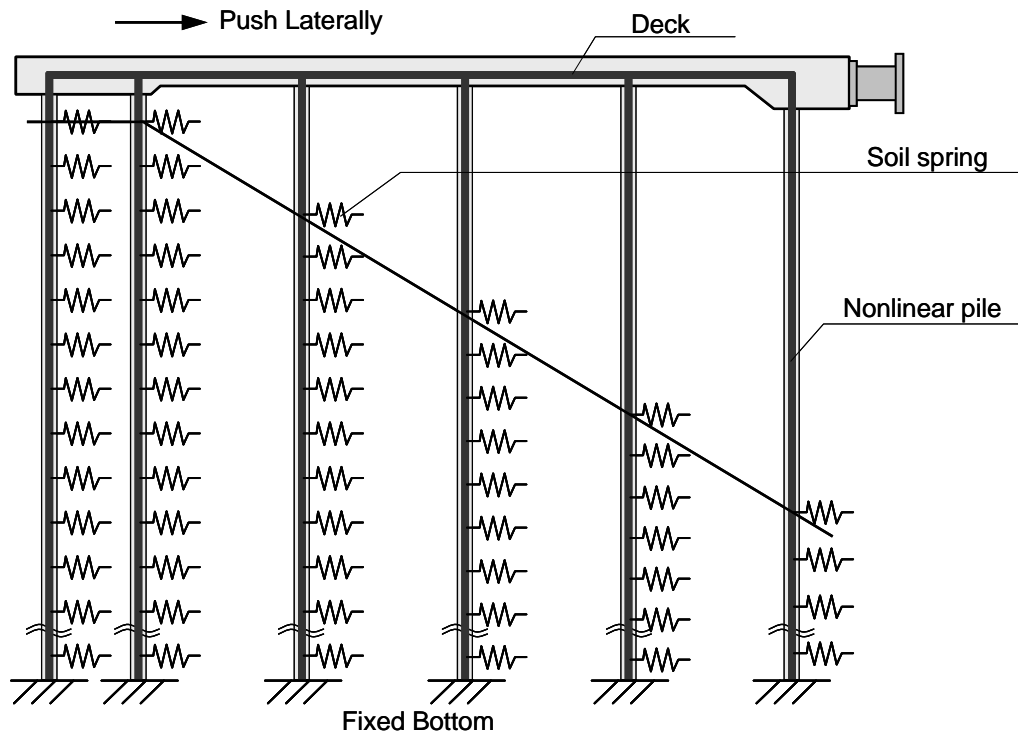


Figure 1-2 An example of model for pushover analysis in the current design



Figure 1-3 Site location

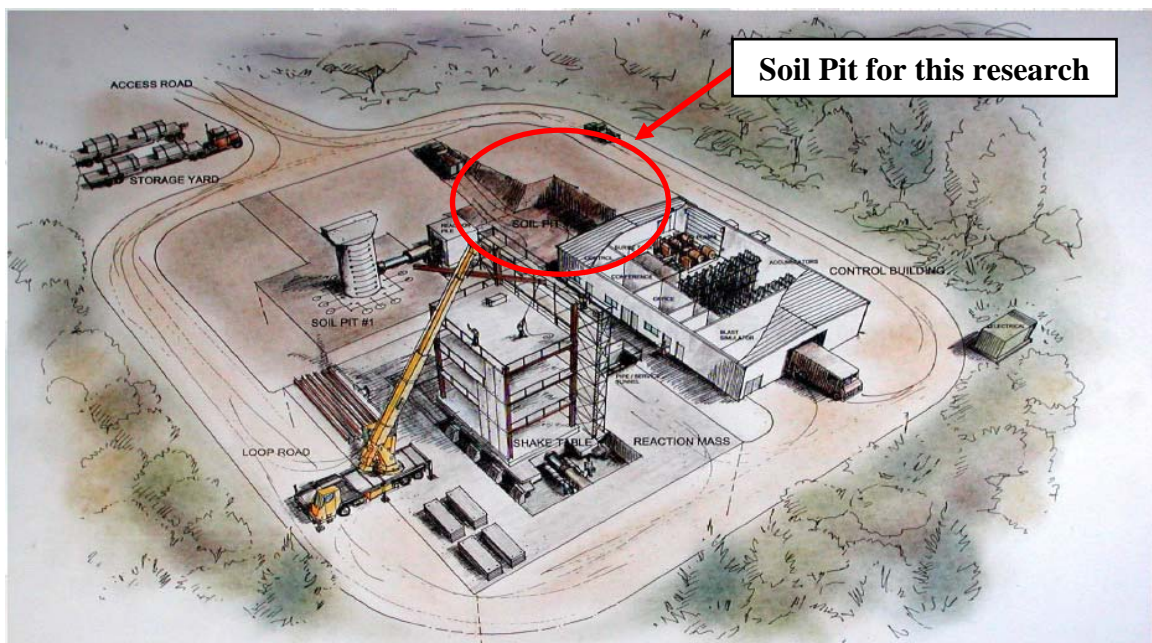


Figure 1-4 Location of soil pit for this research at the site

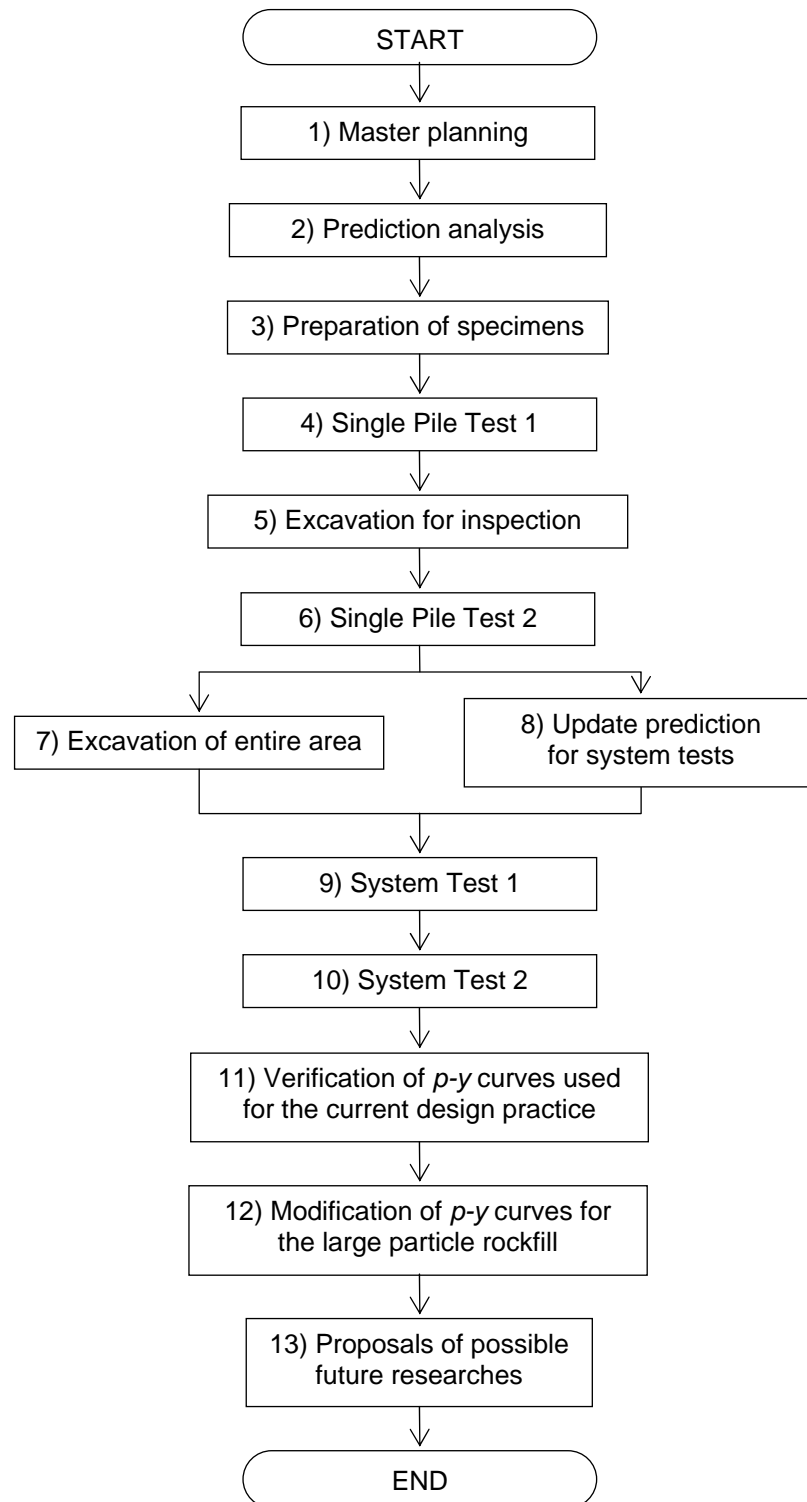


Figure 1-5 Flow chart of the research

2 LITERATURE REVIEW

The origin of interest in laterally loaded pile was in the offshore industry. Lateral loads from wind and waves are usually the most critical factor in design of such the structures. Design methodology for piles subjected to lateral loads in offshore structures can be applied to design for a variety of onshore and inland structures including pile-supported wharves and buildings which may be subjected to lateral forces from seismic event, winds, or large permanent lateral movement of soil, such as lateral spreading during liquefaction and landslide.

In the design of laterally loaded piles, there are two important criteria which must be satisfied. 1) The pile must have appropriate resistance with a reasonable factor of safety against the maximum lateral loading that might be applied to it, and 2) the deflection that occurs due to a working load must be in an acceptable range that superstructure can withstand (Poulos and Davis 1980).

There are several numerical methods proposed for laterally loaded pile problems, however, none of them can perfectly represent all factors affecting on lateral soil pile interaction, such as soil and pile properties. One of the most popular procedures used for design of piles subjected to lateral loading in earthquake engineering is a pushover analysis providing stress condition along piles and load-displacement relationship of soil-pile-structure system in interest. In this analytical methodology, two different possible loading conditions have to be considered for design; inertial force at pile top and kinematic force from ground movement (Port of Los Angeles 2004). The inertial input lateral displacement and load used for pile design can be appropriately estimated based on spectral displacement and acceleration at fundamental-mode period and damping ratio of the structure. Also, the kinematic input load and displacement can be obtained with slope stability analysis with finite element method (Martin 2005), or Newmark sliding block method (Newmark 1965).

The origin of pushover analysis on pile installed into soil was that of a transversely loaded thin elastic beam, supported by a series of linear springs, called as Winkler spring

method, acting along the length of the beam (Winkler 1867, Hetenyi 1946, Barber 1953, Matlock and Reese 1960, and Davisson and Gill 1963); the linear springs represent sub-grade reaction from surrounding soil. Because of its simplicity, this method was widely used in foundation engineering. However, when design of piles subjected to lateral load became to require that displacement of pile is within allowable range, pushover analysis with linear springs could not satisfy demands for reasonable displacement-based design because strong seismic motion induces large pile deflection and high nonlinearity of soil behavior. Therefore, nonlinear soil pile interaction is needed to be taken into account in order to simulate behavior of laterally loaded piles more accurately. A series of nonlinear soil dependent stiffness springs, known as p - y curves, backcalculated based on the results from full-scale lateral pile load tests were replaced the linear soil springs for a better representation of actual soil behaviors (e.g., Matlock 1970, Reese *et al.* 1974, Reese and Welch 1975, Reese *et al.* 1975, and Ismael 1990). Pile nonlinearity also can be easily taken into account by using nonlinear moment curvature relationship of the pile. As a result, the pushover analysis with the nonlinear p - y curves (p - y method) is one of the most acceptable methods widely used in design of laterally loaded piles at present.

Recently approved seismic design code for port facilities (Port of Los Angeles 2004) is also adopting the p - y method. The design code requires considering two types of loadings from soil-pile interaction as mentioned above; one is loading associated with the inertial response of the superstructure and the wharf deck inducing pile moments at the pile-deck joint and in the upper level of the embankment or dike, and the other is kinematic loading from permanent ground deformation inducing pile moments in the deep seated levels of the embankment or dike foundation soils. The code gives p - y curves of rockfill developed from a field test for design of pile-supported wharf structures under lateral loading (Section 2.1.4).

In this chapter, a summary of p - y method and several examples of p - y curves currently used for cohesionless material are reviewed. It is followed by a review of previous experimental and numerical works of piles in granular soil subjected to lateral loading performed to gain better understanding about pile-large particle rockfill interaction. Finally, research on the shear behavior of rockfill, a soil type considered in

this research study, is reviewed because soil-pile interaction is significantly related to characteristics of soil itself, as well as properties of pile.

2.1 Winkler Method and the Concept of p - y Curves

The Winkler method, sometimes known as the *subgrade reaction method*, is currently one of the most widely used in design practice of laterally loaded piles and pile-supported wharves. The method was first introduced by Winkler (1867) in order to analyze the response of beams on an elastic subgrade by characterizing the soil as a series of independent linear elastic springs. The concept of this method is illustrated in Figure 2-1. Advantages of this method over the elastic continuum method are; 1) the concept is quite simple to program in finite difference or finite element methods, and 2) soil nonlinearity and multiple soil layers can be easily taken into account replacing linear elastic springs with nonlinear soil dependent springs. The concept can be easily implemented in dynamic analysis in case if appropriate properties of p - y curves for cyclic loading are available. In addition, because of its simplicity, this method did not take time, and the computational cost was significantly less than other more complicated methods in past. Nowadays, performance of personal computers has been significantly improved and it can not be big advantage in general. Disadvantage of this method is the lack of consideration about continuity of soil, but it is not critical missing because the p - y curves include the effect of soil continuum behavior if these springs are properly backcalculated from appropriate experimental works.

Originally, a term of subgrade reaction indicates the pressure per unit area of the contact surface between a loaded beam or slab and the surrounding soil (P). A coefficient of subgrade reaction (k) is a ratio of the soil pressure at any given point (P) to a displacement (y) at the corresponding point.

$$k = \frac{P}{y} \quad (2.1)$$

In order to implement this concept for a laterally loaded pile, the Equation (2.1) has been modified (e.g. Reese and Matlock 1956, and Davisson and Gill 1963) as;

$$K = \frac{P}{y} \quad (2.2)$$

where K is a modulus of subgrade reaction (F/L^2) and p is a soil reaction per unit length of the pile (F/L).

With the subgrade reaction concept, the response of pile subjected to lateral loading can be derived by solving the following fourth order differential equation;

$$E_p I_p \frac{d^4 y}{dz^4} + Ky = 0 \quad (2.3)$$

where E_p is a modulus of elasticity of the pile, I_p is a moment of inertia of the pile, and z is depth. The Equation (2.3) can be solved analytically only in a case of constant modulus of subgrade reaction (K). However, soil behavior is highly nonlinear, and the equation is usually solved numerically using finite difference method to take account of nonlinearity of soil.

Hetenyi (1946) provided solutions for various infinite beams on an elastic Winkler subgrade analytically solving the governing equations. Table 2-1 and Table 2-2 summarize the solutions of lateral pile responses due to the lateral load and moment at pile head, respectively. However, the modulus of subgrade reaction is usually larger at deeper elevation especially in cohesionless friction materials, such as rockfill, the interesting material in this study.

Barber (1953) provided solutions to determine deflection and rotation of piles at the ground surface using the convenient plots for cases with constant soil modulus of subgrade reaction, as well as linearly increasing soil modulus of subgrade reaction with depth. The solutions can reasonably cover behavior of piles in friction materials providing larger reaction at deeper location, but they are only for piles installed in single

type of soil stratum, and piles are usually installed into several types of soil layers in reality.

Matlock and Reese (1960) included several functions of distribution of reaction modulus with depth (e.g. polynomial and power functions). Matlock and Reese also gave solutions for a special soil profile where the modulus of subgrade reaction has some finite value at the ground surface and continues to increase linearly with depth.

Davisson and Gill (1963) extended the Winkler's method to analyze behavior of laterally loaded piles in a multi-layer soil system, which is more realistic, for both free and fixed head conditions and provided results in non-dimensional forms.

The modulus of subgrade reaction can be obtained using results from in-situ test, such as the plate loading test. For design practice, Terzaghi (1955) recommended roughly estimated coefficients of subgrade reaction for stiff clay and sand used for pile response analysis. Terzaghi mentioned that linear relationship between soil pressure and displacement was valid when the soil pressure is smaller than about one-half of bearing stress.

Another method estimating the modulus of subgrade reaction is use of an equation proposed by Vesic (1961) as;

$$K = \frac{0.65E_s}{(1-\mu_s^2)} \left[\frac{E_s D^4}{E_p I_p} \right]^{1/12} \quad (2.4)$$

where E_s is a soil modulus of elasticity, μ_s is a Poisson's ratio of the soil, D is pile diameter, and $E_p I_p$ is a bending stiffness of the pile. Obtaining the soil modulus of elasticity from laboratory or field tests, as well as properties of the pile, the modulus of subgrade reaction can be estimated from the Equation (2.4).

2.1.1 Concept of p - y curves

The solutions based on elastic subgrade reaction theory mentioned above were developed only for a case of linear soil properties. However, in reality, soil behavior is usually highly nonlinear, especially at larger deformations. Nonlinearity of soil behavior is very important for seismic design of soil-structure systems because design earthquake events are usually large and generate strong motion which may result in significantly large deformation. In light of this, the linear soil springs were replaced with a series of nonlinear soil springs, which represent the soil resistance (p) - deflection curves (y), called p - y curves (McClelland and Focht 1958). The p - y curves of various types of soil have been developed and updated based on the backanalysis of results from full- and large-scale lateral pile load tests.

A concept of the p - y curves can be shown as shown in Figure 2-2. It was assumed that the pile was perfectly straight and there was no deflection and residual stress on the pile under initial condition. According to the assumptions, the soil pressure acting to the pile prior to loading can be assumed as uniform earth pressure at rest as shown in Figure 2-2(a). Resultant pressure on the pile is zero under this condition. When the pile is loaded laterally at a certain displacement as shown in Figure 2-2(b), a net soil reaction can be obtained by integration of soil pressures around the pile giving unbalanced force at the displacement. Repeating this process at various displacements, a series of the p - y curves can be obtained at a depth in interest. Because the p - y curves are usually different at different depth, the curves should be defined at specific intervals of depth. Following defining a reasonable set of the p - y curves, the load-displacement curve at the pile top, profiles of pile rotation, bending moment, shear, and soil reaction can be numerically calculated solving the beam equation.

Several researchers have proposed the p - y curves for various soil types based upon backcomputation from full-scale test results. The following sections present brief descriptions of currently available p - y curves for cohesionless friction material, and curves for cohesive soil are neglected herein because interesting material in this study is

rockfill without cohesion. Some of the p - y curves mentioned below have been incorporated in the commercial programs in analyzing behavior of laterally loaded pile, such as *COM624P* (Wang and Reese 1993), *LPILE* (Reese *et al.* 2000), and *FLPIER* (University of Florida 1996).

2.1.2 Reese sand p - y curves

Reese *et al.* (1974) proposed a procedure for developing p - y curves for sand under static and cyclic lateral loadings. The procedure was developed based on the results of tests at Mustang Island with two 2-ft (0.6-m) diameter, flexible driven piles embedded into a deposit of submerged, dense, fine sand. The characteristic shape of the p - y curve is highly nonlinear, but Reese *et al.* concluded they can be described by three straight line portions and a parabolic curve as illustrated in Figure 2-3 (Reese *et al.* 1974). Also, the procedure proposed by Reese *et al.* is summarized in Table 2-3. According to this developing method of the p - y curves, initial modulus of subgrade reaction (K) and ultimate soil resistance (P_u) need to be estimated. The values of initial modulus of subgrade reaction for sand with various relative densities were also suggested by Reese *et al.* (1974).

2.1.3 API sand p - y curves

The method proposed by Reese *et al.* (1974) requires defining some parameters to develop the p - y curves combined parabolic curve and straight lines as shown in Figure 2-3, but it is more convenient and reasonable to define the p - y curves in simple equations for numerical analysis of laterally loaded piles. O'Neill and Murchison (1983) proposed a simplified method for sand p - y curves, which also yielded the results with reasonable accuracy compared to the original p - y curves. These modified p - y curves were accepted by the American Petroleum Institute (API) (API 1987). In the API method, the sand p - y curves were simplified using a hyperbolic tangent function to describe the characteristic

shape of the p - y curves. The developing procedure of p - y curves in the API code is summarized in Table 2-4. The equations determining the ultimate soil pressure were simplified using three coefficients C_1 , C_2 and C_3 as a function of the internal friction angle of sand (Figure 2-4(a)). The initial modulus of subgrade reaction constant was proposed in the graphical form as presented in Figure 2-4(b).

2.1.4 p - y curves used for current wharf design practice

For seismic design of port facilities, the p - y curves for rockfill were developed by the Port of Los Angeles as shown in Figure 2-5 (Martin 2005). Those curves were defined based on a field test, and corresponds to the curves for sand with 38 to 39 degrees of internal friction angle in API sand curves. The soil resistance at ground surface is zero, and becomes larger at deeper elevation.

The seismic code for port facilities approved in 2004 (Port of Los Angeles 2004) recommends lower and upper bound analyses with possible minimum and maximum resistance because there are still some uncertainties in the p - y curves due to rock properties, dike construction method, and sloping dike configuration. The code recommends p -multiplier approach in order to cover these uncertainties, and 0.3 and 2 as the p -multipliers are recommended for the lower and upper bound cases, respectively. The reaction for the upper bound corresponds to the curves for sand with 45 degrees in API standard. More effort needs to be made to clarify influence of each factor.

2.1.5 Backcalculation of p - y curves from lateral load pile tests

Most of p - y curves proposed for various types of soils were developed based on lateral load pile tests including full-, large-scale and centrifuge tests. It is the best method to directly measure load acting on the pile during laterally loading, but it requires large cost and high technology sensing technique. Therefore, strain gage or tiltmeter arrays are usually installed along test piles, and the p - y curves are mathematically or

numerically derived from records on those sensors. There are several methods proposed, and two of them are presented below; one is differentiation method, and the other is curve fitting method.

Figure 2-6 shows a summary of the differentiation method deriving the p - y curves from records on strain gages (Reese and Van Impe 2001). Strain gage arrays along test pile are usually used to calculate a curvature profile along the pile. A bending moment diagram (Figure 2-6(c)) can be computed by multiplying the curvature with bending stiffness of the pile. It is one of the critical factors to define reasonable bending stiffness of the pile in this procedure. Double differentiation of the bending moment diagram produces the soil reaction curve (Figure 2-6(e)). A deflection along the pile (Figure 2-6(a)) can be obtained by double integration of the curvature diagram. Therefore, the soil reaction versus the deflection of the pile, p - y curve, at a given depth can be obtained by backcalculation of test results.

The p - y curves can be also developed by the curve fitting method. This method requires pile pushover analysis with the various p - y curves. Replacing the p - y curves and running analysis many times, the reasonable agreements need to be found between experimental and numerical pile responses, such as load displacement relationship at pile top and deflection profile along pile. The p - y curves providing the best curve fitting can be the most reasonable p - y curves representing interaction of a soil-pile system in interest.

The former method is very useful when smooth strain profiles can be plotted or interpolated (i.e. minor scatterings on the records), and the latter method can provide more reasonable p - y curves if major scatterings are observed in the test results. In the prestressed concrete piles used for this research, strains along the piles showed significant scatterings because the responses of the piles were affected by localized deformation and damage. In addition, nonlinearity of the prestressed concrete piles produces difficulty for defining reasonable bending stiffness of the pile. Therefore, the curve fitting method was adopted for backcalculation of the p - y curves in this study.

2.1.6 Influence of pile properties on p - y curves

The p - y curves represent interaction between pile and surrounding soil of the pile. Therefore, the p - y curves could be affected by pile properties, as well as soil characteristics. In this section, some literature about influence of the pile properties on the p - y curves are introduced. Because most of the research about effects of the pile properties on the p - y curves are based on theories, full- or large-scale experiments need to be performed in future in order to assess them.

2.1.6.1 Pile cross section shape

Pile section shape may be one of possible significant factors affecting on p - y curves. Most of the p - y curves obtained based on experiments are developed for circular section pile, and equivalent diameter of non-circular section pile has to be defined in order to extend application of the p - y curves to non-circular pile.

Reese and Van Impe (2001) introduced a concept of an equivalent diameter of non-circular cross section pile. Figure 2-7 shows conceptual sketches indicating influence of pile cross section on the ultimate resistance of soil. When the pile is deflected rightward in the figure, reaction on the right side, friction on the top and the bottom sides of the pile are generated, and earth pressure acting on the left side of the pile decreases. These forces are shown as arrows in the figure. Assuming that a pile with a circular cross section is equivalent to a rectangular section pile with the identical width and half the depth of diameter of the circular section pile, the equivalent diameter of the rectangular pile can be derived using the following equation;

$$b_{eq} = w \left[\frac{p_{uc} + 2(d - w/2)f}{p_{uc}} \right] \quad (2.5)$$

where b_{eq} is equivalent diameter of rectangular pile, w is width of section, d is depth of section, p_{uc} is ultimate resistance of the circular section with diameter w , and f is side friction of the rectangular pile.

Ashour and Norris (2000) developed theoretical p - y curves for circular and square piles with same width and bending stiffness using a Strain Wedge model (Figure 2-8). Parameters for the Strain Wedge model are related to a three-dimensional passive wedge of soil developing in front of the pile. The p - y curves derived based on the model are shown in Figure 2-9. From this figure, it was found that larger reaction is generated on the rectangular pile than the circular pile in both sand and clay. Difference of the reactions is larger in dense sand and stiff clay than loose sand and soft clay, respectively.

For a square pile, the section depth (d) is equal to the section width (w) in Equation (2.5), and the equivalent pile diameter of the square pile is;

$$b_{eq} = w \left[\frac{p_{uc} + wf}{p_{uc}} \right] \quad (2.6)$$

This equation indicates that the equivalent diameter of the square pile is larger than the diameter of the circular pile, and reaction working on the square pile is larger than that on the circular section pile. Difference of the reactions is dependent on magnitude of side friction (f); i.e. the difference of the reactions is larger in dense sand and stiff clay than loose sand and soft clay. Therefore, the two literature above show qualitatively consistent results.

2.1.6.2 Pile Diameter

Pile diameter, one of the important factors may significantly influence on behavior of laterally loaded piles. For example, the p - y curves accepted by API are function of pile diameter. A few studies on pile diameter effect on clay and one study on cemented sand are available in literature while no study has been conducted on an investigation of pile diameter on the p - y curves for cohesionless soil.

Terzaghi (1955) explained influence of pile diameter on coefficients of subgrade reaction by using a concept of a stress bulb in passive zone as shown in Figure 2-10. Based on this concept, the following equation was developed;

$$k_n = p/y_n = p/ny_1 = k_1/n \quad (2.7)$$

where k_n , k_1 are coefficients of subgrade reaction for pile diameters D and D_1 , $n = D/D_1$ and $p/y_1 = k_1$. It was concluded that the coefficient of subgrade reaction is linearly proportional to inverse of the pile diameter; i.e. the coefficients of subgrade reaction per unit length of the pile is independent of the pile diameter.

Reese *et al.* (1975) backcalculated p - y curves for a 2.1-ft (0.65-m) pile based on experiment at Manor site and used them to predict the behavior of a 0.5 ft (0.15 m) diameter pile. Moment comparison between analysis and experiment showed reasonable agreement; however, the computed deflection of groundline was considerably lower than the measured during the test. No explanation was made about this disagreement, but this result implied that the reaction per unit length of pile may be smaller at smaller diameter pile, and did not match the conclusion of Terzaghi.

O'Neill and Dunnavant (1984) and Dunnavant and O'Neill (1985) conducted the laterally loaded piles with diameters of 0.9 ft, 4.0 ft, and 6.0 ft (0.27 m, 1.22 m and 1.83 m) in an over-consolidated clay site. It was found that deflection at one half of the ultimate soil pressure (y_{50}) became smaller as the pile diameter increased. The Matlock's p - y curves were modified to gain better agreement between measured and computed response.

A series of full-scale lateral loading test of various diameter piles in cemented sand was conducted by Juirnarongrit *et al.* (2005). Figure 2-11 shows a comparison of the p - y curves of all pile diameters at different depths obtained from the full-scale test results. From these figures, it could be found that the backcalculated p - y curves for all the piles are generally similar, and it indicated that effect of the pile diameter on the p - y curves is insignificant for the input displacement range of this test. The lateral resistance on the p - y curves of the 4 ft (1.2 m) diameter pile (No.2) was less than the others, but it could be

because the pile was located close to natural slope at the test site. It should be noted that the p - y curves backcalculated from the test results, did not reach the ultimate resistance.

In conclusion of the past works mentioned above, it is difficult to make a consensus whether pile diameter significantly affects on the p - y curves. In order to clarify this contradiction of the pile diameter effect, more research needs to be continued, especially for cohesionless soils.

2.1.6.3 Bending stiffness

Bending stiffness of pile is also one of the possible factors with influence on the p - y curves. For example, the ultimate reaction from soil around stiffer pile may be larger under kinematic load condition, because the pile can resist more against lateral load due to relative movement of the surrounding soil.

Ashour and Norris (2000) compared theoretical p - y curves for two piles with different bending stiffness using a Strain Wedge model. The other parameters used for the analysis were identified for both the piles. Figure 2-12 shows comparison of the p - y curves obtained in the analysis. From the figures in Figure 2-12, it was concluded that the bending stiffness has significant effect for dense sand and moderate effect for loose sand and stiff clay while it has no effect for soft clay.

The effect of the bending stiffness on the p - y curves may result from soil continuity because the bending stiffness of the pile dominates deflection profile of the pile which determines strain conditions in soil elements adjacent to the pile. There is no empirical evidence about the effect of pile stiffness on the p - y curves, and experimental efforts need to be made.

2.1.6.4 Type of pile

There was no research about effect of pile type on the p - y curves because building identical piles with different material is not realistic; however, it may have some influences on friction and drag force on sides of piles, direction of contact force at the pile surface, and effective pile diameter in cohesionless friction material because different

material has different friction angle between pile and soil. As shown in Table 2-5 (US Army Corps of Engineers 1991), concrete pile usually has larger friction than steel pile because of rougher concrete surface.

Friction or drag force on sides of piles is function of earth pressure on sides of pile and friction angle between pile and soil; i.e. larger friction or drag force may act on concrete piles than steel piles. Different type piles usually have considerably different properties (e.g. bending stiffness, and moment curvature relationship) more significantly affecting on behavior of laterally loaded piles, and type of pile may have relatively minor effect.

The parameters of piles mentioned above may complicatedly relate each other, and are not completely independent. A set of p - y curves backcalculated from full-scale experiments include all the factors of the pile properties. Therefore, the effect of each parameter needs to be carefully considered in order to extend usage of the p - y curves found in the experiments with a certain type of soil and pile to p - y analysis with other kinds of soil and pile.

General concept of p - y analysis, some examples of p - y curves for cohesionless soils used in design practice, calculation methods of p - y curves from test results, and possible properties of piles affecting on soil-pile interaction are described in this section. As mentioned above, most of the proposed p - y curves were derived based on results from full-, large-scale, or centrifuge tests. In the next section, several examples of experimental works about behavior of laterally loaded piles in cohesionless granular soils are reviewed.

2.2 Experimental Works of Pile-Supported Wharf Structure in Rockfill

Recently, deformation-based design becomes more familiar, and large experimental efforts, including full-scale tests, large-scale 1-g shake table tests, and centrifuge tests, have been made in order to develop more sophisticated approaches for design of soil-

pile-superstructure systems. In this section, focusing on cohesionless granular soils, some examples of past experimental works are reviewed.

2.2.1 Full-scale pile test

Numerous full-scale lateral pile load tests have been conducted to understand the behavior of soil-structure interaction, varying from small diameter timber and steel pipe piles to large diameter cast-in-place shafts. Table 2-6 is a list of full-scale single pile and pile group tests in granular soils. According to this table, the p - y curves were developed based on the limited number of the tests, and were adjusted extrapolating for different soil strengths and type. Especially, the number of tests with piles in large-size rockfill is still lacked because rockfill is not commonly used geomaterial for constructions with few exceptions (e.g. rockfill dam and wharf structures).

The measured responses during lateral load tests were compared with the results from analyses using the available methods for estimating the pile responses, such as elastic continuum, subgrade reaction theory, and p - y curve methods in some of the literature. Brief descriptions on some of these full-scale lateral tests are discussed below.

Chai and Hutchinson (1999) conducted full-scale lateral load test with reinforced concrete piles embedded in loose and dense dry sand. The test results indicated that the maximum lateral force of the soil-pile system was not sensitive to the soil density, even though it was commonly believed that dense sand has larger ultimate reaction. However, the depth of maximum moment was shallower in denser sand. Furthermore, the kinematic model based on the equivalent fixed base cantilever concept was proposed in order to simulate the curvature ductility demand. No p - y curves were developed in this study.

Diaz *et al.* (1984) carried out a set of full-scale tests using a part of the real wharf structure embedded in rockfill at the Port of Los Angeles (Figure 2-13). Instrumented octagonal piles were placed in the actual construction site. Lateral force was operated at the pile top with a reaction pile and a hydraulic jack to the test pile, and load displacement relationship could be obtained, as well as the p - y curves (Figure 2-14).

Because the moment profile along the test pile obtained in this experiment was widely scattered as shown in Figure 2-14(a), the back calculated p - y curves based on the moment profile in Figure 2-14(b) did not seem to be well quantified, but it was notable observation that subgrade reaction was not zero even at ground surface with no effective overburden stress, though pure friction material does not have shear strength under zero confinement. It was mentioned that it may be caused by structural interlocking between rock particles. This set of tests was conducted using a single pile located at dike crest with free head condition, and then, no information was available about the behavior of pile on level ground and effect of pile-deck system with partially fixed condition to soil-pile-deck interaction. Because only this test gives available information about laterally loaded pile behavior in large particle rockfill at present, there are many issues which are not well known.

2.2.2 Centrifuge testing

In order to simulate realistic condition of prototype target structures as much as possible, full- and large-scale experiments are the most reasonable, but those experiments require large amount of cost and time. Therefore, centrifuge test device with scaled model has been widely used for geotechnical problems including slope stability, consolidation, and laterally loaded pile (e.g. Boulanger *et al.* 1999, and Abdoun *et al.* 2003). The main advantages of the centrifuge test are enabling to simulate stress condition in soil layers and saving cost and time; however, there are some uncertainties on scaling, and centrifuge test results need to be carefully considered in order to be quantified.

A series of centrifuge tests was carried out by Boland *et al.* (2001a, b) in order to understand the behavior of pile-supported wharves in rockfill. The large-scale centrifuge facility at the University of Davis, one of the largest centrifuge facilities in the world, was used for the series of experiments. Bending stiffness of piles for the centrifuge test were designed following a scale law, and the target prototype 2 ft (0.61 m) diameter

prestressed concrete piles were modeled using 3/8 inch (9.5 mm) aluminum tubing. Gradation of gravel representing large-particle rockfill in prototype structure was also adjusted based on the scale law. The centrifugal acceleration was 40 g, and loads were applied to the test piles with loading pistons and shake table during flying for static and dynamic tests, respectively. Figure 2-15 and Figure 2-16 show cross section of the centrifuge setup of pile group and single pile tests, respectively.

Based on the results from the static load test of the single pile, a set of p - y curves for gravel used for the centrifuge test was backcalculated using a commercial software, FLAC (McCullough and Dickenson 2004). The p - y curves were not backcalculated directly from strain gage array along the test pile; the curves were calculated by the curve fitting method introduced in Section 2.1.5, matching the profiles of moment and deflection from the experiment with those from the numerical results. Figure 2-17 presents comparison of the moment and the deflection profiles. Using 45 degrees of internal friction angle, commonly used for large particle rockfill, the p - y curves of the gravel for the case without modification were defined; however, both the profiles did not agree with the test results.

Therefore, based on the description of Diaz *et al.* (1984), “lateral resistance of rockfill is not zero even at ground surface”, a concept of pseudo cohesion in the gravel was added in the numerical model for the case with modification. Adding 15 kPa (313 psf) of the pseudo cohesion, the profiles of the moment and the deflection obtained from the modified numerical model could reasonably agree with the results recorded in the centrifuge test. In this connection, the concept of the pseudo cohesion in rockfill was also applied by Martin (2005) in design of pile-supported wharf against permanent deformation of rockfill slope. 200 psf (9.6 kPa) was used as the cohesion.

Based on the results from both the full-scale and the centrifuge tests, it was concluded large particle size rock may have additional reaction explained by the pseudo cohesion, as well as reaction from friction. However, available information from full-scale lateral load test of piles in large particle size rockfill is quite short, and there are some remained uncertainties, such as quantification of soil-pile interaction and the effect of downslope

on the p - y curves. Performance of further full- or large-scale tests, the mechanism of reaction generation in rockfill and interaction between pile and rockfill needs to be clarified.

2.3 Shear Behavior of Rockfill

In order to consider soil-pile interaction on a laterally loaded pile in rockfill, shear behavior of large particle rockfill is one of the key factors. There are many research available about large-scale triaxial and direct shear tests of rockfills in literature; most of them were published in the 1970's and the early 80's in order to make more reasonable design of large earth dams. Since demands for the earth dams decreased, the characteristics of the rockfill were not as relevant any more, and new research has not been forthcoming.

Based on past works of triaxial and direct shear tests with different rockfills, it was concluded that the shear behavior of rockfills is dependent on overburden confining stress, dry density, crushing strength of particles, gradation, and particle shape. In this section, past works about some of fundamental parameters affecting on shear behaviors of rockfills are introduced.

2.3.1 Confining pressure

Confining pressure is one of the most important factors affecting on characteristics of rockfill. The Mohr-Coulomb failure criteria assumes constant friction angle, and it is characterized by a straight line passing through the origin and tangent with all of Mohr's circles obtained from triaxial tests under various normal stress conditions; that is, its internal friction angle is constant at any normal stress. According to large amount of triaxial test and direct shear test results (e.g. Marachi *et al.* 1969, and Leps 1970), however, internal friction angle of rockfills is larger at smaller confining pressure, and

becomes smaller as confining pressure increases, and it is commonly believed that it is caused by combination of dilation and rock particle crushing.

Bertacchi and Bellotti (1970) carried out large scale triaxial tests using materials obtained from the crushing of large boulders with about 2 in (5 cm) maximum particle size. Several definitions of friction angle were proposed as shown in Figure 2-18. Figure 2-18(a) shows one of the various definitions of friction angle obtained drawing straight lines tangent to each circle passing the origin, and Figure 2-18(b) presents the other definitions gained plotting a curved failure envelope. In both definitions, it was concluded that friction angles were smaller under larger normal stresses. In addition, drawing a straight line tangent to all the Mohr's circles, another friction angle with apparent cohesion could be defined, and it could be explained by mechanical interlocking of rock particles. This observation is consistent with the concept of the pseudo cohesion as introduced in Section 2.2.

Marsal (1973) also conducted triaxial compression tests of various rockfills using a large testing device. Examples of triaxial test results are shown in Figure 2-19. The figures include Mohr's circles, curved failure envelope, and friction angles (ϕ_0) developed plotting straight lines which pass through the origin and contact each Mohr's circle. In both of the figures, the internal friction angles were 45 degrees at 71 psi (5 kg/cm², 490 kPa), and about 38 degrees at 570 psi (40 kg/cm², 3920 kPa) of normal stress.

For behavior of laterally loaded pile, characteristics of rockfill at low confining pressure are very important, because the pile behavior subjected to lateral load is dominated by only shallower portions of soil; e.g. Reese and Van Impe (2001) suggested 5 to 10 times of pile diameter in depth. This dominant pile length becomes shorter as the soil around the pile has larger stiffness. In a case of the 2 ft diameter pile in very stiff rockfill, it can be 10 to 12 ft, 5 to 6 pile diameters, and the corresponding normal stresses are about 9 to 12 psi (62 to 83 kPa). However, no test results of rockfill under such low confining pressure are available due to difficulties of specimen preparation; i.e. higher cell pressure is needed to make a specimen stand by self.

2.3.2 Gradation

The gradation of frictional material can be one of the factors affecting the shear characteristics. For example, uniformly graded granular material can not achieve high densities as well graded soil, and it results in less shear strength, as well as larger deformation.

Figure 2-19 shows triaxial tests results obtained by Marsal (1973) using San Francisco Basalt with different grain size distributions. The top figure was a set of Mohr's circles for more poorly-graded Basalt with about 2.5 in (6 cm) of the maximum grain size than one with 7 in (18 cm) providing another set of circles shown in the bottom figure. Comparing these figures, a larger friction angle was measured in the well graded rockfill giving the bottom figure in Figure 2-19.

Anagnosti and Popovic (1982) carried out a series of direct shear tests using same cobbles with different gradations in order to gain better understanding about effect of particle size on its shear behavior because large rocks could not be used for element test while they were used in actual construction of rockfill dams. The maximum particle size of cobbles used in their tests was about 1-7 in (2.5-18 cm). Examples of test results are shown in Figure 2-20. Those test results showed larger shear strength in rock with well gradation. This trend on the results is consistent with one from Marsal (1973).

2.3.3 Maximum particle size

The maximum particle size of rockfill used in actual wharf construction is usually more than 1 ft (30 cm), but there is no information about shear behavior of such the large grain size rockfill from element tests. Therefore, the effect of the maximum particle size of the rockfill on the shear behavior needs to be carefully considered.

There is no consensus on the influence of the particle size, but it is generally accepted that rockfill with larger maximum grain size has less strength (e.g. Marachi *et al.* 1969, and Marsal 1973). It can be one of the possible explanations that larger particles can be

crushed at lower stress condition because the probability of a defect in a particle increases with particle size (e.g. Hardin 1986). On the other hand, Charles and Watts (1980) concluded that there is no effect.

Using common sense, it is not always true that fine sand has larger shear strength than large particle rockfill. As mentioned above, shear behavior of rockfill are related to properties of friction, dilation, interlocking and crushing, and each factor may be dependent on the others. These factors may arise from many soil parameters, such as density, gradation, and particle crushing strength. In addition to these soil parameters, boundary condition of specimens in element tests, represented by ratio of specimen size to the maximum grain size, can be a reason of the inconsistent conclusions.

2.3.4 Particle shape

Shape of rock particles also seem to affect on shear behavior of rockfill. Angularity of rock particles may be different from rock type, forming process, and crushing procedure if it is crushed rock from large boulders. The rockfill used for construction of wharf structures is produced by blasting from mother rock and crushing to obtain a gradation. It has coarse angular particles.

Bertacchi and Bellotti (1970) conducted using two types of rock; tonalite and serpentine with very sharp edges and larger porosity than the tonalite. Even though the latter material had larger porosity, it had larger shear strength than the former. It could be explained by structural interlocking at the sharp edges on the particles.

On the other hand, it is likely that spherical shape rocks may have higher crushing strength than rugby ball shaped or angular rocks because the tensile strength of rocks is much smaller than the compressive strength, and the rugby ball shape and the angular rocks have a higher possibility of having a large tensile stress due to eccentric contact forces. In order to more completely discuss the effects of particle angularity on shear behavior of rockfill, both the structural interlocking and the crushing properties need to be simultaneously considered.

2.3.5 Presence of water

Presence of water affects friction, as well as effective vertical stress because friction is proportional to the effective stress in friction material. In addition, Bertacchi and Bellotti (1970) reported that water also affects friction angle, deformation and dilation properties. Figure 2-21 shows stress strain relationships of specimens under dry and submerged conditions from a series of triaxial tests. According to comparison of these figures under dry and saturated-submerged conditions, friction angle in saturated sample was smaller and deformation was larger than dry sample because water has lubricating effect on the surface of rock particles.

Drainage conditions related to pore water pressure build-up during strong ground motion may have some effect on shear behavior of rockfill. In general, large particle size rockfill has high permeability and pore water pressure would dissipate quickly. However, for case if water is supplied from inundated sea wave or heavy rain storm, undrained conditions may be generated even in high permeability rockfill.

2.3.6 Three dimensional failure criteria for cohesionless granular materials

In the mechanics of cohesionless granular materials, it is commonly accepted that shear strength of soil is composed of a shear friction between rock grains and dilation, and interlocking of particles is not. In larger particle size rockfill, higher shear strength is usually observed at the same deformation than one in smaller particle soil under lower confining pressure. It is because soil particles need to climb over the adjacent grains in dilation process to make deformation, and larger energy is needed to do it in larger grain soil than in smaller grain soil. In addition, it is notable that the ultimate shear strength of rockfill is dependent not only on overburden stress, but also on shear and the other stresses induced from pile deflection. Therefore, it sounds more reasonable idea to apply a failure criterion for three-dimensional stress conditions to find the shear strength of rockfill especially under low confinement.

Matsuoka and Nakai (1982), Lade and Duncan (1975) and Lade (1977) developed yield and failure criteria for cohesionless granular materials. Figure 2-22 shows conceptual drawing about characteristics of failure in 3-dimensional stress conditions. Curved failure surfaces for cohesionless soils can be described in the following equation (Lade, 1977);

$$f_p = \left(\frac{I_1^3}{I_3} - 27 \right) \left(\frac{I_1}{p_a} \right)^m \quad (2.8)$$

where, σ_1 , σ_2 , and σ_3 are the principal stresses, $f_p = \eta_1$ at failure and m are soil-dependent parameters, p_a is atmospheric pressure (2117 psf = 101.3 kPa), $I_1 = \sigma_1 + \sigma_2 + \sigma_3$, and $I_3 = \sigma_1 \cdot \sigma_2 \cdot \sigma_3$. In addition, f_p is a parameter related to magnitude of the principal stresses; i. e. stresses at failure can be larger as η_1 is larger. m is also a soil-dependent parameter affecting the non-linearity of the failure envelope; that is, the increment of failure with depth is constant resulting in a straight failure envelope on triaxial plane in Figure 2-22(a) when m is equal to zero, and exhibits more highly non-linearity for larger m .

Table 2-7 summarizes parameters for sand obtained based on laboratory tests (Lade 1977). In this table, η_1 varies about 30 to 300, and m is about 0.01 up to 0.4. Both parameters are larger in denser soil with larger friction angle.

In conclusion, many factors affecting on shear behavior of large particle rockfill could be found, and the shear properties of the rockfill may also influence on soil-pile interaction. Therefore, more experimental work is needed to clarify relationships between those factors, the shear properties of the rockfill, and the soil-pile interaction. Also, rockfill used for pile tests should be the same or reasonably similar as material used for actual construction of wharves in order to simulate equivalent test specimens as actual wharf structures.

2.4 Summary

Based on literature review described above, more research works are needed to develop more a reliable deformation-based design standard which has become more common. Performance of full-scale tests with pile and rockfill used for actual wharves is the most ideal because many factors, such as properties of the soil and the pile, and scale effects, may vary the behavior of laterally loaded pile-soil systems. Following the full-scale tests, numerical analyses should be conducted using results from the tests in order to gain more understanding about pile-rockfill interaction.

Based on the conclusion of the literature review, a series of full-scale lateral loading tests of piles in rockfill followed by backcalculation of a set of p - y curves, were planned. In the next chapter, details of full-scale tests, including design and construction of the test specimens, as well as the instrumentation plan, are presented.

Table 2-1 Summary of solutions for laterally loaded pile subjected to lateral loading in the case of constant subgrade reaction (Hetenyi 1946)

Pile Response	Due to Horizontal Loading, H
Pile Displacement (u)	$u = \left(\frac{2H\beta}{k_h D} \right) \left(\frac{\sinh \beta L \cos \beta z \cosh \beta(L-z) - \sin \beta L \cosh \beta(L-z)}{\sinh^2 \beta L - \sin^2 \beta L} \right)$
Pile Rotation (θ)	$\theta = \left(\frac{2H\beta^2}{k_h D} \right) \left(\frac{1}{\sinh^2 \beta L - \sin^2 \beta L} \right) \left(\sinh \beta L [\sin \beta z \cosh \beta(L-z) + \cos \beta z \sinh \beta(L-z)] \right. \\ \left. + \sin \beta L [\sinh \beta z \cos \beta(L-z) + \cosh \beta z \sin \beta(L-z)] \right)$
Shear Force (Q)	$Q = - \left(\frac{H}{\sinh^2 \beta L - \sin^2 \beta L} \right) \left(\sinh \beta L [\cos \beta z \sinh \beta(L-z) - \sin \beta z \cosh \beta(L-z)] \right. \\ \left. - \sin \beta L [\cosh \beta z \sin \beta(L-z) - \sinh \beta z \cos \beta(L-z)] \right)$
Moment (M)	$M = - \left(\frac{H}{\beta} \right) \left[\frac{\sinh \beta L \sin \beta z \sinh \beta(L-z) - \sin \beta L \sinh \beta z \sin \beta(L-z)}{\sinh^2 \beta L - \sin^2 \beta L} \right]$

where : $\beta = \left(\frac{k_h D}{4E_p I_p} \right)^{1/4}$

- D = Pile Diameter
 $E_p I_p$ = Pile Stiffness
 k_h = Coefficient of Subgrade Reaction
 z = Depth

Table 2-2 Summary of solutions for laterally loaded pile subjected to moment loading in the case of constant subgrade reaction (Hetenyi 1946)

Pile Response	Due to Moment Loading, M_o
Pile Displacement (u)	$u = \frac{2M_o\beta^2}{k_h D} \left(\frac{1}{\sinh^2 \beta L - \sin^2 \beta L} \right)$ $\left(\sinh \beta L [\cosh \beta(L-z) \sin \beta z - \sinh \beta(L-z) \cos \beta z] \right.$ $\left. + \sin \beta L [\sinh \beta z \cos \beta(L-z) - \cosh \beta z \sin \beta(z-L)] \right)$
Pile Rotation (θ)	$\theta = \left(\frac{4M_o\beta^3}{k_h D} \right)$ $\left[\frac{\sinh \beta L \cosh \beta(L-z) \cos \beta z + \sin \beta L \cosh \beta z \cos \beta(L-z)}{\sinh^2 \beta L - \sin^2 \beta L} \right]$
Shear Force (Q)	$M = \frac{M_o}{\sinh^2 \beta L - \sin^2 \beta L} \left(\sinh \beta L \left[\sinh \beta(L-z) \cos \beta z + \cosh \beta(L-z) \sin \beta z \right] \right.$ $\left. - \sin \beta L \left[\sinh \beta z \cos \beta(L-z) + \cosh \beta z \sin \beta(L-z) \right] \right)$
Moment (M)	$Q = \frac{-2M_o\beta}{\sinh^2 \beta L - \sin^2 \beta L} \left[\sin \beta L \sin \beta(L-z) \sin \beta z + \sin \beta L \sinh \beta z \sin \beta(L-z) \right]$

where : $\beta = \left(\frac{k_h D}{4E_p I_p} \right)^{1/4}$

- D = Pile Diameter
 $E_p I_p$ = Pile Stiffness
 k_h = Coefficient of Subgrade Reaction
 z = Depth

Table 2-3 Summary of Procedure in Developing Sand p - y Curves (Reese *et al.* 1974)

1. Preliminary Computation	$\alpha = \frac{\phi}{2}, \beta = 45 + \frac{\phi}{2}, K_0 = 0.4, K_a = \tan^2 \left(45 - \frac{\phi}{2} \right)$
2. Theoretical Ultimate Soil Resistance due to Wedge Failure, p_{st}	$p_{st} = \gamma' z \left[\frac{K_0 z \tan \phi \sin \beta}{\tan(\beta - \phi) \cos \alpha} + \frac{\tan \beta}{\tan(\beta - \phi)} (D + z \tan \beta \tan \alpha) \right] + K_0 z \tan \beta (\tan \phi \sin \beta - \tan \alpha) - K_a D$
3. Theoretical Ultimate Soil Resistance due to Flow Failure, p_{sd}	$p_{sd} = K_a D \gamma' z (\tan^8 \beta - 1) + K_0 D \gamma' z \tan \phi \tan^4 \beta$
4. Govern Theoretical Ultimate Soil Resistance, p_s	$p_s = \text{the smaller of the values given from step 2 and 3}$
5. Ultimate Soil Resistance, p_u	$p_u = \bar{A}_s p_s \text{ for static loading or } p_u = \bar{A}_c p_s \text{ for cyclic loading}$
6. Soil Pressure at $D/60$	$p_m = B_s p_s \text{ for static loading or } p_m = B_c p_s \text{ for cyclic loading}$
7. Establish Initial Straight Line Portion	$p = (kz)y$
8. Establish Parabolic Section of p - y Curves	$p = \bar{C} y^{1/n}, m = \frac{p_u - p_m}{y_u - y_m}, n = \frac{p_m}{m y_m}, \bar{C} = \frac{p_m}{y_m^{1/n}}, y_k = \left(\frac{\bar{C}}{kz} \right)^{n/(n-1)}$

where: $\bar{A}_s, \bar{A}_c =$	Adjustment Coefficient for Static and Cyclic p - y Curves
$B_s, B_c =$	Nondimensional Coefficient for Static and Cyclic p - y Curves
$D =$	Pile Diameter
$k =$	Initial Subgrade Reaction Constant (MN/m ³)
	Loose Sand (Submerge/above water) 5.4/ 6.8
	Medium Dense Sand 16.3/ 24.4
	Dense Sand 34/ 61
$p_{sd} =$	Theoretical Ultimate Soil Resistance due to Flow Failure
$p_{st} =$	Theoretical Ultimate Soil Resistance due to Wedge Failure
$p_s =$	Govern Ultimate Soil Resistance
$p_u =$	Ultimate Soil Resistance
$z =$	Depth
$\phi =$	Friction Angle
$\gamma' =$	Effective Soil Unit Weight for Soil under Water

Table 2-4 Summary of Procedure in Developing API Sand p - y Curves (API 1987)

1. Theoretical Ultimate Soil Resistance due to Wedge Failure, p_{st}	$p_{st} = (C_1 z + C_2 D) \gamma' z$
2. Theoretical Ultimate Soil Resistance due to Flow Failure, p_{sd}	$p_{sd} = C_3 D \gamma' z$
3. Govern Theoretical Ultimate Soil Resistance, p_s	$p_s =$ the smaller of the values given from step 2 and 3
4. Determine Adjustment Coefficient for Static and Cyclic Loading	$\bar{A}_s = \left(3.0 - 0.8 \frac{z}{D} \right) \geq 0.9 \text{ for static lading}$ $\bar{A}_c = 0.9 \text{ for cyclic loading}$
5. Develop Characteristic Shape of p - y Curves	$p = \bar{A} p_s \tanh \left(\frac{kz}{\bar{A} p_u} y \right)$

where: $\bar{A}_s, \bar{A}_c =$ Adjustment Coefficient for Static and Cyclic p - y Curves
 $C_1, C_2, C_3 =$ Coefficients
 $D =$ Pile Diameter
 $k =$ Initial Subgrade Reaction Constant (MN/m³)
 $p_{sd} =$ Theoretical Ultimate Soil Resistance due to Flow Failure
 $p_{st} =$ Theoretical Ultimate Soil Resistance due to Wedge Failure
 $p_s =$ Govern Ultimate Soil Resistance
 $p_u =$ Ultimate Soil Resistance
 $z =$ Depth
 $\phi =$ Friction Angle
 $\gamma' =$ Effective Soil Unit Weight for Soil under Water

Table 2-5 Angle of friction between soil and pile (US Army Corps of Engineers 1991)

<u>Pile Material</u>	<u>δ</u>
Steel	0.67 ϕ to 0.83 ϕ
Concrete	0.90 ϕ to 1.0 ϕ
Timber	0.80 ϕ to 1.0 ϕ

Table 2-6 Summary of full-scale lateral load pile tests in granular soils

		Reference (Year)	Pile Type	Soil condition
Single Pile	1	Chai and Hutchinson (1999)	4 Concrete piles	Loose and dense sand
	2	Ismael (1990)	12 Bored shaft	Medium dense cemented sand
	3	Little and Briaud (1988)	4 Drilled shaft 1 Square prestressed concrete pile 1 Steel pipe pile	Medium dense sand
	4	Morison (1988)	1 Steel pipe pile	Stiff clay and compacted sand
	5	Trucker and Briaud (1988)	2 H-piles	Medium to dense sand
	6	Bhushan <i>et al.</i> (1981)	7 Drilled shaft	Medium to dense sand
	7	Reese <i>et al.</i> (1974)	2 Steel pipe piles	Submerged dense sand
	8	Alizadeh and Davisson (1970)	3 Pipe Piles, 4 H-piles 1 Timber pile, 3 Concrete piles	Medium dense sand
	9	Alizadeh (1969)	4 Timber piles	Sand, and gravel
	10	Davisson and Salley (1969)	4 Drilled shaft	Medium dense sand
	11	McNully (1956)	3 Taper concrete piles	Medium dense silty sand
	12	Ashford and Juirnarongrit (2005)	5 CIDH piles	Cemented sand
	13	Diaz <i>et al.</i> (1984)	2 Prestressed concrete piles	Large size rockfill
Pile Group	14	Rollins et al. (2005)	3x5 steel pile group	Sand
	15	Ashford and Rollins (2002)	3x3 steel pile group	Sand

Table 2-7 Summary of parameters in the constitutive model in three-dimensional stress condition (Lade 1977)

Parameter \ Soil	Sacramento River Sand		Crushed Napa Basalt		Painted Rock Material		Strain Component
Relative Density, D_r (%)	100	38	100	70	100	70	
Void Ratio, e	0.61	0.87	0.53	0.66	0.40	0.48	
Modulus No., K_{ur}	1680	960	1520	900	1580	730	Elastic
Exponent, n	0.57	0.57	0.34	0.38	0.49	0.66	
Poisson's Ratio, ν	0.20	0.20	0.20	0.20	0.20	0.20	
Collapse Modulus, C	0.00023	0.00028	0.00073	0.00120	0.00100	0.00140	Plastic Collapse
Collapse Exponent, p	0.86	0.94	0.74	0.775	0.63	0.644	
Yield Const., η_1	80	28	280	130	101	67	Plastic Expansive
Yield Exponent, m	0.23	0.093	0.423	0.30	0.21	0.16	
P1. Potent. Const., R	-2.95	-1.00	-5.90	-3.03	-2.34	-2.21	
P1. Potent. Const., S	0.44	0.43	0.41	0.40	0.44	0.44	
P1. Potent. Const., t	8.45	0.00	0.00	0.00	2.80	3.10	
Work-Hard. Const., α	3.00	3.00	2.22	2.35	3.45	3.28	
Work-Hard. Const., β	0.060	-0.076	-0.023	-0.046	-0.033	-0.029	
Work-Hard. Const., P	0.12	0.24	0.50	0.35	0.12	0.080	
Work-Hard. Exponent, ℓ	1.16	1.25	1.09	1.23	1.38	1.61	

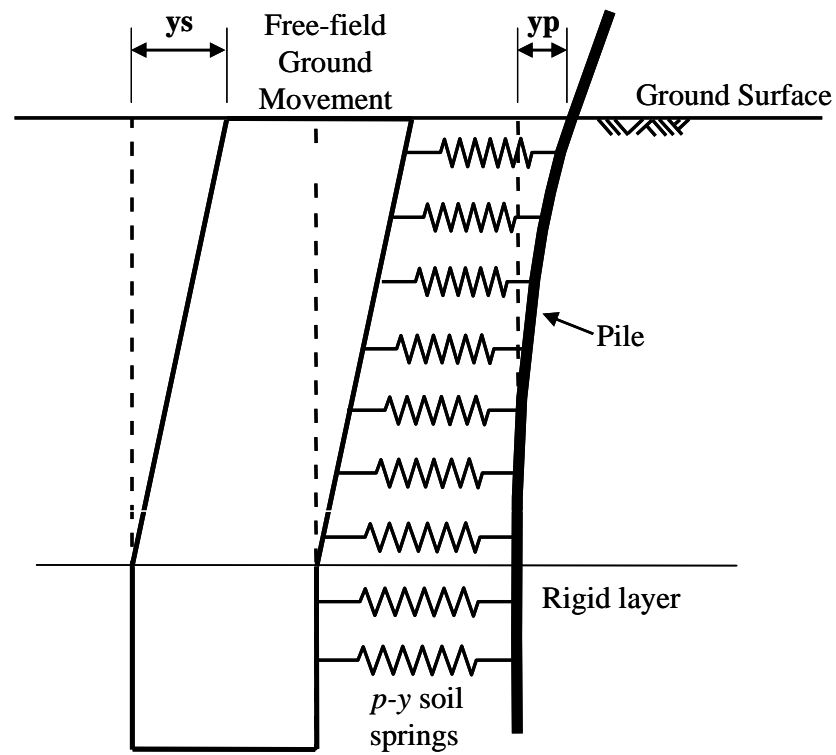


Figure 2-1 Concept of Winkler's spring method for laterally loaded pile

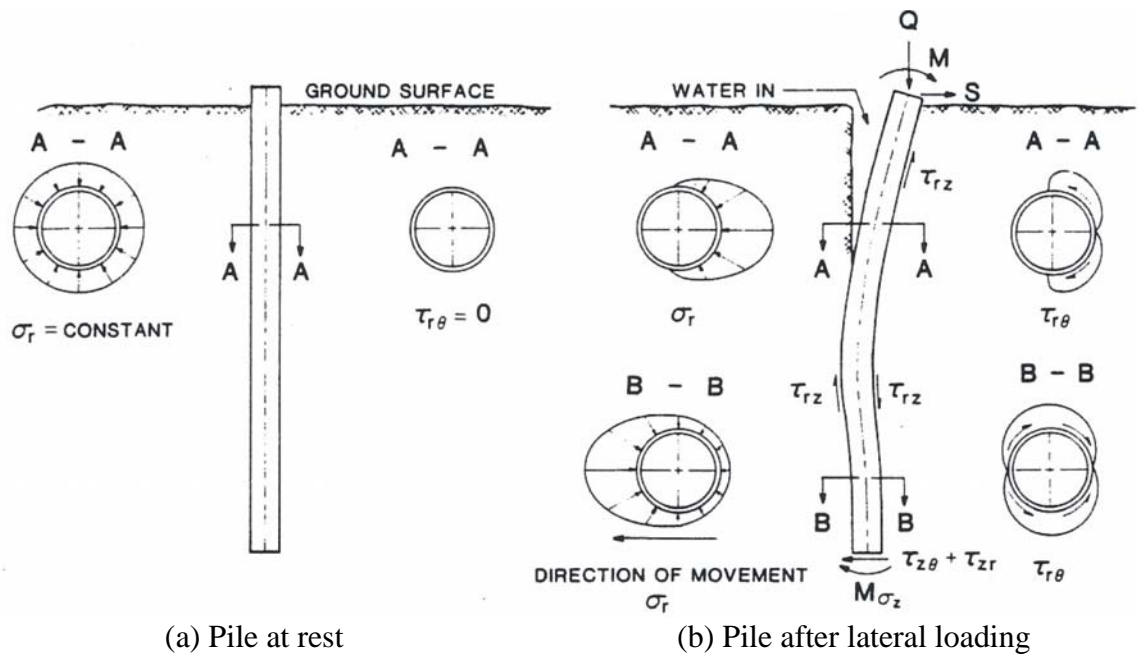


Figure 2-2 Definition of p - y concept (after Dunnivant 1986)

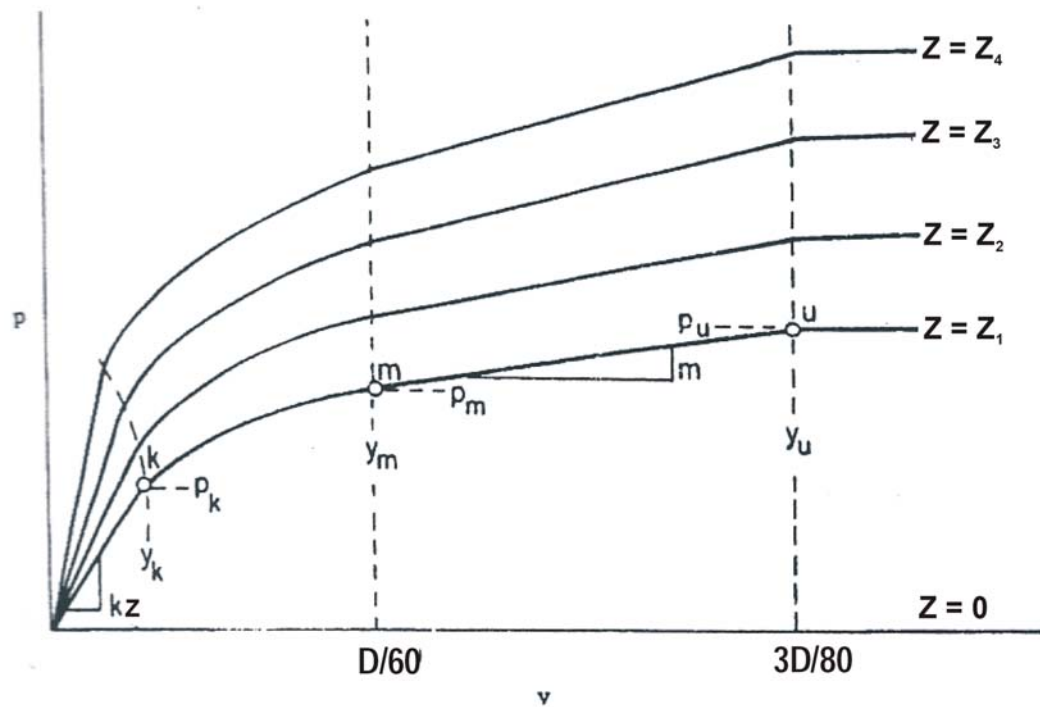


Figure 2-3 Shapes of p - y Curves for Sand (Reese *et al.* 1974)

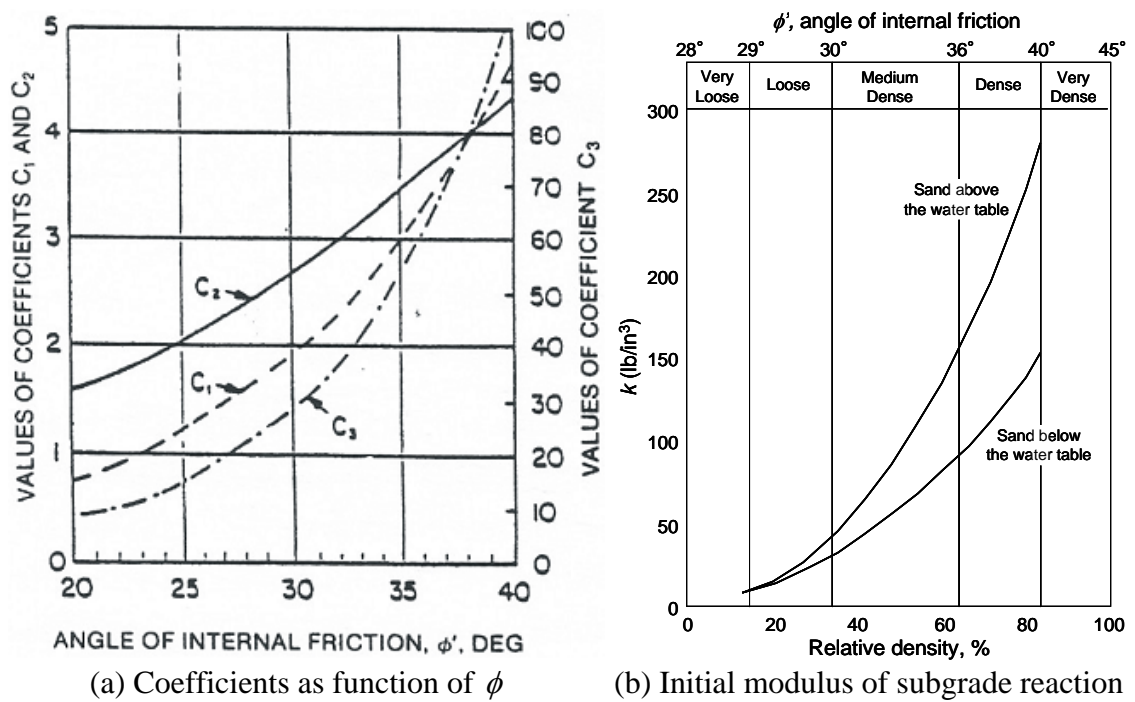


Figure 2-4 Coefficients needed to derive p - y curves for sand (API 1987)

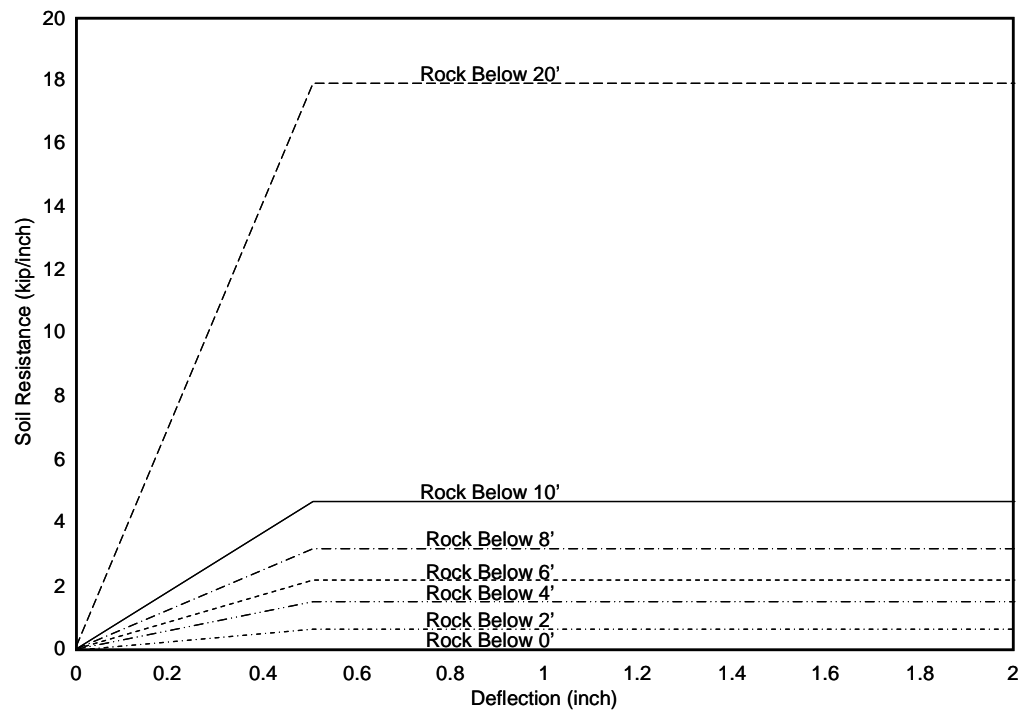


Figure 2-5 p - y curves for the current wharf design (Martin 2005)

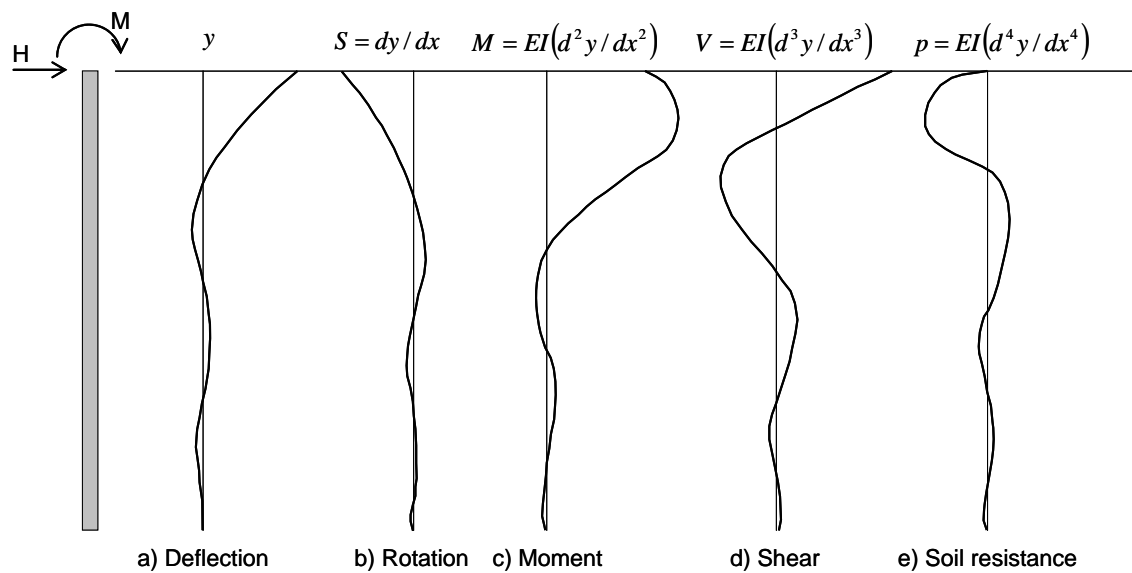


Figure 2-6 Methodology in developing p - y curves (Reese and Van Impe 2001)

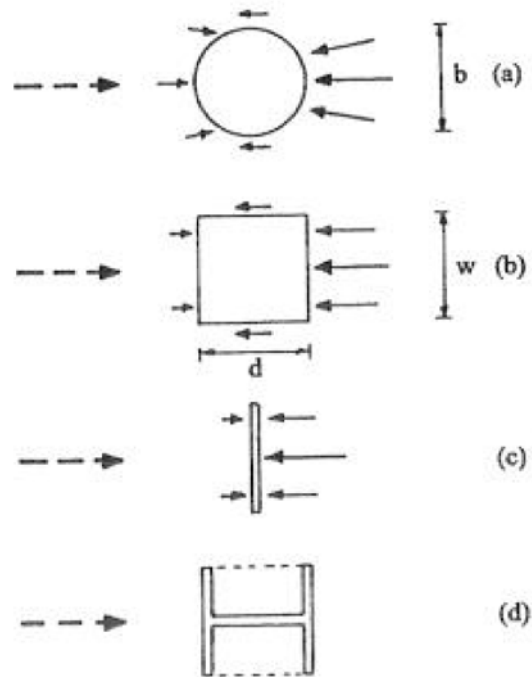


Figure 2-7 Sketches to indicate influence of shape of cross section of pile on the ultimate resistance of soil (Reese and Van Impe 2001)

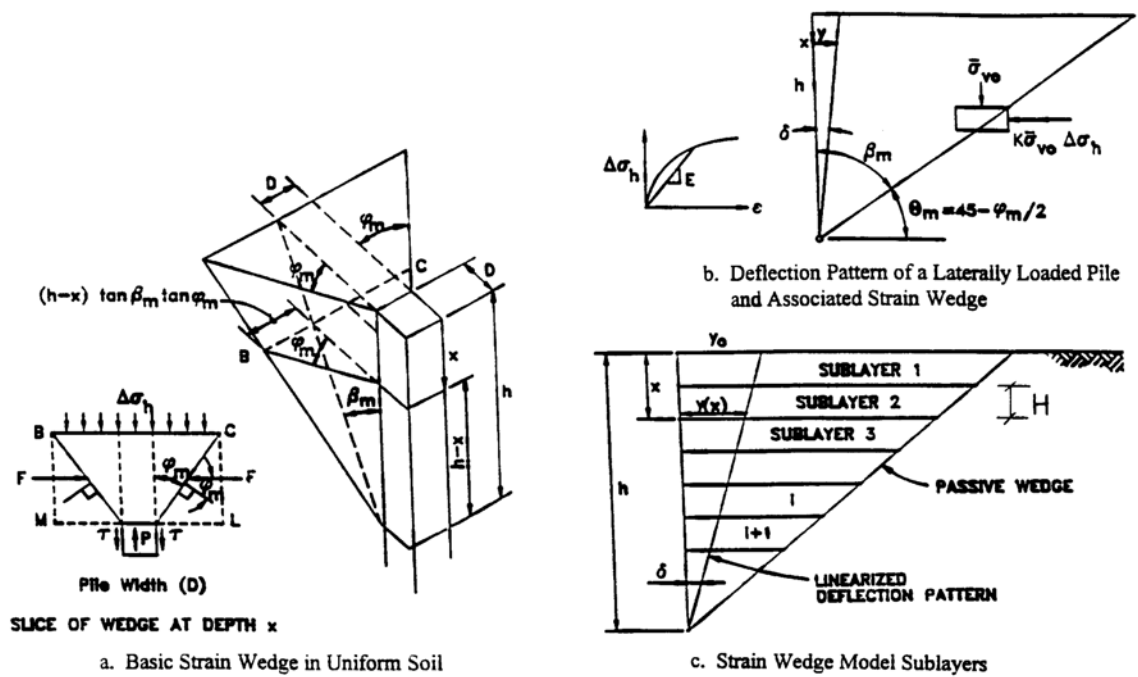


Figure 2-8 Configuration of Strain Wedge model (Ashour and Norris 2000)

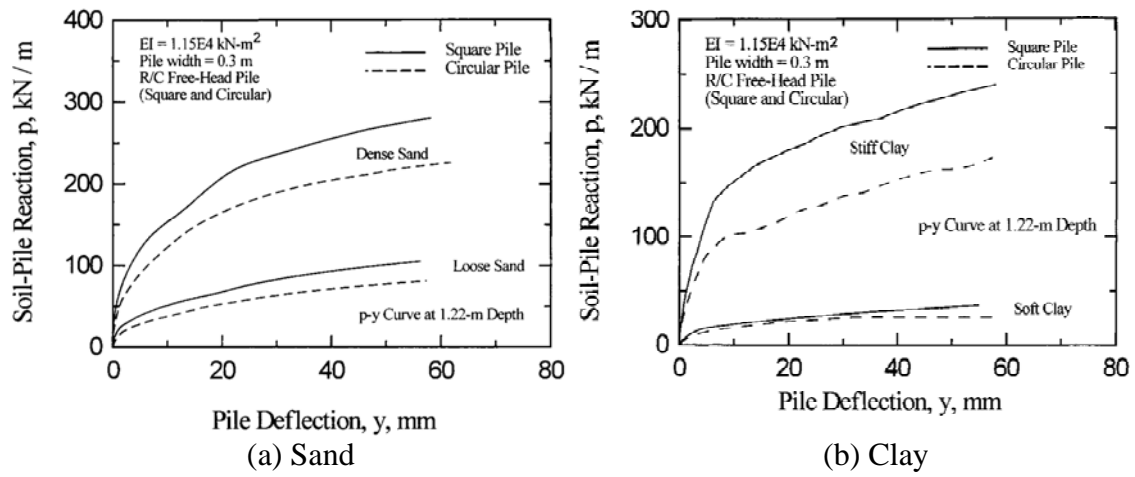


Figure 2-9 Effect of pile cross section shape on p - y curves (Ashour and Norris 2000)

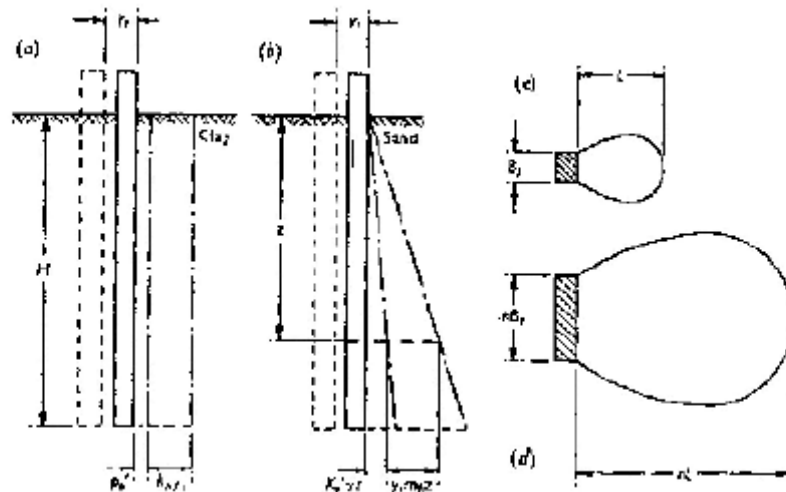


Figure 2-10 Influence of pile diameters on dimensions of bulb pressure (Terzaghi 1995)

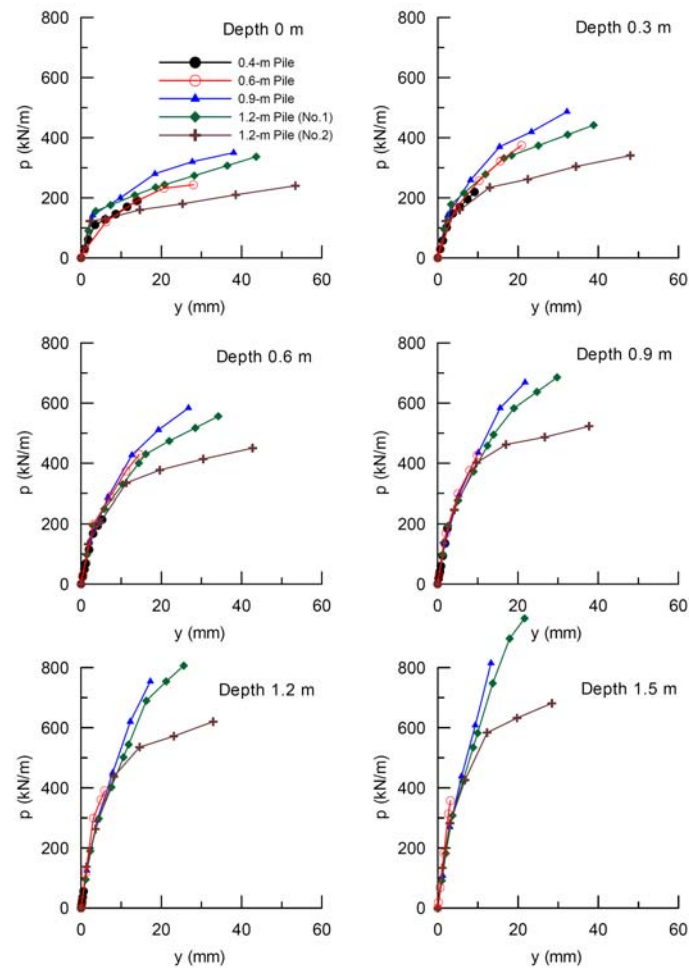


Figure 2-11 Comparison of p - y curves for different pile diameters in cemented sand (Juirnarongrit and Ashford 2005)

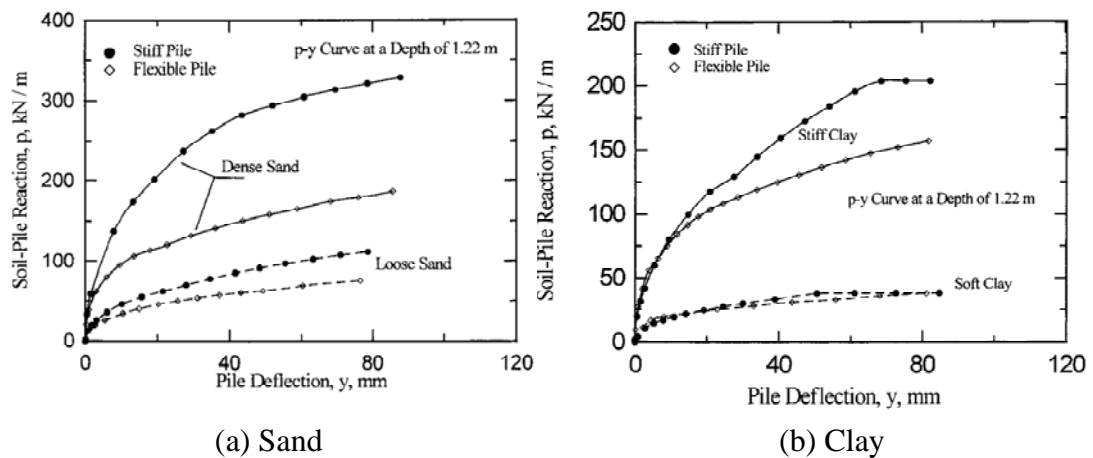


Figure 2-12 Effect of pile bending stiffness on p - y curves (Ashour and Norris 2000)

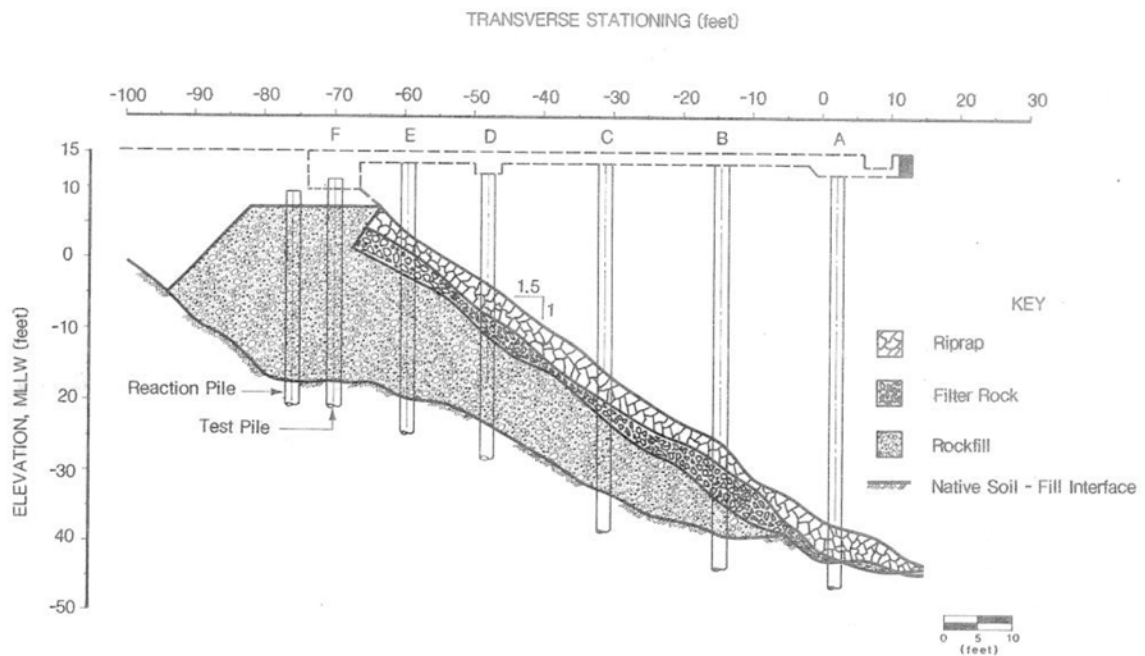


Figure 2-13 Cross section of setup of full-scale test on pile in rockfill (Diaz *et al.* 1984)

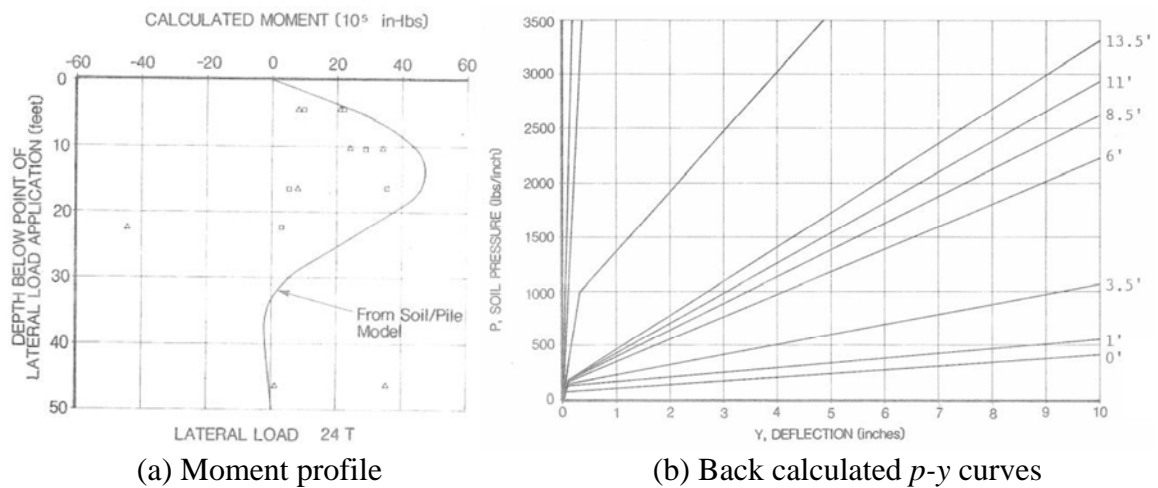


Figure 2-14 Back calculated moment profile and p - y curves for rockfill (Diaz *et al.* 1984)

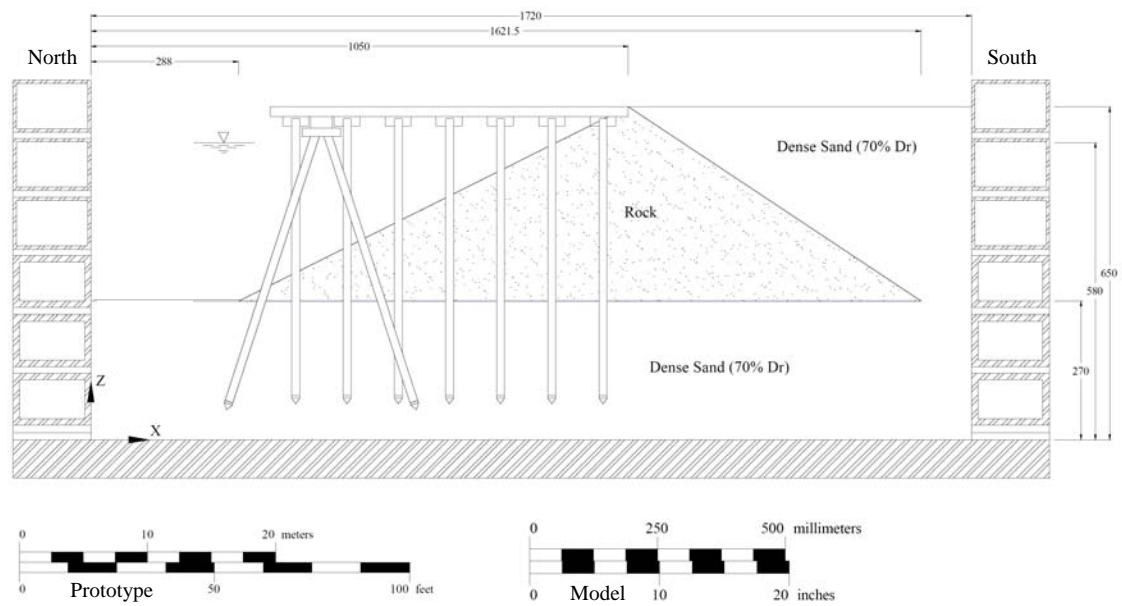


Figure 2-15 Centrifuge model of pile group tests (Boland *et al.* 2001b)

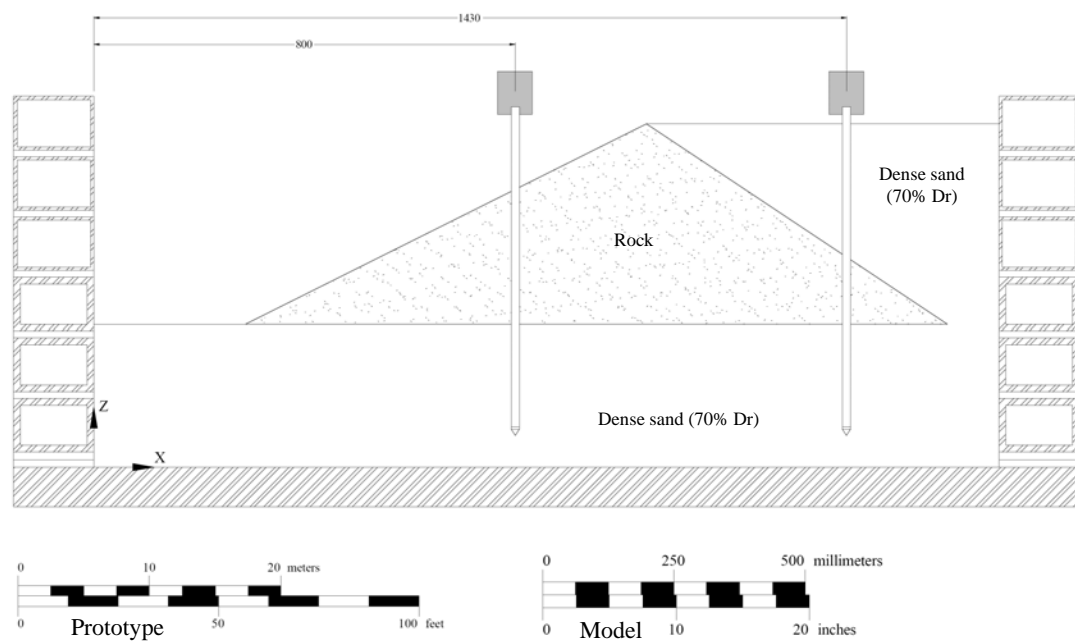


Figure 2-16 Centrifuge model of single pile tests (Boland *et al.* 2001b)

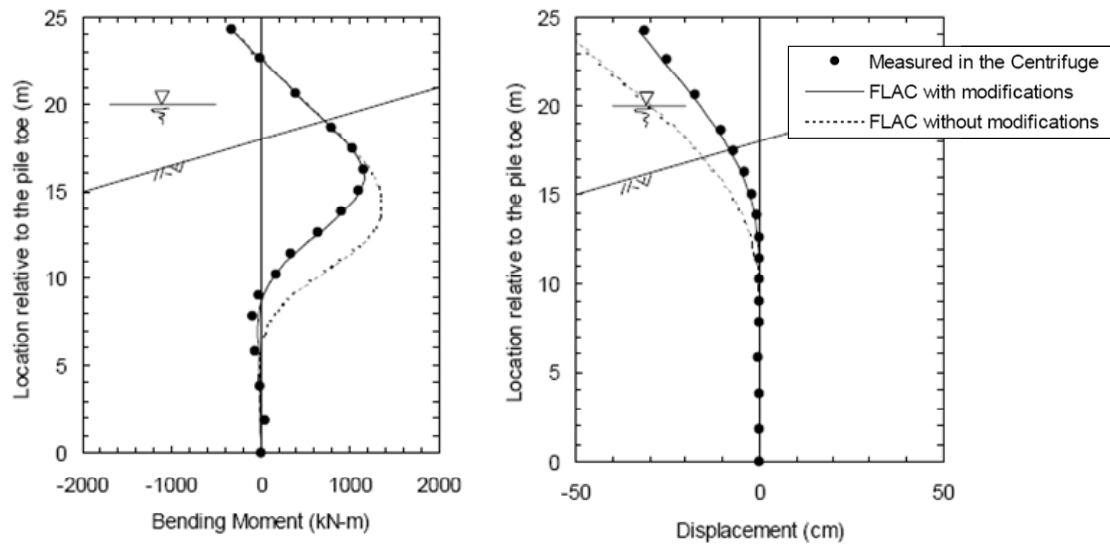
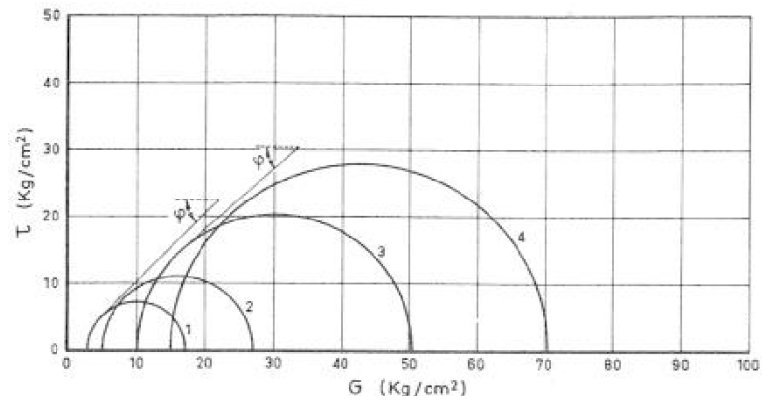
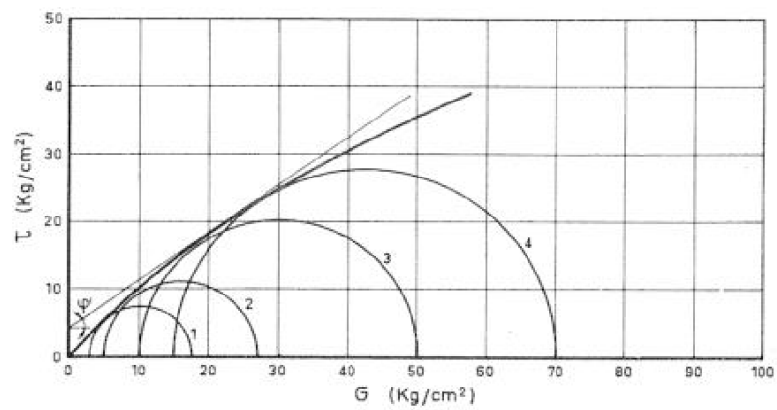


Figure 2-17 Lateral pile response predicted by FLAC (McCullough *et al.* 2004)



(a) Straight lines tangent passing the origin to each circle



(b) Curved envelope and straight line with apparent cohesion

Figure 2-18 Various definitions of failure envelope (Bertacchi and Bellotti 1970)

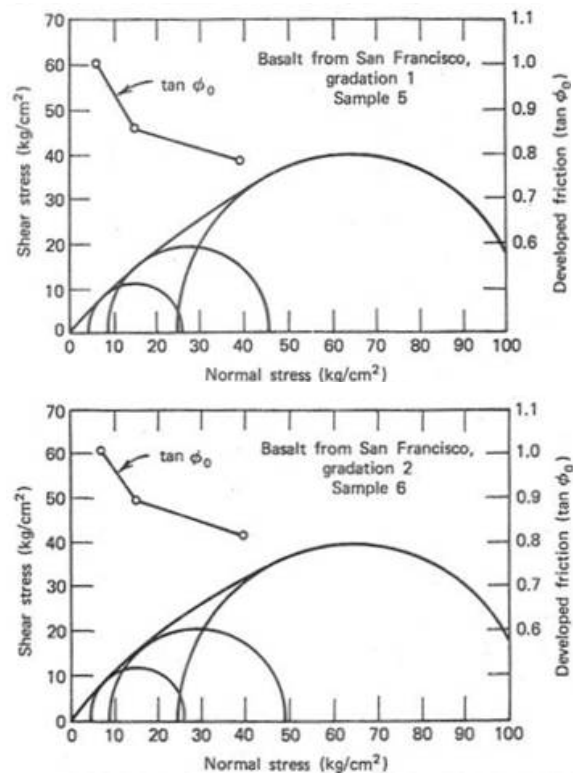


Figure 2-19 Examples of results from triaxial test for rockfill (Marsal 1973)

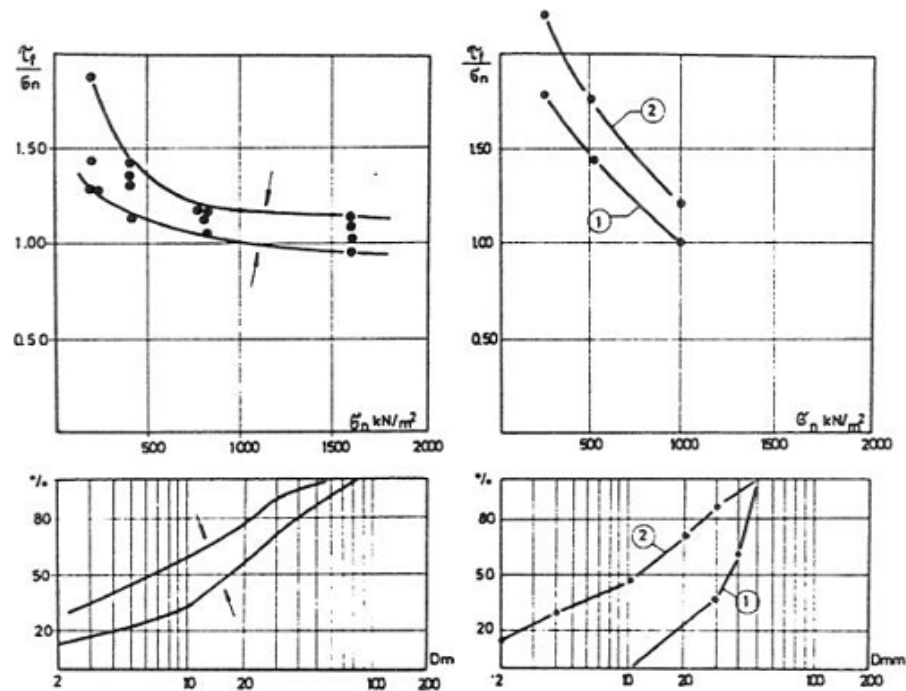


Figure 2-20 Effect of gradation on shear strength (Anagnosti and Popovic 1982)

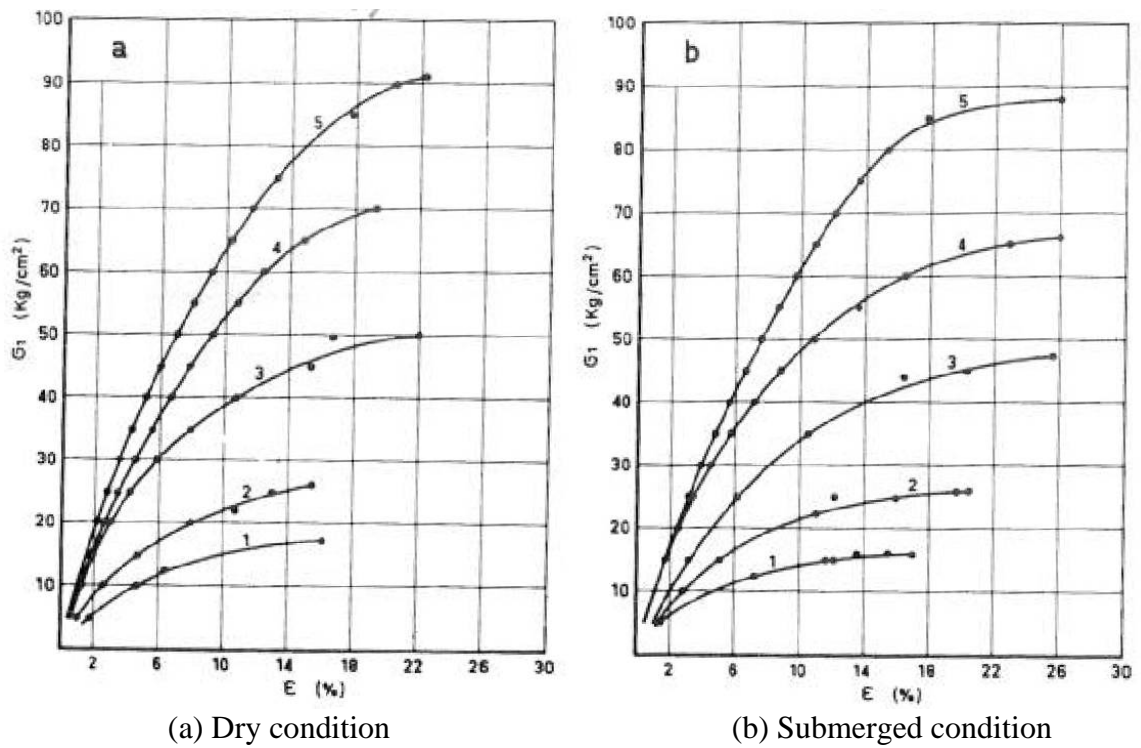


Figure 2-21 Effect of water on shear behavior of rockfill (Bertacchi and Bellotti 1970)

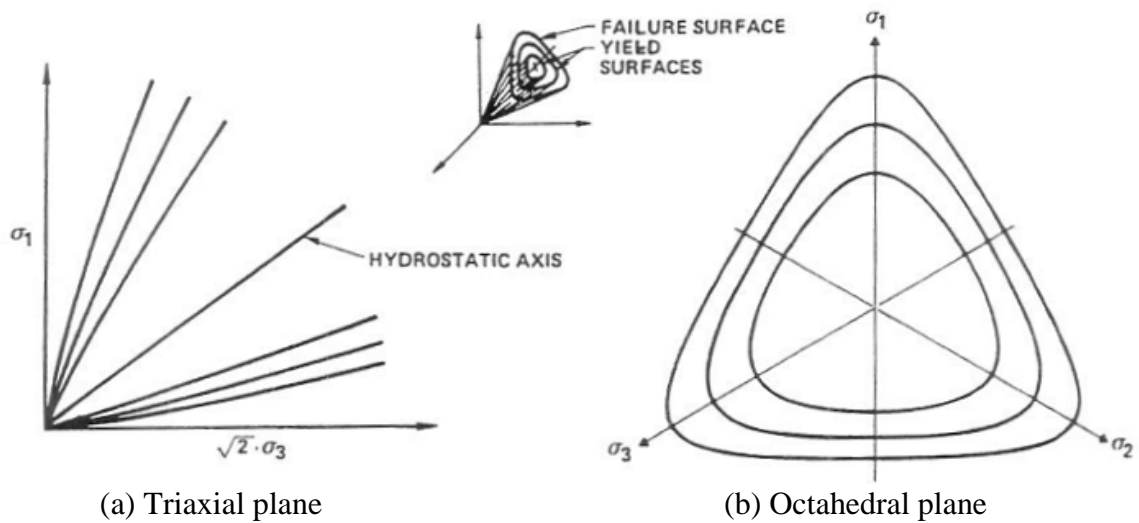


Figure 2-22 Characteristics of failure shown in 3-dimensional stress condition (Lade 1977)

3 DESIGN, CONSTRUCTION AND PROCEDURE OF PILE TEST

In order to achieve the research objectives defined based on the review of past works and the requirements in the current design practice, a test plan needed to be developed with careful consideration. Process of test plan making is composed of design of test specimens and accessories, selection of the best construction methodology and procedure, and development of load protocol.

Prediction analysis of the behavior of the test piles is one of the most important works in the process of the reasonable test plan making. Applying the methodology and the parameters typically used for the current design practice or modified based on the results obtained in the previous test, the laterally loaded pile behaviors were predicted (Sections 3.2 and 3.4).

Based on the prediction results, details of the test plan, such as the test setup, the construction procedures, the locations and the type of instrumentation were developed. The construction process of the test specimens and details of instrumentation are presented in Sections 3.3 and 3.5, respectively.

3.1 Test Plan Update Histories

The test plan was significantly changed two times because some difficulties in construction and unexpected results during the previous tests were observed. Prediction analyses were also conducted whenever the test setup was updated. Therefore, it is reasonable to briefly summarize test plan update histories at the beginning of this chapter. The update histories of the test setup are summarized in Table 3-1; there are two major changes of the test setup.

The original plan in a proposal paper to the Port of Los Angeles (Test Plan 1) had five tests with five individual single piles as shown in Table 3-2 and Figure 3-1. Based on the test setup in the proposal, prediction analyses were conducted to define length of test

piles and locations of sensors. Following the prediction analysis, five test piles were fabricated with sensors embedded in the piles. However, when a detailed construction plan of the test specimens was designed, there were some difficulties found (e.g. construction of large pile caps was needed to make fixed head conditions at the pile tops).

In order to find alternative test plans, analysis of a whole wharf structures was performed. The typical pier structures at the ports in the West Coast of the United States are supported by multi-piles. The piles are interconnected by a 2 to 3 ft (0.61 to 0.91 m) thick concrete deck that constrains the displacement and rotation of the pile heads, and induces the axial load along the piles. Based on the analysis, the most possible critical sections are concentrated on the piles in two landward rows (Figure 3-2), and it is reasonable idea to focus on the piles in these two rows. Therefore, system tests of two interconnected piles can simulate similar condition as that in the actual wharves, and provide more specific information. It is notable that one of the interconnected piles is located on level ground, and the other is placed at the dike crest, identical as piles in the actual wharves.

In addition, a free head single pile test needed to be carried out prior to the system tests with fixed head condition for several reasons even though the single pile with free head condition can not represent boundary conditions in the actual pile-supported wharf structures; i) assessment of accuracy of the prediction analysis, ii) calibration of numerical parameters for simulation analysis, iii) investigation if the locations of the sensors were reasonable and the sensors worked properly, and iv) revision and improvement of test setup plan for the following system tests if problems to be solved were found.

Therefore, the test setup was changed to one single pile test and two coupled-pile tests discussing with engineers at the Port of Los Angeles and technical advisors for this research (Test Plan 2). A list of test cases and test setups for Plan Version 2 is shown in Table 3-3 and Figure 3-3, respectively. All the construction works were made based on Test Plan 2. There was another revision of the test plan after the first Single Pile Test due to unexpected test results observed in the test, and it will be presented in Section 3.4.

3.2 Prediction Analyses Prior to Construction of Test Specimens

As mentioned above, design of test specimens is one of the most critical processes to succeed a series of experiments. In this section, details of prediction analyses prior to the construction of the test piles are described in order to show how the test specimens were designed.

3.2.1 Prediction in the original proposal (Plan Version 1)

The original plan (Plan Version 1) was made for a proposal of this research. It was composed of five individual single pile tests. Prediction analyses were conducted using p - y curves for the lower and the upper bounds; in the lower and upper bounds analyses, the possible lowest and largest reactions from the rockfill needs to be considered, respectively. The p - y curves for the lower bound are 30 percent of the curves for level ground while the p - y curves for the upper bound are 2 times greater than the curves for level ground. The curves for level ground were derived by API standard (API 1987) for cohesionless material with internal friction angle of 45 degrees. *LPILE* (Reese *et al.* 2000), one of the most widely accepted commercial software, was used for the prediction.

Based on the prediction, it was concluded that the horizontal displacement and bending moment for locations deeper than 20 ft (6.10 m) from ground surface were almost zero even in the lower bound analysis. Therefore, 20 ft (6.10 m) long piles from the bottom of soil pit to the ground surface were adopted.

Locations of the dense instrumented zones were also defined from the prediction analyses. Because it is most likely that the critical section develops at the elevation with the maximum moment, the sensors were placed around the location of the maximum moment obtained in the predictions.

3.2.2 Prediction before construction (Plan Version 2)

The test piles were fabricated with sensors embedded at the locations designed based on the predictions in Plan Version 1. However, several difficulties were found during making details of construction plan. In order to avoid the difficulties, several alternative plans were compared and it was found as one of the most reasonable ideas to carry out three separate tests; i.e. the first test, which remained unchanged from the original plan, was carried out in a free head cantilever pile and the other four piles were tested in two coupled pile tests. As the test setup was changed, prediction analysis had to be also updated in order to re-design load protocol, check whether the locations of sensors were reasonable and confirm that lateral resistance of the system would be less than a capacity of an actuator available (Section 3.3.8; 500 kips in compression, and 420 kips in tension).

OpenSees, the Open System for Earthquake Engineering Simulation developed at University of California at Berkeley (McKenna 1997) was used in prediction analyses for Plan Versions 2. Because this application is little complicated, it is used only for research purpose at present. However, it is very powerful tool and it may be used by practitioners in future.

3.2.2.1 Numerical model

Numerical models of pushover analysis for single pile test and system tests are shown in Figure 3-4 and Figure 3-5, respectively. Most parts of these models are based on the current design procedure.

Assuming the concrete footings at the bottom of the piles have no rotation and deflection, the bottom of the soil pit (i.e. the top of the concrete footing) may be fixed in all of horizontal, vertical, and rotational directions. However, numerical analyses were not stable because of large difference of rigidities between fixed bottom and p - y curves just above the bottom in cases of system tests for the lower bound. Therefore, vertically fixed conditions were used at the bottom of the footing and placed p - y curves representing reaction on the footings in order to make stable analyses. Also, a dummy

spring was placed at the top of the pile in order to make structural model stable even after yielding.

The connection is not perfectly fixed; it allows rotation and fails when the rotation reaches certain value. Therefore, rotational springs were included at the connection between the pile top and the load stub to explain the fixity condition referring literature (e.g. Kawamata *et al.* 2006).

Dead weight of piles was ignored, but dead weight of load stubs and steel beam were taken into account on the numerical model. As input motion, lateral displacement was applied at the top of pile.

In the system tests, the leading pile is pushed downward generating compressive force, and the trailing pile is pulled upward inducing tensile force along the pile. Because properties of the prestressed concrete piles and the reinforced concrete connections are dependent on the axial force, it needs to be taken into account in the analysis. Flow chart of the pushover analysis for the system tests is shown in Figure 3-6. In reality, the axial force changes in real time during loading; however, the axial force at the ultimate condition was used for analysis in order to simplify the numerical procedure. It is reasonable simplification because results from parametric analyses with axial force along the piles showed that the axial forces were not sensitive parameters on the pile behaviors.

3.2.2.2 Pile and connection properties

Moment-curvature relationship of the prestressed concrete pile was calculated using a commercial software, called *XTRACT* (TRC/Imbsen Software Systems 2007). Also, moment-rotation relationship at the pile-deck connection was derived by software, *Columna* developed based on full-scale connection tests at University of California at San Diego (Krier *et al.* 2006). Because properties of the prestressed concrete piles and the reinforced concrete connections are dependent on axial force along piles as mentioned in the previous section, the properties were derived at several magnitudes of axial force. When the axial force along the pile was in between axial forces at which the pile and the connection properties were calculated, their properties were defined by linear interpolation of the calculated properties. Figure 3-7 and Figure 3-8 show properties of

the pile and the connection, respectively. According to these figures, the detailed properties of the pile and the connection are smoothly curved with degradation, but these were simplified to multi-linear perfect plastic for analysis; i.e. the numerical model used for the prediction analysis has no degradation, and may not be able to capture the behavior of the piles after the connection or the piles reaches the peak moment.

Eight of #10 dowel rebars were installed 50 inches (1.27 m) from the bottom of the load stubs (refer Figure 3-38), and these bars make the piles stiffer. Used moment-curvature relationship for the section with dowel rebars was 20 percent greater than the section without dowels at any curvature to simplify the analysis. It is reasonable assumption because several parametric analyses were also conducted, and it was found that the moment-curvature for the section with dowel bars did not affect on the behavior of the test piles.

3.2.2.3 Soil-pile springs

The soil-pile springs used were currently used for design of wharf structures (Martin 2005). The p - y curves at various depths are shown in Figure 3-9. As mentioned above, the lower and the upper bound analyses were conducted in order to cover uncertainties of the p - y curves due to rock properties, and dike construction; the possible minimum reaction is used for the lower bound analysis, and the possible maximum reaction is used for the upper bound analysis.

The p -multipliers used herein were 0.3 for the lower bound analysis and 2.0 for the upper bound analysis at any depth referring the current design practice. The p -multipliers used for the prediction analysis of the Plan Version 2 are summarized in Table 3-4. Spacing of springs was a quarter foot, less than one sixth of the pile diameter.

3.2.2.4 Prediction results for Plan Version 2

The prediction results for Single Pile Test are show in Figure 3-10 and Figure 3-11. According to a load displacement curve in the standard case ($m_p = 1.0$) in Figure 3-10, the yielding displacement and lateral resistance of the pile for design of load protocol was

defined as 1.3 inches (3.3 cm) and 65 kips (289 kN), respectively. Figure 3-11 shows profiles of moment and curvature along the pile. From this figure, it was found that locations of the maximum moment from the prediction analyses were within dense instrumented area. It was notable that the critical section may be out of the dense instrumented area if reaction from rockfill is larger than the upper case analysis ($m_p = 2.0$).

The predictions for System Test 1 are shown in Figure 3-12 through Figure 3-14. Based on the predicted load-displacement curves shown in Figure 3-12, the yielding displacement and the lateral resistance for load protocol were defined as 1.1 inches (2.8 cm) and 240 kips (1068 kN), respectively for loading in either direction. Figure 3-13 and Figure 3-14 are profiles of curvature along the piles. These figures show that the locations of critical sections are within the dense instrumented area in all the cases except for the upper bound analysis ($m_p = 2.0$) in pushing toward the downslope. It was less possible assumption that the downslope generates large reaction as the p - y curves defined in the upper bound analysis. Therefore, it was concluded that the most critical section would be in the area with dense sensors.

Figure 3-15 through Figure 3-17 are prediction results for System Test 2. From Figure 3-15, 1.0 inch (2.5 cm) and 275 kips (1223 kN) were used as the yielding displacement and the lateral resistance to design a load protocol for System Test 2. The possible maximum lateral resistance of the system was 350 kips (1557 kN) shown in the upper bound analysis, and it was less than the capacity of the available actuator in tension (refer Section 3.3.8). The profiles of curvatures shown in Figure 3-16 and Figure 3-17 also have the same trend as the prediction for System Test 1. Because of the same reason mentioned above, the upper bound analysis was assumed as a less possible scenario for loading toward the downslope.

In conclusion of the prediction analyses for Plan Version 2, the load protocols were designed. Also, it could be verified that the locations of the dense sensor zones and the capacity of the actuator available satisfied the required specifications. Therefore, it was decided to build the test specimens based on Plan Version 2.

3.3 Construction of Test Specimens and Test Procedures

Based on Test Plan Version 2 mentioned in Section 3.2.2, three individual tests were proposed in order to achieve the test goals defined at the beginning of this research; i.e. one single pile test with a cantilever pile and two system tests with coupled piles. However, in order to improve construction practice, period, and cost performance, there were some reasonable changes, such as using gravel as alternative of the rockfill. In this section, the construction revisions are described, as well as details of construction including procedures, specifications, and dimensions. In addition, details of device and accessories used for the tests are presented.

3.3.1 General descriptions of test setup

Section views of Single Pile Test, and System Tests 1 and 2 are shown in Figure 3-18 through Figure 3-20. In the system tests, the lateral loading induces axial forces along the piles; i.e. a compressive axial force is induced along a leading pile while an uplift tensile force is generated along a trailing pile when the system is laterally loaded. In real wharves, piles are very long and the friction between pile and soil constrains the system against vertical movements. The test piles were significantly shorter and friction around piles against uplift force was significantly smaller relative to the piles of the actual wharves. In order to prevent uplift of the test piles, the piles were embedded into 3 ft (1.07 m) long concrete footings at the bottom. Details of the footing are mentioned below and the design is attached in Appendix-A.

The pile lengths were 20 ft (6.10 m) of embedment into the rockfill based on the prediction pushover analysis (Section 3.2.1), plus 3 ft (1.07 m) of the footing, plus 1.5 ft (0.46 m) for P3, 3.5 ft (1.07 m) for P1, P2, and P5 or 5.5 ft (1.68 m) for P4 of a clearance between the ground surface and the bottom of the load stub, plus 2 inch (5.1 cm) of embedment into the load stub in the initial test setup in the original plan, Plan Version 1. As mentioned above, however, several difficulties and inconveniences in construction

were found during making detailed construction plan and the test setup needed to be updated. After evaluating several alternatives, it was decided to carry out three separate tests. The first test, which remained unchanged from the original plan, was carried out with a free head cantilever pile (P1 in Figure 3-18). The other four piles were arranged in two separate coupled pile system tests (P2-P4 and P3-P5 in Figure 3-18) interconnecting two piles with an instrumented steel beam. This test setup required much simpler construction and also had the advantage of representing boundary conditions of piles at actual wharves (Plan Version 2). The piles were placed to accommodate the coupled tests, with 1.5 ft (0.46 m) and 3.5 ft (1.07 m) height between the ground level and the bottom of the load stub.

3.3.2 Construction procedure

Construction flow of the test specimens is shown in Figure 3-21. This chart includes design of the revision of the test plan and adjustment of the test setup. The test piles were fabricated in a pile fabricator, Utility Vault in Fontana, California. Piles at the Port of Los Angeles are installed through the rockfill dike with strong vibration and jetting; however, it is not reasonable method in this research work because installation of pile through very hard rockfill requires a large powerful pile driver. In addition, sensors placed in the test piles may be damaged during installation. Therefore, the test piles were installed into a pre-excavated soil pit. After completion of the pile installation, the soil pit was filled with gravel and rockfill, and the load stubs at the top of the piles were constructed. During the soil pit excavation and the pile installation, the other accessories such as an instrumented steel beam and a concrete spacer block were fabricated. Cables from the sensors were also connected to data acquisition system, and all the test elements were placed at their correct locations at the last moment of the test preparation. Details of each construction work are described in the following sections.

3.3.3 Test piles

Properties of piles may affect on soil-pile interaction as introduced in Section 2.1.6. In order to eliminate effects of these factors, the test piles used in this research had identical specifications of piles typically used for actual wharf structures in the West Coast of the United States except for pile length (see above for details of the pile length).

The test piles were fabricated at the plant of Utility Vault in Fontana, California providing piles for actual wharf constructions at the Port of Los Angeles. Figure 3-22 shows procedures to build the test piles. Standard concrete usually needs to be compacted by vibrators, but the vibration compaction method was not appropriate for the test piles because the fragile sensors inside the piles could be damaged by the vibration. Therefore, Self Compaction Concrete (SCC) was used for the test piles. This concrete is highly fluid and does not require vibration to fill formwork uniformly (Figure 3-22(f)).

Properties of the test pile are summarized in Table 3-5. The piles were prestressed and had an octagonal section with a diameter of 2 ft (0.61 m) as shown in Figure 3-23. The piles were reinforced with sixteen 0.6 inch (15 mm) diameter A416 prestress strands with an area of 0.215 in^2 (140 mm^2). The ultimate strength was 270 ksi (1860 MPa), the yield strength was 216 ksi (1490 MPa) and the stress after losses was estimated as 153 ksi (1055 MPa). The effective prestress in the concrete was 1137 psi (8 MPa). The transversal reinforcement consisted of 0.51 inch (13 mm) diameter W20, A82 steel with yield strength of 70 ksi (480 MPa) and 2.5 in pitches (63.5 mm). The design concrete strength was 7.0 ksi (48 MPa) and the actual concrete strength of the test piles was 9.1 ksi (63 MPa) in 28 day.

3.3.4 Soil pit

An example of boring log at the test site is shown in Figure 3-24. According to this log, the soil at the site is dense to very dense clayey sand with more than 50 blow counts in standard penetration test.

Figure 3-25 shows the location of newly excavated soil pit for this research. The soil pit was located on the south side of the concrete reaction wall. Detailed dimensions of the pit are also shown in Figure 3-26. The dimensions of the pit are 42 ft (12.80 m) by 44 ft (13.41 m) at the ground surface with an excavation depth of 20 ft (6.10 m). All the side slopes of the soil pit were 1H: 1V for the first top 4 ft (1.22 m) and 0.75H: 1V below that.

The total volume excavated for the soil pit was approximately 530 cubic yards (405 m³). The access road to the bottom of the pit was also prepared on the east side, and its volume was about 320 cubic yards (245 m³). All the excavated soil was hauled from the construction site. Photos of excavation are shown in Figure 3-27.

3.3.5 Pile installation

The concrete piles were placed at the locations specified in Figure 3-28. Three of the pile tips were placed at 23 ft (7.01 m) and two of them were placed at 25 ft (7.62 m) below the original ground surface, and reinforced concrete footings were placed at the base to stabilize the piles and fix their locations during backfilling the soil pit. Details of the footing of the test piles are shown in Figure 3-29.

In design concept of the footings against up-lift force (Appendix-A), connection between the piles and the footing concrete was assumed strong enough even though there was no reinforcement rebars connecting the footings to the piles. In order to satisfy this assumption, sandblasting on portions of the piles embedded into the concrete footings was carried out to increase friction between the piles and the footings. The required strength of footing concrete was 3.0 ksi (21 MPa) to avoid critical failure at the pile-footing connections. The actual strength at the day of Single Pile Test 1 was 4.0 ksi (28 MPa) in compression test of the concrete cylinders casted when the footings were built, and satisfied the requirement in the design.

The locations of the test piles should be as exact as possible because the actuator needed to be precisely placed between the pile caps and the reaction wall. The tolerance allowed for the final locations of the piles was less than ± 2 in (5.1 cm) from the design

drawing at the top of the pile. In order to ensure that error of the pile locations was within the tolerances, four steel beams were placed to fix the pile top locations as shown in Figure 3-30. First, three concrete blocks were placed as foundations of the steel beams. Following that, the steel beams in the north-south direction were placed at the exact locations, and fixed to the concrete blocks and the reaction wall. Finally, the beams in the east-west direction were placed and fixed to the beams in north-south direction with fillet welding. In addition, performing surveys when the test piles were installed and fixed the pile tops to the steel beams, the pile head locations were monitored. The beams fixing the pile tops were removed when depth of backfilling reached 7 ft (2.13 m) from the bottom of the soil pit.

As-built locations of the test piles are shown in Table 3-6. All the errors of the test pile locations were less than the tolerances. Photos of pile installation procedures are shown in Figure 3-31.

3.3.6 Backfilling

In order to find more reasonable understanding about pile-large particle rockfill interaction occurring at actual wharves, it is the most reliable to install the test piles into the rockfill used for actual constructions of the wharves. However, rather than transport the rockfill material from Catalina Island typically used in Los Angeles area, it was decided to use a similar, locally available material in San Diego County because of large transportation cost.

The matching material had limited availability and the available volume of the material was less than that needed to fill the entire soil pit. According to Reese and Van Impe (2001), the soil-pile interaction is concentrated on the top 5 to 10 times of pile diameter deep from the ground surface. This depth significantly affecting on pile behavior becomes shallower as soil around the pile is stiffer; i.e. the most significant depth of the 2 ft (0.61 m) diameter test piles in the very rigid rockfill can be 5 to 6 times of the pile diameter, and 10 to 12 ft deep (3.05 to 3.66 m) from the ground surface in this

study. Therefore, it could be reasonably assumed that backfilling of the bottom 7 ft (2.13 m) of the soil pit with smaller particle gravel had negligibly minor effect on the pile behavior. The 13 ft (3.96 m) thick rockfill was placed directly on the top of the gravel.

The gravel used to fill the bottom 7 ft (2.13 m) was angular-shaped with $\frac{3}{4}$ to 1 in (1.9 to 2.5 cm) of diameter and the rockfill was No.2 backing aggregate from Hanson Aggregates. The specification of the rockfill is provided in Appendix-B and the gradation of the rockfill is shown in Figure 3-32 with typical regulation of the rockfill used for actual wharf construction. According to this figure, the rockfill used for this test seemed poorly-graded than the regulation, but small particles of rockfill may be washed out during placement of the rockfill into water in actual constructions on the sea. A likely gradation of the rockfill after small particles are washed out is also shown in Figure 3-32. Based on these gradation curves, it could be assumed that gradation of the rockfill used for this research reasonably agreed with one of the rockfill in the actual marine structures. It is notable that this difference may affect on behaviors of the pile-soil system somewhat.

The first stage of backfilling was the placement of the gravel for the first 7 ft (2.13 m) from the bottom of the soil pit (Figure 3-33). Because piles of actual wharves are installed with strong vibration through the rockfill and the vibration may compact the rockfill to some extent, the gravel layer placed at the first stage in this experiment should be also compacted with vibration to simulate effect of pile driving to some extent. However, no compaction was required at this stage because it was reasonably assumed that this gravel does not affect on behaviors of the test piles.

At the second stage (Figure 3-34), the rockfill was placed in approximately horizontal layers in between 9 and 12 in (22.9 and 30.5 cm) thick in order to input constant vibration energy. Device used to compact the rockfill are summarized in Table 3-7. Hand-operated plate tamper was used for the first 3 layers of compaction, corresponding to 7 ft to 9.5 ft (2.29 to 2.90 m) from the bottom of the pit, with a minimum of four passes over the entire surface, since heavy equipment could not yet access the bottom of the pit. The hand tamper used was MVC-88GHW from Mikasa Sangyo Co., Ltd.; 211 lb (940 N) in operating weight, and 3450 lb (15.3 kN) in centrifugal force. Since the working space became wide, a heavy vibro-roller was used to compact the rest of layers, with a

minimum of one pass over the entire surface. The vibro-roller used was CP-433E from MacAllister Machinery Company, Inc.; 100 hp in gross power, 15,750 lb (70 kN) in operating weight, and 15,000 to 30,000 lb (67 to 133 kN) in centrifugal force. Slope angle of the rockfill on the south side was 1 5/8H: 1V, identical as that of actual wharves at the Port of Los Angeles.

Because external sensors were placed at the pile surface in order to obtain structural behaviors of the prestressed concrete piles, gravel used for the backfilling of the bottom 7 ft (2.13 m) was placed around the sensors to prevent damage of the sensors during back filling, as shown in Figure 3-35. The access road was also backfilled with soil stored at the test site. There was no specification for the compaction of the access road, but a wheel loader passed over the soil several times to keep workability. Photos of backfilling are shown in Figure 3-36.

3.3.7 Connections and load stubs

After the completion of backfilling, concrete load stubs were built on the top of the test piles. The detailed information of the load stubs and connections between the pile tops and the load stubs are shown in Figure 3-37 and Figure 3-38, respectively.

Eight #10 dowel bars were used to connect the pile with the load stub through grouted corrugated tubes (Figure 3-37 and Figure 3-38). The concrete grout was made of neat cement, and water. The water cement ratio was 0.4. The dowels were placed immediately after grouting. The design code specifies requirement of grouting material by mixture of grouting, but there is no specification of strength. Based on compression tests of cylinders, strength of the grouting material was 6.4 ksi (44 MPa) at the day of Single Pile Test 1.

Concrete used for the load stubs was normal weight standard mix. Required strength of the concrete was 5.0 ksi (34 MPa), and the actual strength was 6.6 ksi (46 MPa) at the day of Single Pile Test 1. The maximum aggregate size was less than 1 in (2.5 cm). Slump was limited to 3 to 4 in (7.6 to 10.2 cm). Steel grade was ASTM A706, Gr 60.

Dimensions of the load stubs and locations of PVC sleeves for placement of an actuator or a steel beam are very critical for the test setup and error should be less than ± 1 in (2.5 cm) from the design drawing. Referring a corner of the reaction wall, these dimensions and locations were carefully monitored, and all the errors were within tolerance. Photos of building connections and load stubs are shown in Figure 3-39.

3.3.8 Concrete spacer, steel beam, and actuator

Figure 3-40 shows detailed dimensions of a concrete block spacer to be placed between the reaction wall and the actuator as shown in Figure 3-20. Steel fiber reinforced concrete was used with the concrete strength at 28 days of not less than 3 ksi (21 MPa) without reinforcement. The minimum required amount of steel fiber was 51 lbs/yd³ (297 N/m³). The maximum aggregate size was 1 in (2.5 cm). Since, the dimensions of concrete block and pipe location are very critical for the test setup, and their error was less than ± 1 in (2.5 cm) from the design drawing. Eye bolts were placed at the top side of concrete block for lifting purpose. Aspect of the concrete spacer block is shown in Figure 3-41.

The details and aspect of the steel beam for system tests are shown in Figure 3-42 and Figure 3-43, respectively. It is composed of two steel girder plates at the both ends and a wide flange beam W24x176. The steel girder end plates are fixed to the beam with welding. One quarter inch of fillet weld on the both sides of the web and complete joint penetration groove weld for both flanges were used. Instrumentation on the beam is described in Section 3.5.

The hydraulic actuator used to operate the lateral force is shown in Figure 3-44. The maximum stroke is ± 24 in (± 0.61 m) and the maximum load capacity is 500 kips (2.2 MN) in compression, and 420 kips (1.9 MN) in tension. It has a displacement transducer and a ΔP type pressure meter. Photos of the actuator setup for the single pile test and the system tests are shown in Figure 3-45 and Figure 3-46, respectively.

3.3.9 Data acquisition system

A total of about 350 sensors at the maximum were connected to data acquisition systems to collect and process the data during the tests. The system used was the SCXI system manufactured by National Instruments. It consisted of SCXI-1520 modules, together with SCXI-1314 front mounting terminal blocks. The sampling rate was 10 Hz. The data acquisition system used in this research is shown in Figure 3-47.

3.3.10 Testing and load protocol

Testing was performed statically applying lateral load and displacement at the top of the piles with the hydraulic actuator. Amplitudes of target load and displacement were defined based on a yielding load and a yielding displacement obtained in prediction analyses.

The proposed load protocol is shown in Figure 3-48(a). There are two phases of loading; load controlled loading in the first phase followed by the displacement controlled loading in the second phase. Because bending stiffness of concrete piles is much higher in smaller displacement range and increment of displacement is quite sensitive to the behavior of the system as shown in Figure 3-48(b), load controlled loading is more reasonable in the first phase. In the second phase, displacement controlled loading is more reliable because of the opposite reason. At the second stage, two cycles of loading were followed by a reduced displacement cycle in order to capture the inner hysteretic behaviors of the system.

As the prediction and actual response of the test pile could be different, the experimental lateral load displacement envelope was compared with the predicted envelopes using the p - y curves with various p -multipliers in real time. This comparison served to define which set of the p - y curves had the best agreement with the experimental results, and update the load protocol for the following loading cycles.

3.3.11 Excavation for Single Pile Test 2

In Single Pile Test 1, large curvature was observed at shallower depth than expected. Therefore, the critical section at which the maximum moment was observed was out of the zone with dense instrumentation. Because the purposes of the first single pile test was to calibrate the sensors placed in the densely instrumented area, which could detect concentrated local damage, as well as to gain fundamental information on behavior of piles in the rockfill, the critical section needed to be in the area with more sensors. In order to shift the critical section into the densely instrumented depth, the rockfill around the pile used for Single Pile Test 1 was excavated as shown in Figure 3-49. The maximum depth of excavation was 3 ft (0.91 m) and slope was 1 5/8H: 1V, identical as prototype wharves at the Port of Los Angeles.

3.4 Revision of Test Plan using Single Pile Test Results

In the first two single pile tests, a considerably large difference between the prediction and the test results was observed; i.e. shear strength of the pile was much larger than predicted. Because capacity of a coupled-pile with 1.5 ft (0.46 m) long above the ground surface in Plan Version 2 may exceed capacity of the actuator available, the test setup of the following system tests needed to be updated again.

There was significant limitation for updating the test setup because the test piles were already in the rockfill, and the other test elements were also already constructed. There was no other acceptable option than excavation around the piles in order to increase pile length above the ground surface and reduce the lateral resistance of the systems. Because the system test with 3.5 ft (1.07 m) clearance between the bottom of the load stub and the ground surface had the closest dimensions to the target actual wharf structure in this research, it was the most important test setup. Therefore, 2 ft (0.61 m) excavation was carried out to change clearance from 3.5 ft (1.07 m) and 1.5 ft (0.46 m) to 5.5 ft (1.68 m)

and 3.5 ft (1.07 m), respectively (Test Plan Version 3). A list of the test cases is shown in Table 3-8 and the updated test setup is shown in Figure 3-50.

3.4.1 Revised prediction following the single pile tests (Plan Version 3)

As the test setup was revised again, load protocol for the following tests had to be updated. Also, it needed to be checked whether the locations of the densely instrumented area were reasonable, and the lateral resistance of the system was less than the actuator capacity.

3.4.1.1 Numerical model and material properties for Plan Version 3

Numerical model and procedure, and all the material properties used herein were exactly same as those used for the prediction analysis for Plan Version 2 except for elevation of the ground surface. According to the test results obtained in the single pile tests, it was found that the reaction from the rockfill was much larger than the prediction with the p - y curves used for the current design practice. Based on a preliminary backcalculation, two and five times larger p - y curves of the standard curves recommended for the current design could provide reasonable rotation profiles along the pile and the load displacement curve at the pile top, respectively. Therefore, the p -multipliers (m_p) used for the prediction of Plan Version 3 were 1, 2 and 5 instead of 0.5, 1, and 2. The p -multipliers used for the updated prediction are summarized in Table 3-9.

3.4.1.2 Prediction results for Plan Version 3

The predictions for System Test 1 for Plan Version 3 are shown in Figure 3-51 through Figure 3-53. Based on Figure 3-51, the yielding displacement and the lateral resistance for load protocol were defined as 1.4 inches (3.6 cm) and 280 kips (1246 kN), respectively for loading in either direction. Also, in the most critical case with five times of reaction (Figure 3-51), the lateral resistance of the system is about 340 kips (1512 kN), which is less than the capacity of the available actuator. In addition, Figure 3-52 and

Figure 3-53 show that the most possible location of the critical section is within the dense instrumented area in all the cases except for the case with $m_p = 5.0$ in pushing toward downslope. It is similar trend observed in the prediction for Test Plan Version 2, and it was regarded as unlikely scenario.

Figure 3-54 through Figure 3-56 are prediction results for System Test 2. According to Figure 3-54, the yielding displacement and the lateral resistance were defined as 1.5 inches (3.8 cm) and 220 kips (979 kN), respectively. Also, it could be verified that the locations of the sensors were reasonable (Figure 3-55 and Figure 3-56), same as the prediction for System Test 1.

3.4.2 Excavation for System Tests

Based on the prediction analysis for Plan Version 3, 2 ft (0.61 m) excavation of the entire soil pit could satisfy all the requirements. Therefore, the top 2 ft (0.61 m) of the rockfill was removed before the system tests using a wheel loader. Figure 3-57 shows photos during and after excavation. The original ground surface was shown in the broken lines in the figure. Also, the section of the test setup after excavation is shown in Figure 3-50.

3.5 Description and Calibration Test of Sensors

The most important objectives of the full-scale experiments in this research were verification and modification of the p - y curves. In order to achieve these objectives, it was very important to capture the load displacement relationship of the test piles, and the response along the piles, such as profiles of rotation, deflection, and moment. Records obtained during testing would be used for backcalculation analysis of the p - y curves.

The displacement and lateral force at the pile top could be measured by displacement transducers and a ΔP -type pressure meter on the hydraulic actuator (Section 3.3.8).

Records on these sensors could provide the load displacement curves of the structural system.

Tiltmeters and strain gages were installed along the test piles. The tiltmeters were one of the most appropriate sensors to find rotation, displacement and curvature profiles for the pile (Section 3.5.1). The tiltmeters, however, were not sensitive to concentrated local damage in surface concrete, such as cracking and spalling of the surface concrete because they were installed at the center of the core concrete inside of spiral transversal reinforcements in the test piles. To make up this disadvantage of the tiltmeters, the strain gages were embedded during pile fabrication (Section 3.5.2). Because of difficulty in direct placement of the strain gages on the prestressing strands, the strain gages were placed on auxiliary bars at different locations across the pile section.

Several string-activate potentiometers were also placed at various locations on the load stub to measure the displacement at the pile top as backup data of the displacement transducer on the actuator, as well as to monitor torsion and rotation of the cap (Section 3.5.3). For the system test, it was needed to place an instrumented steel beam connecting the piles in order to know how lateral force was distributed to each pile. Eight full-bridge gages and six single strain gages were placed on the steel beam. Prior to the lateral load testing of the piles, calibration test of the instrumented steel beam was carried out (Section 3.5.4).

In this section, type and location of the instrumentation used, and a brief description of newly developed tiltmeter housing are described. Calibration test setup and results of the instrumented steel beam are also described.

3.5.1 Removable tiltmeters

Tiltmeters are a capacitance-based sensor used for monitoring changes in the rotation of a structure. When the sensor is rotated about its sensitive axis, it provides an exceedingly linear variation in capacitance, which is electronically converted into angular data.

Data from a series of the tiltmeters along the pile can be used to determine profiles of pile displacement and curvature, as well as rotation. The pile displacement profile can be calculated from the integration of measured pile rotation along the length, and average curvature can be also obtained dividing the measured rotation by the spacing of the sensors. Tiltmeter is one of the most appropriate instrumentation to obtain behavior of entire pile, however, as mentioned above, it is not proper sensor to detect local phenomenon in surface concrete such as cracking and spalling because the tiltmeters were installed inside of the transverse reinforcement. Therefore, both the tiltmeter and the strain gages should be used when local phenomenon is expected.

For installation of the tiltmeters, it would be costly if the tiltmeters were sacrificially embedded into the piles because the embedded sensors can not be reused. A better approach is to install tiltmeters in special tubes embedded in the concrete piles, remove the sensors after testing, and reuse them for the next testing. Because it was expected that the tiltmeters could not be removed because of large deformation along the test piles, a special housing of tiltmeters was designed. This newly-designed housing of tiltmeters is shown in Figure 3-58. The housing has a wheeling system that can guide tiltmeters to the desired depth through the grooves of inclinometer casing as shown in Figure 3-59. A series of tiltmeters can be installed inside the casing by linking them with aluminum bars as shown in Figure 3-60. Fabrication of this housing is considerably cheaper than a cost of sensor itself. Because they can be reused after each test implementing this method, only 31 sensors are necessary for all the tests instead of 85 sensors in case if all the tiltmeters were embedded in the concrete piles. In addition to cost reduction, damage on the sensors during pile driving can be avoided. Also, the condition of sensors can be checked just before testing, and a sensor can be replaced easily if it is out of order.

Locations of the tiltmeters for each test are shown in Figure 3-61 through Figure 3-63. The tiltmeters were placed every 1 to 2 ft. More sensors were placed where large deflection was expected. The sensor used was SPECTROTILT, analog electronic inclinometer fabricated by HY-LINE (Figure 3-58).

3.5.2 Strain gages

As mentioned above, the tiltmeters are not appropriate sensor to detect concentrated local damage in surface concrete including cracking and spalling because they were installed at center of the core concrete inside of the transversal reinforcement. Therefore, a series of strain gages was also installed along the piles in order to complement the data from the tiltmeters (Figure 3-64).

Because large change of pile responses was expected around the most possible critical section, more strain gages were placed around a depth of the maximum moment defined in prediction analysis. Ideally, the gages should be directly glued to pre-stressing strands, but it is not feasible because of the small working space in the pre-existing formwork. Therefore, strain on the pre-stressing strands was monitored indirectly based on the strain of auxiliary #3 steel bars located strategically right besides the most demanded strands at the extreme confined concrete distance from the center of the pile section (refer the right drawing in Figure 3-65). The curvature of the test piles can be estimated by assuming that the plain sections remain plain. FLA-5 fabricated by Tokyo Sokki Kenkyujo was used as gages along the piles. Locations of the strain gages for Single Pile Test, System Test 1, and System Test 2 are shown in Figure 3-65, Figure 3-66, and Figure 3-67, respectively.

3.5.3 String-activated linear potentiometers

Several string-activated linear potentiometers were placed on the load stubs as backup sensors in order to reduce the risk of data missing. Aspect of string pot used for this series of the tests is shown in Figure 3-68, and locations of the potentiometers for Single Pile Test, System Tests 1 and 2 are shown in Figure 3-69, Figure 3-70, and Figure 3-71, respectively. Prior to the tests, all the potentiometers were calibrated in order to obtain more accurate correlation factors. The string-activated liner potentiometers used in this research were manufactured by Calesco and the model number was PT8101; some of potentiometers have 30 in (76 cm) stroke and the others have 50 in (127 cm) stroke.

3.5.4 Instrumented steel beam

The piles in the System Tests 1 and 2 were interconnected with an instrumented steel beam as shown in Figure 3-20. In order to compare actual individual response of each pile with numerical results, it is necessary to understand distribution of lateral load and axial force on each pile. A calibration test of the beam was carried out prior to the tests so that the strains measured on the beam during the pile system test could be reasonably converted into stresses on the piles.

The steel beam was instrumented as shown in Figure 3-72. Strain gages B-1 through B-8 were full-bridge gages composed of four strain gages, and gages B-9 through B-14 were single quarter gage working like tri-axial rosette gage. The strain gages used were FLA-5 fabricated by Tokyo Sokki Kenkyujo.

The calibration test of the steel beam was conducted at the test site. Hence, in order to calibrate the strain gages at both ends of the beam, a static load was applied at one end first, and the beam was flipped over horizontally and applied load at the other end. The steel beam was fixed on the reaction wall with prestressed bars and pushed up by using a hydraulic jack as shown in Figure 3-73 and Figure 3-74 in order to obtain relationship between measured strain on the placed gages and the applied load. The jack used was hollow cylinder, RCH1003 fabricated by ENERPAC; loading capacity is 220 kips (980 kN) and stroke is 3 in (7.6 cm). Applied load was calculated from measured hydraulic pump pressure.

Shear force can be calculated by using records on the triaxial gages at the center of the beam. Because shear stress in the section of wide flange is not uniform, the recorded strain has to be correlated. Based on dimensions of used wide flange, strain at the center of the web is 1.13 times larger than the average as shown in Figure 3-75. Calibration result of the gages at the center of the beam is shown in Figure 3-76. Test result is greatly matched with the correlated theoretical value.

Moment can also be derived from records at the ends of the beam. An example of calibration results of these gages for moment is shown in Figure 3-77. Obtained strain from moment during calibration reasonably agreed with theoretical value.

3.5.5 Other sensors

More sensors were placed on the test piles in order to gain behaviors of prestressed concrete piles including development of in-ground spalling, and behaviors of the connection between the pile and the load stub. Detailed information of those sensors is available elsewhere (Kawamata *et al.*, 2007), and brief descriptions of these sensors are provided herein.

Two types of sensors detecting in-ground spalling were developed; one was named spalling sensor composed of a linear potentiometer and two plates, and the other is instrumented rubber bands composed of double rubber bands and two strain gages. When cover concrete spalls out, these sensors can detect a jump of displacement or strain. The former sensor was embedded in concrete of the test piles, and the latter sensors were placed outside of the test piles. Because the instrumented rubber bands may be damaged when large particle rocks hit the sensors during the backfilling, smaller particle size gravels were manually placed around the sensors (refer Figure 3-35).

Strain gages were also installed on the dowel bars at the connection in order to obtain moment at the connection of the piles used for the system tests; the strain gages along the dowel bars were not needed for single pile tests because the pile head condition was free head for single pile tests, and a jump of moment at the connection would not happen.

Linear potentiometers were placed at the connection between the top of the test piles and the load stubs. Because the test pile for single pile tests behaves as free-head pile and it is obvious the relative rotation between the pile top and the cap would be zero, the potentiometers at the connection were placed only for the system tests.

3.6 Summary

Even though there were two major updates of the test plan, all the construction works were completed well without any accident. Concrete strength for all the test elements satisfied the requirement, and the errors of the test pile locations were within the

tolerance. There was suspicion whether the sensors embedded in the test piles (e.g. strain gages along the piles) work well because the full-scale tests in this research was pendent about a year since the test piles were fabricated. Fortunately, only a few sensors were missing, and most of the sensors worked well. Based on data recorded on the sensors during loading, large amount of information about soil-pile interaction, as well as behavior of soil-pile system could be obtained. In the next chapter, test results shown in raw data on the sensors, and results arranged from the raw data are presented for all the test cases.

Table 3-1 Update histories of test plan

Version of test plan	Works completed	Note / Reference
Version 1: Original Proposal 5 individual single pile	Design pile length and sensor locations < Section 3.2.1 >	Table 3-2 Figure 3-1
	Pile fabrication with designed sensors	Found construction difficulties on the plan in original proposal
	Making details of construction plan	
Version 2: 1st revision 1 single pile / 2 coupled piles	Check analysis of sensor locations for updated condition < Section 3.2.2 >	Table 3-3 Figure 3-3
	Construction of test specimens	Results of the first single pile tests were significantly different from prediction
	Testing with the single pile	
Version 3: 2nd revision with 2 ft excavation	Another single pile test	Table 3-8 Figure 3-50
	Check analysis of sensor locations for updated condition < Section 3.4.1 >	
	Testing with the coupled piles	

Table 3-2 List of the test sets (Plan Version 1)

Test name	Test piles	Boundary condition at the top of piles	Clear space between bottom of cap and ground surface (H)
Single Pile Test 1	P1	Free (level ground)	3.5 ft (1.07 m)
Single Pile Test 2	P2	Fixed (slope)	3.5 ft (1.07 m)
Single Pile Test 3	P3	Fixed (level ground)	3.5 ft (1.07 m)
Single Pile Test 4	P4	Fixed (slope)	5.5 ft (1.68 m)
Single Pile Test 5	P5	Fixed (level ground)	1.5 ft (0.46 m)

Table 3-3 List of the test sets (Plan Version 2)

Test name	Test piles	Boundary condition at the top of piles	Clear space between bottom of cap and ground surface (H)
Single Pile Test	P1	Free	3.5 ft (1.07m)
System Test 1	P2 & P4	Fixed	3.5 ft (1.07m)
System Test 2	P3 & P5	Fixed	1.5 ft (0.46 m)

Table 3-4 Summary of p -multipliers used (Plan Version 2)

Test Setup	Analysis Case	p -multipliers (m_p)		Corresponding analysis case in the current design
		Pile on level ground (m_{p1})	Pile on downslope (m_{p2})	
Single Pile Test	SP-1	0.3	---	Lower bound
	SP-2	1.0	---	Standard
	SP-3	2.0	---	Upper bound
System Tests	SY-1	0.3	0.3	Lower bound
	SY-2	1.0	1.0	Standard case
	SY-3	2.0	2.0	Upper bound

Table 3-5 Properties of test pile

Steel reinforcement	Type	Diameter	Quantity	Ultimate strength	Yielding strength
Prestress strand	A416	0.6 inch (15.2 mm)	16	270 ksi (1860 MPa)	216 ksi (1490 MPa)
Transversal reinforcement	W20	0.51 inch (13 mm)	2.5 inch (63.5 mm) pitches	---	70 ksi (480 MPa)
	Design compressive strength		Actual compressive strength		Effective prestress
Concrete	7.0 ksi (48 MPa)		9.1 ksi (63 MPa)		1137 psi (8 MPa)

Table 3-6 As-built locations of the test piles

Pile	Deviations from the designed pile locations (ft)		
	North-South (+: north, -: south)	East-West (+: east, -: west)	Up-Down (+: up, -: down)
P1	+0.05	+0.01	+0.04
P2	+0.05	± 0.00	+0.04
P3	+0.07	-0.02	+0.02
P4	+0.03	+0.01	+0.06
P5	+0.02	-0.01	+0.07

Table 3-7 Specifications of compaction device

		Gross power	Operating weight	Centrifugal force
Hand-operate plate tamper	MVC-88GHW, Mikasa Sangyo Co., Ltd.	---	211 lb (940 N)	3450 lb (15.3 kN)
Vibro roller	CP-433E, MacAllister Machinery Company, Inc.	100 hp	15,730 lb (70 kN)	15,000-30,000 lb (67-133 kN)

Table 3-8 List of the test sets (Plan Version 3)

Test name	Test piles	Boundary condition at the top of piles	Clear space between bottom of cap and ground surface (H)
Single Pile Test 1	P1	Free	3.5 ft (1.07 m)
Single Pile Test 2	P1	Free	6.5 ft (1.98 m)
System Test 1	P3 & P5	Fixed	3.5 ft (1.07 m)
System Test 2	P2 & P4	Fixed	5.5 ft (1.68 m)

Table 3-9 Summary of p -multipliers used (Plan Version 3)

Test Setup	Analysis Case	p -multipliers (m_p)		Corresponding analysis case in the current design
		Pile on level ground (m_{p1})	Pile on downslope (m_{p2})	
System Tests	SY-4	1.0	1.0	Standard
	SY-5	2.0	2.0	Upper bound
	SY-6	5.0	5.0	--- ¹⁾

- 1) The analysis case, $m_p = 5$ provided the best fitted load displacement curve for Single Pile Test 1

Table 3-10 List of instrumentation

Type of sensor	Location	Data to be obtained	References
Tiltmeter	Whole length of test piles	Profile of rotation along Pile	Figure 3-58 thru. Figure 3-63
Strain gage	Whole length of test piles	Strain of concrete, Profile of bending moment	Figure 3-64 thru. Figure 3-67
String-activated potentiometer	On load stubs	Rotation and displacement of load stub	Figure 3-68 thru. Figure 3-71
Strain gage	Steel beam between piles in system tests	Moment and Shear force on the tops of each pile	Figure 3-72 thru. Figure 3-77
Spalling sensor	Around most possible critical section	Concentrated local damage of concrete piles	Test Report (Kawamata <i>et al.</i> , 2007)
Linear potentiometer	Connection between load stub and pile	Rotation of connection	
Strain gage	On dowel bars of the connection	Strain along dowel rebars	

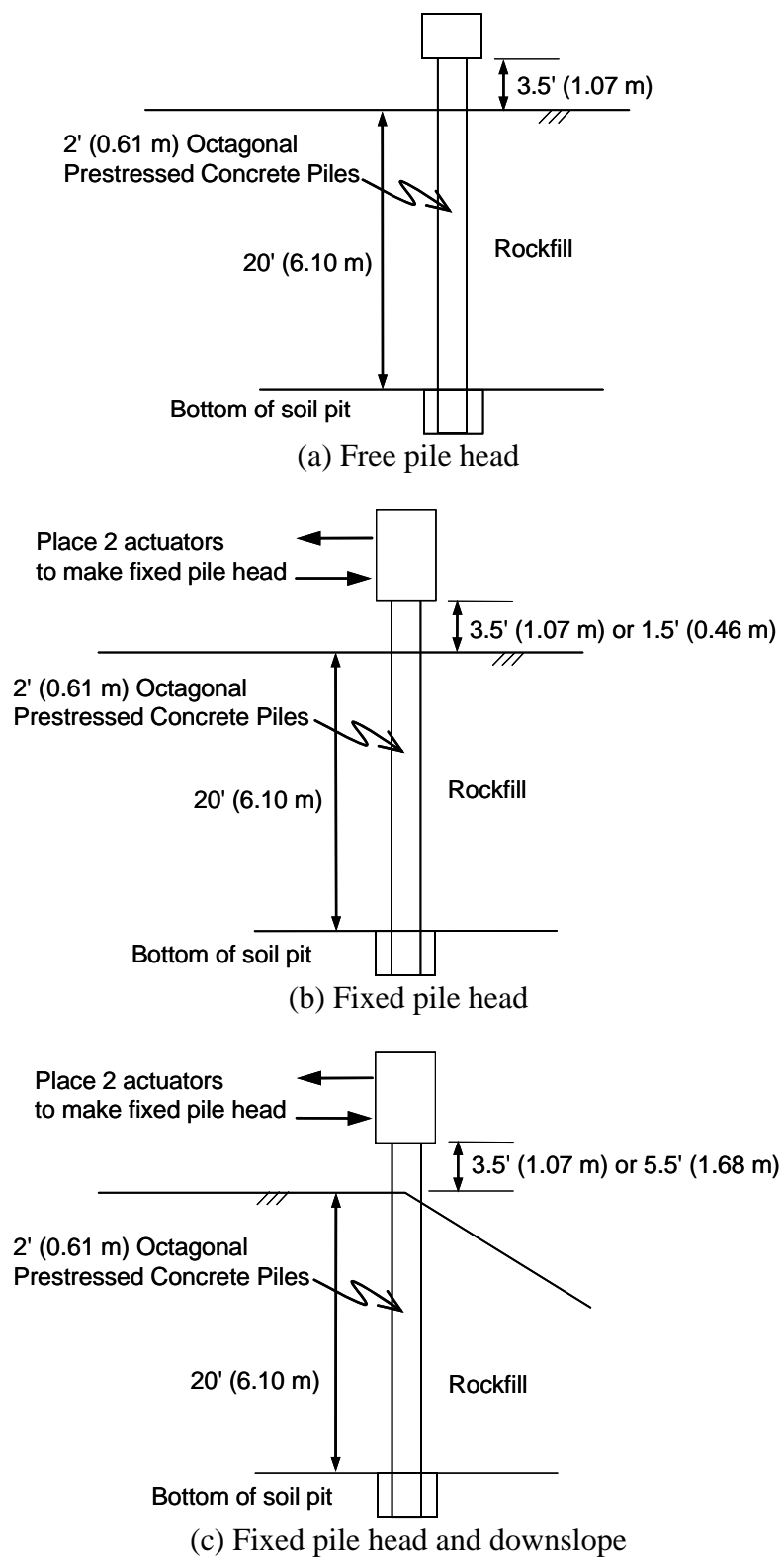


Figure 3-1 Test setup (Plan Version 1)

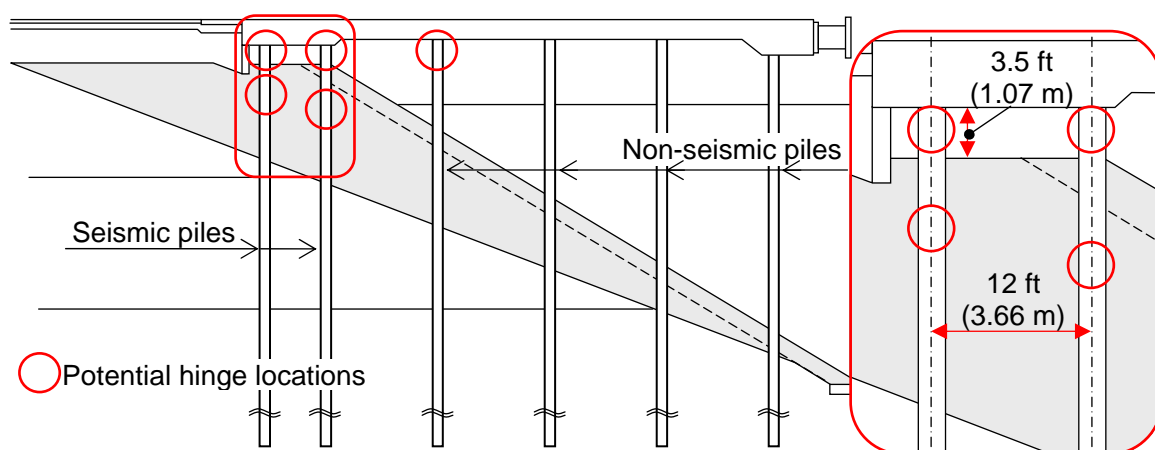


Figure 3-2 Potential hinge locations

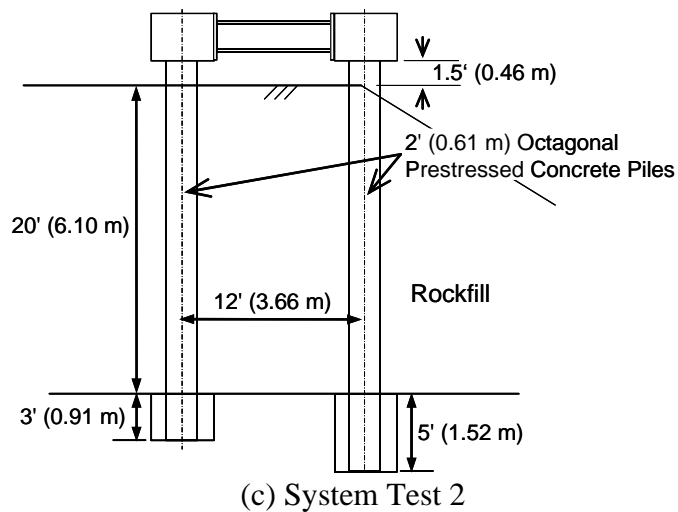
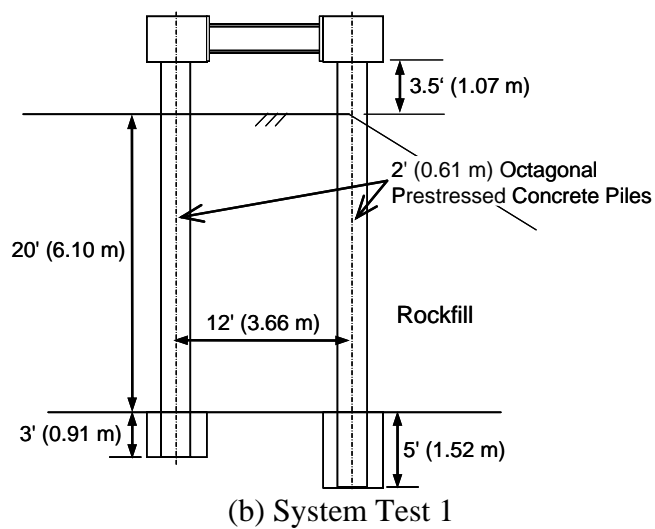
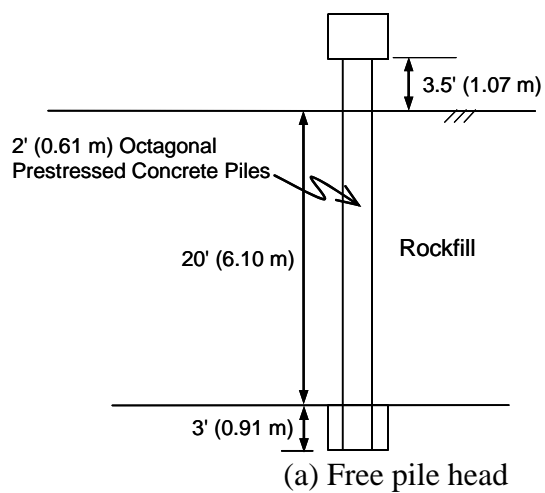


Figure 3-3 Test setup (Plan Version 2)

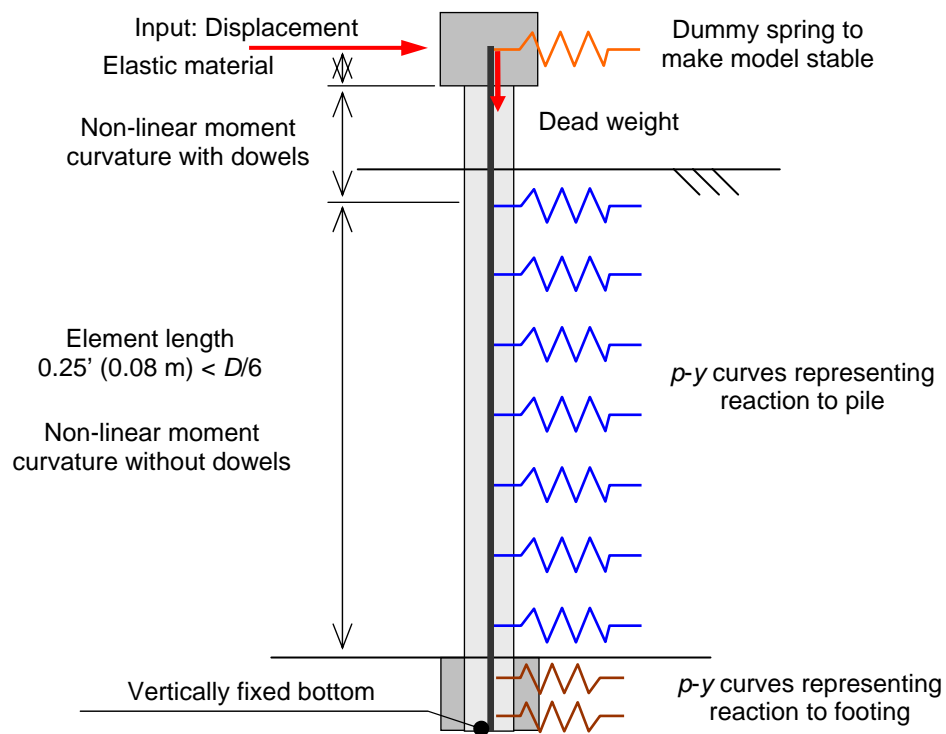


Figure 3-4 Numerical model for single pile tests

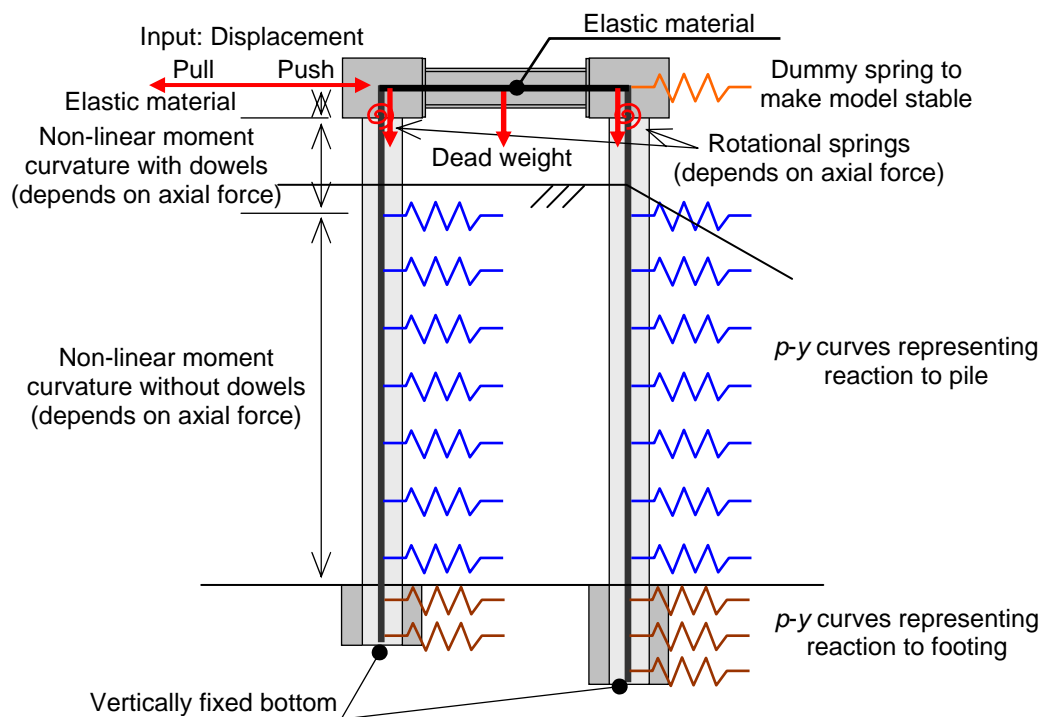


Figure 3-5 Numerical model for system tests

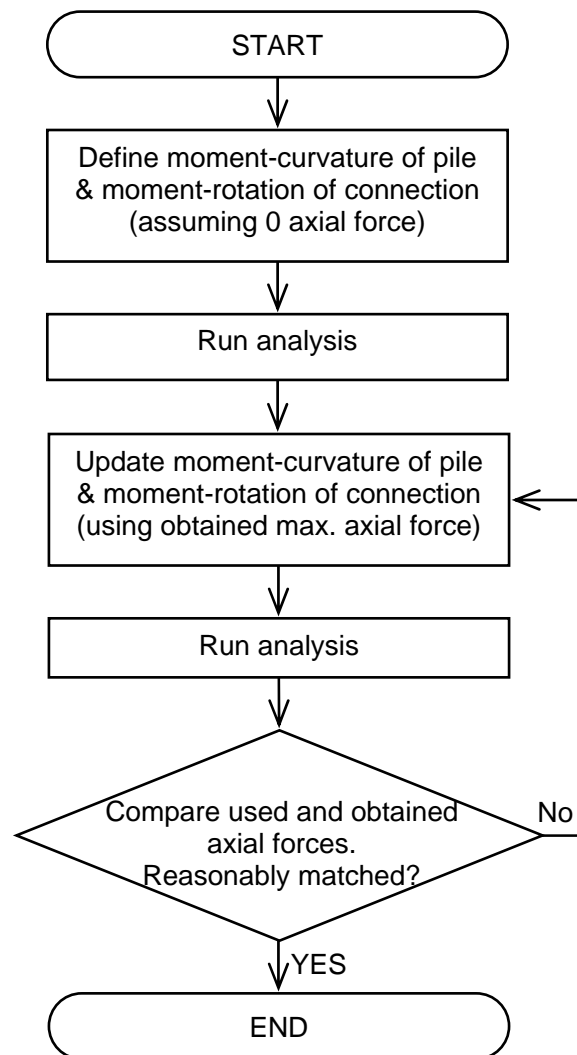


Figure 3-6 Flow chart of analysis for system tests

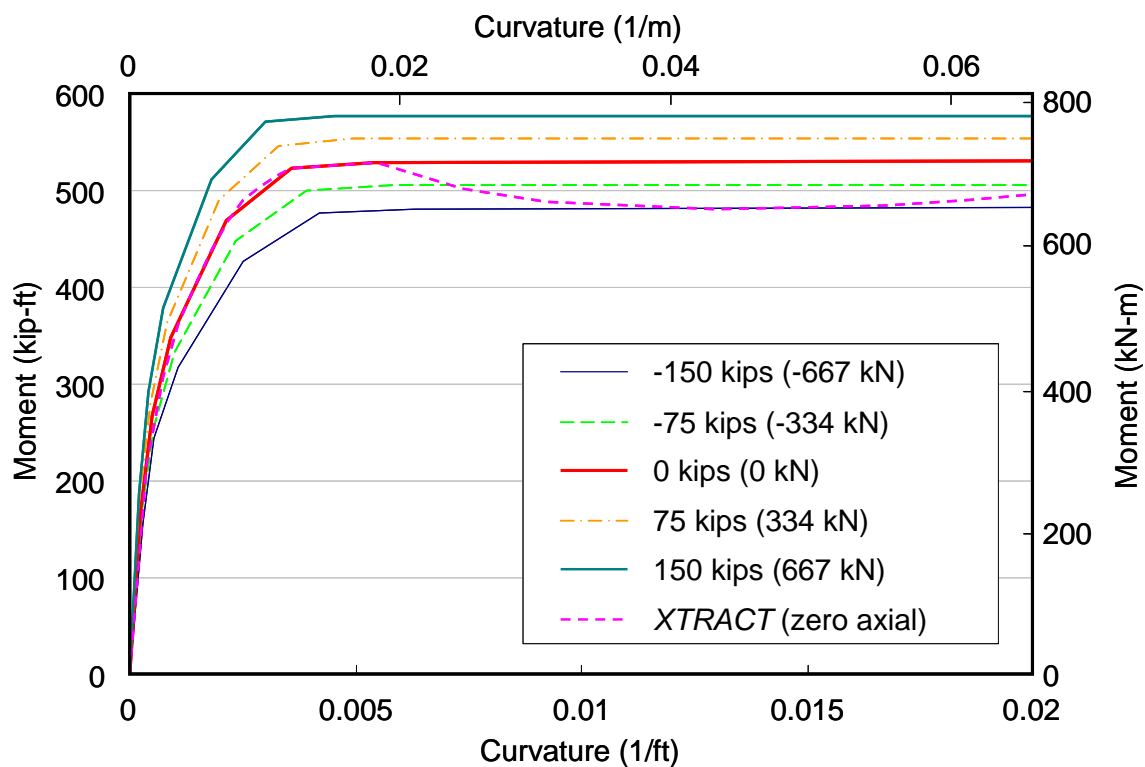


Figure 3-7 Properties of prestressed concrete piles

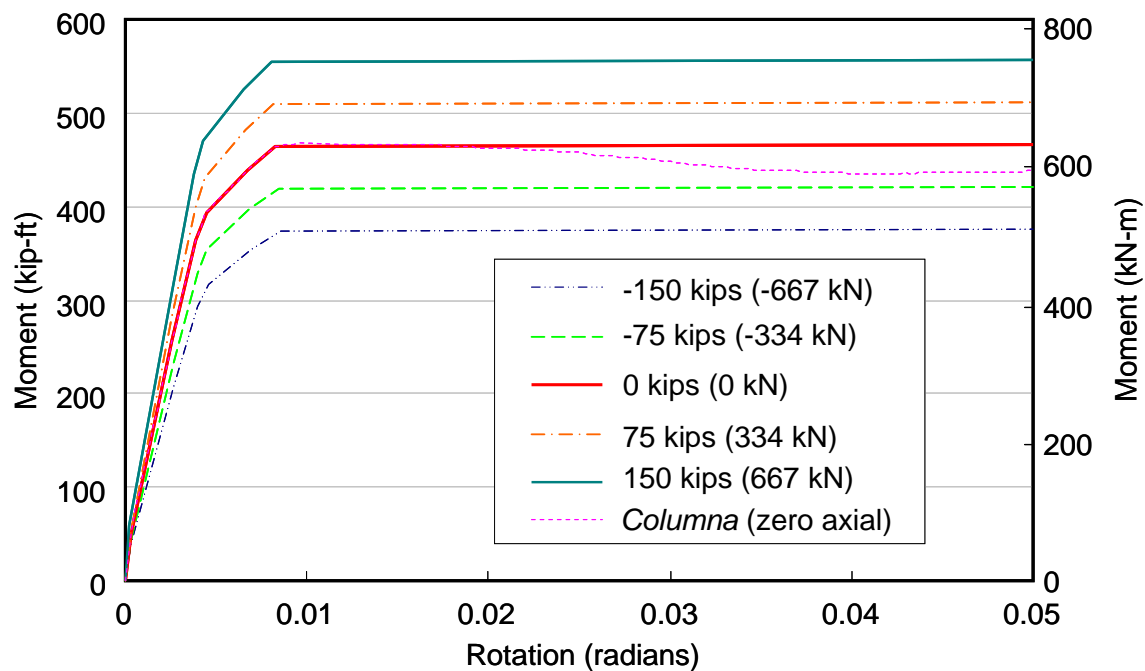


Figure 3-8 Properties of connection between pile and load stub

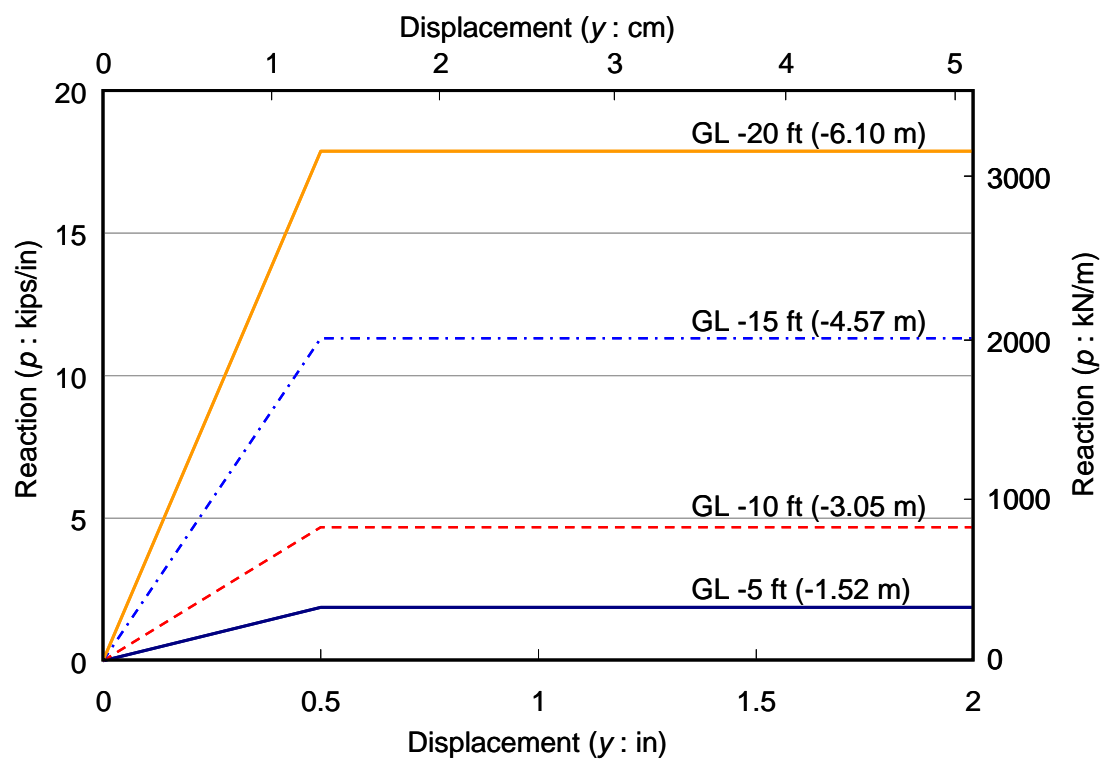


Figure 3-9 Properties of soil-pile springs typically used for wharf design

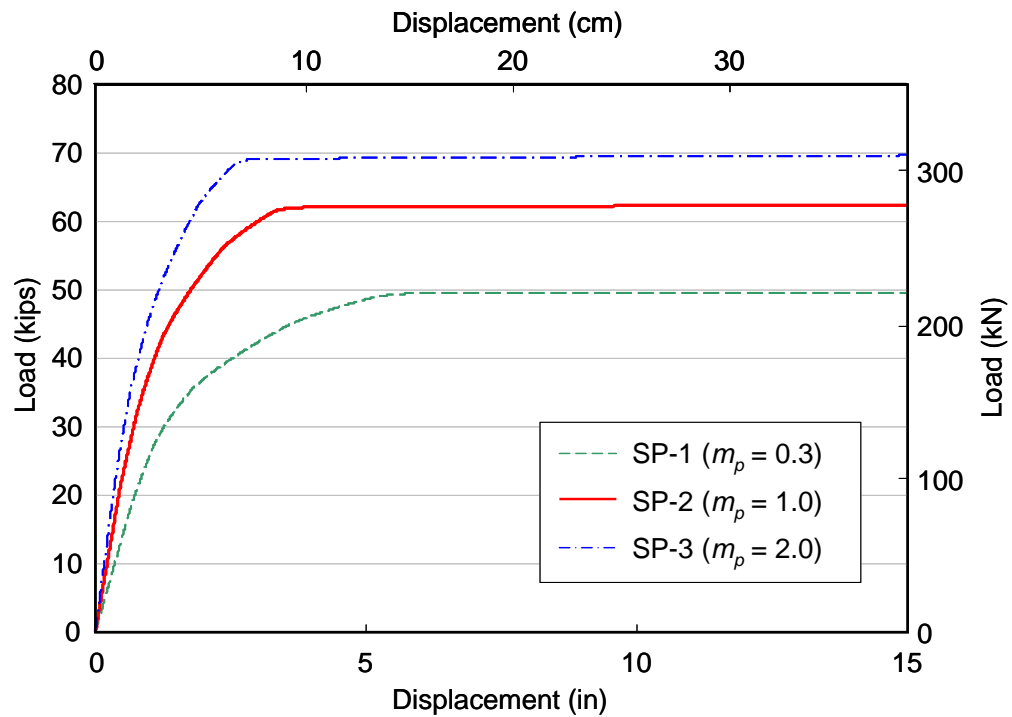


Figure 3-10 Predicted load-displacement curves at pile top (Single Pile Test, Version 2)

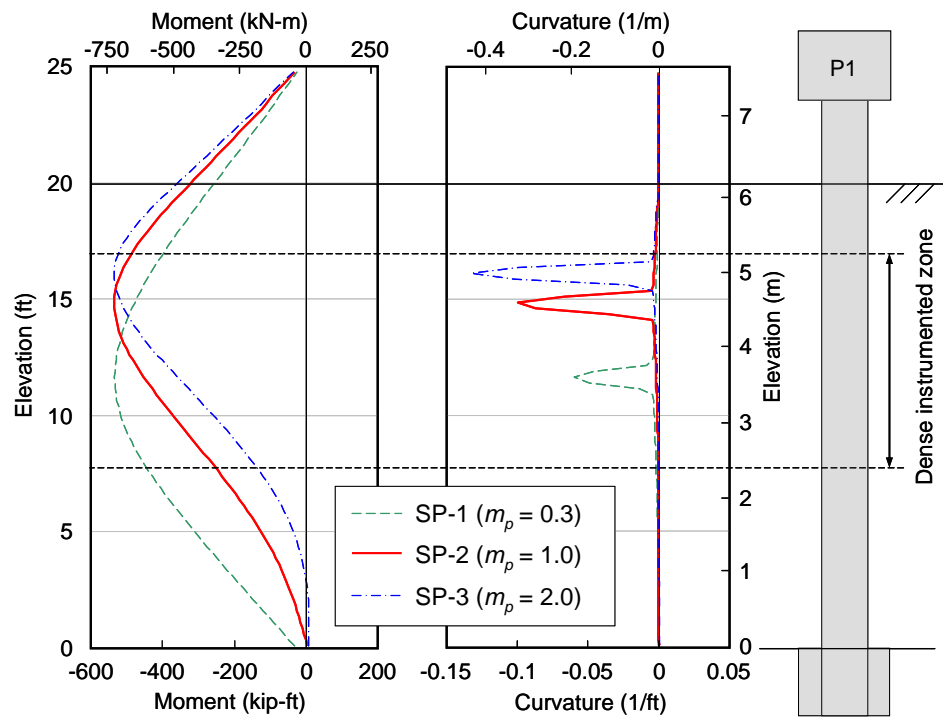


Figure 3-11 Predicted profiles of moment and curvature (Single Pile Test, Version 2)

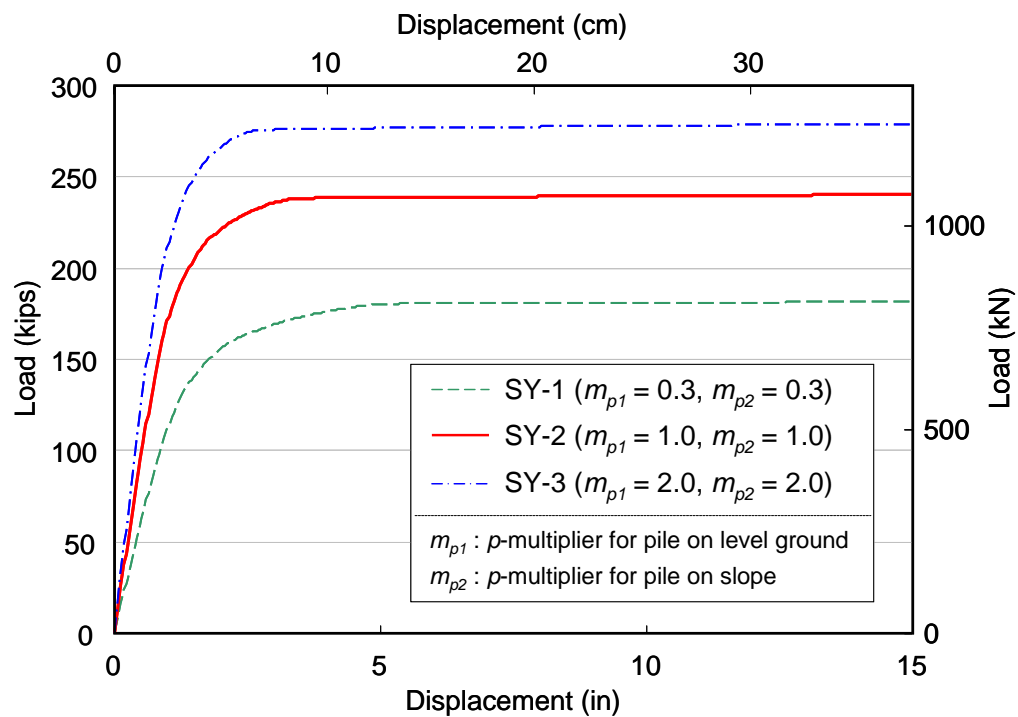


Figure 3-12 Predicted load-displacement curves at pile top (System Test 1, Version 2)

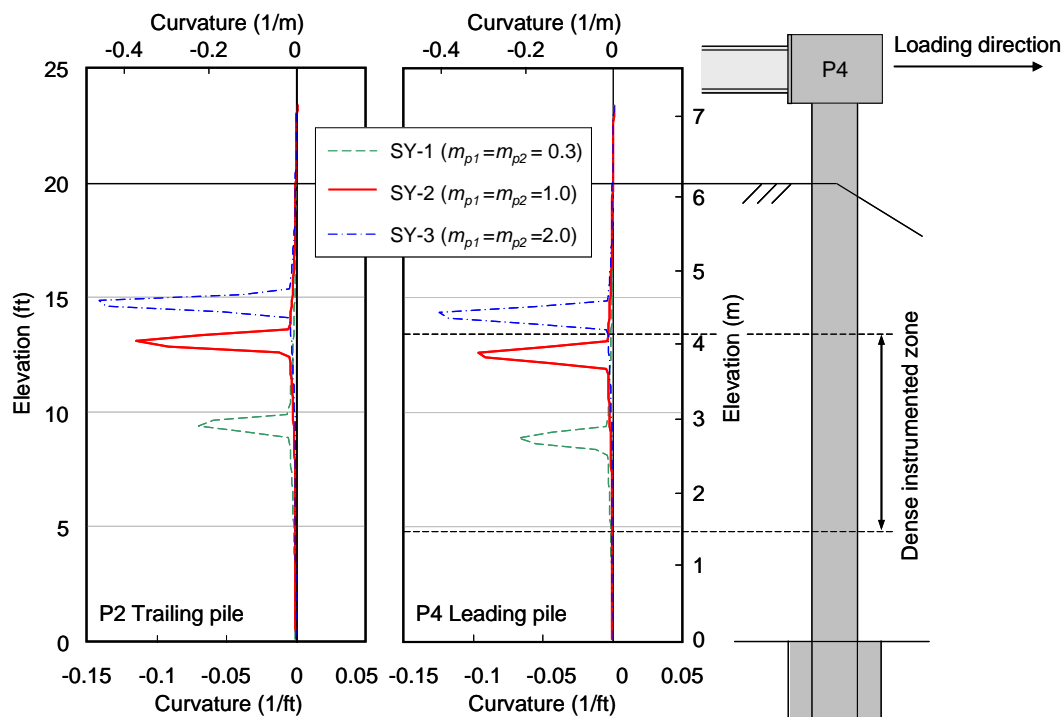


Figure 3-13 Predicted profiles of curvature (Push, System Test 1, Version 2)

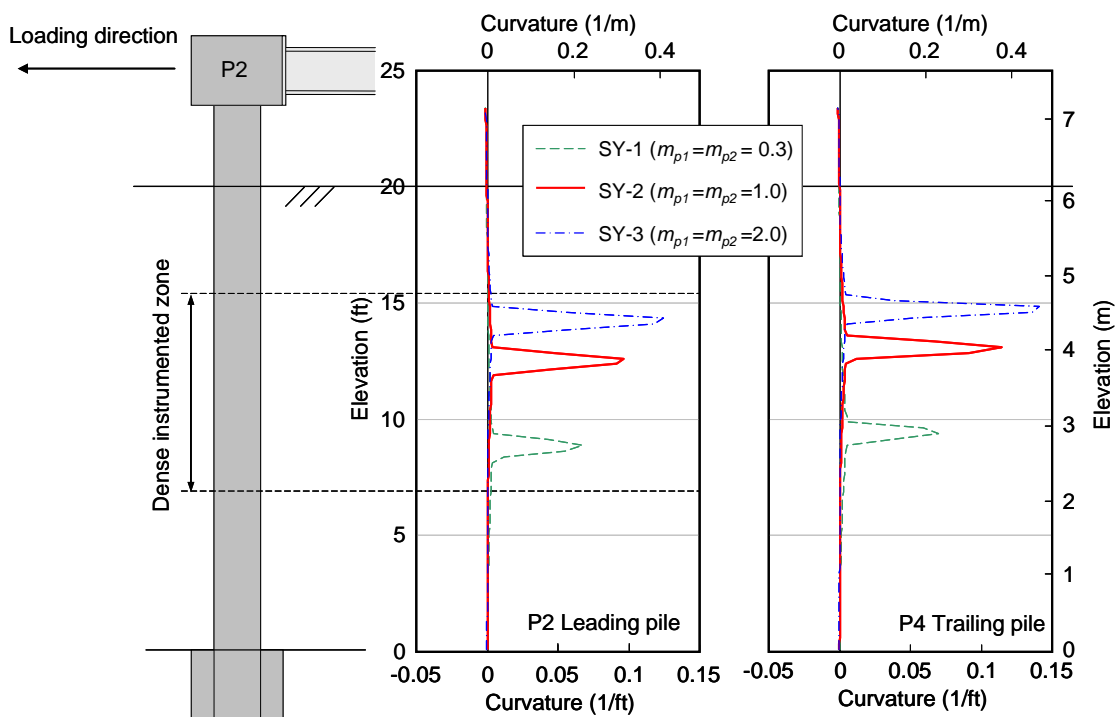


Figure 3-14 Predicted profiles of curvature (Pull, System Test 1, Version 2)

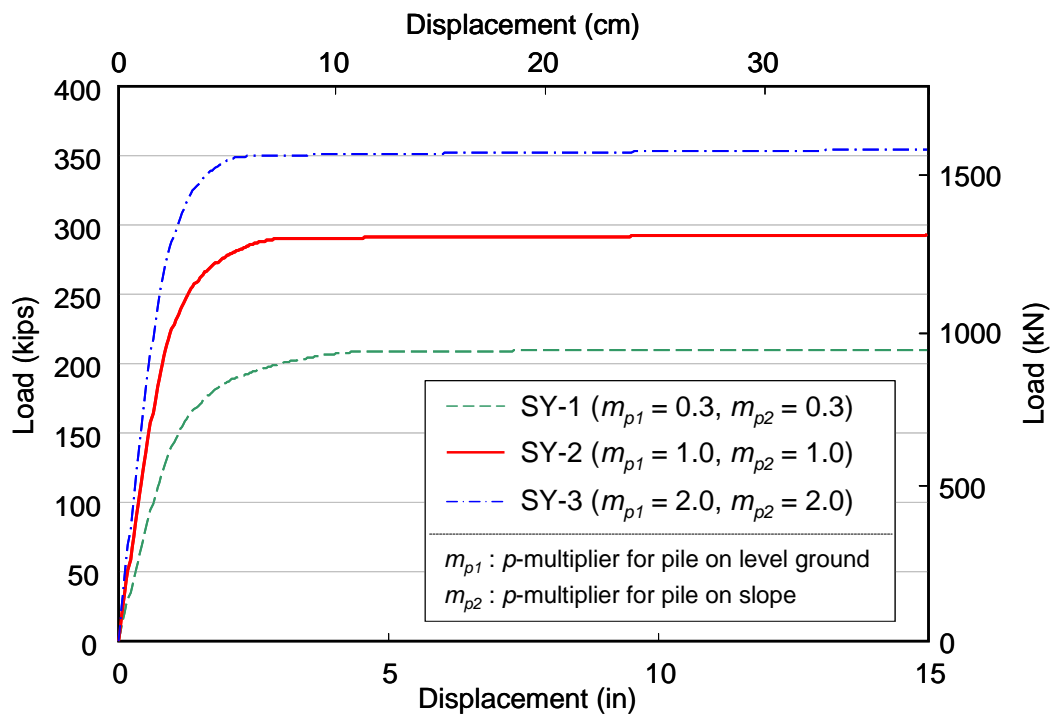


Figure 3-15 Predicted load-displacement curves at pile top (System Test 2, Version 2)

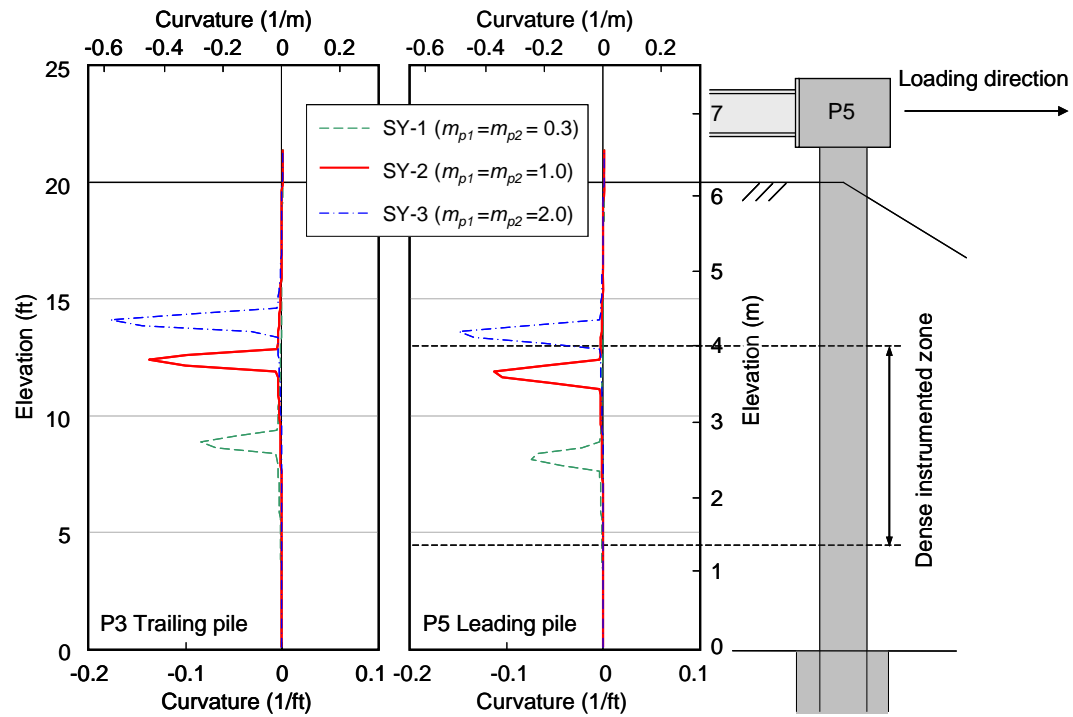


Figure 3-16 Profiles of curvature (Push, System Test 2, Version 2)

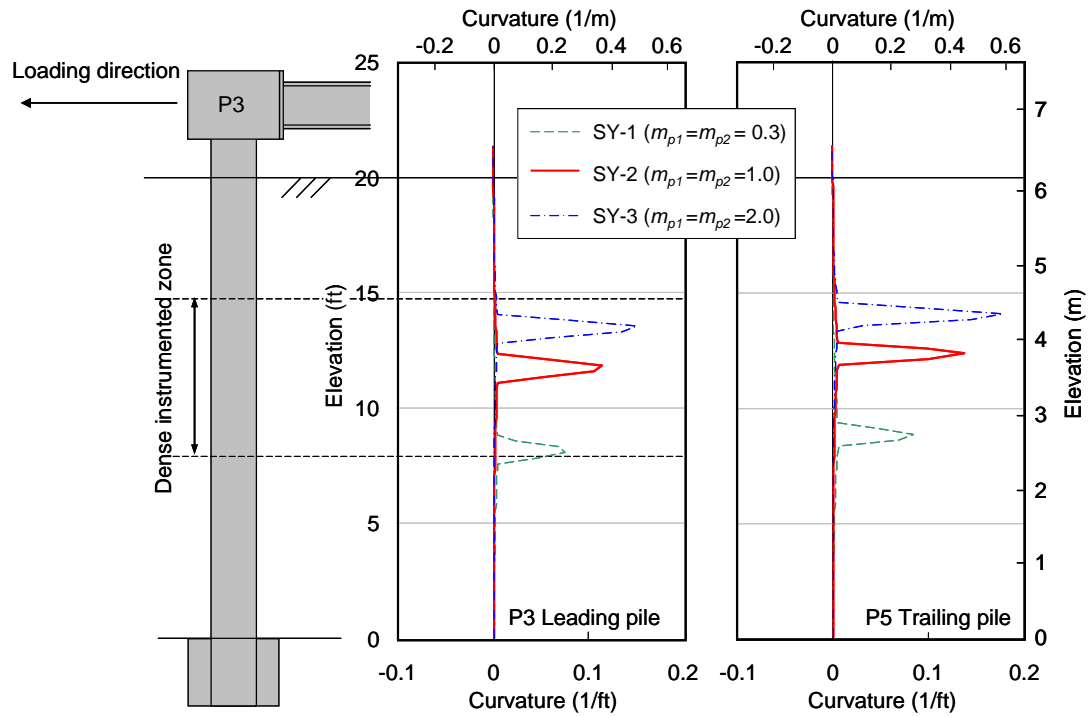


Figure 3-17 Profiles of curvature (Pull, System Test 2, Version 2)

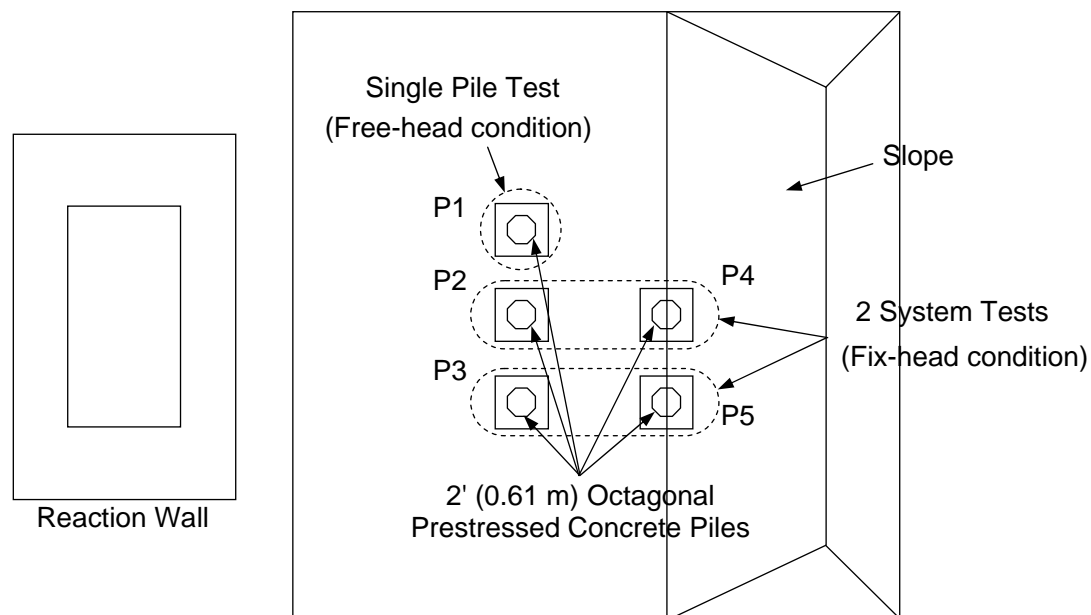


Figure 3-18 Plan view of test set-up

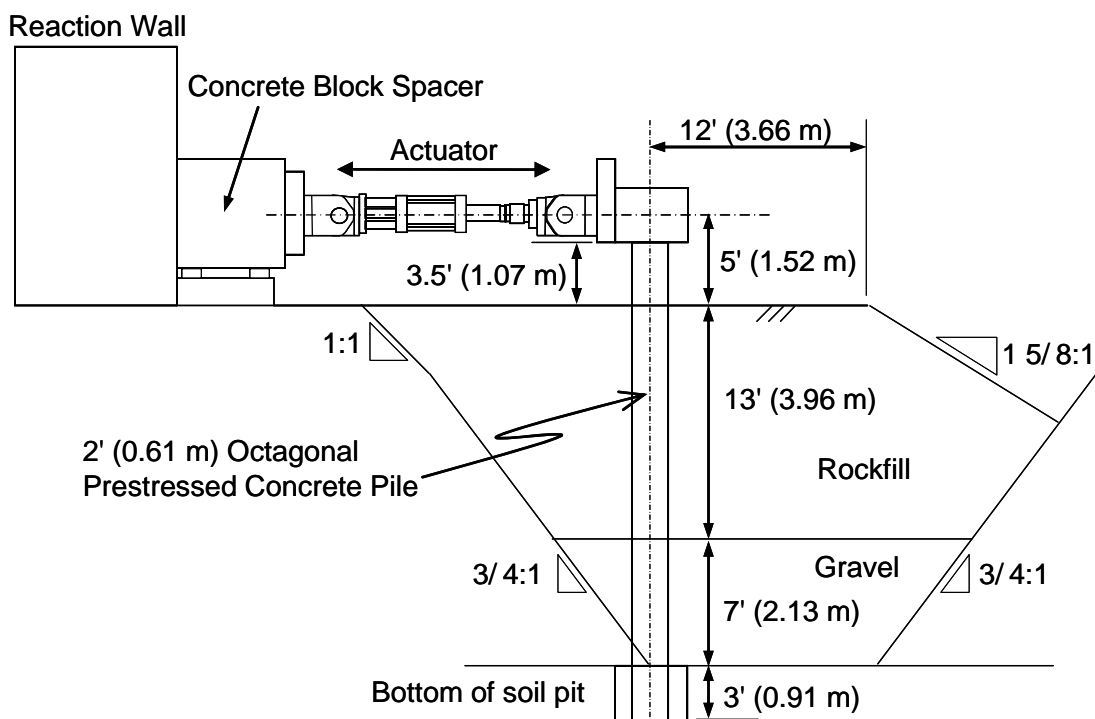
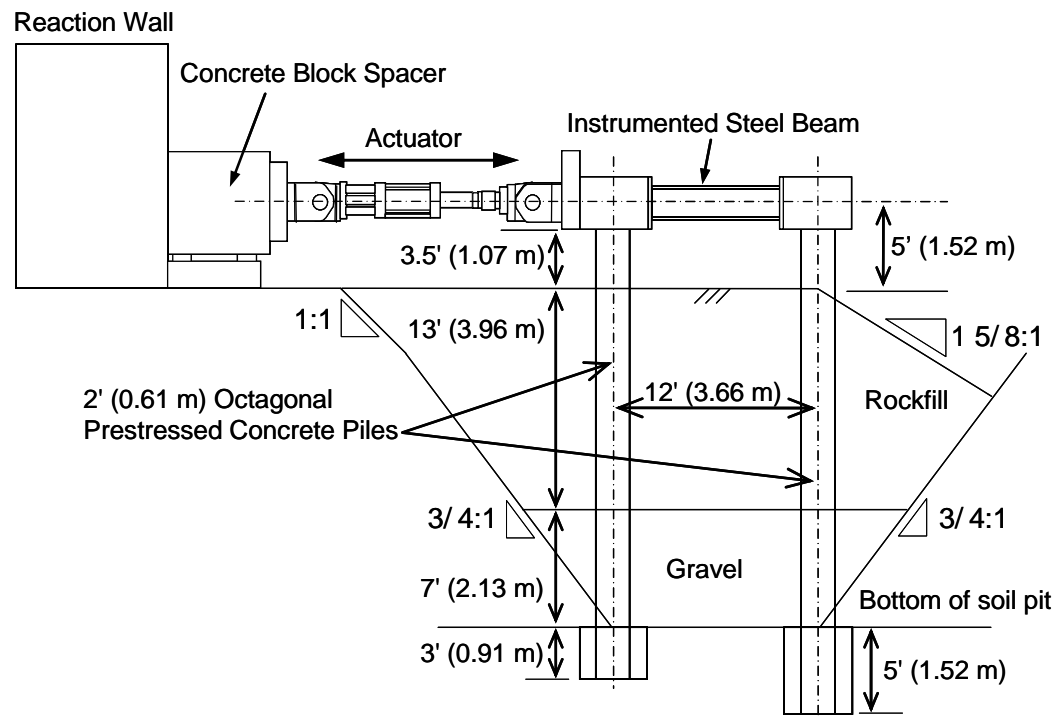
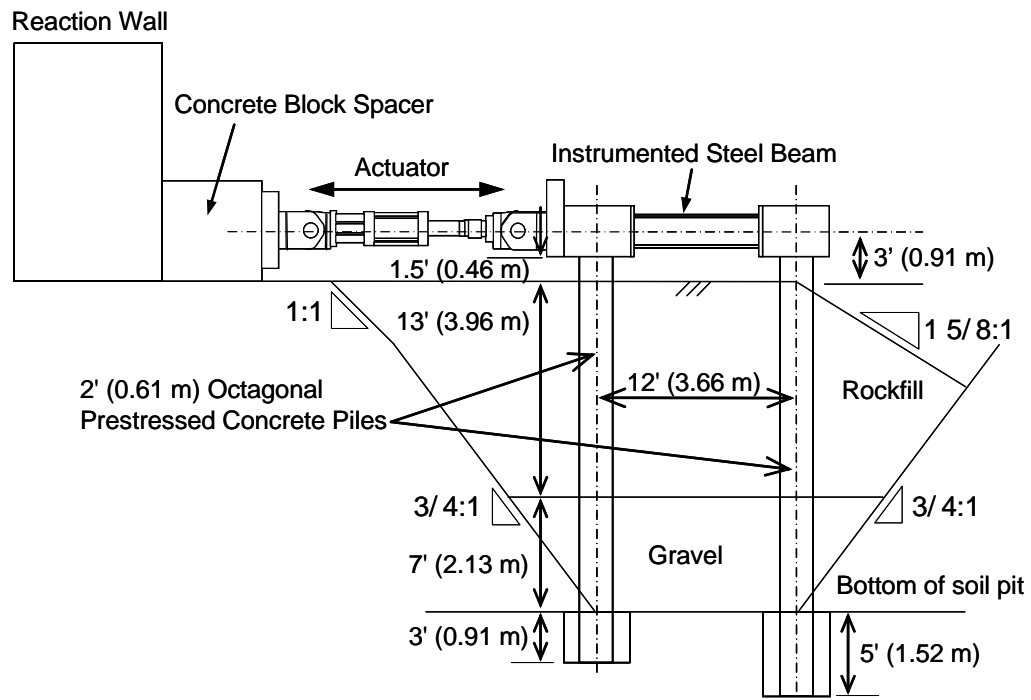


Figure 3-19 Section view for Single Pile Test at completion of construction



(a) System Test 1



(b) System Test 2

Figure 3-20 Test set-up for system tests at completion of construction

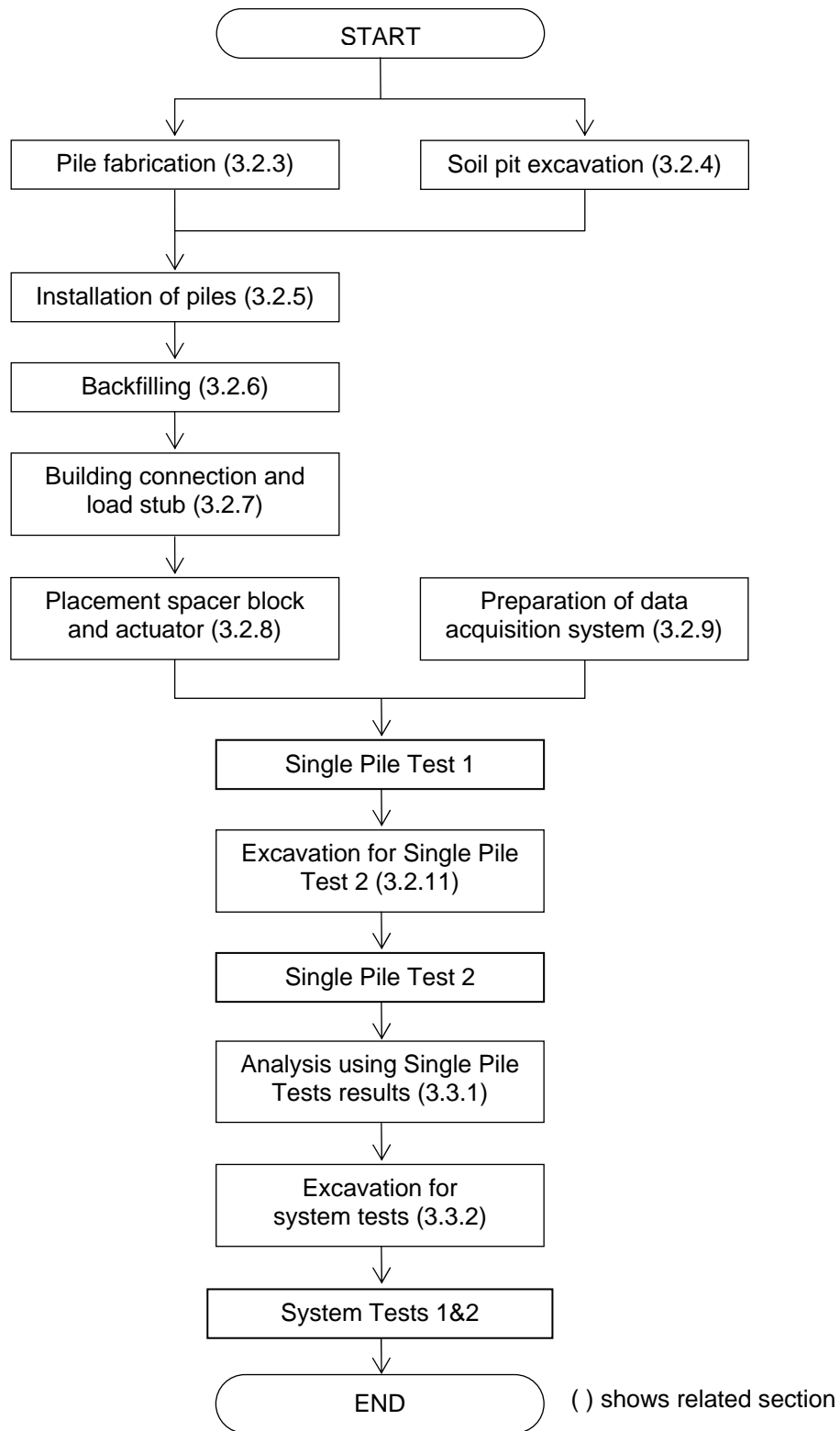


Figure 3-21 Flow chart of construction



(a) Prestress strands before prestressing



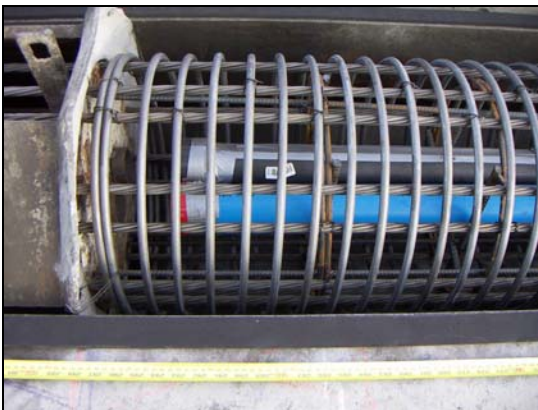
(b) Applying prestressing force on the strands



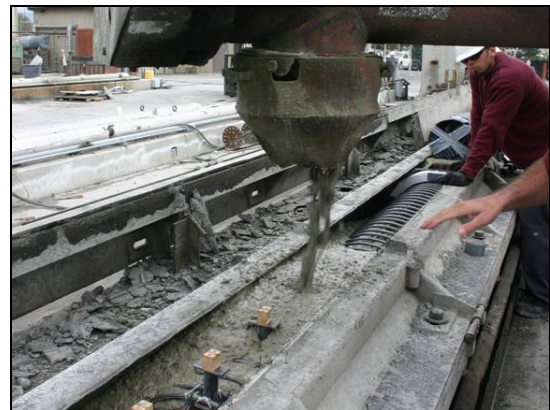
(c) Top of test pile



(d) After placement of spiral

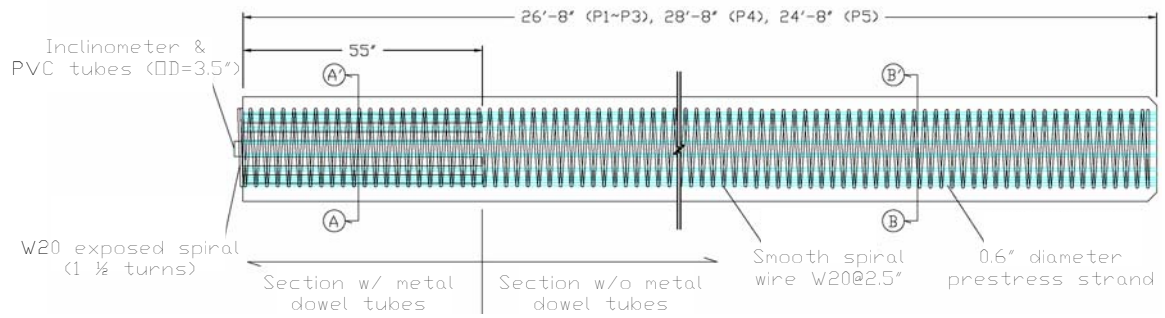


(e) Bottom of test pile

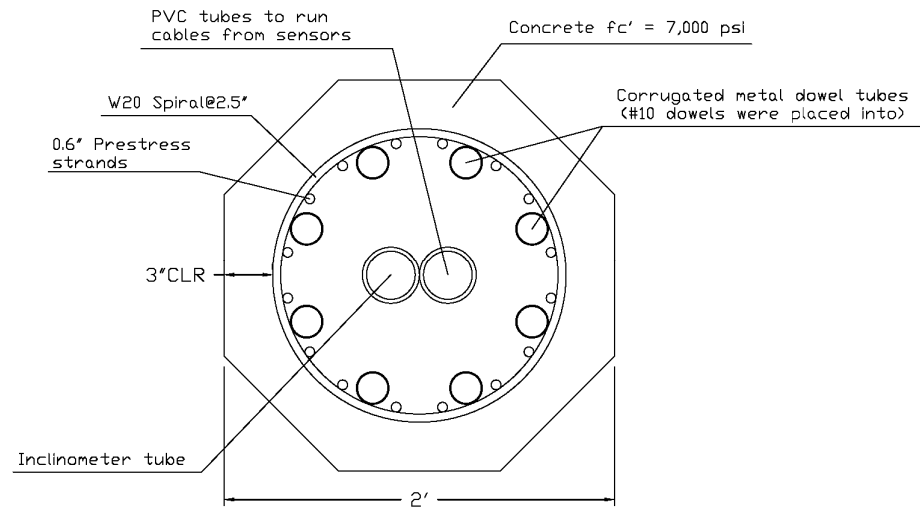


(f) Pouring Self Compaction Concrete

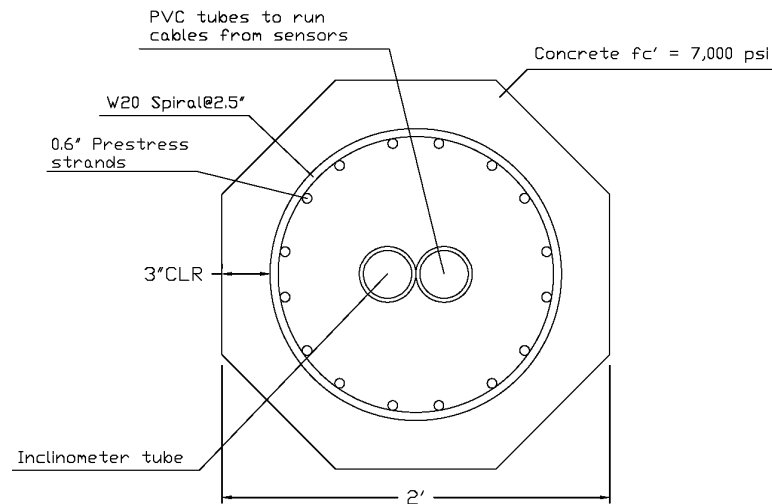
Figure 3-22 Building test piles (Utility Vault at Fontana, CA)



(a) Section along long axis



(b) A-A' section (with dowel tubes)



(c) B-B' section (without dowel tubes)

Figure 3-23 Details of test piles

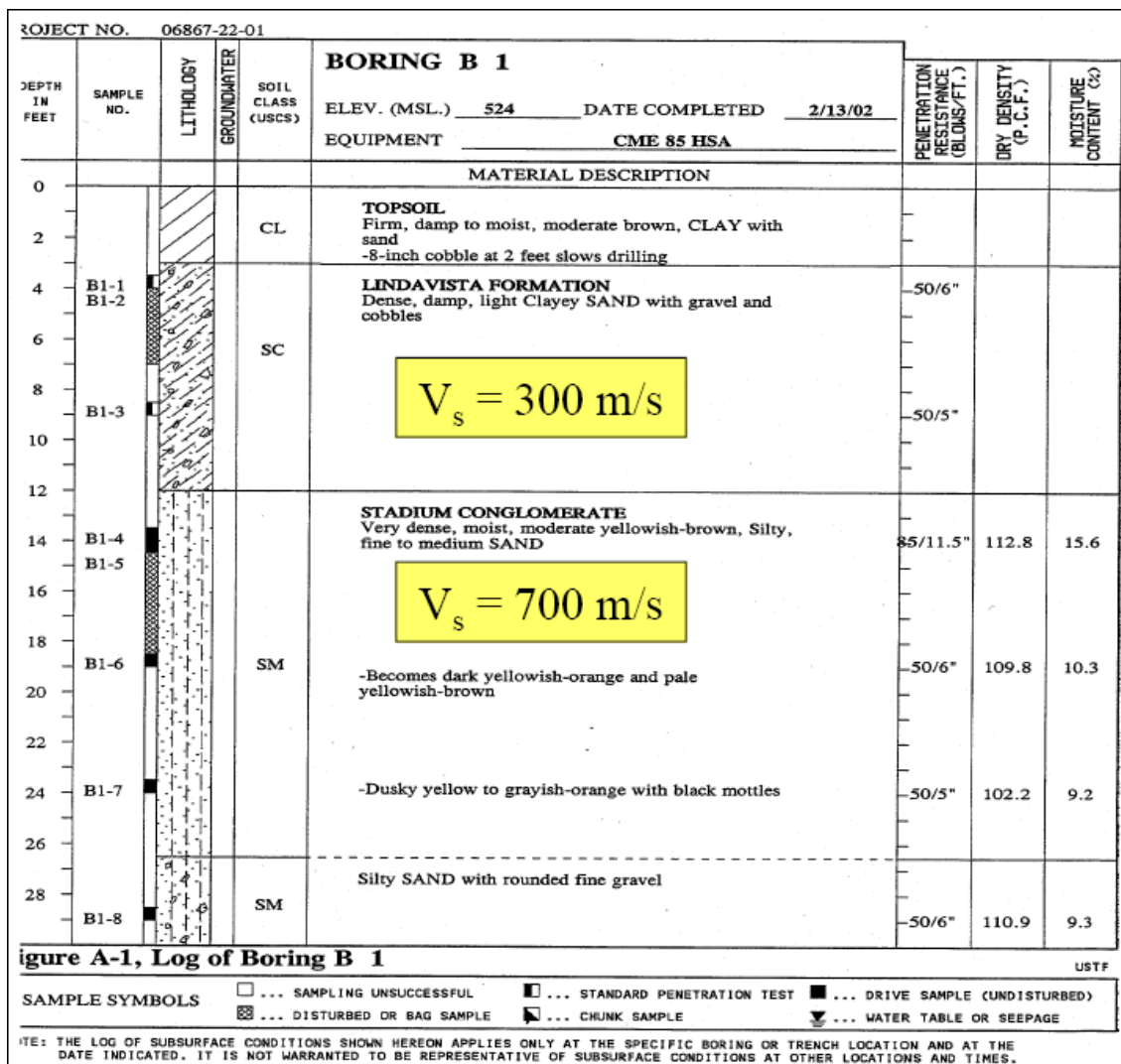


Figure 3-24 Soil boring log at the construction site

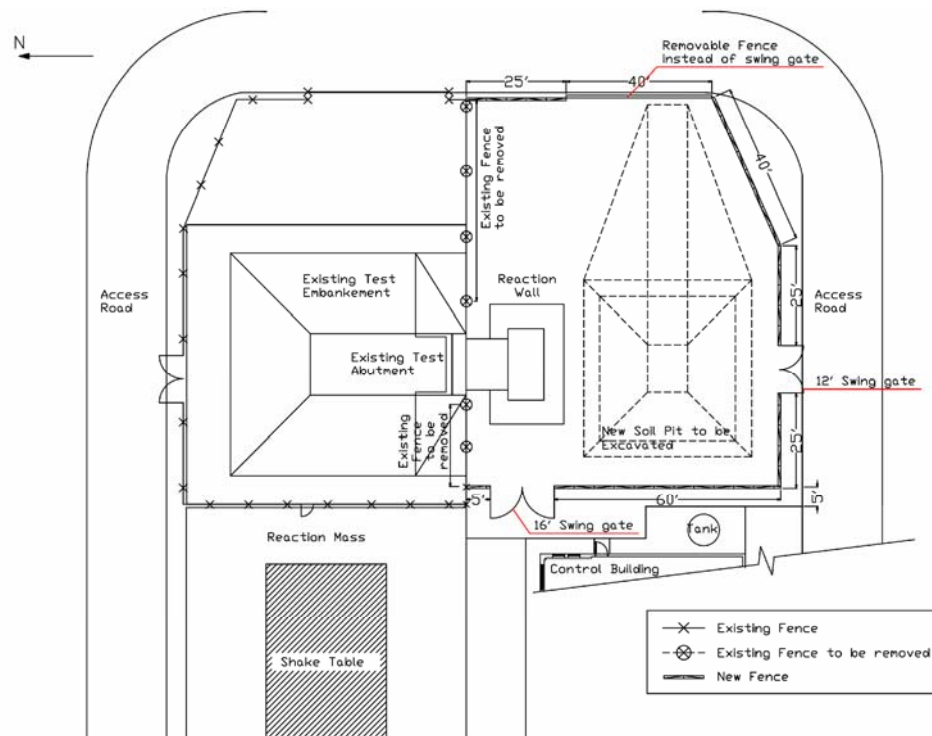


Figure 3-25 Location of newly excavated soil pit

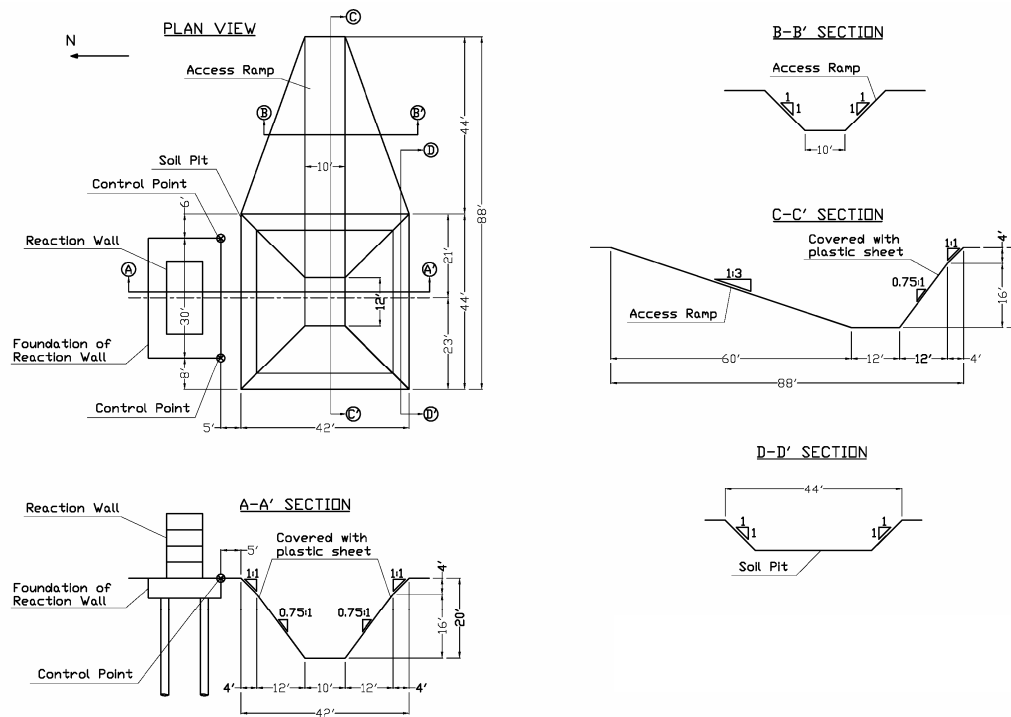


Figure 3-26 Dimensions of newly excavated soil pit



(a) Placing markers



(b) Exporting excavated soil



(c) Excavating



(d) Breaker to remove rigid layer



(e) Excavating



(f) Completion of excavation

Figure 3-27 Excavation of soil pit

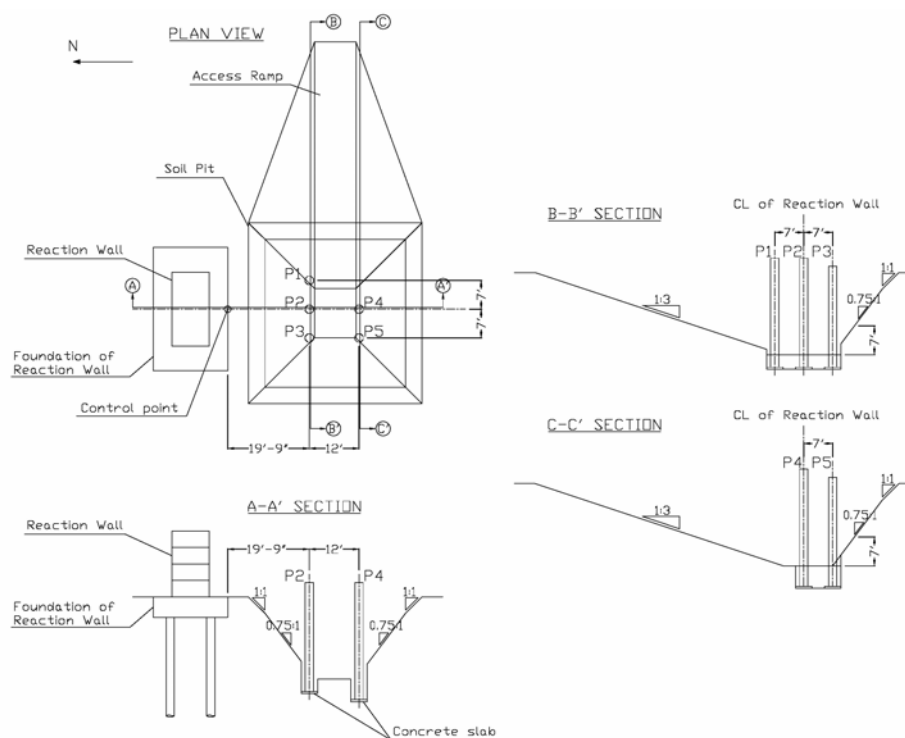


Figure 3-28 Locations of test piles

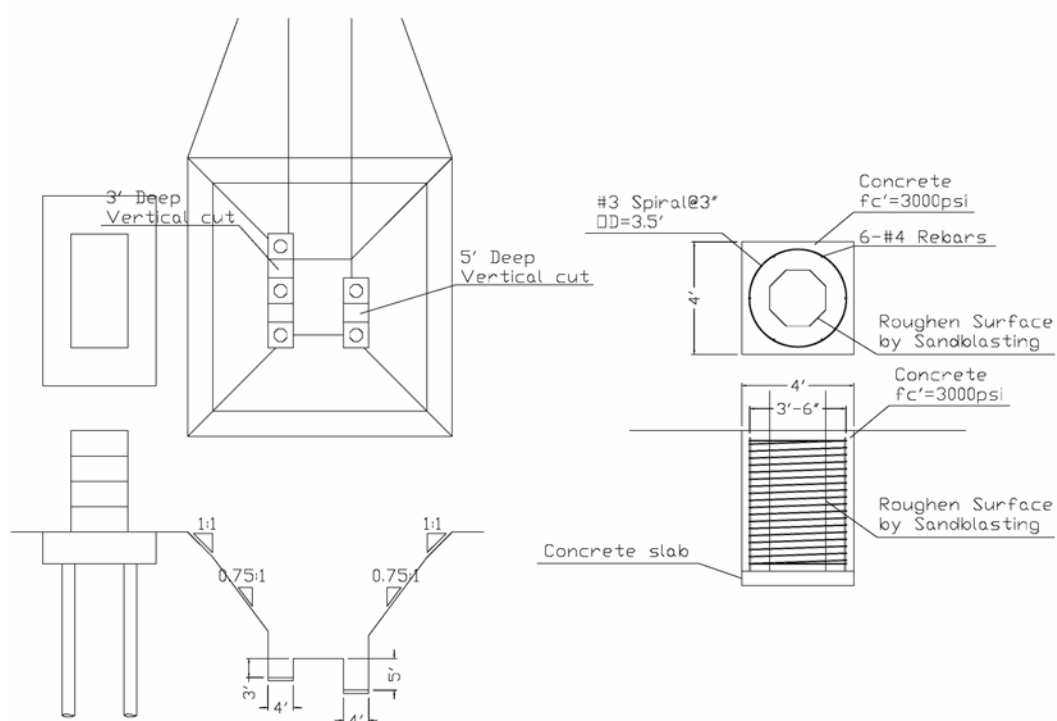


Figure 3-29 Details of footing

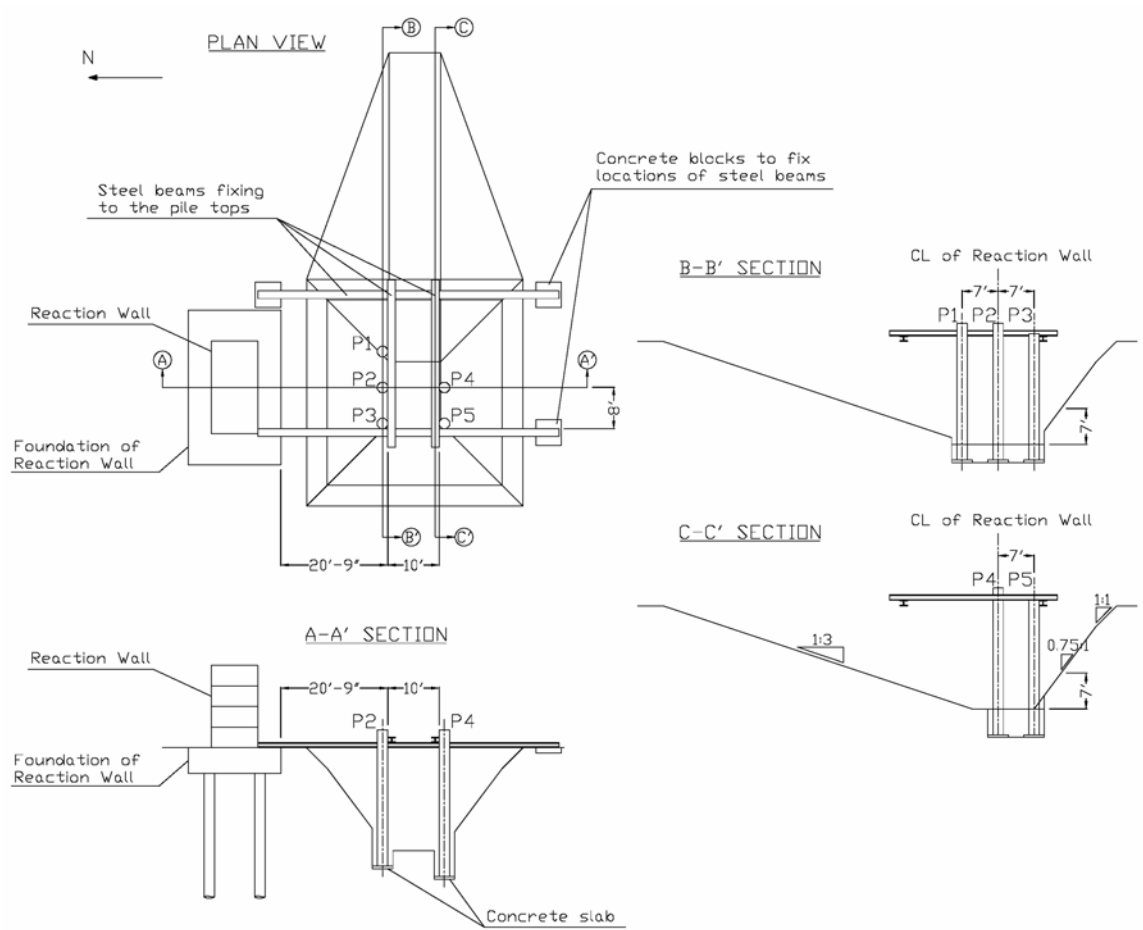


Figure 3-30 Locations of steel beams fixing the pile tops



(a) Excavating trench for footing



(b) Building concrete slab at the bottom



(c) Placing steel beam fixing pile tops



(d) Welding steel beams



(e) Hanging pile



(f) Installed pile fixed to the beam

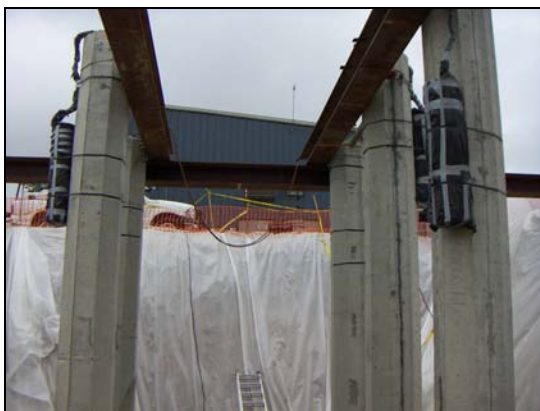
Figure 3-31 Pile installation



(g) Bottom of test pile



(h) Installed piles



(i) Installed piles



(j) Installed piles fixed to the beam



(k) Pouring concrete to the footing



(l) Just after removing formworks

Figure 3-31 Pile installation (continued)

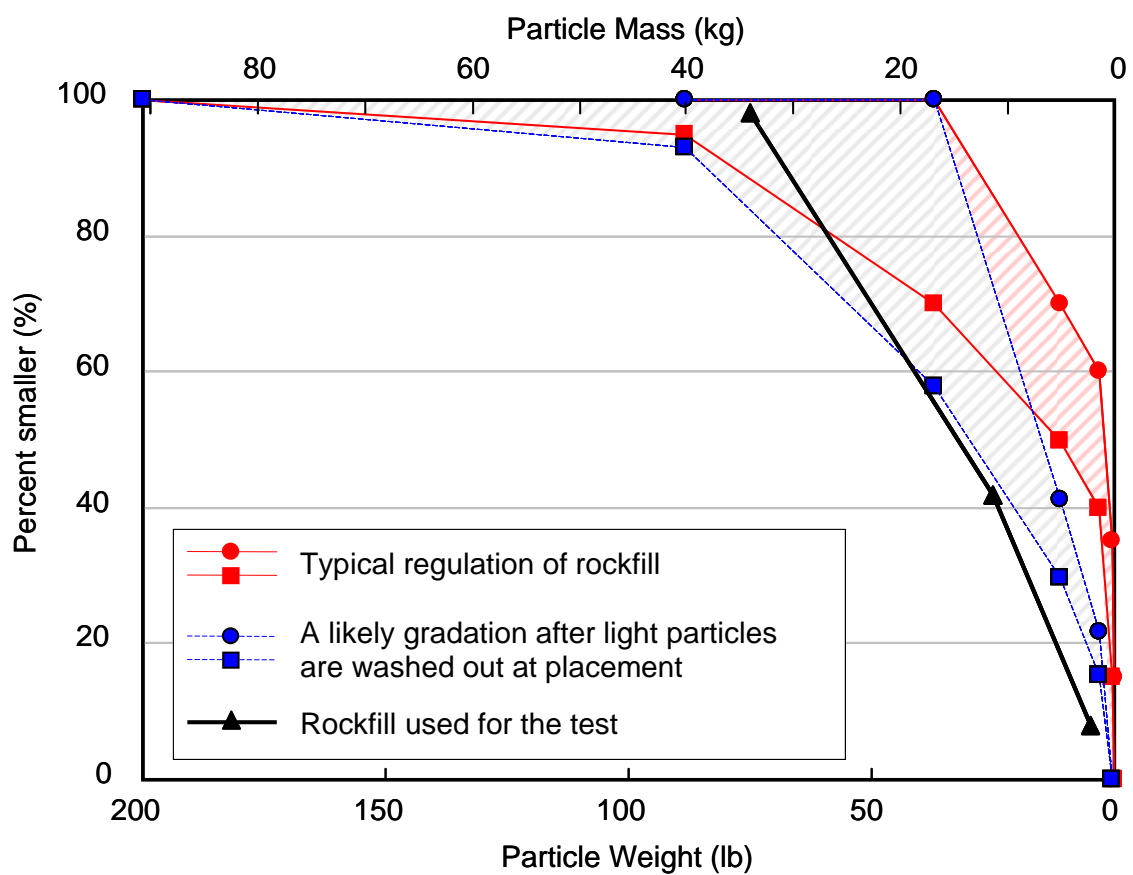


Figure 3-32 Gradation of rockfill

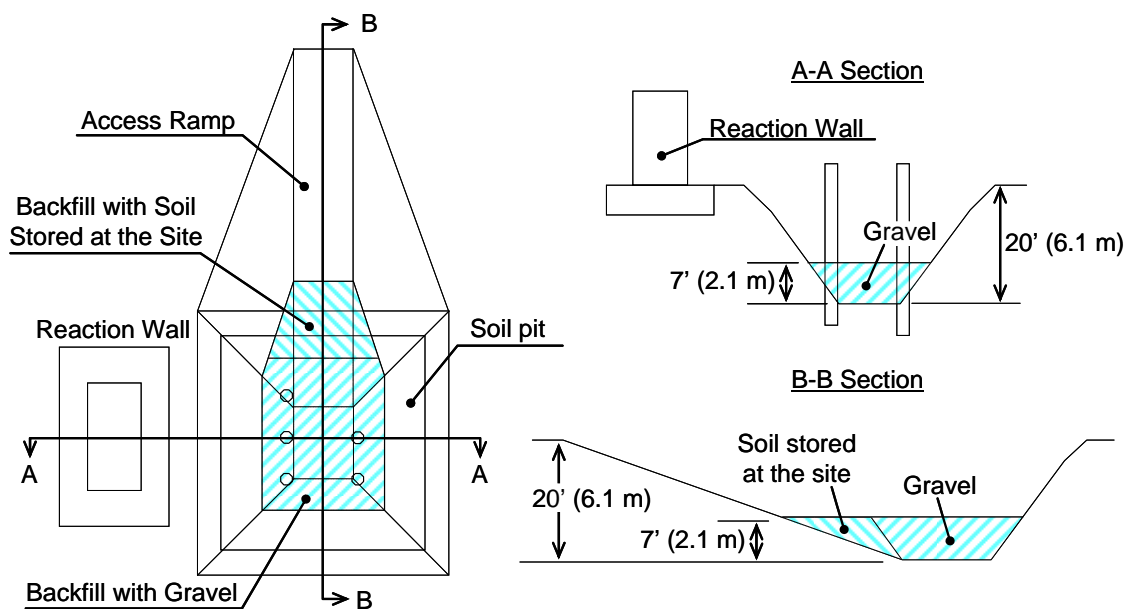


Figure 3-33 Details of backfilling (first stage)

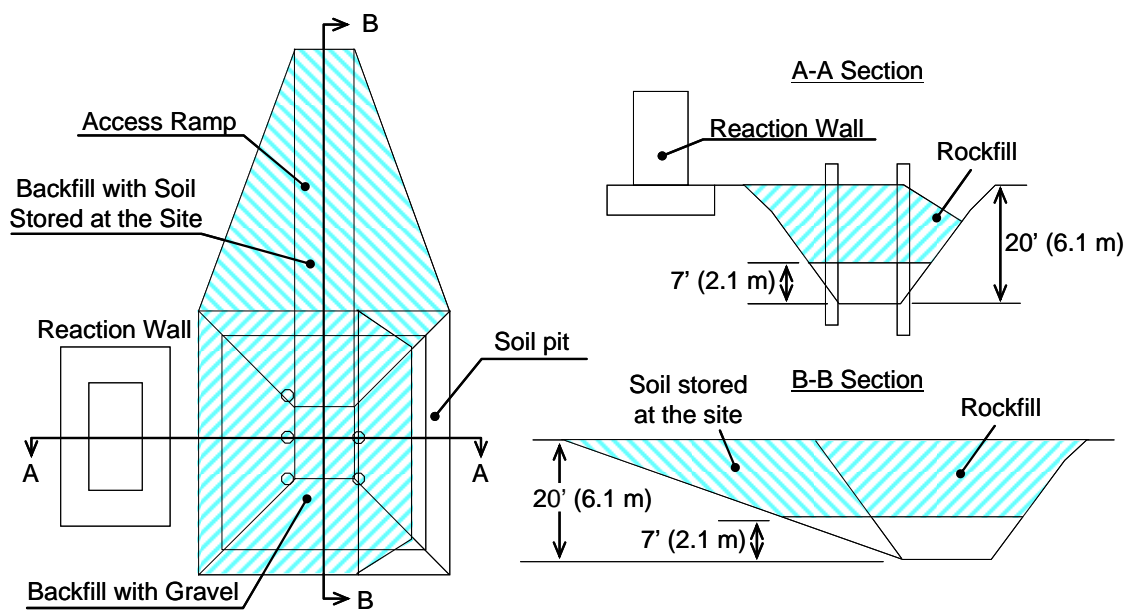


Figure 3-34 Details of backfilling (second stage)

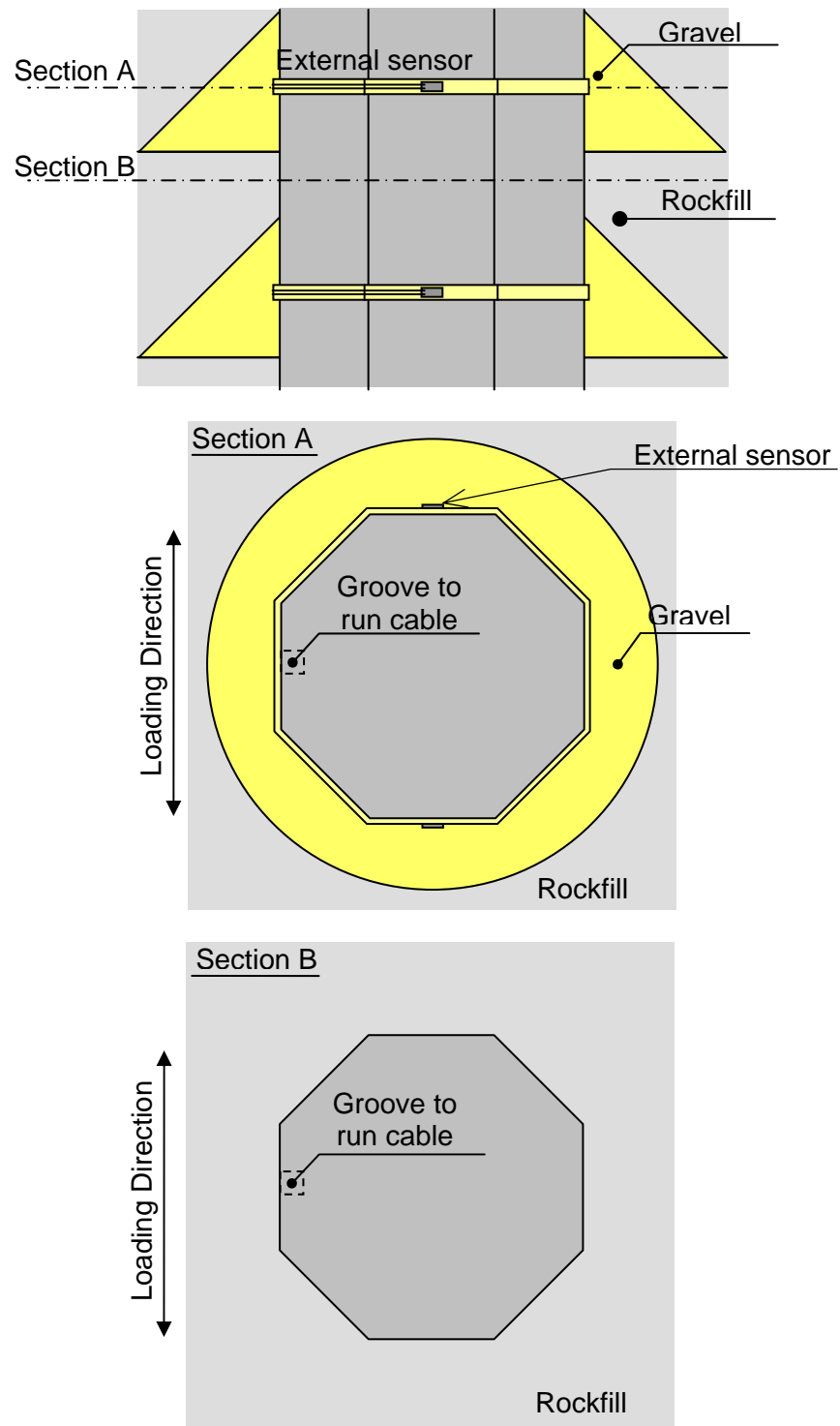


Figure 3-35 Details of backfilling in vicinity of rubber bands



(a) Gravel



(b) Rockfill



(c) Backfilling bottom of the pit with gravel



(d) Backfilling bottom of the pit with gravel



(e) Around the external sensors



(f) Finish the first stage of backfilling

Figure 3-36 Backfilling



(g) Backfilling by hand



(h) Placing gravel around the sensor



(i) Compacting with handy tamper



(j) Compacting with vibro-roller



(k) Gap between the pile and the rockfill



(l) Finish backfilling

Figure 3-36 Backfilling (continued)

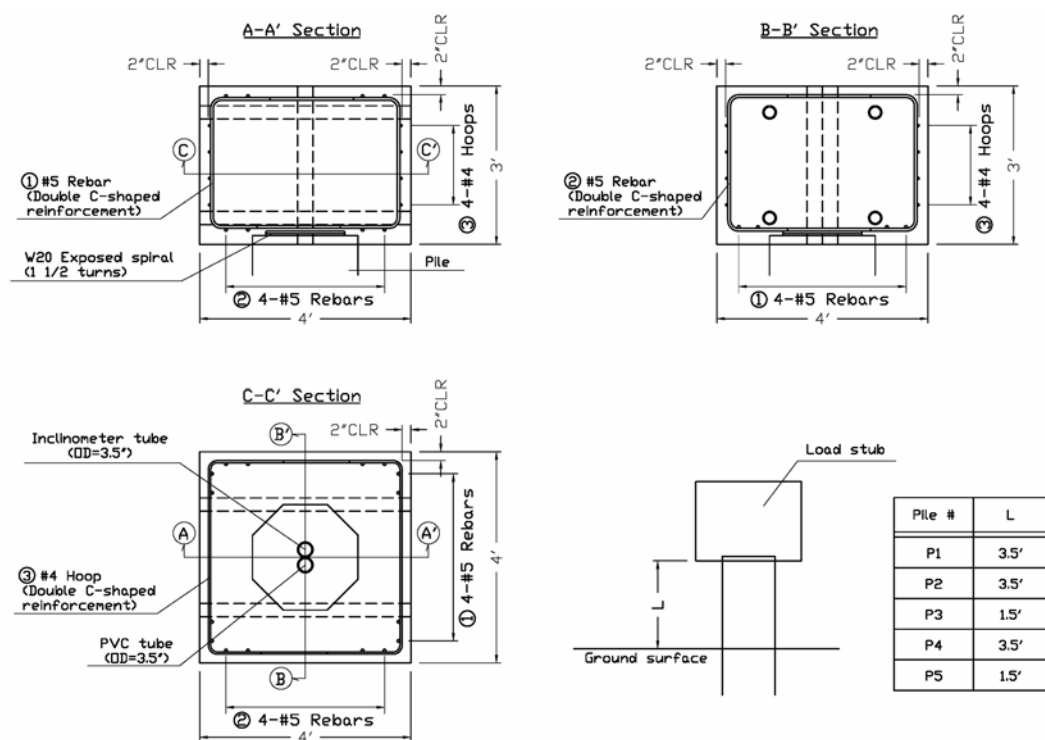


Figure 3-37 Details of load stub

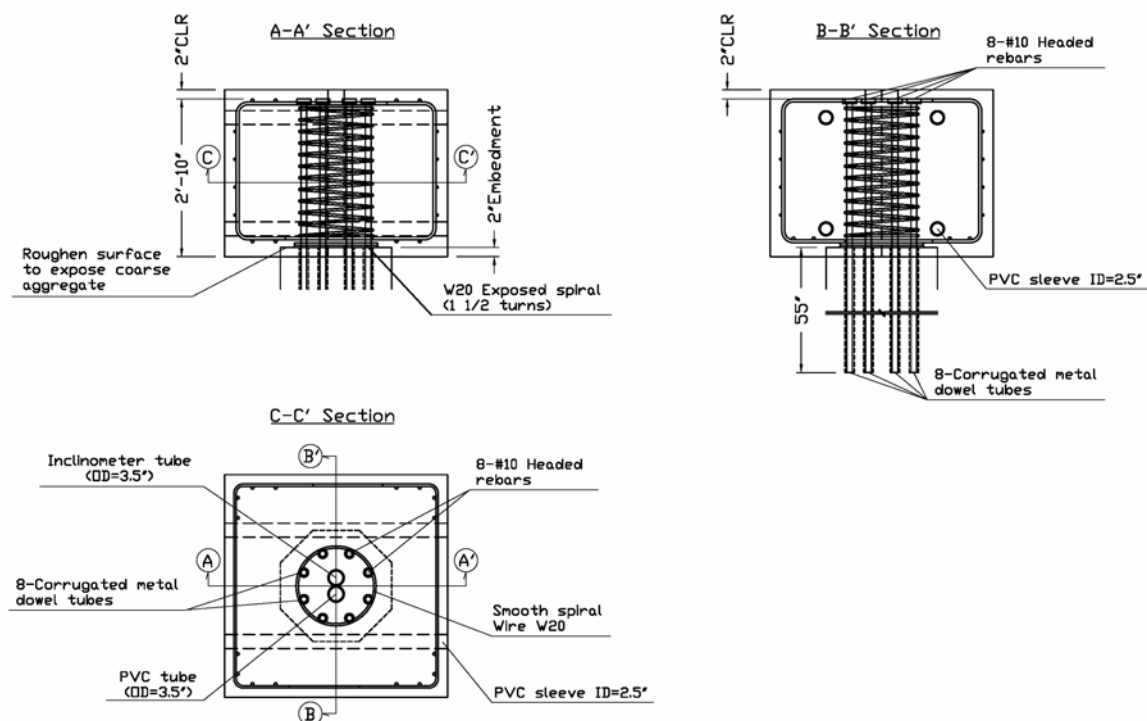


Figure 3-38 Details of connection



(a) Making platform



(b) Making platform



(c) Making platform



(d) Surveyed location of the load stub



(e) Measuring depth of the dowel tube



(f) Mixing grout material

Figure 3-39 Building connections and load stubs



(g) Grouting



(h) Finish installation of the dowels



(i) Just before pouring concrete



(j) Completed making load stubs

Figure 3-39 Building connections and load stubs (continued)

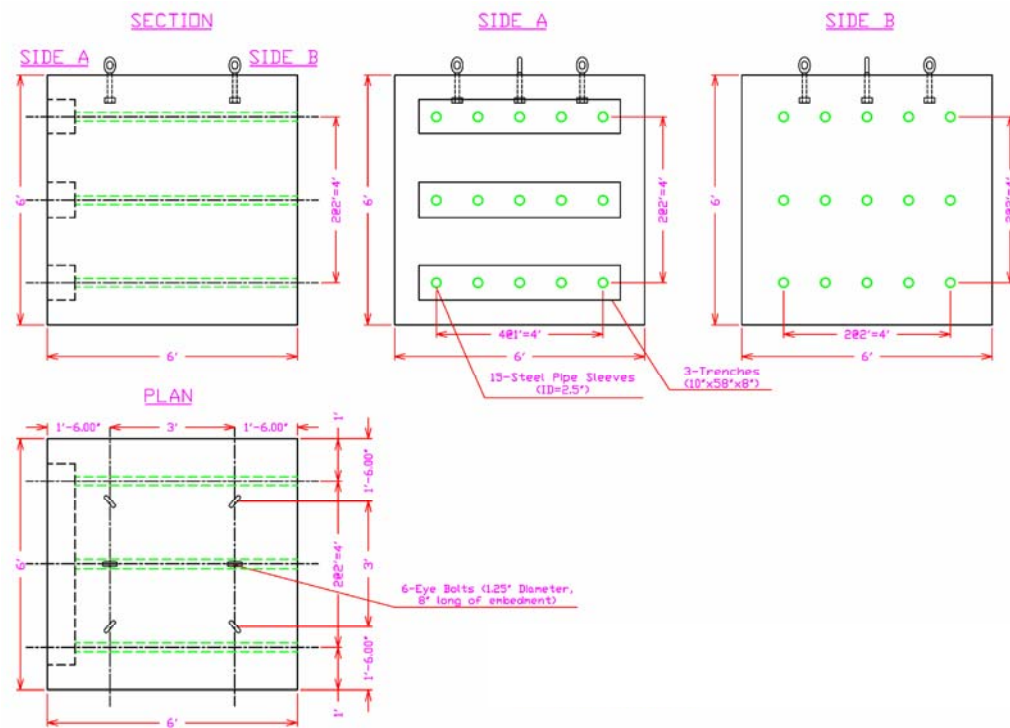


Figure 3-40 Details of concrete spacer block



Figure 3-41 Concrete spacer block

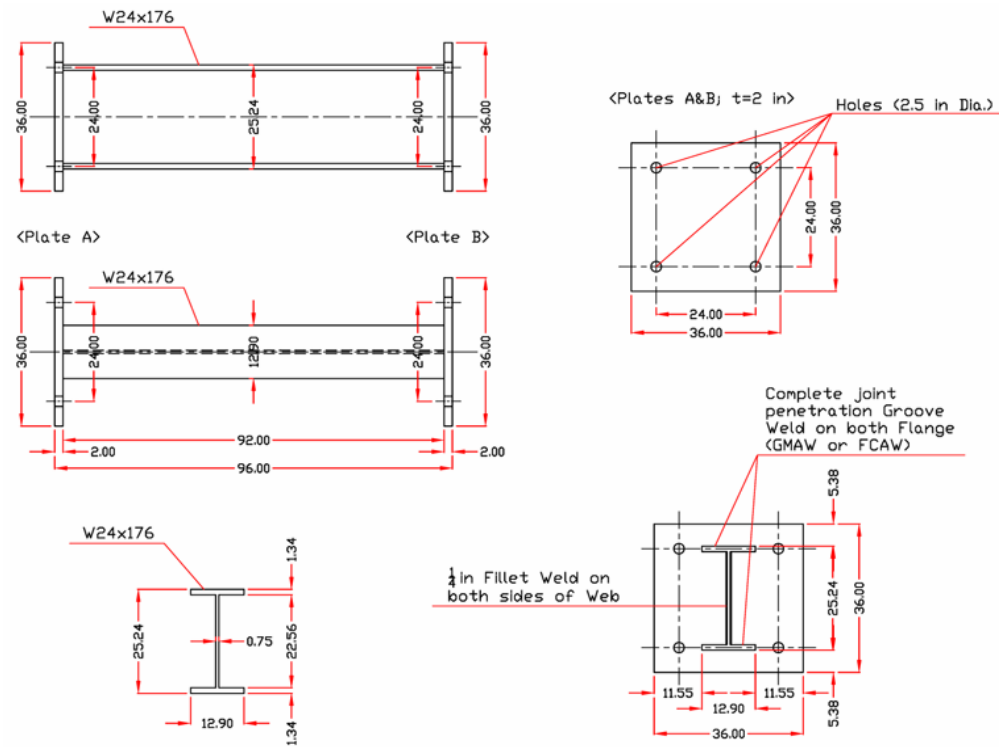


Figure 3-42 Dimension of steel beam



Figure 3-43 Steel beam connecting test piles (before instrumentation)



Figure 3-44 Hydraulic actuator



Figure 3-45 Aspect of test setup for Single Pile Test



Figure 3-46 Aspect of test setup for System Test 1

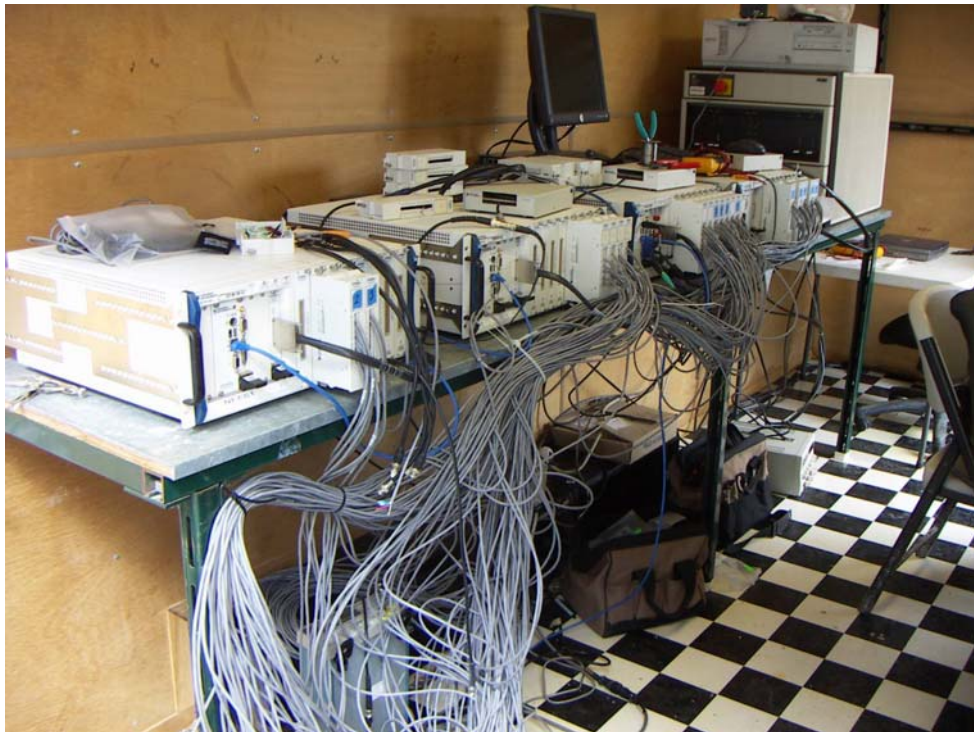
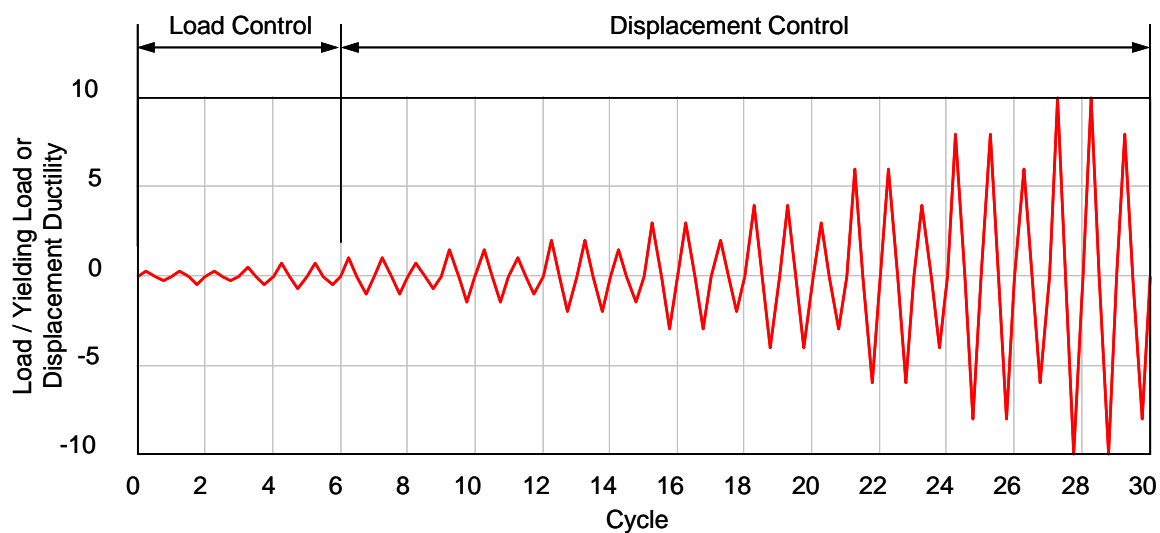
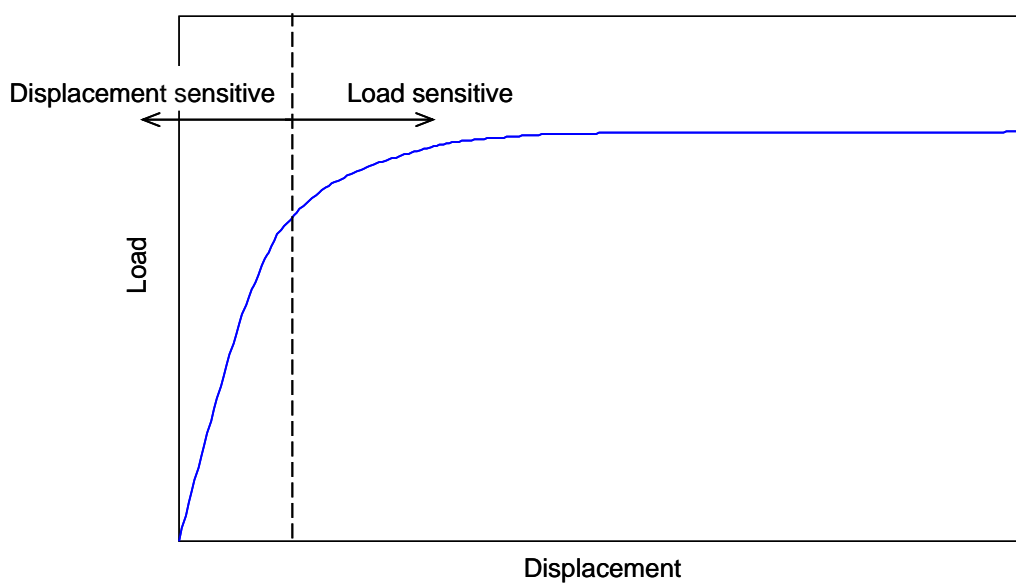


Figure 3-47 Data acquisition system



(a) Two phase load protocol



(b) Expected load displacement curve

Figure 3-48 Load protocol

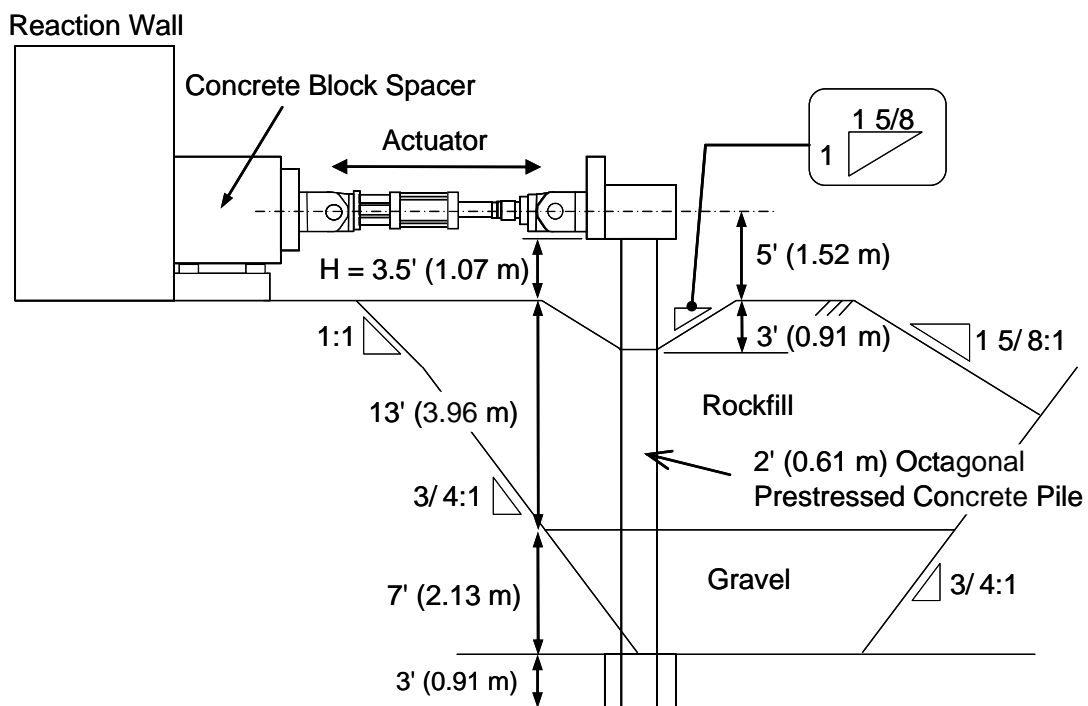


Figure 3-49 Section view for Single Pile Test 2 (after excavation)

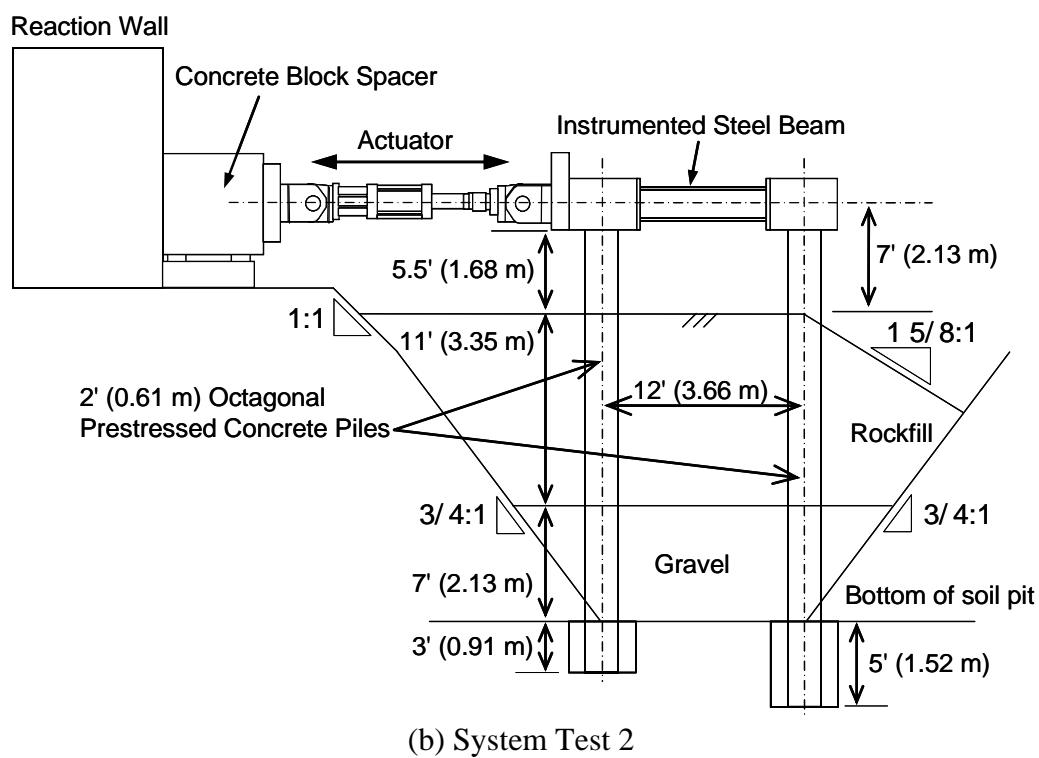
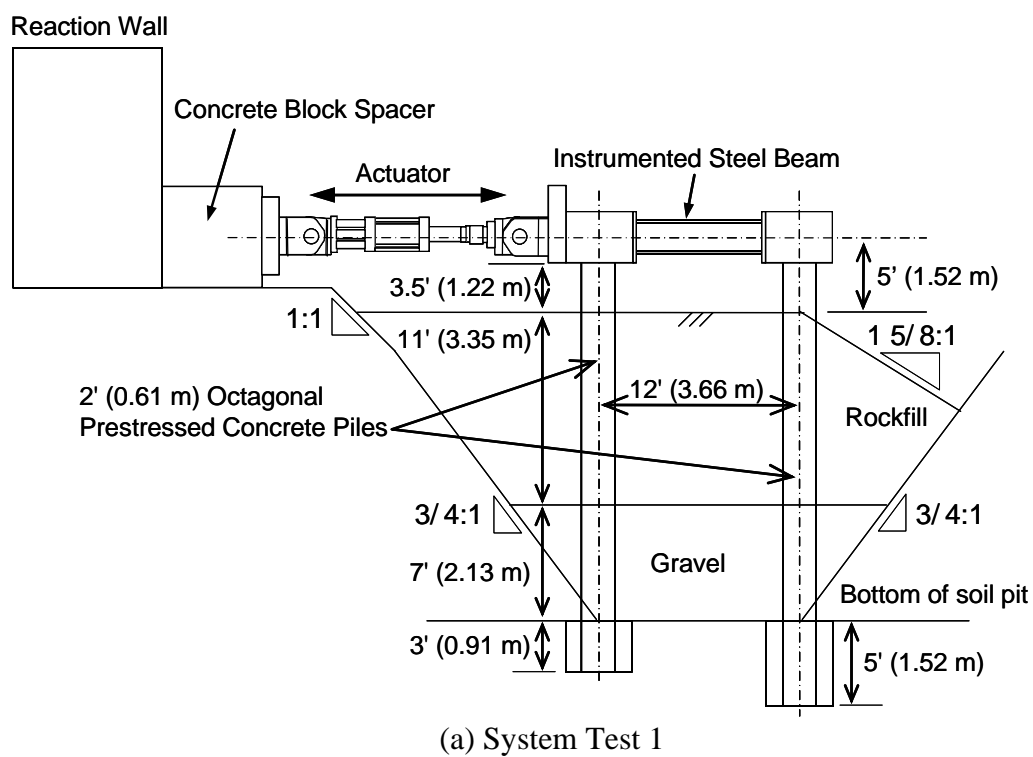


Figure 3-50 Test setup after 2 ft excavation (Plan Version 3)

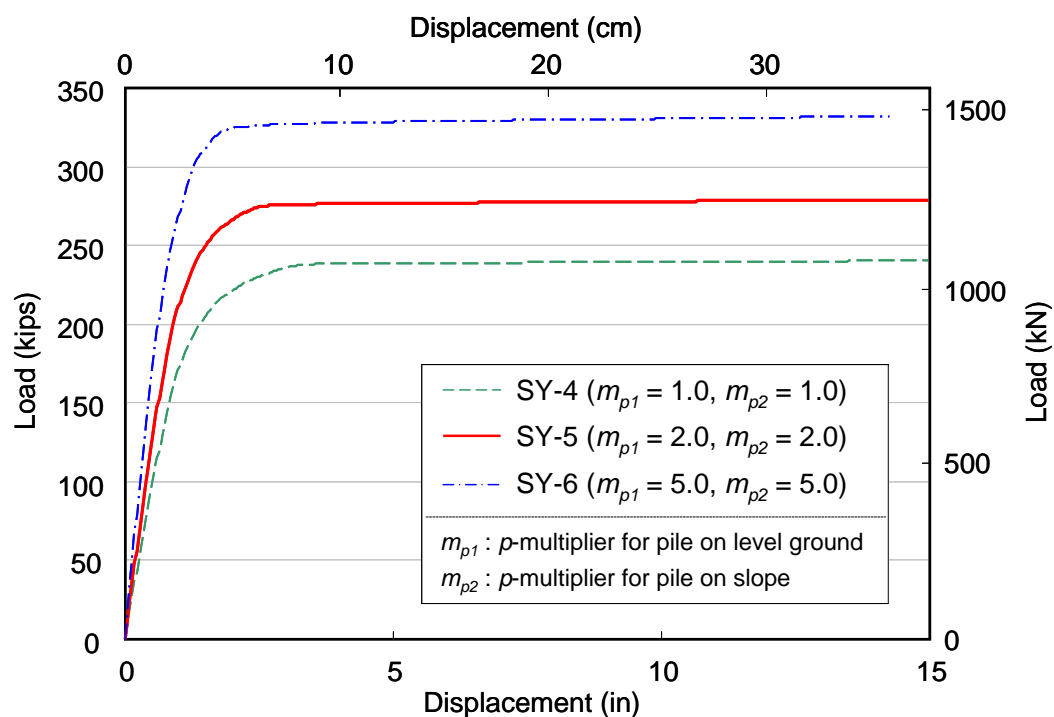


Figure 3-51 Predicted load-displacement curves at pile top (System Test 1, Version 3)

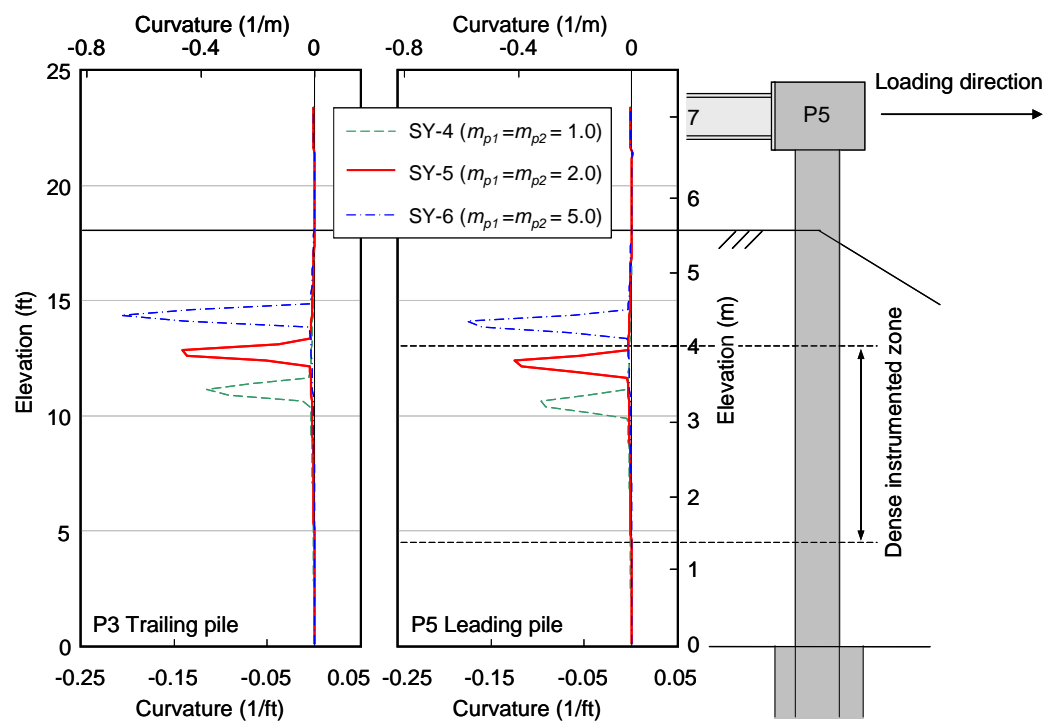


Figure 3-52 Predicted profiles of curvature (Push, System Test 1, Version 3)

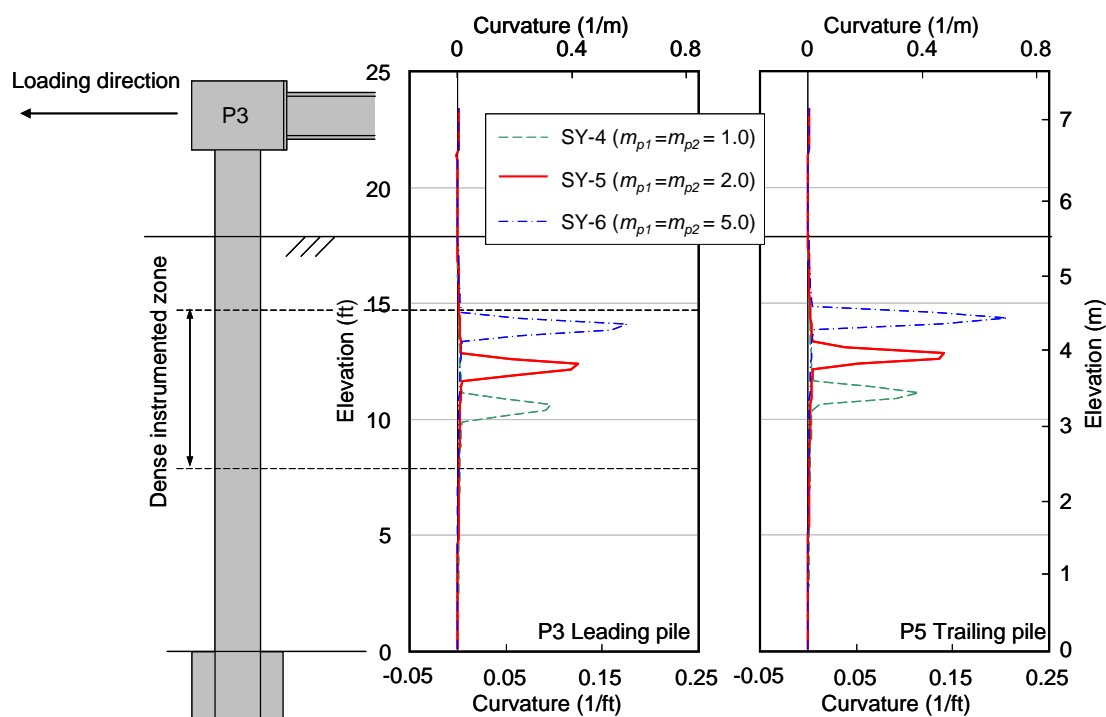


Figure 3-53 Predicted profiles of curvature (Pull, System Test 1, Version 3)

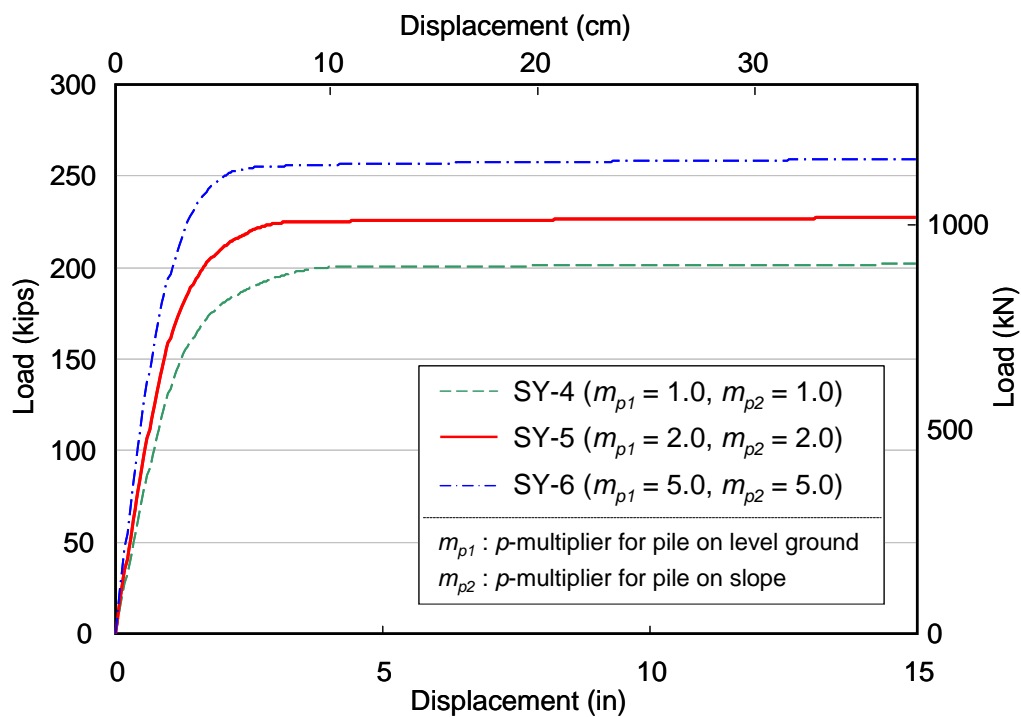


Figure 3-54 Predicted load-displacement curves at pile top (System Test 2, Version 3)

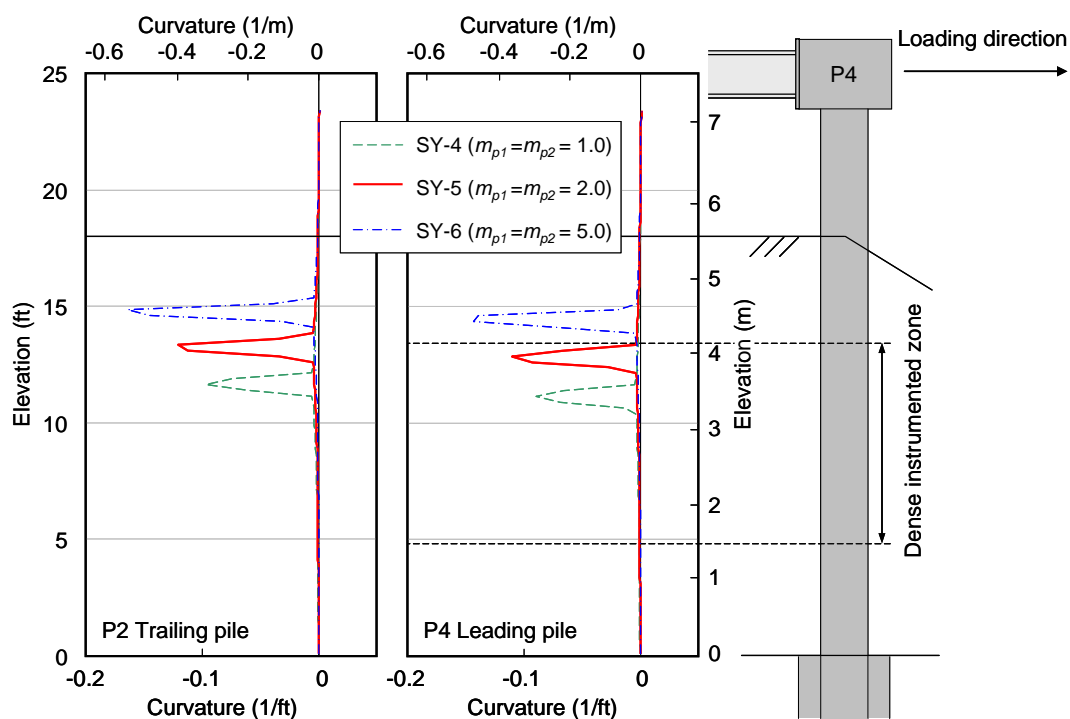


Figure 3-55 Predicted profiles of curvature (Push, System Test 2, Version 3)

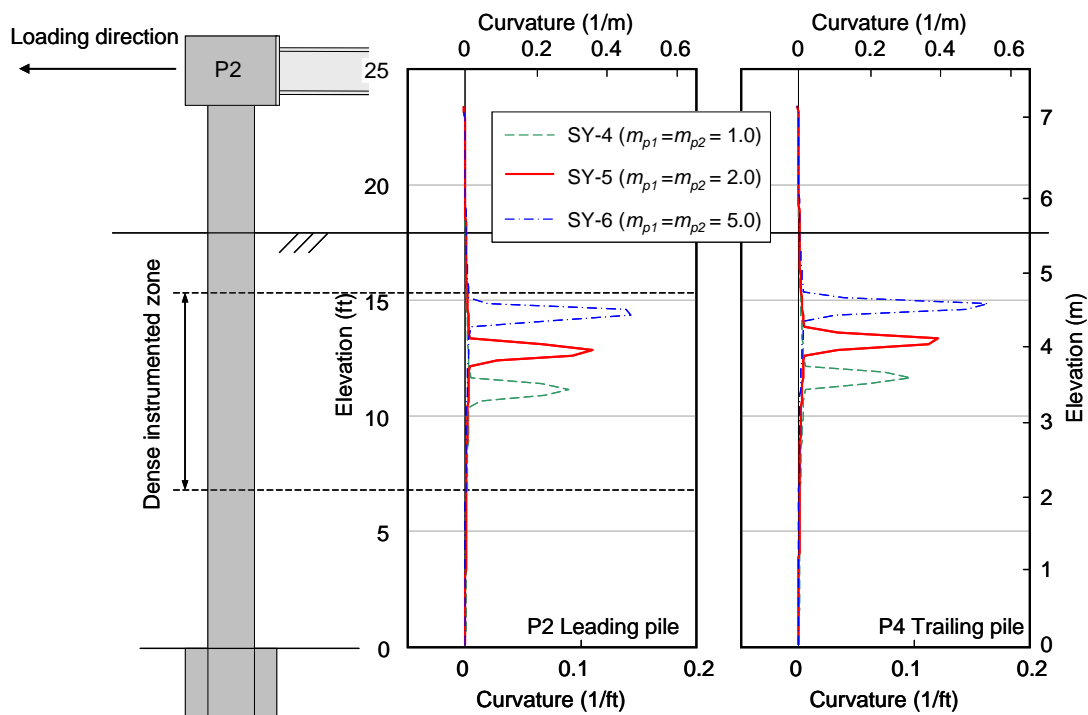


Figure 3-56 Predicted profiles of curvature (Pull, System Test 2, Version 3)



Figure 3-57 Excavation for system tests

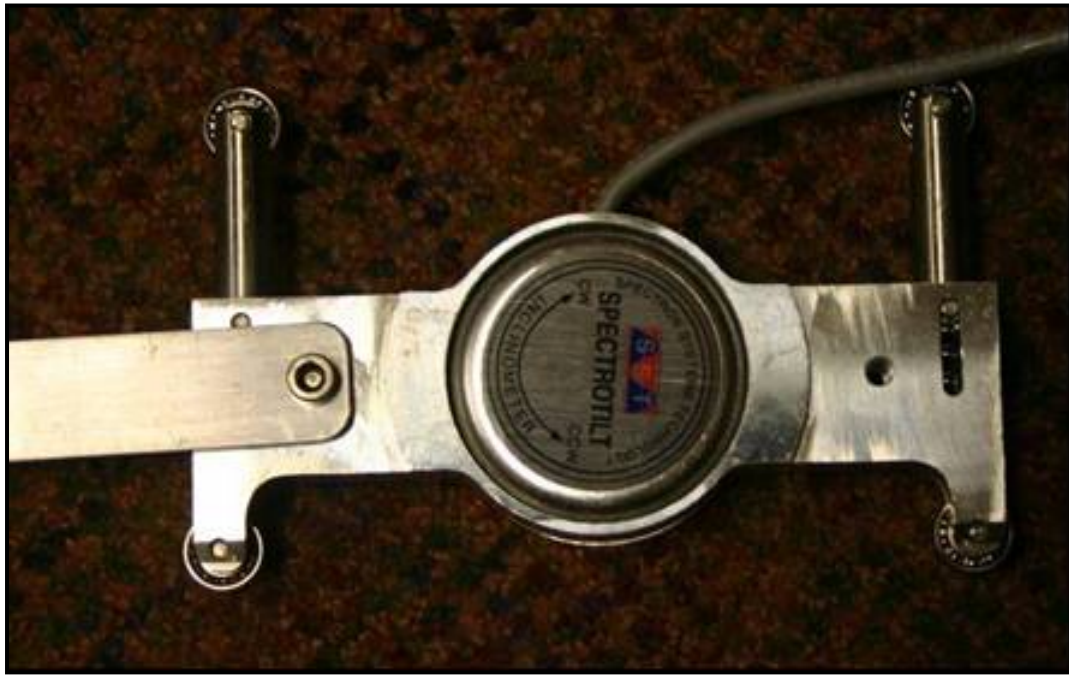


Figure 3-58 Tiltmeter sensor with housing

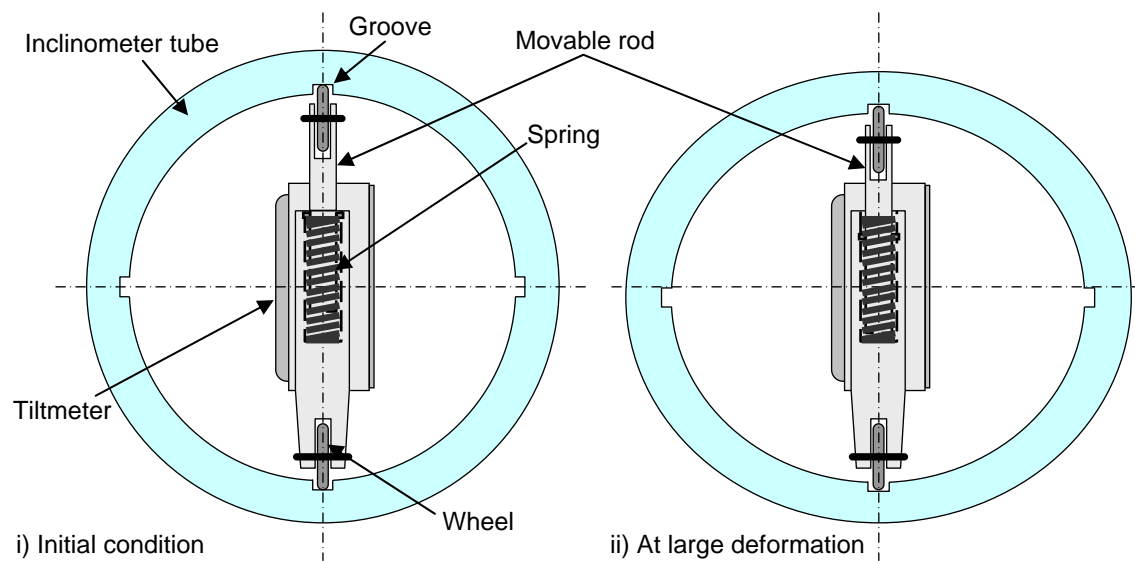


Figure 3-59 Cross section showing tiltmeter inside inclinometer casing



Figure 3-60 Installation of a series of tiltmeters through inclinometer casing

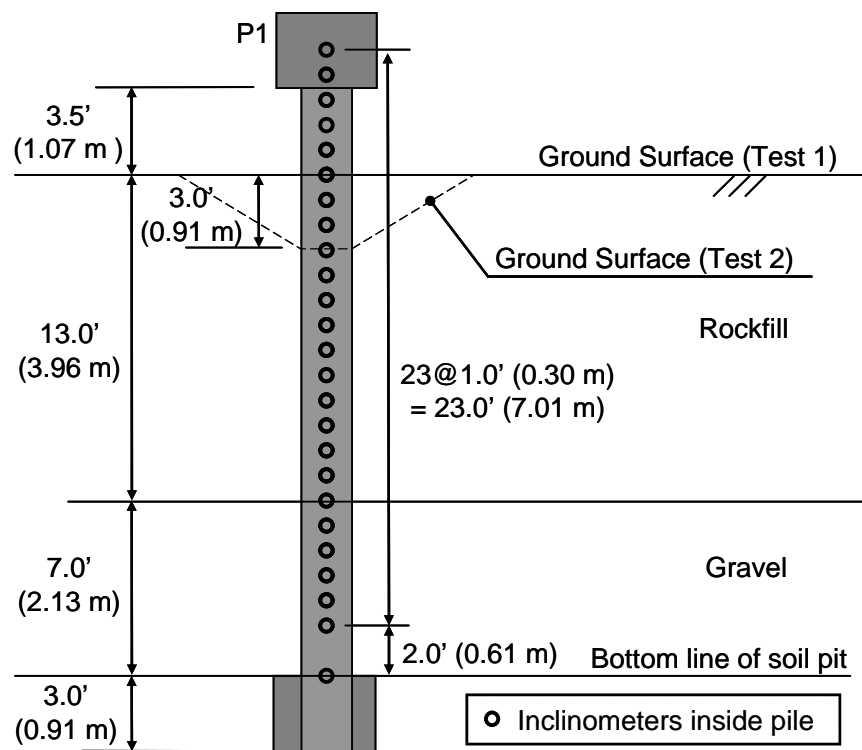


Figure 3-61 Locations of inclinometers for Single Pile Test

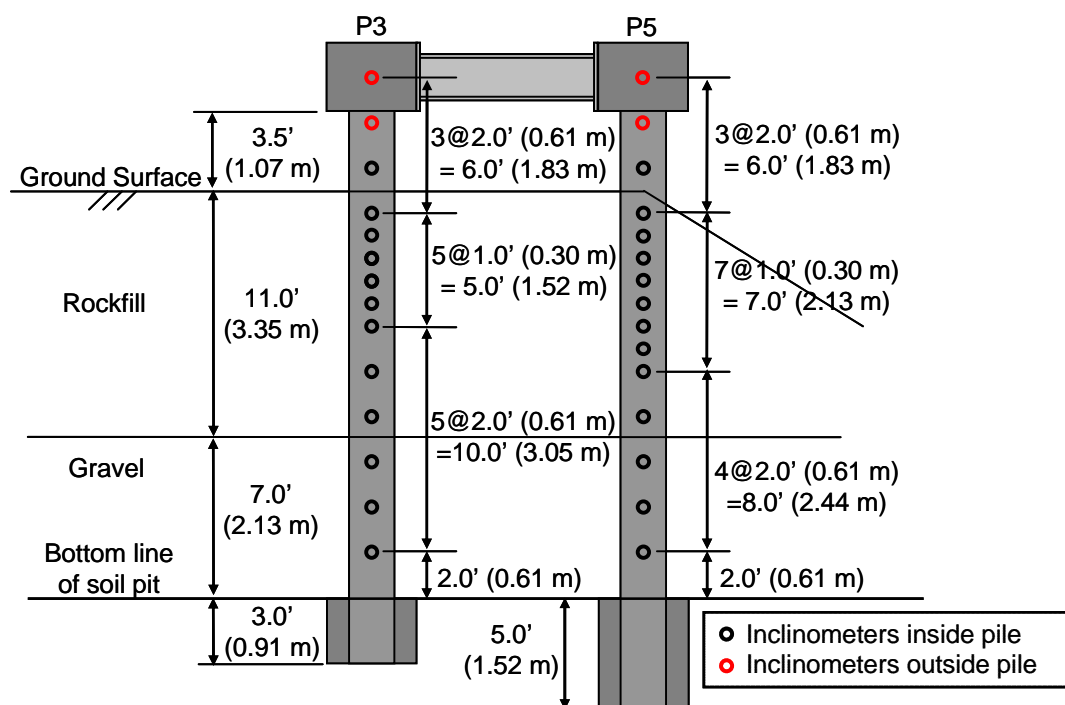


Figure 3-62 Locations of inclinometers for System Test 1

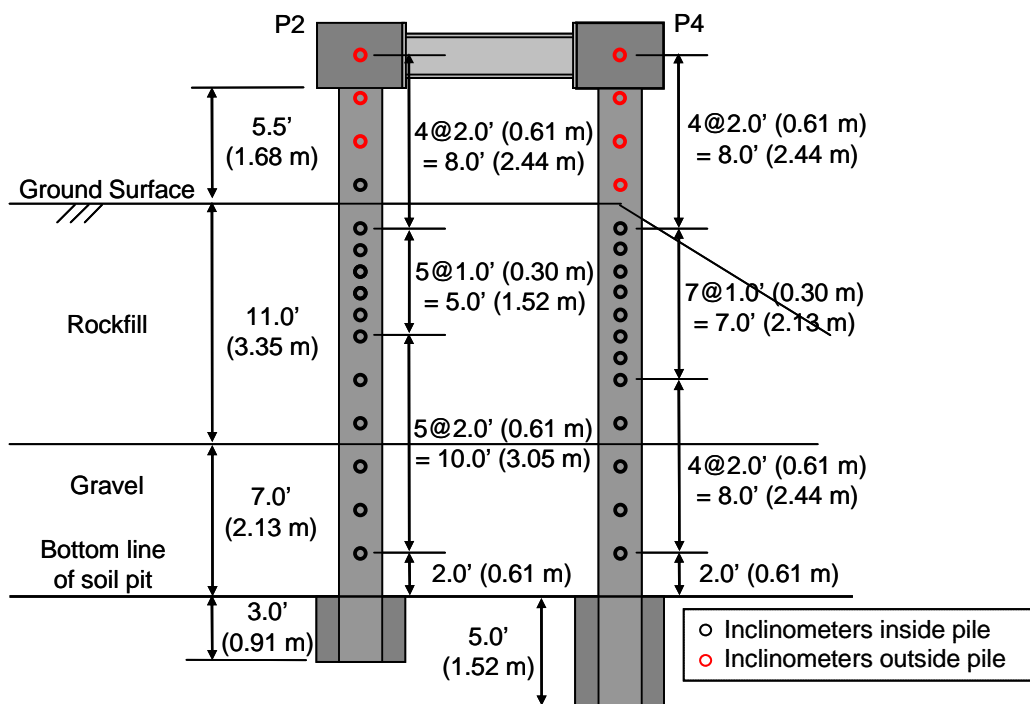


Figure 3-63 Locations of inclinometers for System Test 2

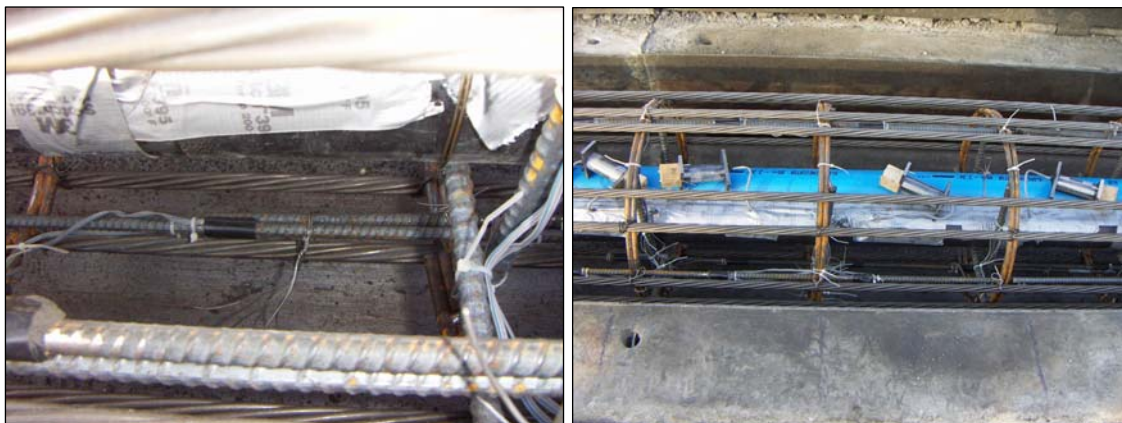


Figure 3-64 Strain gages along additional #3 rebars

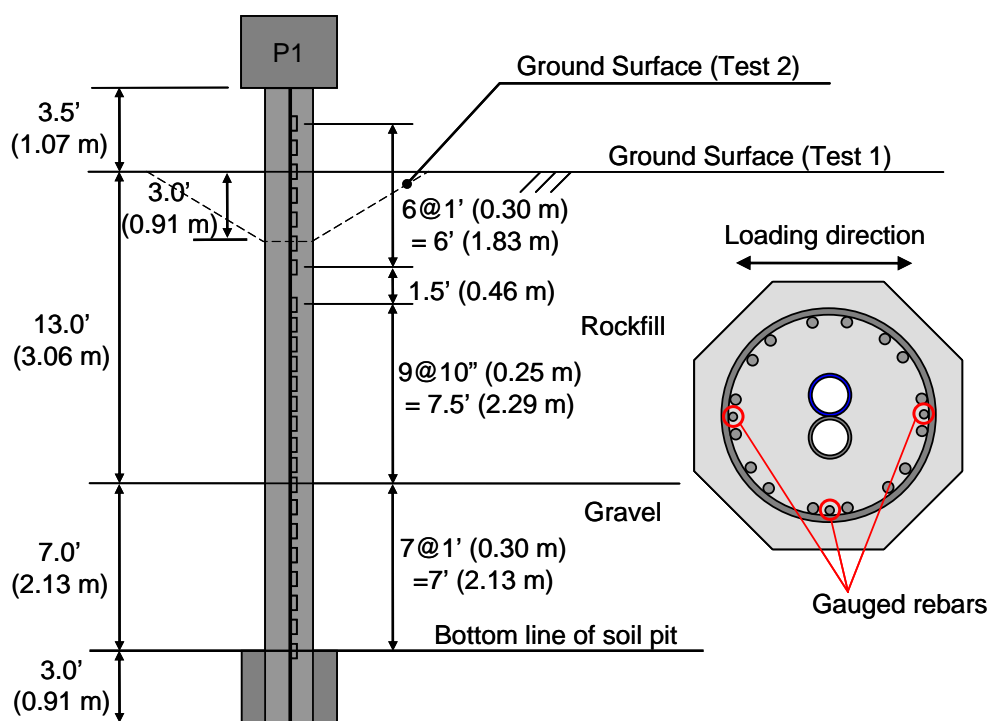


Figure 3-65 Elevations of strain gages along test pile for Single Pile Test

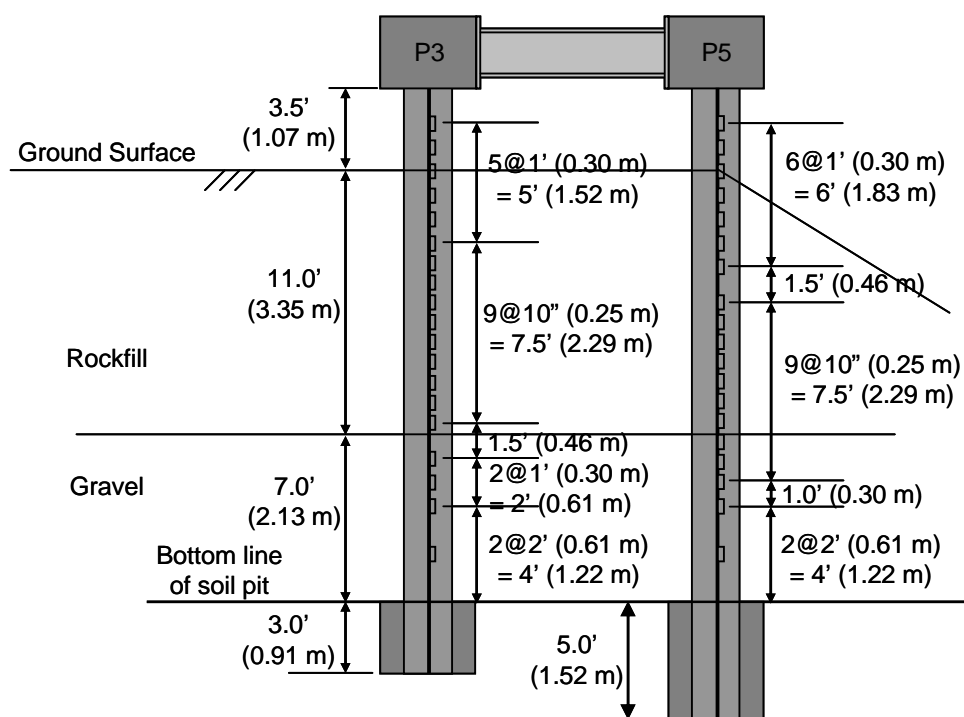


Figure 3-66 Elevations of strain gages along test pile for System Test 1

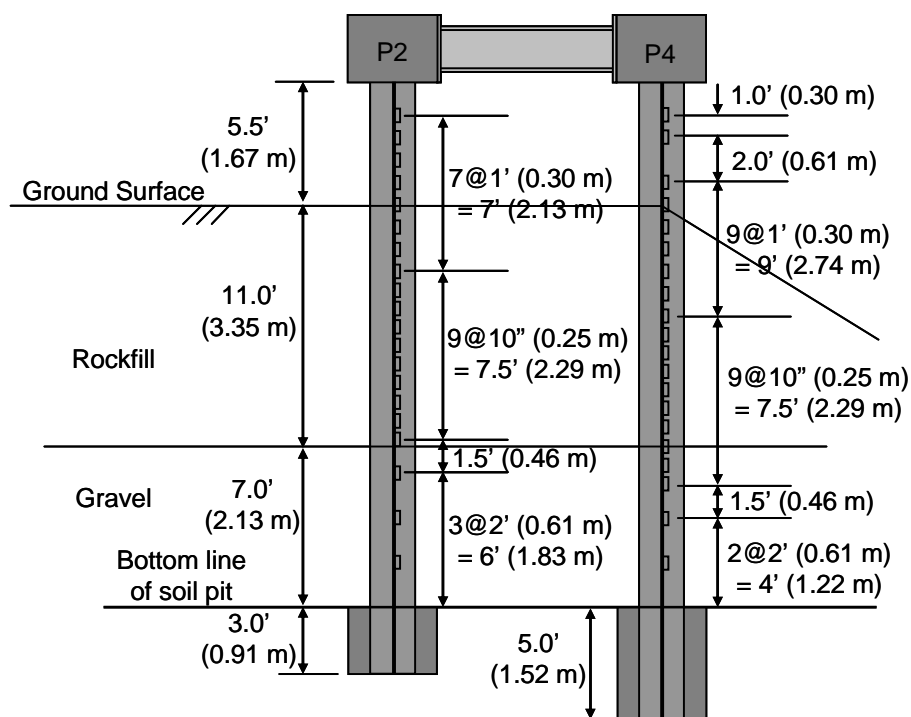


Figure 3-67 Elevations of strain gages along test pile for System Test 2



Figure 3-68 String-activated linear potentiometer

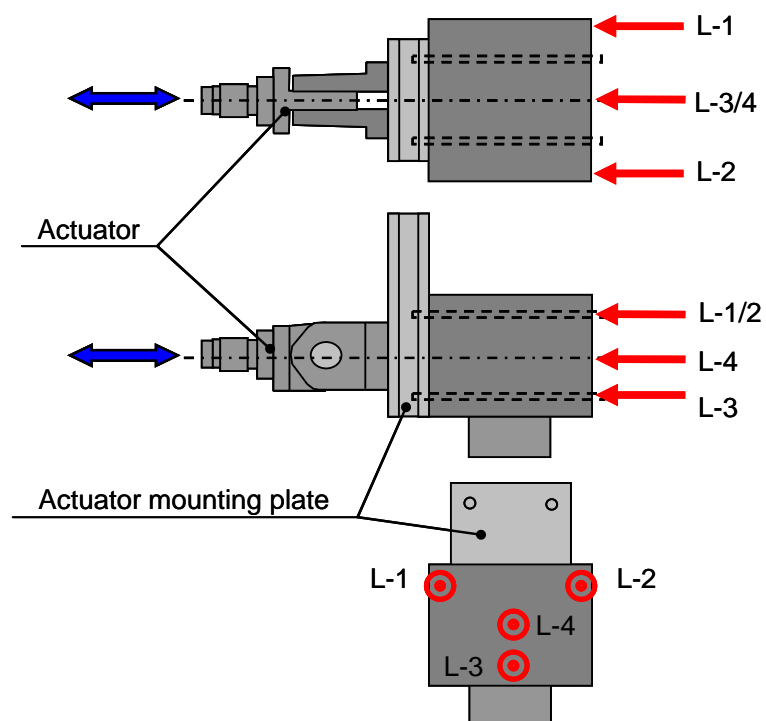


Figure 3-69 Location of linear potentiometers on the load stub for Single Test

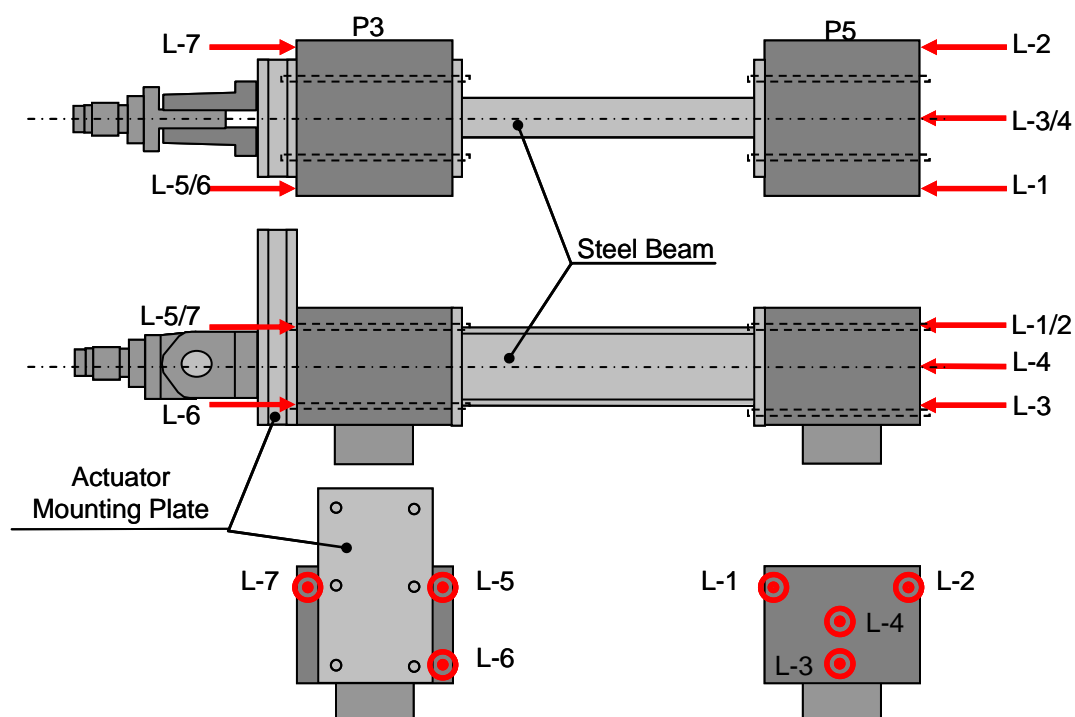


Figure 3-70 Location of linear potentiometers on the load stub for System Test 1

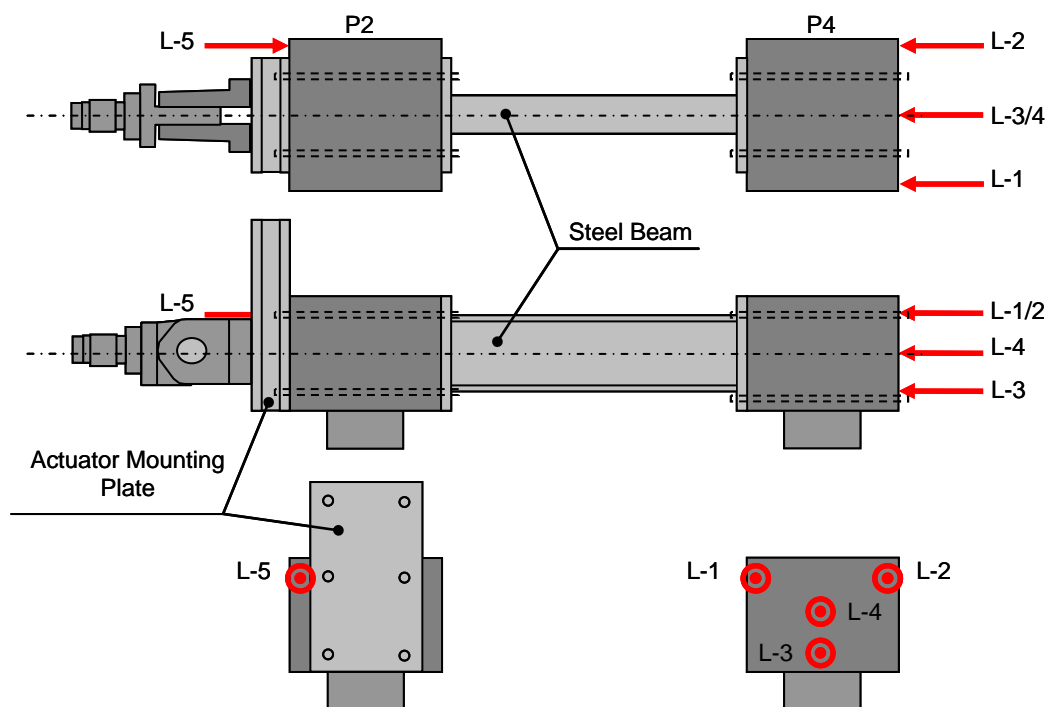


Figure 3-71 Location of linear potentiometers on the load stub for System Test 2

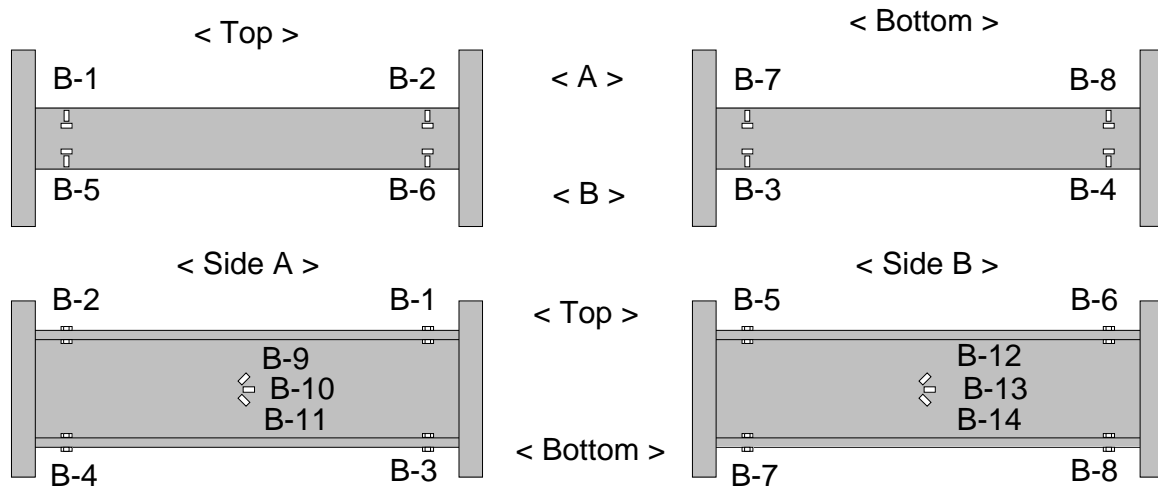


Figure 3-72 Instrumentation plan for steel beam

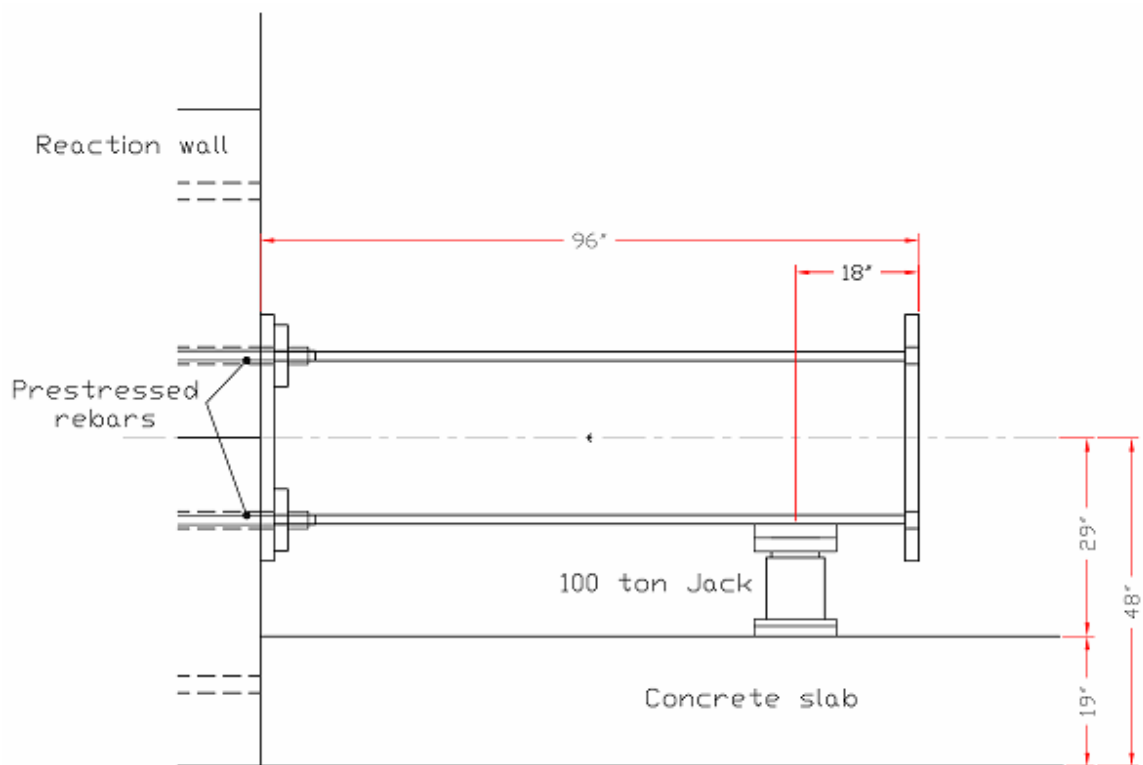


Figure 3-73 Test setup plan for calibration of the steel beam



Figure 3-74 Aspect of test setup for calibration of the steel beam

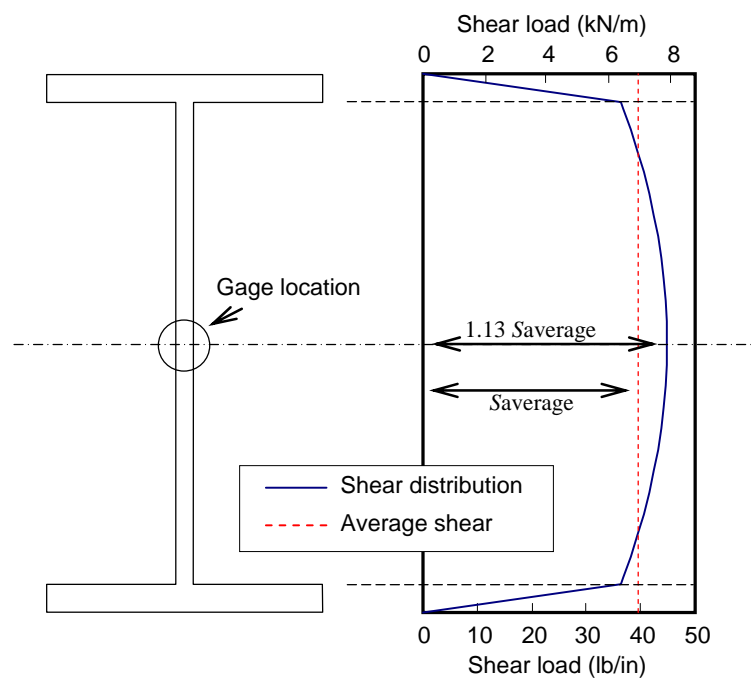


Figure 3-75 Distribution of shear force on wide flange

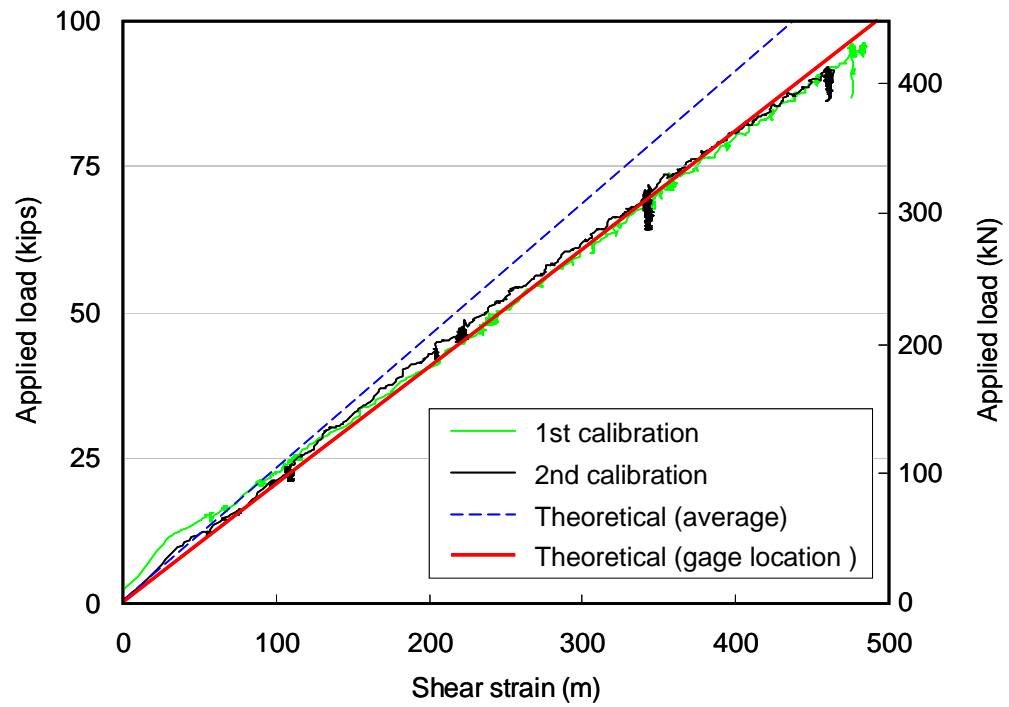


Figure 3-76 Calibration results of steel beam (shear strain)

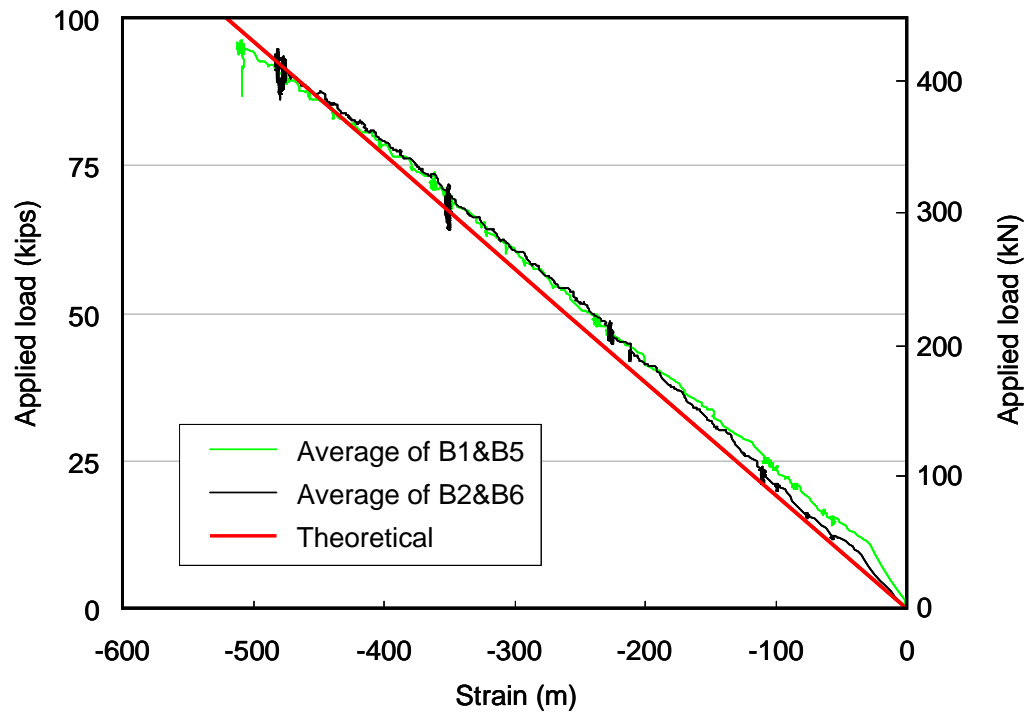


Figure 3-77 Calibration results of steel beam (gages on flange of steel beam)

4 TEST RESULTS

Following completion of all the construction works and the test setup, lateral load tests of the test piles were conducted under four different conditions; i.e. two single pile tests and two system tests with different pile length above ground surface. For all the tests, target loads and displacements were designed based on the prediction analysis conducted prior to the test (Section 3.2.2), and these targets were updated by checking records obtained in the previous cycles of loading during experiment. The actuator load and the displacement were controlled with the load cell and the displacement transducer on the actuator, respectively. The actuator displacement was operated to zero at the end of any loading cycle; i.e. the test pile were loaded back to the initial location.

First of all the tests, a single pile on the level ground with free-head condition was laterally loaded (Single Pile Test 1) in order to obtain fundamental information about soil-pile interaction, calibrate sensors installed, and find any problem or missing to be solved prior to the following system tests. Amplitude of applied lateral load cycles on the pile was carefully increased because it was the first test and there was only little reliable information in past literature.

As a result of the first test, it was observed that the test pile had unexpectedly large lateral resistance, and behaved significantly stiffer than predicted; i.e. the maximum moment along the test pile was observed at shallower depth than predicted. Because the pile response may have large change around the depth showing the maximum moment, sensors were densely installed around the maximum moment location numerically calculated in the prediction analysis. Therefore, the maximum moment location of the test pile may be out of the dense instrumented area if Single Pile Test 1 was continued without any revision of the test setup. In order to shift the critical section into the densely instrumented depth, it was decided to excavate 3 ft (0.91 m) only around the pile and carry out the second phase of single pile test, Single Pile Test 2. This modified setup also gave additional data in order to confirm the findings from the previous test.

Following the Single Pile Tests 1 and 2, the two system tests were conducted with different “stick-up” length (i.e. length above ground surface), 3.5 ft (1.07 m) and 5.5 ft (1.68 m). The setup for the system tests were designed to represent the boundary conditions of the actual pile-supported wharves. In this test setup, the boundary condition at the connection between the pile heads and the load stubs was not free, but “partially” fixed; i.e. the connection is not perfectly fixed because the connection allows rotations which depend on the working rotational moment. The two piles were interconnected with an instrumented steel beam to restrict the displacement at the pile top. When the lateral force is applied at the pile top, compressive force and tensile force are induced along a leading pile and a trailing pile, respectively. The axial force varies from tension to compression as the direction of the lateral force reverses, and affects properties of the piles and the connections. Another important difference from the previous single pile tests was that one of the piles in the system tests was located right at the slope crest. The reaction from the rockfill on the downslope may be significantly lower than that on the level ground. Therefore, the piles on the downslope may behave more flexibly than the piles on level ground. The difference on flexibility of the piles may affect several parameters, such as location of the critical section. The data from all the tests could help on the verification of simulation and back analyses afterwards.

4.1 Single Pile Test 1

Single Pile Test was conducted applying lateral load on P1 in Figure 3-18. The test pile P1 was located 12 ft (3.66 m), corresponding to 6 times of the pile diameter, far from the dike crest. The target loads and displacements applied on the test pile are summarized in Table 4-1. Also, the applied load and displacement time histories are shown in Figure 4-1.

After the first four loading cycles, it was found that the lateral displacements in the original prediction at the applied load levels were significantly overestimated and the bending stiffness of the system was considerably larger than expected. Because of

uncertainties on the pile behavior, the load applied was controlled not only by the load and also by the displacement as a secondary target at Cycle 4. In the initial plan, the test pile would reach yielding at Cycle 4, but the test pile seemed to be able to resist more based on the load displacement curve obtained in the first four cycles of loading. Therefore, the yielding load of the pile was updated from 65 kips (289 kN) to 80 kips (356 kN), and the actuator was also controlled by both the load and the displacement at Cycles 5. Following this cycle of loading, three more cycles were applied on the test pile; however, testing was paused because difference of load displacement curves between the prediction and the experiment became larger and larger as the input displacement became larger.

In addition, Figure 4-1 shows residual shear loads at zero displacement at the end of some loading cycles, and the residual loads became more obvious as amplitude of the input displacement at the pile top increased. One of potential reasons for this may be rearrangement of rock particles filling gap generated by relative movement of the pile to the rockfill during loading.

4.1.1 Load displacement behavior

Based on readings of the sensors on the actuator, the load displacement envelopes for loadings in both pushing toward the downslope and pulling toward the reaction wall are plotted in Figure 4-2. If the downslope decreased the reaction against pile movement, the lateral load in the pushing direction should be lower than that in the pulling direction, but these curves show almost identical responses each other; i.e. the effect of the downslope was not obvious on the behavior of the pile because the pile may be located far from the slope crest. In Figure 4-2, white dots represent the peak values of load-displacement relation in the Cycle 7, 1.9 in (4.8 cm) displacement. The curves show that the maximum load obtained at Cycle 7 was less than at Cycle 5, 1.3 in (3.3 cm) displacement, and it can be explained that non-linearity on the pre-stressed concrete pile and redistribution of the rock particles had already progressed more because larger displacement was operated in

the previous loading Cycle 6, 2.8 in (7.1 cm) because the target displacements were determined in trial and error in this first test.

From the initial load history, the maximum load was reached close to 80 kips at 3.0 in (7.6 cm) displacement. The yielding displacement of the system is located at 1.0 inch approximately based on a bilinear approximation of the envelopes (Figure 4-2).

The hysteretic cycles for the low load cycles show inclined rectangular shape which is typical of friction systems (Figure 4-3). As the load increased, the shape of the hysteretic response keeps the elongated narrow loops (Figure 4-4).

4.1.2 Curvature along test pile

Curvature (ϕ) was obtained from the strain gage readings from the instrumented bars as described by the following equation;

$$\phi = \frac{\varepsilon_i - \varepsilon_j}{x_i - x_j} \quad (4.1)$$

where ε_i and ε_j are strains recorded on the gages on i th and j th bars, and x_i and x_j are distances of i th and j th bars from the pile surface, respectively (Figure 4-5). Totally three sets of the curvatures can be derived, i.e. bars 1 and 2, bars 2 and 3, and bars 1 and 3. Averages of these three sets are used for plotting the curvature profiles.

Figure 4-6 shows the curvature profiles along the pile when the maximum displacements were applied for loading Cycle 5 at which there was no obvious jump of the curvature, and for Cycle 8 with large peak of the curvature in both the pushing and pulling directions. According to this figure, there are curvature concentrations at 3 ft (0.91 m) in the pushing cycle and at 2 ft (0.61 m) in the pulling cycle from ground surface. The maximum curvature was approximately 0.02/ft (0.066/m) which indicated that the section had already passed the elastic range and implied localized damage such as cracking on surface concrete at the depth where the jump of the curvature was observed.

4.1.3 Rotation and deflection along test pile

The rotation and the deflection profiles were plotted from Cycles 5 through 8 in Figure 4-7 in order to track development of the pile response. The profiles in the first four loading cycles were skipped because the response of the pile was not obvious in these cycles. The rotation profiles were obtained from 25 inclinometers installed every foot in a down-hole duct located in the center of the pile section (Section 3.5.1). The displacement profiles were calculated from the integration of the measured rotation along the length assuming that the lateral displacement at the bottom of the pile was zero. The derived displacement at the pile top shows a good agreement with that measured by the displacement transducer on the hydraulic actuator during the test.

4.1.4 Visual inspection

Following the completion of Cycle 8, the rockfill around the pile was manually excavated up to the locations where the maximum strain on the concrete was observed, which was defined as a depth of 2 ft (0.61 m) on the north side, and 3 ft on the south side of the pile (Figure 4-8(a)). No indications of compressive crushing or spalling were observed on the concrete, but minor tensile cracks were observed on both sides of the pile; 2ft (0.61 m) on the north side of the pile and at 3 ft (0.91 m) on the south side of the pile even though the cracks were closed due to prestressing force in the test piles and difficult to be found (Figure 4-8(b)). It shows that the curvature concentrations of the profile indicated the cracks at the pile surface. Also, many pock-marks were observed at the surface of the test pile (Figure 4-8(c)). Those marks indicate existence of strong contacts between the rock particles and the pile, and large point loads at the surface.

During the excavation for this visual inspection, many fractured rock particles were observed (Figure 4-8(d)). Those fractured particles are also apparent evidence of the large point load between the rock grains and the piles. In addition, it was found that contacts between the pile and the rock particles were dense at some elevations as shown in Figure

4-8(e), while the contacts were loose with relatively large voids next to the pile at the other elevations (Figure 4-8(f)). This various density of contacts may imply that large reaction acts on the pile at the dense contact elevations, while relatively low reaction works on the pile at the loose contact depths.

4.2 Single Pile Test 2

Single Pile Test 2 was performed using the same pile used for Single Pie Test 1 (P1 in Figure 3-18). Because the behavior of the test pile was significantly stiffer than predicted, the rockfill around the test pile was excavated 3 ft (0.91 m) deep in maximum as shown in Figure 3-49. Slope of the excavated rockfill was 1 5/8H to 1 V, identical as the slope on the south side of the test site.

Target displacements for any cycle of loading are shown in Table 4-2. Also, applied displacement and load time histories during the test are shown in Figure 4-9. From Figure 4-9, residual shear load could be observed at the end of some loading cycles, but magnitude of the residual shears was less than those observed in Single Pile Test 1. It implied that the residual shear at the pile top was related to soil-pile interaction because the test pile in Single Pile Test 2 had larger height above the ground surface and less significant interaction between the pile and the rockfill than the pile in Single Pile Test 1.

4.2.1 Observations during loading

Damage on the pile could be observed at the ground level where the cracks were observed after Single Pile Test 1. It indicated that the critical section did not shift downward even though increment of pile length above ground surface made the pile more flexible and it results in deeper critical section. It can be imagined that the crack generated in Single Pile Test 1 was expanded during loading in Single Pile Test 2, and induced severe local damage at that elevation. In addition, it may be one of the possible reasons why the maximum lateral forces in the two single pile tests were close each other.

An example of the damaged test pile is shown in Figure 4-10. First, the tensile crack spread into the section. Following that, an inclined shear crack was developed on the side faces of the pile. However, this crack did not affect on the force displacement curve of the system. The maximum load on the envelope was shown when the lateral displacement reached 7 in (17.8 cm) and crushing failure of the concrete cover was observed at a shallow depth.

The final load was applied until a significant drop of the lateral resistance of the pile could be observed in order to gain the ultimate lateral resistance and the maximum displacement capacity of the system. The maximum input displacement was about 15 in (38.1 cm). Damage condition of the test pile after the final load cycle is shown in Figure 4-11. The test pile obviously tilted due to the lateral loading.

4.2.2 Load displacement curve at pile top

The load displacement envelope, hysteretic loops for low load cycles (Cycles 1 through 3) and large amplitude cycles (Cycles 4 through 7) obtained in Single Pile Test 2 are shown in Figure 4-12, Figure 4-13 and Figure 4-14, respectively.

The maximum force and the corresponding displacement for each cycle were plotted as black dots on the envelope. However, significant drop of the lateral load was observed between the first cycle and the second cycle of loading Cycle 6. White dots in the figure show the maximum force and displacement only for the first cycle of loading Cycle 6 before the shear load dropped. As expected, the soil-pile system was more flexible than the previous Single Pile Test 1; however, even though the pile height above ground surface was increased, the lateral load in Single Pile Test 2 reached almost same load recorded in Single Pile Test 1 (refer Figure 4-2).

4.2.3 Curvature along test pile

The curvature profiles at the maximum displacement of each cycle were computed using the strain records along the instrumented bars. The curvature profiles are plotted in Figure 4-15 for loading Cycle 7, at which the maximum curvature was recorded, and for Cycles 4 and 6 to track development of the pile responses. In the pushing cycles (left in Figure 4-15), there were curvature concentrations at two elevations; one was at ground surface and another was 2.5 ft (0.76 m) below ground surface. In the pulling cycles (right in Figure 4-15), two peaks of curvature were also observed at 1 ft above (0.30 m) and 2.5 ft (0.76 m) below ground surface. Comparing with curvature profiles recorded in Single Pile Test 1 (Figure 4-6), it is obvious that the upper peak locations on both sides correspond to the cracking elevation in the previous test, and the lower peaks were developed in Single Pile Test 2.

Curvature profiles based on the tiltmeter records are also shown in Figure 4-16. Comparing with the profiles derived from strain gages (Figure 4-15), it was found that the tiltmeters captured only one peak curvature between two peaks of the curvature from the strain gage readings. It implies that the tiltmeters were not sensitive to the local damage, such as cracks in the surface concrete while the strain gages could capture it.

4.2.4 Rotation and deflection along test pile

Rotation and deflection profiles along the pile are shown in Figure 4-17. From this figure, there is a marked jump on the rotation profiles between the ground level and 2 ft (0.61 m) below the surface. The deflection profiles were calculated from the rotation profiles. The displacements at the pile top obtained from the rotation profiles agreed with the applied displacement on the actuator for lower amplitude; however, difference between the measured and the calculated displacements becomes larger as amplitude of the input displacement increased. One of the reasons for this is spacing of tiltmeters which can not provide continuous rotation profiles along the pile, and it may result in the

offset between the displacements measured on the actuator and calculated from the rotation profiles. For example, two peaks of curvatures indicating concentrated local deformation can be observed in Figure 4-15, but there is only one large jump of rotation in Figure 4-17. It implies that the deflection and the rotation profiles calculated from the tiltmeters do not exaggerate local damage, and reasonably represent entire behavior of the piles. Therefore, the records on the tiltmeters are more appropriate to be used for backcalculation and simulation analysis (Chapter 5).

4.2.5 In-ground inspection during pile demolition

In-ground portions of the test piles were inspected during excavation for demolition of the pile. Initially the excavation was conducted by hand up to a depth of about 18 in (46 cm), and final excavation was carried out with a backhoe (Figure 4-18).

The critical damage on the pile could be observed about 1 to 2 ft (0.30 to 0.61 m) below the ground surface (Figure 4-19). The location of this critical damage agreed with the location of the maximum curvature, at 1.5 ft (0.46 m) below the ground surface, in Figure 4-15 and Figure 4-16.

The lateral resistance of Single Pile Tests 1 and 2 was considerably larger than expected. Based on the results obtained, lateral resistance of coupled-piles used in the following system tests may exceed loading capacity of the actuators available. Therefore, 2 ft (0.61 m) excavation of the entire soil pit was performed prior to System Tests in order to reduce the lateral resistance of the system.

4.3 System Test 1

System Test 1 was performed with coupled-piles, P3 and P5 in the west area of the test site shown in Figure 3-18. The pile P3 was installed on the level ground, 12 ft (3.66 m) far from the dike crest, and the other pile P5 was located at the dike crest (Figure

3-50(a)); i.e. spacing of the piles was also 12 ft (3.66 m) in center-to-center. The height above the ground surface of both the pile was 3.5 ft (1.07 m).

Target loads and displacements for any cycle of loading are summarized in Table 4-3, and the applied load and displacement time histories during test are shown in Figure 4-20. The applied load and displacement were controlled with the load cell, and displacement transducer placed on the actuator. Even though the first three loading cycles were applied in load-controlled, the displacement of loading Cycle 3 was also monitored for a security purpose.

4.3.1 Observations during loading

Development of cracking and surface concrete spalling on the load stubs and the pile heads was tracked during all the loading cycles. Some of notable observations are presented herein, and more details are available in the final report to the project sponsors (Kawamata *et al.*, 2007).

1) Loading Cycle 3

The first crack appeared at the surface of the level ground pile (P3) when the pile was loaded in the downslope direction, and uplift force worked along the pile (Figure 4-21). The similar crack was observed in the pile at the dike crest (P5). There was also a diagonal crack at the deck extending from pile deck interface, right at the pile angle, towards the corner of the cap on the P3. This crack could be observed during loading toward downslope.

2) Loading Cycle 6

As amplitude of the input loading increased, the crack width also became larger and larger. Thin slices of concrete started being crushed and spalled on the compressive side of P3. Several parallel diagonal cracks appeared on the load stubs and reached the edge of the stubs.

3) Loading Cycle 8

The compressive region on P3 showed significant crushing of the cover concrete (Figure 4-22). Also, Figure 4-23 shows that exposed unpainted area of the pile, and its length was about 1 ft (30 cm). It indicated that the rockfill around the test pile was 1 ft (30 cm) settled due to rearrangement of the rockfill particles during loadings, because only portions of the pile above the original ground surface was painted before testing.

4) Loading Cycle 11

The system was loaded in both directions until most of the dowel bars failed and the lateral load capacity considerably dropped. It was possible to hear several dowel breaking and the plastic hinge extreme deterioration. The damage condition of the piles after the final loading is shown in Figure 4-24.

4.3.2 Load displacement curve at pile top

Load displacement envelopes, hysteretic loops for the low loadings (Cycles 1 through 3) and for all the loadings are shown in Figure 4-25, Figure 4-26 and Figure 4-27, respectively. The initial three cycles in the load controlled phase were used to update the yielding displacement for the following displacement controlled phase. Based on the prediction analysis shown in Section 3.4.1, the yielding displacement was defined as 1.4 in (3.6 cm). However, load displacement envelope recorded in the test showed that the average yielding displacement of the system in two directions of loading was about 2.1 in (6.4 cm) as shown in Figure 4-25. One of possible explanations for this difference is that the contact condition between the pile and the rockfill around ground surface is quite sensitive to the initial stiffness of the pile-soil system; i.e. the initial stiffness of the system can be low if void exists between the pile and the rockfill. Recalculated displacement ductility is shown in Table 4-4.

The residual shear loads were observed at the end of some loading cycles even though the test pile was loaded back to the initial location with zero displacement. As mentioned

in the previous section, it may come from rearrangement of the rockfill particles filling gap generated due to relative displacement between the pile and the surrounding soil during cyclic load. Magnitude of residual shear may be dependent on the condition of the redistribution of rock particles, magnitude of the deflection, and deformation profile of the pile.

4.3.3 Shear and axial forces along each pile

Shear and axial forces on each pile can be derived from strain records on the instrumented steel beam. Free body diagram around the pile top and the steel beam is shown in Figure 4-28. Based on this diagram, axial and shear forces at the top of each pile can be calculated using the following equations (refer Figure 4-28 for notations);

$$\begin{cases} S_b = F_{l1} = F_{l2} \\ F_1 = F_{l1} - W_{ls} - W_b / 2 \\ F_2 = -F_{l2} - W_{ls} - W_b / 2 \end{cases} \quad \begin{cases} S_1 = F_a - F_b \\ S_2 = F_b \end{cases} \quad (4.2)$$

Ideally, the raw records should be used to calculate shear and axial force on each pile. However, there were large sudden jump of strains and gradually increased strains on the records on some gages in loading and unloading procedure. No possible reason could be found for the former, and the latter may be caused by thermal strain on the beam and relative displacement between two piles. Because testing started at early morning and one cycle of loading took about 10 to 40 minutes, it was likely that tensile strain was generated due temperature increment on the beam. Compensative gages are usually used in order to eliminate thermal effect, but no compensative gage was placed on the beam for this test. In addition, strain on the beam is very sensitive to relative displacement between the piles; for example, one hundredth inch (0.25 mm) relative displacement induces 100 micro strain along the beam corresponding to about 150 kips (667 kN) of axial load along the beam. However, accuracy of the 50 inch (15.2 cm) stroke string-activated linear potentiometers used is not high enough to measure so small displacement

of the head of the pile on the slope. Therefore, some assumptions have to be made in order to estimate shear and axial load on the piles. It is notable that discussion below is only qualitative, not quantitative because of uncertainties on the records of strain gages on the steel beam.

It was assumed that the upward or downward axial forces along the piles due to lateral loading were zero at the beginning of any loading, and the axial load along the pile could be represented by increment of the axial force during loading because the coupled piles were loaded back to the initial position at the end of any loading cycles and there was no residual displacement in up down direction on the piles. In reality, some residual axial force may exist because of nonlinear pile behaviors, such as concentrated local damage, especially in large input displacement cycles.

The coupled piles had residual shear force at the end of some loading cycles, especially in large displacements loading cycles. As described in Section 4.1, the residual load may result from rearrangement of rock particles filling gap generated due to relative displacement between the pile and the rock grains. The residual load on the pile located on the level ground may differ from that on the pile at the dike crest, but it was assumed herein that the residual shear force on the system was distributed equally on each pile at the beginning of any loading cycles. Because the results at the small displacement loadings gave no residual load at the end, and showed almost identical shear load during loading on each pile, it can be qualitatively reasonable assumption.

Figure 4-29 shows examples of time histories of shear load at the top of P3 and P5 for the loading Cycles 6 and 7, and Figure 4-30 and Figure 4-31 present shear load on each pile at any cycle in pushing and pulling directions, respectively. From these figures, it can be observed that both the piles took almost identical shear force even for pushing toward the downslope.

A couple examples of time histories of axial force along each pile are shown in Figure 4-32, and relationship between the axial force and the displacement at the pile top is presented in Figure 4-33. According to Figure 4-33, the uplift force calculated from strain gage records was 120 to 150 kips in maximum. These measured forces are reasonably matched with calculated uplift force for the footing design (see Appendix-A).

4.3.4 Curvature along test pile

The curvature profiles of the piles in System Test 1 were obtained from the strain gages installed on the three instrumented bars on the pile section. Examples of the curvature profiles are shown in Figure 4-34; the profile for Cycle 9 gave the largest lateral load at the pile top, and the profiles for Cycles 5 and 7 showed development process of the pile responses. As mentioned in Section 3.5.2, these profiles of curvature do not represent entire pile behavior so well, especially for large input displacement, because of concentrated local damage, such as cracking and spalling. However, the peaks of the curvature in the profiles indicate locations of local damage.

One of the most notable observations is that locations of the peak curvature shifted upward as input displacement became larger. This phenomenon is defined as migration of the critical section, and one of the possible mechanisms is shown in Figure 4-35. As shown in Figure 4-8, contacts between the pile and the large particle size rockfill were dense and strong at some elevations, and loose and weak at other elevations. Therefore, zone with few contacts can exist along a pile (Figure 4-35(a)). If the pile is monotonically loaded, the contact between the pile and the rockfill at deeper elevation starts generating strong reaction to the pile, and portions of the pile above that strong contact point deflect. Therefore, large curvature is developed and tensile cracks are generated at the elevation of the strong contact point. As the deflection of the pile becomes larger, the pile starts contacting with another rockfill particle at shallower locations than the first strong contact point, and reaction to the pile at the new contact increases (Figure 4-35(b)). When the reaction force at the newly generated contact point becomes large, deflection of the pile is restricted below the new contact point and the first crack does not expand any more. On the other hand, deflection starts concentrating at the newly generated upper contact point and another cracking is developed there. This procedure of the migration can repeat several times, and it makes the critical section seem to shift upward as amplitude of the input motion becomes larger.

4.3.5 Rotation and deflection along test pile

Rotation profiles for several cycles are shown in Figure 4-36. Assuming the load stubs behave as a rigid body, rotation on the load stub can be also assumed uniform. A jump of rotation was concentrated at the connection between the piles and the load stubs because the connection allowed rotation based on the full-scale connection test (Krier, 2006). Based on the assumptions above, rotation profile along pile should be like shown in Figure 4-36.

From this figure, the inclinometer profile along P3, the pile on level ground, shows an obvious jump of rotation between elevations of 5 to 6 ft (1.5 to 1.8 m) below the ground surface in either direction of loading. The elevation of the rotation jump along P5, the pile at the dike crest, was located at the same elevation as that along P3 for the loading toward the reaction wall. However, the rotation jump for pushing toward the downslope was located 1 ft (0.3 m) deeper than the others. It implies that the pile at the dike crest (P5) behaved more flexibly than the pile on the level ground (P3) when the system was loaded toward the downslope.

Deflection profiles derived from the inclinometer records are shown in Figure 4-37. The derived profiles provides the displacement at the pile top reasonably matching with the displacement measured on the actuator for the initial low amplitude cycles; however, as the displacement increases, the pile top displacement calculated from the inclinometer records tends to underestimate the displacement measured on the actuator. This offset is even larger for the pulling cycles. As mentioned in Section 4.2.4, one of the possible explanations of this displacement offset is localized damage which could not be detected well by the tiltmeters. However, the magnitude of the offset in System Test 1 was significantly larger than that in Single Pile Test 2. Another possible reason is lateral displacement at the connection (i.e. relative displacement of the load stub to the pile top) which can happen only in the system tests. It seems reasonable because the dowel bars connecting the pile and the load stub failed in shear at the final loading cycle, and the relative displacement could gradually increase as the input displacement became larger.

4.3.6 In-ground inspection during pile demolition

The excavation sequence on P3, the pile on the level ground, is presented in Figure 4-38. The first signs of plastic hinge were observed when the excavation reached about 5 ft (1.5 m) from the initial ground level corresponding to the locations previously estimated from the sensor readings. The water was sprayed during excavation in order to damp the test piles revealing the cracks at the surface (Figure 4-39). According to the photos, the cracks on the piles could be observed at multi-elevations. This observation is consistent with the curvature profiles with multi-peaks.

It also could be observed that some of the strands in concrete piles were exposed and fractured. A plastic hinge on P3 in Figure 4-40 provided the severest damage among all the piles used for the system tests.

The damage on the north side of P5, the pile at the dike crest was similar to the damage observed on P3 (Figure 4-41). However, the severely damaged section on the south side of P5 was located at deeper elevation than the critical sections on the others. This observation is also consistent with the strain gage readings, and it was due to higher flexibility of the pile on the downslope.

4.4 System Test 2

System Test 2 was conducted using the other coupled-piles, P2 and P4 shown in Figure 3-18. The section view of System Test 2 was shown in Figure 3-50(b). The pile length above the ground surface of both the piles was 5.5 ft (1.68 m), and spacing of the piles was 12 ft (3.66 m).

The target loads and displacements for any cycle of loading are shown in Table 4-5. The load and displacement time history applied is shown in Figure 4-42. The actuator load and displacement were controlled as described in Section 4.3.

4.4.1 Observations during loading

Cracking and spalling on the surface concrete of the load stubs and the pile heads was traced during all the loading cycles in order to observe development process of damage status. Even though the local damages on the load stub and the pile top are not important in this research because they do not have major effects on the soil-pile interaction, some examples of interesting observations are presented herein. More details are available elsewhere (Kawamata *et al.*, 2007).

1) Loading Cycles 1 to 3

During these initial cycles, several thin cracks were observed. At Cycle 2, the pile deck connection opened at the pile on the level ground (P2) and tension cracks appeared 3 in (7.6 cm) below the connection in both the piles (Figure 4-43). At Cycle 3, the cracks at the connection became more obvious in both the piles. Additional cracks appear at 6 (15.2 cm) in and 18 (45.7 cm) in below the pile deck interface.

2) Loading Cycle 6

At this stage of loading, minor concrete crushing started happening at P2, the pile on level ground when the pile was in compression (i.e. when the piles were pulled toward the reaction wall). The tensile cracks also appeared on both the piles at 1.0 to 2.0 ft (0.3 to 0.6 m) below the pile-load stub connection (Figure 4-44).

3) Loading Cycle 8

Crushing of concrete is still minor even though it was gradually expanded as amplitude of the input displacement became larger. Also, it could be observed that the rockfill around the test piles settled and the pile height above ground surface increased (Figure 4-45).

4) Loading Cycle 10

Horizontal cracks on the load stub became apparent at 3 in (7.6 cm) above the bottom line. The damage was concentrated on the cracks opened in the previous loading cycles at the load stub and the surface concrete spalled at the connection (Figure 4-46).

5) Loading Cycle 11

At this cycle of loading, the damage of the load stub extended until the cover concrete of the stub was completely lost on the level ground pile (P2). In the pile at the slope (P4), the cover concrete was not totally detached but the residual crack width was considerable. Some dowels were failed at the connection (Figure 4-47).

4.4.2 Load displacement curve at pile top

Load displacement curves, hysteretic loops for Cycles 1 through 3, and all the loading cycles are shown in Figure 4-48, Figure 4-49 and Figure 4-50, respectively. Comparing with the maximum loads observed in System Test 1, there is about 10 to 20% reduction of the lateral resistance in System Test 2 due to 2 ft (0.6 m) longer pile length above the ground surface.

The yielding displacement for the System Test 2 was estimated 1.5 in (3.8 cm) in the prediction analysis. Based on the envelope for all the loading cycles, the more reasonable average yielding displacement of both the loading directions is approximately 2.3 in (5.8 cm) as shown in Figure 4-48. Using this updated yielding displacement, ductility of the system was recalculated (Table 4-6).

4.4.3 Shear and axial forces along each pile

Shear and axial forces along the piles for System Test 2 were calculated using assumptions and equations described in Section 4.3.3. Figure 4-51 shows examples of time histories of shear loads at the top of P2 and P4 for the loading Cycles 6 and 7. Figure

4-52 and Figure 4-53 present load displacement curves on each pile in both the pushing and pulling directions, respectively. Curves for total shear load vs. displacement were also plotted in these figures. From these figures, the pile on the slope seemed to contribute more to react against the shear load than the pile on level ground. However, the records on the strain gages on the beam need to be carefully considered for a quantitative discussion because large offset of the shear load was observed at the end of the loading on the time histories even though no lateral displacement was applied on the actuator (Figure 4-51). The most possible reasons for this shear force offset are axial strain from thermal effect on the beam, relative displacement between the test piles, and combination of these two phenomena as mentioned in Section 4.3.3. Unfortunately, strain due to these factors can not be quantified, and the accurate shear force on each pile can not be estimated. Summarizing all the load displacement curves on each pile for System Tests 1 and 2 (Figure 4-30, Figure 4-31, Figure 4-52, and Figure 4-53), it may be concluded that both the piles on level ground and at the downslope in the system tests may take almost same amount of the shear force.

Examples of the axial force time histories on each pile and axial force-lateral displacement curves are shown in Figure 4-54 and Figure 4-55. Comparing Figure 4-55 with Figure 4-33, the recorded uplift and down drag forces in System Tests 1 and 2 were quite similar as each other.

4.4.4 Curvature along test pile

Figure 4-56 shows profiles of curvature derived from the strain gage arrays along the piles at loading Cycles 5, 7, and 9. It is notable that there seems to be crack openings at quite deep location for the pushing cycles on both the piles; i.e. 9 ft (2.74 m) deep for the pile on the level ground and 11 ft (3.31 m) deep from the ground surface for the pile at the slope crest. Based on the figures, migration of the critical section could be observed; i.e. large curvature was developed at deeper elevation at lower input displacement, and

became shallower as amplitude of the input displacement increased. This phenomenon could be also observed in System Test 1 (refer Section 4.3.4).

4.4.5 Rotation and deflection of pile

Examples of rotation profiles derived based on the tiltmeter records for several cycles are plotted in Figure 4-57. The tiltmeters were taken out from the test piles prior to the final loading because it was not possible to remove them from the top due to the excessive damage at the connection in the previous System Test 1, and it was necessary to cut the piles at the ground level and retrieve the tiltmeters.

The inclinometer profiles along P2, the pile on level ground, show a clear jump of rotation between elevations of 5 ft (1.5 m) and 6 ft (1.8 m) below the ground surface for both the pushing and pulling cycles. The jump of rotation along P4, the pile on the slope, was located at the same elevation as that on P2 for the pulling, while it was located at 1 ft (0.3 m) deeper elevation for the pushing due to higher flexibility of the pile loaded toward the downslope.

The displacement at the pile top calculated from the inclinometer records (Figure 4-58) match relatively well when the applied displacements at the top were low; however, the displacement estimated from the inclinometers tends to underestimate the displacement measured at the pile top as the displacement increases. It could be because the inclinometers can not measure concentrated local deformation due to cracking or spalling so well. Also, the relative displacement between the pile and the load stub can be another reason as mentioned in Section 4.3.5.

4.4.6 In-ground inspection during pile demolition

The sequence of excavation around P2, the pile on the level ground, is shown in Figure 4-59. White bands on the pile in the photos are external sensors detecting spalling of surface concrete, which were installed in the dense instrumented area (refer Section

3.5.5). Some of cracking and spalling could be observed in the area. Because the rubber bands used for the external sensors generated confinement on crushed concrete chunk, surface concrete dropped off from the pile when the sensors were removed (Figure 4-60).

Figure 4-61 shows the excavation sequence on the north side of P4, the pile on the slope. Location of the upper crack on the pile corresponded to the elevation of the top peak curvature on the profile (Figure 4-56). The cover concrete at the plastic hinge on the north side of the pile was removed manually as shown in Figure 4-62. The transversal confining steel was visible but there was no sign of damage on the strands.

Both System Tests 1 and 2 were completed without any trouble. The maximum lateral loads on the actuator were about 360 kips (1600 kN) in the System Test 1, and 270 kips (1200 kN) in the System Test 2. Based on these values, it can be guessed that lateral resistance of coupled-piles probably exceeded capacity of the actuator, 420 kips (1870 kN) in tension, if the 2 ft (0.61 m) excavation was not carried out. It can prove that the test plan was appropriately updated.

4.5 Summary

Even though the first single pile test gave results against the original prediction analyses, possible troubles due to these unexpected responses could be solved making reasonable update of the test plan. As a result, all the tests were performed reasonably well. In order to find the appropriate update, preliminary prediction analyses were carried out after Single Pile Tests (Section 3.4.1), but details of pile-soil interaction (e.g. verification and modification of the p - y curves currently used for design practice, and mechanism of reaction generation in rockfill) were not discussed yet. In order to gain better understanding about the pile-large particle rockfill interaction, a series of pushover analyses was conducted. Details of the numerical analyses including numerical model and parameters used are described in the next chapter.

Table 4-1 Target displacement and load for Single Pile Test 1

Loading Cycle	1	2	3	4	5	6	7	8
Testing Date	Apr. 2	Apr. 3					Apr. 4	
Target displacement (in.)	---	---	---	0.85 ¹⁾	1.3	2.8	1.9	3.6
Target load (kips)	15	30	40	65	80	---	---	---
Number of cycles	2						1	2

1) Secondary displacement control value

Table 4-2 Target displacement and load for Single Pile Test 2

Loading Cycle	1	2	3	4	5	6	7
Testing Date	May. 22						
Target displacement (in.)	1.4	2.1	2.8	4.2	5.6	8.4	--- ¹⁾
Target load (kips)	---	---	---	---	---	---	---
Number of cycles	3 ²⁾						---

1) Keep pushing until the test pile failed

2) Two cycles of loading followed by one reduced displacement cycle

Table 4-3 Target displacement and load for System Test 1

Loading Cycle	1	2	3	4	5	6	7	8	9	10	11
Testing Date	July. 2			July. 9							
Target displacement (in.)	---	---	1.2 ¹⁾	1.4	2.1	2.8	4.2	5.6	8.5	11.4	--- ²⁾
Target load (kips)	70	140	210	---	---	---	---	---	---	---	---
Number of cycles	2			3 ³⁾							---

1) Secondary displacement control value

2) Keep pushing until the system failed

3) Two cycles of loading followed by one reduced displacement cycle

Table 4-4 Recalculated ductility for System Test 1

Cycle	Nominal Ductility	Recalculated Ductility
4	1.0	0.7
5	1.5	1.0
6	2	1.3
7	3	2.0
8	4	2.7
9	6	4.0
10	8	5.4

Table 4-5 Target displacement and load for System Test 2

Loading Cycle	1	2	3	4	5	6	7	8	9	10	11
Testing Date	Aug. 21			Aug. 24							
Target displacement (in.)	---	---	1.2 ¹⁾	1.5	2.25	3.0	4.5	6.0	9.0	12.0	--- ²⁾
Target load (kips)	60	110	160	---	---	---	---	---	---	---	---
Number of cycles ²⁾	2			3 ³⁾							---

1) Secondary displacement control value

2) Keep pushing until the system failed

3) Two cycles of loading followed by one reduced displacement cycle

Table 4-6 Recalculated ductility for System Test 2

Cycle	Nominal Ductility	Recalculated Ductility
4	1.0	0.7
5	1.5	1.0
6	2	1.3
7	3	2.0
8	4	2.6
9	6	3.9
10	8	5.2

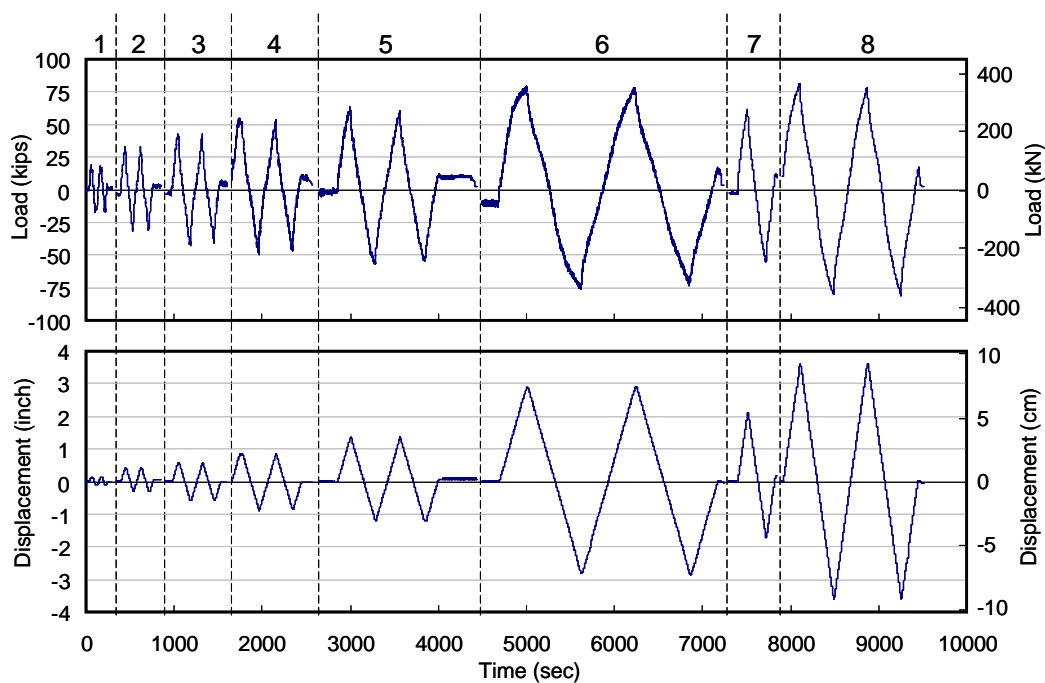


Figure 4-1 Applied load and displacement at the pile top for Single Pile Test 1

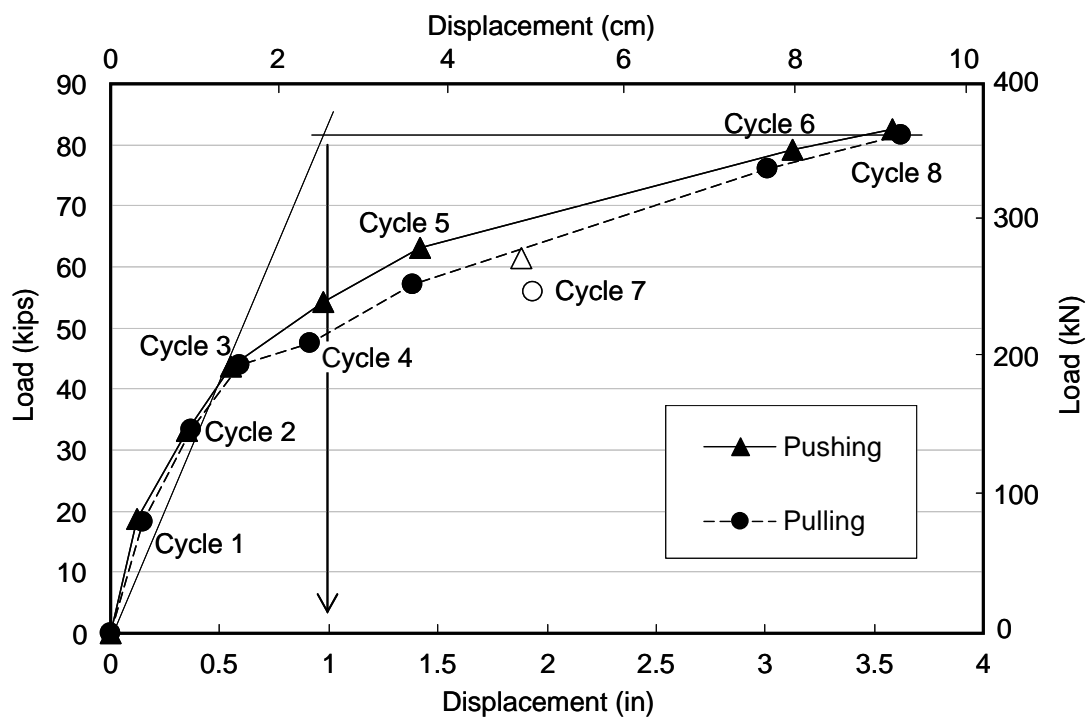


Figure 4-2 Pile top force vs. displacement envelopes (Single Pile Test 1)

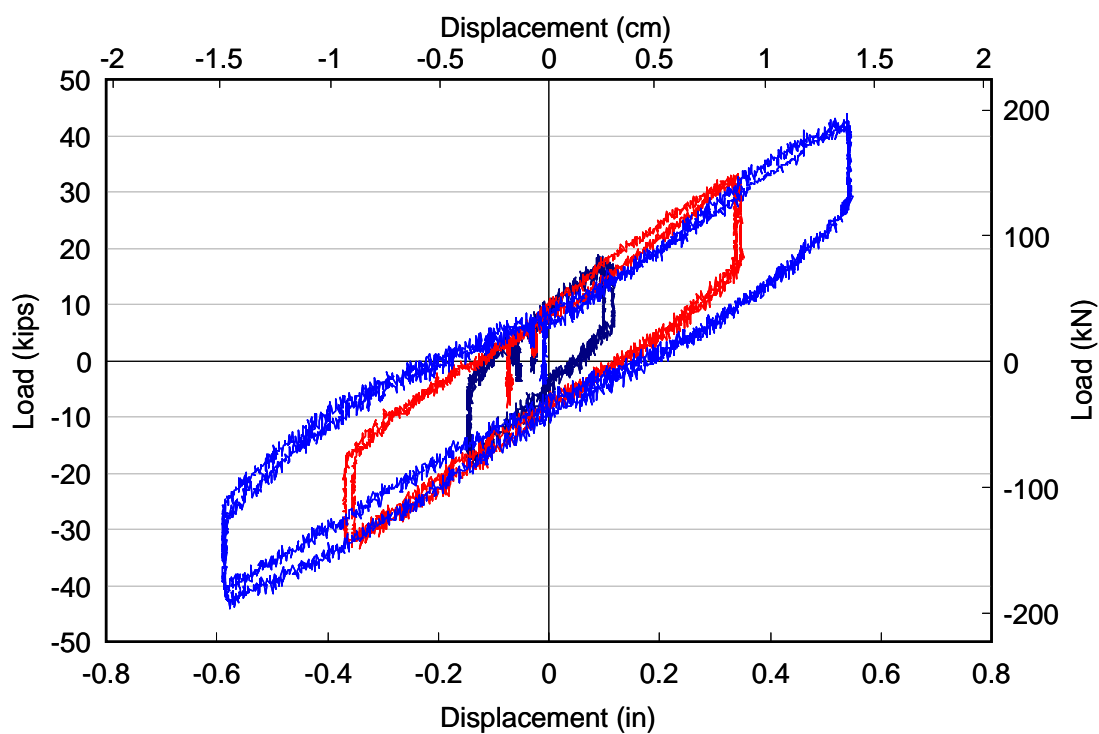


Figure 4-3 Hysteretic loops for Cycles 1 through 5 (Single Pile Test 1)

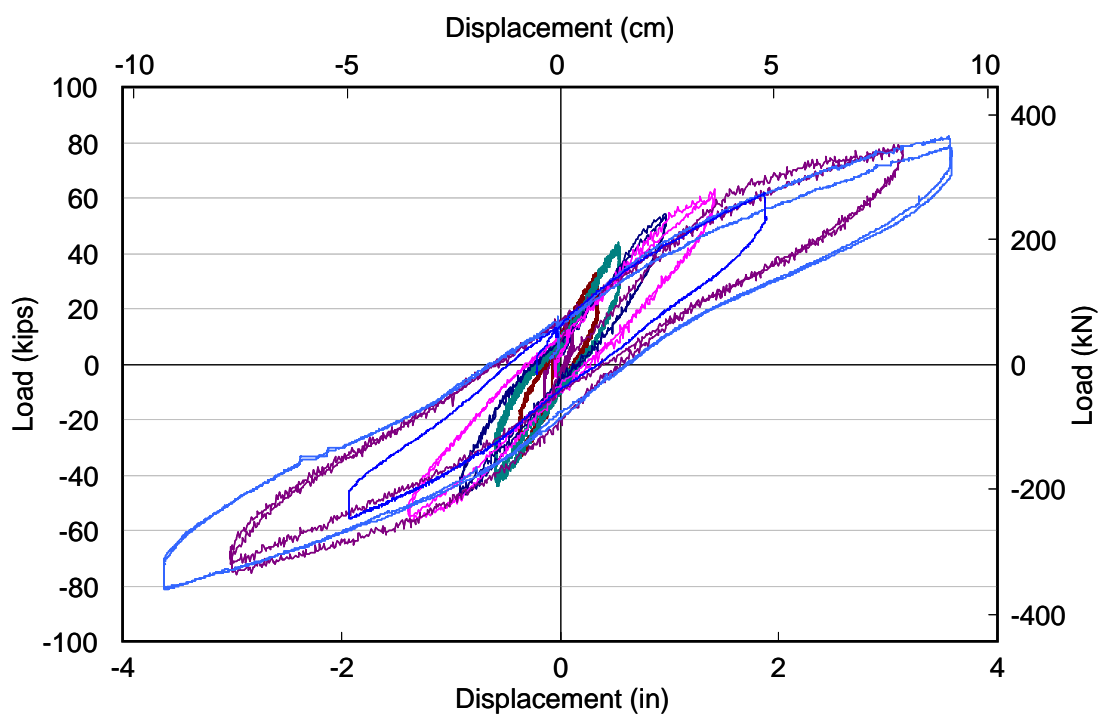


Figure 4-4 Hysteretic loops for all the loadings (Single Pile Test 1)

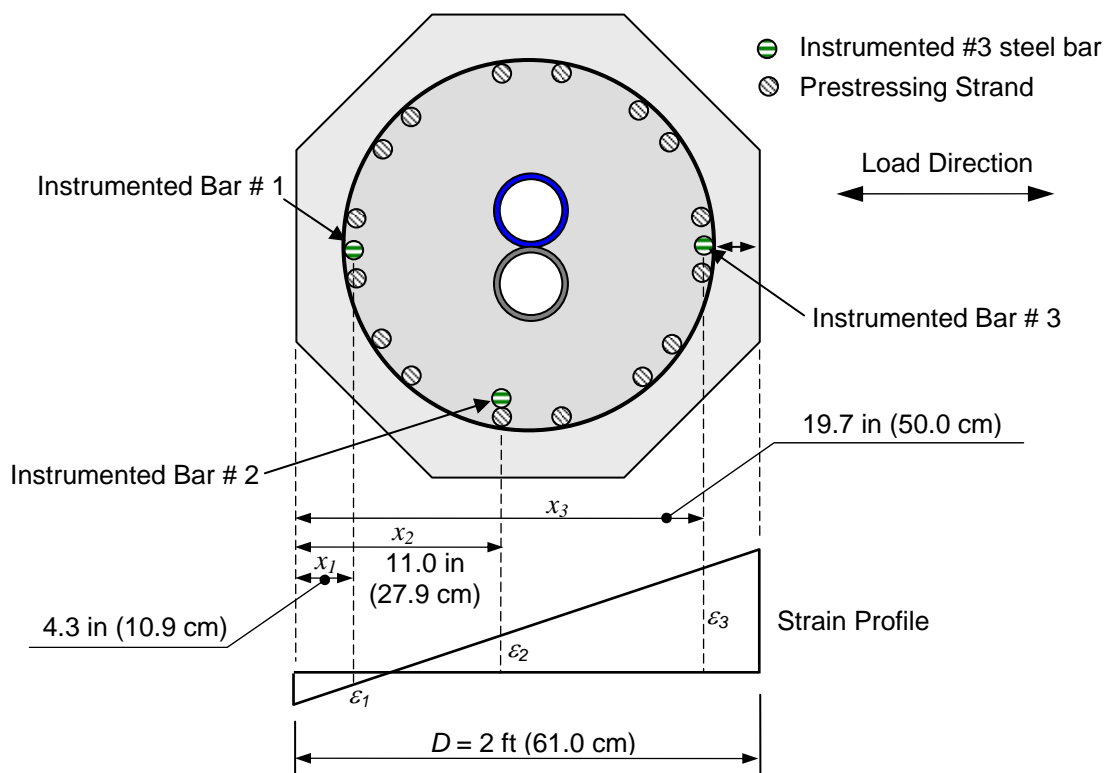


Figure 4-5 Strain distribution to be converted to curvature of the section

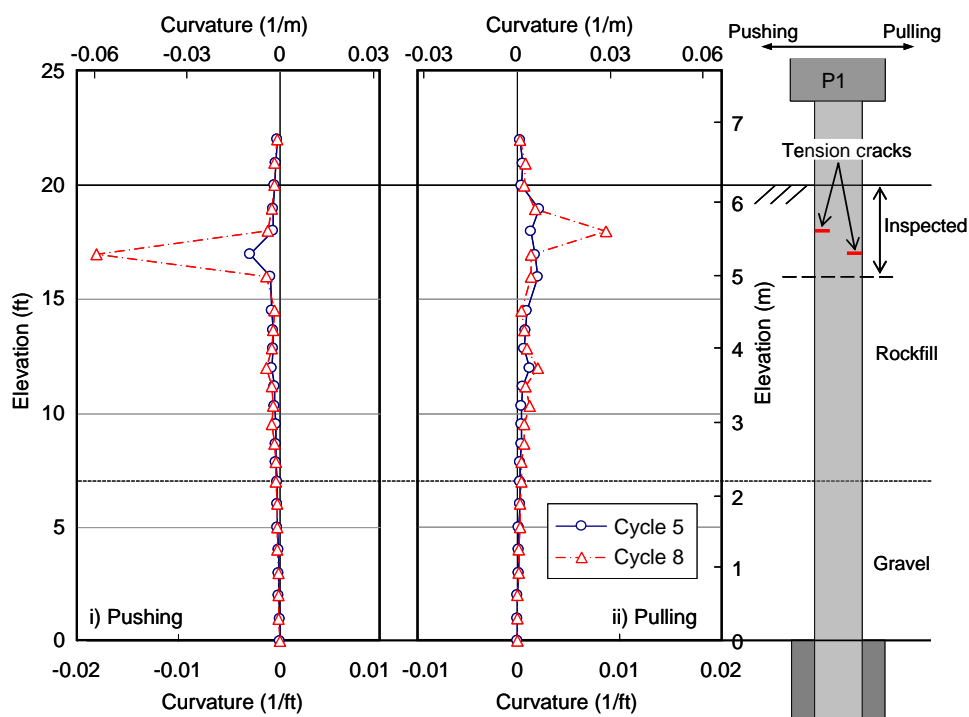


Figure 4-6 Profile of curvature derived from strain gage arrays (Single Pile Test 1)

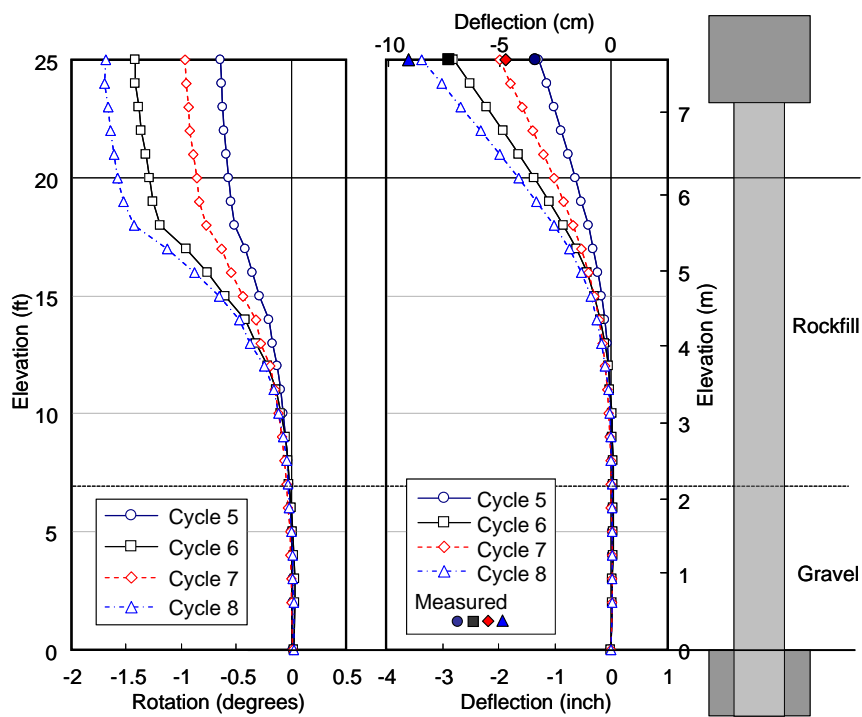


Figure 4-7 Profiles of rotation and deflection derived from tiltmeter readings (Single Pile Test 1)



Figure 4-8 Visual inspection of in-ground parts of test pile (Single Pile Test 1)

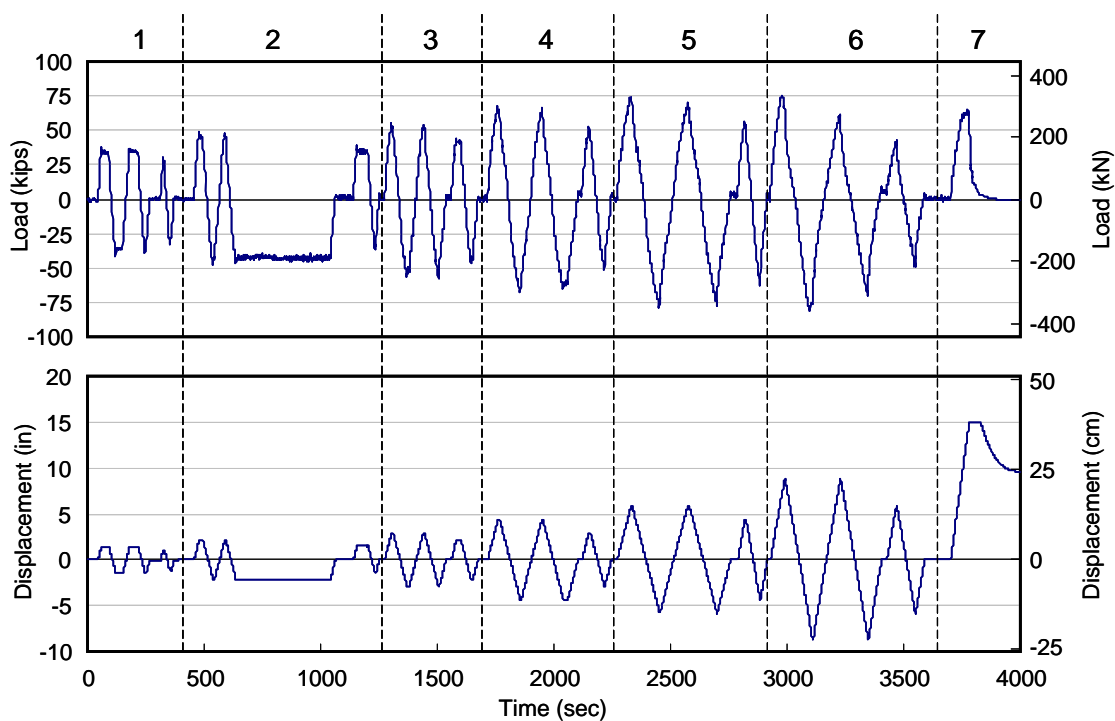


Figure 4-9 Applied load and displacement at the pile top for Single Pile Test 2

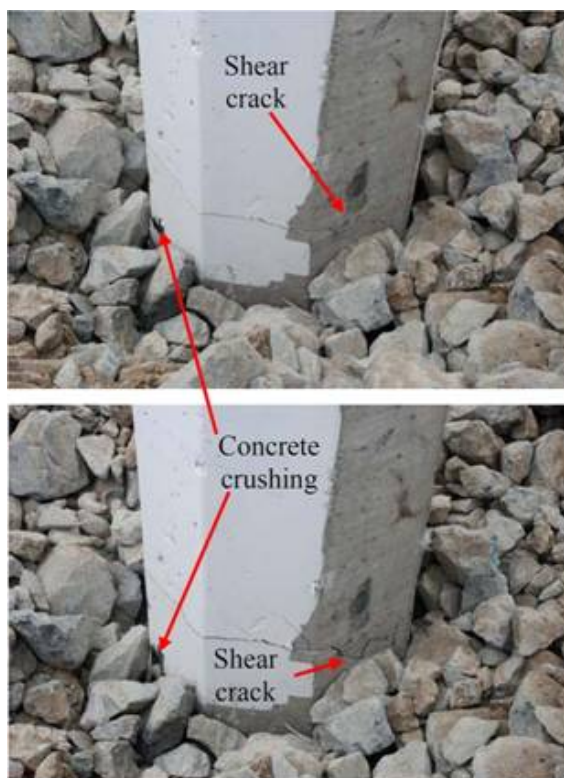


Figure 4-10 Details of the observed damage (Single Pile Test 2)



Figure 4-11 Deformed test pile after all the loading (Single Pile Test 2)

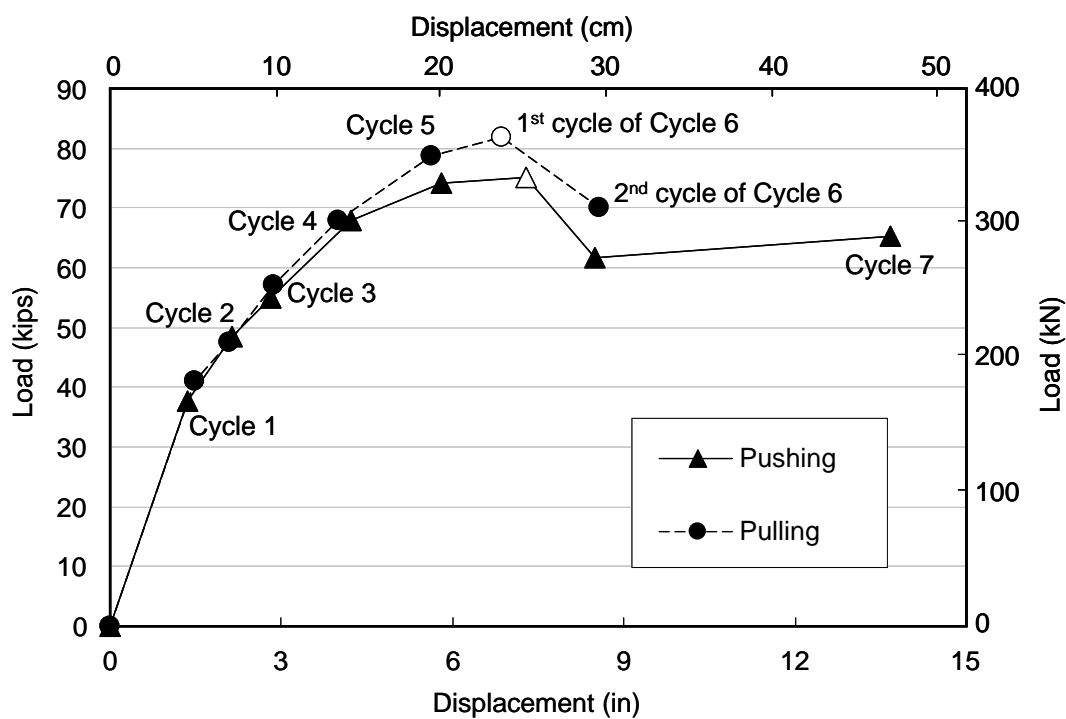


Figure 4-12 Peak lateral load and corresponding displacement at any loading cycles (Single Pile Test 2)

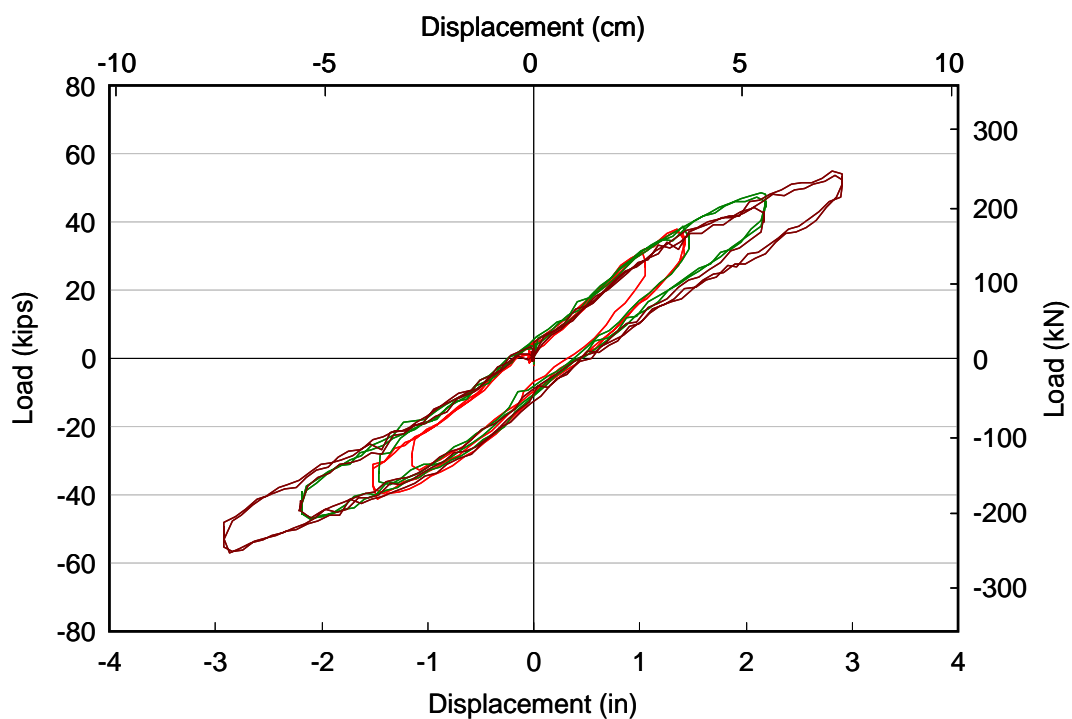


Figure 4-13 Hysteretic loops for Cycles 1 through 3 (Single Pile Test 2)

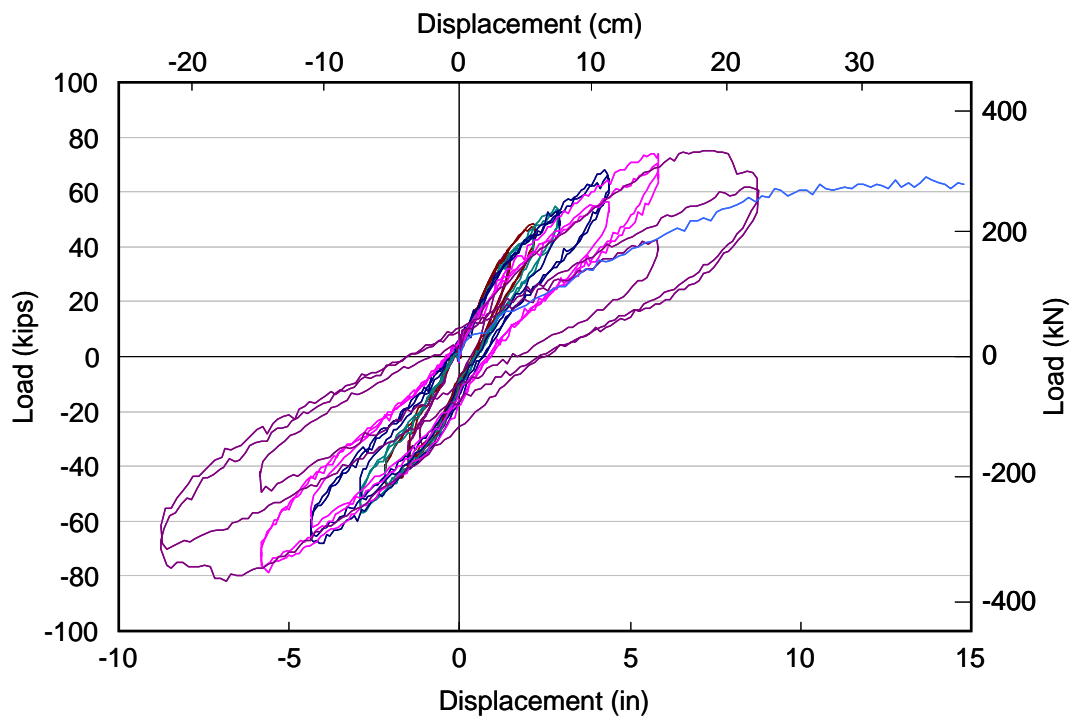


Figure 4-14 Hysteretic loops for Cycles 4 through 7 (Single Pile Test 2)

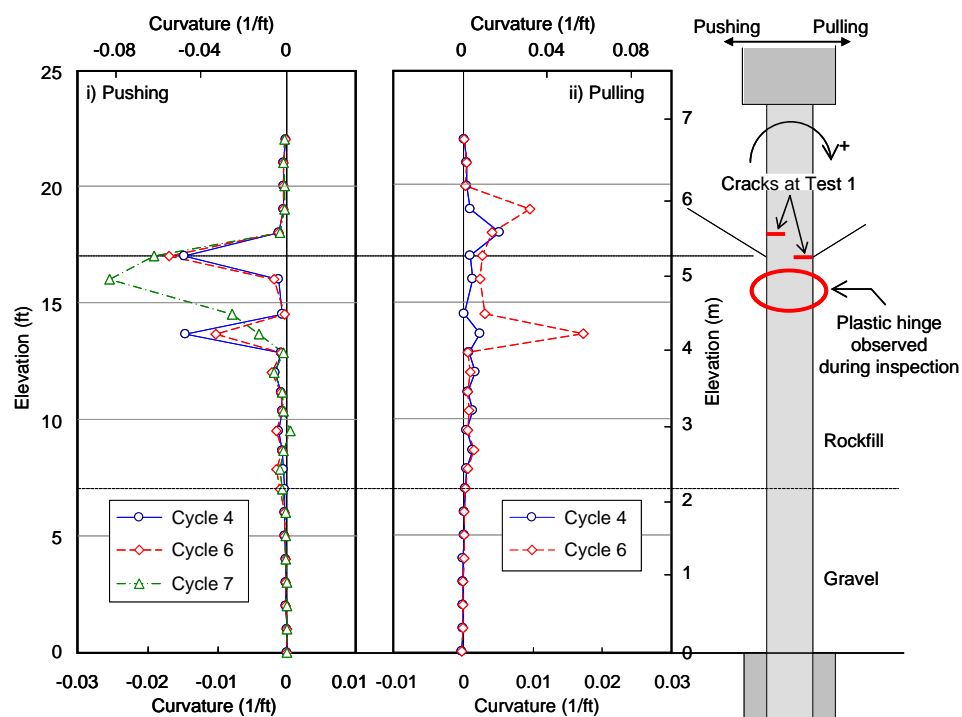


Figure 4-15 Curvature profile derived from array of strain gages (Single Pile Test 2)

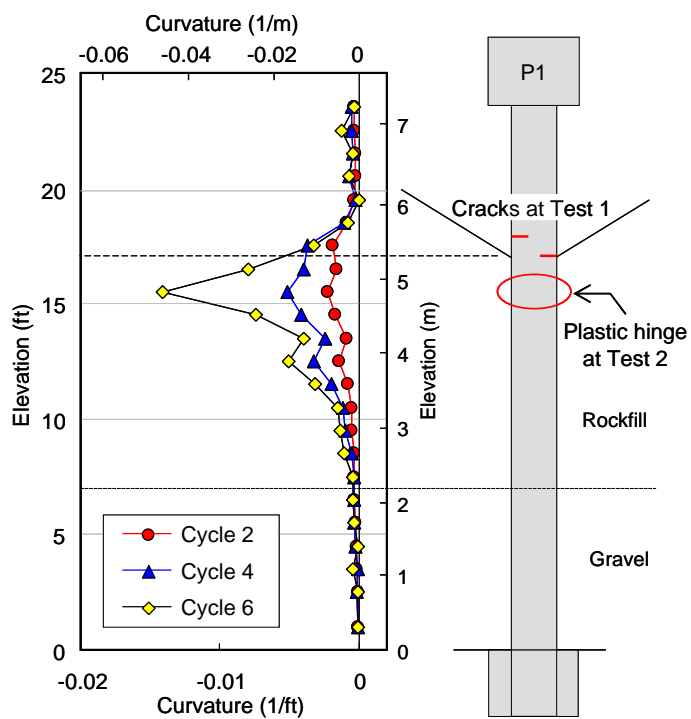


Figure 4-16 Curvature profile derived from records on tiltmeters (Single Pile Test 2)

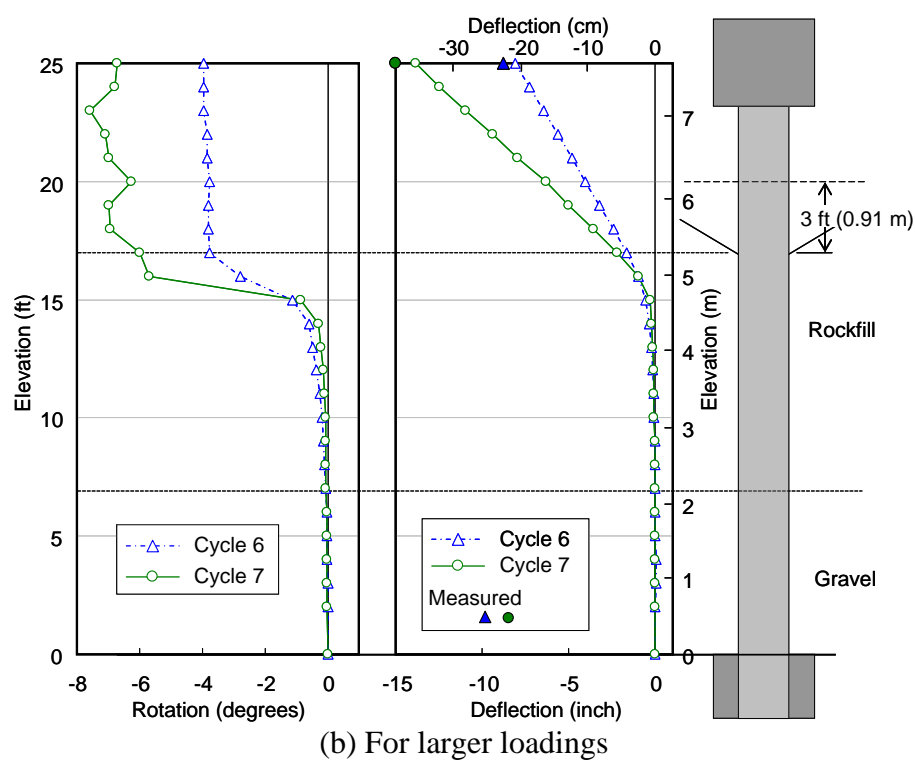
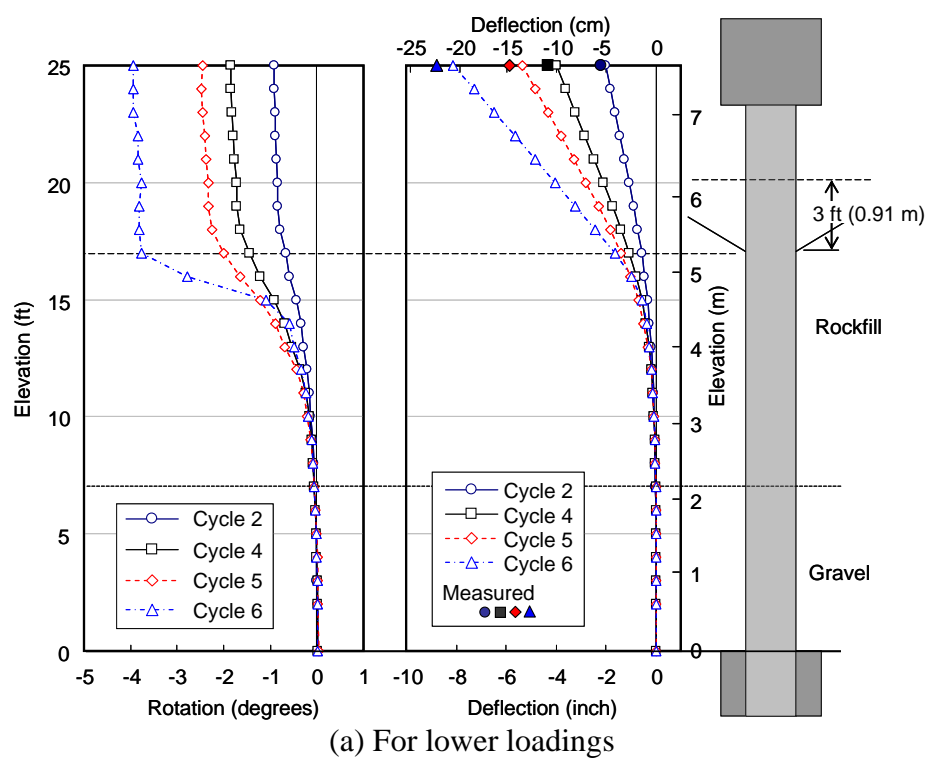


Figure 4-17 Profiles of rotation and deflection derived from rotation (Single Pile Test 2)



Figure 4-18 General view after excavation to 3ft below ground surface (Single Pile Test 2)



Figure 4-19 Exposed in-ground plastic hinge on the north side of the pile (Single Pile Test 2)

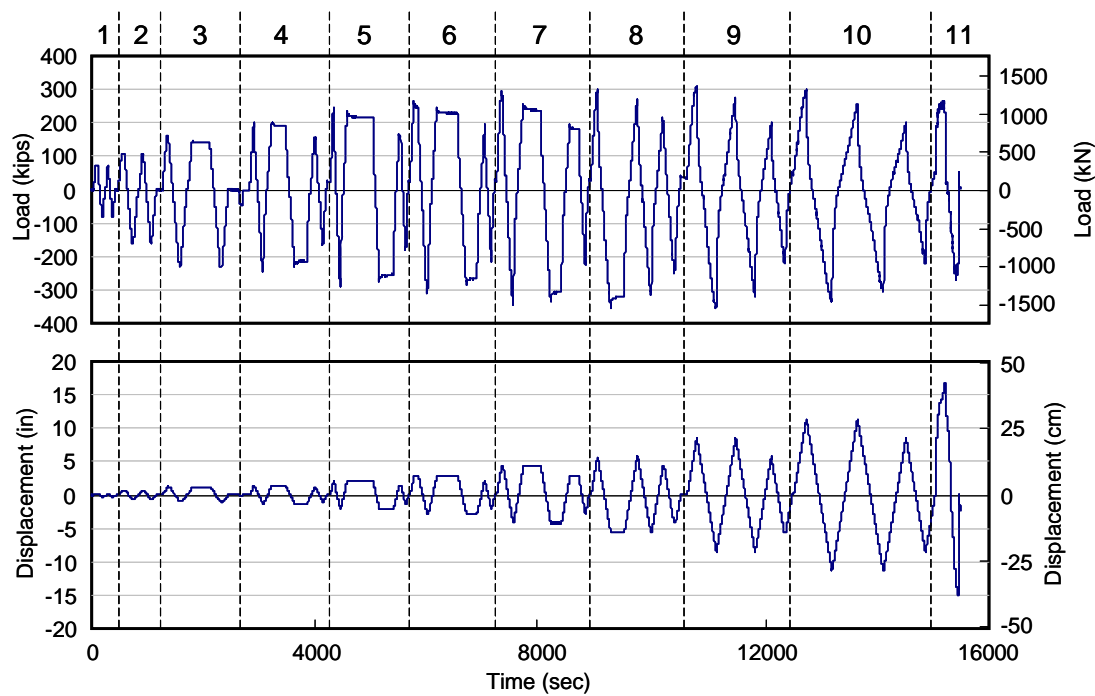


Figure 4-20 Applied load and displacement at the pile top for System Test 1

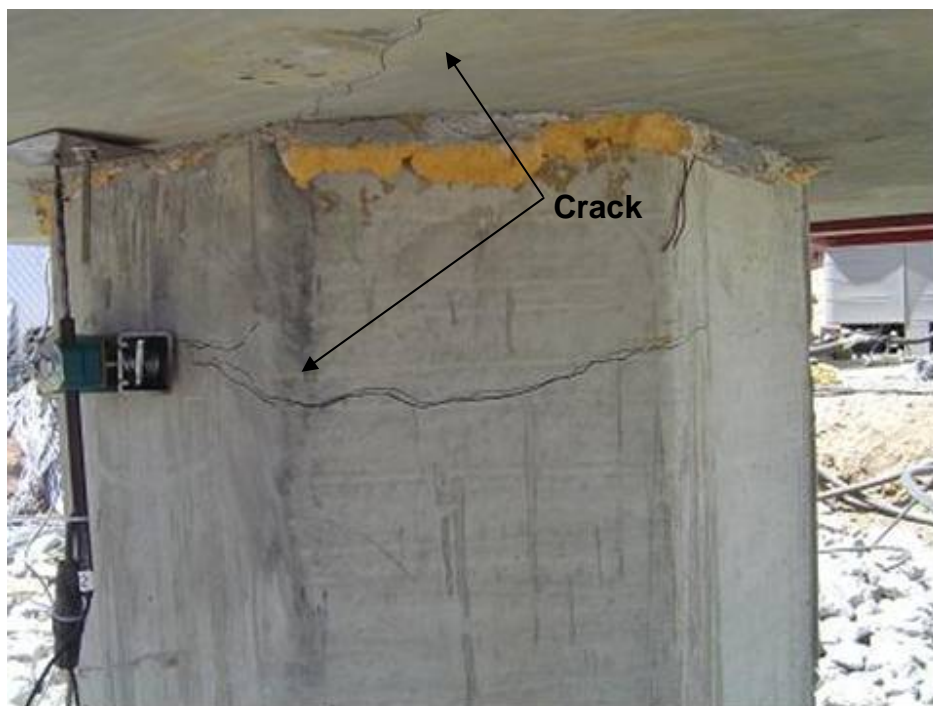


Figure 4-21 Cracks at P3 for loading Cycle 3 (System Test 1)



Figure 4-22 Concrete crushing during Cycle 8 at P3 (System Test 1)



Figure 4-23 Settlement around the test pile (System Test 1)



Figure 4-24 Deformed piles after the final loading (System Test 1)

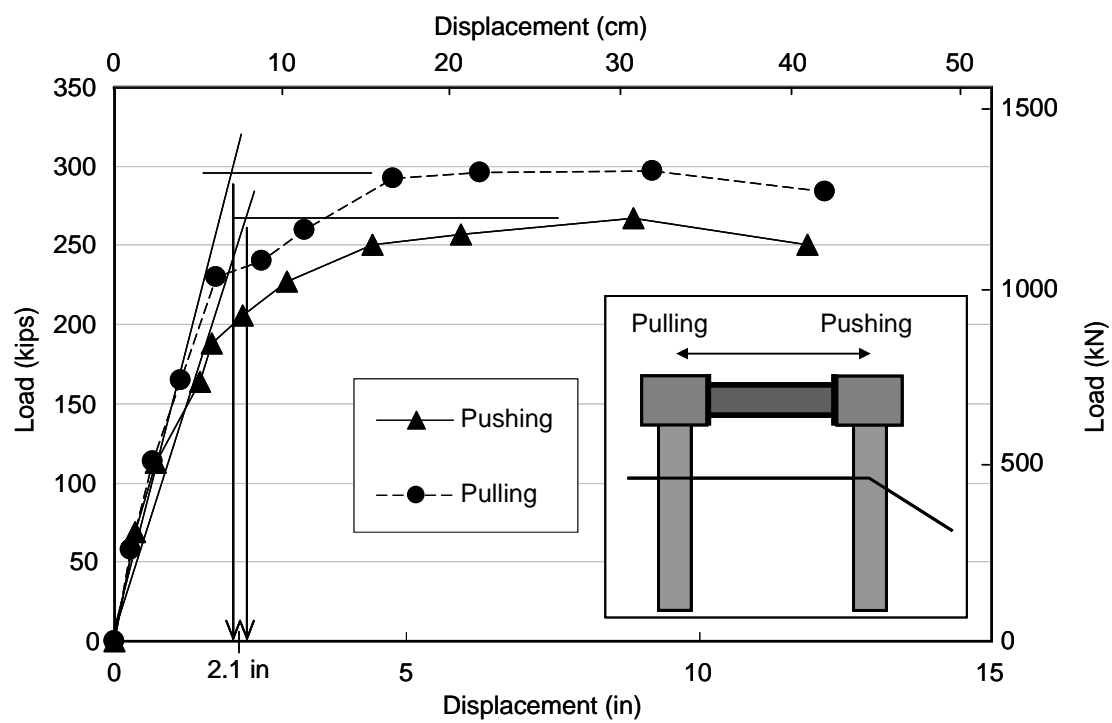


Figure 4-25 Load displacement envelopes (System Test 1)

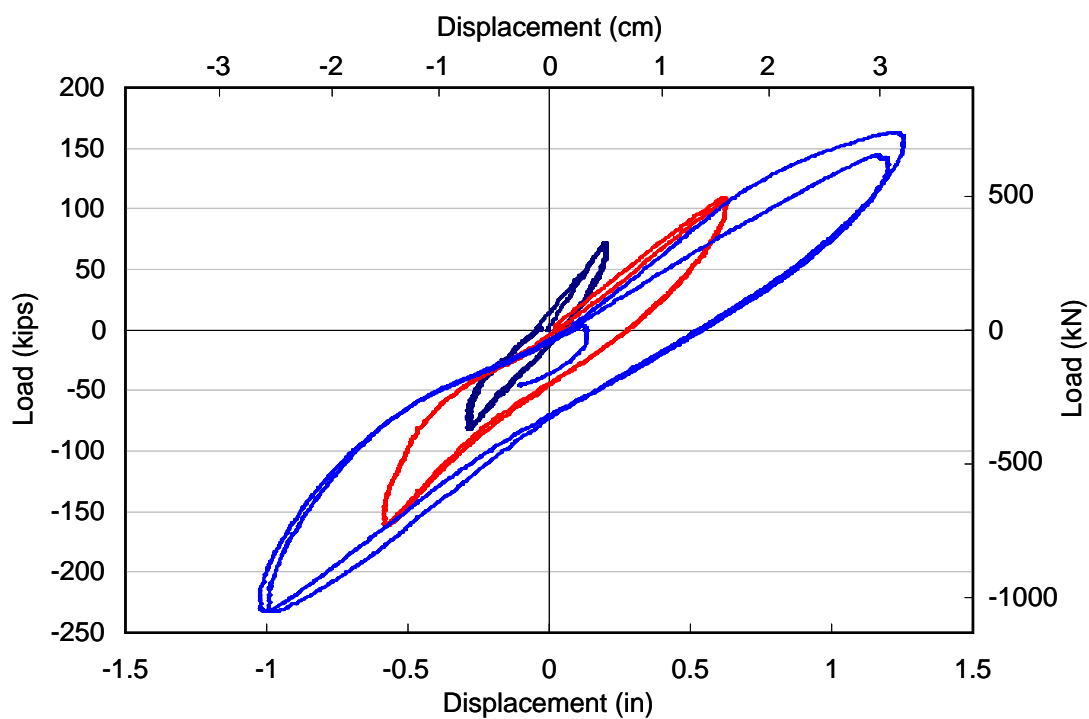


Figure 4-26 Hysteretic loops for Cycles 1 through 3 (System Test 1)

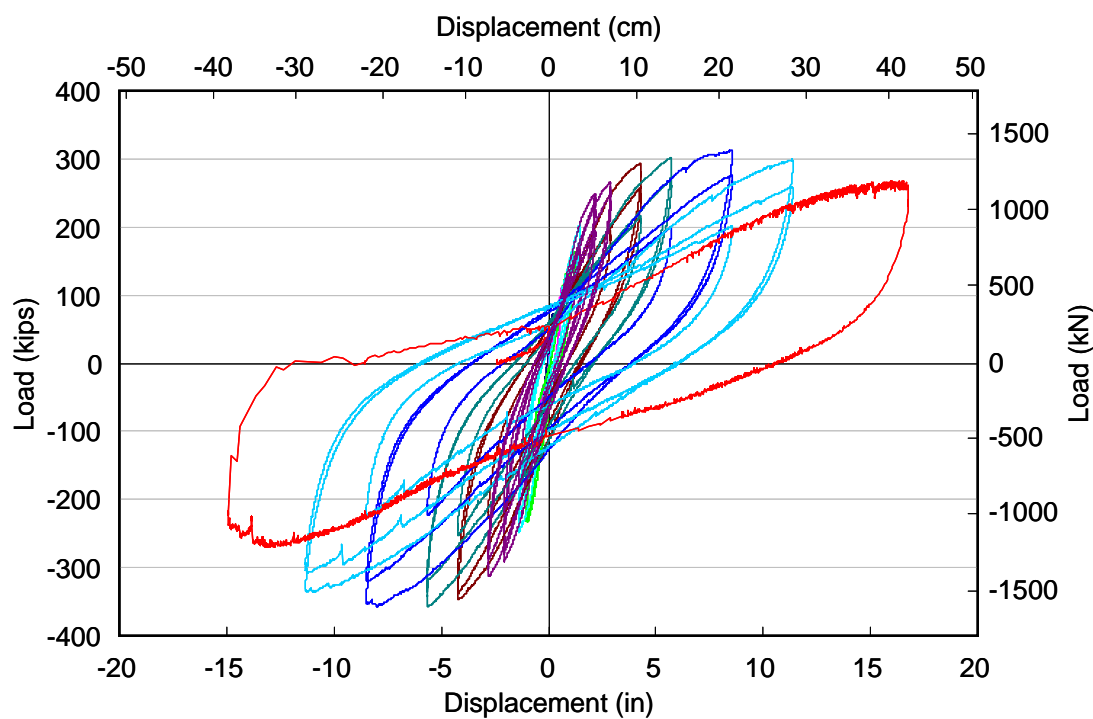


Figure 4-27 Hysteretic loops for all the loading cycles (System Test 1)

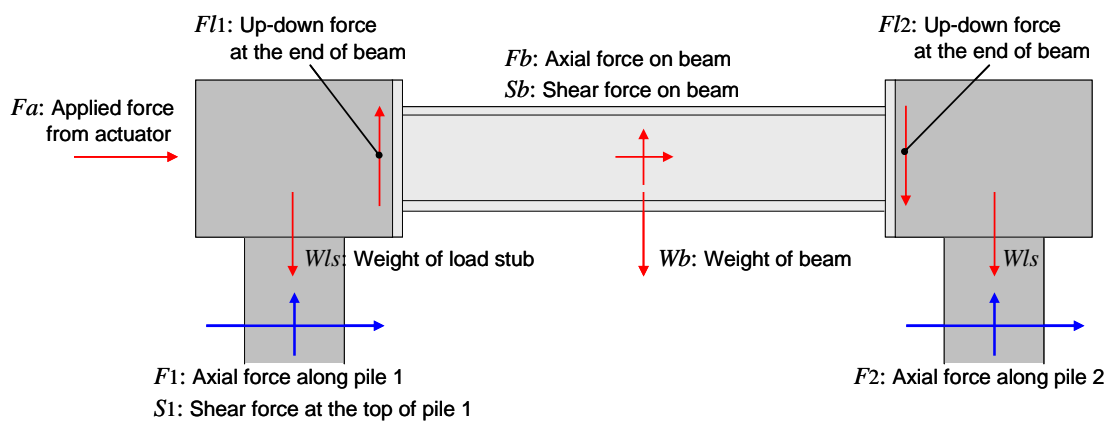


Figure 4-28 Free body diagram of the system tests

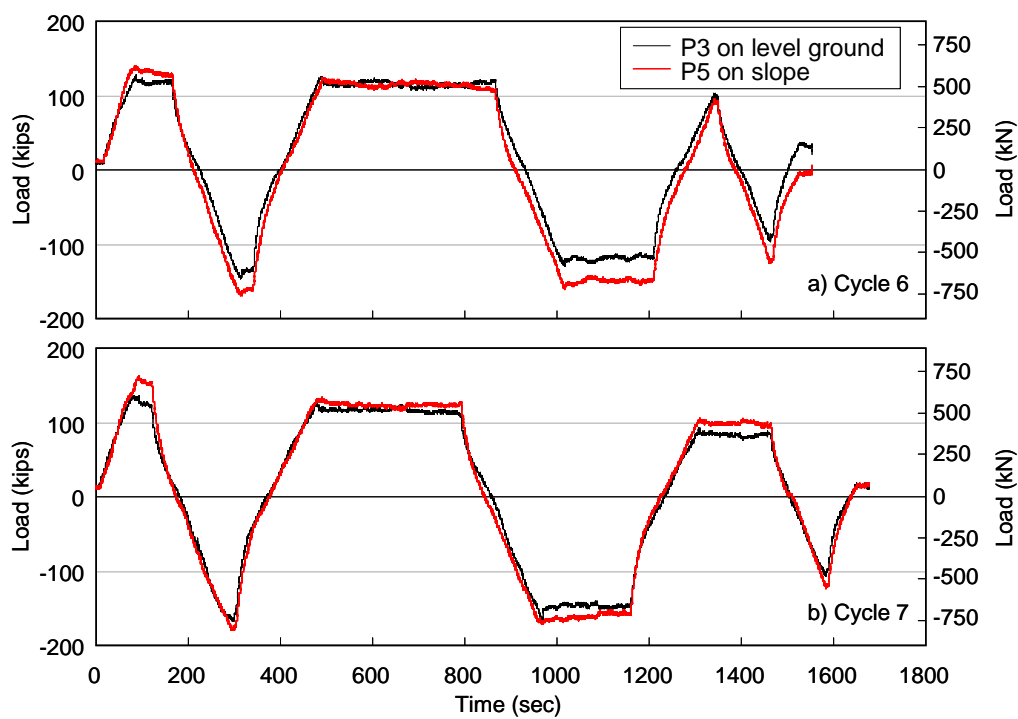


Figure 4-29 Time histories of shear load at each pile top (System Test 1)

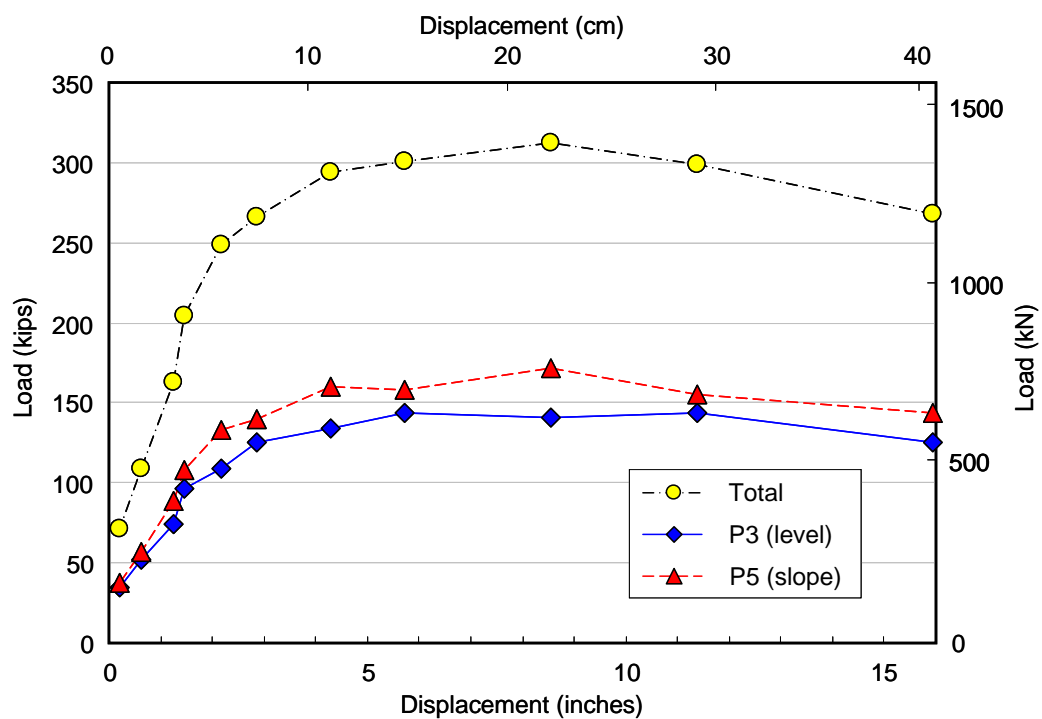


Figure 4-30 Distribution of the shear load (System Test 1, Push)

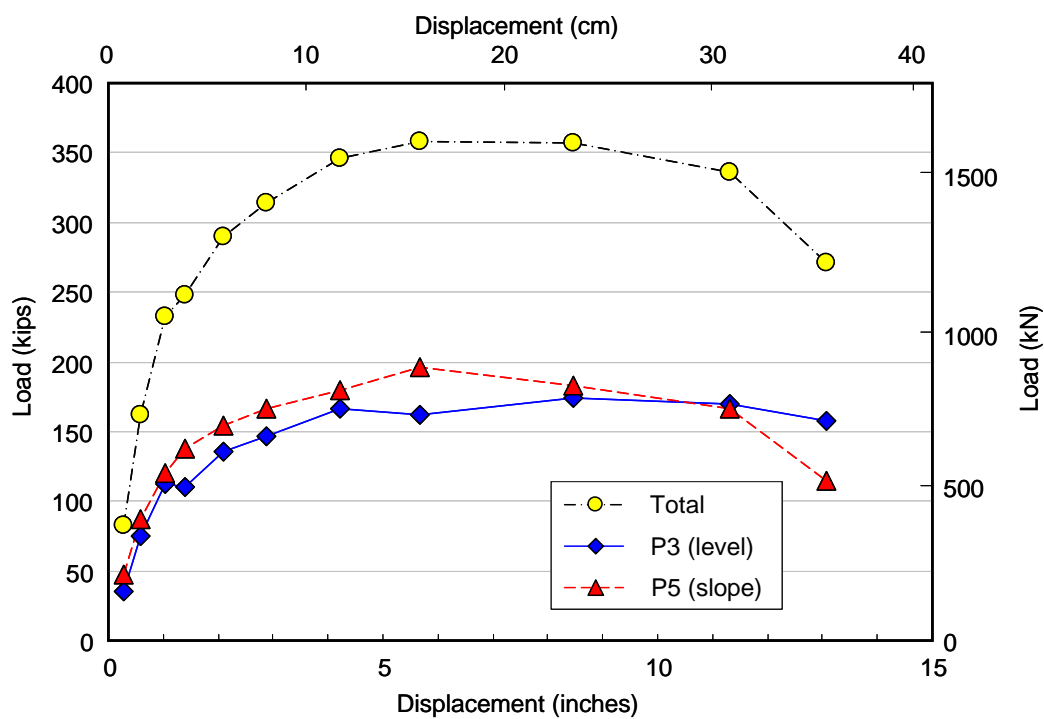


Figure 4-31 Distribution of the shear load (System Test 1, Pull)

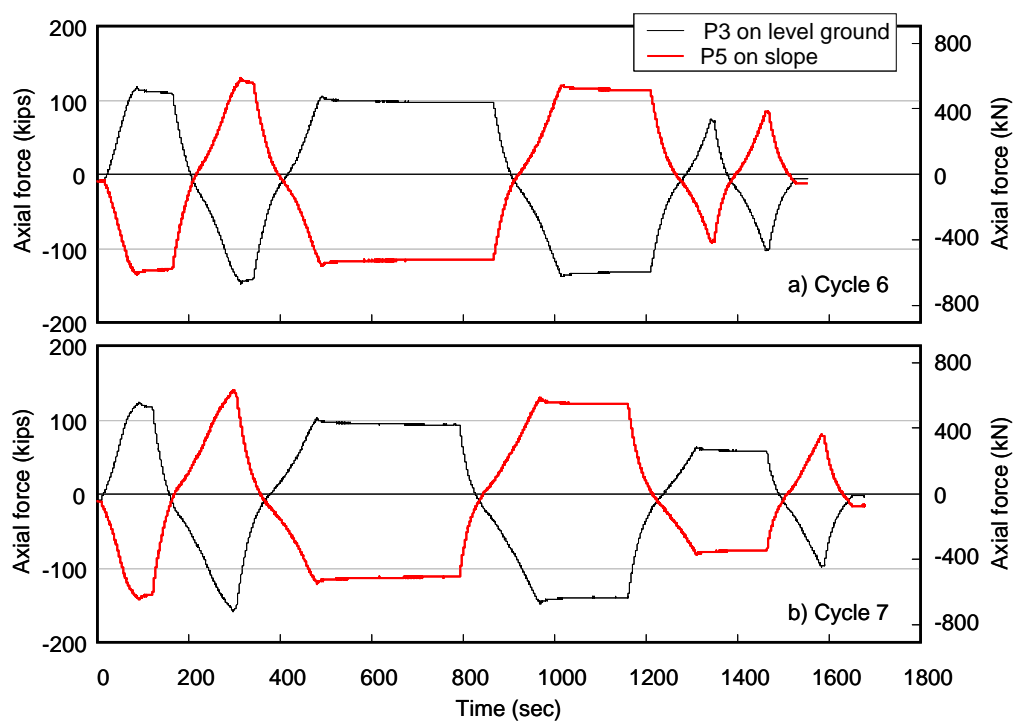


Figure 4-32 Time histories of axial load along each pile (System Test 1)

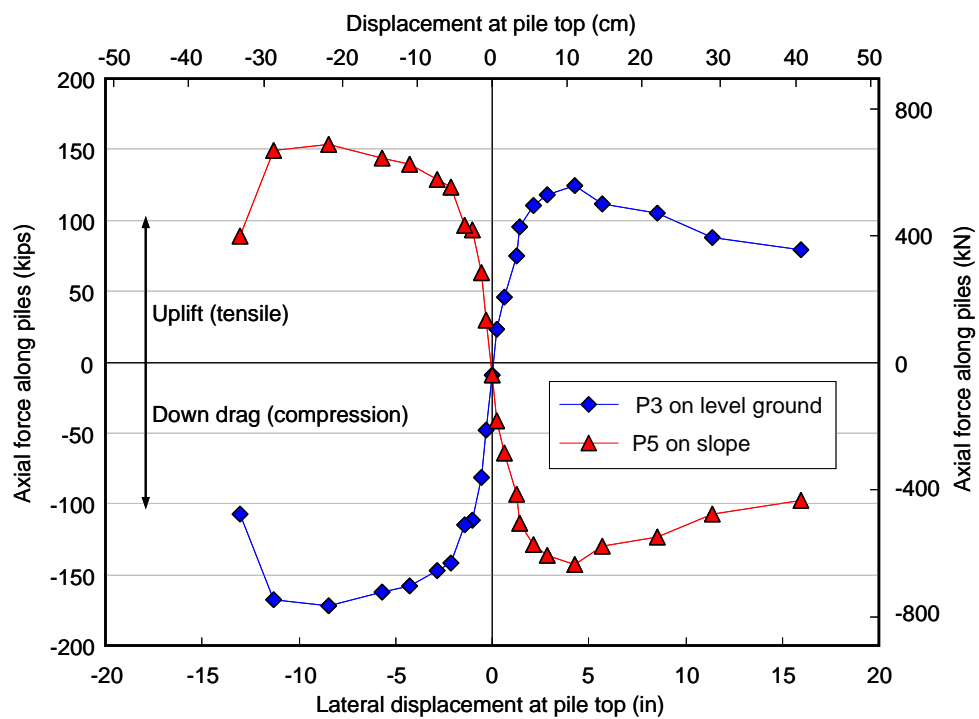
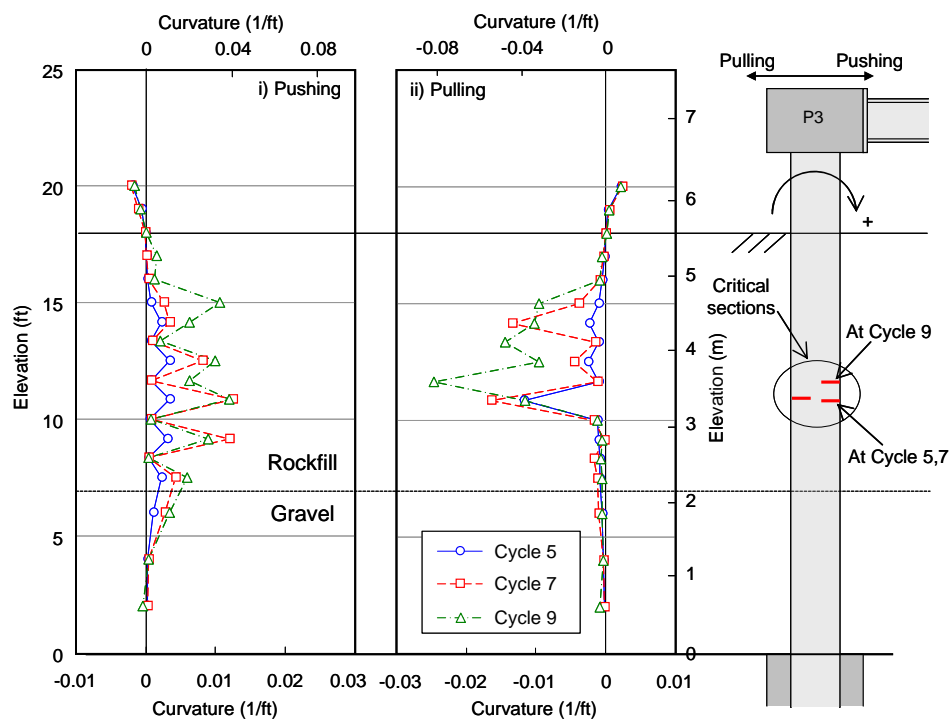
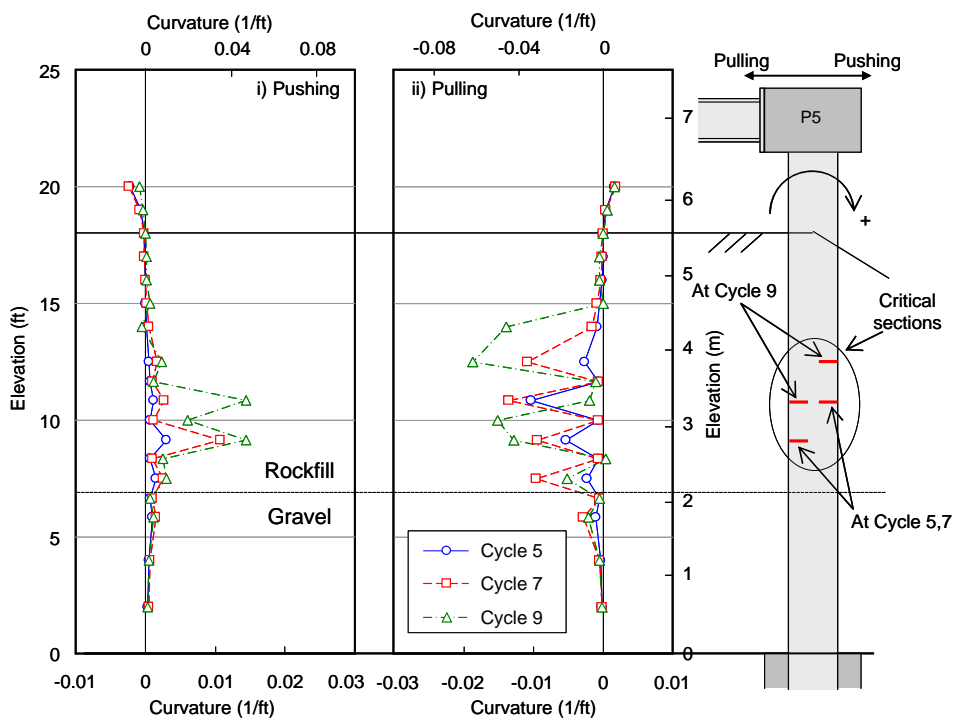


Figure 4-33 Axial force vs. displacement curves on each pile (System Test 1)



(a) P3 on level ground



(b) P5 at the dike crest

Figure 4-34 Profiles of curvature (System Test 1)

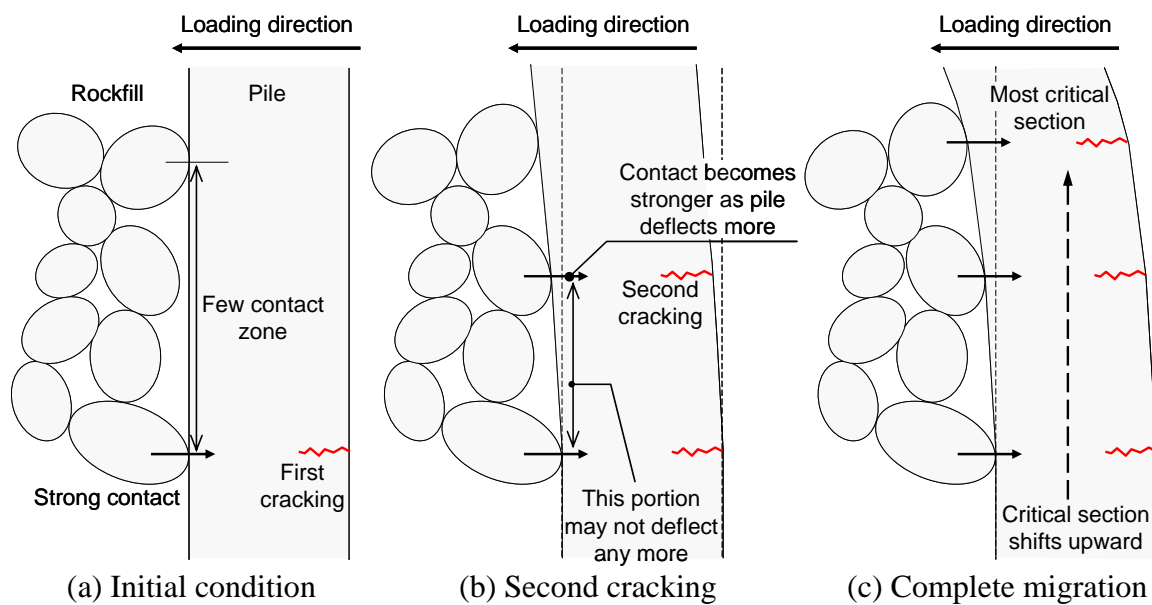
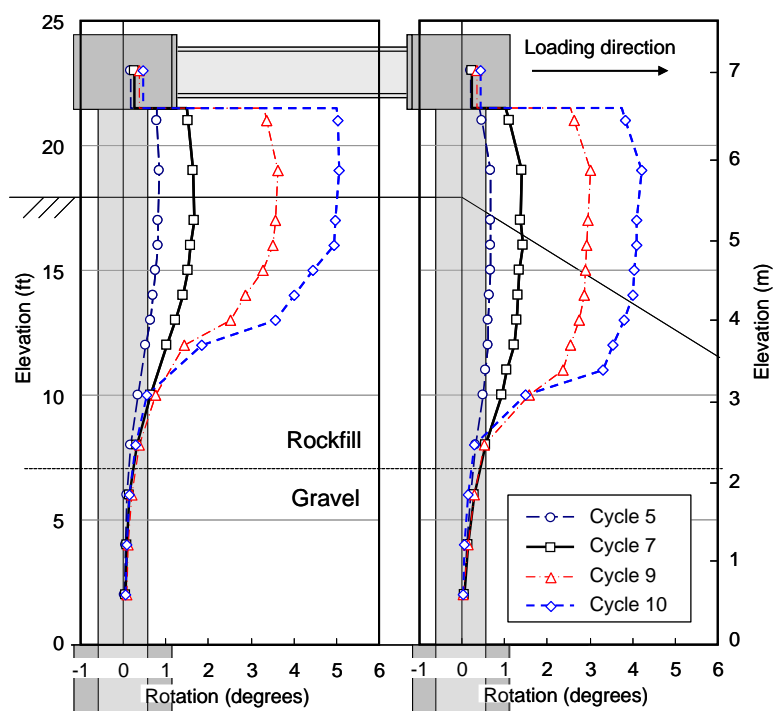
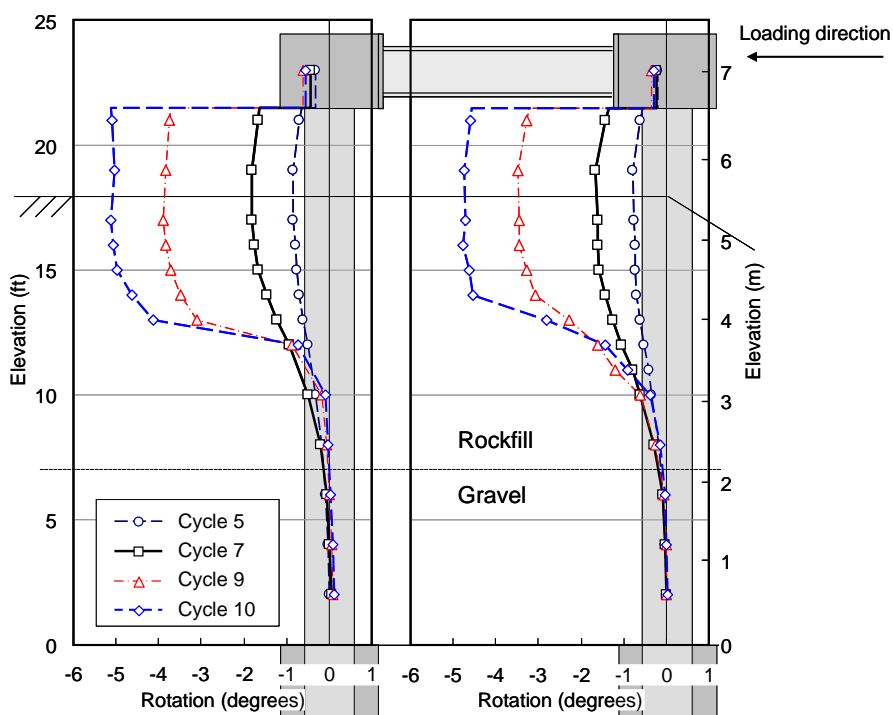


Figure 4-35 Possible mechanism of critical section migration



(a) Pushing toward the downslope



(b) Pulling toward the reaction wall

Figure 4-36 Profiles of rotation (System Test 1)

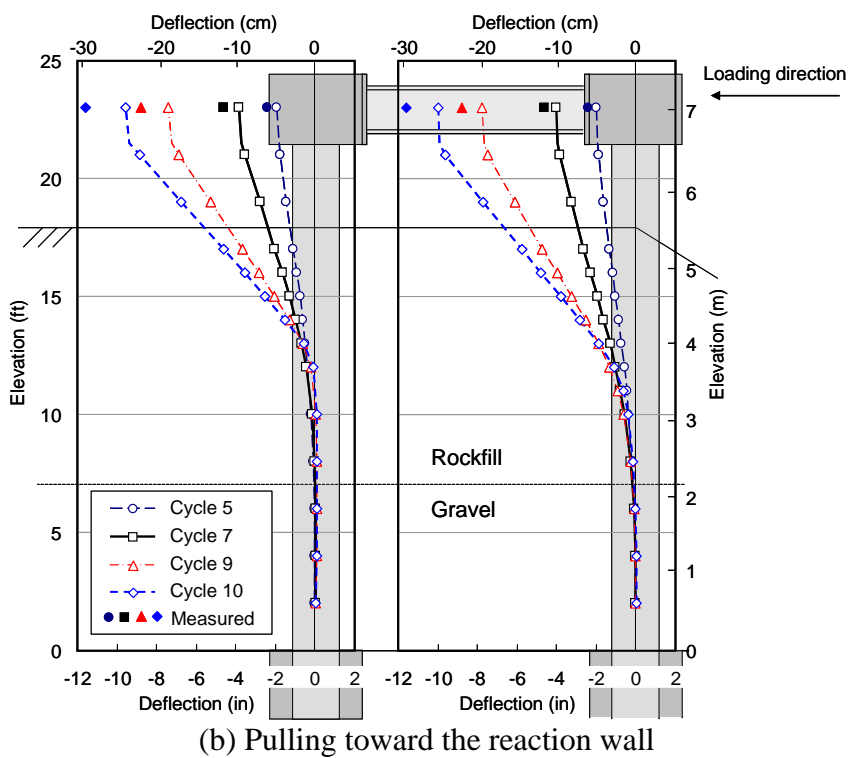
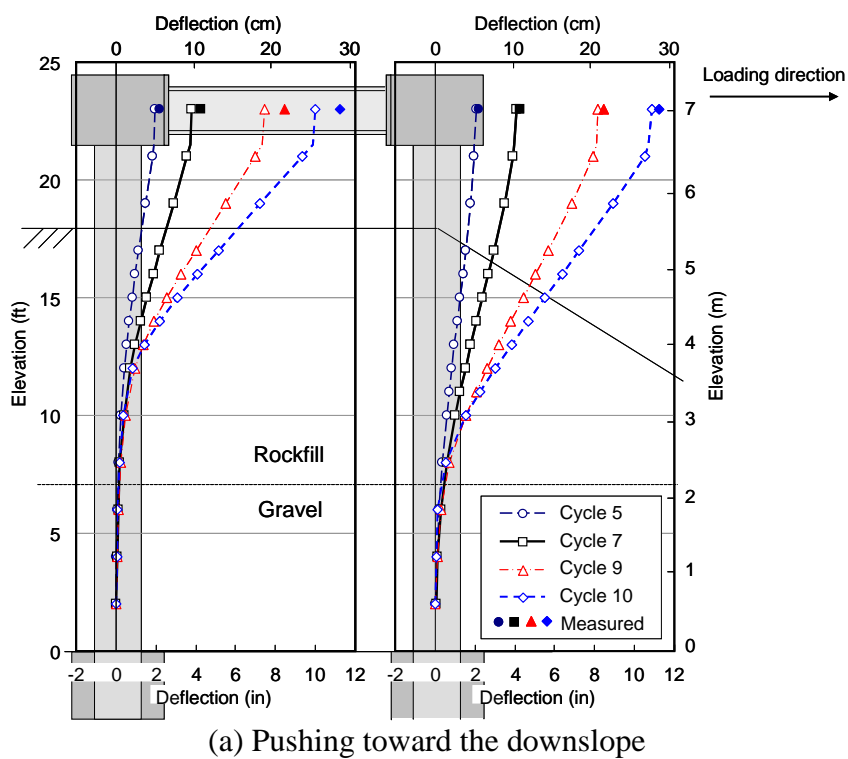


Figure 4-37 Profiles of deflection derived from rotation (System Test 1)

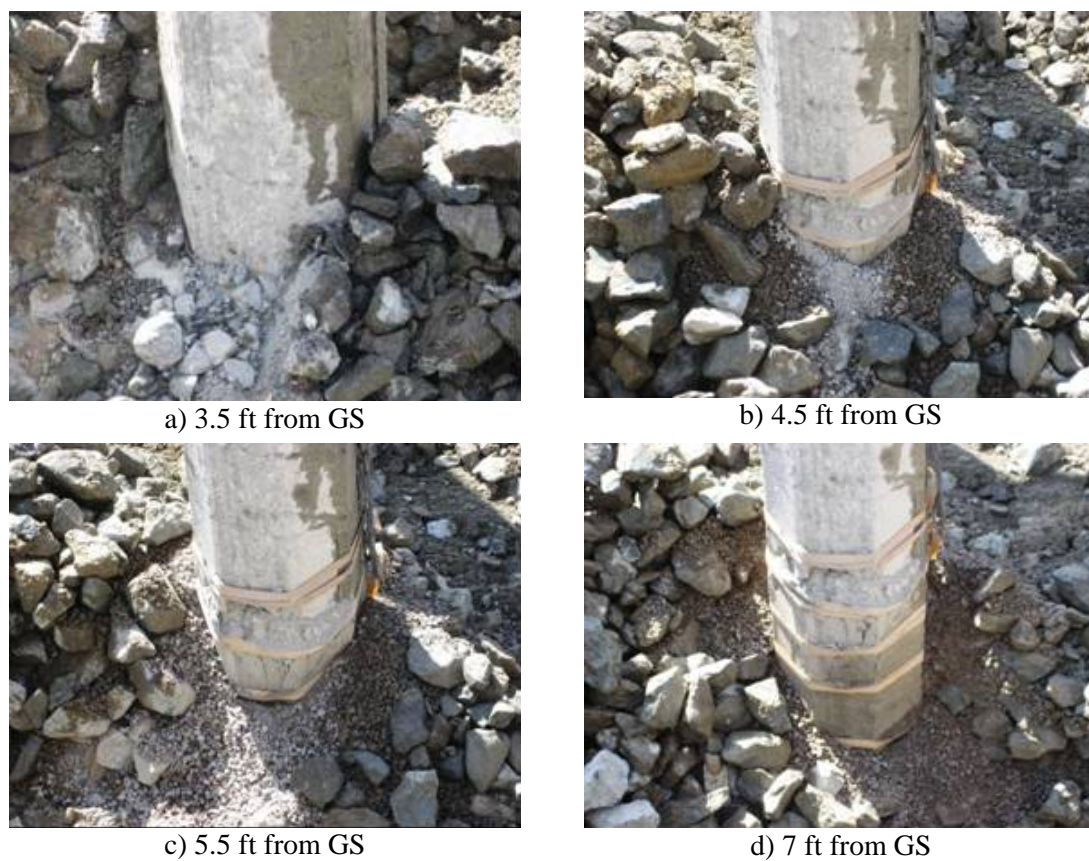


Figure 4-38 Excavation sequence at the north side (System test 1, P3)

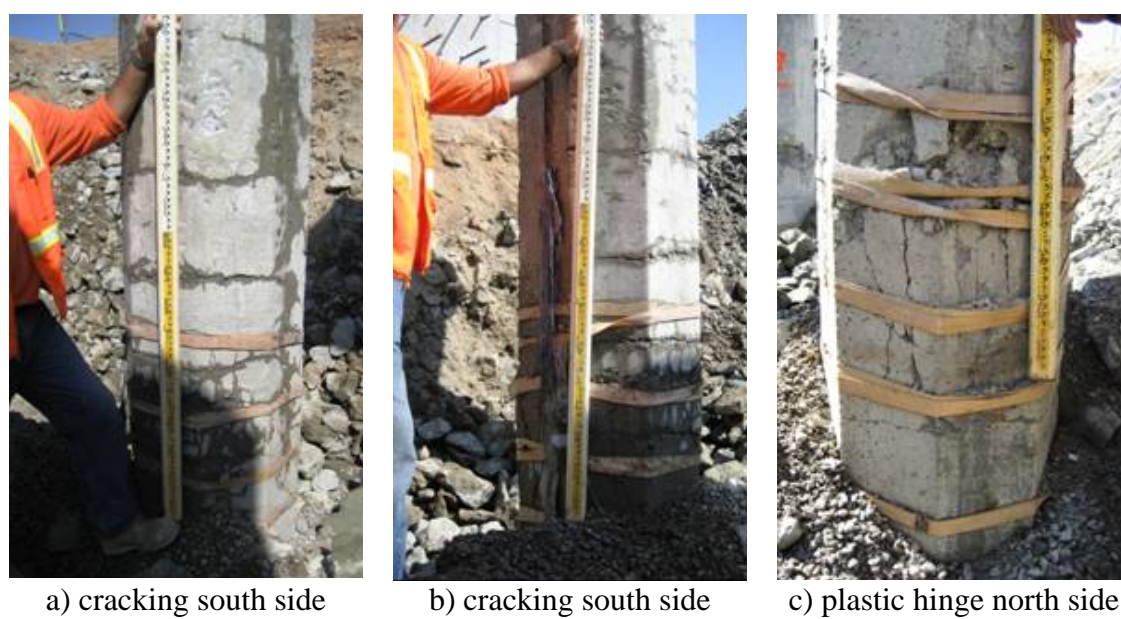


Figure 4-39 Pile inspection during demolition of the piles (System Test 1, P3)



Figure 4-40 Plastic hinge (System Test 1, P3)

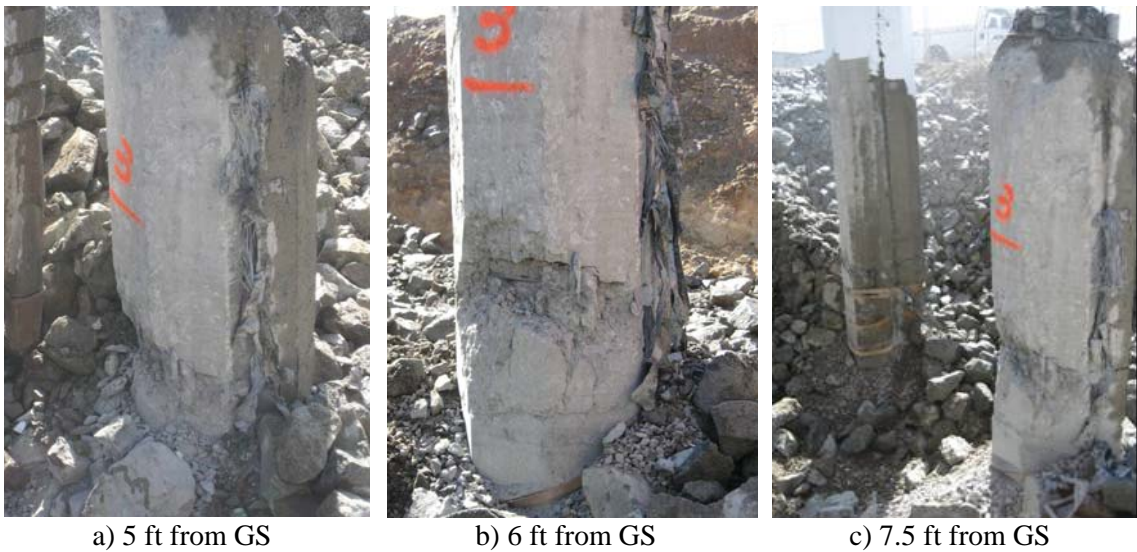


Figure 4-41 Excavation sequence on the north side (System Test 1, P5)

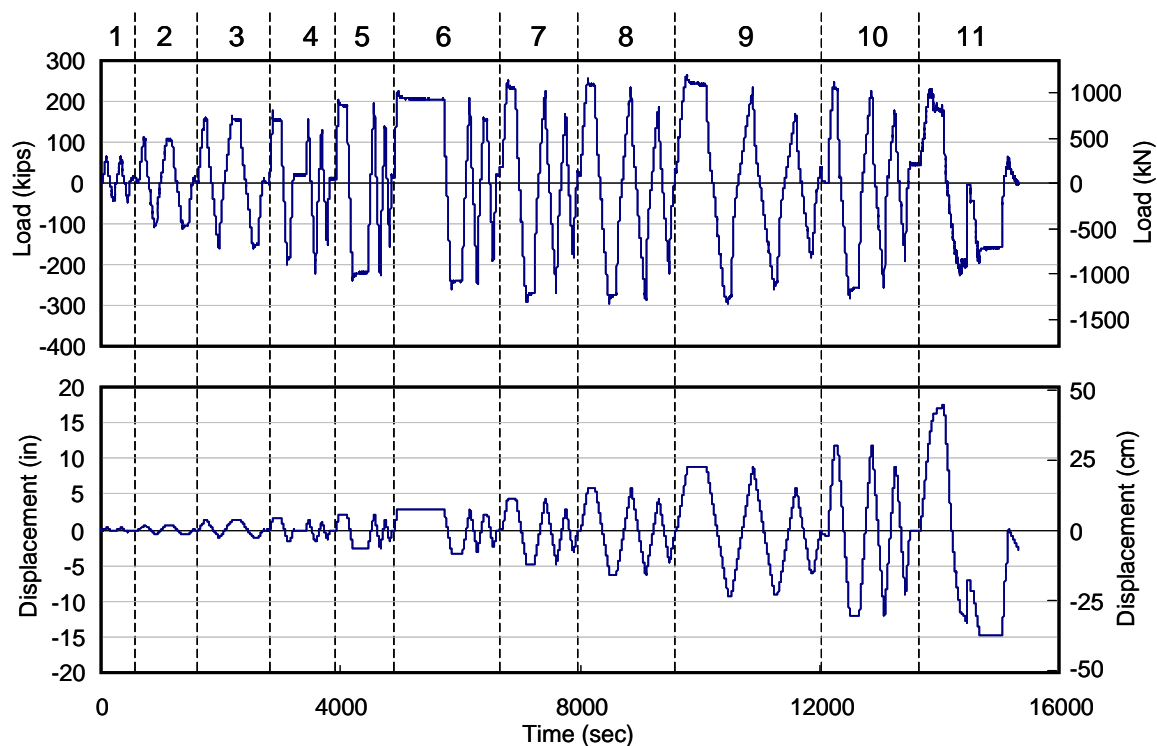


Figure 4-42 Applied load and displacement at the pile top for System Test 2



Figure 4-43 Cracks on P2 and P4 for loading Cycles 1 to 3 (System Test 2)



Figure 4-44 Cracks on P2 and P4 for loading Cycle 6 (System Test 2)



Figure 4-45 Settlement of rockfill around P2 and P4 after Cycle 8 (System Test 2)



Figure 4-46 Spalling at connection of P4 at Cycle 10 (System Test 2)



Figure 4-47 Deformed test piles after the final loading Cycle 11 (System Test 2)

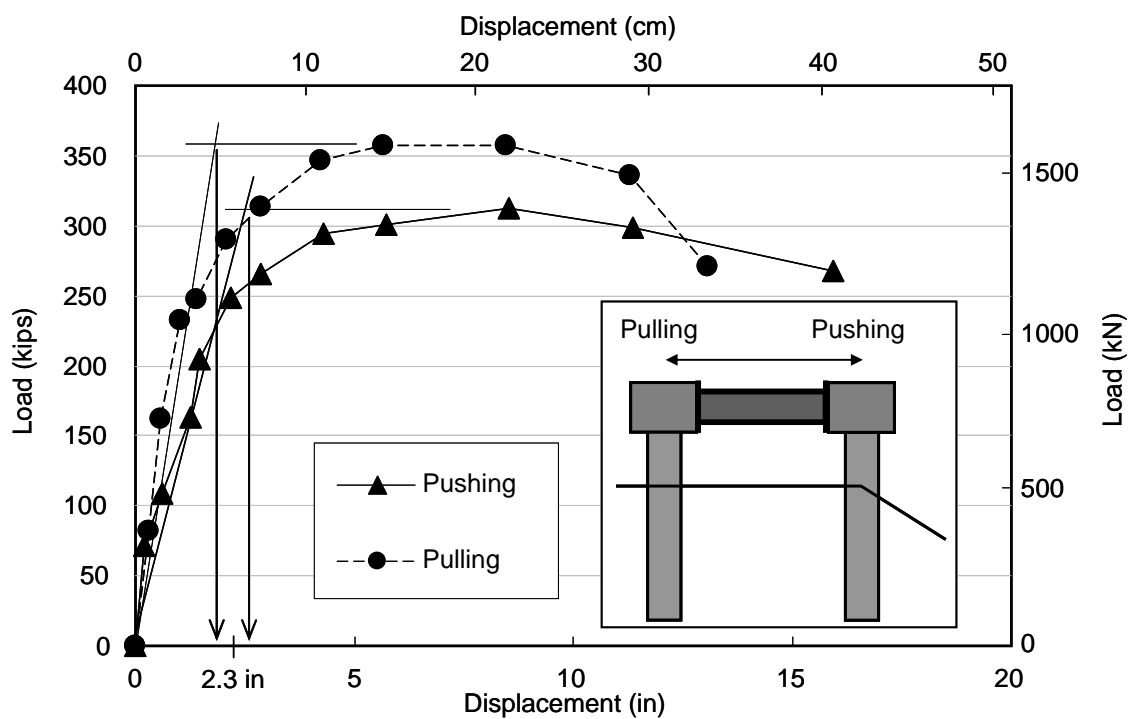


Figure 4-48 Load displacement envelopes (System Test 2)

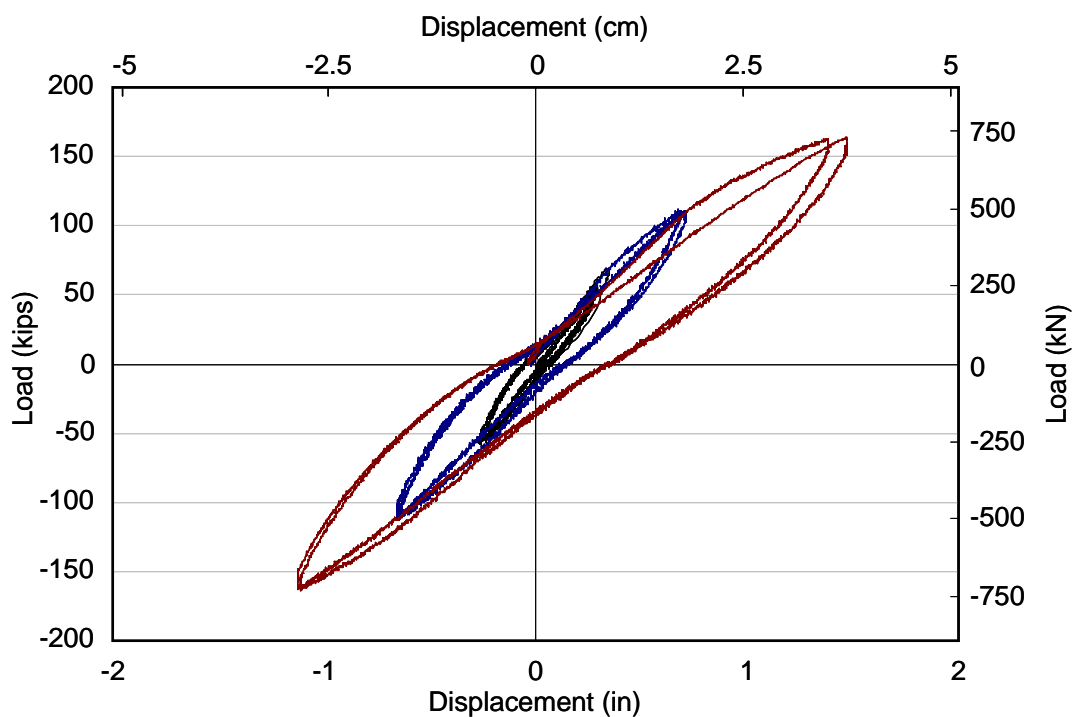


Figure 4-49 Hysteretic loops for Cycles 1 through 3 (System Test 2)

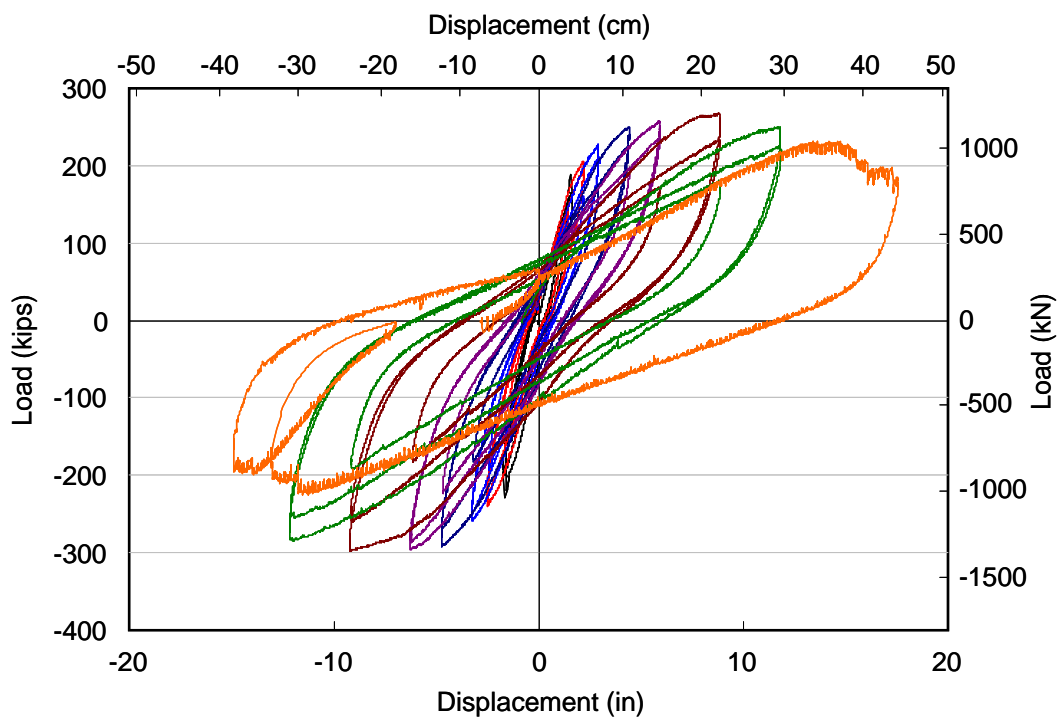


Figure 4-50 Hysteretic loops for all the loadings (System Test 2)

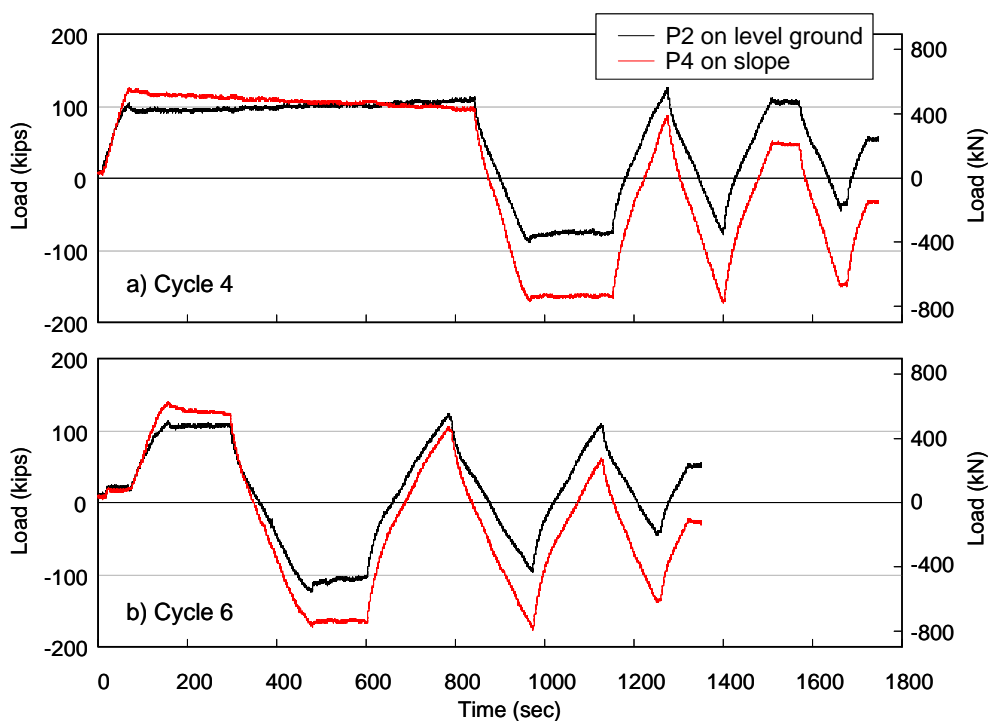


Figure 4-51 Time histories of shear load at each pile top (System Test 2)

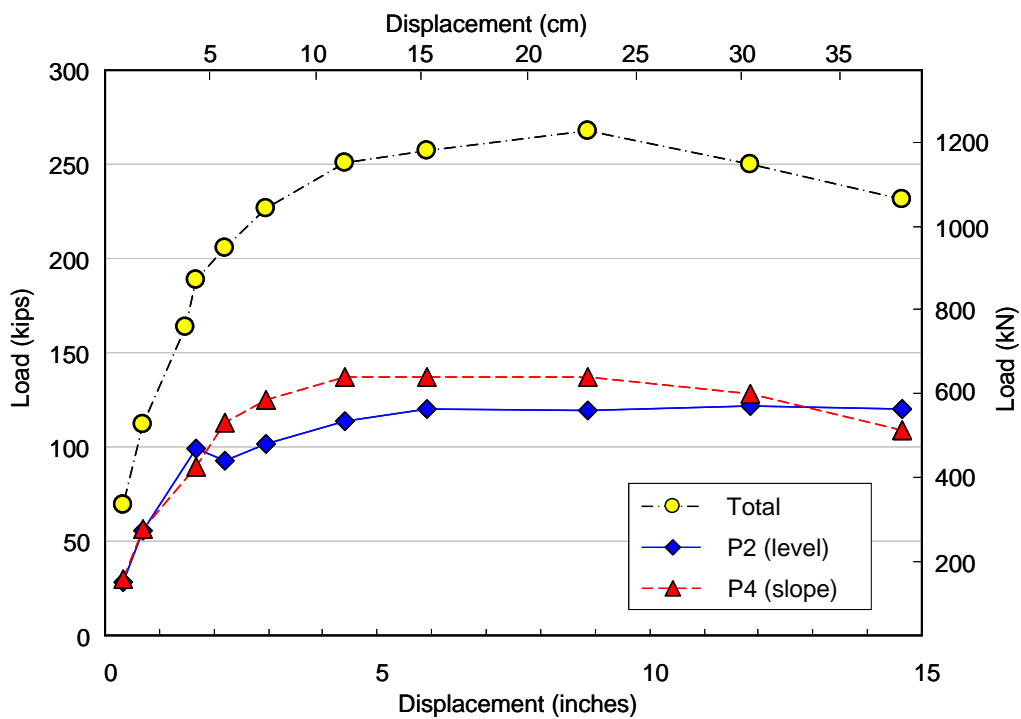


Figure 4-52 Distribution of the shear load (System Test 2, Push)

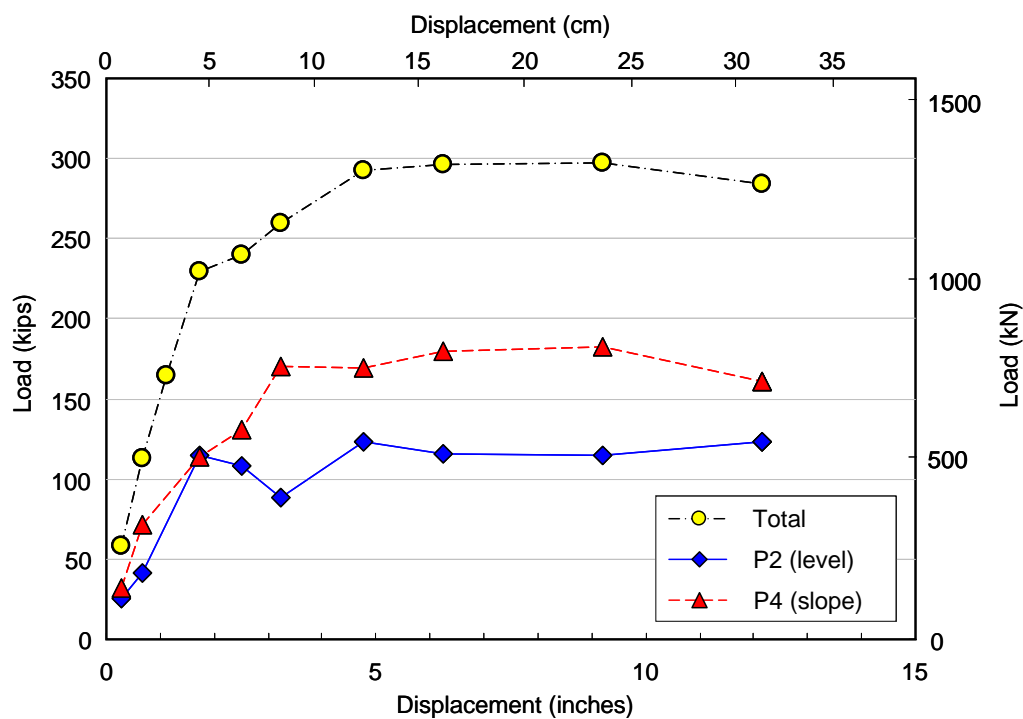


Figure 4-53 Distribution of the shear load (System Test 2, Pull)

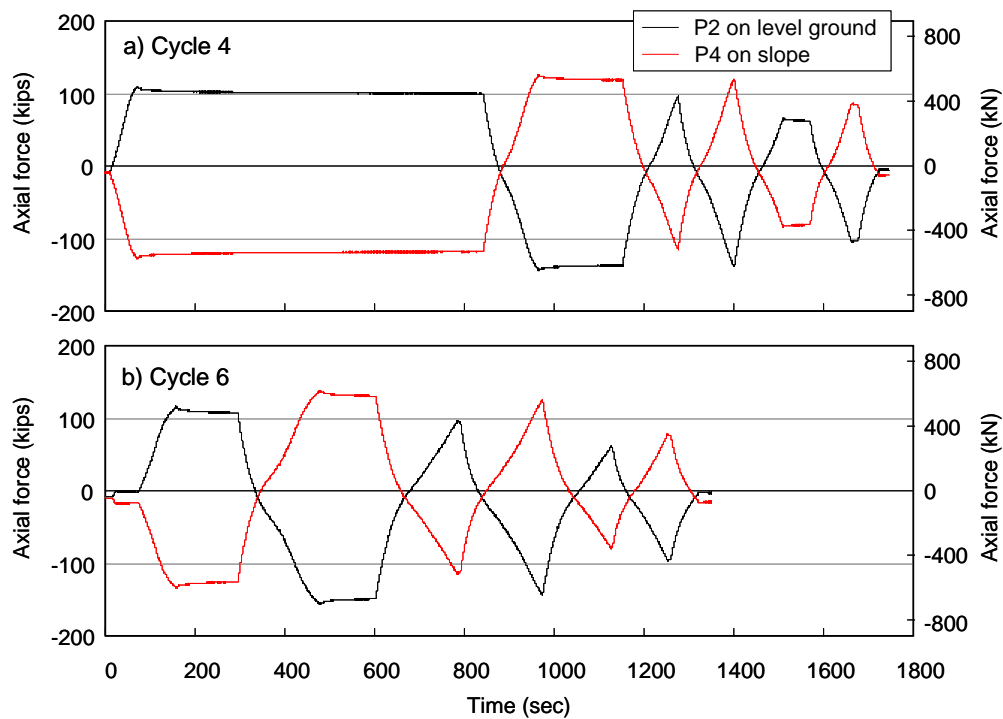


Figure 4-54 Time histories of axial force along each pile (System Test 2)

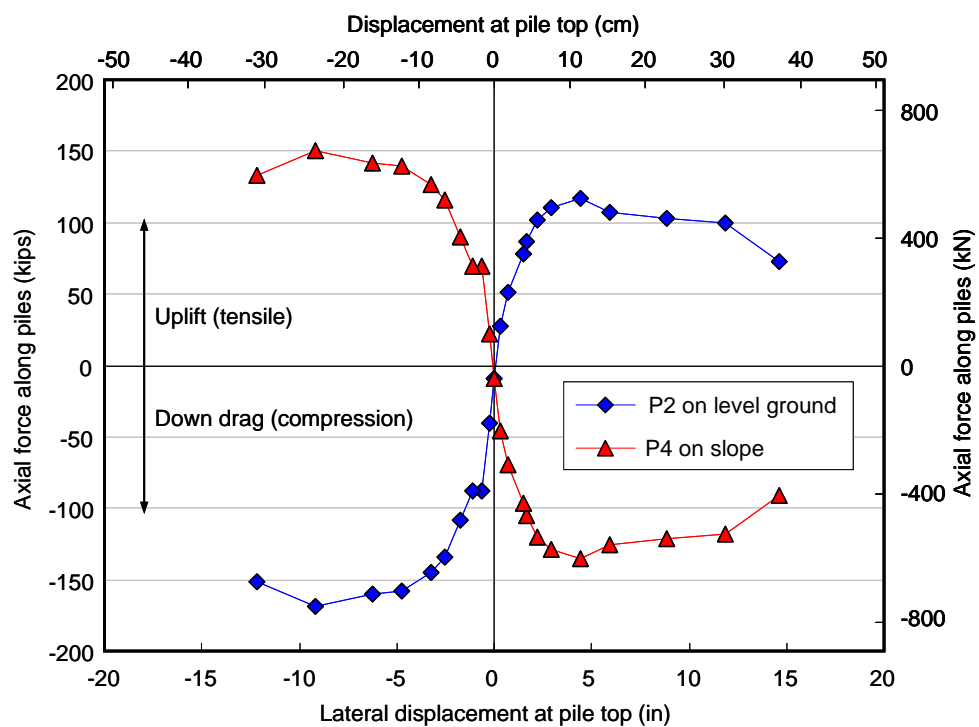


Figure 4-55 Axial load vs. displacement curves on each pile (System Test 2)

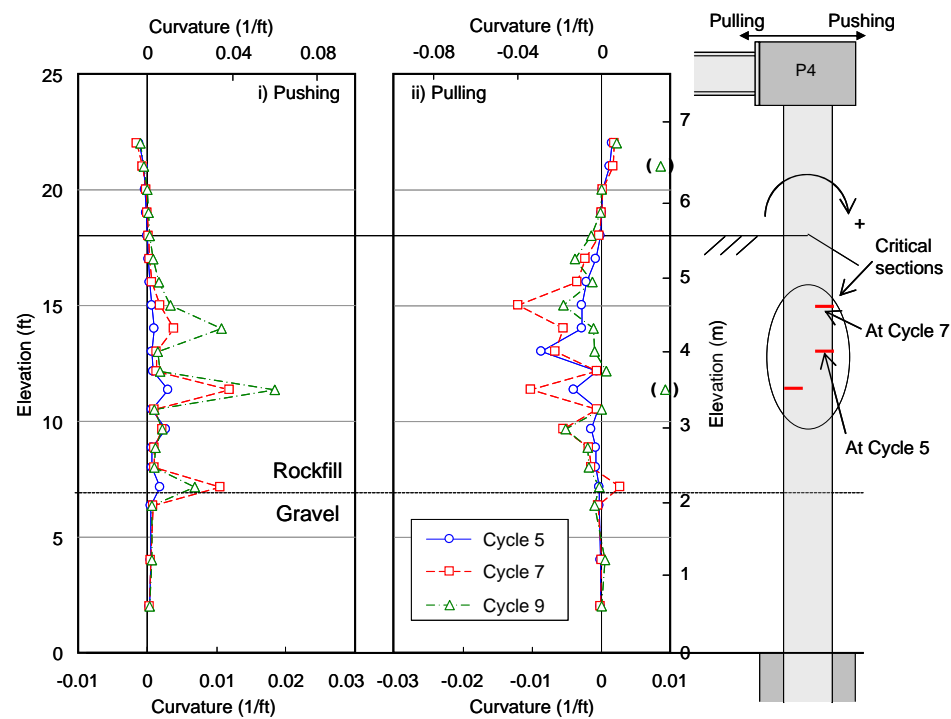
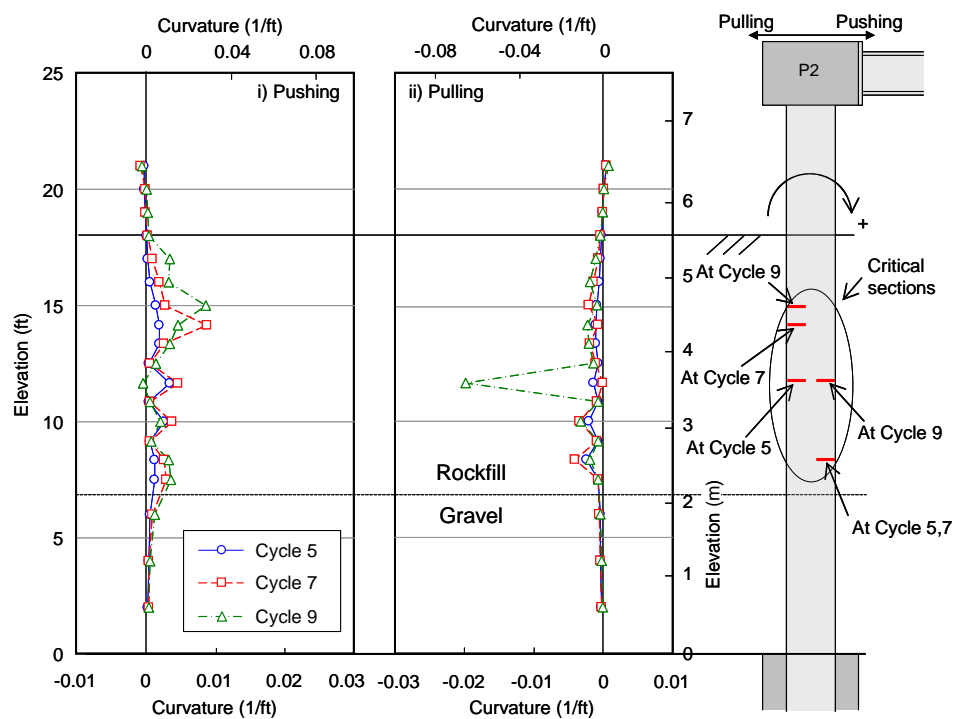
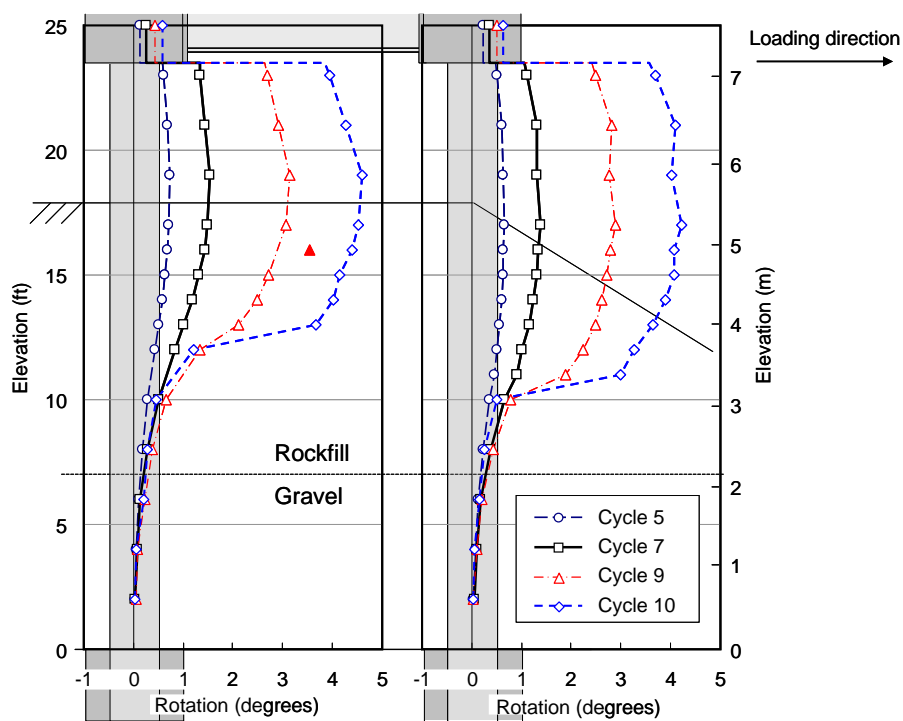
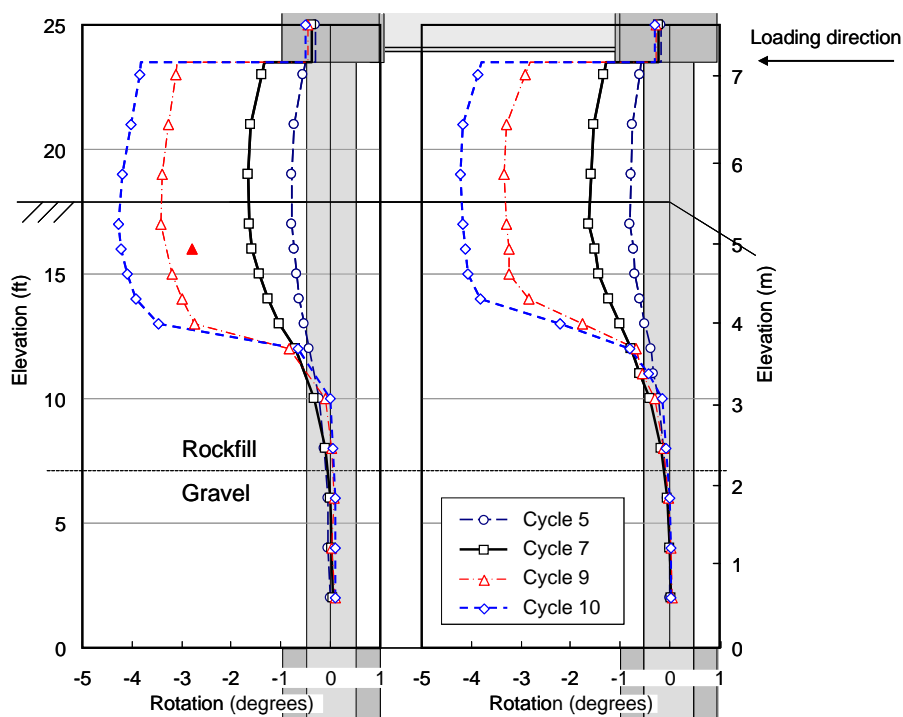


Figure 4-56 Profiles of curvature (System Test 2)



(a) Pushing toward the downslope



(b) Pulling toward the reaction wall

Figure 4-57 Profiles of rotation (System Test 2)

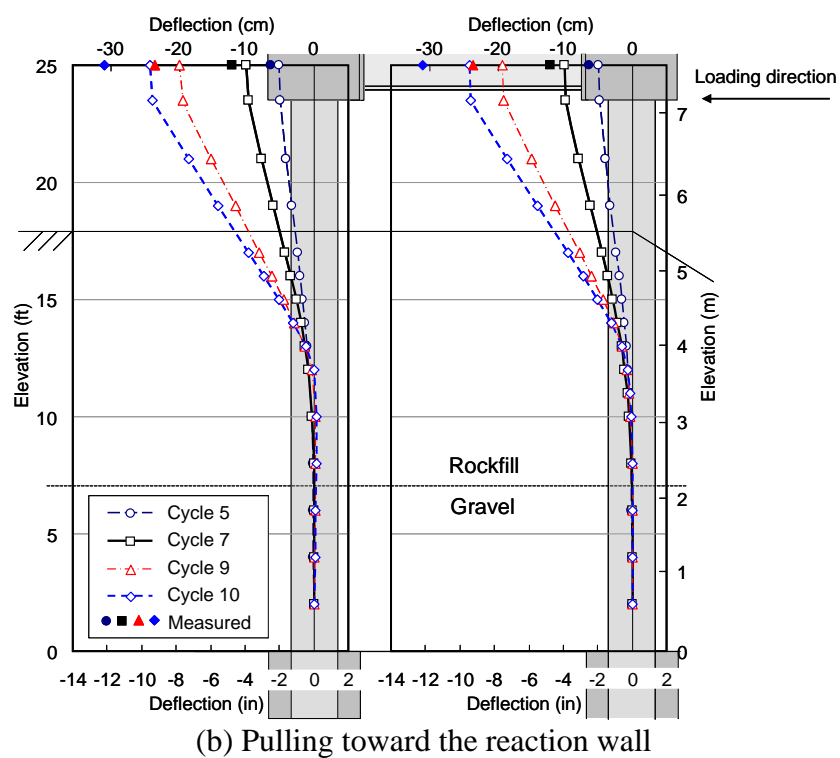
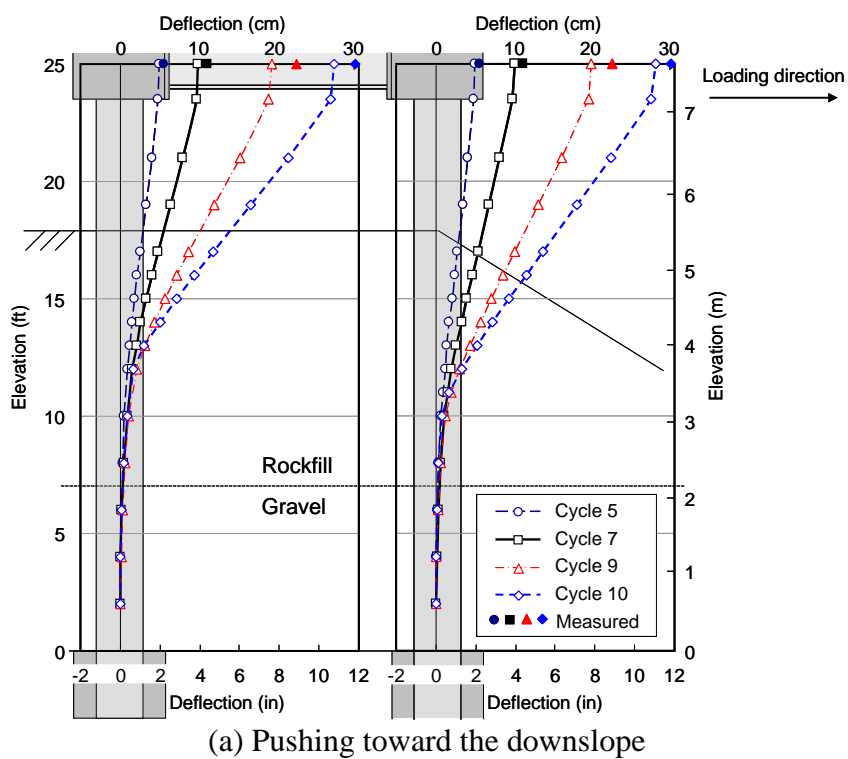


Figure 4-58 Profiles of deflection derived from rotation (System Test 2)

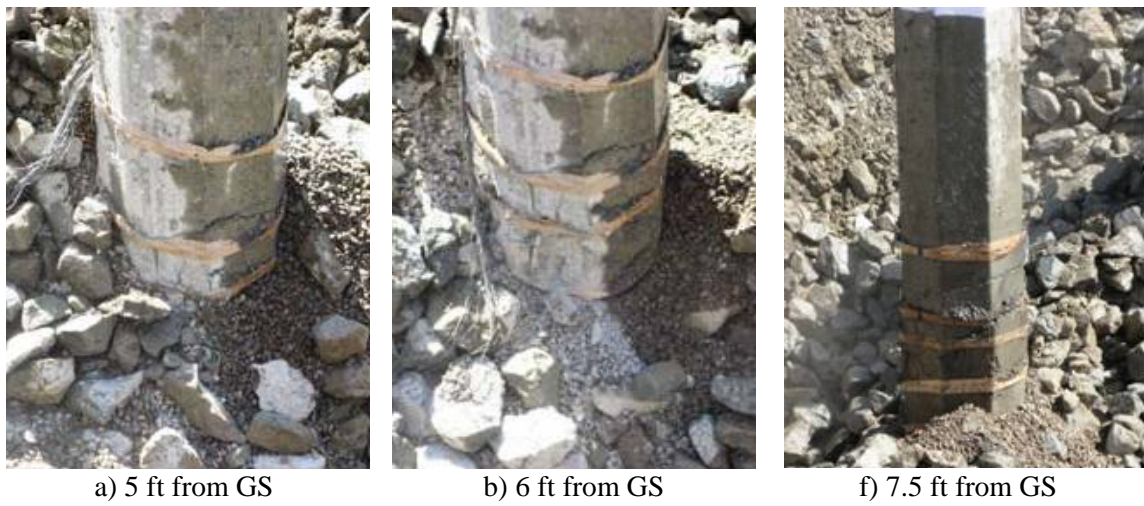


Figure 4-59 Excavation sequence on the north side (System Test 2, P2)



Figure 4-60 Plastic hinge on the north side (System Test 2, P2)

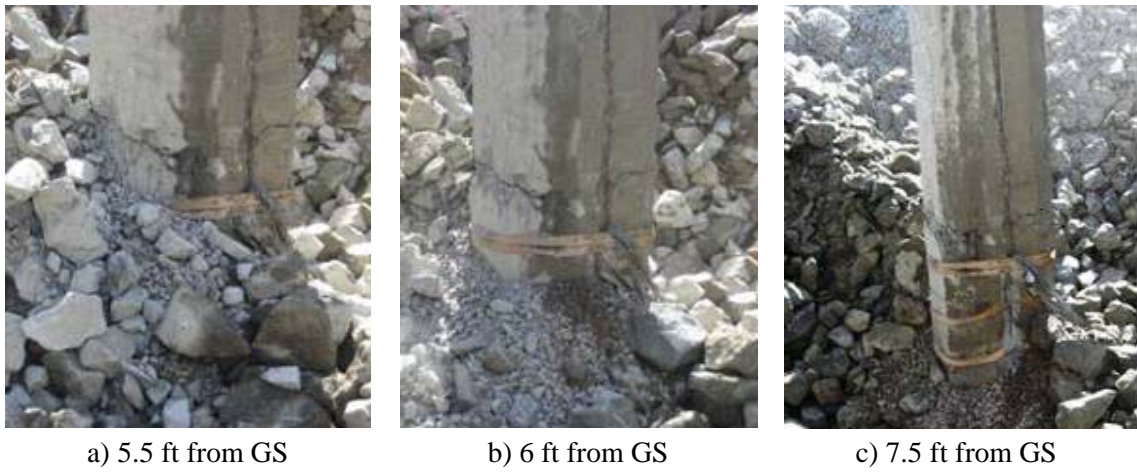


Figure 4-61 Excavation sequence on the north side (System Test 2, P4)



Figure 4-62 Plastic hinge on the north side (System Test 2, P4)

5 ANALYSIS FOR MODIFICATION OF DESIGN

One of the most important objectives of this research is the assessment and possible modification of the p - y curves used for current design of pile-supported wharf structures. In order to achieve this objective, the test results needed to be compared with numerical results derived using the current design procedure.

In the first part of this chapter, the results obtained in the first two single pile tests were compared with numerical results derived using the p - y curves for the current design practice. Based on the comparisons, larger p -multipliers than those currently recommended in the design were used, but this comparison shows that the analytical results using those p - y curves did not agree well with the test results (Section 5.1).

Secondly, past works and observations during and after the loading in this series of experiments were carefully reviewed in order to find reasonable ideas improving the numerical results. Based on the review, apparent reaction due to interlocking between the rock particles and the piles was introduced on the p - y analysis. From comparisons of the test results with numerical results, it was concluded that inclusion of the interlocking effect on the p - y curves could provide reasonable improvements on the numerical results (Section 5.2).

In addition, impact due to consideration of interlocking on behavior of entire wharf structure was estimated in the third part of this chapter. Using the p - y curves backcalculated in this research, a series of pushover analyses of entire wharf structure was conducted. Considering the results in the entire wharf analysis, several recommendations for design practice are provided (Section 5.3).

As the last part of this chapter, a list of the questions and their possible solutions are presented because there are still uncertainties in pile-large particle soil interaction to extend the knowledge found in this research work. Based on the list of uncertainties, possible future research works are also shown in order to gain better understanding and develop more sophisticated design method (Section 5.4).

5.1 Comparison between Test Results and Current Design

Following Single Pile Test 1, prediction analyses for System Tests were updated as shown in Section 3.4.1 using the test results obtained in Single Pile Test 1 because lateral resistance of the pile in Single Pile Test showed significantly larger than originally predicted with a set of the p - y curves used for the current design practice. Because the update of the prediction was performed in order to revise load protocol, estimation of reasonable load displacement relationship at the pile top was the most critical issue at that time, and details of the response of the soil-pile system (e.g. profiles of rotation and curvature, interaction mechanism) were not discussed.

In this section, experimental results including both the load displacement curve and the profiles of the pile responses in Single Pile Tests 1 and 2 were compared with numerical results using the current design methodology with p -multipliers accounting for uncertainties on the soil-pile interaction in order to assess how the current design works. Even though 0.3 and 2 are the p -multipliers currently recommended for the lower and upper bound analyses in design practice, larger multipliers are used herein because of the unexpectedly large lateral resistance of the pile recorded in Single Pile Tests 1 and 2.

5.1.1 Numerical model and parameters

The numerical model used for assessment analysis was exactly same as the model for prediction analysis shown in Figure 3-4. The properties of the pile and the p - y curves used herein were also identical with those used for the prediction (Section 3.2). Three different p -multipliers (m_p) were used; i.e. 1, 2, and 5 as shown in Table 5-1. Based on the updated prediction analyses between Single Pile Tests and System Tests shown in Section 3.4, it was obvious that $m_p = 0.3$ for the lower bound analysis in the current design gave significantly low lateral load at any displacement, and it was replaced with the larger multiplier, $m_p = 5$ providing reasonable lateral loads in the preliminary backcalculation for Single Pile Test 1.

5.1.2 Comparison of the test results and the current design

5.1.2.1 Single Pile Test 1

Comparison of load displacement relationship between test and analysis for Single Pile Test 1 is shown in Figure 5-1. Circle and triangle dots in this figure show the peaks of the shear load at any loading Cycles. The p -multiplier for the upper bound analysis recommended in the current design practice, $m_p = 2$, gave significantly low lateral load. Initial stiffness of the system from the experiments was close to the numerical result with $m_p = 5$. In addition, the result with $m_p = 5$, showed reasonable agreement of the ultimate lateral load with the test result.

Figure 5-2 presents comparison of the rotation profiles along the pile for loading Cycle 8 at which the maximum lateral load was applied in Single Pile Test 1. In order to assess the validity of the numerical results, the rotation profiles for Cycles 5 and 6 are also compared. From these profiles, it was obviously understood that the analysis with $m_p = 2$ provided the best matched results for all the loading cycles. Deflection and curvature profiles along the pile derived from rotation profiles are shown in Figure 5-3 and Figure 5-4, respectively. The curvature profiles from the numerical analysis have quite large peaks because zero stiffness was used after the pile moment reached the ultimate. Therefore, it is difficult to make quantitative discussion, but the curvature profiles from numerical analysis provide qualitative information (i.e. locations of the critical section). Based on these profiles, the analysis with $m_p = 2$ showed the best estimation on the deflection profiles, while the analysis with $m_p = 5$ gave the best solution of the location of the critical section at which the largest curvature along the pile was observed.

5.1.2.2 Single Pile Test 2

Figure 5-5 shows comparison of load displacement curves for Single Pile Test 2. Because the test pile was loaded toward the upslope, it was likely that the reaction from the rockfill is larger than the reaction on level ground. Therefore, the standard case analysis ($m_p = 1.0$) was skipped, and the minimum p -multiplier used herein was 2. From

the figure, it could be observed that even the analysis with $m_p = 5$ significantly underestimated the ultimate lateral load.

Profiles of rotation, deflection and curvature are shown in Figure 5-6, Figure 5-7, and Figure 5-8, respectively. In the same manner as Single Pile Test 1, these profiles are plotted for Cycle 6 showing the maximum pile top displacement and for Cycles 2 and 4 in order to show how close the numerical and test results are. Even though the load displacement curves did not show a good agreement between experimental and numerical results, all the profiles from the analysis with $m_p = 5$ are reasonably matched with the test results.

In conclusion of this section, there are two important findings on verification of the p - y curves used for the current design practice; 1) the p - y curves for the current design can provide reasonable deflection profile if appropriate p -multipliers are used, 2) even using large p -multiplier, the ultimate lateral load was underestimated. Based on these two findings, important factors seem missing in the concept of the p - y curves with p -multiplier approach used for the current design work, and the curves should be updated using experimental results in this study.

5.2 Modification of Numerical Model and Parameters

According to the analyses in the previous section, it was concluded that the numerical analysis with the current design approach did not give reasonable results to simulate the test results. One of the best ways to solve this problem is direct backcalculation of the reaction from the rockfill along the test pile differentiating the moment profiles twice (differentiation method in Section 2.1.5). One of the most important processes to make the backcalculation above is defining appropriate bending stiffness of the pile; however, it is difficult in the prestressed concrete piles because the stiffness of the concrete pile is function of axial load, and curvature due to high nonlinearity of the concrete. In addition, it may be affected by cyclic loading, cracking and spalling. Therefore, the reaction from

the rockfill was backcalculated comparing numerical and experimental results, such as load displacement curve and rotation profile (curve fitting method).

In the first part of this section, important observations during and after testing are summarized to find possible reasons why the model and the parameters used for the current design did not work so well. Based on the possible reasons found, the p - y curves for the rockfill were modified using the test results for Single Pile Test 1. At the last moment of this section, the modified p - y curves were verified comparing the test and numerical results with the modified p - y curves for the other tests.

5.2.1 Notable observations during and after testing

Even though important observations during and after the loading are already described in Chapter 4, it can be still helpful to summarize significant observations again and discuss them in detail in order to find possible mechanisms of pile-large particle rockfill interaction. Notable observations during and after loading found in the entire series of tests were re-summarized in Figure 5-9.

Figure 5-9(a) show fractured rock particles observed adjacent to the test pile in-ground. It indicates that strong contact force generated between the rock particles and the pile broke the rock particles down. Figure 5-9(b) is a photo showing “pock-marks” at the pile surface. These marks are an evidence of strong point load acting to the pile from the surrounding rock grains. Distribution of these pock-marks implies two important things; i) about 10 marks could be observed during inspection with 3 ft (0.9 m) excavation; i.e. the number of contacts was quite few, ii) some marks were found at some elevations, and no mark existed at other elevations. It indicates distribution of contacts was not uniform, and dependent on arrangement of the rockfill particles. Distribution of the rockfill grains seems to have some random factors, and may affect on shear behavior of the piles.

Figure 5-9(c) and (d) show contact conditions at different depth; contacts between the pile and the rock particles are relatively dense at some depths as shown in Figure 5-9(c), while they are quite loose and large void was observed at the other depths shown in

Figure 5-9(d). Because it is assumed that reaction from soil to the pile is uniform at any depth for the common p - y analysis, variation of contact strength is not taken account, but it may be one of the important factors to vary behavior of the pile systems. Settlement of the rockfill around the piles is shown in Figure 5-9(e). Only portions above ground surface of the pile was painted white before loading, unpainted portions of the pile became exposed during loading; i.e. the rockfill around the pile settled. The maximum settlement was about 2 ft (0.6 m). As an example, a sketch of settlement around P5, the pile at the dike crests for System Test 1, is shown in Figure 5-10. It is notable that loading rate may be one of the factors because the settlement progressed quite slowly during loading and such a large settlement may not happen during higher rate loading, such as seismic motion.

Figure 5-9(f) shows a compressed rock particle (arrowed in the figure) between the test pile and adjacent rock grains observed during loading. Deflection of the pile was obviously larger than lateral movement of the adjacent rock particles. This particle compression may generate reaction even under significantly low vertical confinement. Also, it can be reasonably guessed that the pock-marks at the surface of the test pile were developed at the contact points between the test pile and the compressed rock particles.

All the observations above should be reasonably considered in order to gain better understanding about mechanism of reaction generation in the rockfill. However, so many factors can not be discussed under the current condition because of lack of information available about behavior of the laterally loaded piles in the rockfill. Especially, quantitative discussion about random behavior of the pile-soil system requires large statistical data base, and it is not discussed herein.

5.2.2 Assumptions for backcalculation of p - y curves

Considering the observations mentioned above, a set of the p - y curves for the rockfill were backcalculated using curve fitting method introduced in Section 2.1.5. Prior to the backcalculation, it was very important to make reasonable assumptions in order to find

appropriate solutions. Behavior of laterally loaded pile systems is function of pile and connection properties, numerical model, and soil-pile interaction represented by a set of p - y curves. Because all the factors have uncertainties more or less, infinite sets of solutions can be found unless some of these factors above are assumed relatively reasonable comparing the level of their uncertainties.

The property of the prestressed concrete pile was derived with moment curvature analysis using a commercial software widely used for design practice and research. Concrete strength is one of the uncertainties, but it has minor effect on properties of the pile, and quite small effect on interaction of soil-pile systems. The property of the connection was defined based on the full-scale test conducted prior to this study. Concrete strength is also an uncertainty on the connection property, but it does not significantly influence to the connection property because most force at the connection is distributed on dowel bars. The numerical model, composing of a set of nonlinear p - y curves and nonlinear pile elements, is widely used for both design practice and research, and it has been authorized as a reasonable method. On the other hand, pile-large particle soil interaction was defined based on only one full-scale test, and the biggest uncertainty seems to be there.

According to comparisons of uncertainty levels of the factors, it can be assumed that the numerical model and the parameters used in Sections 3.2 and 5.1 are reasonable, and only the soil-pile interaction represented by the p - y curves is poorly-known. Fixing these reasonable factors, backcalculations of the p - y curves are performed below.

5.2.3 Settlement around the test pile

One of the important observations taken account herein is settlement around the test piles. The settlement around the piles may play an important role on the behavior of the laterally loaded piles because the settlement around the pile makes pile length above ground surface longer. Therefore, the pile behaves more flexible, and the ultimate lateral resistance of the pile becomes less.

The effect of the settlement around the pile on the load displacement relationship is shown in Figure 5-11. Ideally, the pile behavior recorded during the test is between numerical results under initial condition without settlement and after loading condition with settlement. However, the actual behavior can be out of the area between these numerical results because the numerical model used herein does not include cyclic effect, randomness of some parameters, and degradation of moment curvature relationship of the piles.

The effect of the settlement was included in analyses only for System Tests because approximately 2 ft (0.61 m) settlement was observed only in System Tests 1 and 2, not for the first two single pile tests. Numerical analyses for cases with 2 ft (0.61 m) settlement were performed removing the p - y curves from the top 2 ft (0.61 m).

5.2.4 Considerations of reaction generation mechanism in rockfill

Rockfill is usually regarded as a cohesionless friction material because it has no cohesion between particles. As mentioned above, however, observations during and after testing showed that structural interlocking between rock particles seems to play an important role on behavior of the laterally loaded pile system in the rockfill. In fact, Diaz *et al.* (1984) mentioned about existence of the interlocking, and some researchers recommended empirically obtained pseudo cohesion in analysis of centrifuge test results in literature (McCullough and Dickenson 2004). In addition, triaxial tests of large particle size rock implied relatively large shear strength even under low confining pressure (e.g. Bertacchi and Bellotti 1970).

Instead of the interlocking concept, there is another possible explanation, shear strength under three-dimensional stress conditions. Based on mechanism of the interlocking, reaction due to interlocking can not be developed unless the rockfill particles are loaded due to any external force, and push back each other. Therefore, it can be considered that interlocking concept is corresponding to shear strength of soil due to increment of shear load from pile deflection under three-dimensional stress condition in

soil mechanics. Increment of the shear stress can be important factor significantly affecting on the shear strength of the soil, especially under very low confinement around the ground surface because the shear stress is considerably larger than the vertical stress. In general, behavior of laterally loaded piles is strongly dependent on properties of shallower portions of soil, and it may be better to define soil parameters from three-dimensional stress conditions.

In this section, concepts of both the interlocking and constitutive model under three-dimensional stress conditions are discussed in detail. In addition, these concepts are used in order to backcalculate the p - y curves for the rockfill, and compared each other at the last.

5.2.4.1 Interlocking concept

First of all, micro-particulate mechanisms in rockfill should be discussed. There are several possible patterns of particle movements in granular materials as shown in Figure 5-12; i.e. a) translation or slippage, b) particle compression, c) rotation, and d) climb over its neighbor particle related to dilation. As mentioned in Section 2.3, it is usually believed that shear strength of soil is composed of shear friction and dilation. Component of shear strength due to shear friction is generated during relative movement of particles, such as slippage and rotation. This component is dependent on effective vertical stress because friction is function of friction coefficient and normal stress at the contact surface. Also, component from dilation is originated by climbing over of soil particles, and the magnitude may be stress-dependent because vertical stress suppresses particle climb over. In addition, compression of particles is another origin of reaction affecting on lateral behavior of the soil-pile system. As observed during testing, when a soil particle is laterally loaded by relative deflection of the pile, and its adjacent soil particles suppress translation and rotation of the particle, the particle would be compressed between the pile and the neighbor particles by “interlocking”. This process can generate reaction working perpendicular to the contact surface. For development of particle compression, existence of particles staying in place is necessary (Figure 5-12(b)).

The compressed particle generating the interlocking force would climb its adjacent particle over when overturning moment at the contact point or upward driving force becomes more than resistance. Therefore, confinement from the adjacent particles is affected by vertical stress, and the rock particles can dilate more easily under low confinement instead of interlock each other. It results that the interlocking force is dependent not only on particle structure, but also on the vertical stress.

Based on the discussion above, a hypothesis can be developed; i.e. the lateral reaction from the rockfill to the piles is a combination of stress-dependent and stress-independent components. Because of different stress dependency of those components, the p - y curves for those reactions need to be separately defined. For convenience, the stress-dependent reaction is defined as “friction” acting parallel to the contact surface between particles, and the other stress-independent reaction is as “interlocking” working perpendicular to the contact surface. Conceptual drawings of friction and interlocking are shown in Figure 5-13.

In order to reduce the number of unknown parameters, it was assumed that the p - y curves used for the current wharf design practice represent the friction component of the reaction. The p - y curves for the interlocking are defined as a bi-linear perfect plastic elastic as shown in Figure 5-14 in order to keep consistency with the p - y curves for the friction. According to this assumption, the p - y curves for the interlocking have two unknown parameters; i.e. the ultimate reaction (p_2) and the displacement when the reaction reaches the ultimate (y_2). The parameter p_2 can be backcalculated comparing ultimate lateral resistances of the system on the load displacement relationship at the pile top. The parameter y_2 can also backcalculated matching stiffness of the system, and rotation profiles along the piles at any loading cycle. These two parameters are not completely independent, but do not significantly influence each other. Therefore, these parameters can be backcalculated almost independently.

The p - y curve for the interlocking component of the reaction was backcalculated comparing the results for Single Pile Test 1. The load displacement curve, the profiles of moment and deflection calculated using the backcalculated p - y curves are shown in the following section. The backcalculated parameters are $p_2 = 2.33$ kips/in (408 kN/m), $y_2 =$

1.75 in (4.45 cm), and the p - y curve for the interlocking is plotted in Figure 5-15 with the stress-dependent p - y curves for the friction. The ultimate reaction of the interlocking component corresponds to one of the friction component at 6 ft (1.83 m) deep. Based on API standard (1987), the lateral capacity of clay is between 8 and 12 times of cohesion of the cohesive soils, and the pseudo cohesion of the rockfill can be calculated from the ultimate reaction p_2 as follows;

$$p_2/d = 8 \sim 12c, \quad c = p_2/d(8 \sim 12) \quad (5.1)$$

where d is pile diameter, and c is pseudo cohesion of the rockfill due to structural interlocking. Substituting $d = 24$ in (0.61 m) and $p_2 = 2.33$ kips/in (408 kN/m), the pseudo cohesion is calculated; $c = 8.1 \sim 12.2$ psi (56 ~ 84 kPa). It is notable that the pseudo cohesion obtained in this study is significantly larger than 2.2 psi (15 kPa) provided in the past work of McCullough and Dickenson (2004). The difference may result from usage of different materials, and scale effect.

5.2.4.2 Constitutive model in three-dimensional stress condition

Another possible explanation of relatively large shear strength in the rockfill under low confining pressure is three dimensional failure criteria for granular cohesionless materials. Making several assumptions, soil-dependent parameters, η_I and m in equation (2.7) were backcalculated, and compared with those parameters for sands in literature in order to discuss about validity of the constitutive model.

A conceptual drawing of the possible stress path in rockfill until the stress condition reaches failure is shown in Figure 5-16 with Lade's failure criteria. As shown in the top-left drawing of Figure 5-16, σ_z is vertical stress, while σ_x and σ_y are horizontal stresses working parallel and perpendicular to the loading direction, respectively. Therefore, σ_x at failure corresponds to ultimate lateral reaction from rockfill to pile. Under initial condition, σ_x and σ_y are stresses at rest, and σ_z is vertical stress derived multiplying unit weight of the rockfill and depth. As deflection of pile in interest becomes larger, σ_x and

σ_y in the rockfill element adjacent to the pile deforms become larger. The vertical stress σ_z may also increase, but the increment of σ_z is relatively low compared to changes of horizontal stresses, so, it can be reasonably assumed that σ_z is constant during lateral loading on the pile. In theory, σ_y can not be larger than maximum passive earth pressure, and σ_y can take a value between earth pressure at rest and the maximum passive earth pressure. Based on classical earth pressure equations with friction angle of 45 degrees, coefficients of earth pressure at rest and passive pressure are about 0.3 and 6, respectively. One of the possible stress paths is shown in Figure 5-16 (curve AB). However, actual stress path may be very complicated because σ_x and σ_y are partially dependent on each other, and then, there are infinite possible paths and it is quite difficult to define σ_y at failure. Since the earth pressure coefficient at failure should be between 0.3 (at rest) and 6 (passive pressure), it is assumed 2 herein for convenience. With those assumptions, the parameters in equation (2.7), η_I and m were backcalculated by fitting load-displacement curves, rotation and deflection profiles obtained in Single Pile Test 1.

Figure 5-17 shows a comparison of ultimate shear resistance profiles used in the current design practice, backcalculated with interlocking concept in the previous section, and backcalculated with the Lade's constitutive model giving the best matched results. From this figure, it can be seen the backcalculated profiles of the ultimate resistance for both of interlocking and Lade's models should be similar at top 10 ft (3.05 m) to make equivalent backcalculation of the pile behaviors. The backcalculated soil-dependent parameters, η_I and m were 4,000,000 and 3.2, respectively. Because variance of η_I and m for smaller particle-size cohesionless soils were 30 to 300 and 0.01 to 0.4, respectively (Lade 1977; refer Section 2.3), the backcalculated parameters for the rockfill used in the experiments are extremely large; especially η_I . It is quite difficult to assess the validity of those large parameters because there is no past work about application of three-dimensional failure criteria for large-particle size rockfill, and more research works and discussions are needed.

5.2.4.3 Comparison of two concepts

Both the concepts mentioned above could give reasonable results comparing with the test results in Single Pile Test 1 even though the parameters of three-dimensional failure criteria are extremely larger than those for sands. It implies that both the concepts can reasonably explain the test results with significantly large lateral loads, and may correspond to each other. Unfortunately, there is no verification which concept is more realistic, and only the interlocking concept is discussed below because of its simplicity.

5.2.5 Pile responses analyzed using backcalculated p - y curves

In the previous section, the p - y curve for interlocking was backcalculated matching the test and numerical results in Single Pile Test 1. First of all, comparison of test and numerical results with the best agreements providing the p - y curve for interlocking for Single Pile Test 1 is presented. Following that, numerical results obtained using the p - y curve of interlocking are compared with experimental results for the rest of the tests (i.e. Single Pile Test 2, System Tests 1 and 2) in order to verify the backcalculated curve more.

In analyses for the system tests, reduction of the interlocking reaction also needs to be considered when the soil-pile system is loaded toward the downslope because the piles at the dike crest behaved more flexibly in the system tests. Figure 5-18 is a conceptual drawing of slope effect on the interlocking. As mentioned above, rock particles staying in place are needed to develop particle compression generating interlocking. In case of the pile on level ground shown in Figure 5-18(a), some particles stay in place, and rock particles next to the pile may be compressed. On the other hand, there are less particles staying in place in case of the pile at the slope crest (Figure 5-18(b)), and it may result in less particle compression and deduction of the interlocking reaction. In this study, the sloping effect on the p - y curve for the interlocking was taken into account defining another p -multiplier, as a function of depth. Figure 5-19 shows a possible profile of the p -multiplier representing slope effect on the interlocking component of reaction. Because the rock particles at the top 2 ft (0.61 m) from ground surface were demolished after all the loading, it is assumed that the interlocking did not fully work at the top 2 ft (0.61 m).

No interlocking at the original dike crest and full interlocking at 2 ft (0.61 m) below ground surface or deeper were used, and linear increment of interlocking was assumed between the dike crest and 2 ft (0.61 m) in depth (Figure 5-19).

Analysis cases are summarized in Table 5-2. The downslope effect on the friction component of the reaction was considered using $m_p = 0.3$ in the case with interlocking reaction.

5.2.5.1 Single Pile Test 1

A comparison of the load displacement relationship between the test and the analysis is shown in Figure 5-20. The cases with $m_p = 2$ underestimated the ultimate resistance of the pile soil system, while the case with $m_p = 5$ and interlocking provided reasonable ultimate resistance. The initial stiffness of the system was slightly underestimated in the case with interlocking, but reasonably agreed with test results in the case with $m_p = 5$.

Figure 5-21 and Figure 5-22 present the profiles of rotation and deflection calculated from rotation profile, respectively. The analysis cases with $m_p = 2$ and interlocking gave reasonably fitted profiles with the experimental records, but the case with $m_p = 5$ did not work well; based on a shape of the profiles, the soil-pile system for this case is stiffer than the profiles from the test. Figure 5-23 shows the curvature profile calculated from the tiltmeter array. Because the moment curvature property of the pile used herein was simplified with zero stiffness after the moment reached the ultimate, the analyses could not provide quantitative profiles, and the values of the maximum curvature in the numerical results were considerably larger than the test results, but the analyses could give reasonable location of the critical section of the pile if the p - y curves used are appropriate. From Figure 5-23, the critical sections in all the numerical cases with $m_p = 5$ were reasonably matched with the depth at which crack was observed.

Based on the comparisons above, the p - y curves with p -multipliers did not provide reasonable results of the load displacement curve and the profiles at the same time, and the inclusion of the depth-independent interlocking reaction could solve this mismatching. In the following sections, the backcalculated p - y curve for the interlocking is verified comparing the experimental and analytical results in the other tests.

5.2.5.2 Single Pile Test 2

Figure 5-24 is comparison of the load displacement curves in the various analysis cases shown in Table 5-2. All the numerical results including the case with interlocking significantly underestimated the ultimate lateral load of the system.

The rotation and deflection profiles for Single Pile 2 are shown in Figure 5-25 and Figure 5-26, respectively. The case with $m_p = 2$ gave slightly large rotation and deflection, but all the analyses could provide reasonable solutions. Figure 5-27 shows the curvature profiles calculated using the records on the tiltmeters. The case with interlocking gave the best location of the critical section, but slightly deeper than that in the test results. In addition, the area with large curvature recorded in the test was wider than the numerical results. It was caused by cracks on the pile generated during the previous Single Pile Test 1.

In summary, the case of the standard p - y curves with interlocking could give the best simulation results even though the ultimate lateral load of the system was significantly underestimated. There are several possible reasons of this underestimation as follows; 1) distribution of rock grains may become considerably denser than the previous Single Pile Test 1 during loading followed by excavation and manual backfill around the pile between Single Pile Tests 1 and 2, 2) the pile could contact with some rock particles above the ground surface when the pile was loaded toward upslope, and those contacts resulted in shorter pile length above the ground surface, 3) damaged portions of the pile in Single Pile Test 2 may not be concentrated because the pile was already cracked in Single Pile Test 1, and damage could be extended to a combination of the damaged portions in Single Pile Tests 1 and 2. It may result in different failure mode of the system, and 4) the pile property needed to be estimated more accurately because the contribution of soil pile interaction on the pile behavior became less dominant as the pile length above ground surface became longer. In fact, some parametric analyses with the p - y curves were conducted in order to clarify the reason, but no reasonable load displacement curve could be met. Therefore, it is likely that the offset of the soil-pile responses in the experiment and the numerical results from unexpected behavior of the pile, not from the soil-pile interaction.

5.2.5.3 System Test 1

The load displacement curves from the experiment and the analysis are compared in Figure 5-28. Even though the upper bound analysis in the current design ($m_p = 2.0$) gave less lateral load in the analysis for Single Pile Test 1, the numerical results from that case were plotted with the results obtained in the case of the interlocking because of the following reasons; 1) the upper bound analysis currently used for design practice should be also assessed comparing the responses of the couple-pile tests, 2) the test results showed that the piles at the dike crest behaved more flexibly (Sections 4.3.5 and 4.4.5), and 3) the numerical case with $m_p = 5.0$ provided stiffer responses than the test results for Single Pile Tests 1. From this figure, it was found that the analyses with $m_p = 2.0$ gave lower lateral resistance of the system especially during pulling toward the reaction wall even in the case without settlement. On the other hand, the numerical case with the interlocking effect provided curves conceptually expected as shown in Figure 5-11, even though the lateral resistance of the pile given in the analysis was slightly less than the test records. This comparison result is consistent with that in Single Pile Test 1.

Figure 5-29 presents comparison of the load displacement curves on each pile between the test and the analysis in the case with the effect of interlocking. The total load displacement relationship is also plotted in the same figure. The numerical results for loading in both the directions were reasonably agreed with the test results; however, the test results showed the pile at the dike crest took larger force than the pile on level ground during the system was pulled toward the reaction wall, while the numerical analysis gave the opposite results. As discussed in Section 4.3.3, the test results are not well-quantitative, and it is concluded that the numerical results are qualitatively matched with the test results.

Figure 5-30 shows comparison of relationships between axial force (down drag and uplift force) along the pile and lateral displacement at the pile top. The numerical results plotted with lines in the figure are obtained in the analysis case with interlocking reaction. Positive axial force means compressive down drag force while negative force represents tensile uplift force. Also, positive displacement at pile top means displacement toward the downslope, and negative value shows displacement toward the reaction wall. Even

though the maximum axial force along the pile was underestimated during loading toward the reaction wall in negative displacement, the analytical results show reasonable axial force vs. pile top displacement relationship.

Figure 5-31 and Figure 5-32 present examples of the rotation profile during pushing and pulling the test piles, respectively. In the concept of the numerical model under the initial condition and after loading conditions with 2 ft (0.61 m) settlement, the experimental data should be between those analytical results. Even though the profiles from the experiments are not perfectly between the profiles in the cases with and without settlement, the analysis with the interlocking p - y curves reasonably worked to simulate the test results. The analysis with $m_p = 2.0$ also could give reasonable results in most of cases except for the case when the piles were loaded toward the downslope. It implies the reduction of the reaction due to the downslope needs to be considered when the pile was loaded toward the downslope. In the large displacement loading cycles, the jump of rotation along the pile in the analysis was sharper than the test results. It is because the bending stiffness of the pile used in the analysis was zero after the moment reaches the ultimate as shown in Figure 3-7 for simplification. In addition, the rotation at the load stub was significantly underestimated in most cases of the analyses. Reason for this is not clear, but there are some possible reasons; 1) the loading direction in the experiment was not perfectly horizontal because of the pile uplift and down drag, and it exaggerated the rotation at the load stub, and 2) relative deformation between the pile top and the load stub gradually increased as the connection failure progressed more, and it may result in additional rotation at the load stub.

Comparison of the deflection profiles calculated integrating rotations along the piles are presented in Figure 5-33 and Figure 5-34. These figures show that the pushover analyses could give fairly agreed profiles of deflection in all the loading cases except for when the test piles were loaded toward the downslope.

The curvature profiles calculated from the tiltmeter arrays were compared with the numerical results in Figure 5-35 and Figure 5-36. The test results were slightly scattered, but the profiles from analysis reasonably matched with the test results. The large curvatures were concentrated in narrower area in the numerical results than in the test

results, and it is also because the moment curvature relationship of the pile used for numerical analysis has no bending stiffness since the moment reaches the ultimate value.

5.2.5.4 System Test 2

Figure 5-37 shows comparison of the load displacement curves at the pile top. From the figures, it was found that the analysis with $m_p = 2.0$ gave significantly underestimated lateral load, while the p - y curves with interlocking concept produced well-matched load displacement relationship even though the maximum lateral load was slightly underestimated when the test piles were pulled toward the reaction wall. The reason of this underestimation can not be clarified, but random rock particle distribution and contact locations can be possible reasons.

The load displacement curves on each pile are plotted in Figure 5-38 with the total load displacement relationship. Because the records of strain gages on the steel beam have some uncertainties as described in Section 4.4.3, the test results were not well-quantitative, but gave qualitative ideas. The numerical results agreed with the test results, and it implies that the numerical analysis can provide at least qualitative results. Also, comparison of the axial force along each pile is shown in Figure 5-39. The figure shows that numerical and the experimental results matched each other even though the maximum down drag and uplift forces were underestimated, especially in the negative displacement at the pile top during pulling the test piles toward the reaction wall. This trend was observed also on the comparison of System Test 1.

Comparison of the rotation profiles are shown in Figure 5-40 and Figure 5-41. From these figures, it was concluded that the numerical results in both the upper bound ($m_p = 2.0$) and the interlocking effect could show reasonable agreement with the test results. As observed in comparison for System Test 1, the rotations at the load stub were underestimated in analysis. Its reason is still unclear, but it may result from the rotation at the connection between the pile top and the load stub. Also, Figure 5-42 and Figure 5-43 are comparison of the deflection profiles, and Figure 5-44 and Figure 5-45 are comparison of the curvature profile, respectively. All the profiles show reasonable agreement between the experimental and the numerical results.

The p - y curve for the interlocking was backcalculated based on the results for Single Pile Test 1. Using the backcalculated p - y curve, pushover analyses were conducted for the rest of the tests (i.e. Single Pile Test 2, System Tests 1 and 2). As a result, it was concluded that the interlocking concept in the rockfill could reasonably explain all the test results, and played an important role on the interaction between the pile and the rockfill.

As shown in Figure 1-1, actual pier type wharf structures are supported by multi-piles. Even though the interlocking had significant effect on the simulation analyses of the single pile and the coupled-pile used in this study, it is still unclear how it affects on design of entire wharf structures. In the next section, pushover analysis of an example whole wharf structure is conducted in order to assess how the interlocking affects on the design of wharf structures, and how the current design works. Based on numerical results of the wharf structure, recommendations for design practice are provided.

5.3 Pushover Analyses for Whole Wharf Structure

Based on the backcalculation of the p - y curves shown in the previous section, consideration of large reaction around the ground surface represented by interlocking effect between rock particles and piles gave more reasonable responses of the laterally loaded piles in rockfill. At the next step, impact of the interlocking reaction on behavior of entire wharf structures should be estimated to assess the importance of the inclusion of the interlocking concept in wharf design practice. If its impact is minor, the p - y curves used for the current design practice are still reasonable even though a concept of reaction generation mechanism without the interlocking in the rockfill is physically unreasonable. On the contrary, more experimental research should be conducted if its impact is significant. Therefore, a series of pushover analyses of an example wharf structure, Berth 100 at the Port of Los Angeles, was carried out using the p - y curves backcalculated in the previous section in order to evaluate the influence of consideration of the interlocking

reaction. Also, several recommendations for design practice are proposed based on the comparison of numerical results of the entire wharf structure.

5.3.1 Numerical model and parameters

Cross-section and pile layout of the target structure in this analysis, Berth 100 at the Port of Los Angeles is shown in Figure 5-46 and Figure 5-47, respectively. The piles in rows A through D are non-seismic piles with lower bending stiffness, and the piles in rows E and F are seismic piles taking more lateral load. In order to support a crane load, the rows A and F have more piles than the others, 2.5 and 3 piles in 20 ft (6.1 m) width along the face line of the wharf.

The numerical model used for a non-linear pushover analysis of this entire wharf is shown in Figure 5-48(a). Even though crane load and live load on the deck are considered in design practice, only the dead load of the deck was considered in this analysis because the axial load along the piles is not a critical parameter, and the purpose of this series of analyses is to estimate difference of various numerical results using the p - y curves used for the current design practice and backcalculated in this study.

In some cases, however, the numerical analysis of the entire wharf model did not converge because of strong nonlinearity of the p - y curves, especially on the piles in rows E and F highly affected by the soil-pile interaction. Therefore, assuming the deck does not rotate and the lateral displacement at each pile top is identical, an individual pile model was developed as shown in Figure 5-48(b). The loads at corresponding displacement on all the piles were summed up in order to calculate the total load of the entire wharf. Because axial load along the piles can not be estimated in the individual pile model, entire wharf analysis was conducted prior to the individual pile analysis in order to calculate ballpark of the axial force and define the properties of the piles and the connections (Figure 5-49). Because the properties of the piles and connections are not sensitive to small difference of the axial force on the piles, it is assumed that the ballpark axial force is reasonable for estimation of the pile and the connection properties.

The properties of the seismic piles and the seismic connections used herein were same as those used for the prediction and the backcalculation mentioned above because the piles used in the tests are identical to piles used for actual construction of wharves. Conducting parametric analysis on the properties of the non-seismic pile and the connection, it was found that their properties had quite minor effect on the numerical results because heights of the non-seismic piles above the ground surface was much larger and soil-pile interaction on the non-seismic piles were less significant than that of the seismic piles. Therefore, 75 % of the bending and the rotational stiffness and the ultimate moment of the seismic pile and connection were used for both the non-seismic piles and connections as rough estimation. Four different p - y curves were used for the rockfill; 1) $m_p = 0.3$ (the lower bound analysis in the current design), 2) $m_p = 1.0$ (the standard analysis), 3) $m_p = 2.0$ (the upper bound analysis), and 4) $m_p = 1.0$ for the pile on level ground, and $m_p = 0.3$ for the piles on downslope with interlocking. Soil parameters used for analysis herein are summarized in Table 5-4. Based on the parameters in the table, the p - y curves for the other soil layers are generated following API standard. It is assumed that the reaction in the liquefiable loose marine sand layer is negligible because shear strength of the layer may decrease due to pore water pressure built-up in design input motion, and a thickness of the layer is less than 3 ft, quite thin relative to the other layers. The p - y curves for all the layers except for the rockfill are identical in any numerical case.

5.3.2 Comparison of results of entire wharf model with various p - y curves

Comparisons of the load displacement curves on the non-seismic piles (rows A through D), seismic piles (rows E and F), and the entire wharf are shown in Figure 5-50, Figure 5-51, and Figure 5-52, respectively. These three figures show the follows; 1) the seismic piles in rows E and F take 80 to 90 % of the total lateral resistance, 2) there are considerable differences between the analytical cases in the load displacement curves on the seismic piles (the analysis with the interlocking shows almost twice greater shear load

than that in the lower bound analysis), while the differences of the loads on the non-seismic piles are insignificant, and 3) all the analysis cases except for the analysis with $m_p = 0.3$ show similar initial behavior up to about 1 in (2.5 cm) displacement at the deck, and difference of curves gradually increases as the deck displacement becomes larger. The first conclusion of this comparison, i.e. that the lateral load acting at the deck is mostly distributed to the piles in rows E and F, was one of the most important verifications that the coupled-pile tests in this research can appropriately represent the entire wharf structure.

Figure 5-53 presents comparison of the deck displacements at any inertial force at the deck. For example, when the inertial force at the deck is 400 kips (1780 kN), the maximum deck displacement was 1.47 in (3.7 cm) given in the lower bound analysis while it is 0.63 in (1.6 cm) in the case with interlocking reaction. Because the possible deck displacement is estimated by the lower bound analysis ($m_p = 0.3$) in the current design practice, the current design gives significantly large deck displacement. On the other hand, the standard ($m_p = 1.0$) and the upper bound analyses ($m_p = 2.0$) give similar deck displacement as that in the case with the interlocking when inertial force at the deck is less than 400 kips (1780 kN) to 500 kips (2225 kN).

Deformed shapes of the entire wharf structure and the top portions of the piles in rows E and F at 2 in (5.1 cm) displacement of the deck are shown in Figure 5-54, Figure 5-55, and Figure 5-56 for the lower bound, the standard, and the upper bound cases, respectively. As a reference, deformed shape calculated in the analysis using the p - y curves with the interlocking is plotted on the same figures. Because magnitude of the deformations is quite small relative to wharf dimensions, 50 times larger deformations are plotted to make the deformed shapes clearer. According to comparisons of these deformed shapes, it can be concluded that the lower bound analysis ($m_p = 0.3$) could not provide reasonably fitted shape with the result from the interlocking case analysis, while the deformation shapes from the standard ($m_p = 1.0$) and the upper bound ($m_p = 2.0$) analyses show good agreements.

Figure 5-57 shows comparison of the moment profiles at 6 in (15.2 cm) displacement at the deck on the pile in row F, the most critical pile of the entire wharf structure. The

upper bound analysis gives the most similar profile as that observed in the analysis with interlocking reaction.

The relationship between the deck displacement and the maximum moment along the pile in row F is shown in Figure 5-58. The lower bound analysis gives the lowest moment at any deck displacement, while the upper bound provided the largest moment. The moments for the standard analysis and the analysis with the interlocking are between the lower and the upper bounds. When the deck displacement is large enough the pile in row F reaches yielding, and the maximum moment becomes the yielding moment of the pile in any case.

Based on the backcalculations of the test results obtained in this study, it can be reasonably assumed that the analysis with the interlocking concept gives the most reasonable predictions. The results of the other analyses, the standard, the lower and the upper bounds used for the current design practice, are compared with the most appropriate results in order to assess validity of the numerical results. Figure 5-59 shows differences of the deck displacements at any inertial force at the deck. The differences of the deck displacement (D , %) in the vertical axis were calculated using;

$$D = \frac{\Delta - \Delta_{\text{int}}}{\Delta_{\text{int}}} \times 100 \quad (5.2)$$

where, Δ is the deck displacement at any inertial force in the standard, the lower or the upper bounds, and Δ_{int} is the deck displacement at corresponding inertial force in the analysis with interlocking. Positive difference shows that the prediction analysis gives larger displacement, and negative value represents less displacement than the most reasonable prediction. According to Figure 5-59, the follows can be concluded; 1) the lower bound analysis ($m_p = 0.3$) gives significantly large displacement, 2) the upper bound analysis ($m_p = 2.0$) provides less displacement (less conservative), and 3) the standard case analysis ($m_p = 1.0$) shows 10 to 20 % larger displacement than the most reasonable value when the inertial force at the deck is less than 450 kips (2002 kN), and

the offset from the most reasonable displacement becomes larger as the inertial force at the deck increases.

In addition, differences of the maximum moment (M , %) along the pile in row F are shown in Figure 5-60. The differences in the vertical axis were derived using;

$$M = \frac{m - m_{\text{int}}}{m_{\text{int}}} \times 100 \quad (5.3)$$

where, m is the maximum moment at any deck displacement in the standard, the lower or upper bounds, and m_{int} is the maximum moment at corresponding deck displacement in the analysis with the interlocking. In Figure 5-60, positive value shows that the numerical case provides larger maximum moment than the most appropriate prediction, and negative difference means the opposite. There are some findings from Figure 5-60 as follows; comparing with the most reasonable results from the analysis with the interlocking, 1) the lower bound analysis ($m_p = 0.3$) shows considerably less moments at any deck displacement, 2) the standard case analysis ($m_p = 1.0$) provides little larger moments in small deck displacement range, but it gives less moments when the deck displacement is between 1 in (2.5 cm) and 4 in (10.2 cm), and 3) the upper bound ($m_p = 2.0$) seems to provide significantly large moments in small deck displacement range, but it gives reasonably larger moments when the displacement at the deck is more than 1 in (2.5 cm).

In order to estimate influence of the interlocking on the design of entire wharf structures, a series of pushover analyses of an example whole wharf structure with various p -multipliers used in the current design practice were performed. The numerical results provided were compared with the most reasonable results from the analysis with the interlocking. Some recommendations for design of pile-supported wharf structures are proposed based on the comparison in the following section.

5.3.3 Conclusions and recommendations for design procedure

The pushover analyses of entire wharf structures were performed, and all the numerical results with p - y curves and p -multipliers used for current design practice were compared with the results using the backcalculated p - y curves in this study. The findings based on the comparisons are;

- a. The p - y curves used for the current design practice give considerably low ultimate lateral resistance of the entire wharf, even in the upper bound analysis ($m_p = 2.0$).
- b. Reasonable deformed shapes and locations of the critical sections can be found by the upper bound ($m_p = 2.0$) and the standard case ($m_p = 1.0$) analyses used for the current design practice.
- c. The p - y curves in the lower bound ($m_p = 0.3$) used for the current design practice significantly overestimate the displacement of the deck at any inertial force. The p - y curves for the standard case analysis provide reasonable displacement of the system if the inertial force at the deck is less than 450 kips (2002 kN). When the inertial force at the deck is more than that, reaction due to interlocking effect in rockfill should be carefully considered.
- d. The upper bound p - y curves ($m_p = 2.0$) seem to give reasonable results in calculation of the maximum moment along the piles at any deck displacement.

Based on the above conclusions, in conjunction with the experimental results, some recommendations can be made to improve the current design practice. It should be kept in mind that these are the first tests of their kind, and these recommendations will likely evolve as more data become available.

- 1) Ideally, consideration of the lateral reaction from rockfill under low confinement represented by the interlocking concept is recommended for design practice.

- 2) In order to estimate the ultimate lateral resistance of wharf structures, appropriate reaction due to interlocking between pile and rock particles should be considered. The p - y curves obtained in this study can be one of the possible options.
- 3) In the current design practice, the intent of the lower bound analysis is to give the maximum displacement of the deck. However, $m_p = 0.3$ used for the lower bound analysis gives significantly large displacement, and it should be replaced with 1.0 if the design inertial force at the deck is less than 400 kips (1780 kN) to 500 kips (2225 kN). When the design load at the deck is more than that, the interlocking effect found in this study should be considered in design analysis.
- 4) The objective of the upper bound analysis is to predict the maximum moment for design purposes. The maximum moment appears to be relatively insensitive to the p -multiplier used. For this reason, $m_p = 2$ used in current practice gives reasonable results. However, this approach greatly underestimates the ultimate lateral resistance of the wharf structures. If the ultimate lateral resistance is important, the interlocking mentioned above should be considered.

The conclusions and recommendations above are appropriate for the rockfill, the piles, and the target structure used for this study. In order to extend information obtained in this research to different types of rockfills and piles, currently existing uncertainties on behavior of laterally loaded piles in the rockfill have to be understood conducting more experimental and numerical works.

In the next section, possible uncertainties significantly affecting on soil-pile interaction are presented. Also, several future research directions are proposed in order to clarify these uncertainties.

5.4 Uncertainties on Pile in Rockfill and Possible Future Research

Research related to large particle size rockfill requires large- or full-scale experiments to obtain results under more realistic conditions. However, only two research of full-scale

tests on piles in rockfill (this research and Diaz *et al.* 1984) were conducted. Scaled tests in centrifuge device were also carried out to simulate behavior of prototype structures (e.g. McCullough *et al.* 2004), but information from large- or full-scale tests is needed to assess a scale effect on characteristics of the rockfill. Even though this research provides much useful information, but more research works are still needed, in order to make more accurate prediction.

Because the tests in this research were carried out with only one type of rockfill and pile under a certain condition, there are still some questions to use the p - y curves obtained in this study for other rockfill materials and piles. A list of the uncertainties can be useful information to show directions of possible future research. In this section, the uncertainties, expected possible solutions, and impacts on behavior of wharves are described. In addition, some examples of possible future research projects are presented at the last of this section.

5.4.1 Uncertainties on laterally loaded pile in rockfill

Even though large amount of useful information could be provided in this study, some reasonable assumptions and simplifications needed to be made because there are still some uncertainties in details of the soil-pile interaction. More research works are necessary in order to reduce these assumptions and make more sophisticated numerical model for design of wharf structures with higher accuracy. In this section, uncertainties found in this study are listed up, and their possible solutions are described.

5.4.1.1 Details of particulate reaction generation mechanism in rockfill

For the backcalculation in Section 5.2, only the additional p - y curves due to stress-independent interlocking were included on the p - y curves in the current design, and the other parameters were assumed reasonable in order to focus on the most significant unknown because currently available information can not define so many parameters. However, particulate reaction mechanism in rockfill may be more complicated. As

mentioned above, shear friction, dilation, structural interlocking, and particle crushing are most possible critical factors, and these factors may be complicatedly correlated to each other.

Based on the observations and the considerations presented in the previous section, the reaction generation mechanism can be imagined as shown in Figure 5-61. Initially, rock particles do not contact each other so strongly due to gaps existing between the particles and the pile (Point 1 in the figure). At this stage, friction between particles may not fully work because of fewer weak contacts and more voids. Initial condition of rock particle distribution around pile may be dependent on conditions of rockfill placement and pile driving method, as well as characteristics of the rockfill, such as gradation, and maximum particle size.

As pile deflection increases, soil volume decreases because of the initial loose condition, contacts between particles become stronger and stronger, and interlocking force gradually becomes larger. This phase can be defined as contractive or densification phase. When the displacement reaches certain level, volume reduction from contraction of grain structures becomes saturated, and soil volume starts increasing (Point 2). At this stage, the contacts between particles become so dense that the friction starts working well. In addition, soil stops contracting and start dilating; i.e. the phase transfers from contractive to dilative phase. However, the particles under lower confining pressure start climbing over the next particle staying in place, and interlocking force can not increase any more (Pass 3 in the figure). On the contrary, the particles at deep elevation can not climb over adjacent particles due to large vertical confining pressure, and larger reaction can be expected from dilation. However, the rock particles will be broken down at certain stress condition and reaction force due to interlocking or dilation may suddenly drop (Point 4). Because the fractured rock particles can fill smaller gap and contract grain structures, reaction may rise up again. This reaction increase due to contraction of fractured particles followed by reaction drop from particle breakage may be repeated.

Figure 5-62 is one of the simplified p - y curves for pushover analysis with consideration of the possible mechanism mentioned above. This p - y curve model has

some unknown parameters, and more experimental and numerical works are required in order to define these parameters.

5.4.1.2 Gradation, particle size, and particle shape

As shown in Figure 3-32, the rockfill used in this research was poorly-graded than that used for the actual wharves at the Port of Los Angeles. Better-graded soil can be generally denser and compacted more; i.e. better-graded soils usually have higher internal friction angle and larger friction. In fact, some researchers (e.g. Marsal 1973) reported that well-graded rockfills could have larger shear strength than poorly-graded if both were compacted to their maximum density because the well-graded material can have greater density (Section 2.3).

In addition, gradation of rockfill may also affect on particle crushing properties. It is more likely that eccentric contact force acts on rock particles in poorly-graded soils because there are more voids like shown in Figure 5-63. Usually, compressive strength of rock particle is four or more times greater than its tensile strength, and particles in poorly-graded rockfills have more chances to be crushed because of eccentric load generating large tensile stress on the rock particles (Figure 5-63). On the contrary, eccentric contact force does not seem to occur so frequently on rock particles in dense rockfill because of more contact points. Therefore, the rockfill typically used for actual construction of wharves may have larger reaction than the rockfill used in this research.

Also, particle size seems a possible factor significantly affecting on shear behavior of rockfill. Considering degrees of freedom on particle movements, it can be imagined that fine particles can move to small void, and frequently redistribute, instead of interlock each other. Because of that, interlocking may not be important in shear properties of fine particle soils. On the other hand, larger particles require larger displacement to make equivalent redistribution as that in finer particle soils. Therefore, larger particles may be more compressed and generate larger interlocking. It results that interlocking is negligible in fine sand, and it should be taken into account in large particle rockfill. However, large rock particles generally have less crushing strength because the probability if a defect in a particle increases with particle size. Therefore, the magnitude of the interlocking may be

dependent on both the particle size and the crushing strength, and these factors are related each other. Assuming crushing strength of rock particle is large enough, a possible relationship between particle size and the ratio of interlocking to friction is shown in Figure 5-64.

Shape of particle also has influence on interlocking. Rounded particle may be able to slip smoothly on its neighbor because of its rounded shape, whereas angular particles may be caught by sharp edges of the adjacent particles. Therefore, it can be imagined that angular particle soil generates larger interlocking. It is also shown in Figure 5-64. In reality, crushing strength of rock grain is usually lower as particle is larger or as particle is more angular (see section 2.3), and the relationship between interlocking and friction in particle size and shape may be more complicated.

5.4.1.3 Presence of water

Presence of water affects shear behavior of rockfill because friction is proportional to the effective stress. Also, water may affect friction angle, deformation, and dilation properties as mentioned in Section 2.3; comparing triaxial test results of rockfill under dry and saturated-submerged conditions, it was found that friction angle in saturated sample was lower and deformation was larger than dry sample because water has lubricating effect on the surface of rock particles (Bertacchi and Bellotti 1970).

Because of high permeability of rockfill, probably pore water pressure buildup during earthquake does not generate critical failure, such as liquefaction, but excess pore water pressure induced by earthquake is not zero, especially in case if water is supplied from inundated sea wave, and it may reduce shear strength due to friction of rockfill, as well as effective normal stress.

Water may also affect crushing strength of rock particles. Rock is usually much weaker in tension than in compression, and submerged rock may be stronger than in dry one because water pressure provides compression stress on rock particles and it works as prestressing force.

However, because of size of vessels using large wharves, distance between bottom of deck and water table is usually long, and the critical section may be above water table in

most cases; for example, the critical section is 2 ft (0.61 m) above the water table in Figure 5-57. Therefore, the effect of water on behavior of pile-supported wharves may be minor relative to influence of the other factors.

5.4.1.4 Loading rate

Loading rate may also affect on shear properties of rockfills. Crushing strength and compressive stiffness of rock particles may be larger at higher rate loading; i.e. rockfill has higher potential to generate larger interlocking at higher rate dynamic loading. In addition, settlement around piles may be affected by rate of loading. According to the observations of the settlement around the test piles in this research, the settlement of the rockfill progressed quite slowly. It implies that large settlement does not happen at higher rate loading, and dilation and volume change from redistribution of particles are less than that when the pile is loaded at slower rate. It may be because rock particles have more chances to redistribute at slower loading.

Also, loading rate affects on dilation properties of the rockfills. Yamamuro and Lade (1993) mentioned “higher strain rates do not allow as much time for particle crushing and rearranging and this makes the soil appear less compressive or more dilatant, resulting higher strength” in sand. In addition, larger energy is required to make dilation in larger particle size rockfill. Therefore, it is likely that rock particles may be compressed more intensively at higher rate of loading, and it results in larger interlocking.

Figure 5-65 shows a possible relationship between loading rate, friction and interlocking with definition that friction and interlocking are 1 at very slow loading rate assuming no crushing of the rock particles. Because smaller particles can redistribute at smaller displacement, they may also redistribute in shorter time. Therefore, the loading rate does not significantly affect magnitude of friction and interlocking reaction in smaller particle soil.

5.4.1.5 Loading type

Reaction mechanism for inertial load and force development mechanism for kinematic load are different. Figure 5-66 shows free body diagrams around pile for both the load conditions. It is notable that area of particle compression zone may be much smaller in force development for kinematic load than the other because rock particles around the pile can also move with free-field ground. If the assumption that the interlocking is generated by particle compression in contractive phase as mentioned above, magnitude of the interlocking may be dependent on the area of the particle compression zone. As a result, the interlocking may not rise up in force development for kinematic load, and pseudo cohesion for kinematic and inertial load conditions may differ from each other; i.e. the pseudo cohesion for design under kinematic load condition of rockfill may be less than that obtained in this study, and needs to be carefully defined. Also, less pseudo cohesion may be appropriate for slope stability analysis because the particle compression may happen only around slip surface.

5.4.1.6 Statistical variables on random distribution of rockfill

Random distribution of rock particles may vary parameters for the p - y curves, and provide random lateral capacity, yielding displacement of piles, and location of the maximum moment. Conservatively, the possible maximum and the possible minimum reaction at any depth can be used for the upper and the lower bound analyses in the current design practice; however, it is unlikely that the reaction takes the maximum or the minimum values along an entire pile length, and obtained numerical results are unrealistic.

In order to make more realistic design, a probabilistic approach with probability density function (PDF) can be one of the options. PDF analysis is widely accepted in seismic hazard analysis (e.g. Abrahamson 2000), but there are only few research about probabilistic analysis of contact force between rock particles (e.g. Marsal 1973); however, there is no research about probabilistic analysis of the interaction between large particle size rocks and pile, and no information about statistical variables for random distribution of rock particles affecting the p - y curves.

As shown in Figure 5-9(c), (d) and Figure 5-67, density of contacts is varied in depth due to random arrangement of the rock particles. Figure 5-68 shows a conceptual drawing on variance of the reaction and the particle distribution. In case if a pile is small relative to soil particle size as shown in Figure 5-68(a), the number of contacts at any depth is large, and resultant reaction becomes closer to the number of contacts times average contact force per a contact point. Therefore, it can be reasonable assumption that the reaction is uniform. For relatively small pile, however, randomness of the contact force at a contact point may have large impact on resultant reaction at that depth (see Figure 5-68(b)) because there are several contact points at some elevations and no contact point at the others.

Possible relationship between the relative pile size to the soil particle size and intensity of variance on the pile behavior is shown in Figure 5-69. For small particle soils, random arrangement of the soil particles does not have significant effect on the pile behavior because the number of contacts between the pile and the soil particles is so large that it can be assumed reaction at any depth is not varied. However, as the relative size of the soil particle is larger, locations of the contact between the pile and the soil particles become more various, and the variance of the p - y curves also becomes larger because of less contact points. Randomness of the particle arrangement in rockfill may be varied by the following factors.

a) Gap size

Random distribution of rock particles varies size of gaps between piles and rock particles. As a gap size is larger, initial stiffness of the p - y curves would be lower, and it may result larger displacement at the pile top, especially in low input motion under inertial load condition. On the other hand, drag force under kinematic load condition may be lower at the same free field displacement. The gap size seems dependent on particle gradation, density, and particle shape. Construction methods of pile installation and rockfill placement are also possible factors.

b) Contact location and density

Contact location and density are other important variables due to random arrangement of rock particles. When contact density around the ground surface is low, it may reduce resultant reaction from soil, and result in lower resistance of system. Impact of the random contact location to the system behavior becomes larger as the relative soil particle size to the pile size is larger because the number of contact points may be significantly fewer on piles in larger particle rockfill.

c) Passive wedge

It is commonly believed that reaction working to piles is related to passive failure wedge. When rock particles located along the passive failure surface are small, the size and the shape of the passive wedge may be consistent, but it may be random if the size of grains is large. It may be accompanied by random magnitude of reaction.

d) Relationship between interlocking and friction

Because reactions due to the interlocking and the friction have different generation mechanism as defined above; i.e. the interlocking works perpendicular and the friction does parallel to contact surface of particles, the effect of random rock grain distribution on the interlocking may be different from that on the friction. However, because some parameters, such as density of particles, affect on both of them, impact of random grain distribution on the interlocking and the friction may be partially independent on each other.

Several sets of full- or large-scale experiments are needed in order to gain large amount of statistical information about the effect of the random distribution to numerical parameters. However, it requires large costs to conduct so many sets of tests with large piles. Discrete finite element analysis can be one of its alternatives. It may be able to provide supplemental information about the statistical parameters of the p - y curves, though at least several full-scale tests are required to assess the numerical results. Examples of possible future research are described in the next section.

An example of expected results from PDF analysis is shown in Figure 5-70. The results, such as load displacement relationship, yielding displacement, and location of critical section, are also described in PDF. Based on this analysis, practitioners can choose the best solution of wharf design with reliability demand, e.g. 95 % reliable displacement of the pile top, and 80 % reliable maximum moment along the pile.

In order to show potential of PDF analyses as probabilistic design, Monte-Carlo simulation analyses of a single pile model were conducted with three cases of random variables; i.e. 1) Contact strength representing all the random factors on the ultimate reaction, 2) Size of gap, 3) A combination of 1 and 2. All the random variables are described in p -multipliers. As mentioned above, it may be more realistic to define random p -multipliers for interlocking and friction separately, but the same p -multipliers were used for both the variables at a depth to simplify the analysis. The numerical model used for the PDF analysis was exactly same as the analysis for Single Pile Test 1 except for the random p -y curves (refer Figure 3-4).

Unfortunately, there is no reasonable statistical information available about rock properties now. Therefore, probability density functions of the contact strength and the gap size used herein are assumed uniform distribution, one of the simplest distributions, as shown in Figure 5-71 and Figure 5-72, respectively. It is assumed that the reaction at each elevation is varied from 0 to 2 times of the p -y curves backcalculated in this study (Figure 5-71). Also, Figure 5-72 shows that no reaction is generated at smaller displacement due to the gap between the pile and the rock grains, and the gap size is assumed varied from 0 to 1 in (2.5 cm). Based on these probability density functions, random p -multipliers were independently generated for all the elevations, and pushover analyses were carried out 500 times by repetition of replacing the p -y curves and running analyses.

Figure 5-73 through Figure 5-75 show the results of Monte-Carlo simulation analysis for all the three cases. In these figures, two results are shown in histogram and normal distribution curve for each case; 1) Lateral load at 1 ft (0.3 m) displacement at pile top. 2) Lateral displacement at 50 kip (222 kN) load at pile top.

Figure 5-73 indicates that both the lateral load and the displacement are varied in certain range, and their median values are very close to them obtained from analysis using the average p - y curves at any depth. The probability density function of lateral load at 1 ft shows relatively wide distribution, while the function of lateral displacement at 50 kip load has relatively narrow and sharp shape. It is notable that the minimum load and the maximum displacement in the PDF analysis are much larger and smaller than ones in the lower bound analysis; i.e. the lower bound analysis gives significantly large displacement at the pile top and low lateral resistance of the pile.

Figure 5-74 shows probability density functions obtained from Monte-Carlo simulation with random size of gap. According to Figure 5-74(a), the size of the gap does not affect on the lateral load at 1 ft (0.3 m) displacement because ultimate reaction at any depth is identical as analysis without the gap and 1 ft displacement is so large that the reactions at shallower depth can reach the ultimate values. On the other hand, lateral displacement at 50 kip (222 kN) load is varied in relatively wide range as shown in Figure 5-74(b).

The probability density function of the results for the case with combination of two variables is shown Figure 5-75. The probability density functions for both the lateral load and the displacement have relatively wider foot.

Comparison of the results for all the three cases in normal distribution curves is shown in Figure 5-76. In figures (a) and (b), there are two important observations; 1) contact strength makes the lateral resistance of the system varied in wide range, and it affects the lateral displacement to some extent, 2) the size of the gap affects on the lateral displacement and the initial stiffness of the system, but it does not on the ultimate lateral resistance. In reality, the gap size and the contact strength may be related each other; for example, loose soil may have larger gap and weaker contacts at the same time. Their relation needs to be clarified from analysis of particulate mechanism.

Figure 5-77 shows an example of curvature development sequence obtained in analysis with the combination of two random variables. The first peak of the curvature was found at 15.5 ft (4.72 m) from the bottom of the soil pit, but the other peaks are developed at 16.5 ft (5.03 m) and 17.3 ft (5.27 m) as the displacement at the pile top

becomes larger. As introduced in Figure 4-34 and Figure 4-56, this process is the critical section migration observed in the system tests; i.e. the critical section shifts upward as pile top displacement increased. Even though there are many assumptions in this PDF analysis, it can be one of the verifications that the migration of the critical section is caused by the variance of the gap size along the pile (refer Figure 4-35).

5.4.1.7 Relationship between numerical parameters and in-situ and laboratory tests

Performance of full- or large-scale tests is the best way in order to gain more realistic parameters for analysis, but it may take gigantic amount of cost and time. Therefore, these parameters are usually defined from in-situ and laboratory tests commonly conducted for the current design practice.

Standard Penetration Test (SPT) and Cone Penetration Test (CPT) are the most popular in-situ tests. Results from SPT and CPT are easily available, but can provide quite rough information about shear properties of the soil; e.g. higher SPT N-value “may” mean larger reaction. Some researchers (Marchetti *et al.* 1991) tried using Dilatometer Test (DMT) as a potential in-situ test in order to define more reasonable parameters for behavior of laterally loaded piles. Its advantage is direct measurement of initial stiffness of the soil against lateral force under actual stress condition. However, DMT can not directly provide ultimate reaction from soil, and large amount of data needs to be collected to develop empirical equations converting from DMT results to numerical parameters. On the other hand, the most common laboratory test for laterally loaded pile analysis is triaxial compression test providing cohesion and internal friction angle. These soil parameters are usually used to define the p - y curves for design practice. Also, there are several correlation equations proposed from SPT and CPT results to friction angle or cohesion of the soil, which can be converted to the parameters for the p - y curves.

Unfortunately, SPT, CPT, and DMT are not applicable to large particle size rockfill because their device can not penetrate into the rockfill. Also, there are significant difficulties for laboratory test of the large rockfill; i.e. large test device is needed for laboratory test, and testing takes lots of cost and time.

Ideally, the parameters of the rockfill for numerical analyses need to be reasonably defined from the minimum amount of laboratory tests. In order to do it, constitutive model reasonably fitting with any type of rockfill needs to be developed based on particulate mechanism of granular material and interaction between the pile and the soil, and the model developed is function of only parameters which can be directly obtained in laboratory tests.

5.4.2 Possible future research

The uncertainties on behavior of laterally loaded piles in rockfill are listed up in the previous section. At the next step, more experimental and numerical works are needed in order to find reasonable solutions for the above questions.

The uncertainties and impacts when they can be clarified are summarized in Table 5-5. Among the uncertainties in the table, the particulate reaction mechanism is the most fundamental and important item with the largest impact. All the other uncertainties are related to the particulate mechanism in the rock particles. The statistical parameters of the rockfill due to random distribution of the particles are also important for higher reliability design. The other uncertainties need to be clarified in order to expand interlocking concept to the different materials or/and the different conditions. Especially, loading type and rate are quite interesting research topic because the current design guideline of port facilities requires designs for both the kinematic and the inertial force conditions due to dynamic strong motion during design earthquake events.

Figure 5-78 shows network of possible future research including four types of works, such as analysis, laboratory tests, scaled tests, and full-scale tests. As mentioned above, full-scale tests are one of the best ways to obtain more realistic parameters for analysis; however, it takes much time and cost. Therefore, scaled tests including centrifuge and 1-g shaking table tests, and laboratory tests, such as triaxial and direct shear tests are needed to clarify scaling effects and correlations between results from different type experiments. Analysis is also one of the most important research works in this effective research

network. Numerical research works can calibrate with experimental works can provide supplemental information, such as reasonable prediction with various conditions. Some examples of possible future research are introduced below.

5.4.2.1 Discrete element method (DEM)

Discrete element method (DEM) was developed by Cundall *et al.* (1971), and it is widely used for analysis of the motion of granular material with a large number of particles including geo-material. Based on grain structure of rockfill, it can be one of the options for research about reaction generation mechanism in rockfill. In addition, some of numerical models for crushable soil have been developed (e.g. Jensen *et al.* 2001, and Lobo-Guerrero *et al.* 2005), and then, DEM has high potential to simulate micro behaviors in rockfill, and qualify interaction between pile and rock grains. In reality, interlocking between rock particles is 3-dimensional phenomenon, but numerical results can not be quantified under current condition with fetal shortage of available information. Therefore, 2-dimensional analysis is reasonable enough at present to find fundamental information. Because DEM analysis has some limitations, such as particle shapes, numerical results need to be complemented with experimental works.

Figure 5-79 shows examples of numerical model in DEM analysis for inertial load condition. Conducting parametric analyses with various gradations, slope dimensions, and loading rates, some of fundamental data can be gained.

Main purpose of a numerical model shown in Figure 5-80 is to understand on the effect of loading type. Comparing forces acting to pile for inertial (Figure 5-79(a)) and kinematic (Figure 5-80) load conditions, pseudo cohesion roughly estimated for kinematic load condition can be proposed. However, based on 3-dimensional soil-pile interaction mechanisms shown in Figure 5-66, the difference of pseudo cohesions obtained comparing 2-dimensional numerical results may be underestimated. Combination of 3-dimensional analyses and experiments mentioned below is needed in order to quantify the difference.

Figure 5-81 is an example of numerical model to gain better understandings on influence of relative size of pile to size of rock particles. Making random distributions of

rock ground and running analyses many times, basic data about some statistical parameters may be available.

5.4.2.2 Centrifuge test

As described in Section 2.2.2, centrifuge tests are commonly conducted for soil-pile interaction problems with scaled models. Centrifuge test device can simulate stress condition in soils, and save cost and time because it does not require large size specimens. However, because scale effect of interlocking between pile and large grain rock particles is not clear yet, centrifuge test results have to be compared with results from full- or large-scale tests. In addition, experimental results need to be supplemented with results from numerical analysis in order to gain better understandings what happens on pile in rockfill.

Figure 5-82 is an example of centrifuge test setup for inertial loading. The advantage of usage of glass beads is enabling to make ideal uniform grain size soil. Replacing different size glass beads, effect of grain size to contribution level of interlocking can be clarified. Installation of piles with various dimensions can show how relative pile size to particle size affects on behavior of pile.

Figure 5-83 shows a possible centrifuge test setup for kinematic load. Ground displacement can be inputted using a laminar box and a loading piston. Comparing results for inertial and kinematic loadings with exactly same pile dimension and glass beads diameter, differences on behaviors of pile, soil particles, and their interaction can be understood.

5.4.2.3 Full-scale test

As mentioned in the section of centrifuge test, full- or large-scale tests are needed to verify scale effect on pile in large particle size rockfill. Full- or large-scale tests are most ideal to simulate realistic condition of prototype target structures; however, it takes large cost and time. Therefore, plan of full- and large-scale tests has to be made with careful considerations. Numerical analyses, small-scale tests, and centrifuge tests can provide

useful information in order to make more reasonable test plans of full- or large-scale tests. Also, full-scale test results have to be compared with numerical and scaled test results to complement each other.

An example of full-scale test on reaction generation in rockfill is shown in Figure 5-84. Set of p - y curves for inertial loading can be directly obtained from records of load and displacement on actuator. Changing size of the loading plate and weight on embankment of rockfill, pile size and overburden dependency on p - y curves can be clarified. Also, effect of loading rate to reaction generation can be found applying load in various rates.

Also, full- or large-scale test of laterally loaded pile for kinematic load condition can be conducted using large laminar box and large capacity actuator. Test setup may be similar as a centrifuge test shown in Figure 5-83. From this test setup, relationship between input displacement of rockfill and drag force acting on pile can be derived. The results can be widely used for design practice in future.

5.4.2.4 Laboratory element tests

As mentioned above, numerical parameters for design should be defined from the minimum efforts, such as small-scale laboratory test and element tests including triaxial or direct shear test. In order to achieve this, constitutive model for the p - y curves reasonably fitting to any type of soil needs to be developed based on mechanics of soil and interaction between pile and soil, or empirical data base. There are some differences of parameters between theory and reality, and several sets of in-situ large-scale lateral load pile and laboratory tests are required in order to collect information about empirical correlation between them comparing their results (refer Figure 5-78).

5.5 Summary

Comparing the test results with the numerical results calculated using the p - y curves currently adopted in design of wharf structures, it was concluded that the curves needed

to be modified in order to make more accurate prediction analysis. Based on the observations during and after loading the test piles, the reaction from the rockfill under low confinement seems to have significant effect on the behavior of the laterally loaded soil-pile systems. In order to account for that, the interlocking concept was included into the p - y curves used for current design practice. Magnitude of the interlocking was quantified by backcalculation of the test results. According to comparisons of the test results and the numerical results with the backcalculated interlocking, the inclusion of the interlocking could reasonably improve the numerical results for all the tests.

In order to estimate impact of the interlocking on design of entire wharf structure, a series of pushover analyses with numerical model of an actual whole wharf were also conducted. As a result, the interlocking had significant effects on the behavior of the wharf structure, but the p - y curves used for design practice without the interlocking could reasonably cover possible behaviors of the wharf using appropriate p -multipliers in certain range of design inertial force or displacement at wharf deck.

At the last moment, important uncertainties found through this entire research work were listed up, and some ideas of possible future research were proposed to clarify the uncertainties. In order to make more reliable design analysis and make the understanding obtained in this study applicable for more general issues, more research works need to be performed in future.

Table 5-1 Summary of analysis cases for back analysis with various p -multipliers

Test Setup	Analysis Case	p -multipliers (m_p)	Corresponding analysis case in the current design
Single Pile Tests	SPB-1	1.0	Standard
	SPB-2	2.0	Upper bound
	SPB-3	5.0	--- ¹⁾

- 1) The analysis case with $m_p = 5$ provided the best fitted load displacement curve for Single Pile Test 1.

Table 5-2 Summary of analysis cases for back analysis with interlocking and settlement

Test Setup	Analysis Case	<i>p</i> -multipliers		Interlocking	Settlement ²⁾	Note
		Pile on level ground (m_{pl})	Pile on downslope ¹⁾ (m_{ps})			
Single Pile Tests	SPB-2	2.0	---	No	No	Providing reasonable profiles of pile response
	SPB-3	5.0	---	No	No	Providing reasonable load displacement curve at pile top
	SPB-4	1.0	---	Yes	No	<i>p</i> - <i>y</i> curves ($m_p=1$) + Interlocking
System Tests	SYB-1	2.0	2.0	No	No	Providing reasonable profiles of pile response
		2.0	2.0	No	Yes	
	SYB-2	1.0	0.3	Yes	No	<i>p</i> - <i>y</i> curves ($m_p=1$) + Interlocking + Slope effect
		1.0	0.3	Yes	Yes	

1) *p*-multipliers in this column are used for pile on slope only during loading toward downslope.

2) Soil pile springs at the top 2 ft from the original ground surface were removed in order to represent the condition after loading with 2 ft settlement.

Table 5-3 Summary of analysis cases for entire wharf structure

Analysis Case	p -multipliers on p -y curves for rockfill (m_p)		Consideration of interlocking	Note
	Pile on level ground (m_{pl})	Pile on downslope (m_{ps})		
WS-1	0.3	0.3	No	Lower bound analysis in the current design
WS-2	1.0	1.0	No	Standard analysis in the current design
WS-3	2.0	2.0	No	Upper bound analysis in the current design
WS-4	1.0	0.3	Yes	Standard case + Slope effect + Interlocking (providing the best results in this research)

Table 5-4 Numerical parameters used for analysis on entire wharf behavior

Soil type	Total unit weight pcf (kN/m ³)	Friction angle degrees	Cohesion psf (kPa)
Loose Marine Sand (liquefiable)	120 (18.9)	--- ¹⁾	---
Medium Dense to Dense Marine Sand	125 (19.6)	35	---
Soft to Stiff Lagoonal Clay	110 (17.3)	---	1000 (47.9)
Stiff Lagoonal Clay	115 (18.1)	---	1500 (71.8)

1) No reaction from liquefiable sand is assumed because of effect of pore pressure built-up and small thickness of this layer.

Table 5-5 Summary of important uncertainties on behavior of pile in rockfill

Uncertainty	Impact when it can be clarified
Particulate reaction generation mechanism for inertial / kinematic forces	<ul style="list-style-type: none"> - Gaining the most fundamental and important information - Enabling to make more reasonable assumptions for both of research and designs and directing the other research at the next stage
Gradation of rockfill	<ul style="list-style-type: none"> - Modifying the p-y curves obtained in this study for other rockfills with different gradations
Particle size / Relative particle size to pile	<ul style="list-style-type: none"> - Obtaining better understandings on contribution of interlocking and friction in different particle size soils - Understanding effect of relative size of soil particle to interaction between pile and soil
Effective overburden stress	<ul style="list-style-type: none"> - Clarifying on effective stress dependency of reactions from friction and interlocking
Loading rate	<ul style="list-style-type: none"> - Expanding the p-y curves in this study to the dynamic problems
Loading type	<ul style="list-style-type: none"> - Clarifying differences of p-y curves under different loading condition
Random distribution of rockfill particles	<ul style="list-style-type: none"> - Enabling more reasonable probabilistic design
Relation between element test results and numerical parameters	<ul style="list-style-type: none"> - Defining reasonable numerical parameters for pushover analysis from laboratory element tests

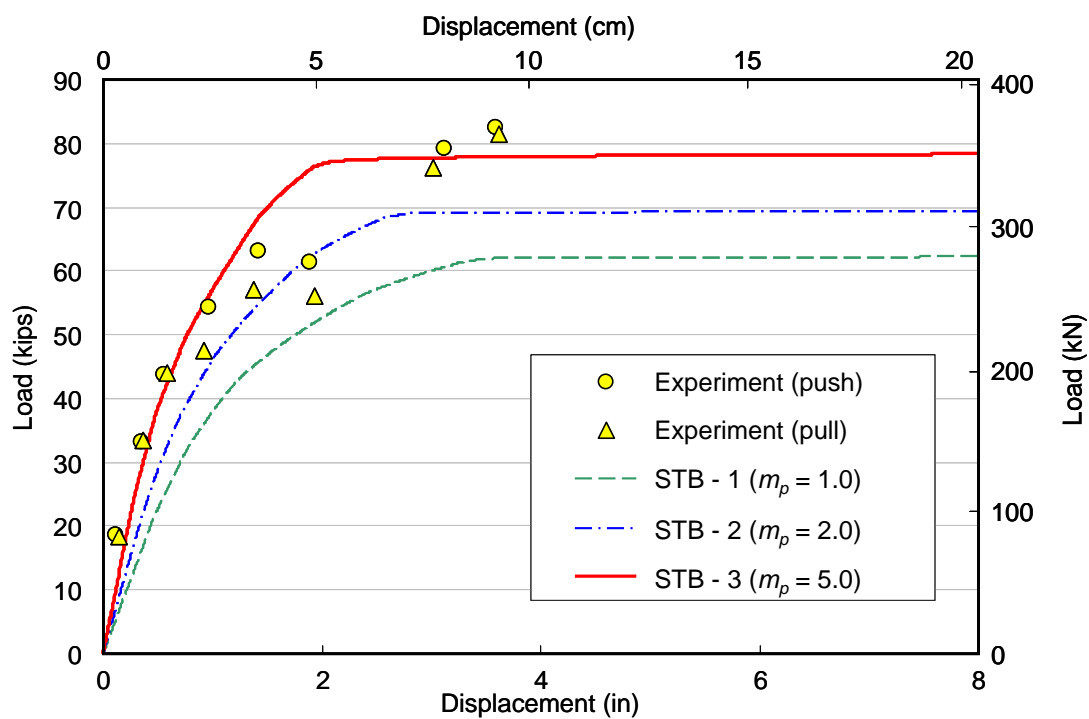


Figure 5-1 Load-displacement curve for Single Pile Test 1 with various p -multipliers

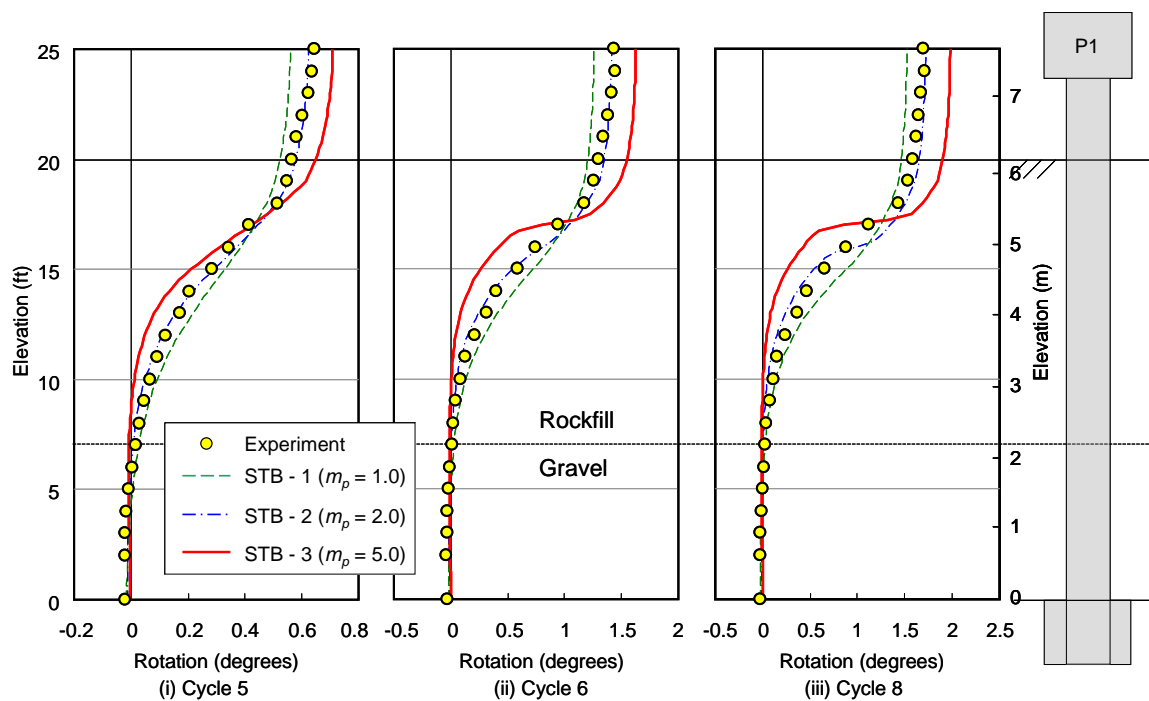


Figure 5-2 Rotation profiles for Single Pile Test 1 with various p -multipliers

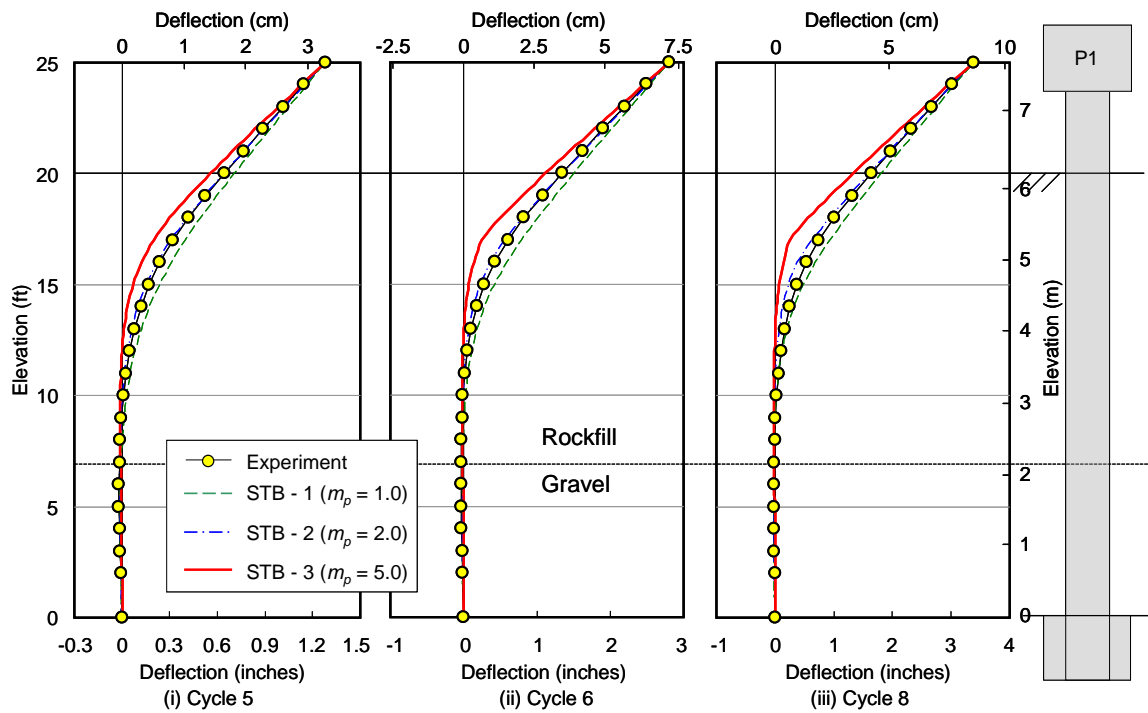


Figure 5-3 Deflection profiles for Single Pile Test 1 with various p -multipliers

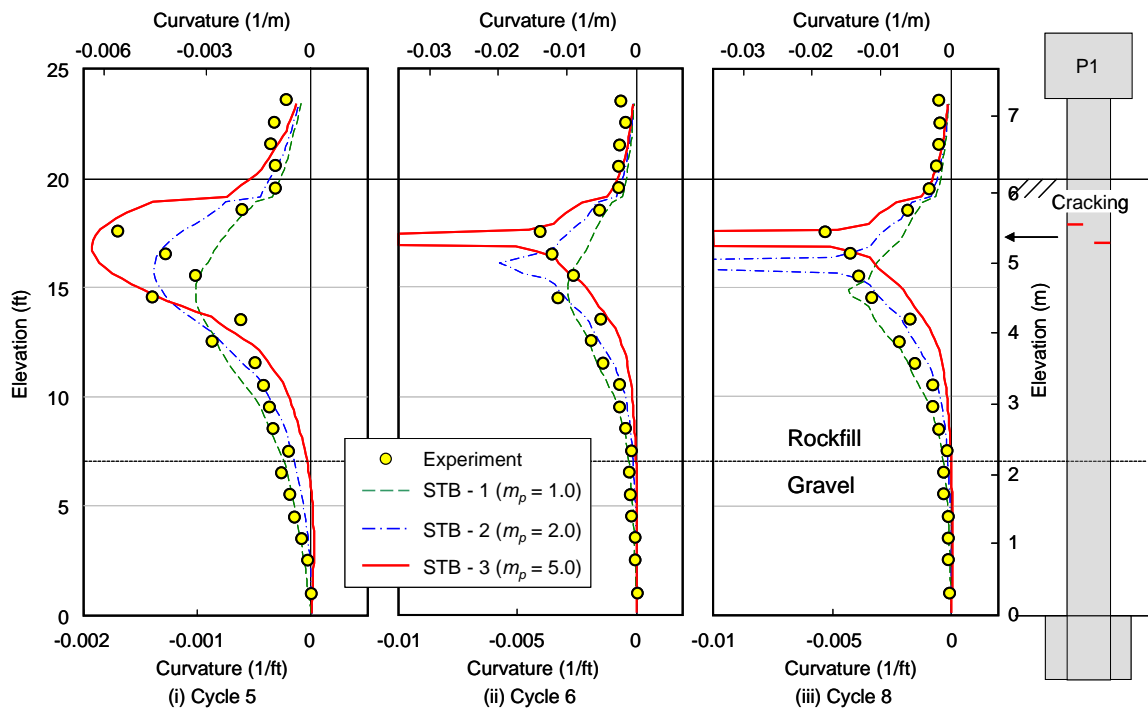


Figure 5-4 Curvature profiles for Single Pile Test 1 with various p -multipliers

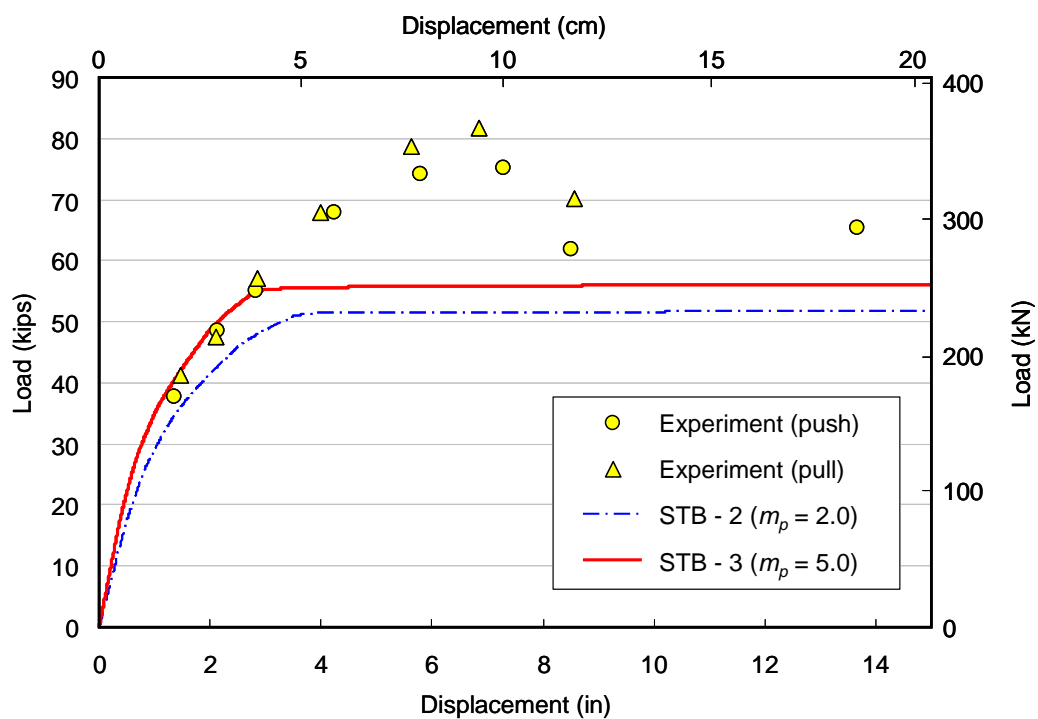


Figure 5-5 Load-displacement curve for Single Pile Test 2 with various p -multipliers

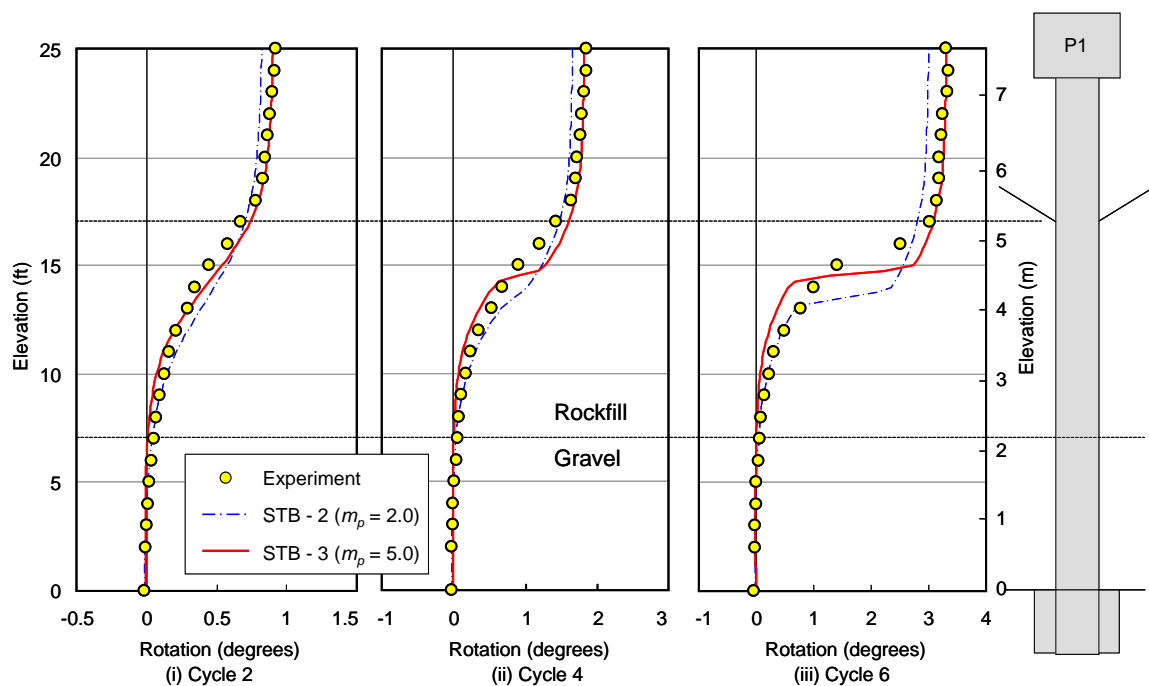


Figure 5-6 Rotation profiles for Single Pile Test 2 with various p -multipliers

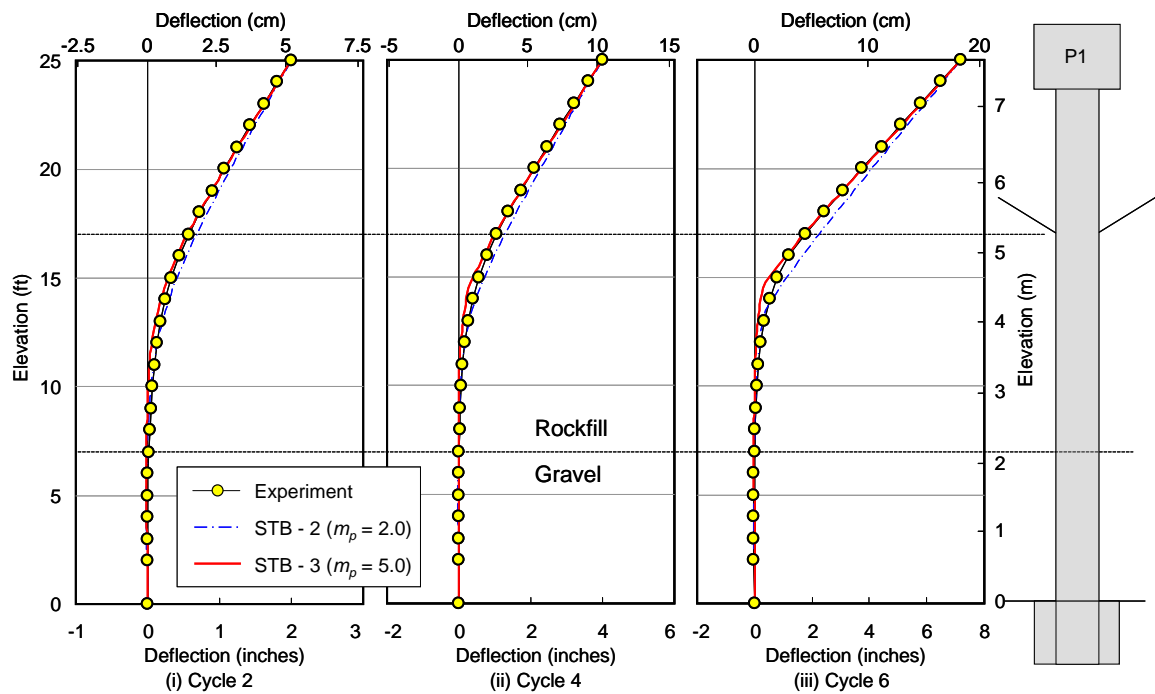


Figure 5-7 Deflection profiles for Single Pile Test 2 with various p -multipliers

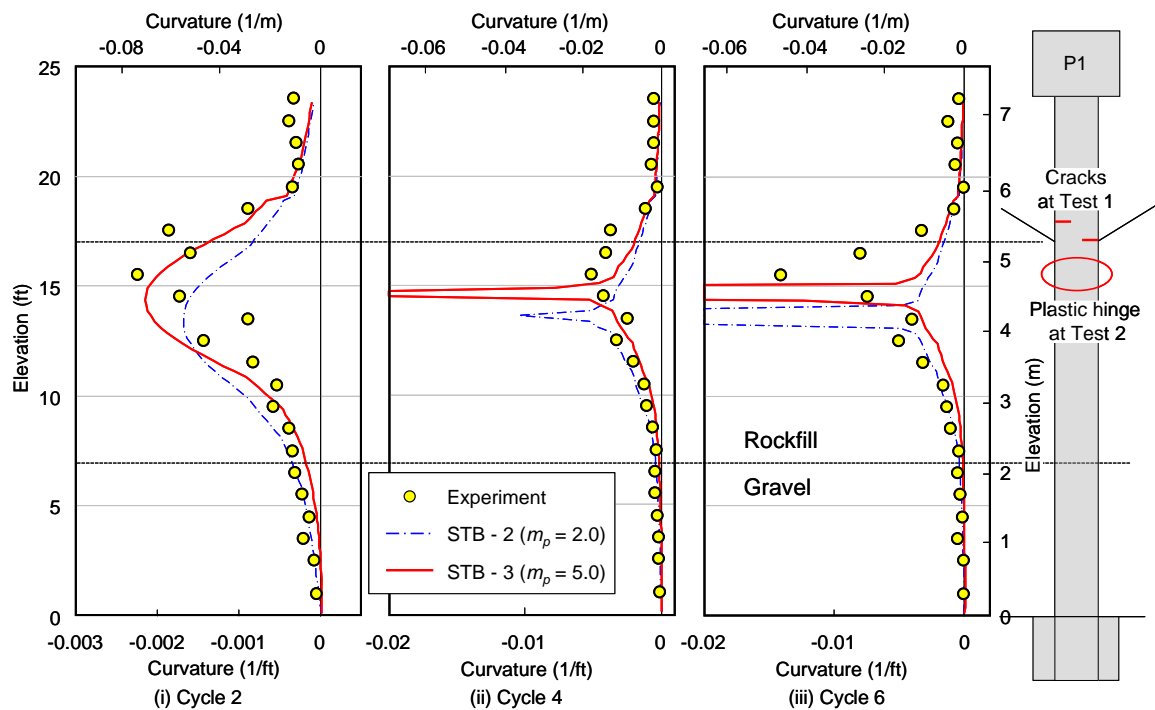


Figure 5-8 Curvature profiles for Single Pile Test 2 with various p -multipliers



(a) Fractured rocks, shows interlocking



(b) Pock-marks, evidence of point load



(c) Relatively dense contact



(d) Gap next to pile



(e) About 18-24 inches settlement



(f) Particle compression during loading

Figure 5-9 Notable observations

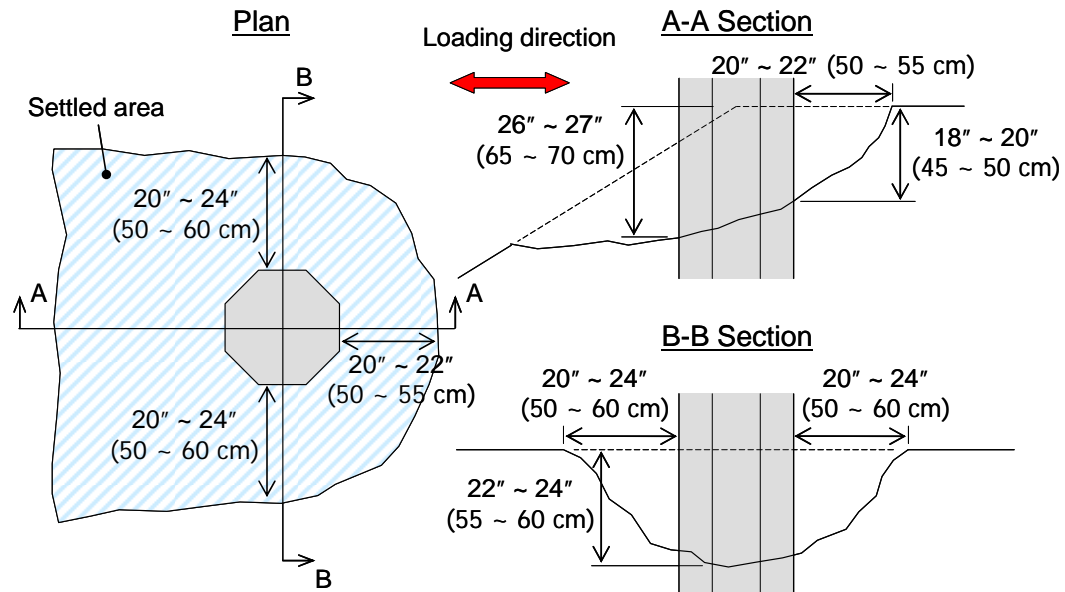


Figure 5-10 Sketch of settlement around P5 after System Test 1

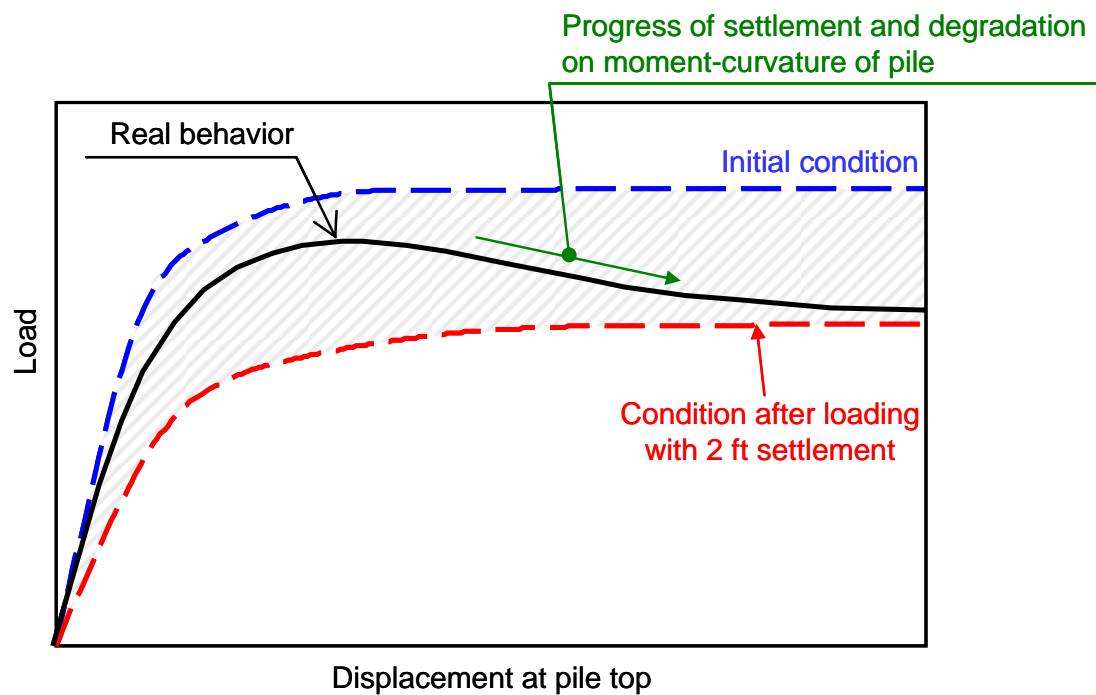


Figure 5-11 Concept of effect of settlement around pile on load displacement curve

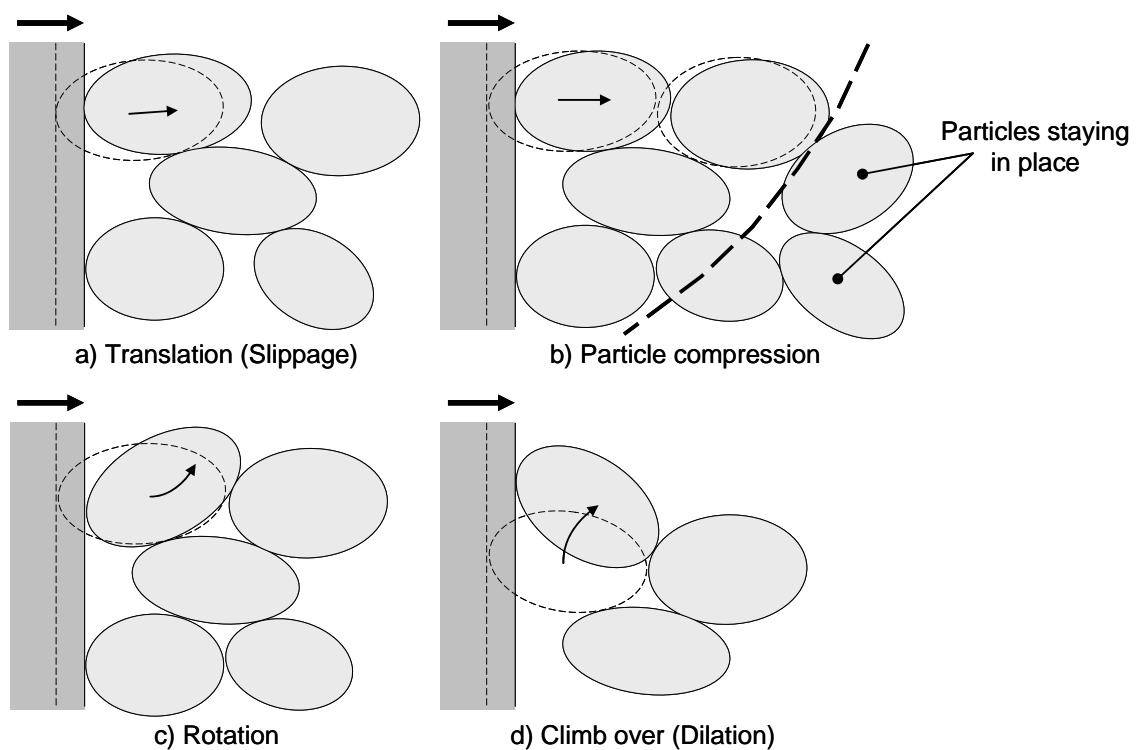


Figure 5-12 Possible particle movements

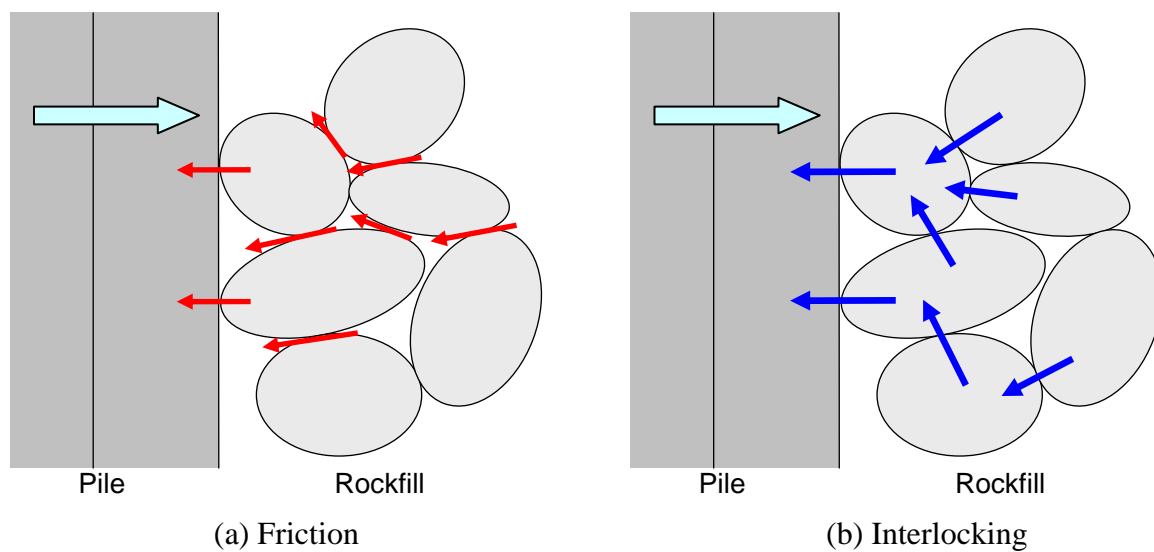


Figure 5-13 Definition of friction and interlocking

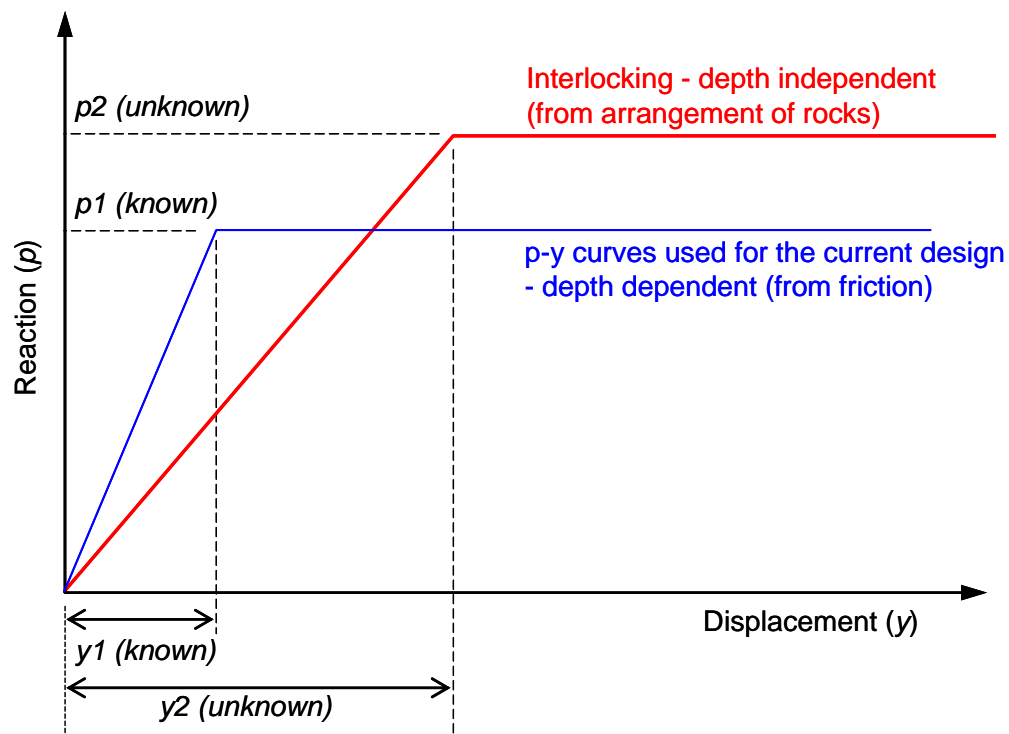


Figure 5-14 Concept on soil-pile spring of friction and depth independent interlocking

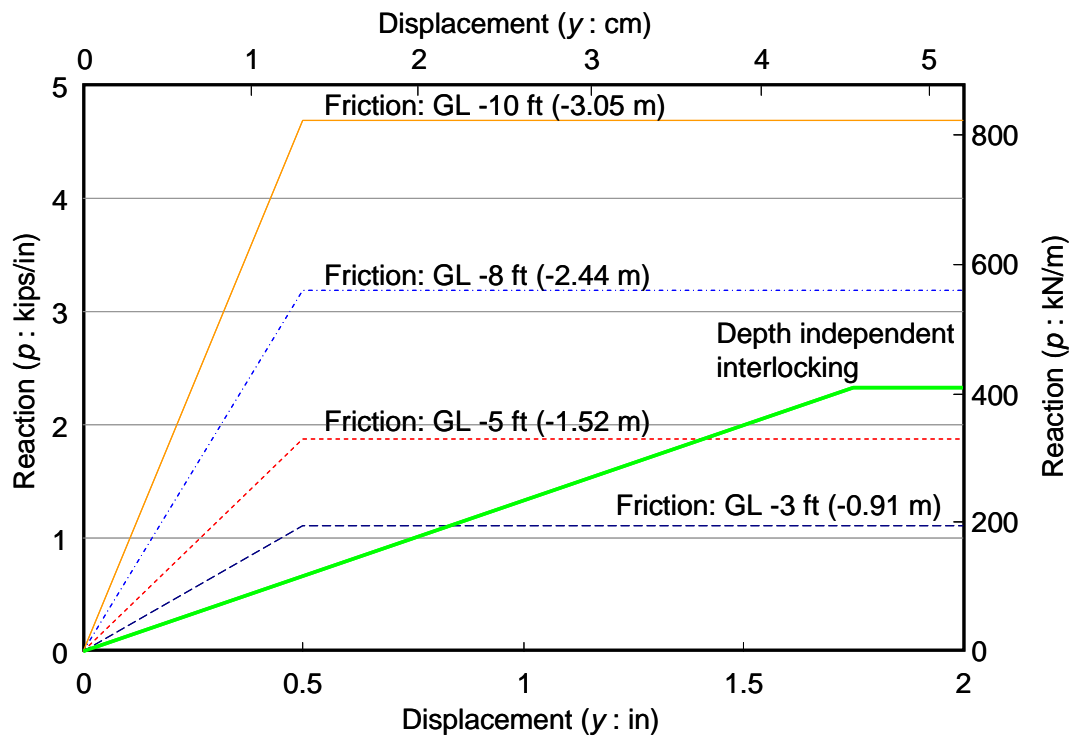


Figure 5-15 Soil-pile springs of friction and depth independent interlocking

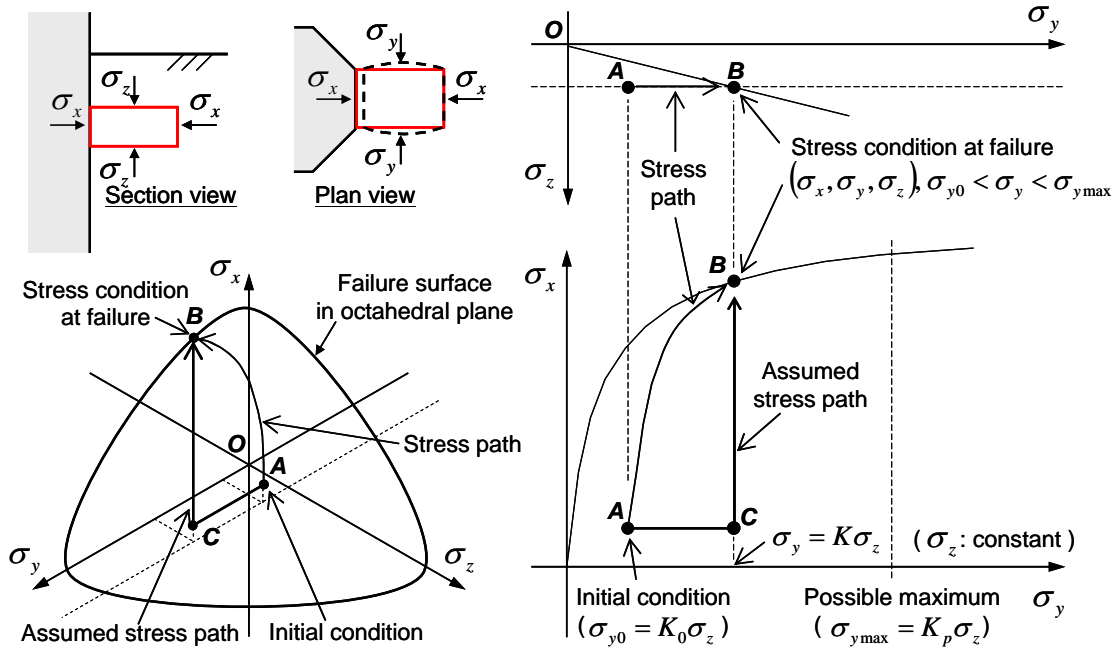


Figure 5-16 Three-dimensional stress pass in rockfill

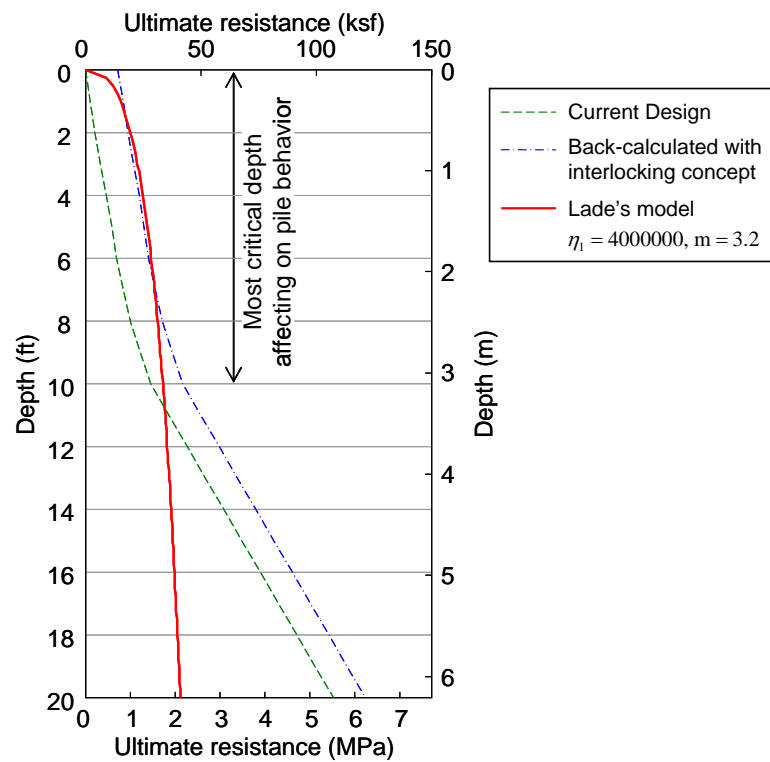


Figure 5-17 Comparison of profiles of ultimate shear resistance

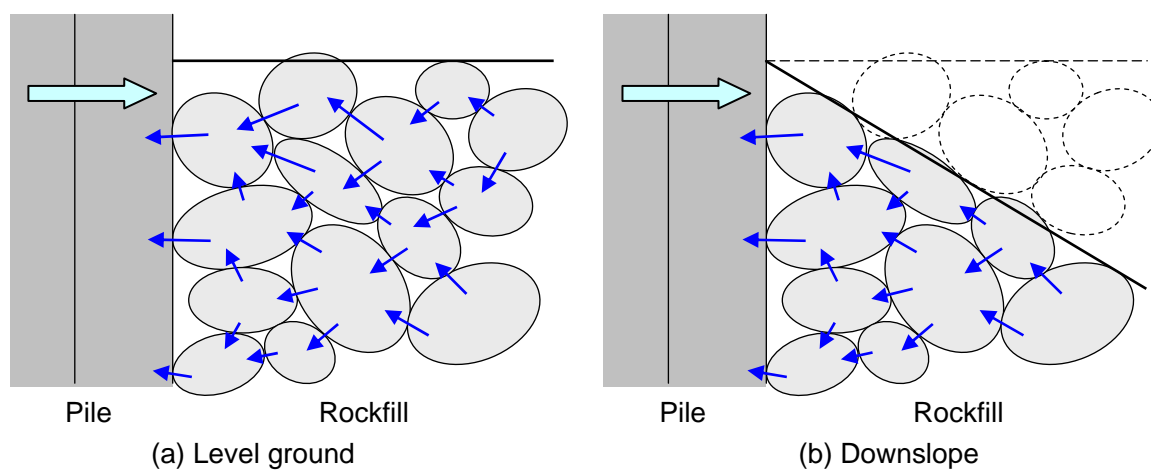


Figure 5-18 Effect of downslope to interlocking

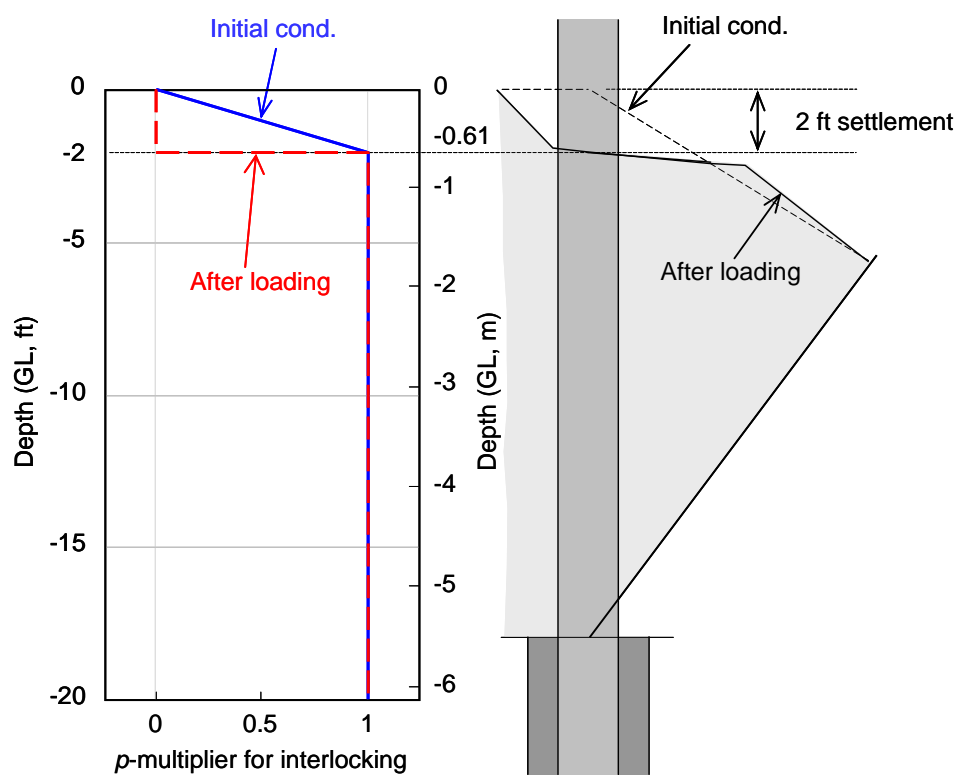


Figure 5-19 Multiplier of interlocking reduction for piles on downslope

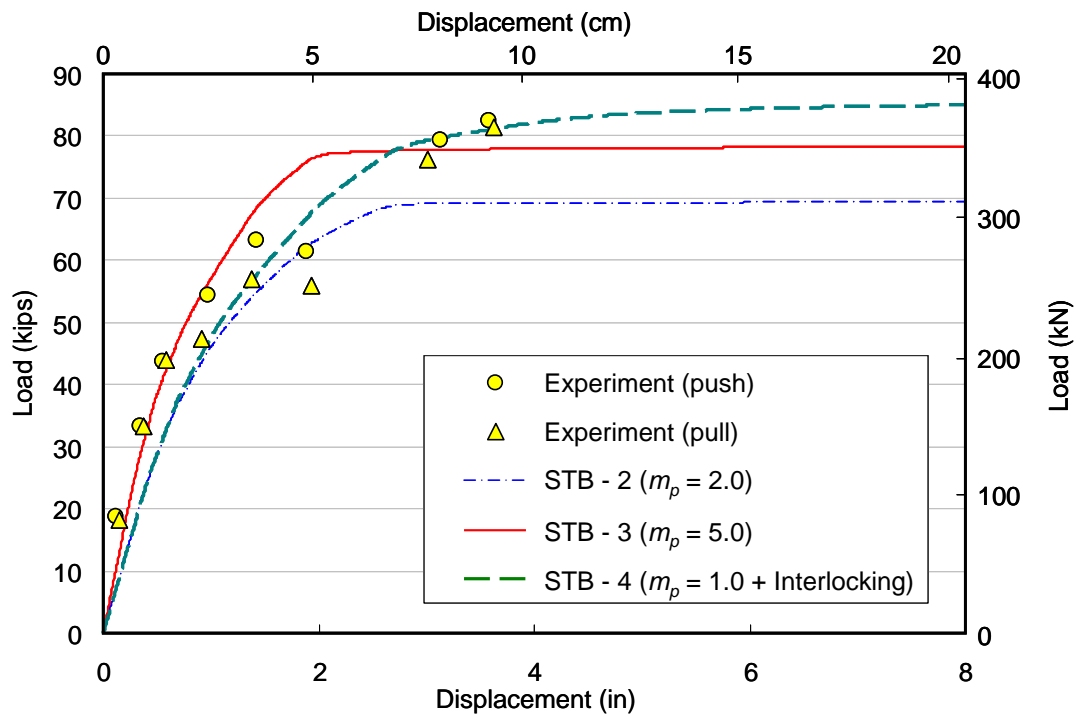


Figure 5-20 Load-displacement curve for Single Pile Test 1 with p -multipliers and interlocking

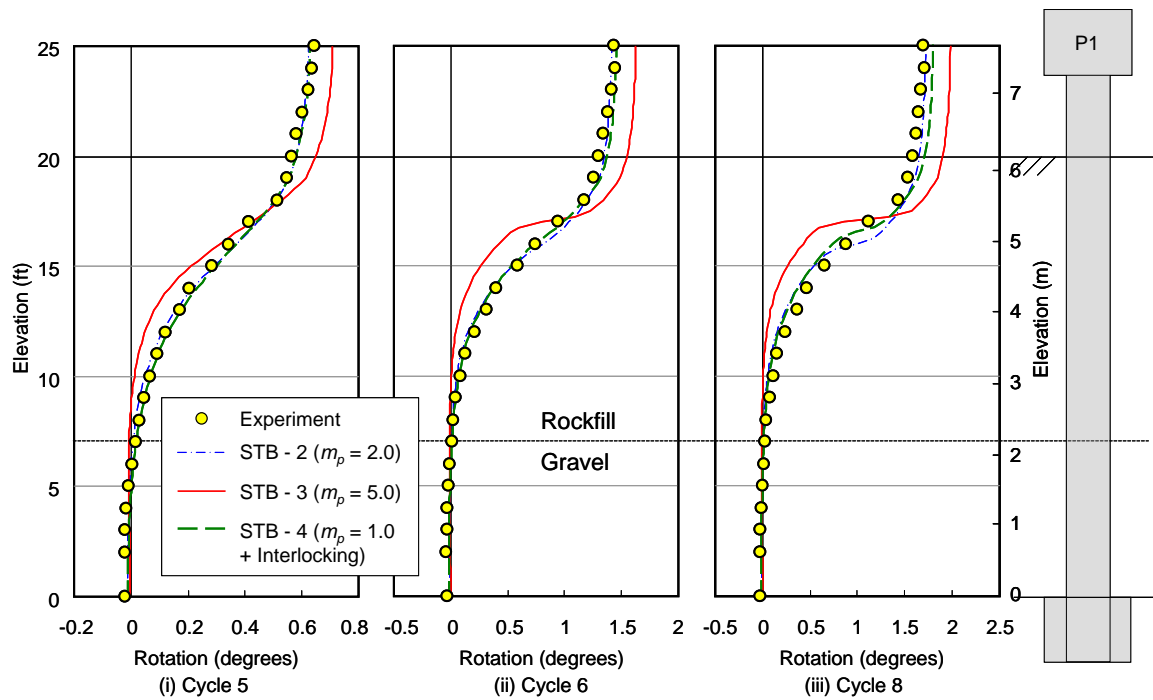


Figure 5-21 Rotation profiles for Single Pile Test 1 with p -multipliers and interlocking

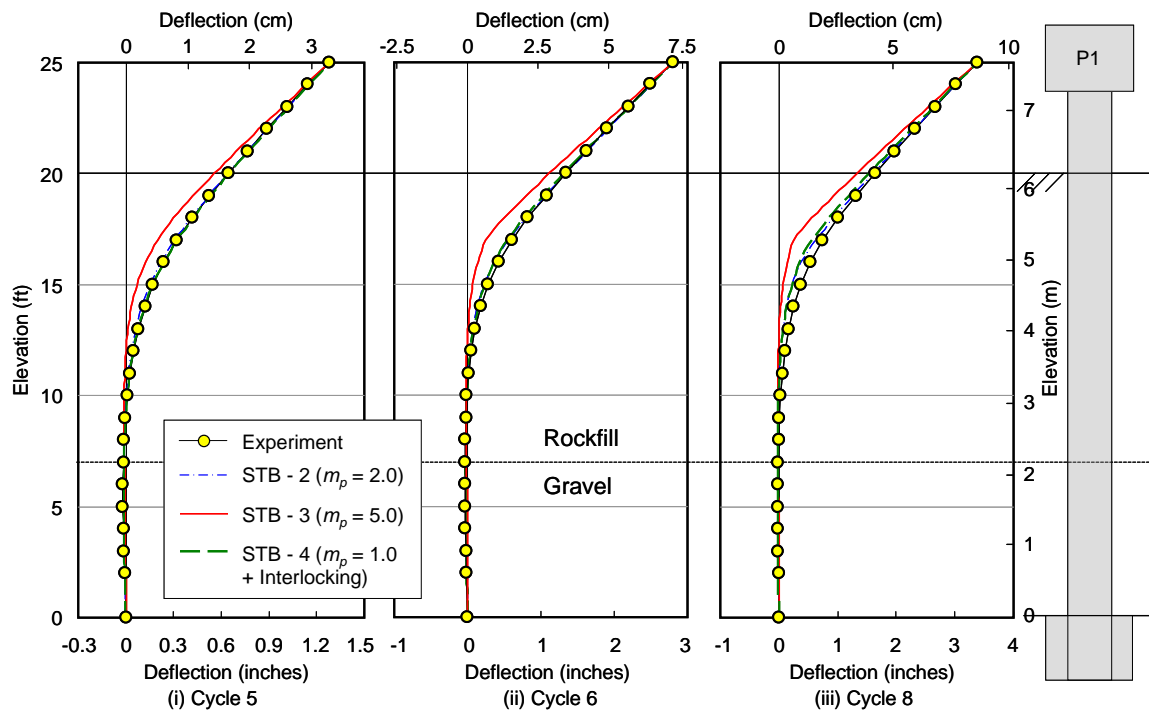


Figure 5-22 Deflection profiles for Single Pile Test 1 with p -multipliers and interlocking

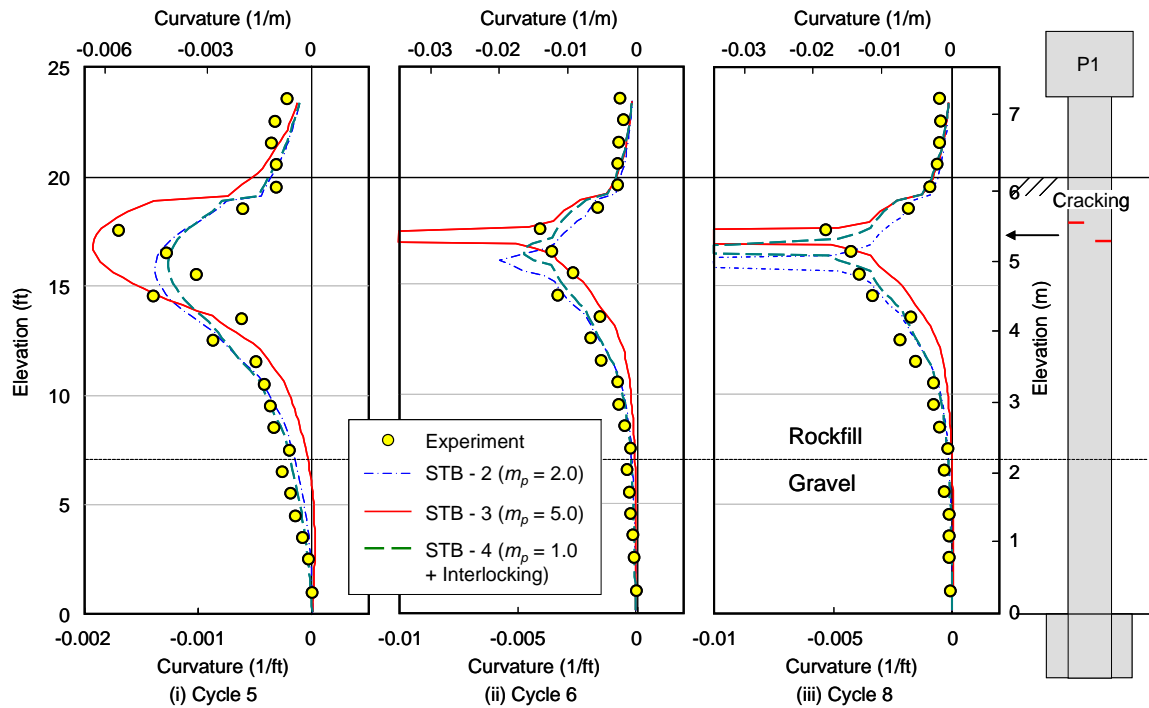


Figure 5-23 Curvature profiles for Single Pile Test 1 with p -multipliers and interlocking

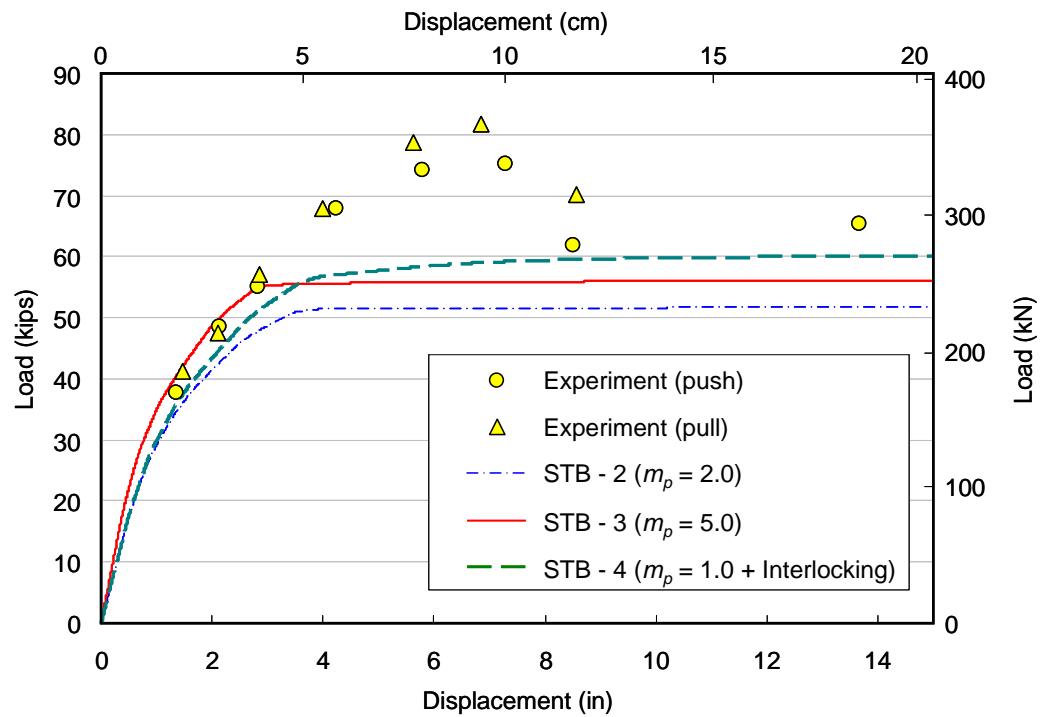


Figure 5-24 Load-displacement curve for Single Pile Test 2 with p -multipliers and interlocking

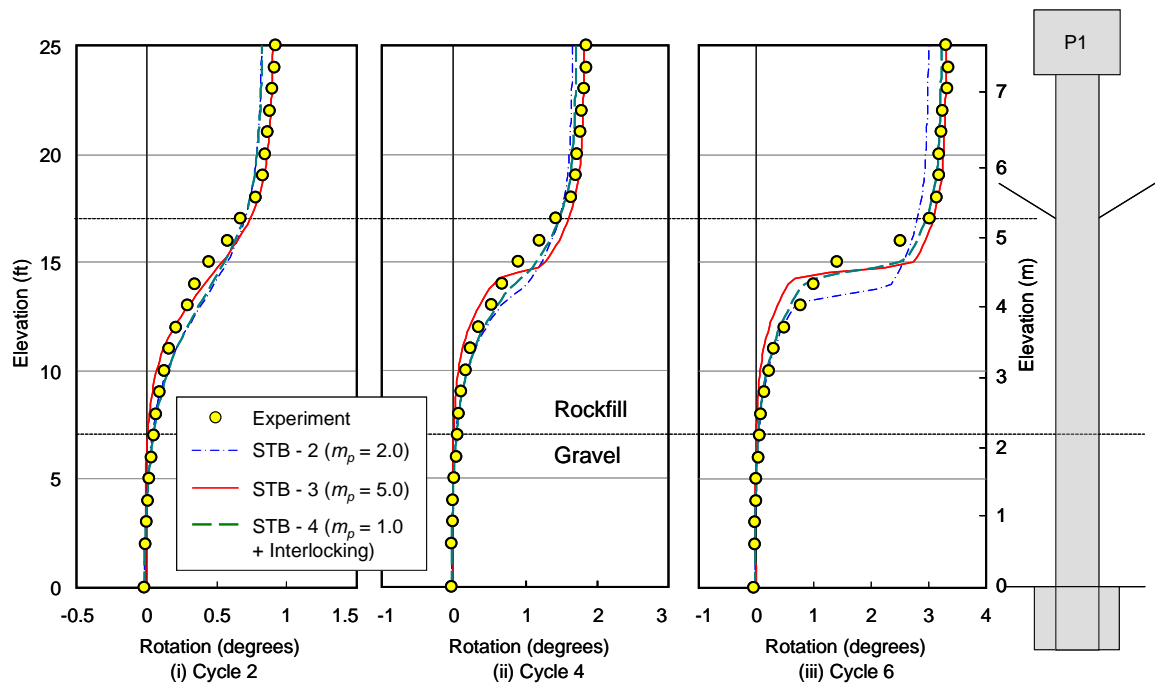


Figure 5-25 Rotation profiles for Single Pile Test 2 with p -multipliers and interlocking

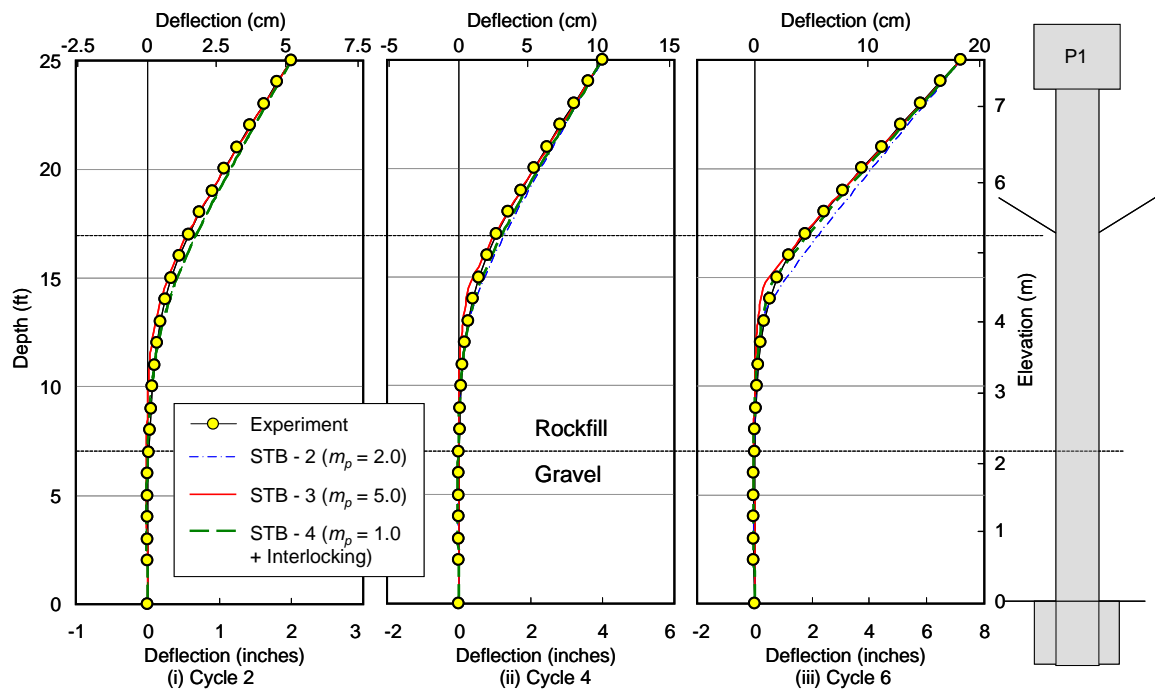


Figure 5-26 Deflection profiles for Single Pile Test 2 with p -multipliers and interlocking

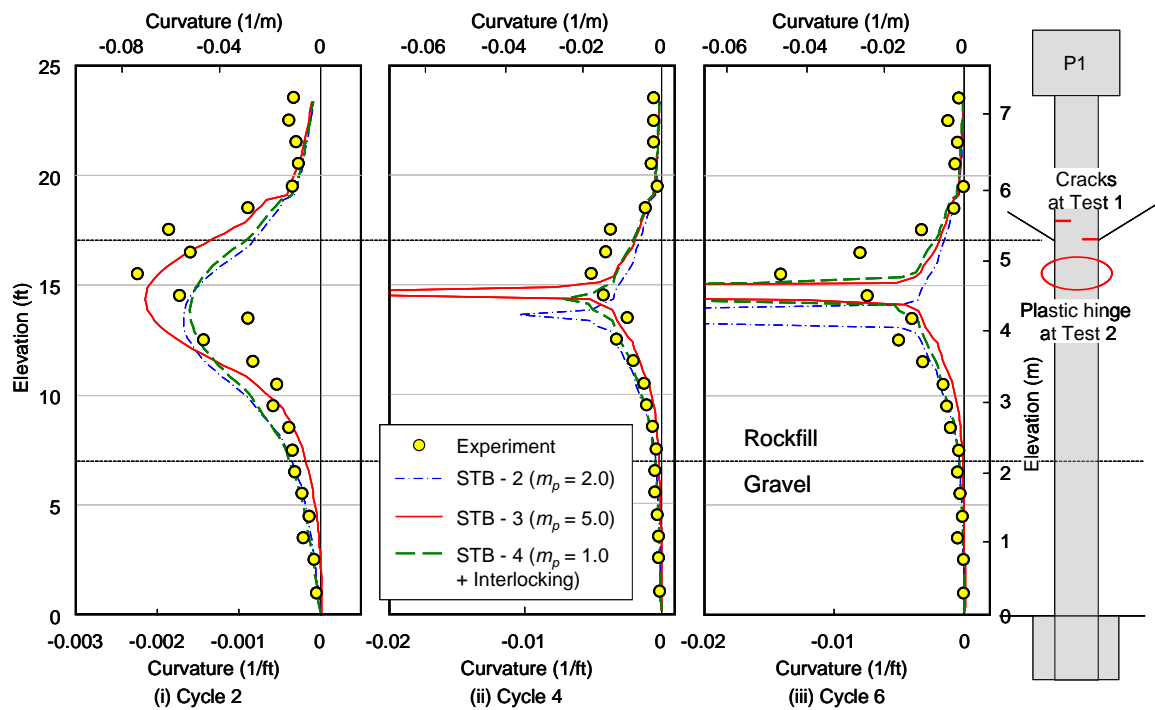


Figure 5-27 Curvature profiles for Single Pile Test 2 with p -multipliers and interlocking

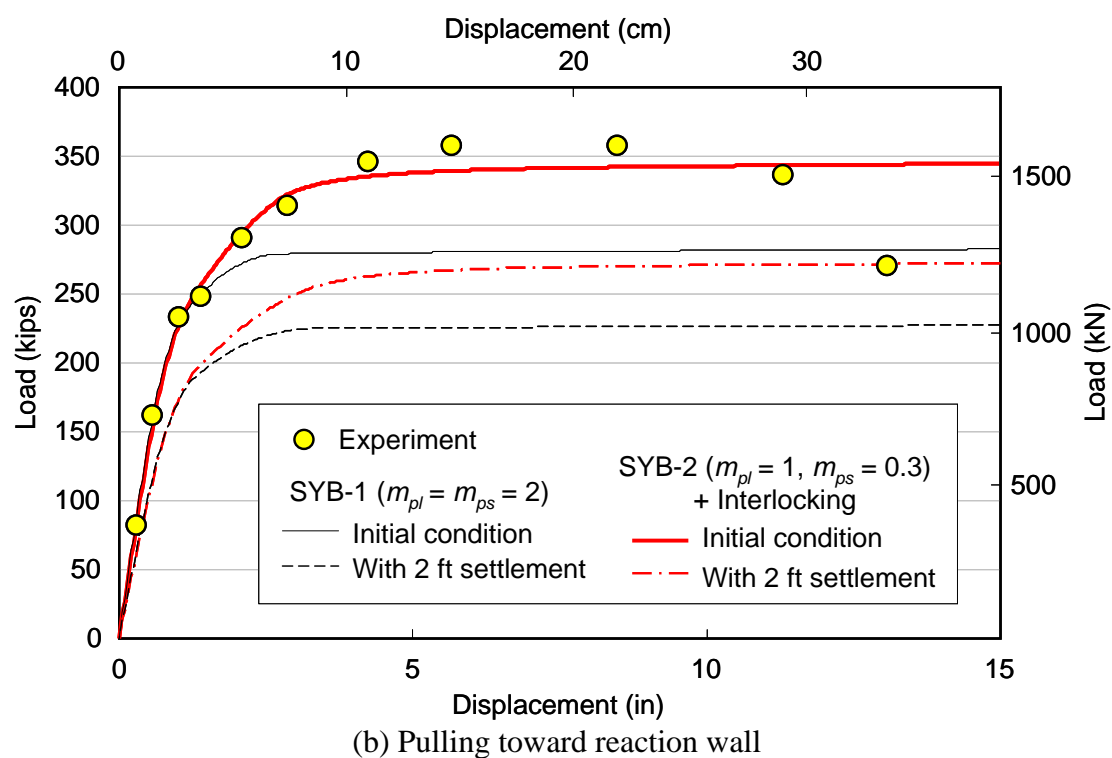
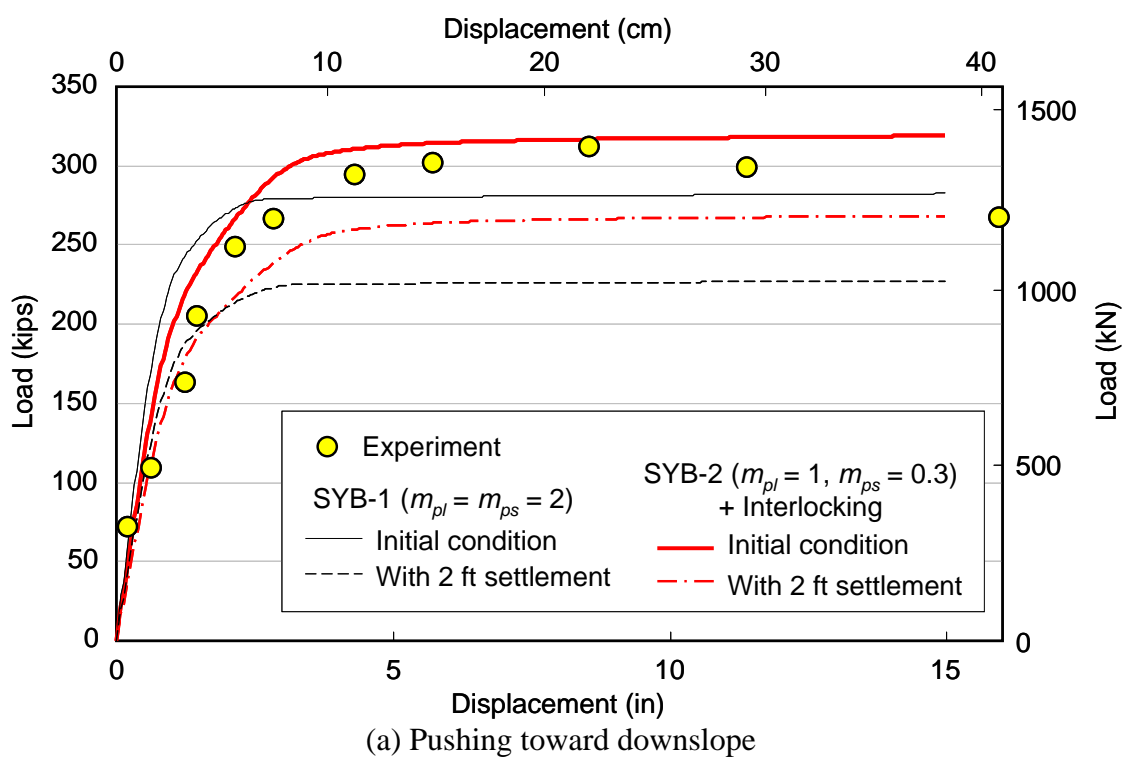


Figure 5-28 Load-displacement curve for System Test 1 with p -multipliers and interlocking

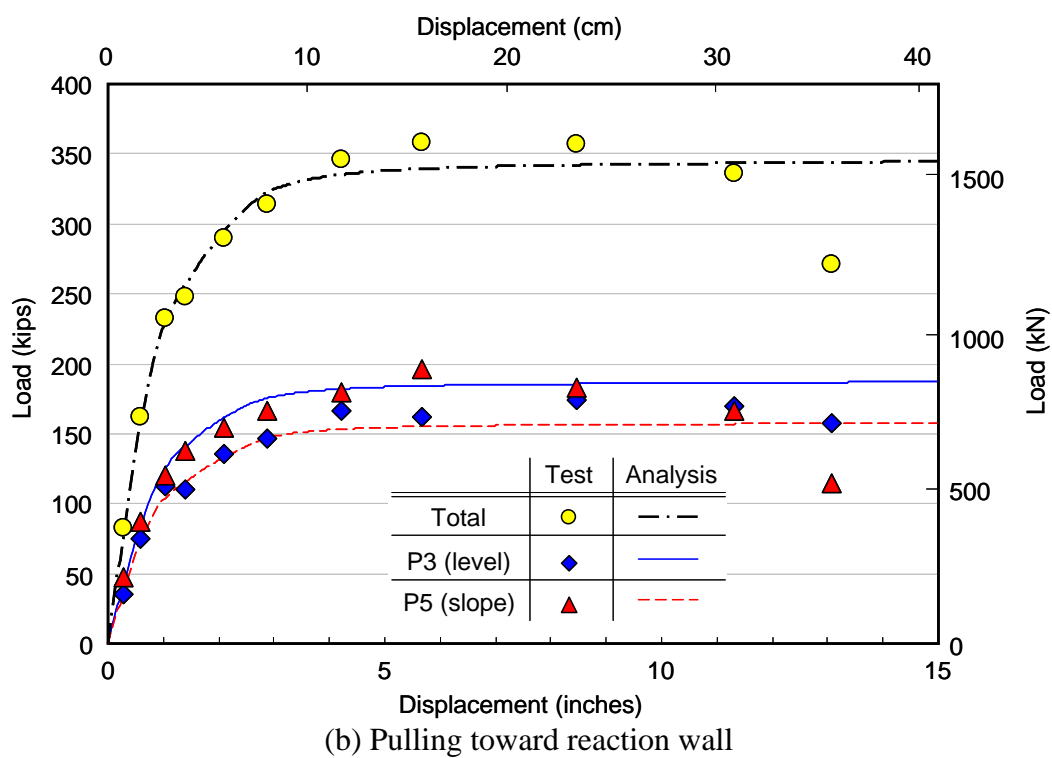
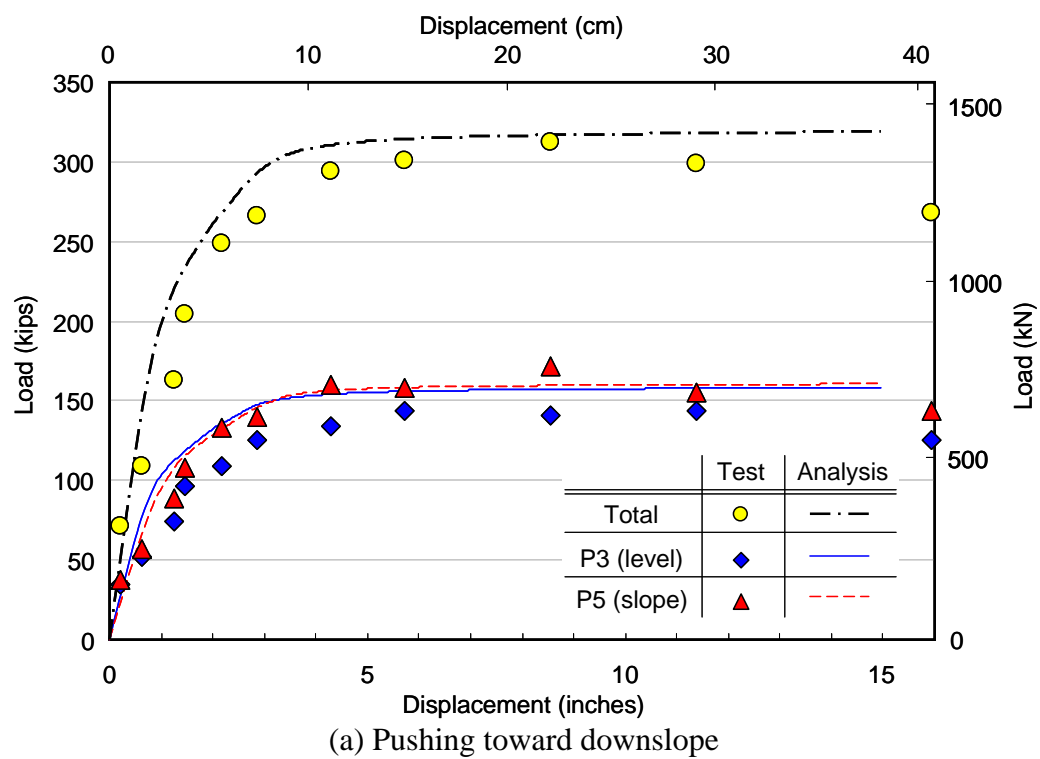


Figure 5-29 Load-displacement curve on each pile for System Test 1 with p -multipliers and interlocking

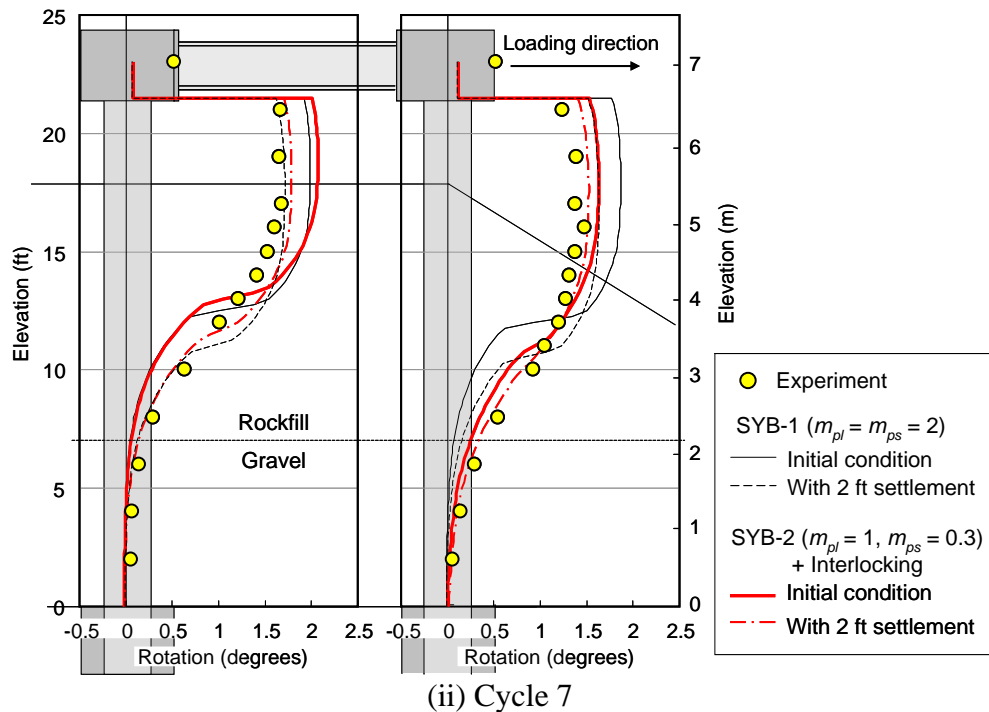
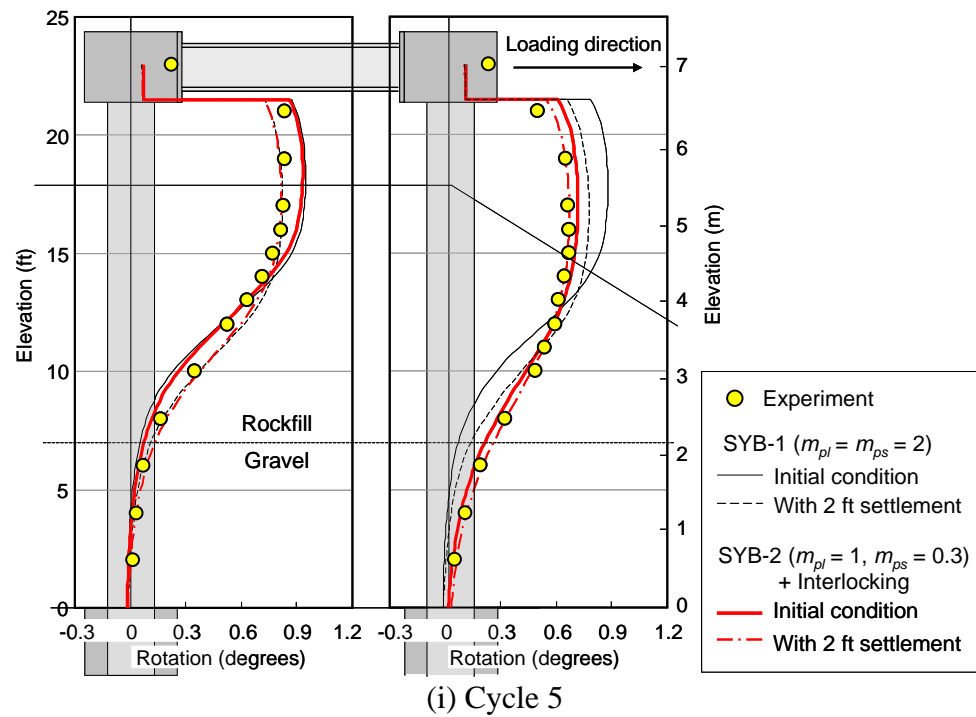


Figure 5-31 Rotation profiles for System Test 1 with p -multipliers and interlocking (pushing)

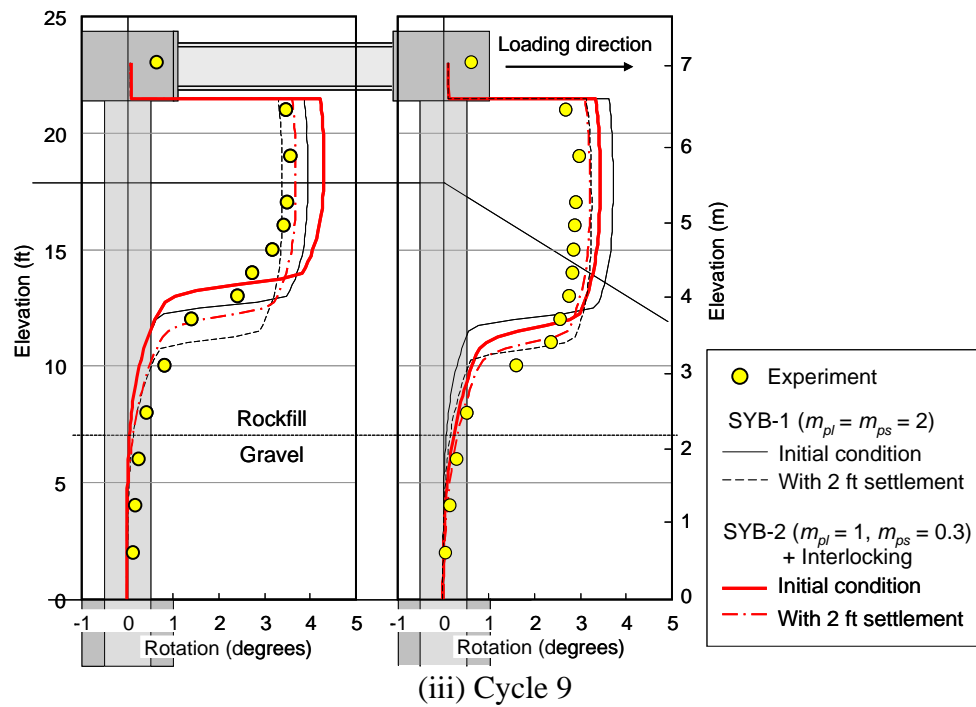


Figure 5-31 Rotation profiles for System Test 1 with p -multipliers and interlocking (pushing: continued)

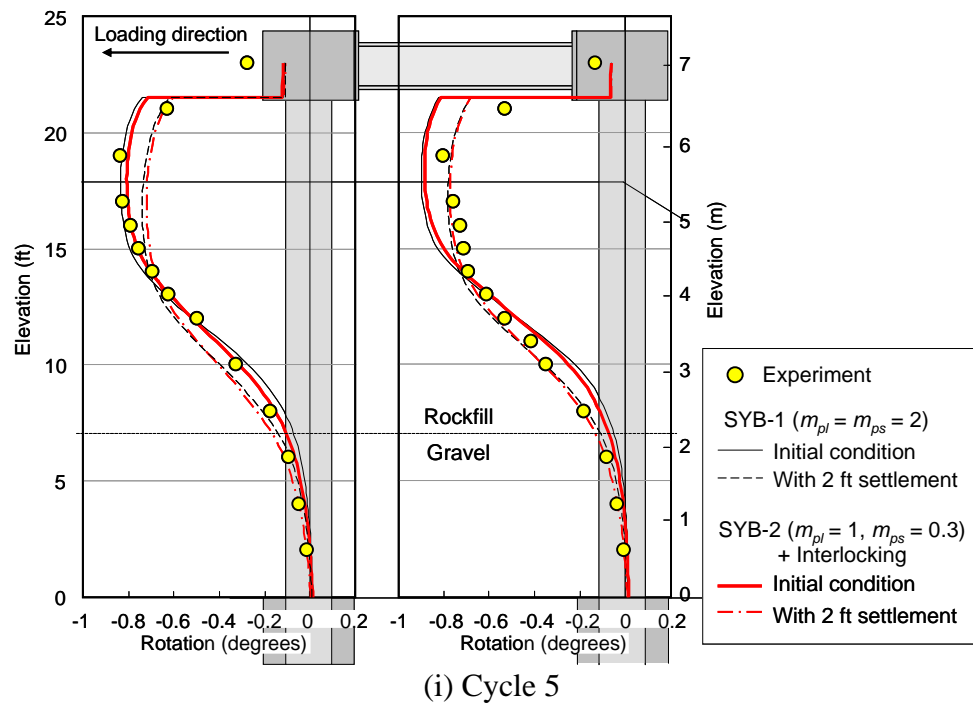


Figure 5-32 Rotation profiles for System Test 1 with p -multipliers and interlocking (pulling)

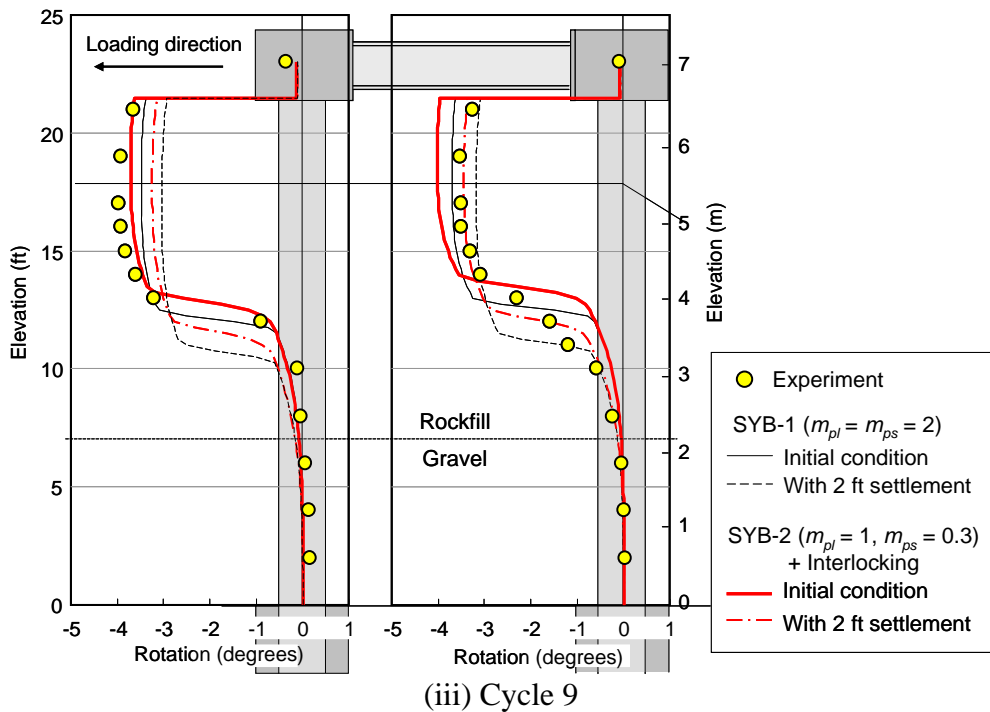
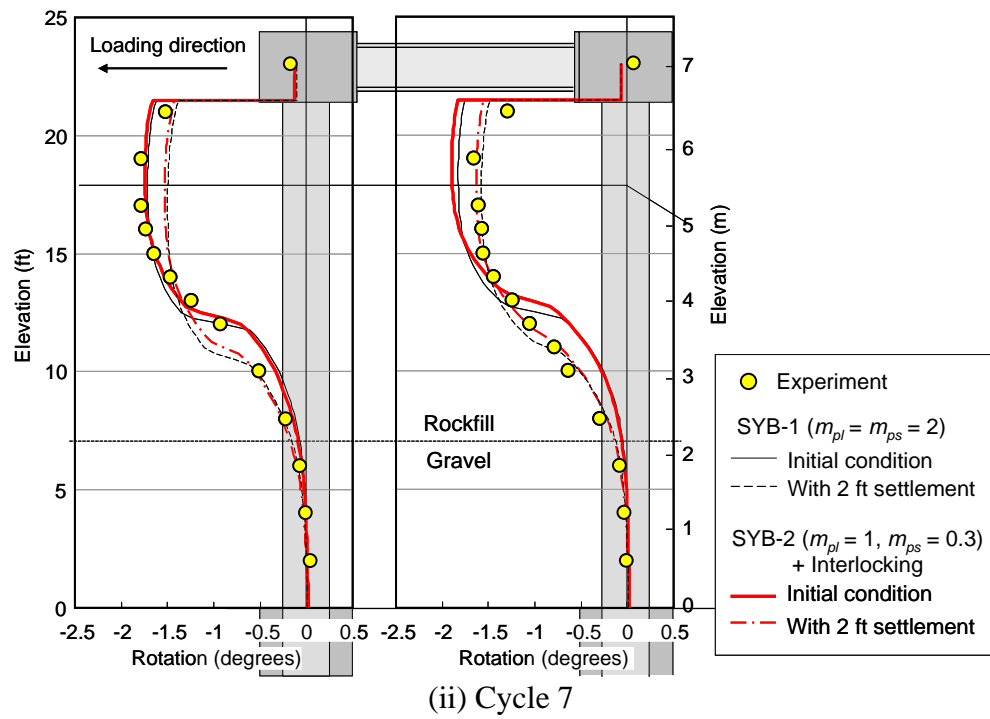


Figure 5-32 Rotation profiles for System Test 1 with p -multipliers and interlocking (pulling: continued)

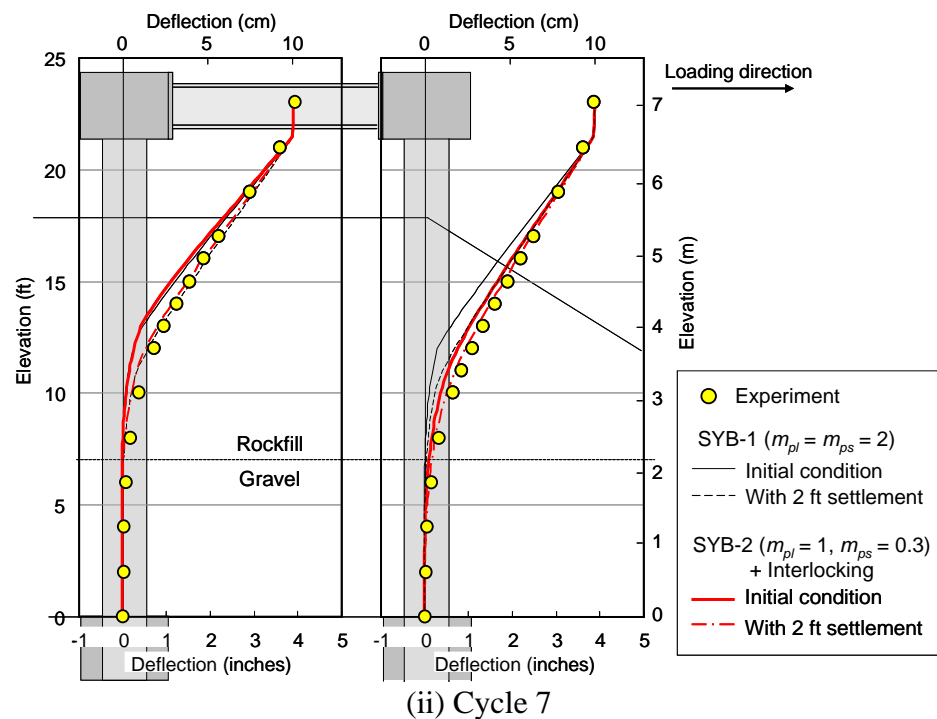
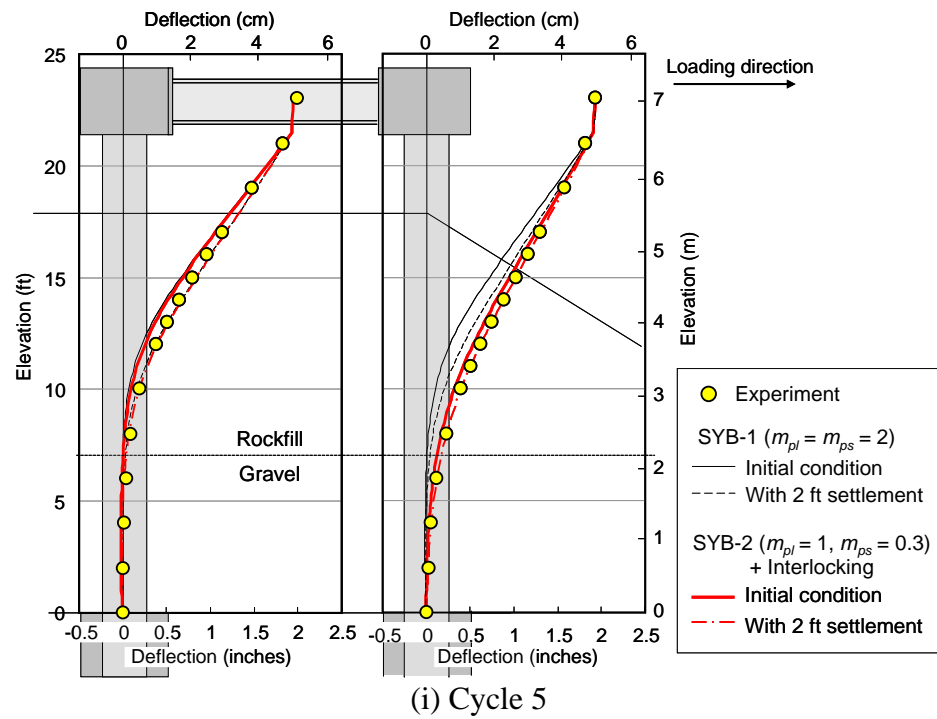


Figure 5-33 Deflection profiles for System Test 1 with p -multipliers and interlocking (pushing)

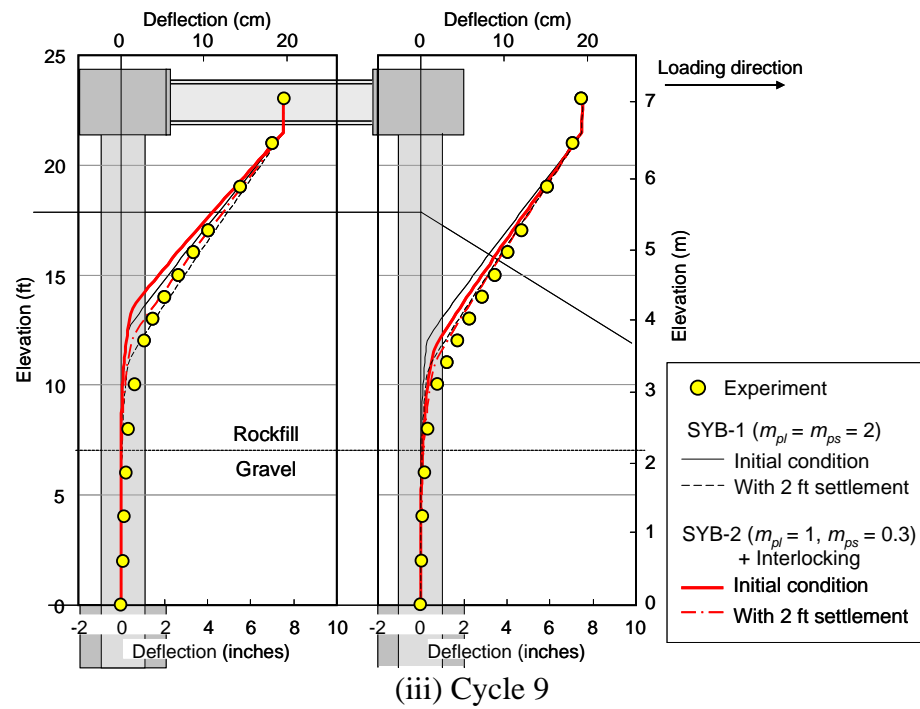


Figure 5-33 Deflection profiles for System Test 1 with p -multipliers and interlocking (pushing: continued)

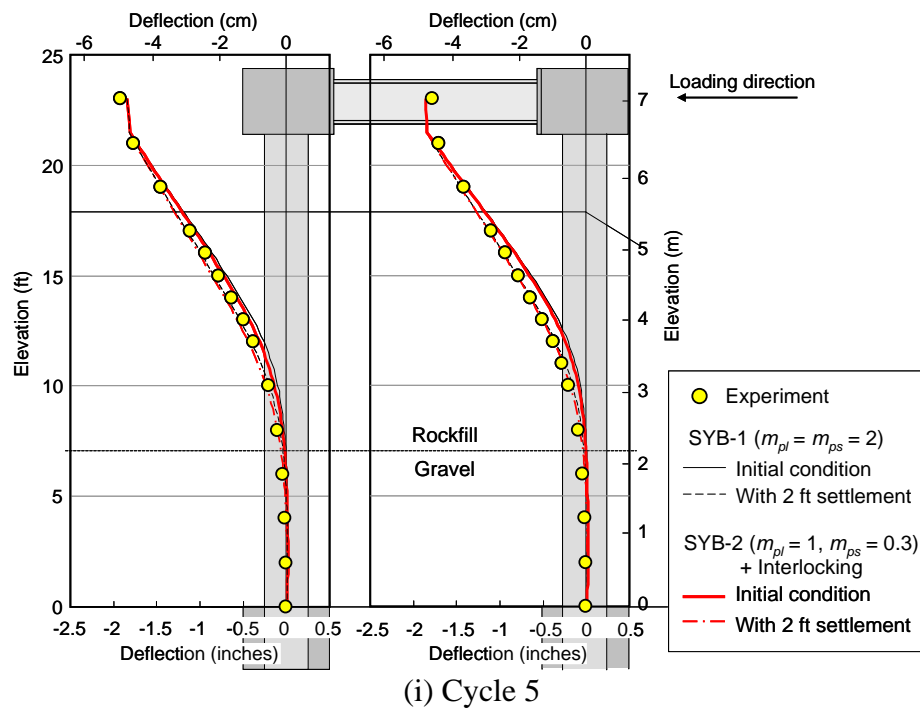


Figure 5-34 Deflection profiles for System Test 1 with p -multipliers and interlocking (pulling)

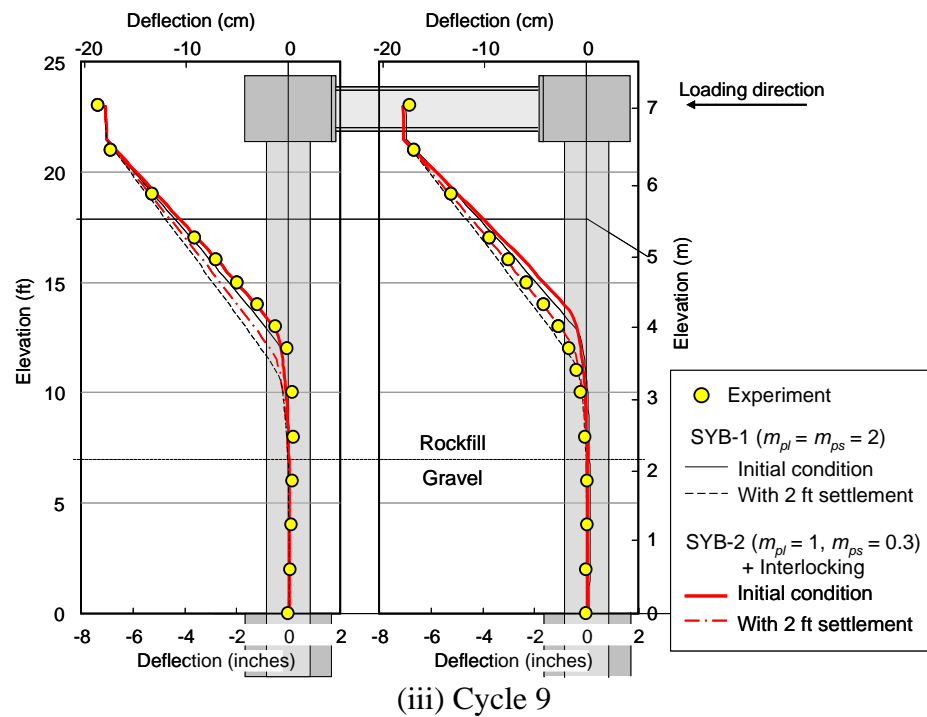
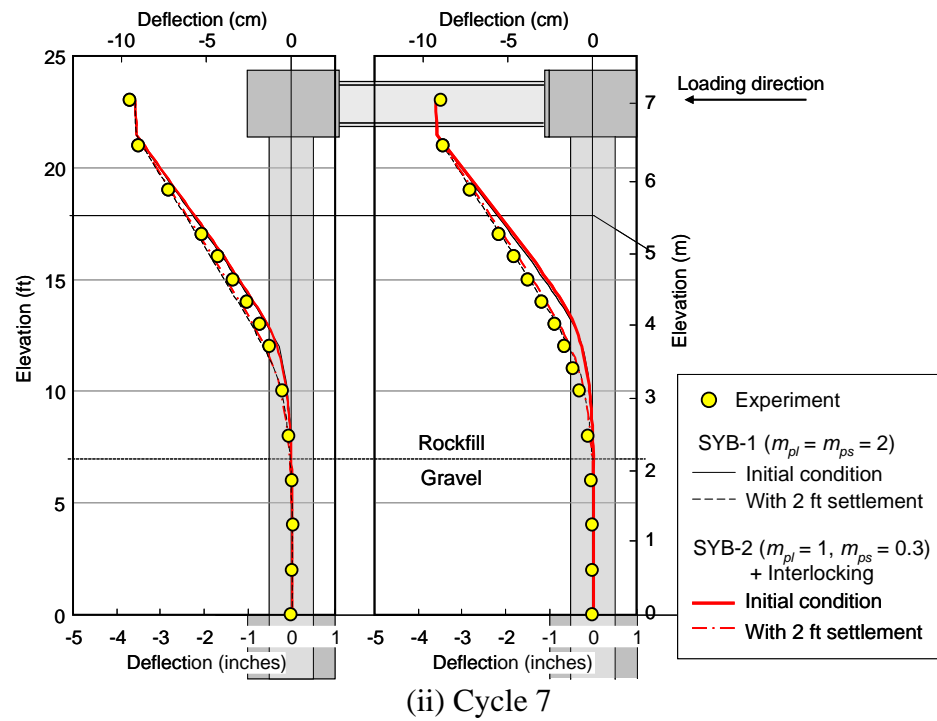


Figure 5-34 Deflection profiles for System Test 1 with p -multipliers and interlocking (pulling: continued)

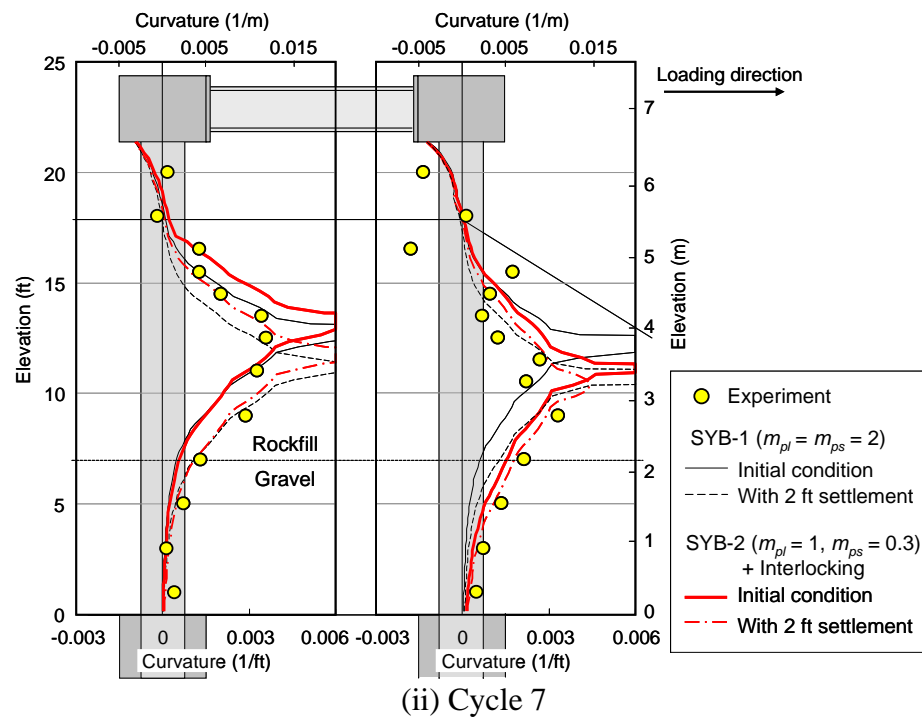
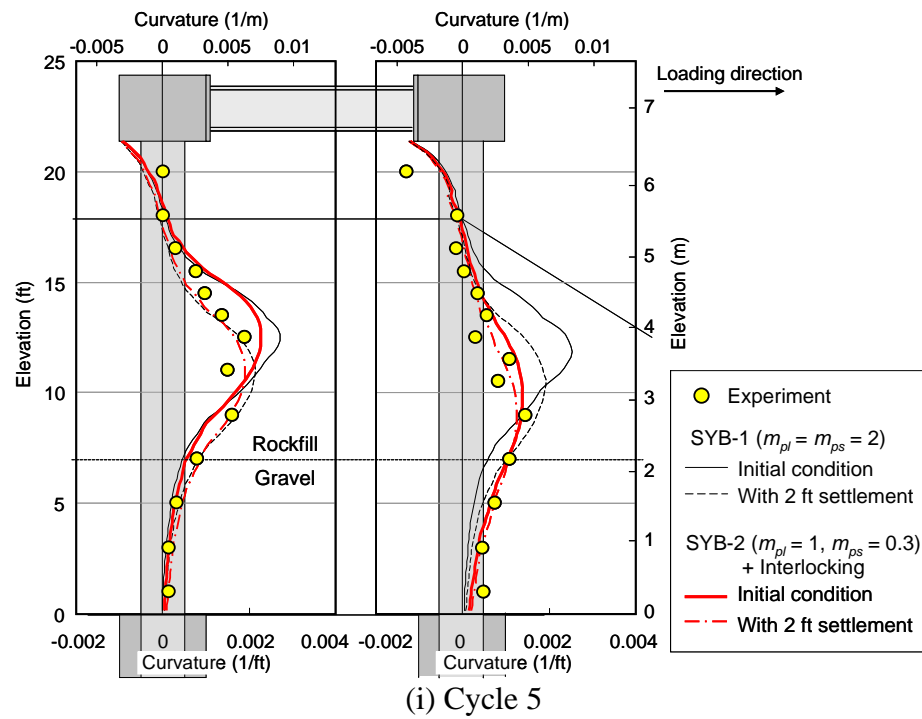


Figure 5-35 Curvature profiles for System Test 1 with p -multipliers and interlocking (pushing)

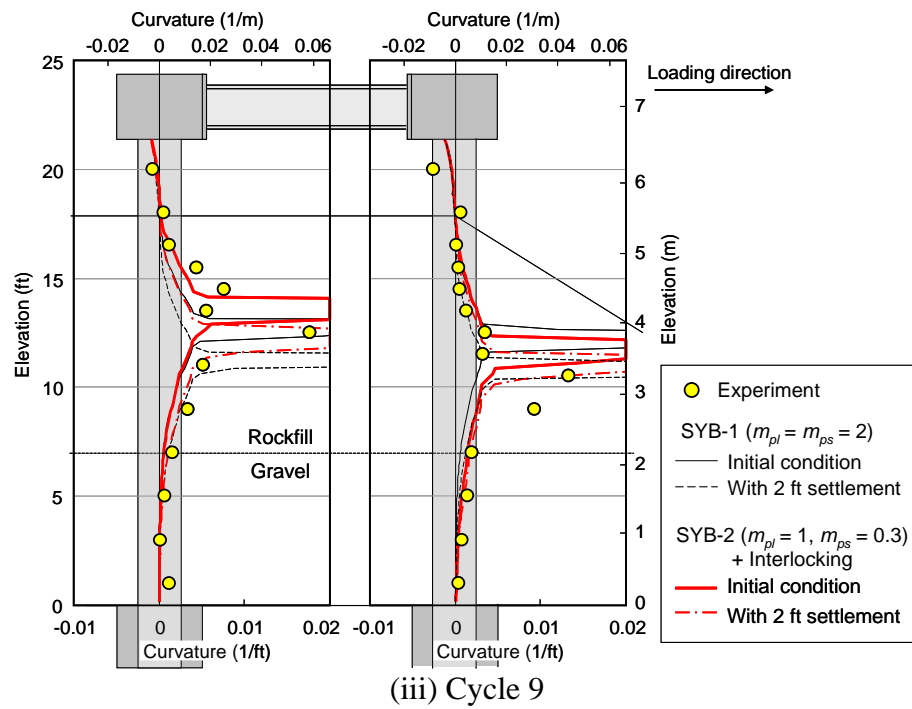


Figure 5-35 Curvature profiles for System Test 1 with p -multipliers and interlocking (pushing: continued)

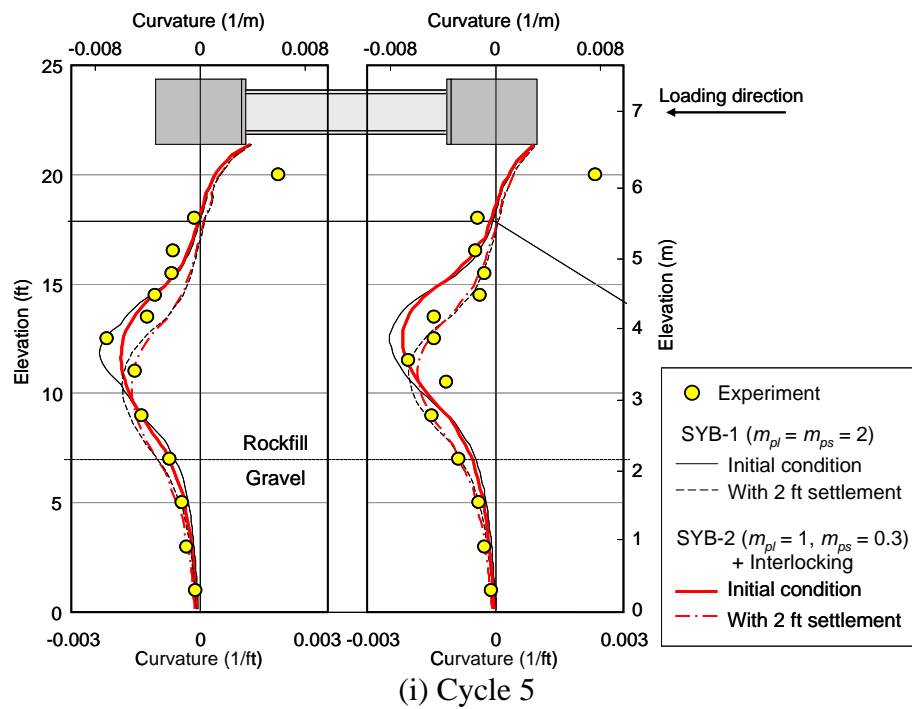


Figure 5-36 Curvature profiles for System Test 1 with p -multipliers and interlocking (pulling)

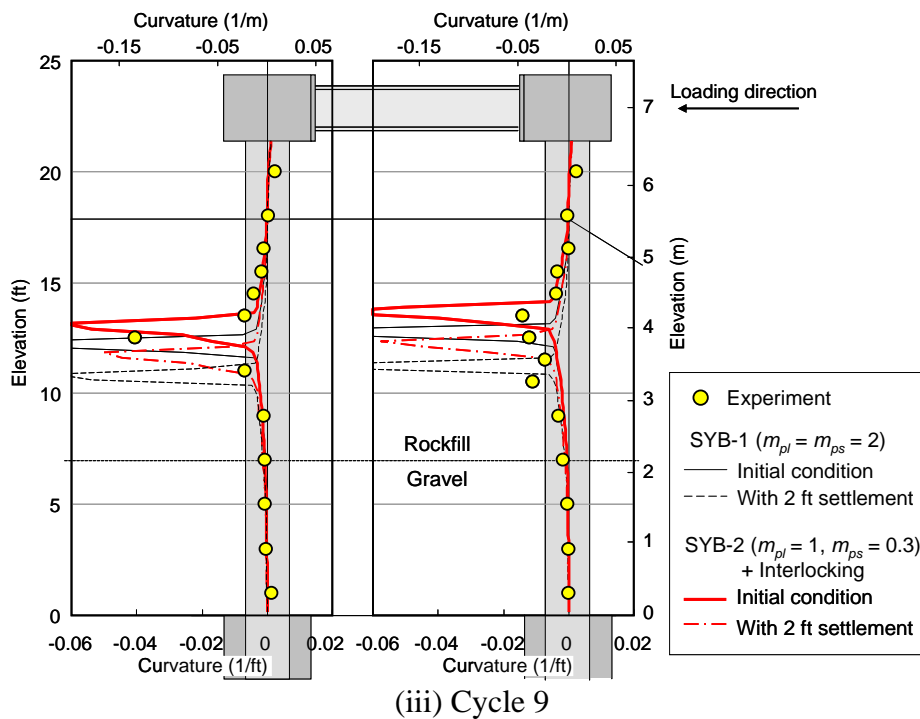
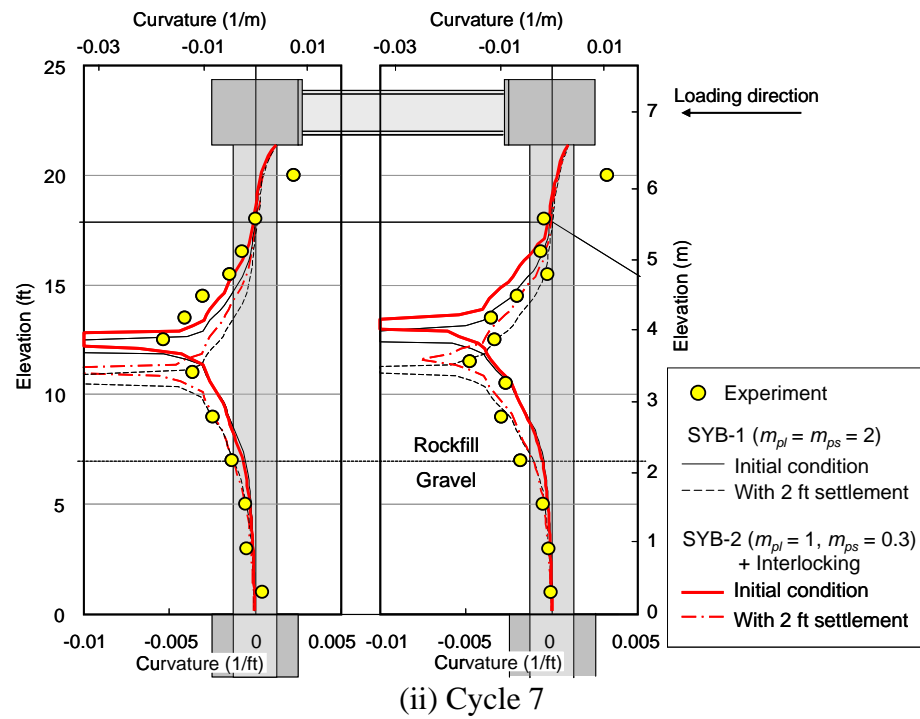
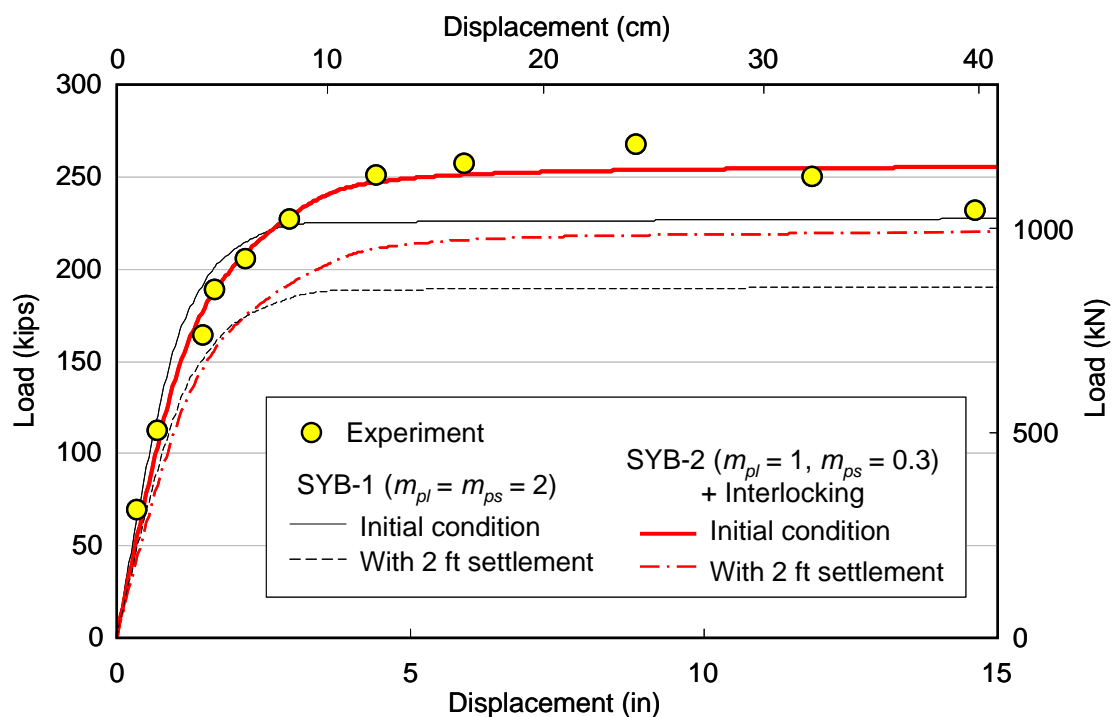
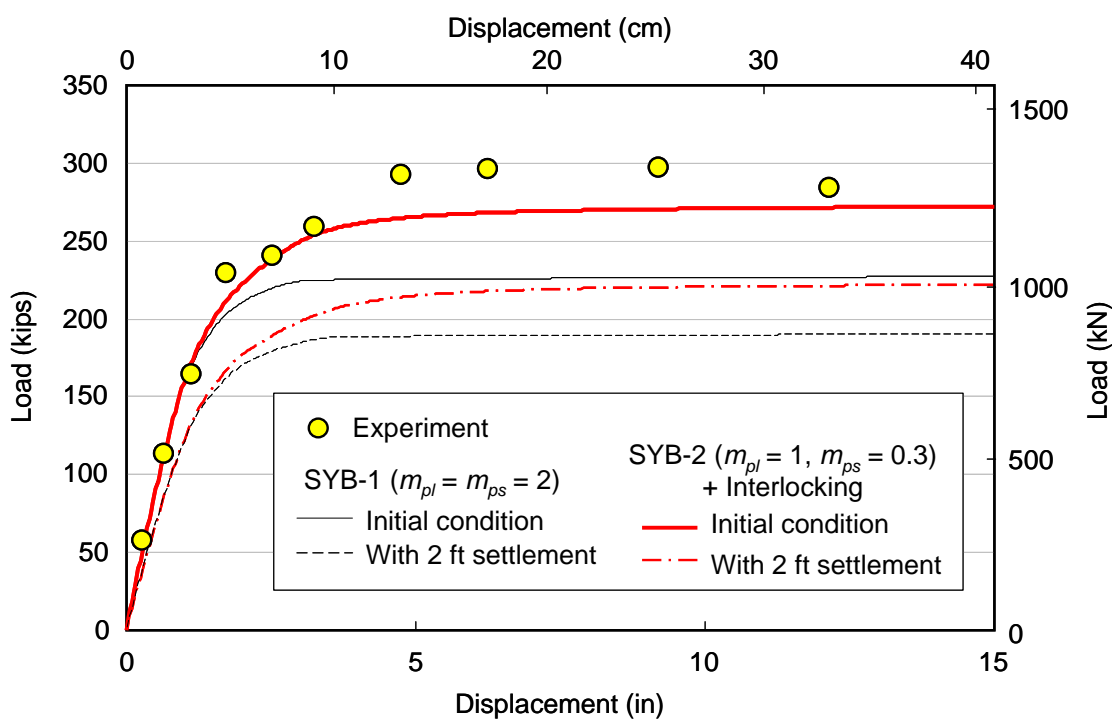


Figure 5-36 Curvature profiles for System Test 1 with p -multipliers and interlocking (pulling: continued)

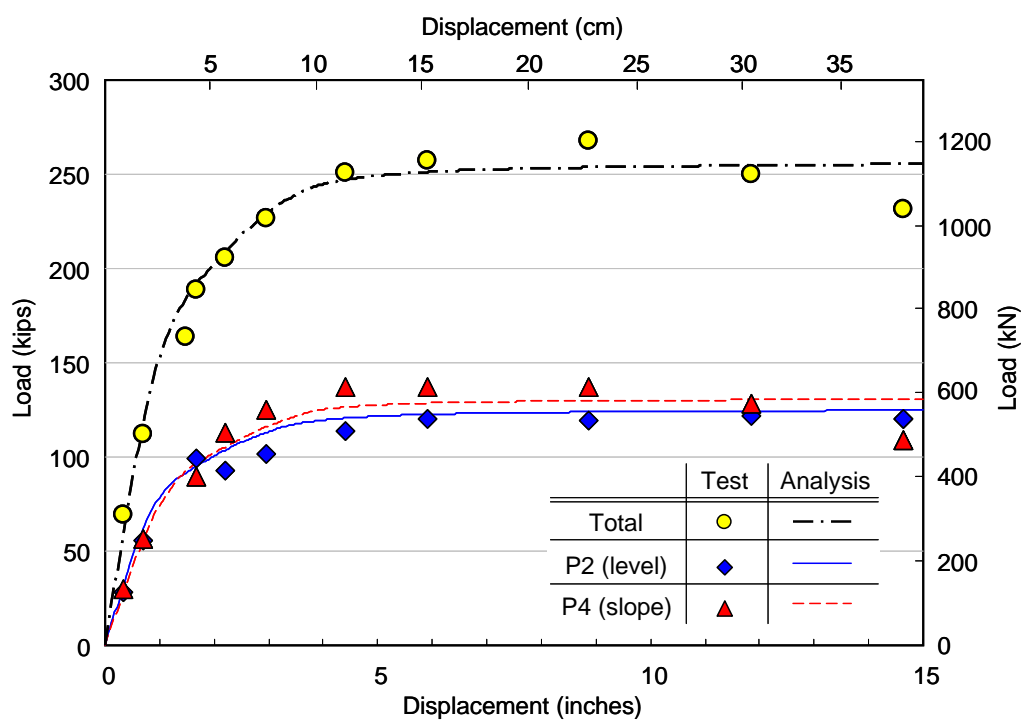


(a) Pushing toward downslope

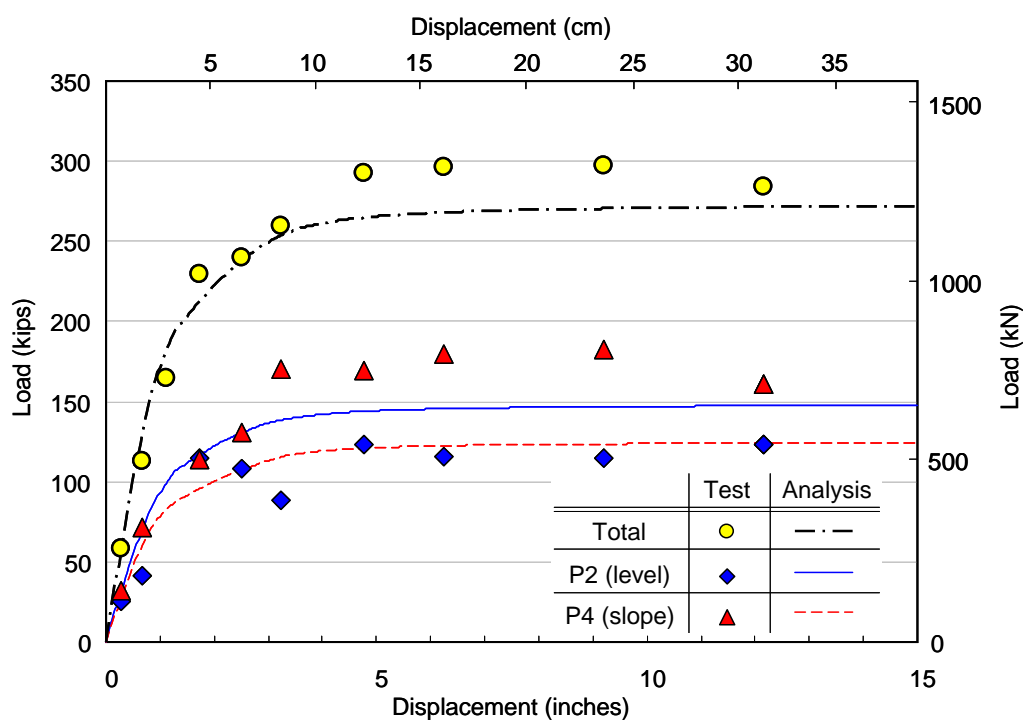


(b) Pulling toward reaction wall

Figure 5-37 Load-displacement curve for System Test 2 with p -multipliers and interlocking



(a) Pushing toward downslope



(b) Pulling toward reaction wall

Figure 5-38 Load-displacement curve on each pile for System Test 2 with p -multipliers and interlocking

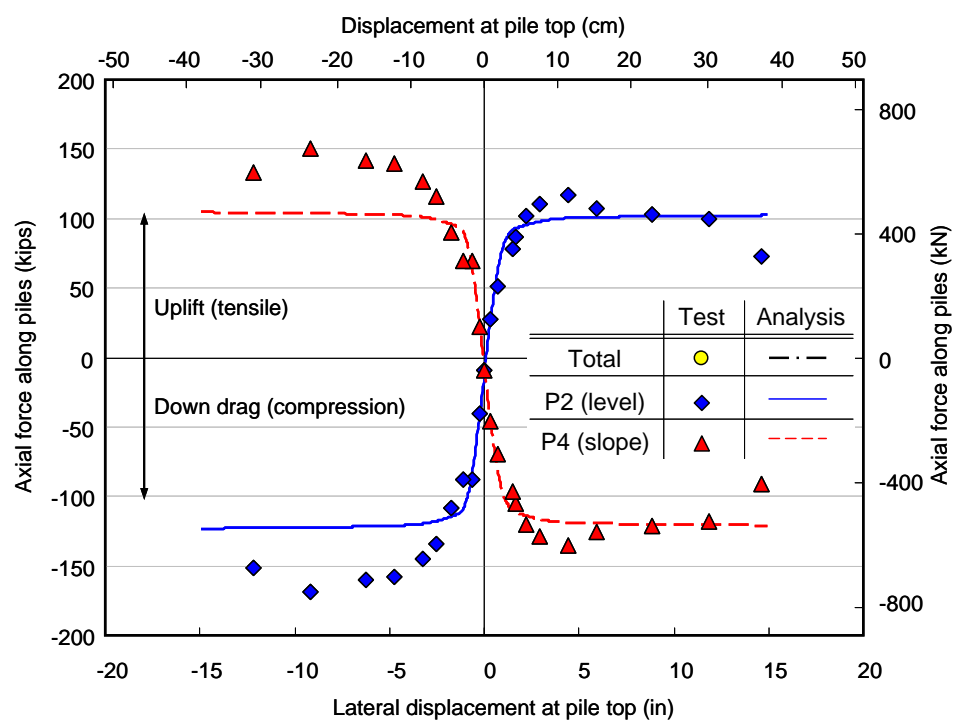


Figure 5-39 Axial force on each pile for System Test 2

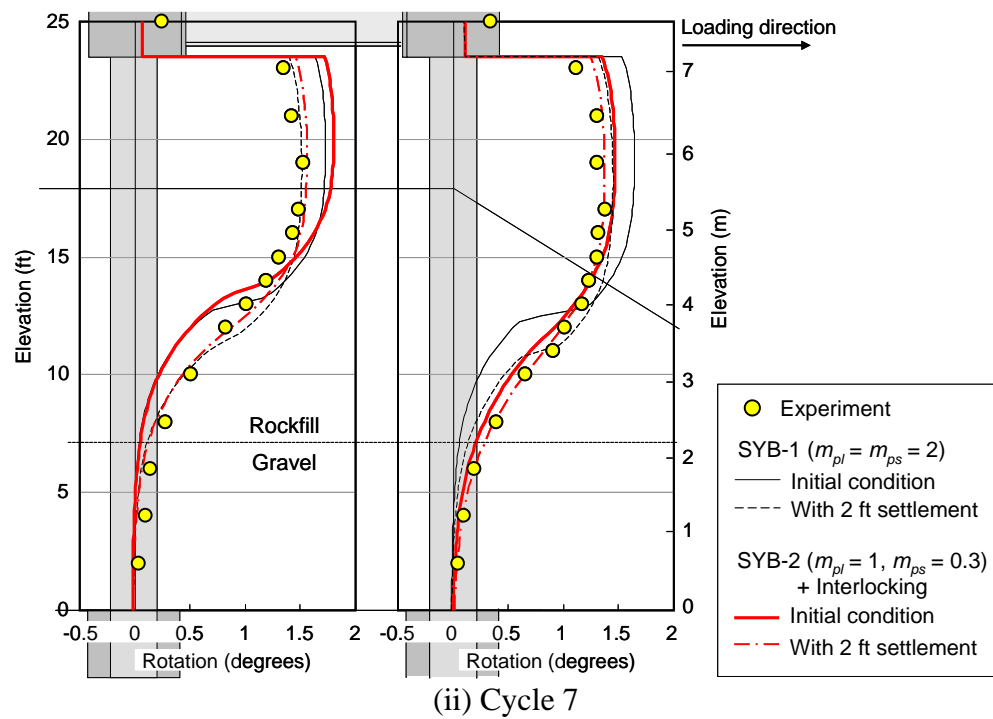
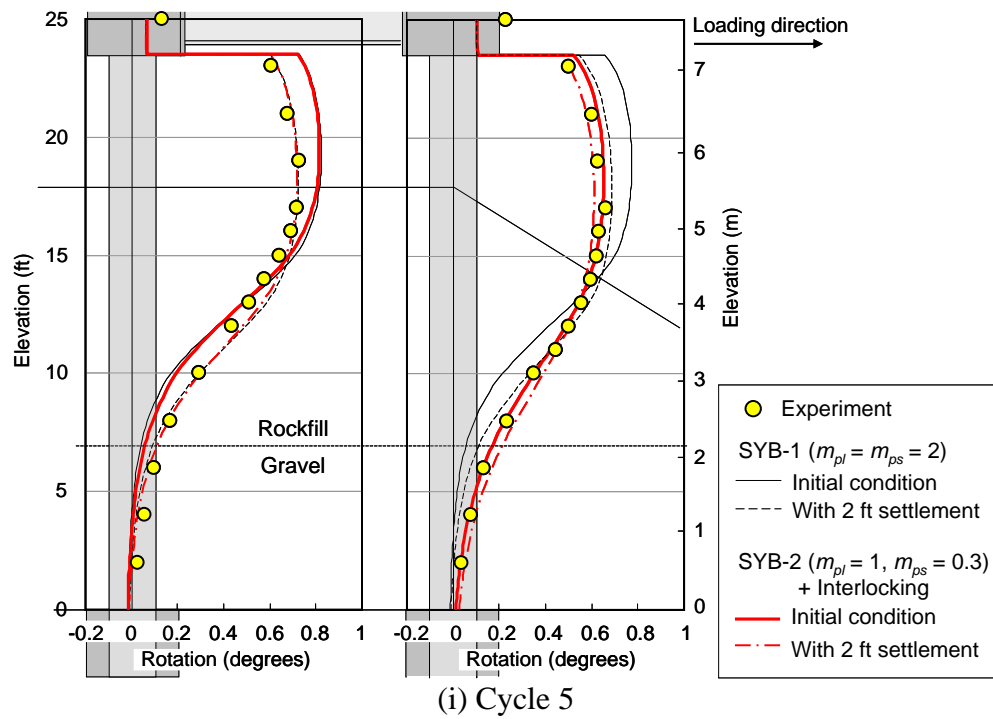


Figure 5-40 Rotation profiles for System Test 2 with p -multipliers and interlocking (pushing)

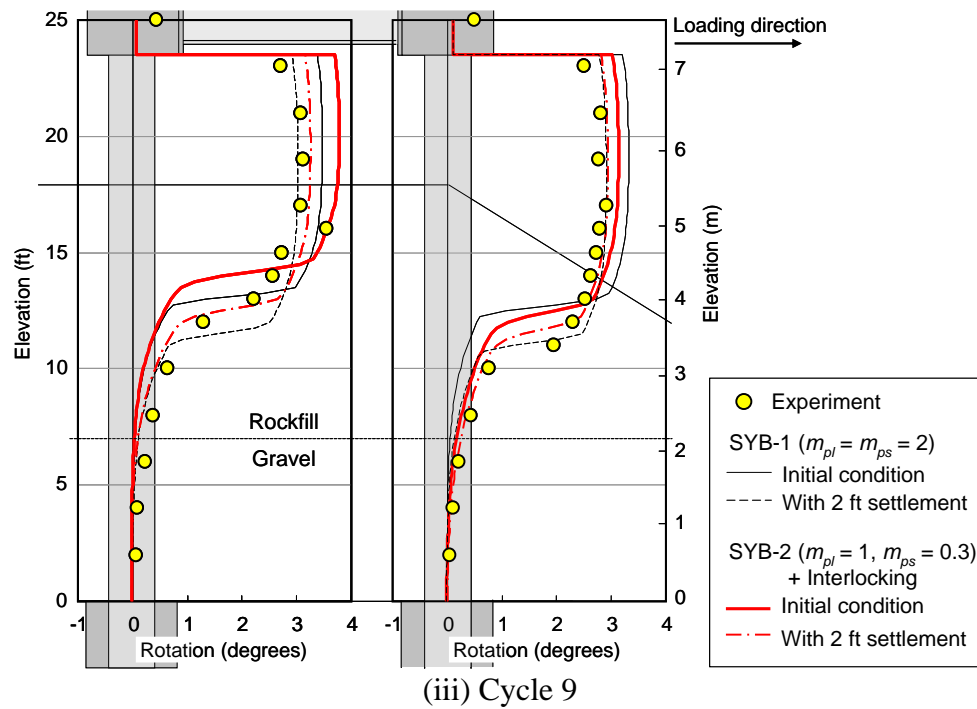


Figure 5-40 Rotation profiles for System Test 2 with p -multipliers and interlocking (pushing: continued)

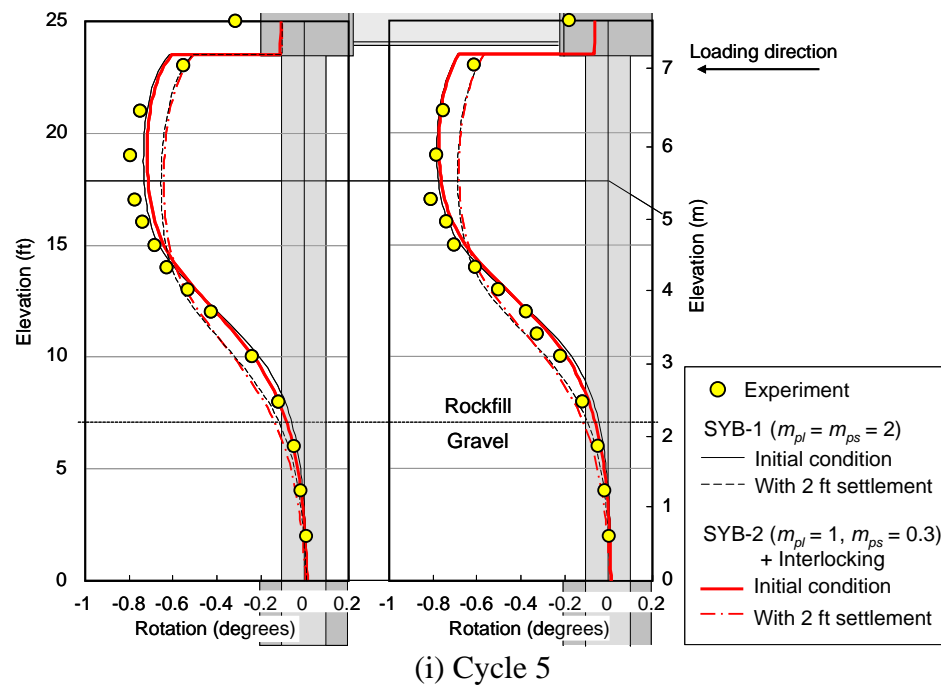


Figure 5-41 Rotation profiles for System Test 2 with p -multipliers and interlocking (pulling)

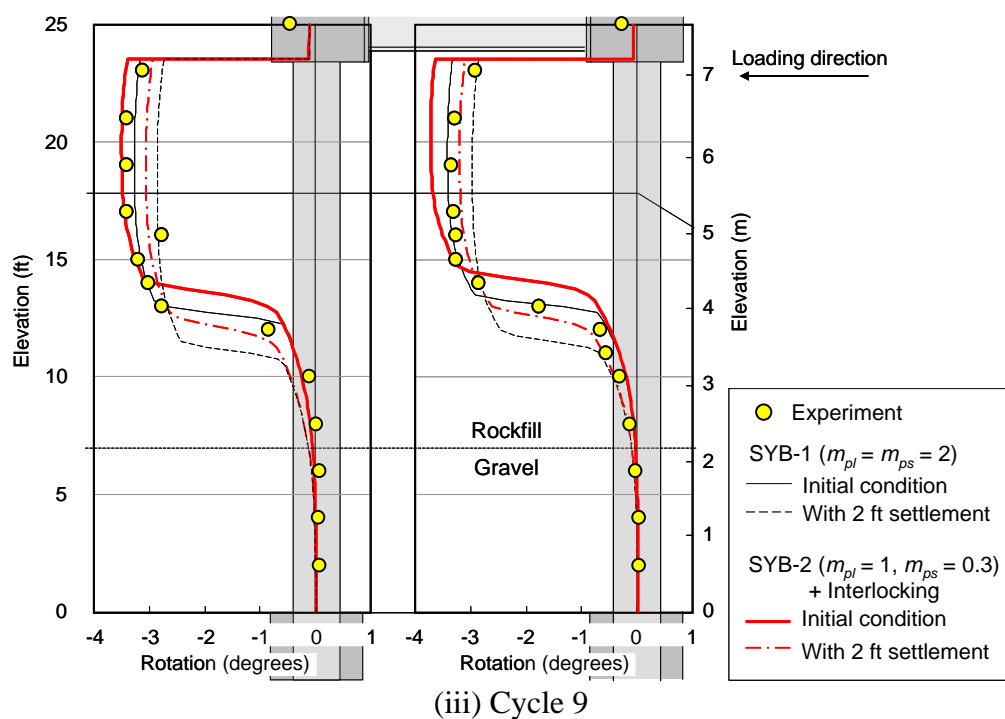
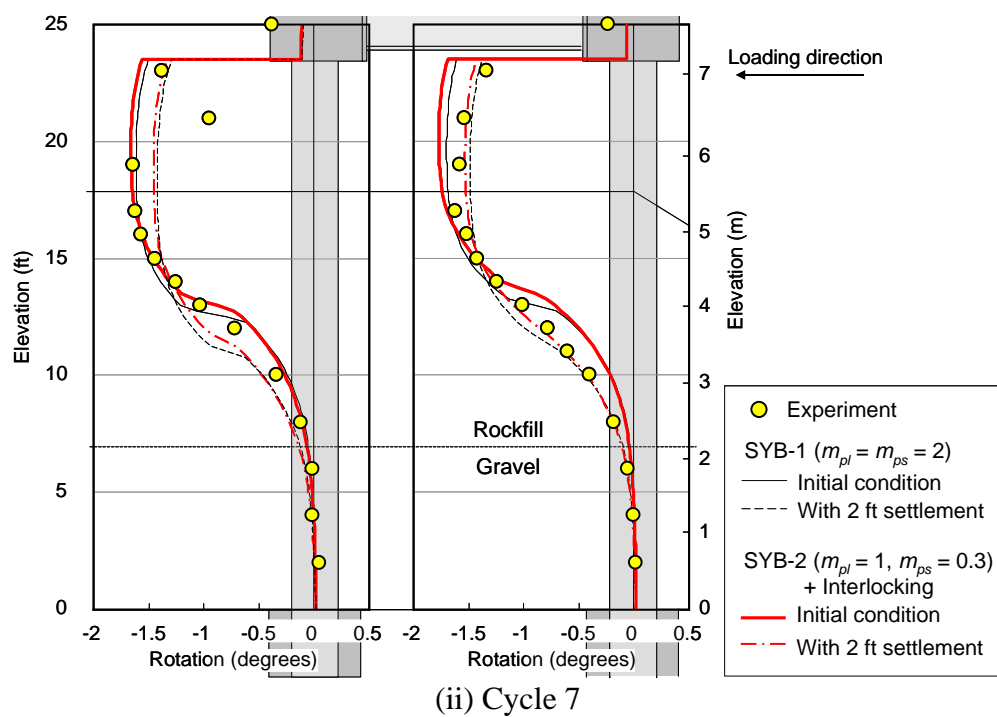


Figure 5-41 Rotation profiles for System Test 2 with p -multipliers and interlocking (pulling: continued)

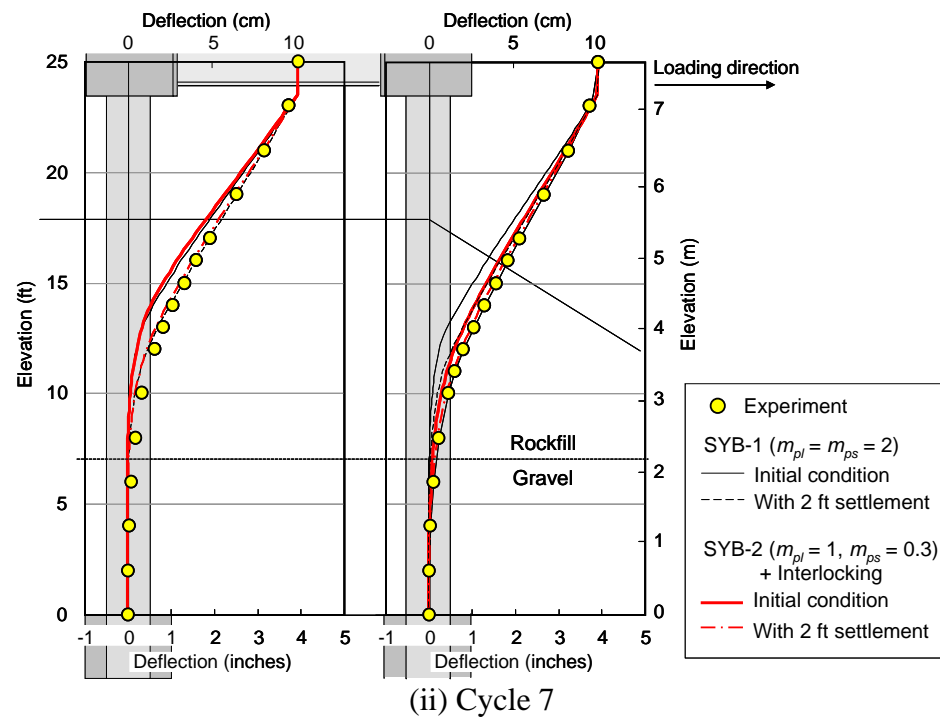
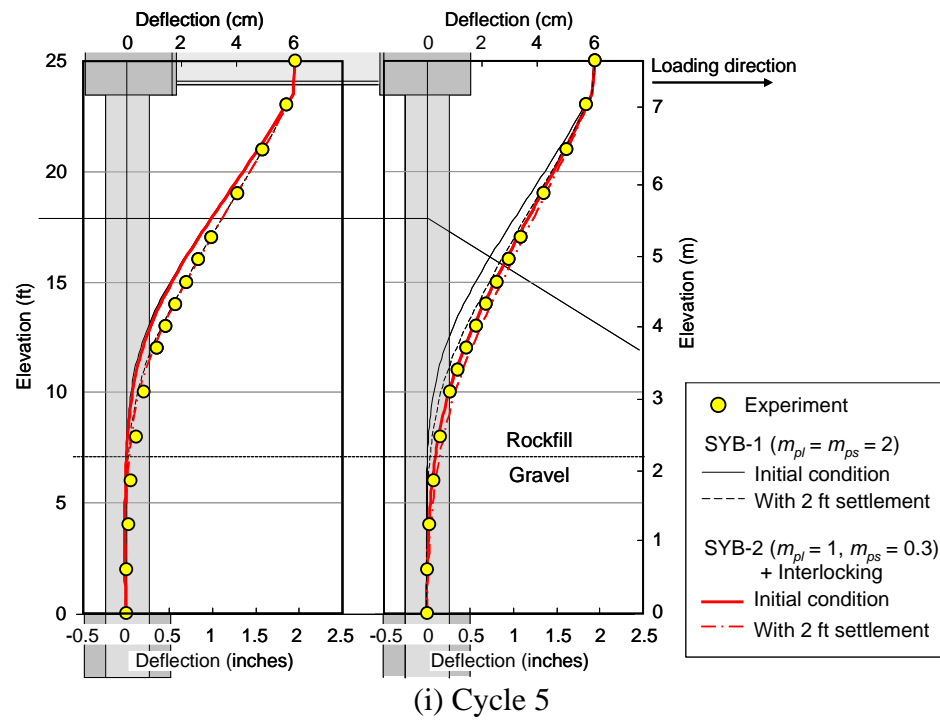


Figure 5-42 Deflection profiles for System Test 2 with p -multipliers and interlocking (pushing)

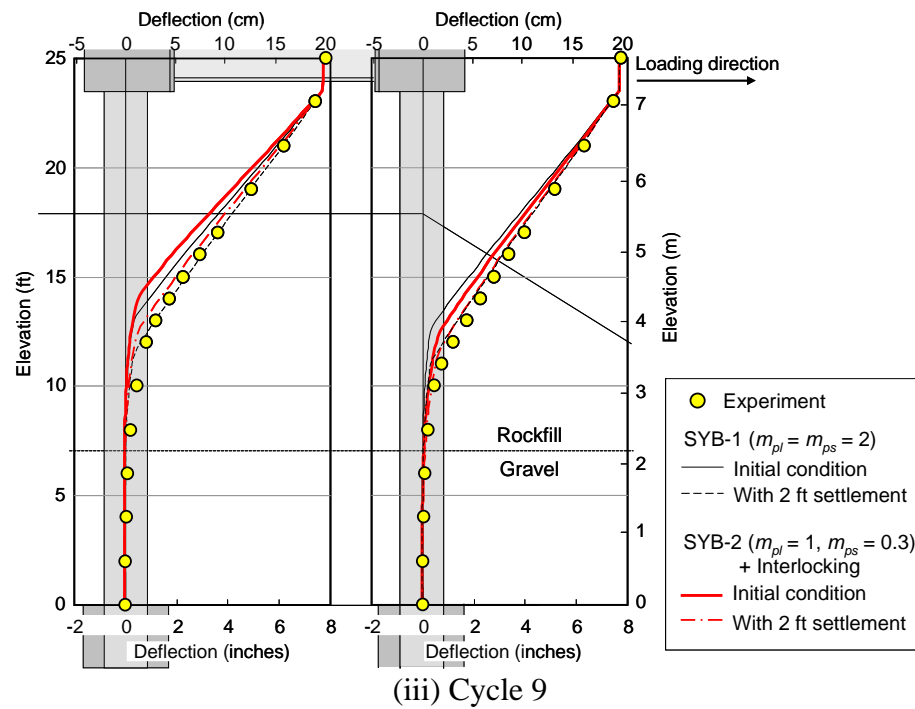


Figure 5-42 Deflection profiles for System Test 2 with p -multipliers and interlocking (pushing: continued)

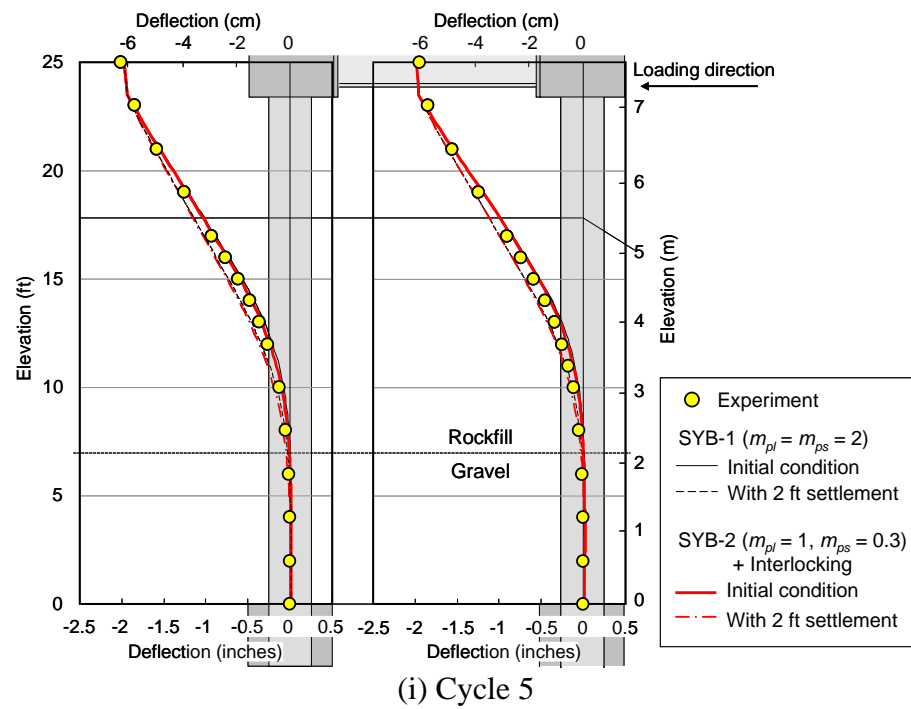


Figure 5-43 Deflection profiles for System Test 2 with p -multipliers and interlocking (pulling)

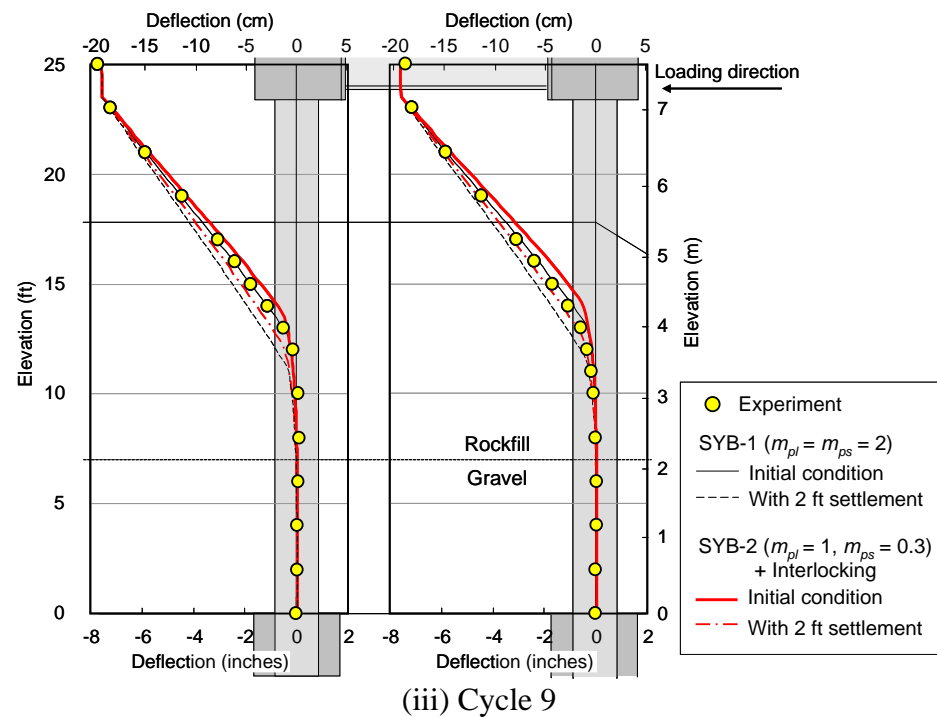
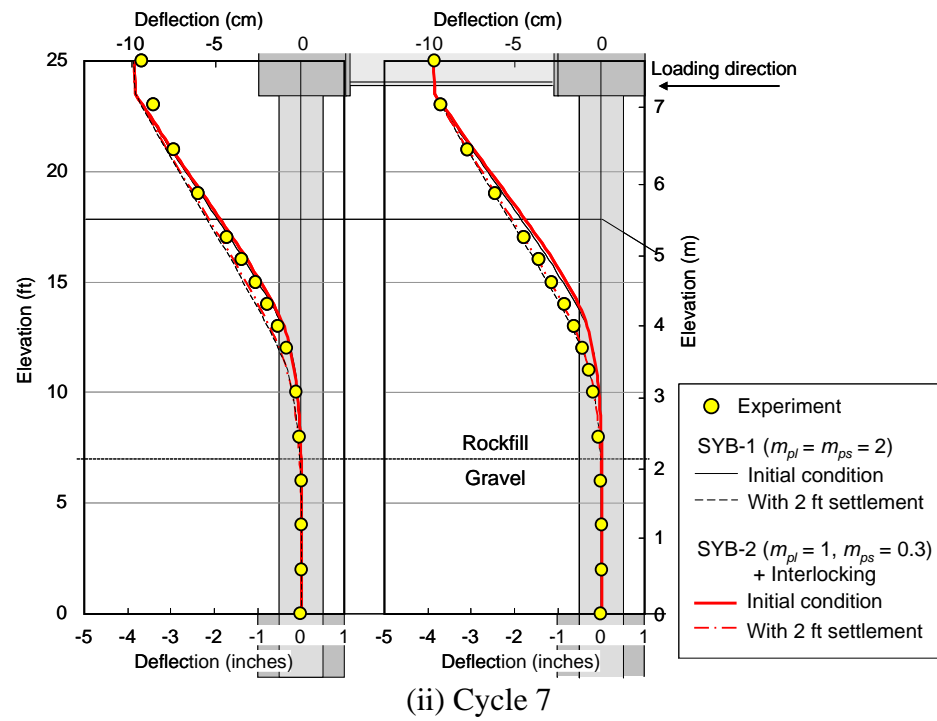


Figure 5-43 Deflection profiles for System Test 2 with p -multipliers and interlocking (pulling: continued)

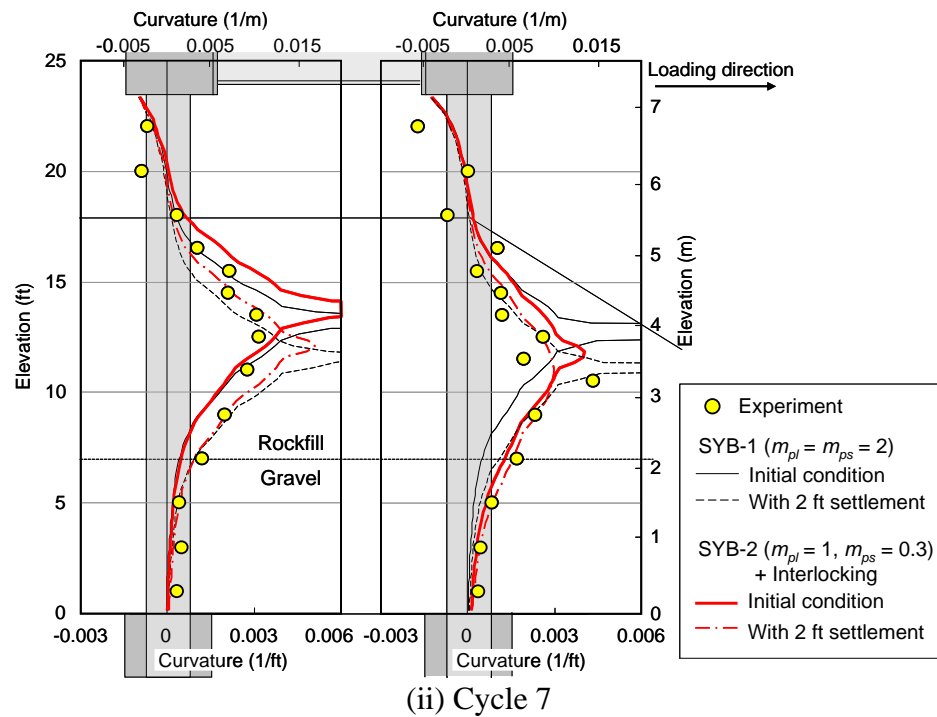
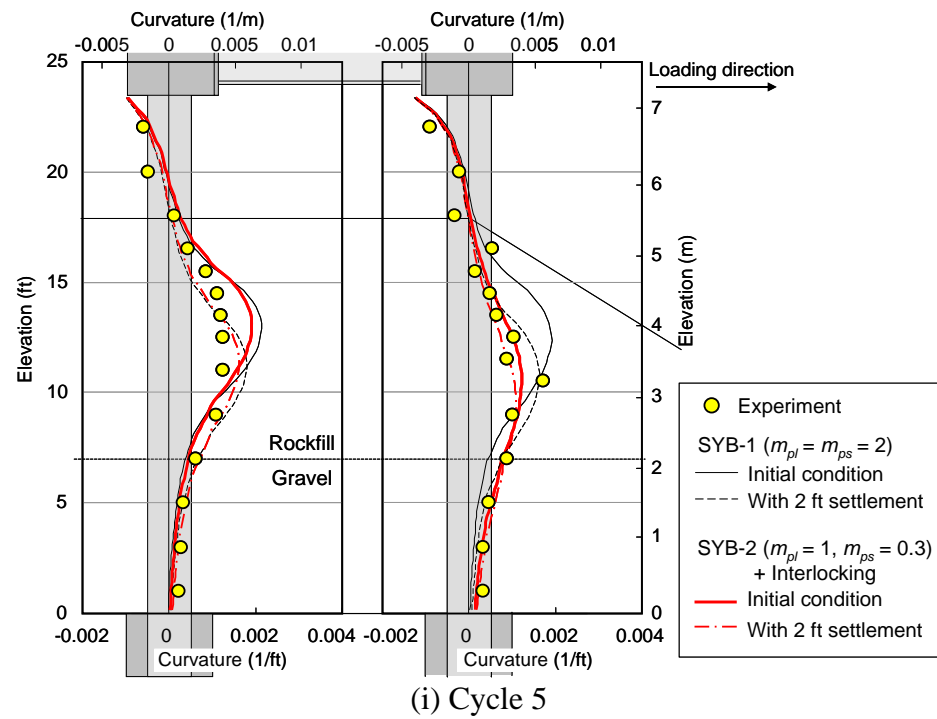


Figure 5-44 Curvature profiles for System Test 2 with p -multipliers and interlocking (pushing)

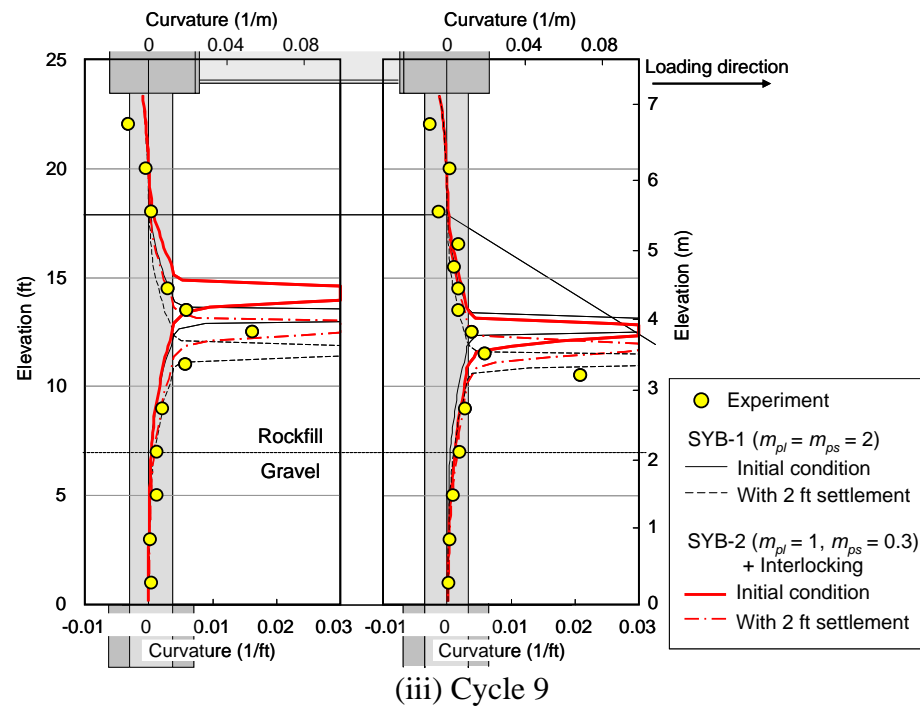


Figure 5-44 Curvature profiles for System Test 2 with p -multipliers and interlocking (pushing: continued)

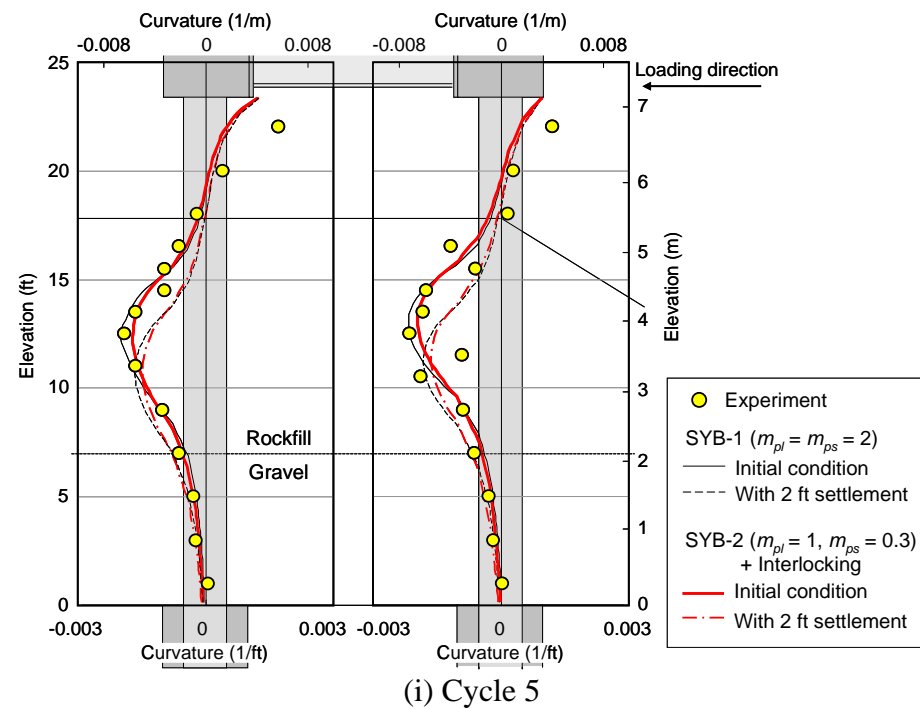


Figure 5-45 Curvature profiles for System Test 2 with p -multipliers and interlocking (pulling)

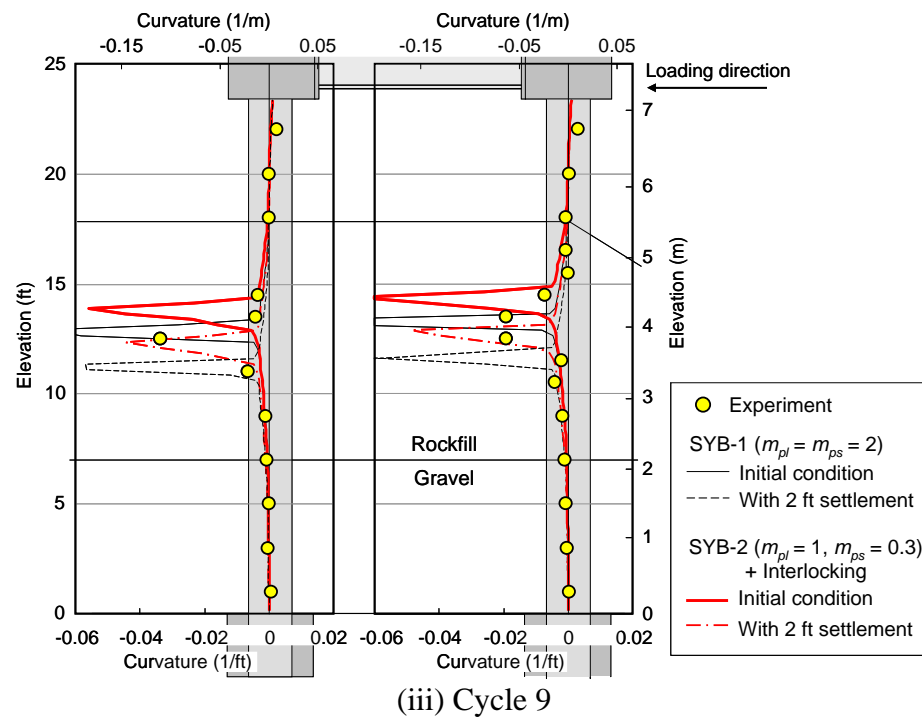
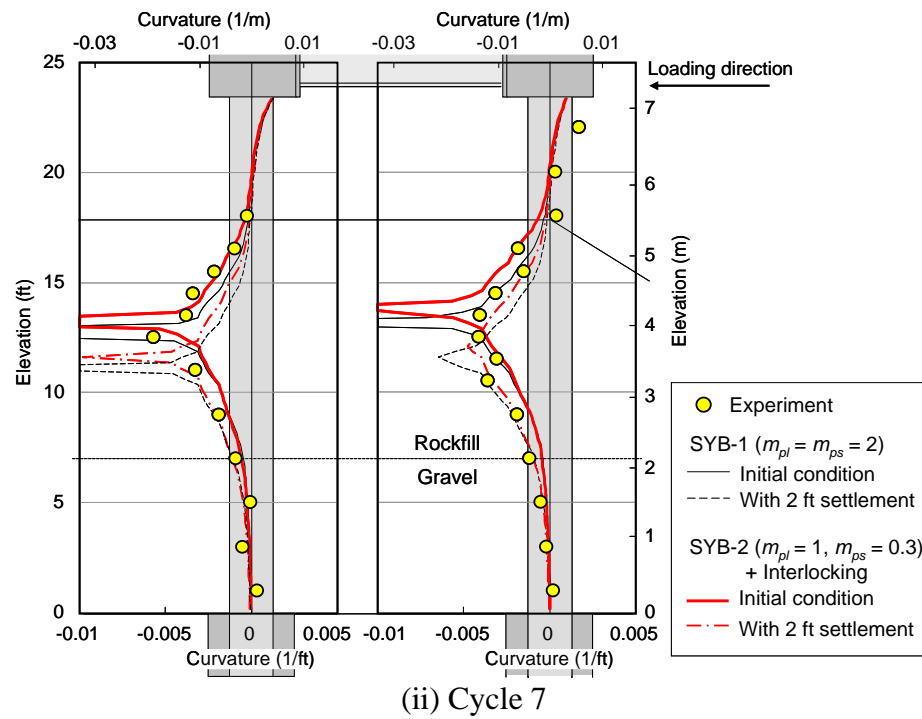


Figure 5-45 Curvature profiles for System Test 2 with p -multipliers and interlocking (pulling: continued)

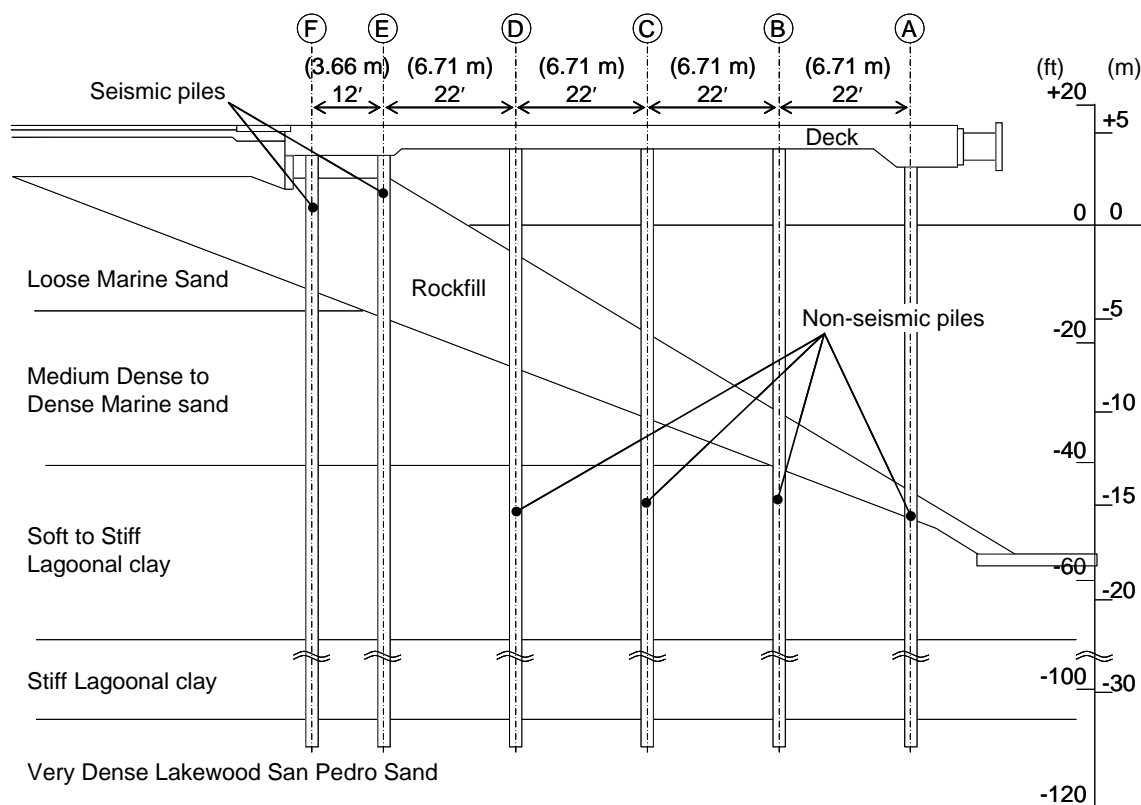


Figure 5-46 Subsurface cross section of Berth 100 at the Port of Los Angeles

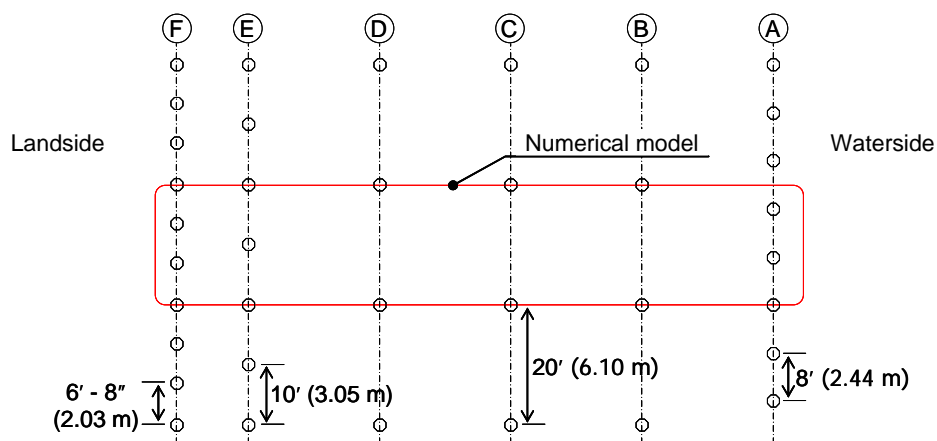


Figure 5-47 Pile layout of Berth 100 at the Port of Los Angeles

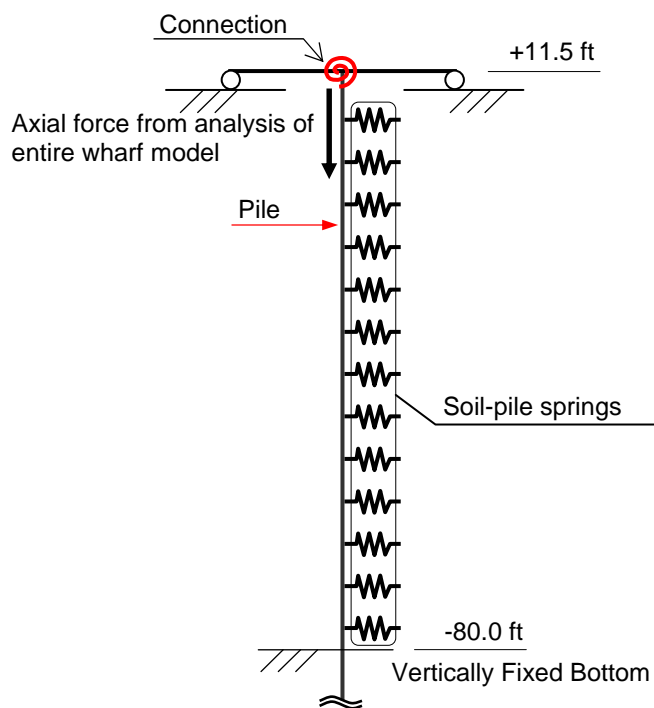
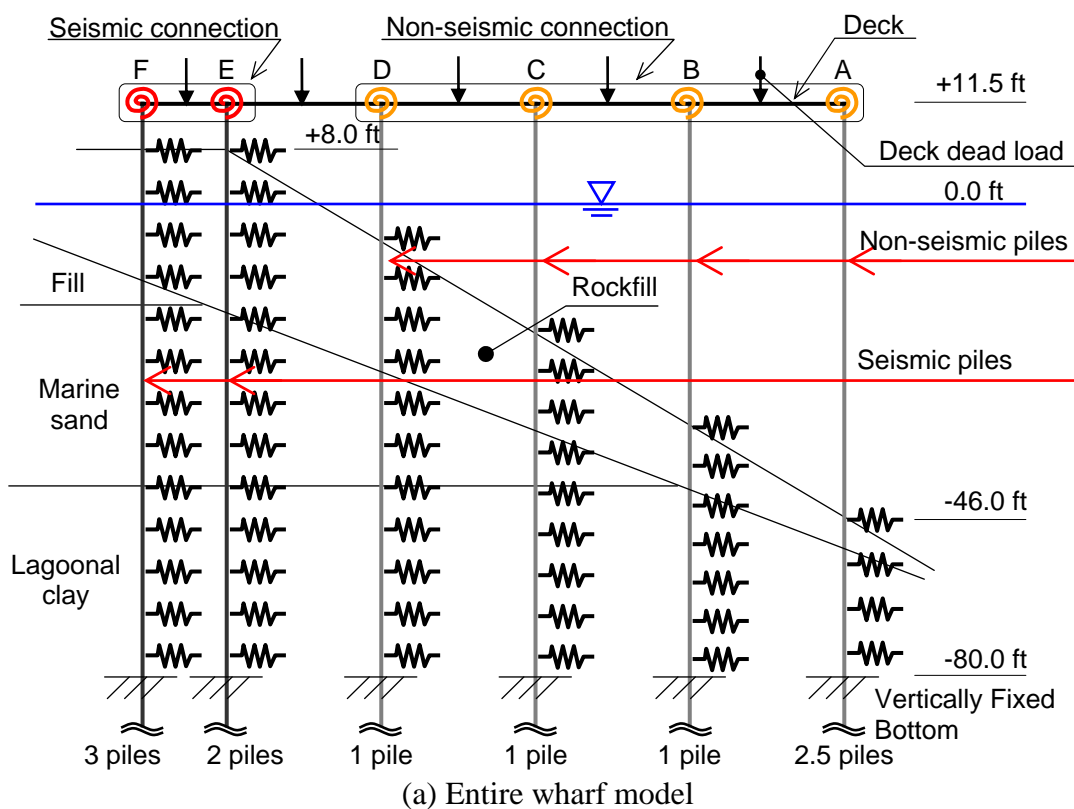


Figure 5-48 Numerical model of entire wharf structure

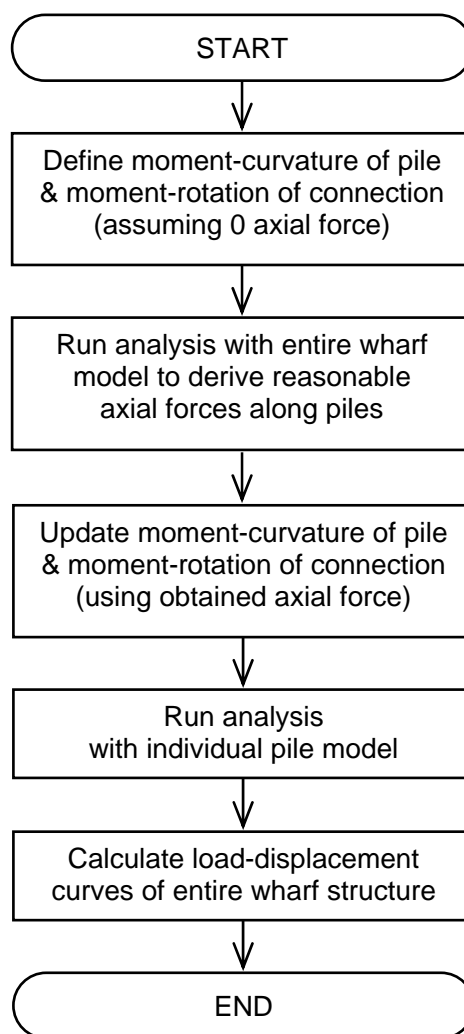


Figure 5-49 Flow chart of analysis for entire wharf structure

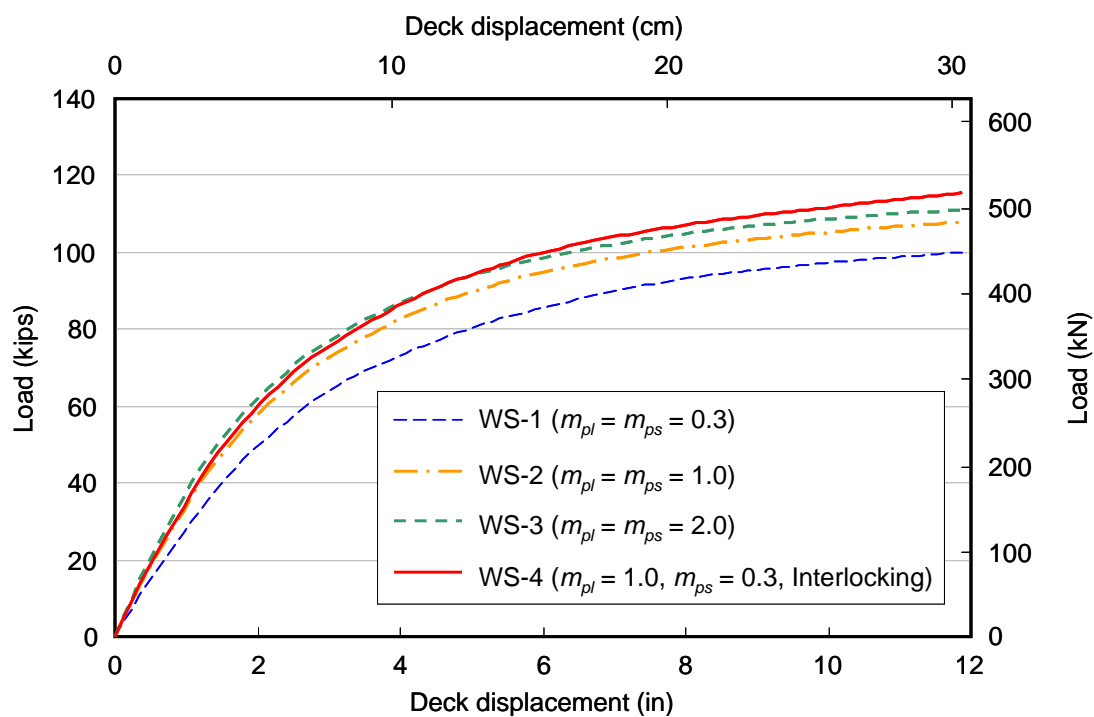


Figure 5-50 Load displacement curves on non-seismic piles (rows A through D)

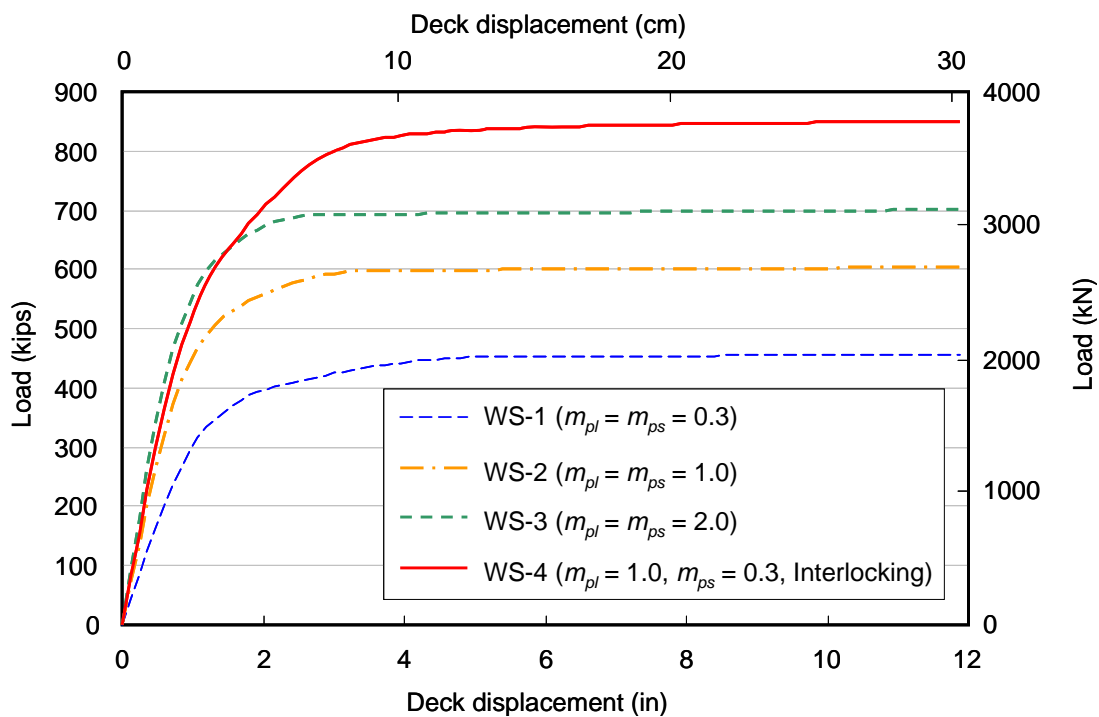


Figure 5-51 Load displacement curves on seismic piles (rows E and F)

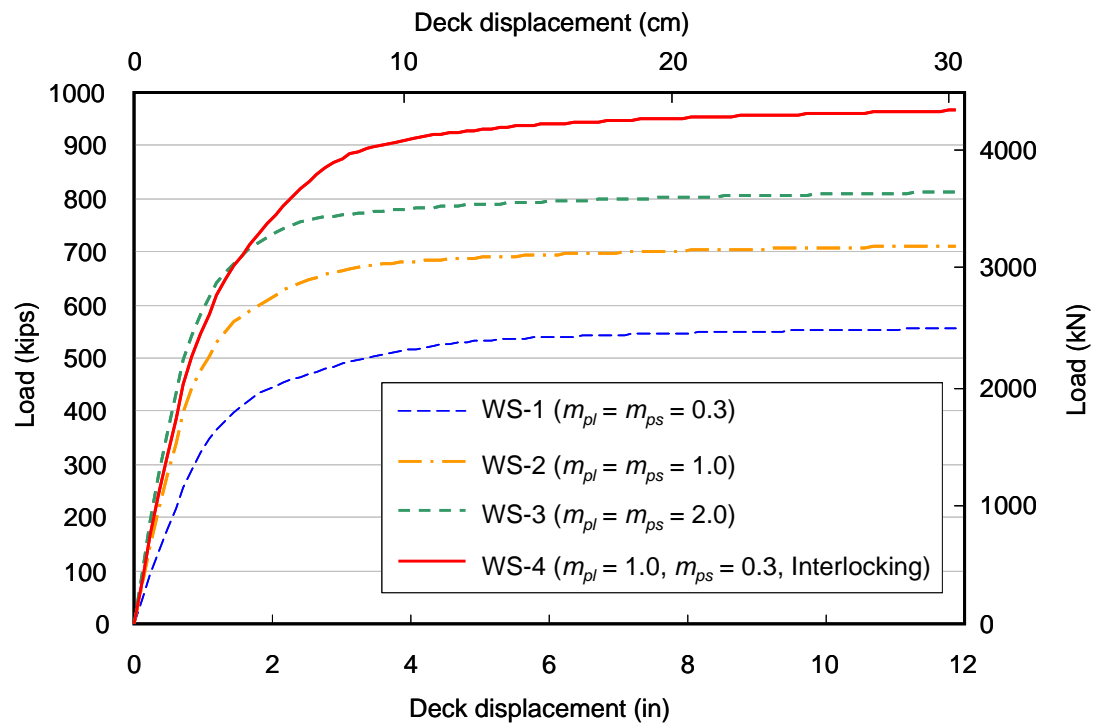


Figure 5-52 Load-displacement curves for entire wharf structure

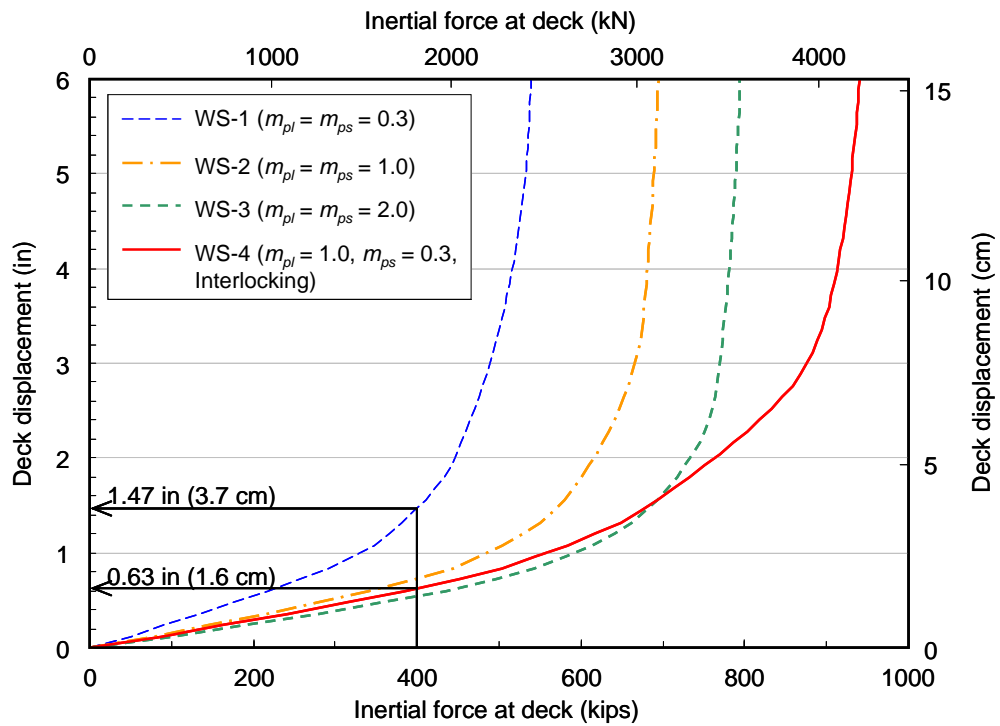


Figure 5-53 Deck displacement at certain inertial force

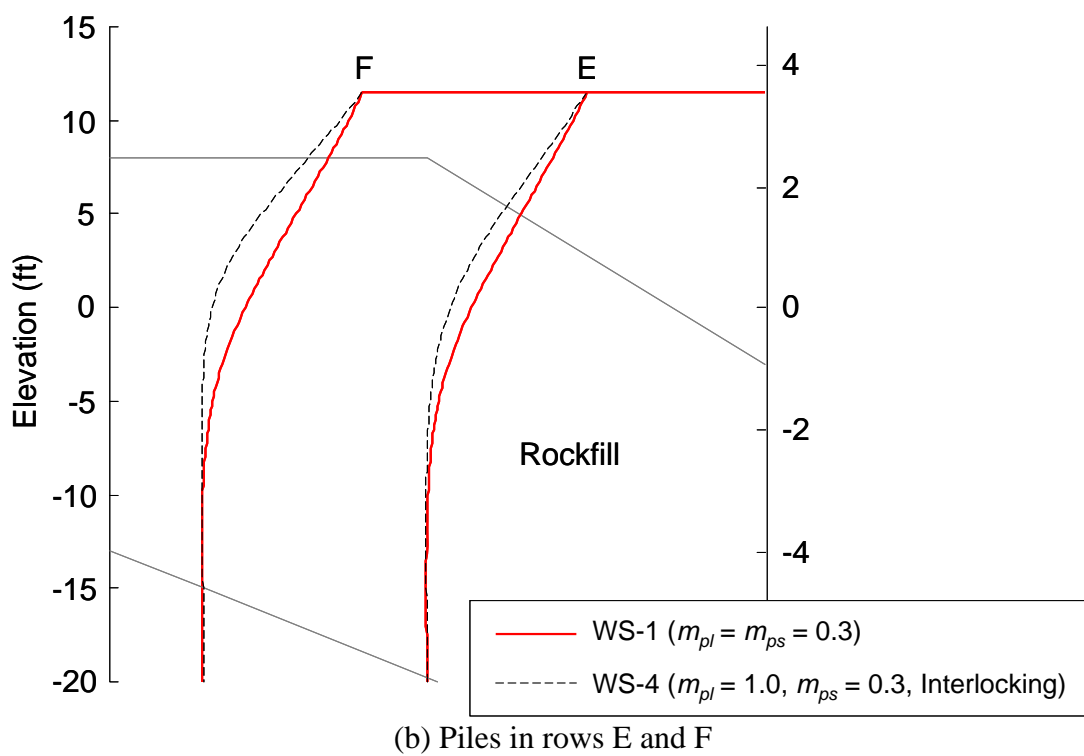
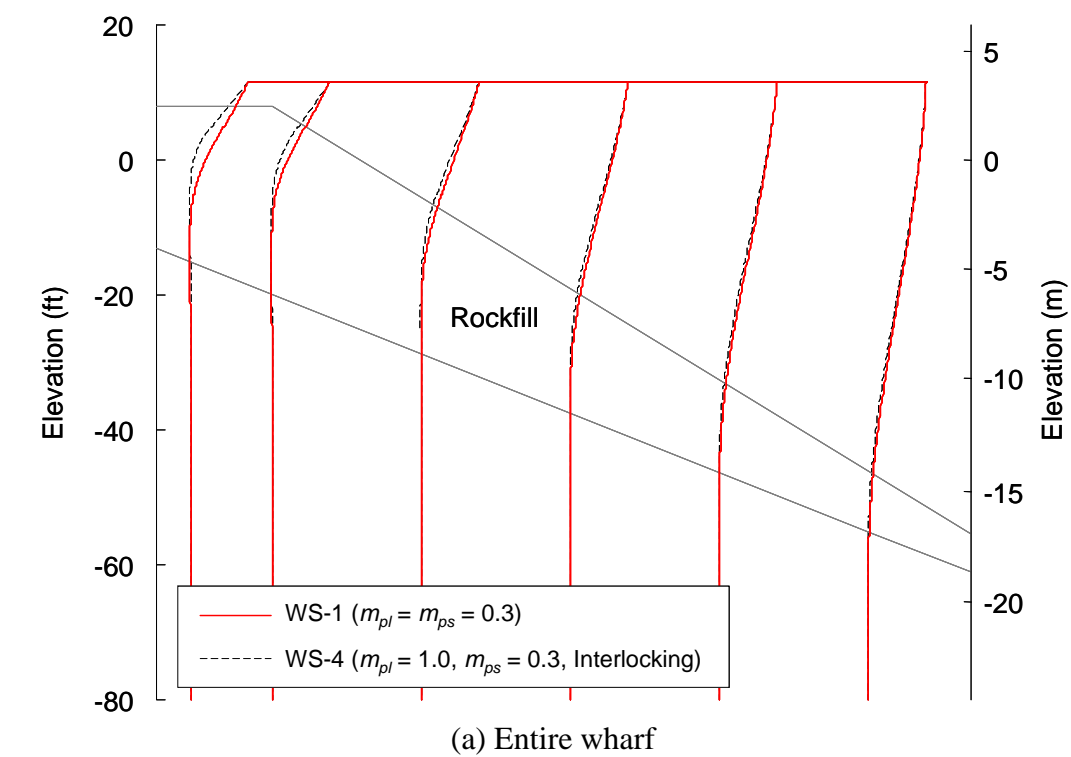


Figure 5-54 Deformed shape (Lower bound, $m_p = 0.3$; multiplied by 50)

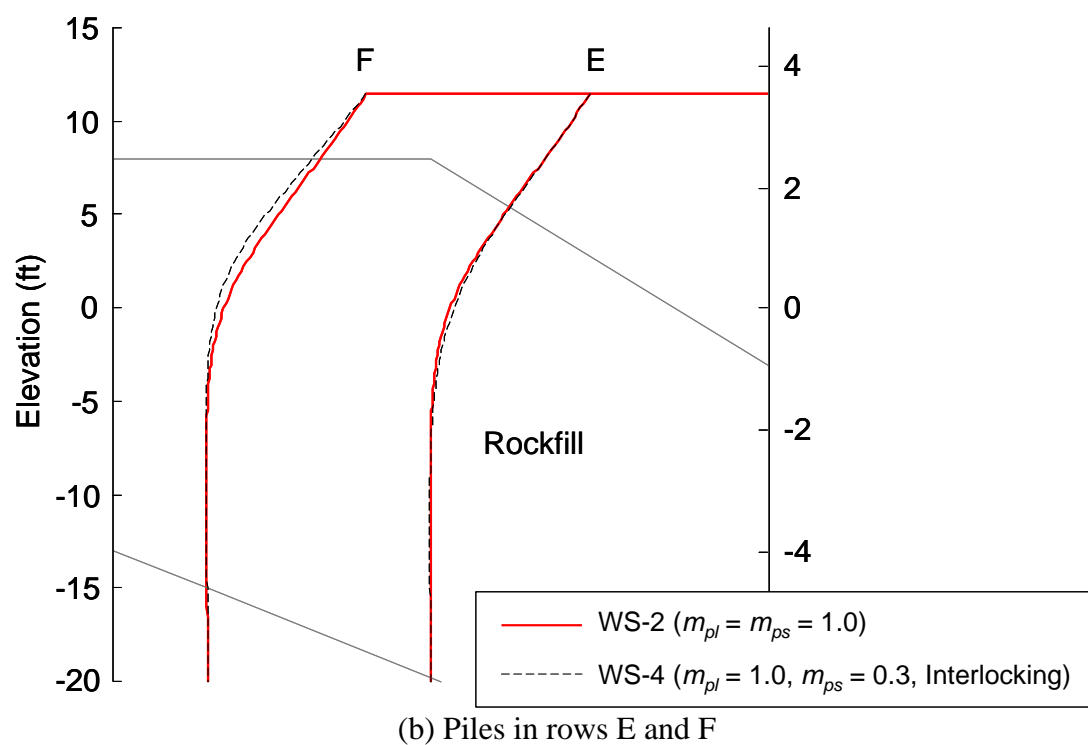
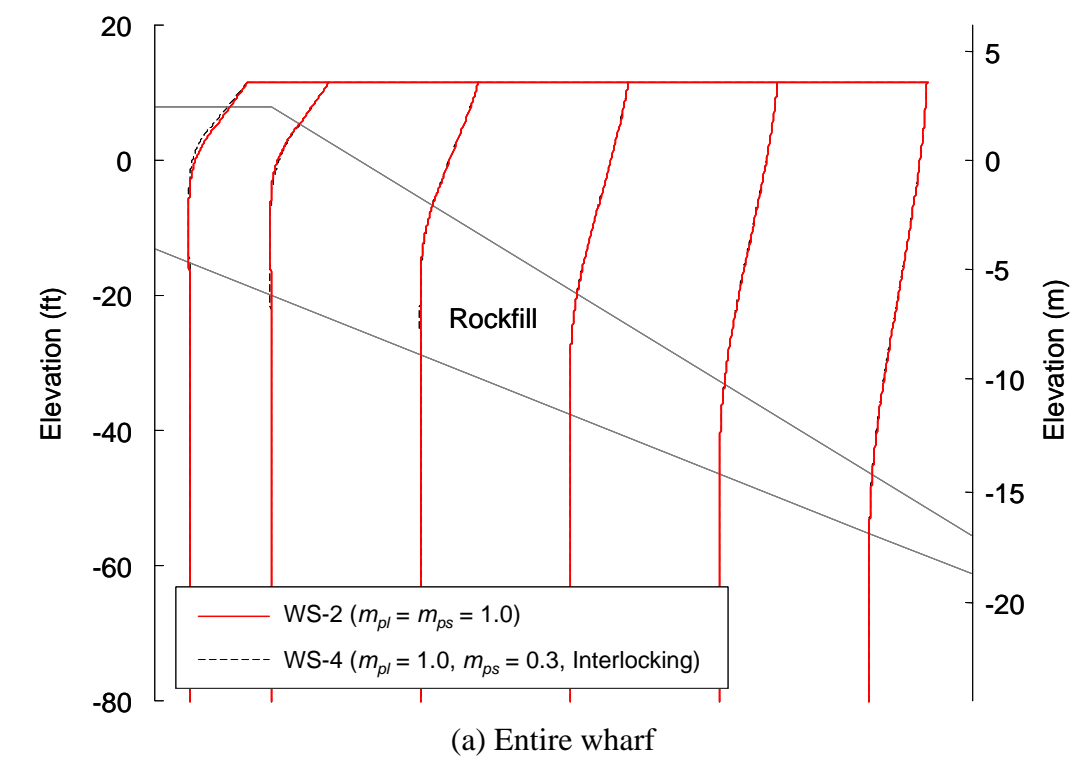


Figure 5-55 Deformed shape (Standard, $m_p = 1.0$; multiplied by 50)

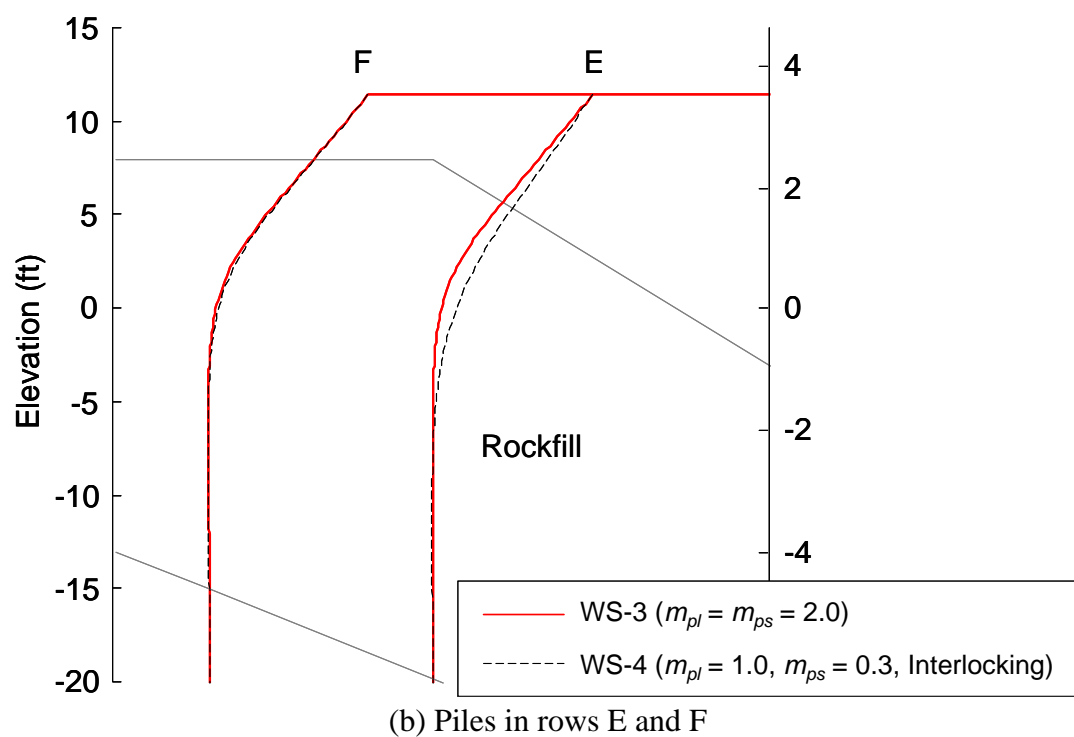
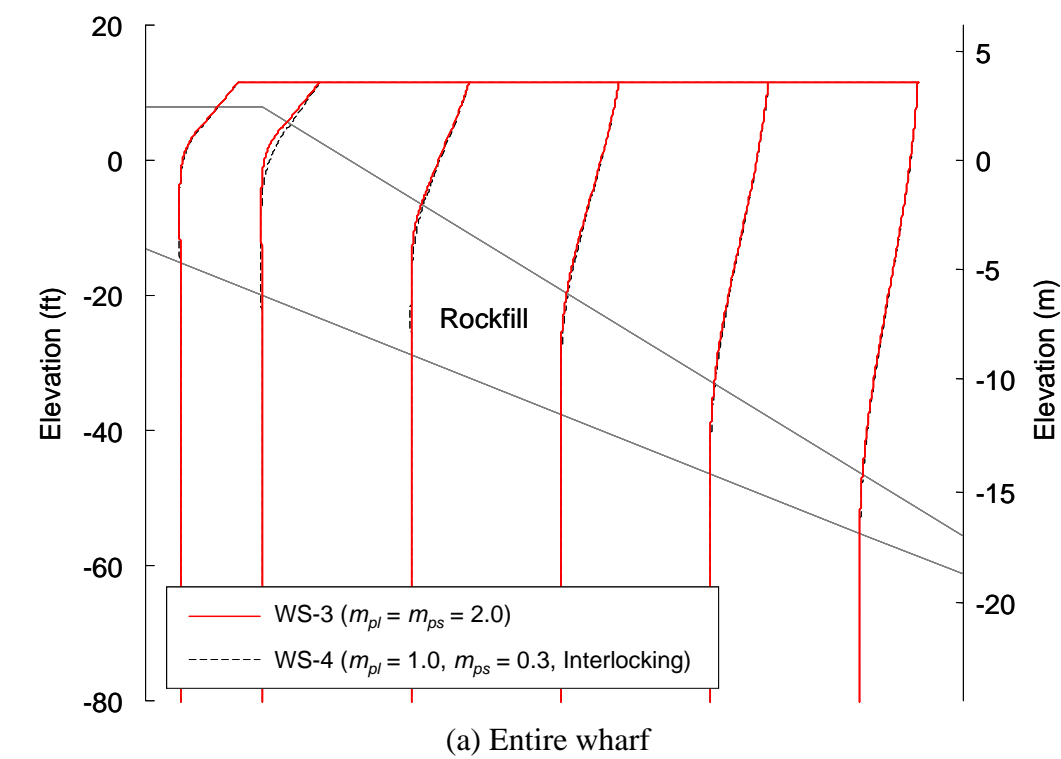


Figure 5-56 Deformed shape (Upper bound, $m_p = 2.0$; multiplied by 50)

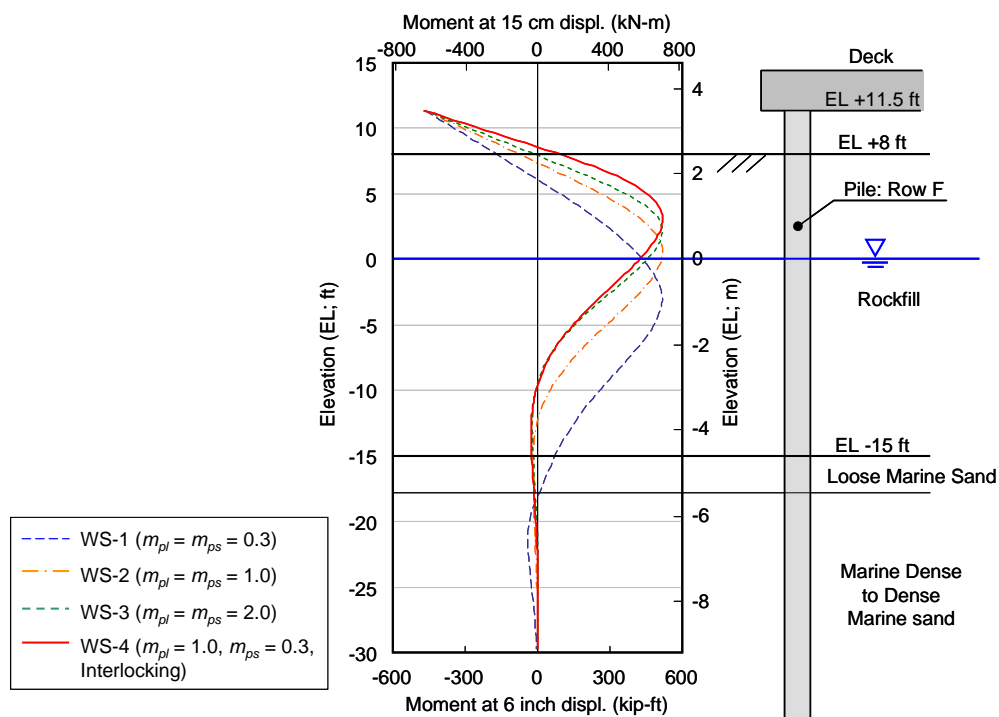


Figure 5-57 Comparison of moment profiles along pile in row F in various analysis cases

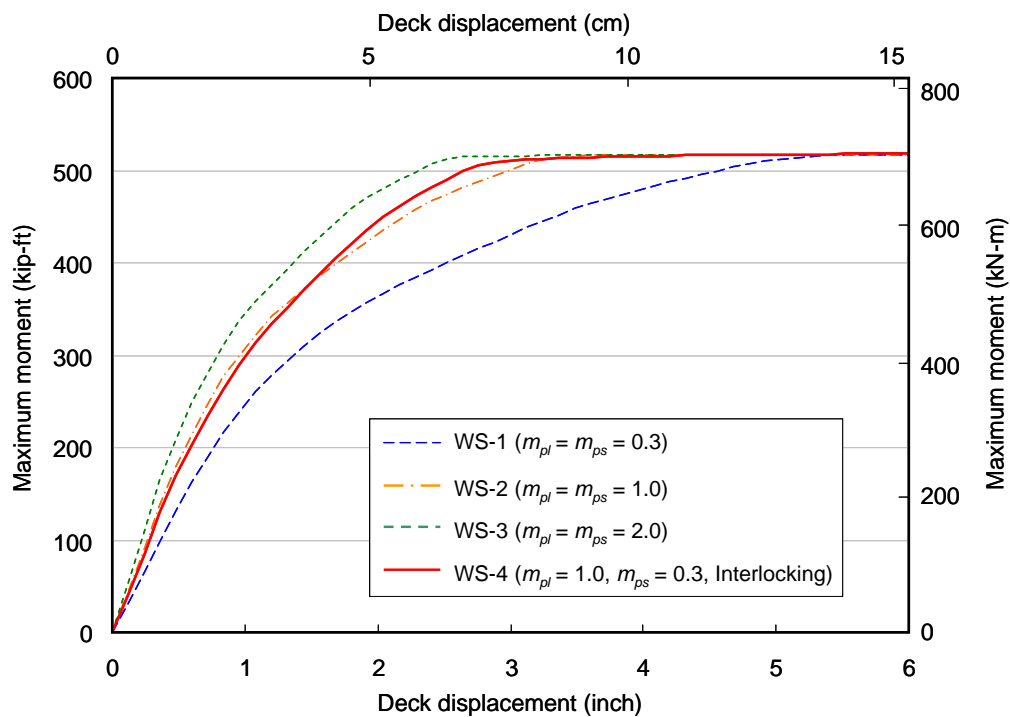


Figure 5-58 Relationship between deck displacement and maximum moment

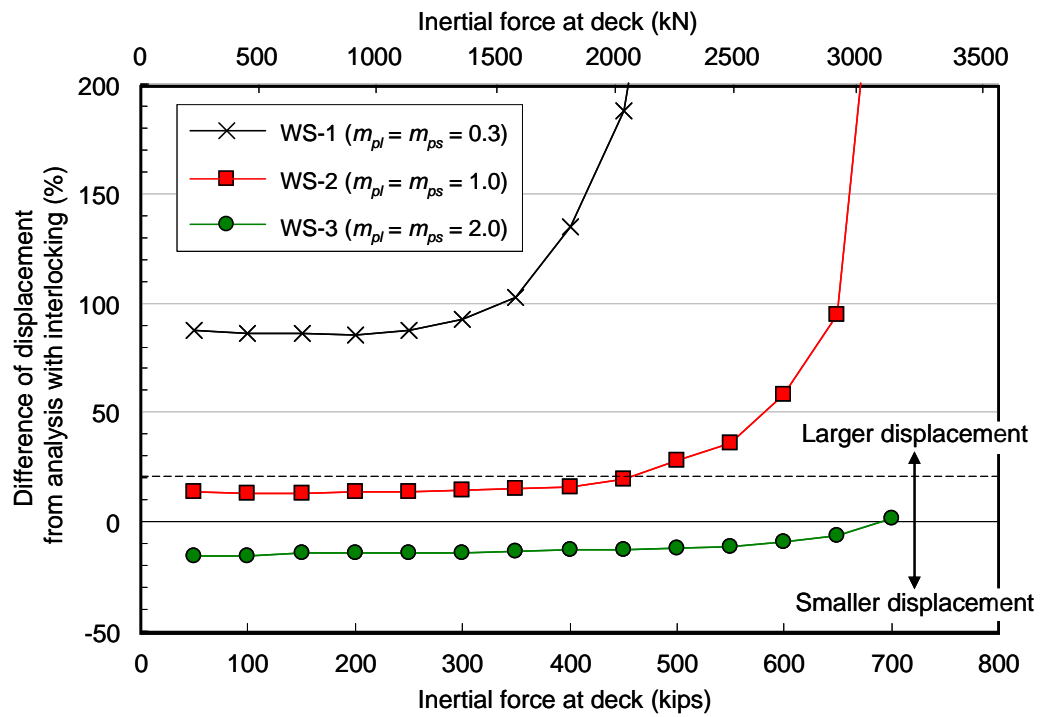


Figure 5-59 Difference of deck displacement among various analysis cases

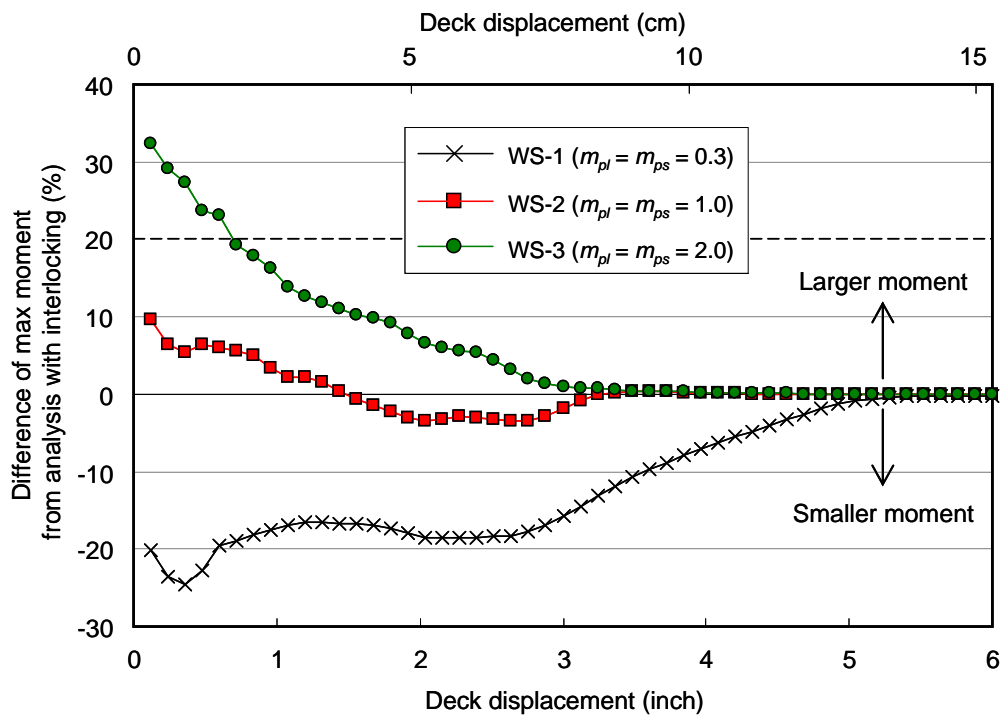


Figure 5-60 Difference of maximum moment among various analysis cases

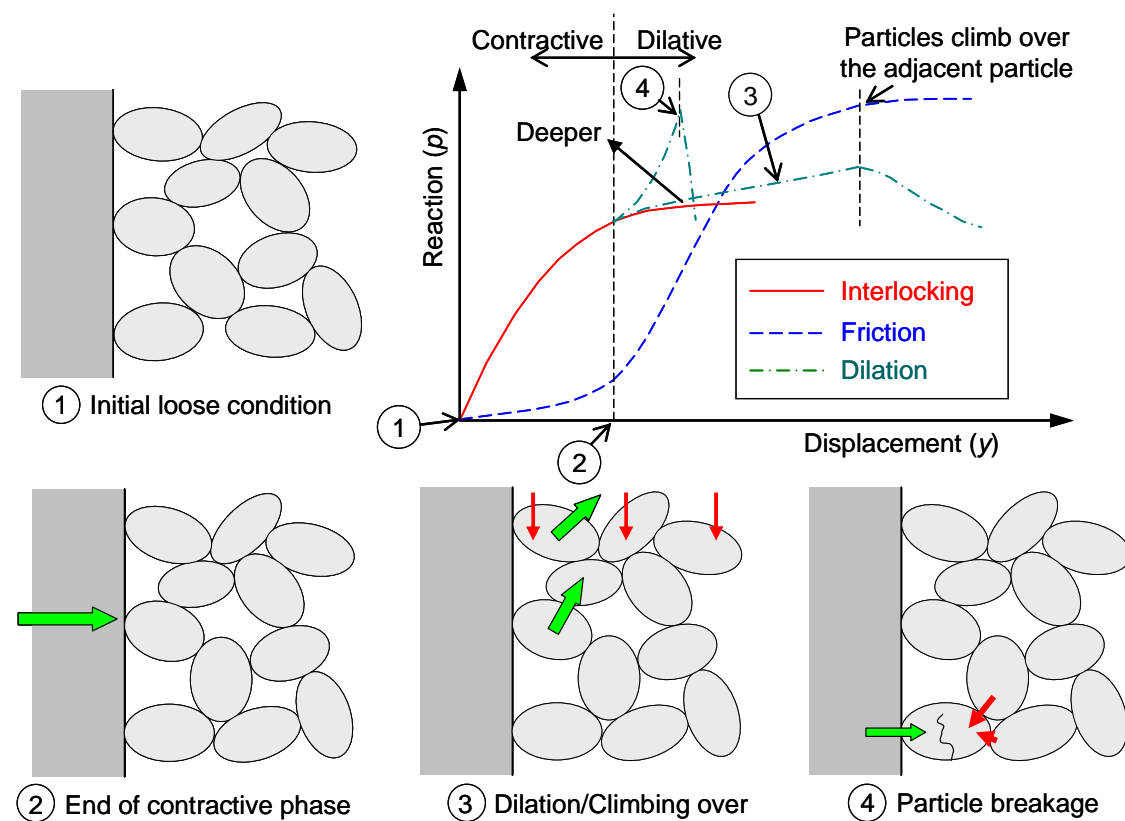
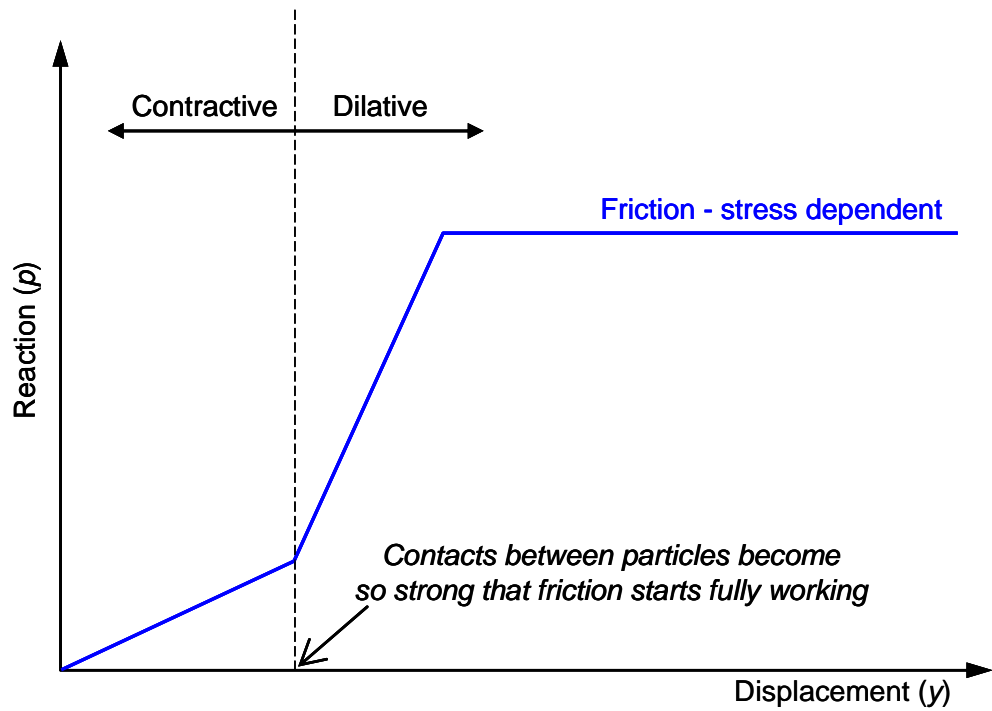
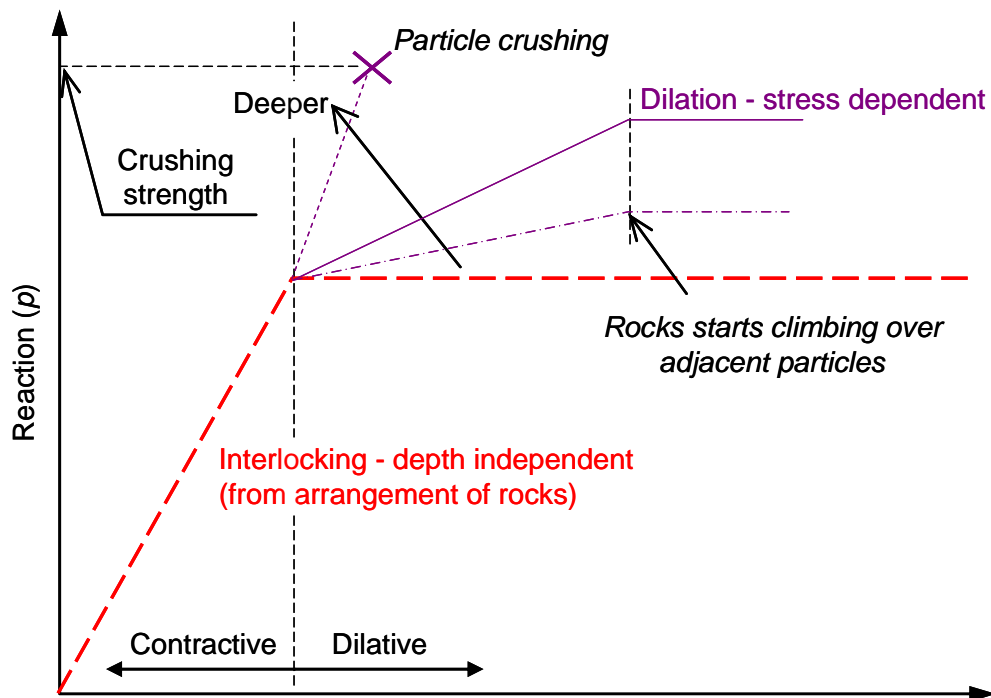


Figure 5-61 Possible mechanism on reaction generation in rockfill



(a) Friction



(b) Interlocking and dilation

Figure 5-62 Simplified p - y curves based on possible reaction generation mechanism in rockfill

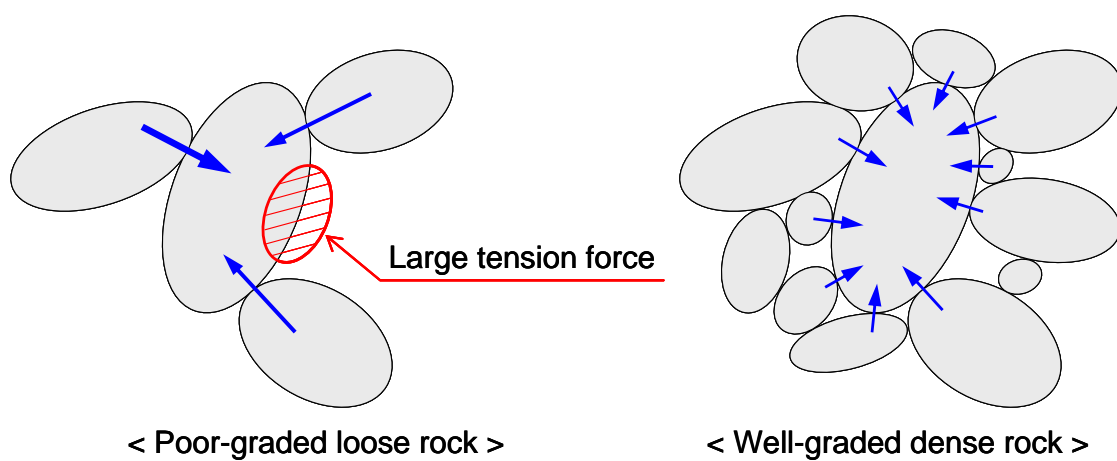


Figure 5-63 Contact forces on a particle in poor- and well-grades rock

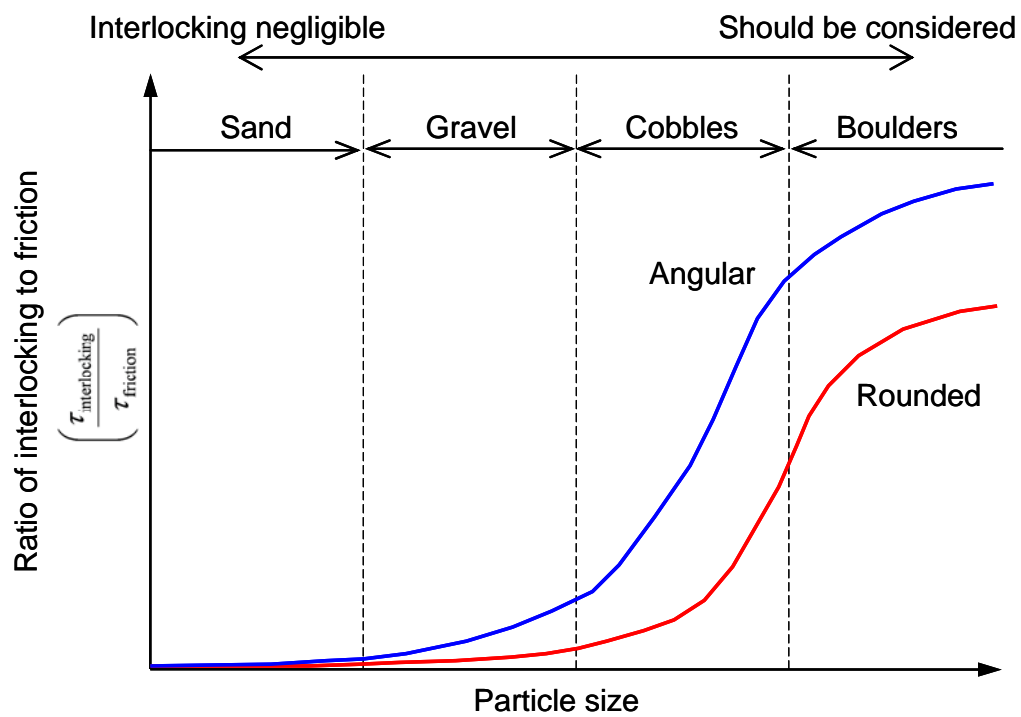


Figure 5-64 Possible relationship between particle size and ratio of interlocking to friction

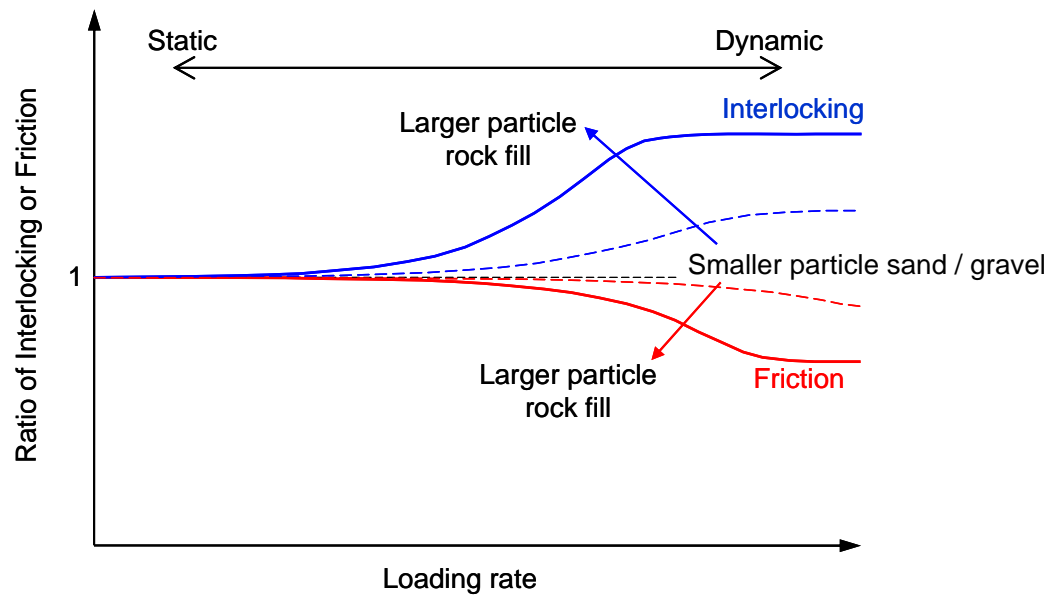
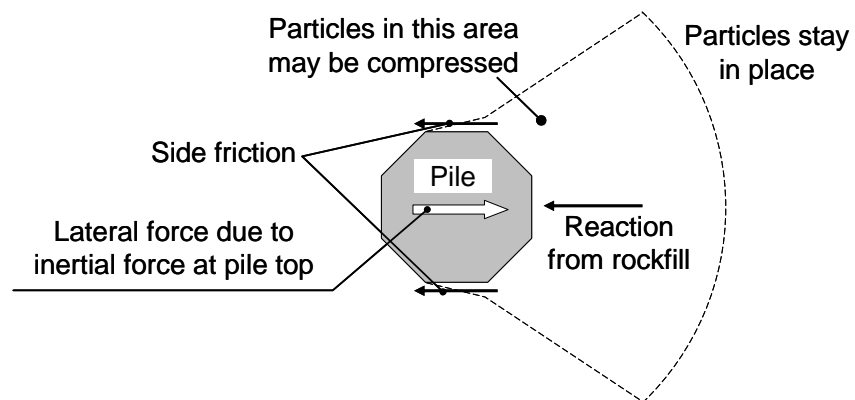
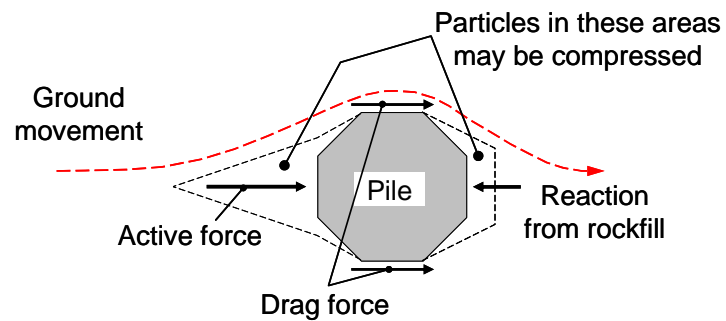


Figure 5-65 Possible relationship between loading rate and friction/interlocking



a) Inertial force



b) Kinematic force

Figure 5-66 Free body diagram around pile

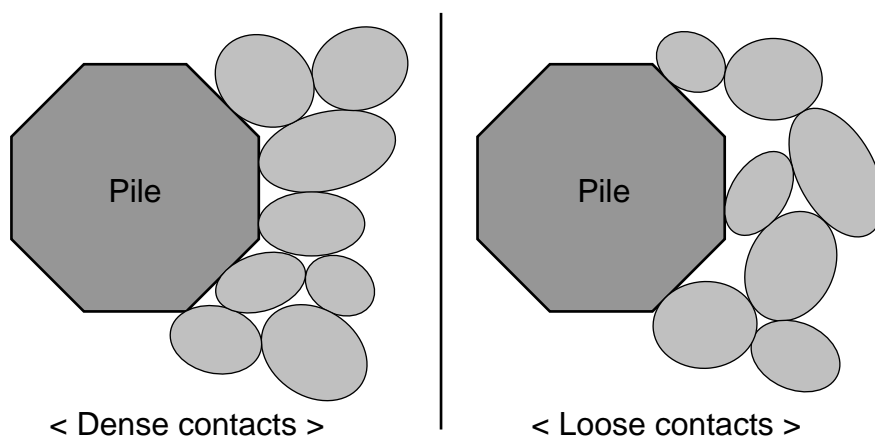


Figure 5-67 Density of contacts in relatively large rockfill

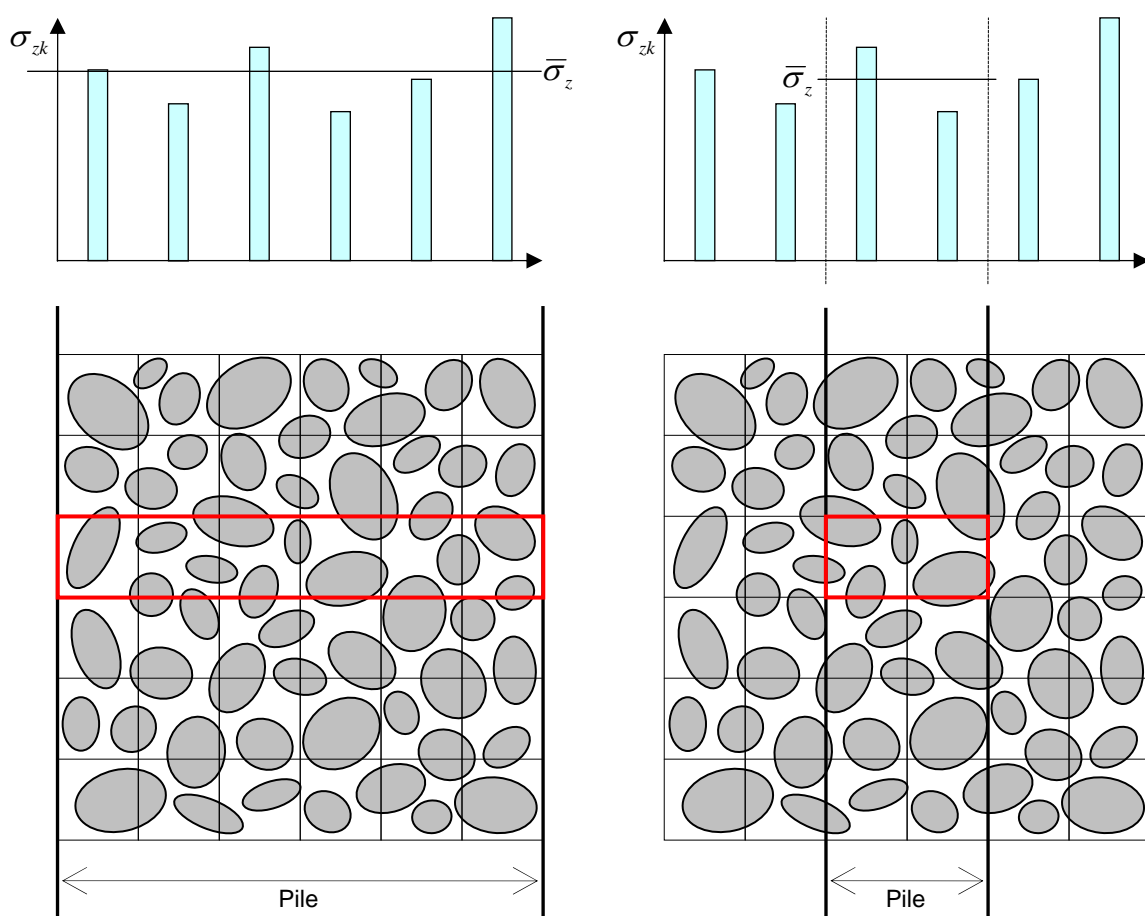


Figure 5-68 Variance of reaction and relative size of soil particles

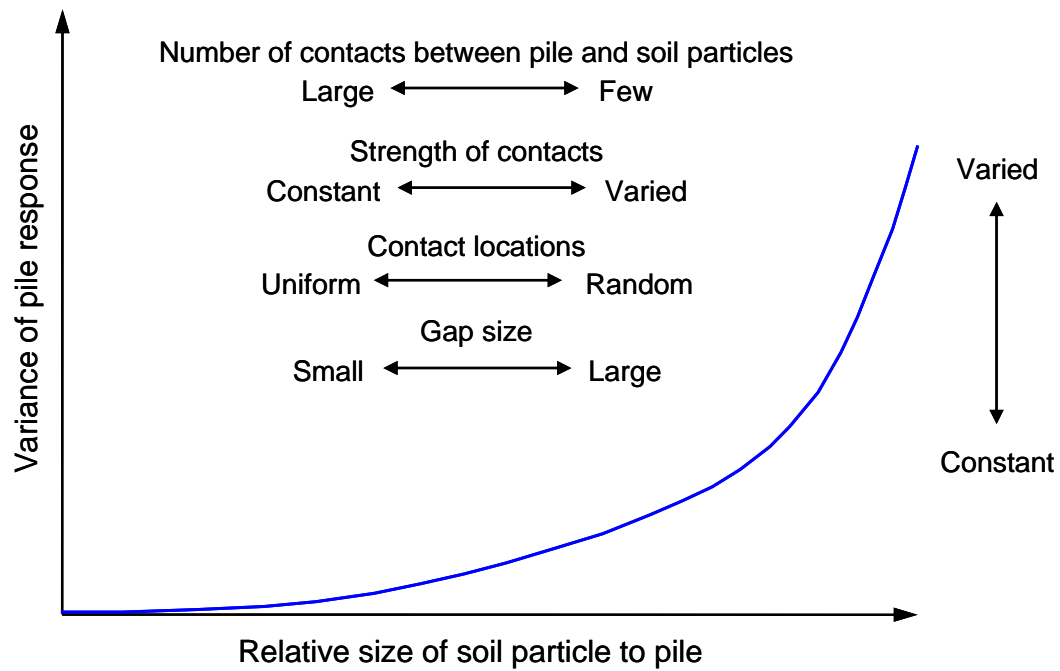


Figure 5-69 Expected relationship between relative size of soil particle and variance of pile response

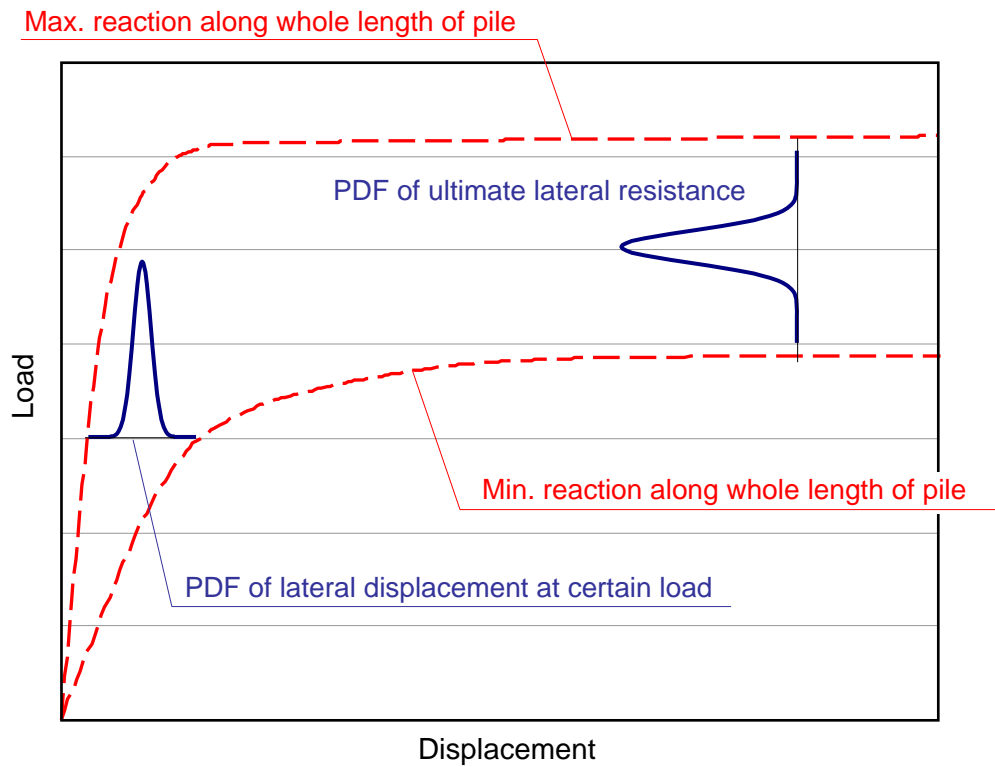


Figure 5-70 Concept of probabilistic analysis on laterally loaded pile response

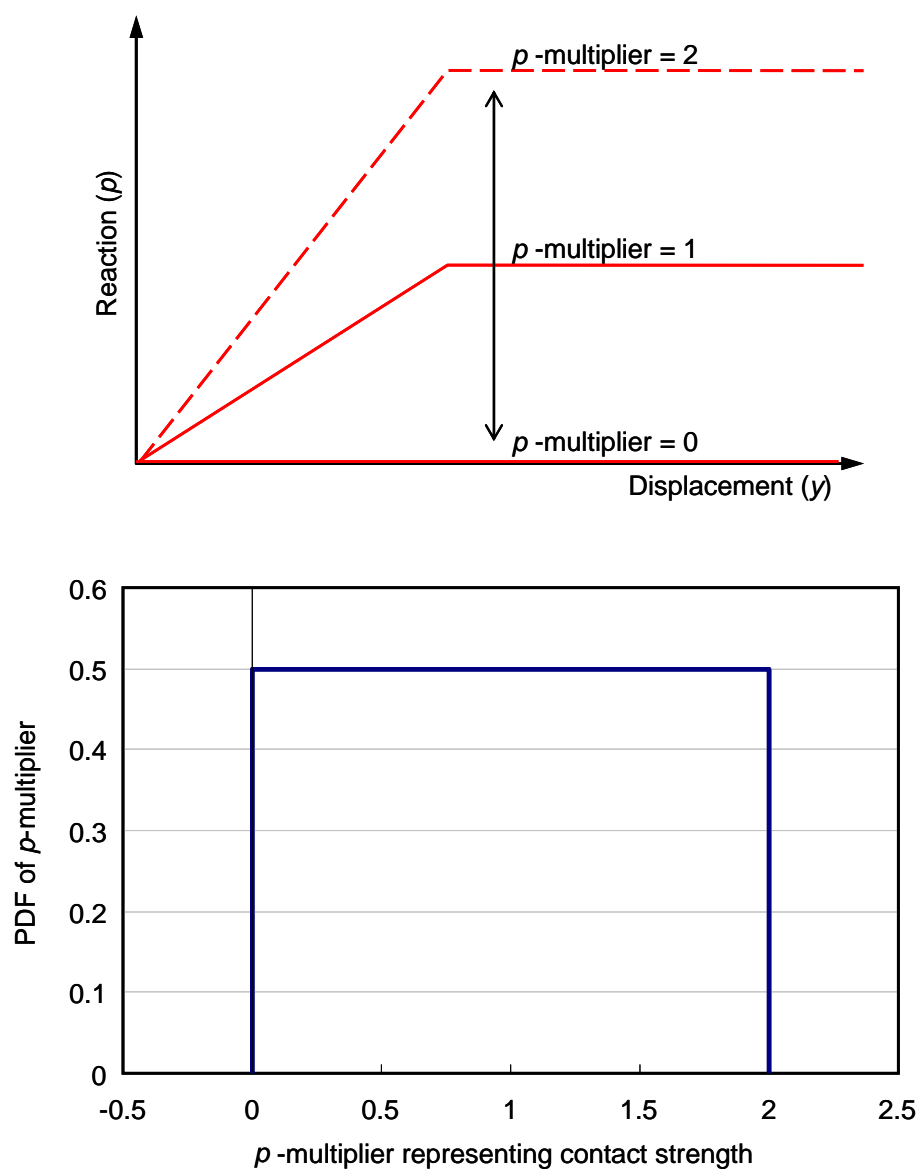


Figure 5-71 Probability density function of p -multiplier representing contact strength

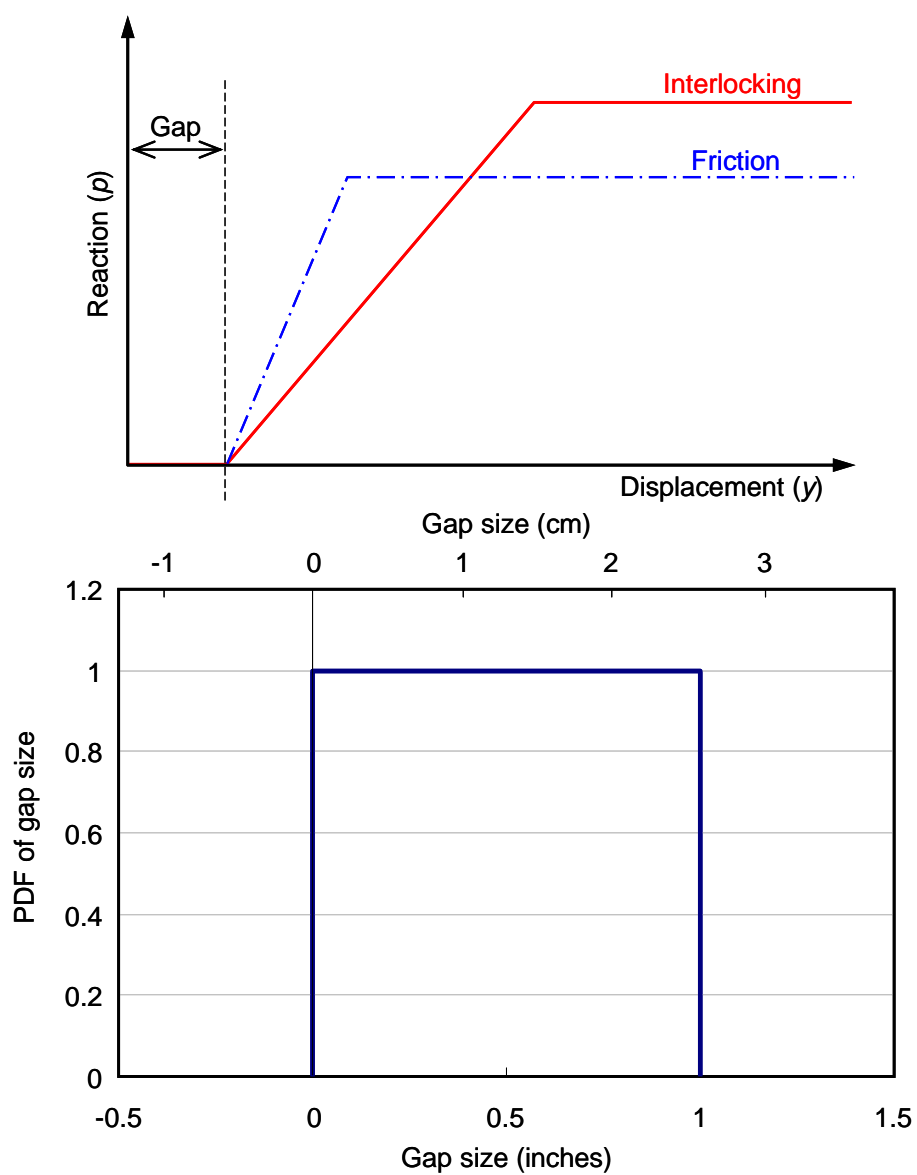


Figure 5-72 Probability density function of gap size

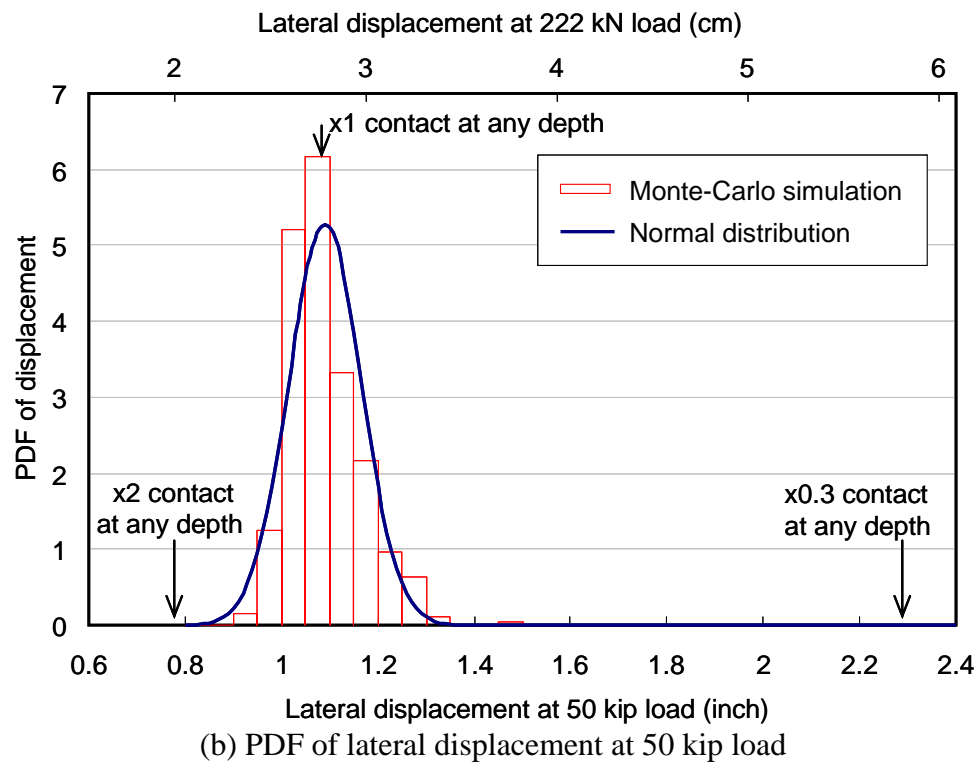
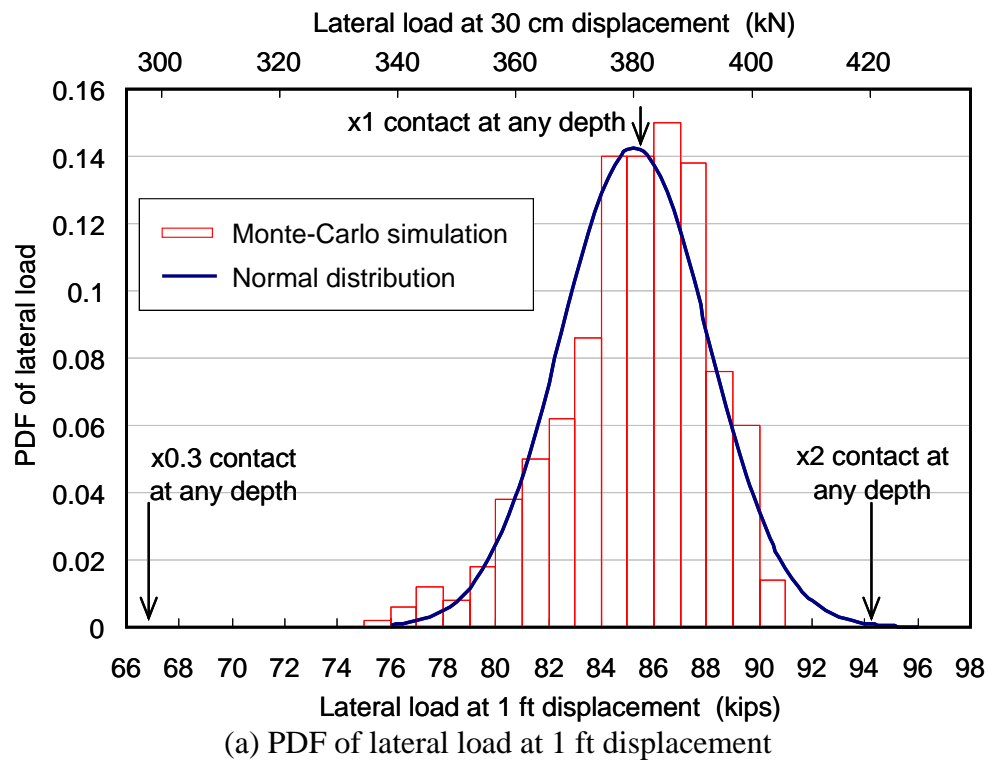


Figure 5-73 Results from Monte-Carlo simulation for random contact strength

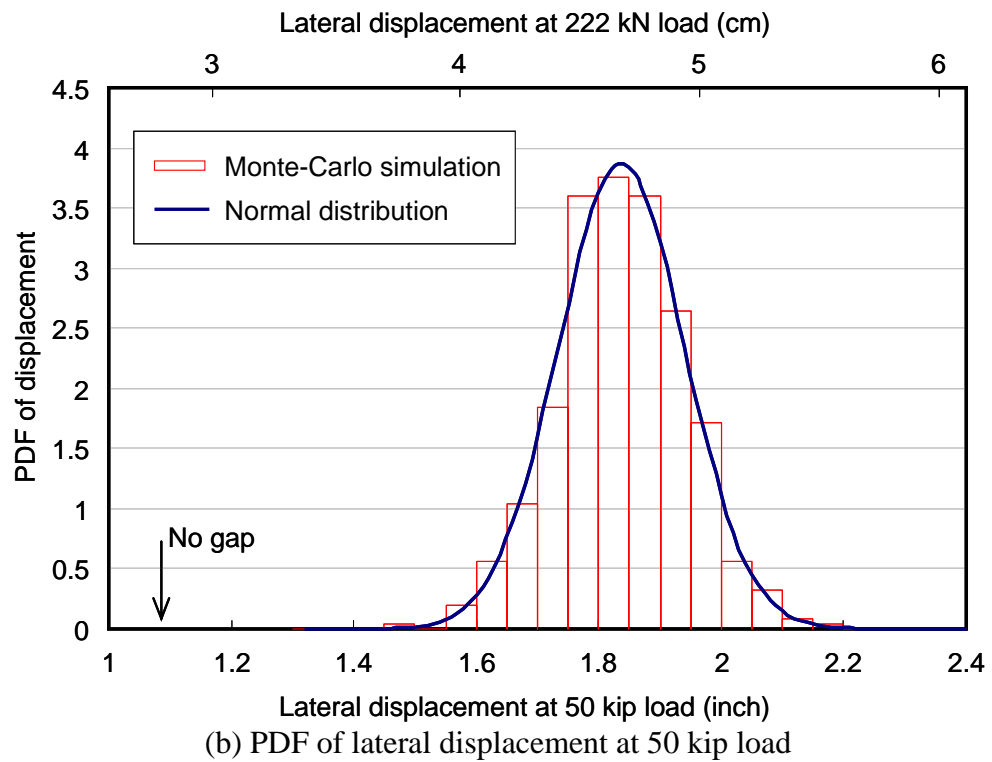
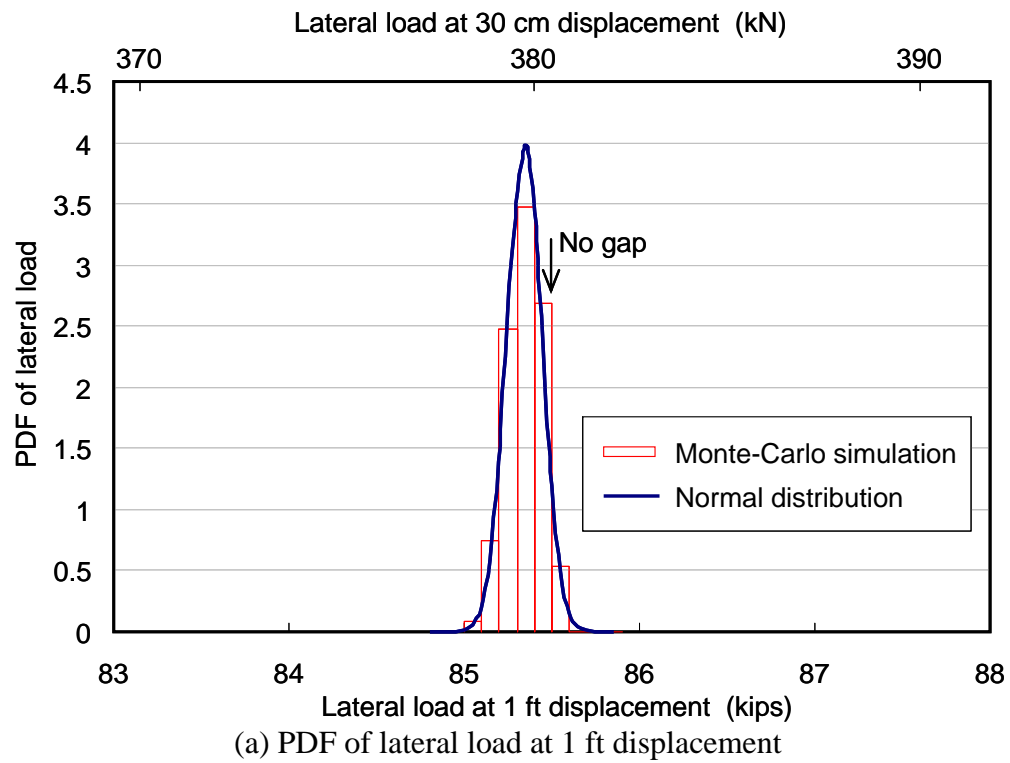


Figure 5-74 Results from Monte-Carlo simulation for random gap size

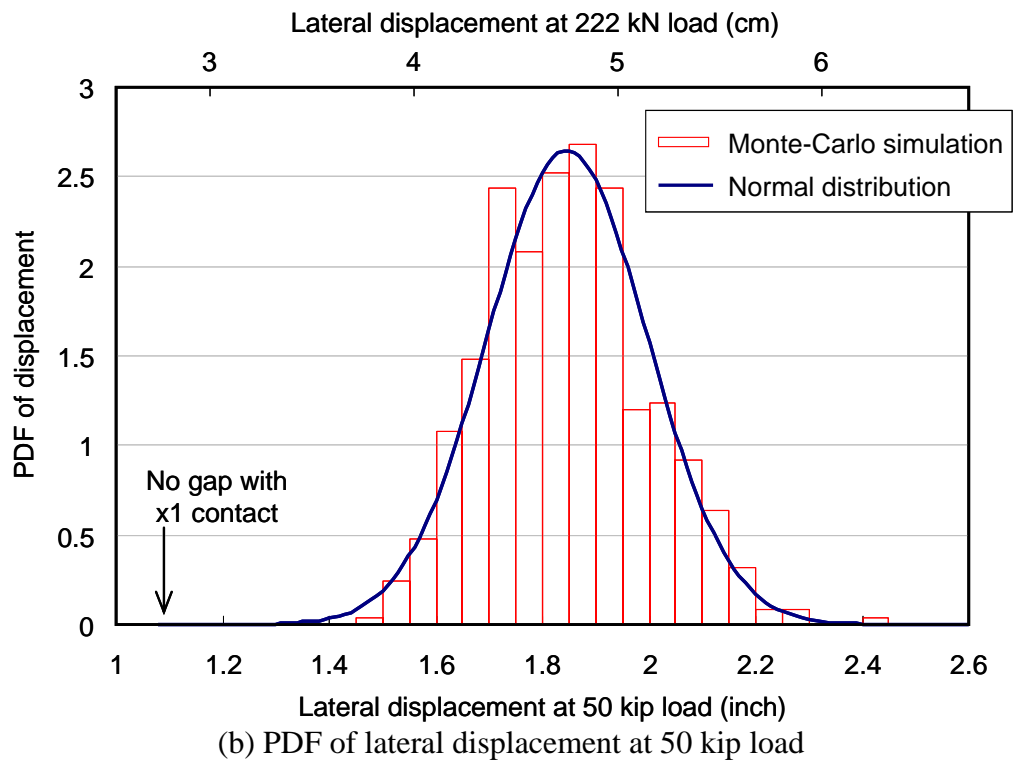
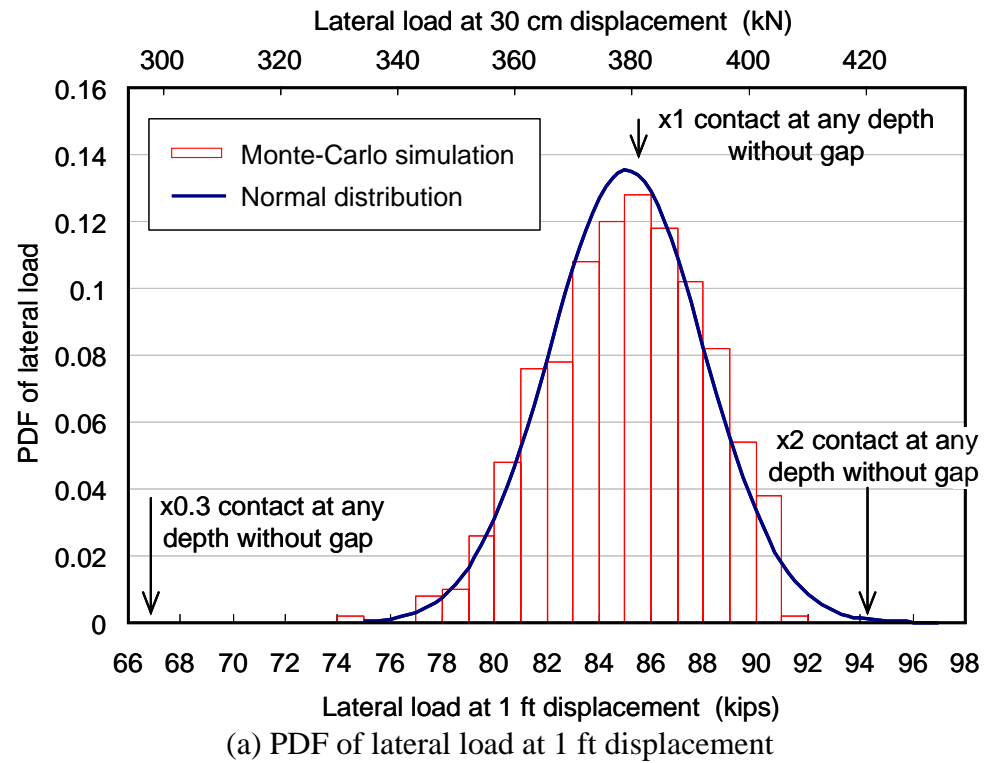
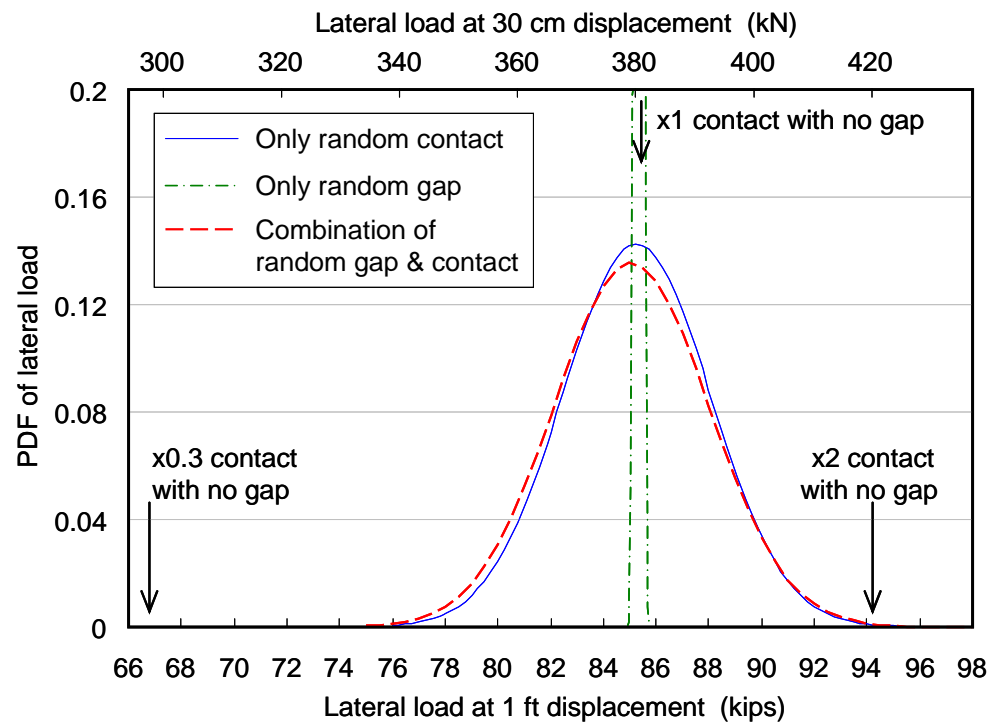
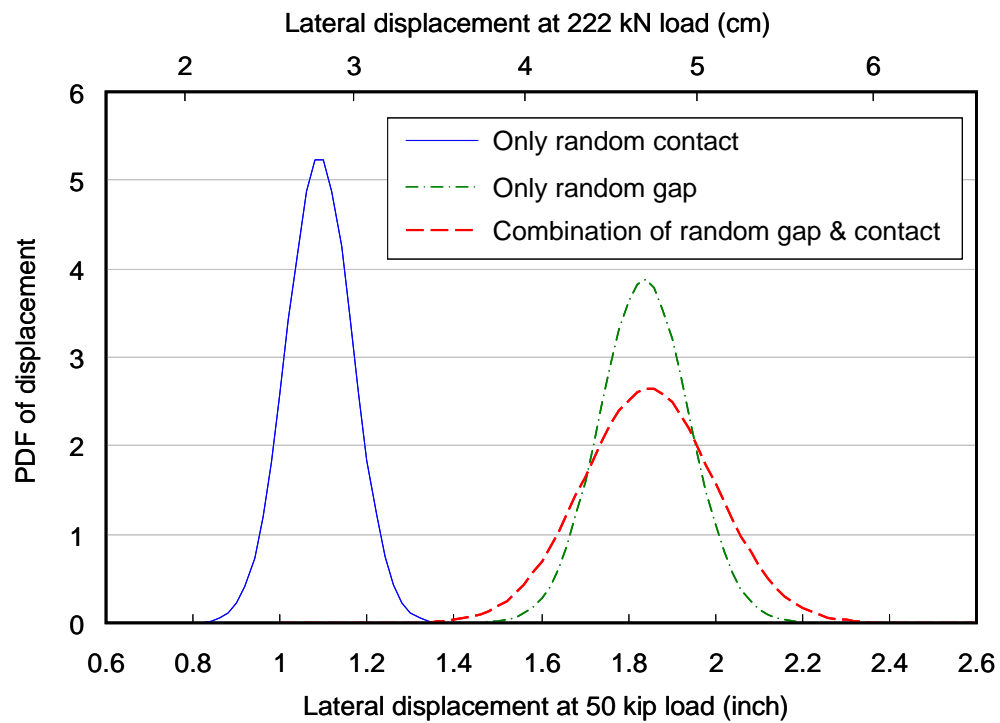


Figure 5-75 Results from Monte-Carlo simulation for random contact and gap size



(a) PDF of lateral load at 1 ft displacement



(b) PDF of lateral displacement at 50 kip load

Figure 5-76 Comparison of PDFs of various analysis cases

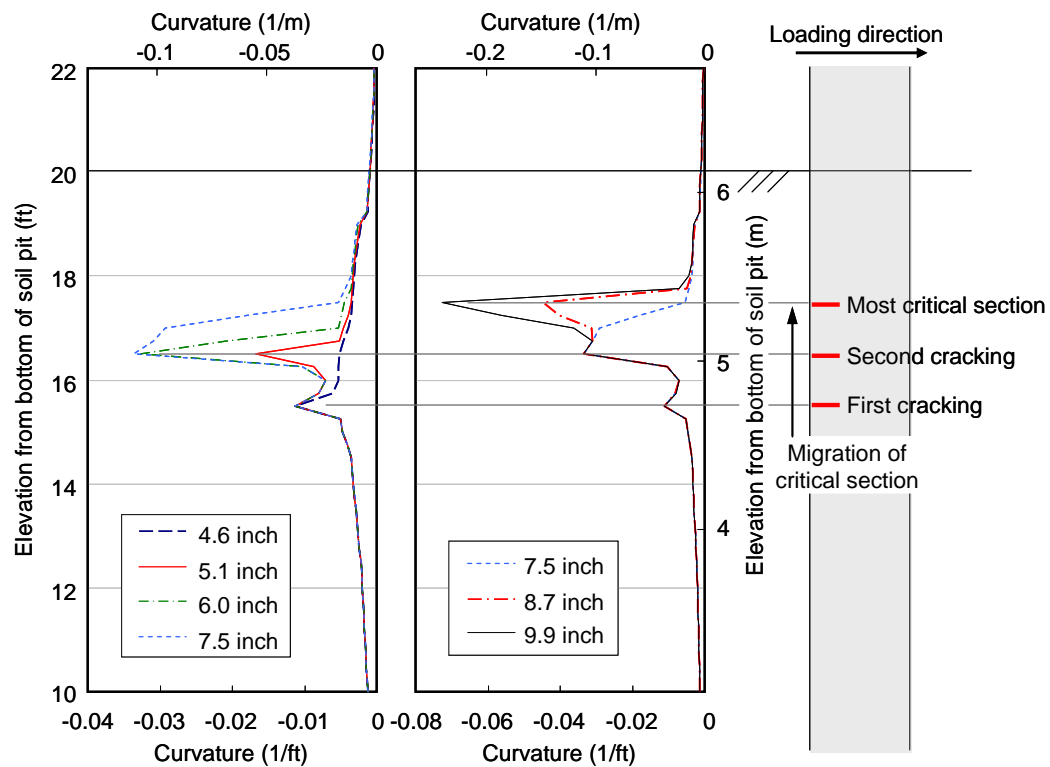


Figure 5-77 An example of critical section migration in analysis

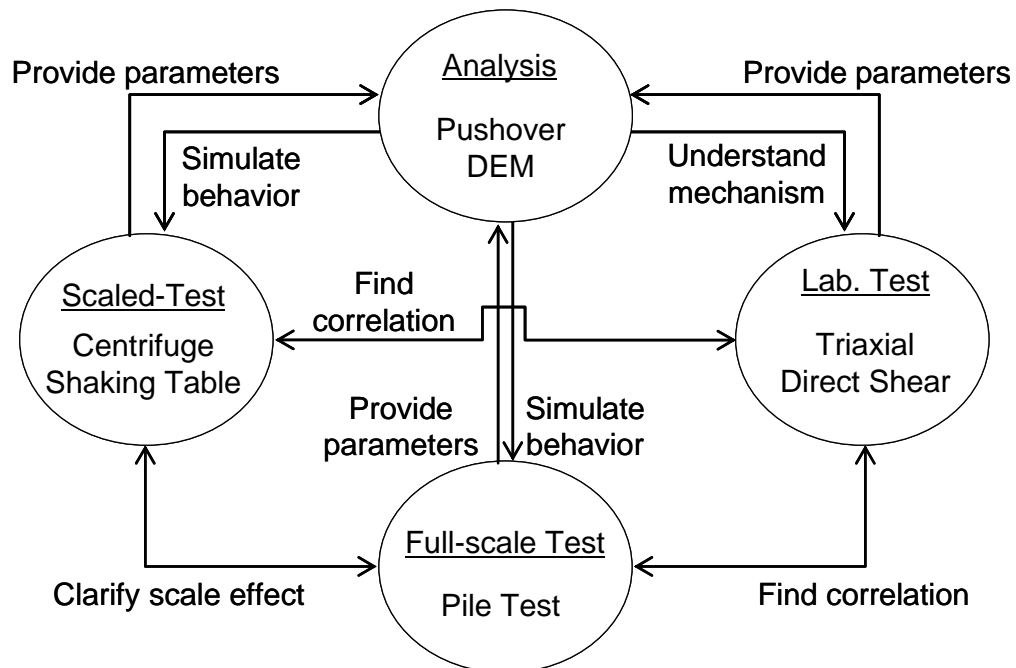


Figure 5-78 Network of experimental and numerical research

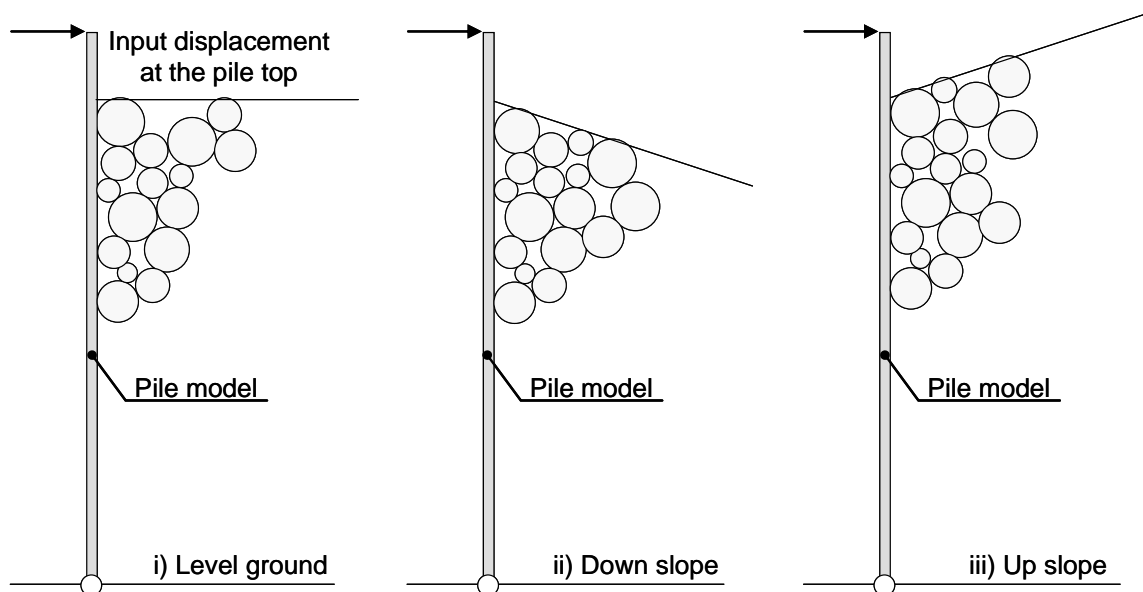


Figure 5-79 Examples of numerical model in DEM on pile behavior for inertial force

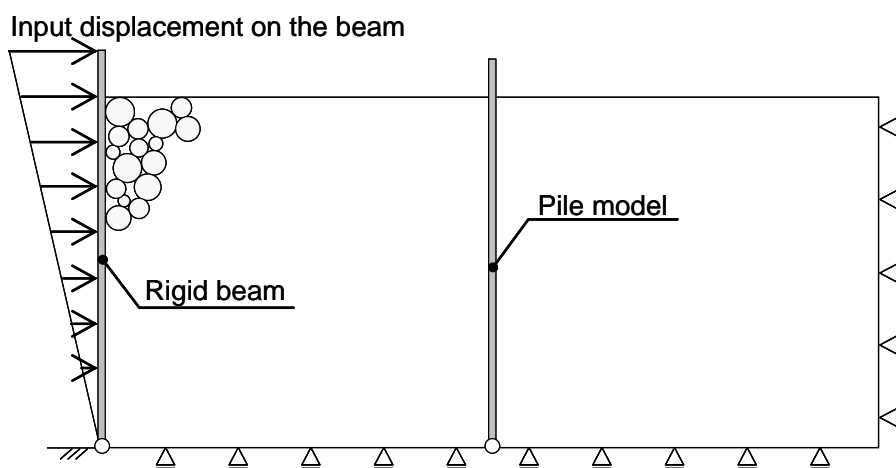


Figure 5-80 An example of numerical model in DEM on pile behavior for kinematic force

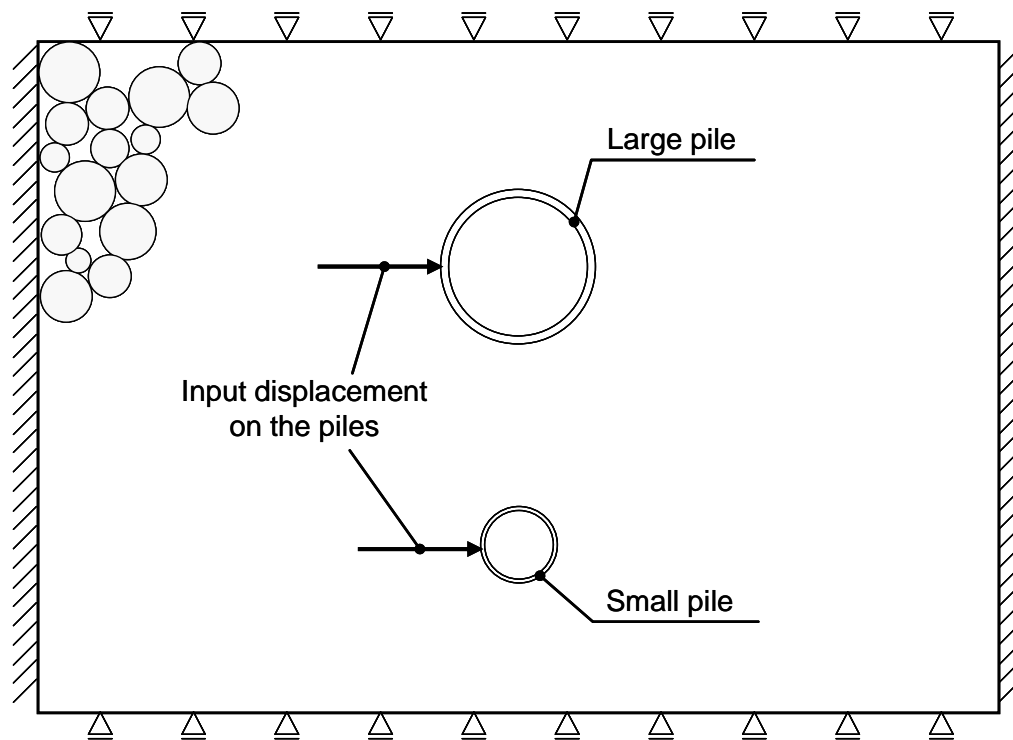


Figure 5-81 An example of numerical model in DEM on relative size of pile to soil particle size

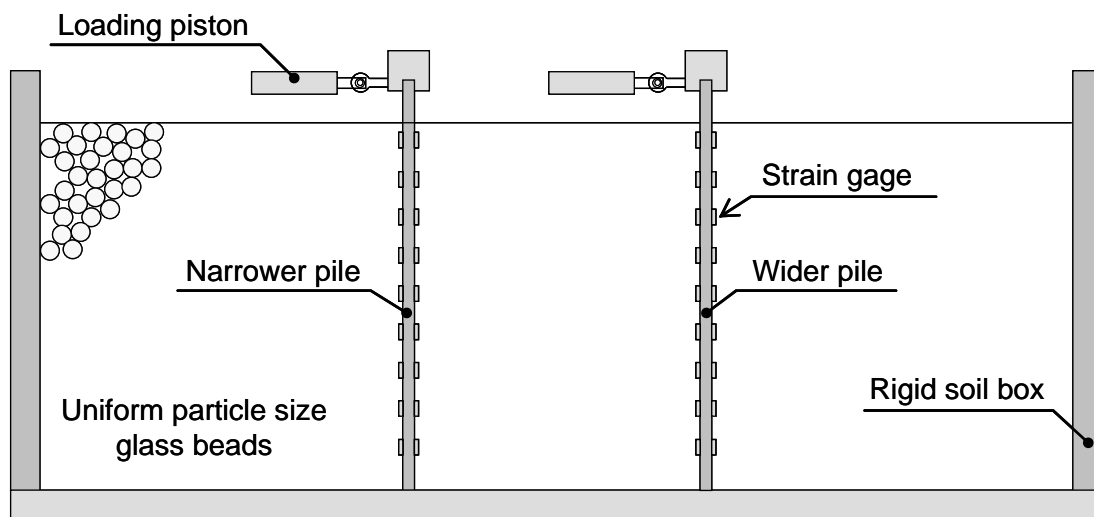


Figure 5-82 An example of setup in centrifuge test on pile behavior for inertial force

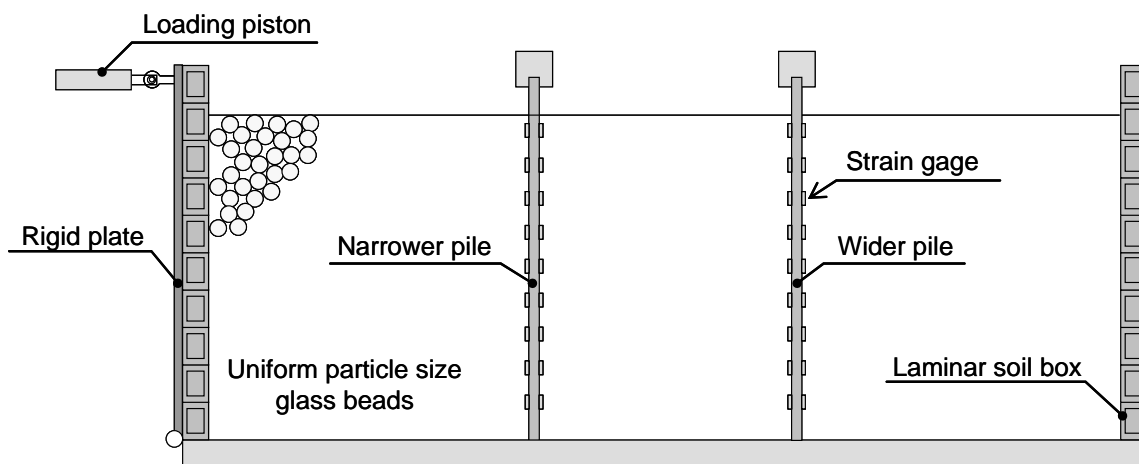


Figure 5-83 An example of setup in centrifuge test on pile behavior for kinematic force

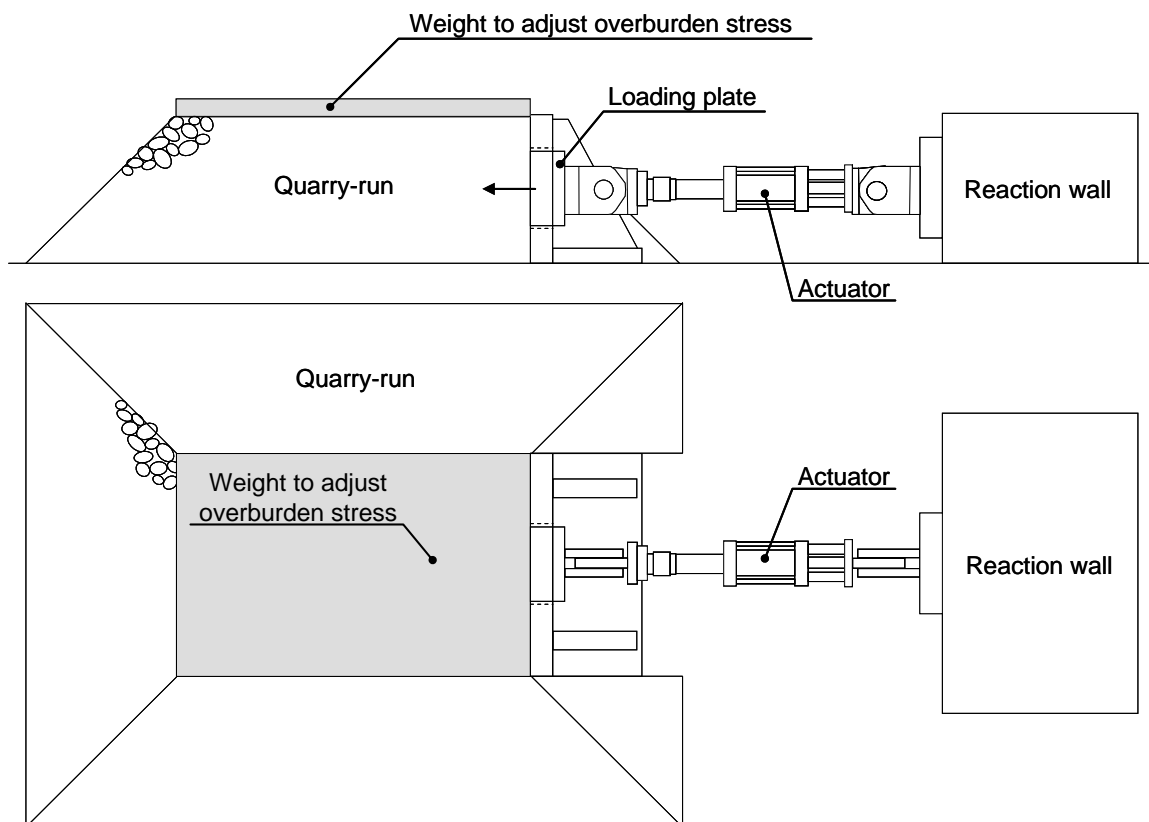


Figure 5-84 An example of setup in full-scale test on p - y curves of rockfill

6 SUMMARY AND CONCLUSIONS

6.1 Summary

Recently, deformation-based design for pile-soil-structure has become more popular, and the design of wharf structures is not an exception. A typical wharf consists of a pile-supported pier type structure, and the piles are usually placed in large particle size rockfill. For development of more reliable and sophisticated design standards for this kind of structure, soil-pile-superstructure interaction is very important, but there was very limited information available about the interaction between pile and rockfill. In order to fill this gap of knowledge, a series of full-scale tests and numerical analyses were performed in this study.

Data obtained in the full-scale tests were analyzed and compared with numerical results obtained using methodology and parameters for the current design practice in order to assess them. According to the comparison between the test and the analysis results, it was concluded that the p - y curves used for the current design gave reasonable, but improvable results. Based on observations during and after the tests, the concept of particle interlocking was added to the p - y curves currently used for design, and it was found that inclusion of the interlocking could improve the numerical results of the pile-soil behavior, such as the load displacement relationship at the pile top and rotation profiles along the piles.

In addition, a pushover analysis of entire wharf structure was conducted using the modified p - y curves with the interlocking concept to estimate the impact of the results in this study. It was concluded that the current design methodology works reasonably well under certain design conditions, but the interlocking should be included for more accurate design of entire wharf structures supported by piles in rockfill. Based on the conclusions, recommendations for design of wharf structures were provided.

Finally, uncertainties on behavior of laterally loaded piles in rockfill were identified. Some examples of possible future research including numerical and experimental were proposed based on the identified uncertainties.

6.2 Conclusions

The main findings of this research study on pile-large particle rockfill interaction based on both of experimental and analytical works are provided as follows:

- 1) The series of full-scale experiments provides a large quantity of useful information about behavior of laterally loaded pile in rockfill.
- 2) The p - y curves used for the current design practice underestimated lateral resistance of the piles, but worked reasonably well to estimate rotation profile along the piles.
- 3) Large reaction under low confinement (i.e. around the ground surface) plays very important role on behavior of laterally loaded pile systems.
- 4) Considering observations during and after the tests, a hypothesis was developed; i.e. the reaction from rockfill is a combination of both friction and interlocking between rock particles. Based on this hypothesis, a stress-independent reaction due to the interlocking was added to the current design methodology, and improved the performance of analysis.
- 5) The pseudo-cohesion due to the interlocking of rock particles backcalculated from the results in this series of full-scale tests is significantly larger than that proposed from centrifuge test results (McCullough and Dickenson 2004). The difference may result from usage of different materials, and scale-effects.
- 6) In the coupled pile tests, both the pile on the level ground and the pile at the slope crest took almost same shear load even in loading toward the downslope, even though the pile at the slope crest exhibited more flexibly. Inclusion of the

interlocking concept can reasonably explain about all the pile responses reasonably well.

- 7) The critical sections along the piles shifted upward as amplitude of input motion became larger. This may be caused by a zone with few or weak contacts between the pile and the rock grains.
- 8) Consideration of the interlocking concept has significant impact on estimation of performance of entire wharf structures. Therefore, inclusion of the interlocking effect is strongly recommended to make more reasonable design.
- 9) In order to estimate behavior of entire wharf structures, the current design methodology with p -multiplier approach can be alternative if design condition is within a certain range. For estimation of possible deck displacement and bending moment along piles using the methodology used for the current design practice, 1 and 2 are recommended as p -multipliers for the lower and the upper bound analyses, respectively. However, this approach gives significantly low ultimate lateral resistance of wharf structures, and interlocking should be considered if the lateral resistance is critical factor in design.
- 10) More numerical and experimental efforts, such as discrete element analysis, centrifuge test, and full-scale test, are needed in order to gain better understanding about particulate reaction mechanism in rockfill and extend knowledge obtained in this study to the different types of soils and piles.

REFERENCES

- Abdoun, T., Dobry, R., O'Rourke, T. D., and Goh, S. H. (2003), "Pile Response to Lateral Spreads: Centrifuge Modeling", *Journal of Geotechnical and Geoenvironmental Engineering*, pp. 869-878, October
- Abrahamson, N. A. (2000), "State of the practice of seismic hazard evaluation", *GeoEng 2000*, Melbourne, Australia
- American Petroleum Institute (API) (1987), "Recommended practice for planning, designing, and constructing fixed offshore platforms", *API Recommended Practice 2A (RP-2A)*, 17th edition
- Anagnosti, P., and Popovic, M. (1982), "Evaluation of shear strength for coarse-grained granular materials", *14th Congress on Large Dams*, Rio de Janeiro, ICOLD, Vol. Q.55, pp. 753-767
- Ashour, M. and Norris, G. (2000), "Modeling Lateral Soil-Pile Response based on Soil-Pile Interaction", *Journal of Geotechnical and Geoenvironmental Engineering*, pp. 420-428, May
- Ashford, S.A., and Juirnarongrit, T. (2004), "Performance of Lifelines Subjected to Lateral Spreading", Report No. SSRP-04/18, Department of Structural Engineering, University of California at San Diego, San Diego, California
- Barber, E. S. (1953), "Discussion to paper by S. M. Gleser", ASTM, STP 154, pp. 94-101
- Bertacchi, P., and Bellotti, R. (1970), "Experimental Research on Materials for Rockfill Dams", Montreal, International Conference of Large Dams, Vol. Q36, pp. 511-529
- Blandon, C.A. (2007), "Seismic Analysis and Design of Pile Supported Wharves" PhD Dissertation, ROSE School, University of Pavia, Italy
- Boland, J. C., Schlechter, S. M., McCullough, N. J., Dickenson, S. E., Kutter, B. L., and Wilson, D. W. (2001a), "Data Report: Pile-Supported Wharf Centrifuge Model (SMS02)", Geotechnical Engineering Group, Department of Civil, Construction and Environmental Engineering, Oregon State University
- Boland, J. C., Schlechter, S. M., McCullough, N. J., Dickenson, S. E., Kutter, B. L., and Wilson, D. W. (2001b), "Data Report: Pile-Supported Wharf Centrifuge Model (JCB01)", Geotechnical Engineering Group, Department of Civil, Construction and Environmental Engineering, Oregon State University

- Boulanger, R. W., Curras, C. J., Kutter, B. L., Wilson, D. W., and Abghari, A. (1999), "Seismic Soil-Pile-Structure Interaction Experiments and Analyses", *Journal of Geotechnical and Geoenvironmental Engineering*, pp. 750-759, September
- Charles, J. A., and Watts, K. S. (1980), "The influence of confining pressure on the shear strength of compacted rockfill", *Geotechnique*, 30, pp.353-367
- Coleman, J. and Spacone, E. (2001), "Localization Issues in Force-Based Frame Elements", *Journal of Structural Engineering*, November,
- Cundall, P. A., and Strack, O. D. L. (1971), "A discrete numerical model for granular assemblies", *Geotechnique*, 29, No.1, pp. 47-65
- Davisson, M. T., and Gill, H. L. (1963), "Laterally loaded piles in a layered soil", *Journal of Soil Mechanics and Foundations*, ASCE, 89(3), pp. 63-94
- Diaz, G. M., Patton, B. W., Armstrong, G. L., and Joolazadeh, M. (1984), "Lateral Load Tests of Piles in Sloping Rock Fill", Proceedings of the Analysis and Design of Pile Foundations Conference. J.R. Meyer editor. Held at the ASCE National Convention, San Francisco, California, October 1-5. pp 214-231
- Dunnivant, T. W., and O'Neill, M. W. (1985), "Performance analysis and interpretation of a lateral load test of a 72-inch-diameter bored pile in overconsolidated clay", *Report UHCE 85-4*, Department of Civil Engineering, University of Houston, Texas, 57 p.
- Hardin, B. O. (1985), "Crushing of Soil Particles", *Journal of Geotechnical Engineering*, Vol. 111, No. 10, October, pp. 1177-1182
- Hetenyi, M. (1946), *Beams on Elastic Foundations*, University of Michigan Press, Ann Arbor, Michigan.
- Ismael, N. F. (1990), "Behavior of laterally loaded bored piles in cemented sands", *Journal of Geotechnical Engineering*, ASCE, 116(11), pp. 1678-1699
- Jaradat, O. A. Arulmoli, A. (2005) "Port of Los Angeles Seismic Code: Case Study", POLA Seismic Code Workshop, Los Angeles, September 13
- Jensen, R. P., Plesha, M. E., Edil, T. B., Bosscher, P. J., and Kahla, N. B. (2001), "DEM simulation of particle damage in granular media-structure interface", *International Journal of Geomechanics* 1, No. 1, pp. 23-39.
- Juirnarongrit, T., and Ashford, S. A. (2005), "Effect of Pile Diameter on the Modulus of Sub-grade Reaction", Report No. SSRP-2001/22, Department of Structural Engineering, University of California at San Diego

- Juirnarongrit, T., and Ashford, S. A. (2004), "Performance of lifelines subjected to lateral spreading", Report No. SSRP-04/18, Department of Structural Engineering, University of California at San Diego
- Kawamata, Y., Ashford, S. A., and Juirnarongrit, T. (2006), "Numerical simulation of soil-foundation interaction subjected to lateral spreading", 5th National Seismic Conference for Bridges and Highways, San Francisco, September 18-20
- Kawamata, Y., Blandon, C. A., Ashford, S. A., and Restrepo, J. I. (2007), "Seismic Performance of Container Wharf Piles", Report No. TR-2007/06, Department of Structural Engineering, University of California at San Diego
- Krier, C. J., Restrepo, J. I., Blandon, C. A. (2006), "Seismic Testing of Full-Scale Precast Prestressed Pile to Deck Connections", Report No. SSRP-2006/26, Department of Structural Engineering, University of California at San Diego
- Lade, P. V., and Duncan, J. M. (1975), "Elastoplastic Stress-Strain Theory for Cohesionless Soil", *Journal of the Geotechnical Engineering Division*, October, pp. 1027-1052
- Lade, P. V. (1977), "Elasto-plastic Stress-Strain Theory for Cohesionless Soil with Curved Yield Surfaces", *International Journal of Solids Structures*, Vol. 13, pp. 1019-1035
- Leps, T. M. (1970), "Review of shearing strength of rockfill", *Journal of the Soil Mechanics and Foundations Division*, 96 (SM4), pp.1159-1170
- Lobo-Guerrero, S. and Vallejo, L. E. (2005), "DEM analysis of crushing around driven piles in granular materials", *Geotechnique* 55, No. 8, pp. 617-623
- Marachi, N. D., Chan, C. K., Seed, H. B., and Duncan, J. M. (1969), "Strength and Deformation Characteristics of Rockfill Materials", *TE-69-5*, Department of Civil Engineering, University of California at Berkeley
- Marsal, R. J. (1973), "Mechanical properties of rockfill", *Embankment-Dam Engineering Casagrande Volume*, Willey & Sons, N.Y., pp. 109-201
- Martin, G. (2005), "Port of Los Angeles Seismic Code: Presentation on Geotechnical Aspects", POLA Seismic Code Workshop, Los Angeles, September 13.
- Matlock, H. and Reese, L. C. (1960), "Generalized solutions for laterally loaded piles", *Journal of Soil Mechanics and Foundations, Div.*, ASCE, 86(5), pp. 63-91.

- Matlock, H. (1970), "Correlations for design of laterally loaded piles in soft clay", *Proceeding of 2nd Annual Offshore Technology Conference, Paper No. OTC 1204*, Houston, Texas, pp. 577-594.
- Matsuoka, H., and Nakai, T. (1982), "Deformation and failure of granular materials", *Symposium on Deformation and Failure of Granular Materials*, Delft, Aug. 31-Sept. 3, Balkema, pp. 253-263.
- McCullough, N., and Dickenson, S. (2004), "The Behavior of Piles in Sloping Rock Fill at Marginal Wharves", *Ports 2004*, May 23-26, Houston, Texas.
- McKenna, F. (1997), "Object oriented finite element analysis: Frameworks for analysis algorithms and parallel computing", PhD Thesis, University of California at Berkeley.
- Merchetti, S. Totani, G., Calabrese, M., and Monaco, P. (1991), "P-y curves from DMT data for piles driven in clay", *Proceeding of International Conference on Piling and Deep Foundations*, DFI, Stresa, Vol. 1: pp.263-272.
- Newmark, N.M. (1965), "Effects of earthquakes on dams and embankment", *Geotechnique*, 15(2), pp. 139-160
- O'Neill, M. W., and Dunnavant, T. W. (1984), "A study of effect of scale, velocity, and cyclic degradability on laterally loaded single piles in overconsolidated clay", *Report UHCE 84-7*, Department of Civil Engineering, University of Houston, Texas, 368 p.
- Port of Los Angeles (2004), "POLA Code for Seismic Design, Upgrade, and Repair of Container Wharves", California, May
- Poulos, H. G., and Davis, E. H. (1980), *Pile Foundation Analysis and Design*, John Wiley, New York
- Reese, L. C., Cox, W. R., and Koop, F. D. (1974), "Analysis of laterally loaded piles in sand," *Proceeding of 6th Offshore Technology Conference, Paper 2080*, Houston, Texas, pp. 473-483.
- Reese, L. C., Cox, W. R. and Koop, F. D. (1975), "Field testing and analysis of laterally loaded piles in stiff clay", *Proceeding of 7th Offshore Technology Conf., Paper No. OTC 2321*, Houston, Texas, pp. 671-690.
- Reese, L. C., and Van Impe, W. F. (2001), *Single Piles and Pile Groups under Lateral Loading*, Balkema, Rotterdam, Brookfield
- Reese, L. C., and Welch, R. C. (1975), "Lateral loading of deep foundation in stiff clay", *Journal of Geotechnical Engineering Division*, ASCE, 101(7), pp. 633-649

Reese, L.C., Wang, S. T., Isenhower, W. M., and Arrellaga, J. A. (2000), *Computer Program LPILE Plus Version 4.0 Technical Manual*, Ensoft, Inc., Austin, Texas.

Terzaghi, K. (1955), "Evaluation of coefficients of subgrade reaction", *Geotechnique*, 5(4), pp. 297-326

TRC/Imbsen Software Systems (2007), *XTRACT v3.0.8*, Rancho Cordova, CA

University of Florida (1996). *User's Manual for FLORIDA-PIER Program*, Dept. of Civil Engineering, University of Florida, Gainesville

US Army Corps of Engineers (1991), *Design of Pile Foundations*, Washington, DC

Vesic, A. S. (1961), "Beam on elastic subgrade and the Winkler hypothesis", *Proceeding of 5th International Conference Soil Mechanics and Foundation Engineering*, Paris, Vol. 1, pp. 845-850

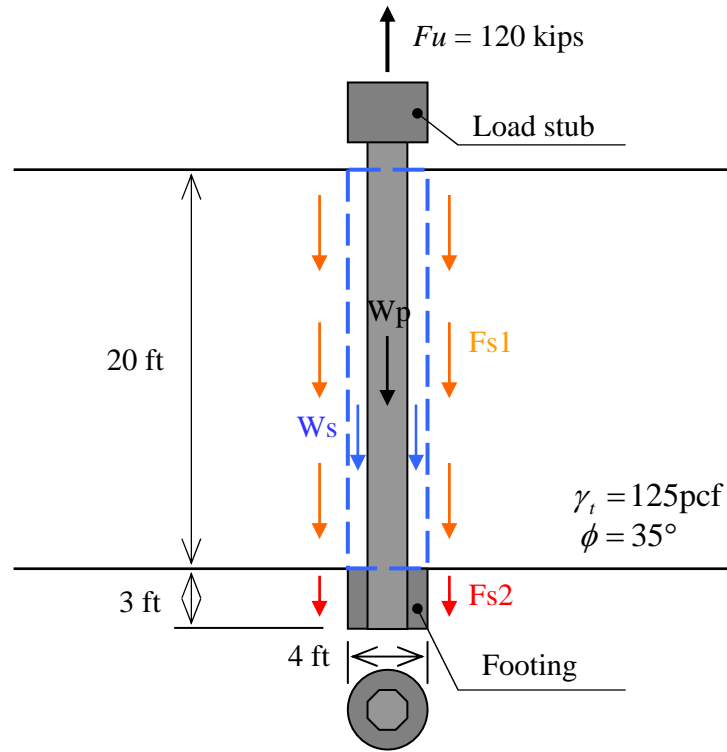
Wang, S. and Reese, L. C. (1993), "COM624P-Laterally loaded pile analysis program for the microcomputer, version 2.0", *FHWA-SA-91-048*, U.S. DOT, Federal Highway Administration

Winkler, E. (1867), "Die lehre von elasticzitat and festigkeit (on elasticity and fixity)", *Prague*, 182 p

Yamamuro, J. A., and Lade, P. V. (1993), "Effects of Strain Rate on Instability of Granular Soils", *ASTM Geotechnical Testing Journal*, Vol. 16, pp. 304-313

Appendix-A Uplift capacity of pile

Method A (Cylindrical shape - Conservative Estimate)



Q_u : Ultimate resistance against uplift force

$$= F_{s1} + F_{s2} + W_p + W_s$$

W_p : Weight of Footing + Weight of Pile + Weight of Load Stub

$$= 150 \text{ pcf} \left[\pi (4 \text{ ft})^2 / 4 (3 \text{ ft}) + \pi (2 \text{ ft})^2 / 4 (21.5 \text{ ft}) + (4 \text{ ft})(4 \text{ ft})(3 \text{ ft}) \right] = 23 \text{ kips}$$

W_s : Weight of soil resisting uplift force

$$= 125 \text{ pcf} \left\{ \pi \left[(4 \text{ ft})^2 - (2 \text{ ft})^2 \right] / 4 (20 \text{ ft}) \right\} = 23 \text{ kips}$$

F_{s1} : Friction along pile

$$= A S_1 K_0 \sigma'_v \tan \phi = [\pi (4 \text{ ft})(20 \text{ ft})] (1 - \sin 35^\circ) (125 \text{ pcf} (10 \text{ ft})) \tan 35^\circ = 94 \text{ kips}$$

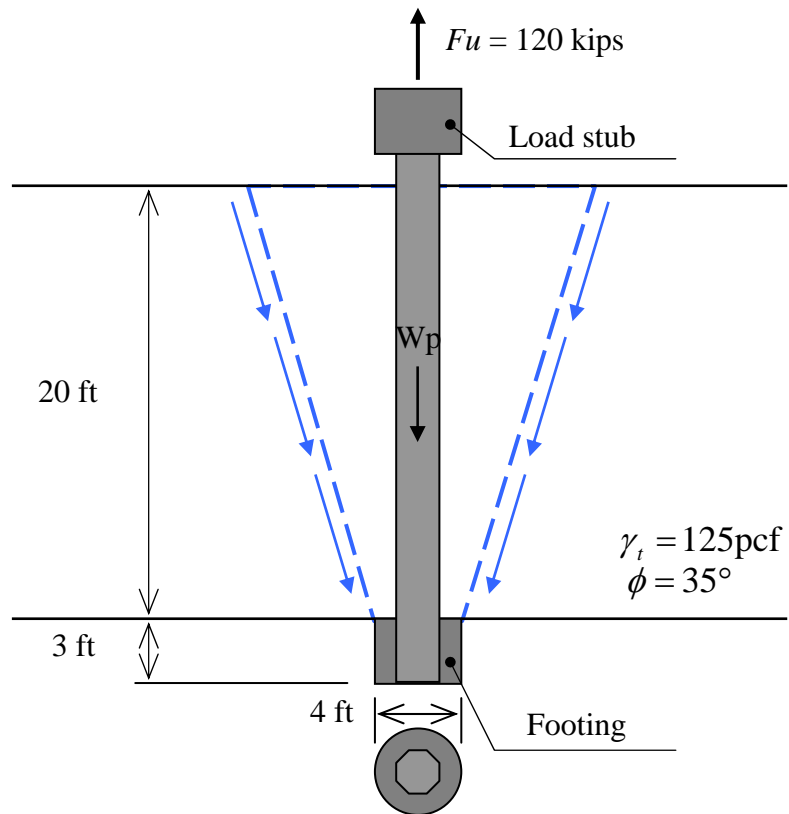
F_{s2} : Friction along footing

$$= A S_2 K_0 \sigma'_v \tan \phi = [\pi (4 \text{ ft})(3 \text{ ft})] (1 - \sin 35^\circ) (125 \text{ pcf} (21.5 \text{ ft})) \tan (0.7 \times 35^\circ) = 20 \text{ kips}$$

$$Q_u = 23 + 23 + 94 + 20 = 160 \text{ kips}$$

$$FS = Q_u / F_u = 160 \text{ kips} / 120 \text{ kips} = 1.33$$

Method B (Meyerhof and Adams, 1968 and Das and Seeley, 1975)



Q_u : Ultimate resistance against uplift force

$$= B_q AE \gamma_t L + W_p$$

B_q : Breakout factor = 10 for $\phi = 35^\circ$

$$Q_u = 10 \pi (4^2 / 4) (125 \text{ pcf}) (20 \text{ ft}) + 23 \text{ kips} = 337 \text{ kips}$$

$$FS = Q_u / F_u = 337 \text{ kips} / 120 \text{ kips} = 2.81$$

Appendix-B Specification of Rockfill

Rock Mass		No. 2 Backing % larger than
Standard	Metric	
75 lbs	34 kg	2
25 lbs	11 kg	58
5 lbs	2.2 kg	92
Durability Index (Cal 229)		78
Bulk Specific Gravity Oven Dry (ASTM C127)		2.72
Bulk Specific Gravity SSD (ASTM C127)		2.75
Apparent Specific Gravity (Cal 206)		2.79
Percent Absorption (Cal 206)		0.9
Sodium Sulfate Soundness (ASTM C88)		
Total % loss by weight		2.1

**Visual approval by project engineer is required.

June 2005



Hanson Aggregates
 Pacific Southwest Region
 P.O. Box 639069
 San Diego, CA 92163-9069
 Tel (858) 715-5611
 Fax (858) 715-5601
 www.hansonplc.com

**LABORATORY TESTING OF No. 2 BACKING AGGREGATE
 OTAY QUARRY PLANT**

Sieve Analysis (ASTM C136 and C117)

THIS PAGE LEFT BLANK